MARTIN MARIETTA ENERGY SYSTEMS LIBRARIES
3 4456 0322247 5

ORNL-3452
UC-10 – Chemical Separations Processes
for Plutonium and Uranium
TID-4500 (22nd ed.)

CHEMICAL TECHNOLOGY DIVISION
ANNUAL PROGRESS REPORT
FOR PERIOD ENDING MAY 31, 1963

CENTRAL RESEARCH LIBRARY
DOCUMENT COLLECTION
LIBRARY LOAN COPY
DO NOT TRANSFER TO ANOTHER PERSON
If you wish someone else to see this
document, send in name with document
and the library will arrange a loan.

OAK RIDGE NATIONAL LABORATORY
operated by
UNION CARBIDE CORPORATION
for the
U.S. ATOMIC ENERGY COMMISSION

Printed in USA. Price: $3.50 Available from the
Office of Technical Services
U. S. Department of Commerce
Washington 25, D. C.

LEGAL NOTICE

This report was prepared as an account of Government sponsored work. Neither the United States, nor the Commission, nor any person acting on behalf of the Commission:

A. Makes any warranty or representation, expressed or implied, with respect to the accuracy, completeness, or usefulness of the information contained in this report, or that the use of any information, apparatus, method, or process disclosed in this report may not infringe privately owned rights; or

B. Assumes any liabilities with respect to the use of, or for damages resulting from the use of any information, apparatus, method, or process disclosed in this report.

As used in the above, "person acting on behalf of the Commission" includes any employee or contractor of the Commission, or employee of such contractor, to the extent that such employee or contractor of the Commission, or employee of such contractor prepares, disseminates, or provides access to, any information pursuant to his employment or contract with the Commission, or his employment with such contractor.

ORNL-3452

Contract No. W-7405-eng-26

CHEMICAL TECHNOLOGY DIVISION

ANNUAL PROGRESS REPORT

For Period Ending May 31, 1963

F. L. Culler – Division Director
J. C. Bresee – Assistant Director
D. E. Ferguson – Assistant Director
R. G. Wymer – Chemical Development Section A Chief
R. E. Blanco – Chemical Development Section B Chief
K. B. Brown – Chemical Development Section C Chief
M. E. Whatley – Unit Operations Section Chief
H. E. Goeller – Process Design Section Chief
R. E. Brooksbank – Pilot Plant Section Chief

DATE ISSUED

SEP 13 1963

OAK RIDGE NATIONAL LABORATORY
Oak Ridge, Tennessee
operated by
UNION CARBIDE CORPORATION
for the
U. S. ATOMIC ENERGY COMMISSION

MARTIN MARIETTA ENERGY SYSYEMS LIBRARIES

3 4456 0322247 5

Summary

1. POWER REACTOR FUEL PROCESSING

1.1 Processes for Uranium and Thorium Carbide Fuels

The preparation of uranium and thorium carbides and their subsequent hydrolysis in water and other aqueous reagents were studied. Nearly single-phase uranium monocarbide (UC) was prepared by an arc-melting method (samples prepared by Metals and Ceramics Division). Preparation of uranium dicarbide, however, resulted in the preparation of $UC_{1.85}$, not stoichiometric UC_2. Hydrolysis at 80°C of as-cast uranium-carbon alloys with compositions between UC and $UC_{1.85}$ yielded complex mixtures of gaseous hydrocarbons, hydrogen, and a solid tetravalent oxide. Waxes were formed when the alloy contained either U_2C_3 or $UC_{1.85}$. As the C/U ratio in the carbide increased from 1 to 1.85, the methane concentration in the gas decreased, and the amounts of hydrogen, C_2- to C_8-hydrocarbons, and wax increased.

Thorium dicarbide had a composition of $ThC_{1.95}$. Hydrolysis products of ThC and water were the same as those found for UC. Thorium dicarbide when contacted with water produced more alkynes and less wax than those obtained with $UC_{1.85}$.

Soluble organic species, primarily acids, were produced during the dissolution of uranium carbides in nitric acid. The dissolution of UC left 20 to 40% of the carbide carbon in solution, mainly as oxalic acid. Other organic acids such as mellitic (benzene hexacarboxylic acid) and higher-molecular-weight species were also found in the solution.

The UO_2 slurry obtained by hydrolysis of UC was easily dissolved in boiling 8 *M* HNO_3. The raw solution was an unsatisfactory feed for Purex solvent extraction because the organic acids acted as strong emulsifiers and complexing agents for uranyl nitrate. However, treatment of the solution with $KMnO_4$ or $Ce(NH_4)_2(NO_3)_6$ to oxidize the organic acids did provide a satisfactory feed.

1.2 Hot-Cell Tests on Sulfex and Zirflex Processes

Nineteen hot-cell demonstrations of the Sulfex process for decladding stainless-steel-clad UO_2 fuel in boiling 4 *M* H_2SO_4 were made with prototype Yankee Atomic Reactor fuel specimens irradiated up to 28,200 Mwd/ton. The exposed uranium dioxide was washed with water and dissolved in boiling 4 *M* HNO_3 to provide a feed suitable for a modified Purex solvent extraction process. Stainless steel dissolution rates averaged 2 mg min^{-1} cm^{-2}, which were comparable to those obtained with unirradiated specimens. Complete decladding required about 5 hr. Soluble losses of uranium and plutonium to the decladding solution averaged about 0.05%. The decladding solutions required filtration to remove undissolved scale and uranium dioxide fines. Core dissolution in boiling 4 *M* HNO_3 was completed in about 6 hr, about the time required for unirradiated uranium dioxide.

The solvent extraction performance of feeds at irradiation levels up to 28,200 Mwd/ton was acceptable when highly purified solvent was used on a once-through basis.

1.3 Processes for Breeder Reactor Fuels

The dissolution rates of high-density UO_2, PuO_2, and UO_2-PuO_2 pellets were determined as a function of acid, nitrate, fluoride, and aluminum concentrations, with and without various oxidizing agents. The dissolution rate (in mg min^{-1} cm^{-2}) of UO_2 pellets of 95% theoretical density prepared by Davison Chemical Company was defined by the equation, log (rate) = 2.1 log (NO_3) − 0.68. Pellets of the same density but from different sources varied widely in their rate of dissolution. The dissolution rate of PuO_2 pellets, 90% of theoretical density, prepared by Nuclear Materials and Equipment Corporation in 14 *M* HNO_3–0.1 *M* HF was 2.1 mg min^{-1} cm^{-2}; without fluoride it was 0.006 mg min^{-1} cm^{-2}. The addition of 3 moles of aluminum per mole of fluoride eliminated the rate-increasing effect of the fluoride. The dissolution rate of pellets prepared from coprecipitated PuO_2-UO_2 may be calculated from the rates of the pure components.

Ionic plutonium (but not plutonium polymer) was successfully adsorbed from nitrate solutions on zirconium phosphate or zirconium-phosphate-silicate.

A chemical flowsheet was developed for the reprocessing of U^{233} for fuel recycle by extraction with di-sec-butylphenyl phosphonate (DSBPP). The factor for U^{233} decontamination from daughters of U^{232} was greater than 100, and the nitrate-to-uranium ratio in the product was less than 2.3. In engineering studies of this system in 2-in.-diam pulsed columns, the flow capacity of the compound extraction-scrub column varied from 490 to 1340 gal hr^{-1} ft^{-2} as the frequency decreased from 90 to 35 cpm. The stage efficiency expressed as HETS was 2.1 ft at 70 cpm for uranium extraction, 4.6 to 6.2 ft at 50 cpm for thorium scrubbing, and 4.2 ft at 70 cpm for uranium stripping. The separation factor between uranium and thorium was higher with DSBPP than with TBP, but the DSBPP in diethylbenzene was less stable chemically than TBP in *n*-dodecane.

Rate studies indicated that a 4-kg sphere of uranium metal will dissolve in 1.5 *M* $Th(NO_3)_4$–4 *M* HNO_3 in about 68 hr.

In laboratory studies on the adsorption of protactinium from nitrate solutions, unfired Vycor was loaded to greater than 10 mg of Pa^{231} per gram of glass. In one test, about 80% of the protactinium was recovered at a concentration equivalent to 120 times the feed concentration by eluting with 0.5 *M* oxalic acid. The remainder of the protactinium was recovered at lower concentrations. Decontamination factors of protactinium from thorium, uranium, ruthenium, zirconium-niobium, and total rare earths of 6300, 1.59×10^4, 40×10^3, 3, and 5.8×10^5, respectively, were obtained in tracer experiments. The presence of $2\frac{1}{2}$ moles of aluminum per mole of fluoride reduced the fluoride corrosion of the glass by a factor of 50. The use of $7\frac{1}{2}$ moles of aluminum per mole of fluoride increased the adsorption distribution coefficient to that of fluoride-free solutions. The distribution coefficient of Pa^{233} between laboratory-prepared silica gel and nitric acid is three times that of unfired Vycor and more than five times that of commercial silica gel.

Protactinium-containing synthetic dissolver and solvent extraction feed solutions were prepared to determine the long-term solution stability of protactinium. These solutions simulated those that would be obtained from Consolidated Edison Thorium Reactor fuel irradiated to 18,000 Mwd/metric ton and cooled for ten days. The dissolver solution was 0.5 *M* in thorium and had a Pa^{231} concentration of 70 mg/liter; the feed solution had a thorium concentration of 40 g/liter and a Pa^{231} concentration of 90 mg/liter. These solutions showed no change other than a ±10% scatter in the analytical values after standing one month at room temperature in plastic containers, or a ±6% scatter after contacting type 347 stainless steel (2 cm^2 per milliliter of solution) for one week.

In other solvent extraction experiments the combining ratio of tributyl phosphate (TBP) to thorium nitrate was measured and is believed to be 4. The extraction of uranium from acid-deficient aluminum nitrate by a given concentration of TBP may be expressed solely as a function of the pH of the solution. Over the range 0.5 to 4 *M* HF, the uranium distribution coefficient with 30% TBP remains constant at 1 when the nitrate-to-fluoride ratio is 3.5. The distribution coefficient of protactinium tracer between fluoride-free 5 *M* HNO_3 and 30% TBP is 4. The protactinium is completely complexed and is not extracted when the solution is 0.02 *M* in HF.

1.4 Corrosion Studies

In corrosion studies on aqueous processes for reactor fuels done in the Reactor Chemistry Division, no material tested was satisfactorily resistant to HNO_3-HF mixtures at all temperatures and compositions. Corronel 230 was the most generally acceptable material tested. Aluminum corroded at very low rates in mixed acid when the HNO_3 was $\geqq$15.6 *M* and HF was $\geqq$1 *M*, but rates became catastrophic at lower HNO_3 concentrations. Corronel was also the most satisfactory material tested in a reprocessing cycle consisting of oxidation of fluoride-contaminated graphite at 800°C followed by digestion in 5 *M* HNO_3. Rates on Corronel were about 0.1 mil/month for 22 cycles vs 19.6, 7.5, 9, and 8 mils/month, respectively, for type 304L stainless steel, Carpenter 20, Haynes 25, and Nichrome V. Prefilmed titanium exposed in nitric-fluoboric acid solutions containing Cr(VI) employed for zirconium dissolution corroded at overall rates of 4.14 to 7.75 mils/month after defilming; after about 70 hr of exposure, pitting occurred.

1.5 Mechanical Processing

A shear-and-leach apparatus, which consists of a 250-ton, horizontally actuated prototype shear, rotary-drum conveyor-feeder, and rotary-drum leacher, was successfully operated. A series of shear-leach runs were made in which UO_2 was leached from ½-, 1-, and 1½-in.-long sections of unirradiated ORNL Mark I, 36-tube prototype fuel assemblies with 7 to 8 *M* HNO_3 as the dissolvent. The results obtained in these tests showed that leaching of UO_2 from sheared sections of stainless steel tubing in a rotary-drum leacher is feasible. Almost no undissolved UO_2 or stainless steel fines were carried out of the leacher in the product stream, and the UO_2 was completely leached from the stainless steel hulls in 4 hr, as determined by visual inspection and chemical analysis of the hulls.

Bench-scale batch studies on the leaching of UO_2-ThO_2 from sheared ½-in.-long sections of stainless-steel-clad fuel, in Thorex dissolvent, show that suspension of fines is essential to good dissolution.

Complete particle-size-distribution data were obtained for ½-, 1-, and 1½-in.-long sheared sections of ORNL Mark I stainless-steel-clad porcelain, UO_2, and UO_2-ThO_2 and for Zircaloy-2-clad UO_2. The amounts of particles discharged from both UO_2 and ThO_2-UO_2 fuel rods are about equal, slightly more being discharged from ThO_2-UO_2 cores.

The life of the stepped moving blade of the 250-ton shear was estimated from shearing tests to be 10,000 cuts if the blade is reversible. The dimensions of the steps should be proportioned according to the size of the fuel assembly being sheared.

An investigation of remote maintenance of the shear was initiated. Extraction tools were designed and built for remote removal and installation of the gags, fixed-blade holder, and the moving blade in the shear housing, using the feed mechanism hydraulic cylinders as the moving force.

Stainless-steel-clad and Zircaloy-2-clad UO_2 fuel specimens, irradiated to 16,000 and 17,000 Mwd/ton, respectively, were sheared into 1-in. and ½-in. lengths to determine whether the particle-size distribution of the UO_2 fines was the same as for unirradiated fuel. One-inch cuts with the irradiated specimens resulted in about 4 to 6% of the UO_2 particles being less than 2000 μ; similar results were obtained with unirradiated specimens. Shearing of the irradiated stainless-steel-clad specimens was characterized by clean-cut edges, in contrast to the torn edges of the more ductile unirradiated material.

In a continuation of evaluation of methods for safely handling sodium- and NaK-bonded fuels, design studies and limited experiments were made of various methods for removing inert end adapters from fuel clusters that use spiral-wound wire on the fuel rods as spacers. These studies included potting of fuel rod ends in fusible metal or epoxy resins, followed by friction sawing; and mechanically clamping an assembly and mill sawing the end adapters. Partial removal of jacketing to release or expose the sodium or NaK bond was investigated. An orbital shearing device with a rotary shearing motion was designed, built, tested, and found to be promising. Equipment was also designed and built to evaluate the shearing of this type fuel, followed by disposal of sodium and NaK by dispersion in oil and reaction of the dispersion with water under an inert-gas blanket.

1.6 Chloride Volatility Process Development

This section is reported in ORNL-3452, suppl 1.

1.7 Rover Fuel Processing Development

This section is reported in ORNL-3452, suppl 2 (classified).

2. FLUORIDE VOLATILITY PROCESSING

2.1 Processing of Uranium-Zirconium Alloy Fuel

The decontamination of the equipment in cell 1 of the Volatility Pilot Plant was demonstrated following a six-run series on 5- to 6.5-yr decayed zirconium-uranium alloy fuel. The decontamination program, as developed in laboratory studies, included a simulated-fuel dissolution run, a molten-salt flush, and extensive cleaning of process equipment with water and circulating and static decontaminating solutions [0.35 *M* ammonium oxalate, 0.03 to 0.10 *M* $Al(NO_3)_3$–0.10 to 0.01 *M* HNO_3, and 5-1-1 to 5-2-2 wt % NaOH–H_2O_2–sodium

tartrate]. Ammonium fluoborate was added as a nuclear poison to the initial ammonium oxalate wash.

The general activity levels in cell 1 were 30 to 60 millirems/hr, and residual equipment activity was sufficiently low after decontamination to permit direct maintenance. However, nickel weld filler metal 61 (INCO-61) in the L-nickel fluorinator was severely attacked. A laboratory-scale simulation of the pilot-plant decontamination procedure showed that INCO-61 welds in nickel were vulnerable and that INOR-8 base metal and weld filler metal of the hydrofluorinator were not unduly attacked.

Metallographic examination of samples of L-nickel removed from the lower part of the fluorinator revealed attack on the base metal at the rate of 0.38 mil/hr based on 57.7 hr of fluorine exposure time, including the decontamination procedure.

During examination following aqueous decontamination, a crack was found near the bottom of the hydrofluorinator. The leak probably occurred during the first run of the long-decayed six-run series. About 20 in. of the lower portions of the vessel was replaced. Specimens from the damaged portion were examined metallographically and subjected to tensile-strength tests. The cracks through which salt leaked were of external origin and related to the attachment of thermocouple sheaths to the vessel, during which operation the hydrofluorinator wall was overheated and embrittled. There was no indication that salt corrosion of the interior of the vessel was a factor in initiating the cracks or of embrittlement. Rather, fabrication of the hydrofluorinator from one of the substandard heats which were susceptible to microfissuring and to damage by high temperature may have been a factor in the crack formation.

Following decontamination of the equipment, the pilot plant was modified to (1) improve product purity by the addition of a magnesium fluoride bed for technetium and neptunium removal, (2) allow convenient recycle of off-specification product, (3) provide a solids rod-out device in the hydrofluorinator off-gas line, and (4) add the shielding needed for future higher radiation levels.

After the modifications, five runs with cold and irradiated zirconium-uranium alloy were completed. Alloy dissolution rates ranged from 2.0 to 2.9 kg/hr for three cold runs, during which HF utilization efficiencies per pass through the dissolver were 24 to 34%. Greater dissolution rates and HF utilization efficiencies were obtained during the processing of 13-month- and 6-month-decayed alloy (3.7 and 3.4 kg/hr, and 49 and 41%, respectively), although the higher rate may not have been a result of the extent of fuel burnup.

The product recovery operations were successful, although HF contamination of the product was appreciable (up to 30 wt %) during cold runs. Conversely, the product from the first hot run was free from HF, while the product from the second run had 0.5% HF contamination. Average fluorine utilization efficiencies were 5% during cold runs and 14 and 7% during the runs with 13-month- and 6-month-decayed alloy (runs R-7 and R-8). Nonrecoverable uranium losses, mainly to the waste salt, during all fluorinations were less than 0.46%. Total cation impurity levels in the product during cold runs were about 3200 ppm, or ten times higher than AEC specifications. However, cation specifications were met during run R-7 on 13-month-decayed alloy (total cations less than 171 ppm). The UF_6 product from runs R-7 and R-8 met AEC specifications for gamma activity. The product natural beta activity is being evaluated for both hot runs to determine if AEC beta specifications were also met. Significantly, molybdenum contamination of the product was only 9 and 43 ppm during runs R-7 and R-8, as a result of a selective desorption procedure. A higher total cation level (less than 712 ppm) was obtained during run R-8.

The decontamination of uranium from fission products was excellent during runs R-7 and R-8. Overall process decontamination factors ranged from greater than 10^8 to nearly 10^{11} for volatile fission products (Sb^{125}, Te, Ru^{106}, and Nb^{95}), and from greater than 10^9 to greater than 10^{10} for nonvolatile fission products (Zr^{95}, Sr^{90}, and Cs^{137}) during run R-8 on 6-month-decayed fuel. Generally lower DF's were obtained during run R-7 on 13-month-decayed fuel. Trace quantities of volatile fission products reached the MgF_2 trap during both runs, probably due to entrainment rather than to absorber breakthrough since Cs^{137} was also collected. The MgF_2 trap was effective for Tc^{99} removal during runs R-7 and R-8 (less than 1 and 4 ppm, respectively, in the product), but less effective for Np^{237} removal (4 and 48 ppm, respectively, in the product).

The performance of pilot-plant equipment was generally satisfactory during all runs. All difficulties encountered were relatively minor, and in

each case it was possible to continue operations or to repair or modify the equipment.

Results of the metallographic examination of five groups of corrosion rods exposed in the pilot-plant fluorinator were received during the year. Nickel filler metal 61 (INCO-61), E-nickel, nickel–5 Fe, nickel–1 Al, INOR-8, and HyMu 80 all showed significantly improved performance over L-nickel and thus are possible materials of construction for a fluorination vessel.

2.2 Volatilization and Recovery of Plutonium Hexafluoride

Plutonium hexafluoride was fluorinated from a 31-24-45 mole % $LiF-NaF-ZrF_4$ melt containing about 1000 ppm plutonium, at rates similar to those obtained for a concentration of 2 ppm. The volatilization rate has a first-order dependence on concentration, with reaction half-times of about 5.3 hr at 500°C and 3.0 hr at 600°C. In a recent test, preliminary results indicated a reduction of the reaction half-time to 1.5 hr by the use of fluorine at 40 psig, which is an acceptable rate for process use provided pressurized fluorine does not also increase markedly the vessel-corrosion rates. Neither violent salt agitation nor intermittent additions of UF_4 increased the rate of PuF_6 volatilization. Material balances of 95 to 100% were obtained in all the fluorination tests conducted with about 1000 ppm of plutonium and 55 mg of total plutonium present. In addition to the CaF_2 previously studied, high-surface-area LiF and MgF_2 both showed high effectiveness for trapping volatilized PuF_6.

2.3 Preparation and Absorption of Tellurium Hexafluoride

Observations made in the course of attempting to prepare TeF_6, a volatile fission product fluoride present in processing short-decayed fuel, indicated that it is readily reduced by nickel at less than 300°C. Thus, in the fused-salt fluorination step much of this fission product is retained on the relatively cool upper walls of the fluorination reactor. In studying the absorption of TeF_6 in 10% aqueous KOH, a 12% TeF_6 mixture in fluorine was passed through two 20-in.-long × 1-in.-diam columns, in series, packed with $\frac{1}{4}$-in. Alundum Berl saddles with an absorption of 46, 68, and 67% of the tellurium, respectively, at 25, 50, and 70°C.

2.4 Process Engineering Studies

Single-vessel hydrofluorination-fluorination and salt recycle are being evaluated on an engineering scale. Dissolution experiments with Zircaloy-2 and zirconium-uranium alloy elements indicated that salt recycle has no significant effects on rate and also showed that filtration and/or settling steps for salt purification are not required. Corrosion rates measured during a series of single-vessel dissolutions and fluorinations in INOR-8 vessels, on either a laboratory or engineering scale, were not significantly different from the sum of the rates noted when the two process steps were conducted in separate vessels. The alloys HyMu 80 (Alloy 79-4), Ni–5 Fe, and Ni–1 Al showed some possibility of providing corrosion rates lower than those for INOR-8, the material of construction for the present pilot-plant hydrofluorinator.

The data on the sorption of UF_6 from a flowing stream of UF_6-N_2 by beds of $\frac{1}{8}$-in.-diam NaF pellets in the temperature range 29 to 100°C and at UF_6 concentrations of 0.57 to 8.5 mole % UF_6 were correlated by use of a mathematical model that took into account the effect of temperature, UF_6 concentration, gas flow rate, and pellet characteristics. The experimental data were obtained by measuring the weight gained by a single layer of NaF pellets at various temperatures and during prescribed times. Calculational methods based on this model were developed for predicting simultaneous sorption of volatile fluorides such as UF_6 and MoF_6 by fixed beds of NaF.

2.5 Other Corrosion Studies

Based on the promising results reported last year for Alloy 79-4, an attempt was made to determine whether this composition was optimum for hydrofluorination conditions. Somewhat inconclusive results were obtained by exposing INOR-8, HyMu 80, and experimental alloys to 50.5-37.5-12.5 mole % $NaF-LiF-BeF_2$ and to 37.5-37.5-25 mole % $NaF-LiF-ZrF_4$. These tests were done with HF, but without zirconium dissolution. At 650°C, HyMu 80, Ni–10 Mo, and Ni–10 Mo–5 Fe corroded less than INOR-8.

In studies comparing the 36.9-27.0-27.0-9.1 mole % $NaF-LiF-ZrF_4-BeF_2$ mixture at 500°C with the highly corrosive 50.5-37.0-12.5 mole % NaF-LiF-

BeF_2 mixture at 650°C, the former was found to be only slightly corrosive. Initial Zircaloy-2 dissolution rates were significantly lower than the rates caused by the NaF-LiF-BeF_2 melt.

2.6 Processing of Uranium-Aluminum Alloy Fuel

This section is reported in ORNL-3452, suppl 1.

3. WASTE TREATMENT AND DISPOSAL

3.1 Pot Calcination of High-Level Waste

Engineering Studies. – Eleven engineering-scale tests were made with simulated waste of the following types: TBP-25, five tests; Purex and formaldehyde-treated waste, 1965 (FTW-65), six tests. Feeding the calciner pot by gravity feed (gravity head of 10 ft) was a satisfactory alternative to pump feeding directly from the evaporator. A cyclone mercury trap operating at 150 to 200°C in the calciner off-gas line retained only 10 to 17% of the mercury. The distribution of ruthenium in the closed loop of the evaporator-calciner system was determined in a test with Purex FTW-65 waste with nonradioactive ruthenium (0.09 g/liter). Only 0.03% of the ruthenium escaped from the evaporator, and 10% remained in the evaporator heel. Average feed rates to the loop system were 15 to 26 liters/hr for TBP-25 waste and 26 to 68 liters/hr for Purex FTW-65 waste, depending on the presence or absence of organic in the waste and the degree to which the pot had been filled with calcined solids. Sulfate was easily retained in the calciner pot by adding calcium nitrate solution to produce a 10% stoichiometric excess of calcium and sodium over the sulfate.

Mechanical Development. – The mechanical development program was completed at the Lockheed Nuclear Products Facility–Georgia Nuclear Laboratory, and the demonstration equipment was disassembled and shipped to Hanford. Two types of permanent seals were developed for calcination pots, the reliability of remote operation and equipment maintenance was demonstrated, and heat transfer data were obtained under simulated process conditions. Recommendations for design changes to improve the performance of the equipment and facilitate remote maintenance were made by the Georgia Nuclear Laboratory.

Pilot-Plant Design. – A pilot plant to demonstrate the pot calcination of radioactive wastes is being designed by Hanford laboratories in cooperation with ORNL for installation in the new Hanford Fuels Recycle Pilot Plant building. Studies at ORNL included shielding calculations, process flowsheet and equipment reviews, design of a pump loop for testing pumps under simulated process conditions, and calculations to determine the influence of fission product heat on the operation of the pot calciner.

Laboratory Studies. – Fixation experiments on high-sulfate Purex waste produced nonglassy, apparently insoluble products that retained as much as 98% of the sulfate. Hanford FTW-65 waste solution could be reduced in volume by a factor of 4 before solids began to appear; semiengineering-scale fixation of this waste gave a volume reduction greater than 30, resulting in a strong, apparently insoluble product that lost less than 2% of the sulfate present during the fixation process. Fixation products with softening temperatures as low as 700°C were prepared from FTW-65 waste by varying the additives and the percentage of waste oxides.

Darex wastes, fixed as glassy solids or as ceramics, were leached at rates of about 1.3×10^{-6} and 4×10^{-3} g cm^{-2} day^{-1} for a glass containing 15.3% waste oxides and a ceramic containing 25% waste oxides respectively. Phosphite did not suppress ruthenium volatility when pot operation employed a slowly rising liquid level. Entrainment during a TBP-25 fixation run in a 4-in.-diam pot was about 0.1%. A TBP-25 glass heated in a sealed pot at 900°C for 24 days produced a vacuum; the product was glassy at the end of the heating period. Semicontinuous, semiengineering-scale fixation of Darex waste as a ceramic containing 25% waste oxides produced an exceedingly hard and strong product, giving a volume reduction factor of 5.1.

Corrosion studies showed that type 304L stainless steel is a satisfactory material of construction for both the fixation pot and the pot head.

Accurate methods were developed for measuring the thermal conductivity of powders, and the variation of k was correlated with the theoretical density of the material.

Hot-Cell Demonstration with Radioactive Waste. – Equipment is being constructed for semi-pilot-plant-scale demonstration of the pot-calcination process, using radioactive wastes obtained from the Hanford Purex and Idaho TBP-25 plants. Both calcination

and glass formation will be tested, and the stability of the products will be determined.

3.2 Treatment of Low-Level Waste

Scavenging-Precipitation Ion Exchange Process. – Seven additional runs were completed in the 600-gph pilot plant for testing the scavenging-precipitation ion exchange process for waste-water processing. The process achieved significantly better decontamination of Sr^{90} and Cs^{137} than the lime-soda process (currently used at ORNL) during a five-month demonstration on process waste water. Decontamination factors for Sr^{90} and Cs^{137} ranged from 2000 to 12,000 and from 77 to 3400, respectively, in 12 demonstration runs. In all but two runs the average activity of the process effluent was less than 3% of the MPC_w values for all isotopes with respect to continuous occupational exposure.

The presence of hexametaphosphate in the waste-water feed decreased hardness precipitation (calcium and magnesium), thereby causing a premature breakthrough of Sr^{90} to the ion exchange column effluent in two of the runs. However, making the feed 0.005 *M* in Na_2CO_3 in the precipitation step reduced the detrimental effect of the phosphate. Three methods for preventing hardness supersaturation in the precipitation step were developed on a laboratory scale: (1) the addition of sodium carbonate to aid complete precipitation in the clarifier, (2) the ion exchange removal of high residual hardness in the stream exiting the clarifier, and (3) the removal of phosphates from the untreated neutral waste with alumina prior to precipitation. The choice of an optimal method for a given low-level waste stream may depend on the level of phosphate contamination.

Foam Separation. – Foam separation was studied as a method for decontaminating process waste water, and both one- and two-step processes are being developed. The two-step process employs a slowly agitated, upflow sludge column and a countercurrent foam column. Calcium is precipitated as the carbonate (by making the water 0.005 *M* each in NaOH and Na_2CO_3) and is retained in the sludge column; the clear effluent is fed to the foam column. Laboratory-scale experiments with spiked tap water gave overall strontium decontamination factors of 1000 to greater than 10,000; decontamination factors across the foam column were in excess of 100. Initial results from experiments with ORNL process waste water gave strontium decontamination factors across the foam column in excess of 15, 20, and 200. The one-step process is a simplified version of the two-step process. Calcium is precipitated as the orthophosphate in a small mixer, and solution and solids are fed to the foam column, where both flotation and foam separation occur. Strontium decontamination factors with simulated and actual ORNL waste water gave, respectively, values of 1000 for simulated waste and 200 to 300 with ORNL waste.

Engineering studies showed HTU_x values as low as 1 cm in a 6-in.-diam foam separation column for liquid flows up to 100 gal ft^{-2} hr^{-1} when conditions were selected to give uniformly sized bubbles and to avoid channeling. The performance of centrifugal, sonic whistle, and cyclone foam breakers was measured. A 24-in.-diam foam column and a surfactant recovery system were studied to determine design specifications for larger units.

3.3 Engineering, Economics, and Safety Evaluations

A study undertaken to evaluate the economics and safety associated with alternative methods of waste management in a nuclear power industry showed that the costs for the interim storage of solidified wastes for periods of 1 to 30 yr ranged from 0.0015 to 0.0048 mill/kwh (electrical) for calcined, acid Purex and Thorex wastes, and 0.0018 to 0.0063 mill/kwh (electrical) for calcined, reacidified Purex and Thorex wastes. The interim storage of acid wastes as solids costs less than storage of the same wastes as liquids, but the reverse is true for neutralized wastes.

The effects of fission product removal on total waste-management costs, which are the sums of the costs of interim storage, pot calcination, shipping, and final disposal in salt mines, were estimated according to optimistic expectations of future processes for separating the fission products. The cost of managing wastes that are 90 to 99% depleted in fission products is about 70% as much as the cost of managing wastes with no fission products removed. The difference, about $400 per metric ton of uranium processed, is not enough to pay for the separation and handling of fission products. Fission product removal must be justified

and paid for by the market for fission product radiation or heat sources, with only a marginal credit from reduced costs of ultimate waste disposal.

4. TRANSURANIUM ELEMENT PROCESSING

The Transuranium Processing Plant (TRU) and High Flux Isotope Reactor (HFIR) are being built to produce gram quantities of many of the heavier actinide elements for research purposes. Development of the chemical processes and equipment for separating and isolating these elements as well as the design of TRU are under the direction of the Chemical Technology Division.

Target material for HFIR irradiation will be prepared from plutonium-aluminum alloy irradiated to a greater than 99.9% burnup of Pu^{239}. The irradiations and the recovery of the residual plutonium (Pu^{242}) by conventional solvent extraction or anion exchange procedures are being done at Savannah River. Recovery of Am^{243} and Cm^{244} in the raffinate by either anion exchange or tertiary amine extraction from neutral nitrate salts and the final purification of Am^{243} and Cm^{244} by the Tramex (Transuranium amine extraction) Process will be done here.

Irradiated HFIR targets will be processed by separation of the actinides from fission products by the Tramex Process. Subsequently, the actinides will be split into an americium-curium fraction and a transcurium fraction by extraction with di-sec-butylphenyl phosphonate. Berkelium will be isolated by extraction of Bk^{4+} with dialkylphosphate from nitric acid solution, and the individual elements in the group Cf-Es-Fm will be separated by chromatographic elution from an organic anion exchange resin.

4.1 Chemical Process Development

Satisfactory results were obtained in laboratory tests of the Tramex Process for separating transplutonium elements from fission products, corrosion products, and materials used in target fabrication. This process is useful for recovering all known transplutonium elements as a group from irradiated HFIR targets and also for isolating Cm^{242} and Am^{241} from irradiated cermets of AmO_2 and aluminum. Ruthenium decontamination factors in laboratory tests under these conditions were greater than 10^4. Zirconium, niobium, and rare-earth decontamination factors were $\gtrsim 10^4$. The only contaminants investigated that follow the transplutonium elements through the process are nickel, Ag^{111}, and possibly Te^{132}. Precipitating the oxalates or hydroxides of the heavy elements effects a satisfactory separation from nickel. Tests with rare earths as substitutes for the heavy elements gave better than a 99% recovery, with nickel decontamination factors of about 300. For most processing, Ag^{111} and Te^{132} will not present any problems because of their short half-lives.

The Tramex Process was modified in three respects: (1) aluminum chloride was included in the feed since aluminum is present in the target material; (2) the concentration of the hydrochloric acid in the stripping solution was increased to 8 *M* to improve zirconium, niobium, and iron decontamination; and (3) a scrub of freshly prepared Alamine 336·HNO_2 was added to the stripping section to improve ruthenium decontamination.

Results of testing the Tramex Process in a batch countercurrent extraction at a solution activity level of 4 w/liter (from Cm^{242}) indicate no difficulties. Distribution coefficients were in agreement with tracer-level studies, and phase separation was as good as or better than that obtained in the absence of activity. Radiation stability of the solvent, 0.6 *M* Alamine 336·HCl–diethylbenzene (DEB), was confirmed in a batch test for a total exposure to alpha radiation of about 300 whr/liter. The curium distribution coefficient decreased 30% but was still large enough for a satisfactory process.

Stable Tramex feeds of low acidity were prepared on a 1- to 2-liter scale in laboratory glassware by simply distilling off excess acid and water. Loss of acid in Tramex feed by radiolysis at a high activity level poses a potentially serious problem. Preliminary data indicate that feed solutions at the proposed operating level (10 w/liter) will lose acid at the rate of about 0.1 mole $liter^{-1}$ day^{-1}, making adjusted feeds stable for less than a day unless acid is replenished. Readjustment of the acid concentration by bubbling HCl gas through the solution results in an equilibrium acid concentration that is higher than permitted. Acid addition with dilute HCl-air mixtures will be investigated.

A careful investigation of the effect of $AlCl_3$, LiCl, and HCl concentrations in Tramex feed on

americium, europium, and acid distribution coefficients is in progress. Concentrations must be very carefully controlled. For example, the americium distribution coefficient between 0.6 Alamine 336·HCl–DEB and 10 *M* LiCl–0.1 *M* $AlCl_3$–0.02 *M* HCl is about 4. This distribution coefficient was decreased to 1 either by increasing the acid concentration to 0.135 *M* or by decreasing the $AlCl_3$-LiCl salt concentration to 9.5 *N*.

In the phosphonate process for splitting transplutonium elements into an americium-curium fraction and a transcurium fraction, solvent diluent has an important effect. A correlation has been noted between the dielectric constant of the solvent used to dilute 2-ethylhexyl phenylphosphonic acid [2-EH(ØP)A] and distribution coefficients of americium and curium into 1 *M* 2-EH(ØP)A from 1 *M* HCl. The californium distribution coefficient decreased from 45 for heptane diluent (dielectric constant, 1.9) to 3 for toluene diluent (dielectric constant, 2.4). Americium distribution coefficients with these two diluents were 0.37 and 0.028 respectively.

Complete separation of americium and californium was demonstrated in a test in which americium was preferentially stripped into 1.9 *M* HCl from a column of 2-EH(ØP)A adsorbed on powdered glass.

Precipitation methods and ion exchange methods are being investigated for the separation of americium from the curium. A 2.5-g sample of Am^{241} contaminated with lanthanum, cerium, iron, and calcium was purified by precipitating $KAmO_2CO_3$ from 3 *M* K_2CO_3. The precipitate contained 99.6% of the americium, free of all contaminants except cerium. This method can be used to separate americium from curium, which will remain in solution.

With –270-mesh anion resin, gassing (caused by high alpha activity levels) was controlled well enough by column pressurization to accomplish satisfactory americium-curium separation by ion exchange at activity levels equivalent to 0.4 to 1 mg of Cf^{252}. Elution from cation exchange resin with ammonium α-hydroxyisobutyrate gave a product containing 96% of the curium free of americium, and elution from anion exchange resin with 4 *M* $LiNO_3$ gave a product containing 99% of the curium free of americium. Separation of Cf-Es-Fm was not possible by elution from anion exchange resin with 4.4 *M* $LiNO_3$ because of an unexpected reversal in elution positions of the transcurium elements.

The extraction of americium, curium, and rare earths into tertiary amine from neutral nitrate solution is an attractive method for producing a chloride product that can be readily adjusted to Tramex feed conditions. In a laboratory demonstration, curium recovery of 99.8% was achieved with 1 *M* $Al(NO_3)_3$ feed containing Cm^{242} and $Ru^{103-106}$ tracers. About 60% of the ruthenium was extracted, but most of this remained in the solvent during stripping, giving an overall ruthenium decontamination factor of about 1000. The curium product solution contained 2.4 *M* HCl and <0.01 *M* HNO_3. In another laboratory mixer-settler test with a feed of 2 *M* $Al(NO_3)_3$ containing 5 g/liter of rare earths and 1 g/liter of iron, nickel, and chromium, the rare-earth losses were 0.005%; iron, nickel, and chromium extraction was undetectable. The aluminum decontamination factor was 300. With different diluents, americium distribution coefficients varied from 0.53 to 38, and americium-curium separation factors varied from 1.23 to 2.06 for the system 0.6 *M* Alamine 336·HNO_3 vs 3 *M* $LiNO_3$–1 *M* $Al(NO_3)_3$. Diethylbenzene is the recommended diluent.

Methods for separating actinides and lanthanides in carbonate solutions are being investigated in scouting tests. It may be possible to separate americium and curium from most lanthanides either by extracting the lanthanides into quaternary amines or by loading them on strong-base anion exchange resin from dilute carbonate solutions. However, group separation of actinides and lanthanides does not appear possible since the heavy actinides have larger distribution coefficients than the light lanthanides. Distribution coefficients between 30% Aliquat 336 in DEB and 0.5 *M* $NaHCO_3$ were as follows: Am, 0.52; Cm, 0.65; Cf, 2.03; Es, 2.51; Ce, 1.0; and Eu, 4.8. Since there is a possibility that cerium was tetravalent in these tests, the results may be somewhat misleading. Furthermore, the practical application of this method is limited by low solubilities of actinides and lanthanides in the dilute carbonate solutions.

A method was investigated for preparing PuO_2-aluminum cermets for use in HFIR target prototypes. When PuO_2 particles less than 10 μ in diameter are mixed with –325-mesh aluminum powder and pressed into cermets, the oxide phase is continuous, and the thermal conductivity of the pellet is low. With PuO_2 particles ranging from 20 to 200 μ, the aluminum phase is continuous, and conductivity is satisfactory for irradiation in high neutron

fluxes. Dense, coarse particles were prepared by precipitating $Pu(OH)_4$, washing, drying at 150°C, and firing at 1200°C to produce a glassy solid with a density of 10.99 (96% of theoretical) and particles 1 to 3 mm in diameter. Careful grinding and screening should produce a satisfactory product.

4.2 Development of Pulsed Columns

The solvent extraction contactors chosen for the Transuranium (TRU) Facility are small pulsed columns (about $1\frac{1}{2}$ in. in diameter by 6 ft high) with feed capacity in the order of 1 to 2 liters/hr. Development work was continued in the past year with a newly acquired set of three $\frac{3}{4}$-in. glass columns with Teflon process lines and tantalum pulse plates.

Since the rare-earth scrub section of the Tramex flowsheet is believed to be the slowest mass-transfer step of all the processes proposed for TRU, studies have been concentrated on this problem. Stage heights ranged from 17 to 37 in., the lowest being obtained with coalescence sections in the column.

Hydraulic characteristics of all sections of both the Tramex and phosphonate flowsheets were studied and found to be satisfactory.

4.3 Process Equipment Design

Complete equipment and engineering flowsheets were developed for the primary processes, and detailed design of equipment components was started. Corrosion and cost data accumulated within the past year led to the decision not to use Hastelloy C for low-temperature service, but to go to a more-corrosion-resistant all-Zircaloy-2 piping system. In nearly all environments, corrosion rates for Zircaloy-2 are only a tenth as high as the rates for Hastelloy C. Waste tanks will still be of Hastelloy C, whereas evaporators will be tantalum lined, and product storage tanks may be either tantalum lined or of all-welded Zircaloy-2. To date, detailed design of the following items has been completed:

1. process pumps for use in sampling, as feed pumps and for product transfer,
2. disconnects for makeup of all mechanical joints,
3. a 12-unit sampler station,
4. the dissolver,
5. the first-cycle solvent extraction equipment rack.

Overall design is about 20% complete as of July 1.

4.4 TRU Facility Design

Detailed design of the TRU building structure was completed in February 1963 and advertised for bid. The low bidder (at $2,586,000, compared with the engineering estimate of $2,716,700) is expected to start construction in mid-June for scheduled completion in April 1965. The procurement of materials for the use of the lump-sum contractor, including special materials such as Hastelloy, valves, eductors, etc., and the hydrous iron ore aggregate for the special shielding concrete, is progressing on the schedule established by the critical-path analysis of the overall project.

Design of the important mechanical equipment components for the building, such as the conveyor for intercell transfers and the equipment transfer case for removing cubicle equipment, was nearly completed. Mockups of both are under test.

4.5 Experimental Engineering Studies

Many of the unique design features of the Transuranium Processing Plant cell-cubicle arrangement must be tested and developed in a full-scale mockup. The basic mockup structure for two cells was installed.

After minor alterations the automatic port closure on the conveyor worked well, and there was little wear during 1000 cycles of operation. Tests showed a need for modifications of an intercell pass-through design and of the extended-reach manipulator tongs. Tests of equipment-rack handling, maintenance of the lighting system, and manipulators are partially complete.

A prototype diaphragm sampler pump demonstrated adequate performance and life for Hastelloy C or Zircaloy-2 diaphragms. Two electric impact wrenches, used in conjunction with eight torque-limiting extensions made by machining standard socket wrench extensions to give thinner, springlike cross sections, proved satisfactory for applying recommended torques to all sizes of bolts required.

Tantalum disconnects made by forming the conical sealing surfaces directly on the tubing itself leaked excessively, but a successful joint was made from machined pieces joined to the tubes by a rolling operation. Burnishing the cone surfaces with hardened rollers improved the surface finish so that the joint was leak-tight even after several make and break cycles. Misalignment of the sealing surfaces of the disconnect clamps, due to strain induced by the cantilevered load, was corrected by machining the upper contact surface at an angle of 1.5°.

Initial attempts to form tantalum bellows for process valve stem seals by magneforming, explosive forming, and hydraulic forming were not successful. However, a vendor has been found who may be able to supply the bellows.

4.6 TRU – Evaluation of Protective Coatings

Tests were made on 54 protective coatings potentially useful in the TRU facility to determine radiation resistance and ease of decontamination. At a dose of 4×10^9 r, four coatings (all epoxy or epoxy-phenolic formulations) exposed in deionized water and 29 exposed in air were still serviceable. Fiberglas fabric reinforced coatings retained greater impact resistance. Decontamination factors, determined following simple water flushing and a 3 *M* HNO_3 acid scrub, averaged 1850 for the polyesters, 990 for the vinyls, 870 for the epoxies, and 410 for the modified phenolics.

4.7 Calculations for the Irradiation of Prototype HFIR Targets

Calculations for irradiating three prototype TRU HFIR targets in the MTR were completed.

5. CURIUM PROCESSING

5.1 Flowsheet Tests for the Processing of Pu^{242}, Americium, and Curium

The recovery of 30 g of plutonium and 4 g of transuranium elements from highly irradiated Pu-Al alloy fuel rods was completed in a pilot-plant study of flowsheets featuring anion exchange separation methods. The purpose of the program was the separation and recovery of quantities of the plutonium and transuranics suitable for studies of their nuclear properties and the development of processes for the further separation of the transuranium elements from each other.

The process was conducted according to a flowsheet which includes dissolution of the fuel rods in 6 *M* HNO_3 catalyzed with 0.05 *M* Hg^{2+} and 0.03 *M* F^-, coagulation of the soluble silica by digestion at 80° with 10 ppm of gelatin, clarification, valence adjustment of the plutonium to the tetravalent state, nitric acid concentration adjustment to 7.0 *M*, followed by sorption on Permutit SK ion exchange resin, scrubbing sorbed aluminum and fission products from the resin with 7.0 *M* HNO_3–0.01 *M* F^- followed by elution of the plutonium with 0.7 *M* H^+. The plutonium was further purified by readjustment of the plutonium valence to 4 and the acid concentration to 7.0 *M* and repeating the ion exchange step. Further processing of the aluminum-bearing wastes from the first ion exchange cycle to recover the transuranium element included evaporation of the waste until the boiling temperature reached 140°C, acid and aluminum concentration adjustment, clarification, and sorption of the rare earths and transuranium elements on Dowex 1-X10 ion exchange resin, scrubbing sorbed aluminum and light fission products from the bed with 8 *M* $LiNO_3$, and elution of the rare earth fraction containing the transuranium elements with 0.7 *M* HNO_3.

Plutonium product suitable as feed for the isotopic separation process was recovered. The plutonium assayed 75% Pu^{242}. Gross decontamination from fission products averaged 2×10^5. Measured process losses across two ion exchange cycles totaled 8% of the feed. Abnormally high sorption losses were obtained in the first cycle, in which a significant fraction of the plutonium was irreversibly sorbed on the resin along with Ru^{106}, Rh^{106}, and Pd.

The rare earth fraction contained the transuranium elements decontaminated from aluminum by a factor of 70 and from light fission products by a factor of 10. Overall recoveries of greater than 95% were demonstrated under optimum conditions. Losses in the ion exchange process, which were dependent on salt concentration but independent of acid deficiency over the range 0.1–1.0 *N*, were 0.2 and 0.4%, respectively, during sorption and scrubbing. High recovery of the product hinged on the effective washing of the filter cake during the clarification step; as much as 25 to 30% of the transuranium elements was retained in the cake under some operating conditions. Colloidal $Al(OH)_3$ present in ion exchange feeds in which the acid deficiency exceeded 1.0 *N* interfered with the mechanical operation of the ion exchange system.

5.2 The Curium Production Facility

The high-level solvent extraction development facility for the Transuranium Program, located in cells 3 and 4 of Building 4507, is being modified to supply multigram quantities of Cm^{242} free of fission products to the Isotopes Division for the fabrication of heat sources such as SNAP 13, SNAP 11, and others, and Surveyor lunar probes, which are unmanned instrument packages designed for soft landings on the moon. The facility will be used also to demonstrate process chemistry for the Transuranium Program, its original purpose. The highly radioactive acid chloride process solutions will be handled in tantalum or glass equipment and designed for remote manipulation and maintenance through use of the same concepts of equipment racks and disconnects that are to be employed in the TRU Facility. The special containment features which are required of all alpha-gamma cells, such as seals on openings and access ports, were previously incorporated into the facility and are adequate for the curium production work.

The first gram quantities of Am^{243} and Cm^{244} from the Transuranium plutonium irradiation will be recovered in this Facility in the coming six-months period, using fission product Am-Cm concentrates isolated by du Pont at Savannah River. An experimental heat source of the long-lived Cm^{244} will be made. Subsequently, for the experimental heat, Cm^{242} will be produced for the SNAP-13 (4 g) and SNAP-11 (12 g) programs, and routine curium production will follow. Curium-242 has a specific heat generation rate of 120 w/g and decays with a 162.5-day half-life. Space available in cell 3, Building 4507, will be equipped for laboratory-scale special development work for the TRU program to continue. Techniques for isolating the individual transuranium elements (Am, Cm, Bk, Cf, Es, and Fm) will be developed at essentially the full-gamma-activity levels to be encountered in the TRU program. Only traces of elements heavier than Cm will be available in these solutions, so that shielding for neutrons is no problem. All work in these cells, including the "production" oriented work for Cm^{242}, will provide an excellent check on the chemicals systems to be used in the Transuranium Facility.

5.3 Calculations Regarding the Irradiation of Gram Quantities of Americium-241

Engineering calculations for irradiating gram quantities of Am^{241} in the Oak Ridge Research Reactor were completed. They are based on an average perturbed thermal neutron flux of 3.0×10^{14}, a peak-to-average thermal flux ratio of 1.2, and an irradiation time of 50 days. If a 100% release of the gaseous fission products is assumed, the maximum stress in the aluminum capsule is 500 psi.

6. THORIUM FUEL-CYCLE DEVELOPMENT

6.1 Sol-Gel Process Development

The sol-gel process was developed to convert thorium nitrate to dense ThO_2 particles, and uranyl and thorium nitrates to uranium-thorium oxide particles suitable for loading into fuel tubes by vibratory compaction. The radioactivity of the decay daughters of the U^{232} contaminant in U^{233} and Th^{228} in recycled thorium fuels makes it necessary to process these fuels to oxides behind shielding, and the combination of the sol-gel process and vibratory compaction provides a comparatively simple system, readily adaptable to remote operation.

The major emphasis in the development of the sol-gel process has been to optimize it for the demonstration of the full-scale preparation of 10 kg of $U^{233}O_2$-ThO_2 (uranium/thorium weight ratio, 3/97) per day. This will be done in the Kilorod Facility, a pilot plant with a capacity of ten fuel rods per day. The facility is being used to prepare 1000 fuel rods clad with Zircaloy-2 for zero-power criticality experiments at the Brookhaven National Laboratory. Engineering equipment was designed and successfully operated for each step of the sol-gel process at full scale, by using U^{238} nitrate as a stand-in. In this campaign about 200 kg of $U^{238}O_2$-ThO_2 was prepared for vibratory-compaction studies. Five runs with U^{238} nitrate were made in the Kilorod Facility with only minor difficulties.

The steps in the sol-gel process, including denitration of thorium nitrate, dispersion of the denitrated thorium to a sol, formation of the gel

by evaporation, and firing to dense oxide particles having properties suitable for vibratory compaction, were shown to be flexible. The steam denitration of thorium nitrate solution gave thoria that was equally as dispersible as the oxide from thorium nitrate crystals. A dispersible mixed oxide containing up to 5% uranium was prepared by steam denitration. In the preparation of the sol of a 3% UO_2-ThO_2, oxide concentrations up to 5 *M* gave satisfactory gels when evaporated. Comminution (prior to firing) of gel particles to sizes suitable for vibratory compaction was shown in the laboratory to be feasible. On the laboratory scale, firing the gel in an inert gas (argon or nitrogen) was shown to produce particles satisfactory with respect to density, oxygen/total metal (oxygen/uranium plus thorium) mole ratio, and release of gases upon heating to 1200°C in vacuum.

Sol-gel thoria and 3% UO_2-ThO_2 spheres about 0.5 cm in diameter were prepared that had attrition rates as low as 0.005 %/hr in a standard spouted-bed test. Microspheres of these oxides with diameters of about 100 μ were also prepared.

6.2 Properties of Sol-Gel Oxides

All analytical and photographic evidence indicates that sol-gel uranium-thorium oxide products containing up to 10 mole % uranium are homogeneous solids, probably solid solutions. They can be made uniform in the U/(U + Th) mole ratio from particle to particle and from batch to batch. Particles have densities between 99 and 99.8% of the theoretical value. The closed porosity, measuring less than 1% of the volume of the solid, is uniformly distributed throughout in about equal-sized pores. When optimally sized, these oxides can be vibratorily packed to (90 ± 1)% of theoretical density in fuel tubes from ¼ to ½ in. in diameter.

Sol-gel oxides are quite free from contaminants that parasitically capture neutrons. The analysis of one large batch showed that the impurities had a total macroscopic neutron absorption cross section equivalent to that of 5 ppm boron. The O/U ratios (calculated on the assumption that the O/Th ratio = 2) varied from 2.02 to 2.5, depending on the furnace atmosphere in which the gels were calcined. The volume of gas released by heating to 1200°C in vacuum varied from 0.002 to 0.4 std cm^3/g and depended on the atmosphere in which the oxide was calcined and the grinding applied after calcination. It was shown to be possible to hold the gas evolution, particularly hydrogen, oxygen, and water, to a value low enough to prevent excessive corrosion of the Zircaloy-2 cladding while the element is in service.

Thirty-two irradiation-test capsules were fabricated by vibratory compaction: 27 from enriched-uranium sol-gel oxide and 5 from arc-fused oxide. These have been or are being irradiated in the NRX, MTR, and ORR. The in-pile tests have been completed on 18 capsules, and the accumulated results show the sol-gel oxide to be a satisfactory reactor fuel. For the 16 capsules that were irradiated in the NRX and in the MTR with burnups of 5000 to 17,000 Mwd per metric ton of Th + U, linear heat ratings from 25,000 to 45,000 Btu hr^{-1} ft^{-1}, a clad temperature of about 200°F, and average fuel temperatures of 2000 to 2500°F, no significant dimensional changes in the capsules nor evidences of sintering of fuel were observed. Irradiation tests and subsequent evaluations are being pursued as part of the joint effort of the Metals and Ceramics and the Chemical Technology Divisions.

6.3 The Kilorod Facility

Cold and low-activity-level runs were completed in the Kilorod Facility (a thoria-urania fuel fabrication facility for use with U^{233}).

Thorium and gross-gamma decontamination factors of 1100 to 25,000 and 100 to 500, respectively, were measured during shakedown tests of the solvent extraction system used to purify the U^{233} feed for the program. Satisfactory sol-gel feed (NO_3^-/U ratio less than 2.5) was obtained, as well as low uranium losses (less than 0.07% to the extraction-column waste). A 4-kg piece of U^{233} metal was dissolved in 40 hr.

Sixty-five kilograms of specification-grade thoria–natural urania was prepared in the sol-gel line during six shakedown runs. This material was successfully processed through powder conditioning and vibratory compacting into the rods. The density of the packed powder was 9.0 g/cm^3.

Calculations were made of the expected gamma dose rates to the hands from operations at each step of the Kilorod process. A maximum hand-exposure case was evaluated in which a single operator performed all operations in the Kilorod Facility over a two-week period. A maximum gamma dose to hands of 1000 millirems was estimated to be received during the second week of the operating cycle.

The Kilorod Facility is being operated jointly by the Chemical Technology Division and the Metals and Ceramics Division.

6.4 Application of Sol-Gel Process to Preparation of ThC_2 and ThC_2-UC_2

Carbon, having a particle size of 90 A and a specific surface area of 670 m^2/g, was dispersed in sols of thoria or uranium-thorium oxide at carbon-to-metal mole ratios of 4.3 to 6.8 to form stable, mixed sols. By evaporation of these sols to gels, and calcination of the gels, complete conversion to the dicarbides was obtained at a temperature as low as 1580°C. Conversions were obtained in times as short as $1\frac{1}{4}$ hr at 1750 to 1800°C. Studies of the kinetics of carburization of thoria indicate the reaction to be first order or pseudo first order with respect to ThO_2. Arrhenius plots were straight lines between 1500 and 1800°C, and apparent activation energies ranged from 110 to 170 kcal per mole of ThO_2.

Initial experiments in forming uranium-thorium oxide–carbon mixed sols to spheres of 100 to 250 μ diameter in carbon tetrachloride and setting them to gels by the addition of isopropyl alcohol gave a high yield of spheres in the desirable size range. The system promises to give an easily controlled method of forming sol-gel spheres. Several problems in the reproducibility of preparation of sols having closely defined viscosity must be solved before the process can be scaled up successfully.

6.5 Design of Thorium-Uranium Fuel-Cycle Development Facility

Title I design of the Thorium-Uranium Fuel-Cycle Development Facility was completed. The facility will consist of four large operating cells having a total inside area of 2120 ft^2, plus two supporting cells and a glove maintenance room, together with the necessary operating areas and other facilities. Shielding will be of normal concrete $5\frac{1}{2}$ ft thick. The cells will be equipped with window liners on 8-ft centers, half of which will be plugged and half equipped with zinc bromide viewing windows. In-cell cranes and electromechanical arms are provided to facilitate equipment maintenance, removal, and replacement by remote means.

Process equipment will be provided for the sol-gel vibratory-compaction method of fabricating fuel rods. This system is to be designed such that it can fabricate rods ranging in diameter from 0.25 to 0.75 in. and in length from 3 to 10 ft. Changes from one rod configuration to another can be accomplished by replacing various fixtures on the basic machines. The equipment for this process will occupy only about half the cell space, leaving the remaining space available for another process equipment line.

7. CHEMISTRY OF LANTHANIDES AND TRANSPLUTONIUM ELEMENTS

7.1 Extraction of Trivalent Lanthanides and Actinides

Study of the separations chemistry of the lanthanides and the transplutonium elements is continuing, with two main objectives: (1) finding an efficient actinide-lanthanide separation that does not require use of chloride and (2) developing separations for the individual transplutonium elements. Part of this section is reported in ORNL-3452, suppl 1.

7.2 Extraction of Hexavalent Americium

Extraction of Am(III) was greater than that of Am(VI) by factors greater than 10^4 with D2EHPA from dilute HNO_3; up to 100 with trioctylphosphine oxide from lithium nitrate; and up to 30 with tributyl phosphate (TBP) from sodium nitrate. Extraction by D2EHPA should be applicable to the separation of curium from americium as Am(VI), since Cm(III) is usually still more extractable than Am(III).

8. SOLVENT EXTRACTION TECHNOLOGY

8.1 Final-Cycle Plutonium Recovery by Amine Extraction

Batch equilibration tests with both aged and fresh Purex plant solutions showed that the aged but not the fresh plant solutions contain zirconium-niobium species highly extractable by the hydrocarbon diluents used with amines and other extractants. The amounts of zirconium-niobium species extractable from the aged solutions were sufficient to account for the low decontamination previously obtained when aged plant solution was used in continuous countercurrent demonstration of the flowsheet. Batch cascade tests with fresh plant solution showed separation and decontamination factors high enough for use in the projected purification process.

8.2 Metal Nitrate Extraction by Amines

Continued studies on amine extraction of nitrato nitrosylruthenium complexes showed extractions by a quaternary amine to be qualitatively similar to those previously reported with a tertiary amine, but extractions by a primary amine to be considerably different, increasing continuously with increasing nitric acid concentration from 1 to 10 *M*. Extraction coefficients were about 0.001, 0.1, and 1 at 1 *M* HNO_3, and 0.05, 0.006, and 0.02 at 10 *M* HNO_3 with (respectively) primary, tertiary, and quaternary at about 0.25 *M* in toluene.

8.3 Metal Chloride Extraction by Amines

Data were obtained for the extraction with amines of twenty different metals from HCl and LiCl–0.2 *M* HCl solutions over the range 0.5 to 10 *M* total chloride. With few exceptions, the extraction power of the amines for the various metals varied in the order: Aliquat 336 (quaternary amine) > Alamine 336 (tertiary amine) > Amberlite LA-1 (secondary amine) > Primene JM (primary amine). For most metals the extraction coefficients increased with an increase in chloride concentration.

8.4 Metal Fluoride Extraction by Amines

Extraction of uranium(VI) and niobium from hydrofluoric acid by amines decreased with increased hydrofluoric acid concentration. The primary amine extracted uranium best, and the tertiary amine extracted niobium best. Extractions of both metals were poorest with the secondary amine.

8.5 Extraction Performance of Degraded Process Extractants

The stability of Amsco 125-82 (aliphatic hydrocarbon) against nitric acid was improved by pretreatment with concentrated sulfuric acid or by preliminary nitric acid degradation followed by treatment with sulfuric acid. The sulfuric acid apparently destroyed the sites otherwise reactive to nitric acid by sulfonation to sulfuric acid–soluble by-products or by rearrangement of the molecule to a more stable configuration. After treatment, the Amsco could be degraded with nitric acid but at a consistently low rate, about the same as that for the relatively stable *n*-dodecane.

Use with tributyl phosphate of diethylbenzenes, butylbenzene, or trimethylbenzenes, rather than aliphatic diluents, gave improved performance with regard to radiation stability, uranium extraction power, and separation of uranium from fission products.

The isomers of diethylbenzene varied in stability against side-chain degradation by nitric acid, and in order of decreasing stability were: meta > ortho >> para. The meta isomer was about as stable as *n*-dodecane. Several polymethylbenzenes were equally stable.

8.6 Separation of Alkali Metals

Favorable separations of alkali metals were obtained by extracting with substituted phenols from alkaline solutions. With 4-sec-butyl-2(α-methylbenzyl)phenol (BAMBP), the order of extractability was Cs > Rb > K > Na > Li, and separation factors were ~20 for both cesium/rubidium and rubidium/potassium. Combining a small concentration of di(2-ethylhexyl)phosphoric acid with BAMBP greatly enhanced alkali metal extractions from neutral or slightly acidic liquors where extraction with BAMBP alone is inappreciable. Extractions were also synergized by combining dinonylnaphthalenesulfonic acid, dodecylphosphoric acid, or Neo-Tridecanoic acid with phenols.

8.7 Cesium Recovery from Ores

The phenol extraction (Phenex) process was applied to the recovery of cesium from ores and its separation from other alkali metals. The cesium in pollucite ore was solubilized by roasting the ore with Na_2CO_3-NaCl at 800°C and leaching with water. Greater than 99% of the cesium was recovered from this solution by extracting with 1 *M* 4-*sec*-butyl-2(α-methylbenzyl)phenol (BAMBP) in diisopropylbenzene and stripping with hydrochloric acid. Overall decontamination factors (leach liquor to strip product) for cesium were 230 from Rb, 610 from K, 16,000 from Na, >10 from Li, and >3000 from Si. Cesium was also recovered effectively with BAMBP from a water solution of Alkarb, which is an alkali metal carbonate by-product of the lithium industry.

8.8 Acid Recovery by Amine Extraction

Preliminary tests showed the potential utility of tertiary amines for recovery and purification of phosphoric acid from the highly contaminated wet-process acid produced in the fertilizer industry. Water-stripping the amine yields a product more than 1.5 *M* in H_3PO_4 and almost free of iron and aluminum.

8.9 Extraction of Niobium and Tantalum from Alkaline Solutions

Quaternary ammonium compounds, for example, Aliquat 336, extracted niobium and tantalum from alkaline solutions. Niobium was extracted preferentially (niobium/tantalum separation factor, 5 to 10) in some tests with pure solutions, but no appreciable separation of the elements was obtained in tests with practicable ore liquors. Solutions of Na_2CO_3, NaOH, $(NH_4)_2CO_3$, K_2CO_3, chloride salts, and nitrate salts were effective stripping agents.

8.10 New Extractants

A number of amides,

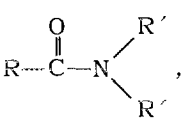

covering a range of structures, were examined with regard to their extraction of uranium, thorium, and several other solutes from nitric acid solutions. In comparison with tributyl phosphate (TBP), the *N*,*N*-dialkylamides extract in the same manner, are somewhat weaker uranium extractants, but have potential for considerably greater selectivity. Extracted uranium was stripped with water or with dilute nitric acid. The amides resemble TBP in synergistically enhancing uranium extraction by di(2-ethylhexyl)phosphoric acid. Uranium extraction power vs nitric acid concentration varied considerably with amides made from differing fatty acids, and, like TBP, the coefficients for any one amide varied by only about a factor of 2 in the acidity range 2 to 7 *M* HNO_3. In contrast, the thorium extraction power varied only slightly with chain length of the fatty acids, but the amide coefficients increased over three times as fast as those with TBP in the acidity range 2 to 6 *M* HNO_3. Branched-chain amides showed much lower extractions but higher indicated selectivity for uranium. Extraction was low for uranium and thorium from hydrochloric and sulfuric acid solutions, and for strontium and cesium from nitrate solutions. Nitric acid was extracted readily.

A systematic survey was started of cation-exchange extraction by high-molecular-weight carboxylic acids, including some specially synthesized and some of recent commercial availability. The constants, $K = (H^+)(MA)/(M^+)(HA)$ for the neutralization reaction $\underset{\cdots}{HA} + M^+ \rightleftharpoons \underset{\cdots}{MA} + H^+$ (dots indicate the organic phase), measured at half-neutralization in two-phase titration, ranged from 10^{-10} to 4×10^{-6}.

Hydroxamic acids,

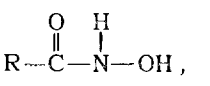

showed potential for extraction of zirconium, niobium, hafnium, and strontium. The available acids decomposed when exposed to nitric acid or alkaline solutions but appeared stable in extraction from hydrochloric acid, suggesting usefulness in non-oxidizing acid systems.

A bicyclic or "cage-structure" phosphate ester, the bicyclic phosphate of 1,1,1-trimethylolnonane, showed high extraction power for thorium and high selectivity for thorium over uranium.

8.11 Fundamental Studies on Solvent Extraction Equilibria and Kinetics

In continued studies of alkaline earth extraction by di(2-ethylhexyl)phosphate ($[HA]_2$ + NaA) in benzene, the generalized equation,

$$Sr^{2+} + (n/y)[aHA \cdot bNaA]_y \rightleftharpoons SrA_2 \cdot (n-2)[\alpha HA \cdot \beta NaA] + iH^+ + jNa^+ ,$$

$$a + b = 1, \quad \alpha + \beta = 1, \quad i + j = 2,$$

proved to be a suitable model for strontium extraction when the extractant ranged from the acid form to the 50% salt form, with n experimentally found in the range of 4 to 6. When the extractant is nearly all in the acid form this becomes

$$Sr^{2+} + [HA]_2 \rightleftharpoons SrA_2 \cdot 4HA + 2H^+ .$$

The corresponding reaction for sodium extraction was also confirmed,

$$Na^+ + 2[HA]_2 \rightleftharpoons NaA \cdot 3HA + H^+ .$$

These extracted species are of particular interest since their stoichiometry is markedly different from that found in most other metal species extracted by di(2-ethylhexyl)phosphate. The choice of diluent affects strontium extraction by shifting the pH of maximum extraction, and in some cases (e.g., n-nonane plus TBP) by synergistic enhancement.

Formation constants were evaluated for the thorium trisulfate and tetrasulfate anionic complexes on the basis of amine extraction equilibrium data:

$$K_{23} = [Th(SO_4)_3^{2-}]/[Th(SO_4)_2][SO_4^{2-}] = 5.7 \pm 1.2,$$

$$K_{24} = [Th(SO_4)_4^{4-}]/[Th(SO_4)_2][SO_4^{2-}]^2 = 0.054 \pm 0.009,$$

$$K_{34} = [Th(SO_4)_4^{4-}]/[Th(SO_4)_3^{2-}][SO_4^{2-}] = 0.009 \pm 0.003,$$

evaluated at zero ionic strength. A general method was developed for this evaluation, using the essential feature of experimentally maintained constant chemical potentials of extractable species in the aqueous phase, controlled and monitored by constant composition of the equilibrium organic phase.

Continued transfer-rate measurements of tagged sulfate from amine solution to aqueous sulfate solution, with uranium absent, present and extracting, or already at equilibrium, gave evidence that both neutral complex transfer and ion transfer contribute to the uranium transfer, the former predominating in extraction from low-sulfate solutions, where little of the uranyl ion is complexed, and the latter becoming important at higher sulfate concentrations, where most of the uranium exists in anionic complexes.

Direct precise measurement of diluent vapor-pressure differences showed increasing polymerization of di(2-ethylhexyl)-phosphate (HA,NaA) solutions in benzene as the proportion of salt form increased, from $[HA]_2$ to $[NaA]_{13}$ at 0.1 M and from $[HA]_2$ to $[NaA]_{50}$ at 0.25 M ΣA. The same technique was used to measure the activity coefficients of triphenylmethane in benzene, varying from 0.98 at 0.014 m to 0.74 at 0.33 m. With this as the reference solute, the activity coefficients of azobenzene and of tri-n-octylamine were determined by isopiestic balancing, varying from 0.96 at 0.0134 m to 0.67 at 0.346 m, and from 0.98 at 0.021 m to 0.55 at 0.354 m respectively.

8.12 Engineering Equipment Studies

The use of solvent extraction to concentrate valuable materials from dilute solutions requires operation at high flow ratios. Pulsed columns show promise in that the stage heights for uranium extraction by tributyl phosphate at a flow ratio of 100:1 was only 2 to 3 times that at a more conventional ratio of 5:1.

Knowledge of the maximum and minimum hydraulic pressure at the base of a pulsed column is needed for design of the pulser and external piping. The variation of orifice coefficients (calculated from maximum and minimum pressure) of nozzle plates with pulse frequency and direction of flow was determined to be not significantly different from that for conventional sieve plates.

9. FISSION PRODUCT RECOVERY

9.1 Cesium

Continued study confirmed the utility of the Phenex process for recovering cesium from alkaline Purex wastes by extracting with substituted phenols and stripping with dilute acid. Of a large number of phenols screened, best performance was given by 4-sec-butyl-2 (α-methylbenzyl) phenol (BAMBP) and 4-chloro-2-benzylphenol (Santophen-1). In a batch countercurrent test with Santophen-1 in diisopropylbenzene diluent, >99.7% of the cesium was recovered from simulated Purex 1WW waste (tartrate complexed and adjusted to pH 12.3) in six extraction and two scrub stages. The extract was stripped with 0.1 *M* HNO_3 to give a product solution with ~5 g of cesium per liter. The overall cesium/sodium decontamination factor for the experiment was $\sim 6 \times 10^4$. The process has also been applied to the treatment of alkaline liquors produced by sorbing cesium from acid wastes with ammonium molybdophosphate (AMP) and dissolving the AMP in caustic.

9.2 Strontium and Rare Earths

The di (2-ethylhexyl) phosphoric acid (D2EHPA) extraction process for recovering strontium and mixed rare earths gives efficient separation of yttrium from the rare earths in the nitric acid stripping cycle. Batch countercurrent tests indicated that the yttrium content of the rare-earths product would be <2% of the amount in the original waste solution. Comparison of tartrate and citrate as complexing agents for the Purex 1WW feed showed that results are strongly dependent on feed-adjustment procedures. More efficient extractions of strontium and rare earths were obtained from tartrate-complexed than with citrate-complexed feeds.

9.3 Other Strontium Extractions

This section is reported in ORNL-3452, suppl 1.

9.4 Zirconium-Niobium

Efficiencies in the extraction of zirconium-niobium from Purex 1WW solution with D2EHPA and stripping with oxalic acid were greatly improved by increasing the temperature.

9.5 Extractions from Purex-Waste Concentrate with Amines

In a batch countercurrent test, most of the acid, iron, zirconium-niobium, and ruthenium were extracted with a primary amine (Primene JM) from simulated Purex waste while extracting only ~5% of the cerium. More than 98% of the cerium was then extracted from the solution with Primene JM, leaving a raffinate that would be highly amenable to treatment for strontium and cesium recovery.

10. URANIUM PROCESSING

10.1 Radium Removal from Uranium-Mill Waste Streams

In studies on the column adsorption of Ra^{226} from simulated, neutralized waste streams from uranium mills, the capacities to 5% radium breakthrough were ~2000 column volumes for clinoptilolite (natural zeolite) and 6000 column volumes for Decalso (synthetic zeolite). Ammonium nitrate was an efficient eluting agent.

10.2 Amine Extraction of Uranium from Sulfate-Chloride Liquors

The uranium extraction power of the *N*-benzyl secondary amines is sufficiently strong that they can be applied to the treatment of chloride-containing sulfate liquors of the type produced in plants that use the salt-roast acid-leach process for uranium-vanadium recovery.

11. THORIUM RECOVERY FROM GRANITIC ROCKS

Three drill-core samples to depths of 500 to 600 ft in the Conway granite formations in New Hampshire showed uniform thorium concentration and thorium leachability with depth. The thorium reserve in the outer 600 ft of the main Conway mass has been estimated at 21 million tons. The uranium reserve in the rock is probably a fourth to a fifth of the thorium reserve. Process studies indicate that about two-thirds of

the thorium and a smaller fraction of the uranium can be recovered by an acid leach–solvent extraction flowsheet for an average cost of less than $75 per pound of thorium plus uranium. Thorite, huttonite, and zircon were identified as the major carriers of thorium in Conway granite.

12. PROTACTINIUM CHEMISTRY

The investigation of the chemistry of protactinium has been concerned primarily with extraction of Pa(V) from sulfuric acid solutions by organic amine solutions and by anion exchange resins. The extractability of Pa(V) from sulfuric acid is qualitatively related to the base strength of the amine; extraction coefficients for different amines vary over several orders of magnitude. An observed marked decrease in the extraction of protactinium with increasing aqueous acidity may be due at least partly to changes in the composition of the organic phase, particularly the decrease in sulfate ion concentration, as well as to changes in the aqueous protactinium complex. Extraction coefficients obtained with Dowex 1 resin and with dilute trilaurylamine, at conditions giving relatively low extraction, increase very rapidly with the aqueous protactinium concentrations above about 10^5 counts min^{-1} ml^{-1} (Pa^{231}) in 2.5 *M* H_2SO_4. These observations are consistent with a reversible polymerization of Pa(V) in one or both phases, with both the polymer and the simpler species being extracted, and the polymer being more extractable.

13. EFFECTS OF REACTOR IRRADIATION ON ThO_2

Thoria pellet and powder preparations irradiated in D_2O and dry in the LITR to exposures of 2.5×10^{18} fissions/gram were examined to determine irradiation effects. The preparations included P-82 thoria pellets; sintered thoria compacts; shaped, arc-fused thoria pellets; sol-gel thoria particles; Houdry thoria spheres (44 to 74 μ); arc-fused thoria fragments (44 to 74 μ); and 1600°C-fired thoria powder (DT-46). The purpose of the experiment was to determine the influence of the method of preparation and the physical condition of the product on the irradiation effects and on effects associated with the presence of water. Radiation effects were evaluated in terms of visual examination, material balances, wear tests, impact fracture tests, and x-ray and metallographic examination. Principal attention was paid to the P-82 pellets.

13.1 Irradiation Effects on P-82 Thoria Pellets

The P-82 pellets irradiated under D_2O and dry showed minor weight losses but did not appear to suffer structural damage. A portion of the pellets irradiated in the vapor phase, however, showed a significant weight loss as well as considerable surface and structural damage. Wear tests showed that the pellets irradiated under D_2O and dry had enhanced attrition resistance. The surface of the P-82 pellets was found to contain an aluminum/thorium weight ratio of 0.08, in contrast with an average aluminum content of 0.02% for whole pellets, which may account for the marked stability of the P-82 pellet under irradiation.

13.2 Irradiation Effects in Thoria Pellets Prepared by a Pressing and Firing Procedure Different from That for P-82 Pellets

The thoria pellets prepared by a method different from that for the P-82 pellets suffered considerable damage upon being irradiated in D_2O, despite their higher initial density. Those irradiated dry appeared undamaged.

13.3 Irradiation Effects on Other Thoria Preparations

The arc-fused pellets and sol-gel-prepared particles irradiated under D_2O and dry did not appear on visual inspection to be significantly damaged by the irradiation. No gross changes were observed in the Houdry spheres and in the ground, arc-fused materials. Wet-irradiated 1600°-fired thoria powder was transformed into a porous plug contaminated with corrosion products; the dry-irradiated material had formed a chalky plug.

13.4 Results of X-Ray and Metallographic Examination of Irradiated Thoria: P-82 Pellets, Arc-Fused Pellets, and Sol-Gel-Prepared Particles

X-ray diffraction measurements on the P-82, arc-fused, and sol-gel-prepared materials indicated that relatively little change had occurred as a result

of the irradiation, indicative of the marked resistance of cubic structures to radiation damage.

Polished sections at low magnification of the unirradiated and irradiated P-82 and arc-fused materials were similar. The irradiated sol-gel-prepared material exhibited extensive fracturing. At high magnification the polished and etched sections of all irradiated and unirradiated materials were similar.

14. RADIATION EFFECTS ON CATALYSTS

Attempts to alter the catalytic activity of $MgSO_4$ and $MgSO_4$-Na_2SO_4 by the addition of trace impurities failed, providing further evidence that the previously reported effects were caused by the presence of radioactive sulfur. The overall reaction order for the dehydration of cyclohexanol on these catalysts was found to be 1.

15. HIGH-TEMPERATURE CHEMISTRY

15.1 High-Temperature, High-Pressure Spectrophotometer System

Design of the high-temperature, high-pressure spectrophotometer system by a subcontractor was completed and the subcontract terminated. The prototype absorption cell is undergoing testing.

15.2 Miniature Circulating-Loop System and Digital Data Output System for the Cary Spectrophotometer

A spectrophotometer, Cary model 14 CMR, was installed and equipped with the previously constructed digital data output system. It is operable with solutions at temperatures up to 95°C. Valve and support problems encountered with the miniature circulating-loop system, designed for operation with liquids up to 170°C and 200 psi, have been solved.

15.3 Measurement of Liquid Densities at High Temperatures and High Pressures

An autoclave and facility designed for the accurate measurement of liquid densities at high temperatures and high pressures was built. It should be possible to determine densities of solutions at 370 to 371°C within a maximum error of 0.6% with this system. The error will be less at lower temperatures.

15.4 Computer Programs for Spectrophotometric Studies

A computer program for the analysis of spectrophotometric absorption data for dynamic multicomponent systems was written and tested. Concentration-time data for each component of the reacting system can be obtained to within a relative error of ±0.1% over the entire course of the reaction. Output may be tabulated and/or plotted on the Calcomp graphical plotter.

A set of computer programs and subroutines was written for the least-squares convolution smoothing of the noise and random fluctuations from digitized spectral data obtained from the spectrophotometer digital data output system. The fitting is done for each point over a 3- to 15-point range, utilizing a cubic function. The smoothed-data output may be in the form of tables, punched cards, or Calcomp graphical plotting.

16. MECHANISMS OF SEPARATIONS PROCESSES

For the purpose of developing a mathematical description of extraction of nitric acid and uranyl nitrate from aqueous solutions by tributyl phosphate (TBP)–hydrocarbon diluent solutions, activities of water, nitric acid, uranyl nitrate, and TBP are being obtained by transpirational vapor-pressure techniques. The activity of water and the stoichiometric, molecular, and ionic activity coefficients of nitric acid were obtained for 0 to 100% acid by combining new data with literature data. Measured vapor pressures of TBP over water–nitric acid–TBP solutions were used to calculate a value of 1.75 for the equilibrium constant, K/y_{TN}, for extraction of nitric acid by TBP. Water and nitric acid activities over the three-component system water–nitric acid–uranyl nitrate were measured. From these data the activities of uranyl nitrate will be calculated.

17. ION EXCHANGE

17.1 Radiation Damage to Ion Exchange Resins

The anion exchange resin, Dowex 1 (50 to 100 mesh) in the hydroxyl form, lost more than 90%

of its strong-base capacity in a flowing-water system after an exposure of 1.3×10^8 r in a Co^{60} gamma irradiation source – about half the dose reported in the literature for this resin in a static system for a comparable loss of capacity. Analysis of data from the irradiation of Dowex 50W cation exchange resin indicated that degradation occurs, initially, by cleavage of the active sulfonate groups and is followed by the breakup of the resin matrix into water-soluble products and small, noncentrifugable particles with a molecular weight of several million.

17.2 Studies of the Separation of Some Fission Products by Ion Exchange

Citrate at pH 2.5 (usually citrate is used at higher pH's) was evaluated as a complexer of impurity cations in the ion exchange recovery of rare earths and strontium fission products from radioactive wastes like Hanford Purex 1WW. Experimental distribution coefficient data, obtained from Dowex 50W-X8 (100- to 200-mesh) cation resin pre-equilibrated at pH 2.5 and waste solution treated with 1.5 moles of citrate per mole of combined Al^{3+}, Fe^{3+}, and Cr^{3+} (impurity cations), indicated that (1) bulk trivalent cation impurities were effectively complexed and remained in solution; (2) resin capacity for strontium and rare earths increased as waste acidity was lowered by dilution; and (3) at a reasonable waste dilution factor of 20, separation factors were favorable, being: K_d^{Sr}/K_d^{Fe}, >200; K_d^{Ce}/K_d^{Fe}, >600; and K_d^{Ce}/K_d^{Sr}, ~3.

18. CHEMICAL ENGINEERING RESEARCH

18.1 Development of High-Speed Contactors: The Stacked-Clone Contactor

Eight geometrically distinct designs of the stacked-clone contactor, a high-throughput, low-holdup solvent extraction device, were tested for capacity and stage efficiency with uranyl nitrate–1 *M* sodium nitrate–18% TBP–Amsco. Within each design, the effects of the diameter and length of the vortex finder were studied, as was the area of the feed port. With Mark I, a ¾-in.-diam conical design (the others were 1½-in.-diam funnel-shaped designs), the effects of different underflow baffling and underflow chamber volumes were also studied.

The need for an underflow-chamber arrangement providing symmetrical radial flow to the pump, mixing opportunity, and preservation of the organic vortex is indicated.

The original design, the Mark I contactor, gave combined flow capacities of 2.0 liters/min at 70% efficiency. The Mark XI contactor, the latest design of a series, gave capacities of 4.5 liters/min at 60 to 70% efficiency. This corresponds to a retention time of both phases per theoretical stage of about 4 sec.

The Mark XI design represents a useful and practical prototype high-speed contactor for radiochemical processing.

18.2 Studies on Coalescence in Solvent Extraction Systems

Studies of the effect of ionizing radiation on coalescence rates in liquid-liquid solvent extraction systems have been undertaken. Fast protons, alpha particles, or fission fragments may be produced in the vicinity of the interdrop membrane by the neutron irradiation of hydrogen, Li^6, or U^{235} in the aqueous phase. Preliminary experiments show no effect of recoil protons on the coalescence of water drops in benzene, in agreement with theory.

18.3 Dynamics of Gas-Liquid Contacting in Packed Towers

In studies of the dynamics of contacting gases and liquids in packed columns, experiments were conducted on an air-CO_2-water system using ¼- and ⅝-in. ceramic Raschig rings. Both direct sinusoidal and pulse forcing of the entering gas composition were used, and good agreement was obtained between the two perturbation methods in terms of the resulting amplitude ratios and phase shifts. A simplified theoretical dynamic model indicated that dynamic behavior is primarily influenced by the absorption factor, the number of transfer units, and the time required for the phases to traverse one transfer unit. Further experimental data must be obtained, including measurements on the distribution of velocities, before mathematical models for packed columns can be evaluated.

19. GAS-COOLED REACTOR COOLANT PURIFICATION

19.1 Oxidation of Hydrogen, Carbon Monoxide, and Methane by Fixed Beds of Copper Oxide Pellets

The investigation of the kinetics of the oxidation of small amounts of H_2, CO, and CH_4 (impurities) in a flowing stream of helium by fixed beds of porous pellets of copper oxide is continuing. Two forms of copper oxide were tested: porous pellets made by compaction, and a mixture of powdered copper oxide, alumina, and silica, extruded into pellets. The oxidation of the impurities is a proposed first step in the purification of the helium before its use as a coolant for the Gas-Cooled Reactor. Two types of CuO have been tested in the following range of conditions: temperature, 400 to 600°C; pressure, 10.2 to 300 atm; mass flow rate of the gas, 0.0058 to 0.050 g cm^{-2} sec^{-1}; and contaminant concentration, 0.0008 to 1.21 vol %. The rate controlling factors for the three contaminants are: (1) mass transfer of the H_2 or CO from the bulk gas stream to the CuO reaction site, and (2) reaction surface in the CuO particles for the oxidation of the CH_4. Computer solutions of the mathematical models were made, and correlation of the experimental and model-predicted results will be the basis for reactor design.

19.2 Characterization of Aerosols by a Light-Scattering Technique

An experimental investigation was started on the characterization of aerosols by determining particle-size distribution and concentration in gas streams by means of a light-scattering technique. The detecting cell for this device was made, and instruments are being procured. An aerosol generator was developed for use in calibrating the detector.

20. EQUIPMENT DECONTAMINATION STUDIES

Laboratory tests showed that stainless steel blowers and piping exposed to contaminated helium at the operating temperatures of the Experimental Gas-Cooled Reactor can probably be adequately decontaminated, without damage, by hot oxalic acid solutions containing fluoride and hydrogen peroxide. These mixtures were superior to many others for decontaminating, for dissolving oxide films, and for brightening the surfaces of heated stainless steels. The search for improved methods is continuing.

21. FUEL SHIPPING STUDIES

21.1 Fuel Carrier Drop Tests

As a part of the Laboratory's Reactor Evaluation Program, experimental and cost studies were made on the shipping of irradiated reactor fuels to a fuel-processing plant. The experimental work involved the dropping of 1.4- and 6-ton model casks from heights up to 28 ft in order to evaluate a section of the proposed AEC regulations on fuel shipping. Flat drops from 15 ft resulted in little or no damage, but corner and "piston" drops from this height did result in minor damage. Thus it appears that, except for the piston-impact provisions, the regulations can be satisfactorily met by careful cask design.

21.2 Fuel Shipping Cost Studies

Shipping cost studies indicated that, for a domestic-fuel-discharge rate of 3 tons of natural uranium per day, the truck shipping cost for a 2350-mile round trip with a 25-ton cask would be about $1.30 per kilogram of uranium for an irradiation level of 8500 Mwd/ton. Rail costs are higher by almost a factor of 2. The shipping of the same fuel from Italy to southern California by chartered boat was estimated to cost only $1.25 per kilogram of uranium.

22. CHEMICAL APPLICATION OF NUCLEAR EXPLOSIVES (PROJECT COACH)

22.1 Recovery of Isotopes from Coach Event

A flowsheet was developed for the recovery of the few grams of transplutonium isotopes (to be produced in the Coach nuclear detonation) from the 10,000 to 35,000 tons of salt in which it will be dispersed. In this flowsheet the mined and crushed salt is dissolved in 2.5 lb of water per pound of salt; and the insoluble material, containing 99% of the transplutonic isotopes and fission

products, is separated from the brine. The separated insolubles are dissolved in nitric or hydrochloric acid. Oxalic acid is then added to the acid leach to precipitate about 1% of the dissolved calcium; the calcium oxalate, which carries the transplutonics quantitatively, is separated and probably dried for shipment to an AEC site for further processing. Scavenging by ferric hydroxide as a means of carrying the transplutonics was unsatisfactory.

22.2 Jet Sampling and Bubble-Tapping Studies

Two support studies were made at Frankford Arsenal. The first showed the feasibility of jetting uranium targets with velocities sufficient to outrun the shock wave from an underground nuclear explosion. The second study indicated that conventional explosives in a radial pipe from the nuclear device can provide sufficient counterpressures to keep a sampling pipe open during and after the nuclear detonation.

23. PREPARATION OF URANIUM-232

The preparation of U^{232} for neutron cross section measurements was completed. A total of 32.9 mg of U^{232} containing from 180 to 350 ppm U^{233} was prepared previously, and 1.04 g of U^{232} containing 0.72 wt % U^{233} was prepared during the past year. The U^{232} was produced by the neutron irradiation of approximately 45 g of Pa^{231} irradiated as an Al-Pa_2O_5 cermet. Chemical separation was accomplished by two cycles of anion exchange from mixed HCl-HF solution, followed by a uranium extraction into 20% TBP from 6 *M* HNO_3.

24. ASSISTANCE PROGRAMS

The Chemical Technology Division continued to provide assistance to others on several projects.

24.1 Eurochemic Assistance

This program was continued at ORNL by providing the U.S. Technical Advisor, E. M. Shank, to Eurochemic for the construction phase of the Eurochemic Plant at Mol, Belgium, and for the subsequent startup period. ORNL also continued to coordinate the exchange of data between Eurochemic and the United States.

The Eurochemic staff is rapidly increasing and employed a total of 195 people at the end of 1961. The Eurochemic Plant is currently estimated to cost $24,670,000.

24.2 High Radiation Level Analytical Laboratory

The Division is continuing to provide the technical liaison for this facility for the Analytical Chemistry Division. Last year the Foster and Creighton Company of Nashville, Tennessee, was selected as the prime contractor and began construction in July 1962 following preconstruction site preparation work by the H. K. Ferguson Company. Construction of the facility is now scheduled for completion early in 1964.

24.3 Plant-Waste-System Improvements

The division continued to provide technical liaison to the Operations Division on this project. The plant waste improvements currently being designed and built are (1) a separate Melton Valley collection and transfer system for low- and intermediate-activity-level waste, (2) an intermediate- and high-activity-level waste evaporator, and (3) a pair of 50,000-gal, high-activity-level, water-cooled, stainless steel, acid-waste storage tanks. Construction of the first project and the structural facilities for the other two were started in March 1963 by the Rentenbach Construction Company and are scheduled for completion by December 1963. Design of process equipment for the evaporator facility is complete; this equipment is being fabricated at ORNL. Design of the waste storage tanks was also completed, and they will be made outside the Laboratory. The evaporator and waste tanks are scheduled to be ready for use by December 1964.

24.4 Molten-Salt Converter Reactor (MSCR) Fuel-Processing Study

The MSCR fuel-processing design study and cost estimate made jointly with the Reactor Division and presented previously was expanded to determine the economics in recovering the protactinium in the waste salt after the first processing. This

new study showed that at a plant capacity of about 3 kg of U^{235} per day an annual saving of $150,000 could be achieved by discarding the protactinium.

24.5 Interim Alpha Laboratory, Building 3019

An interim alpha laboratory for joint use by the Chemical Technology and Metals and Ceramics Divisions was designed and is being built in the basement of Building 3019.

24.6 Fuel Cycle for Large Desalination Reactors

Fuel cycle costs were evaluated for a variety of reactor stations for the production of water and possibly electricity. The base case studied was a heavy-water-moderated, light-water-cooled, natural-uranium reactor using the nested tube element. Fuel cycle throughputs ranged from 1 to 30 short tons of uranium per day. The fuel cycle costs were also determined for the same fuel element (*a*) when the irradiated fuel was discarded rather than processed at 10 and 30 tons per day, and (*b*) when plutonium and depleted uranium replaced the natural uranium at 1 to 30 tons per day. An attempt was made to examine on a comparable basis a partially enriched uranium fuel of the Dresden type at 10 tons per day.

These studies indicated:

1. Unit costs are rapidly reduced by increase in production requirements.
2. Natural-uranium fuels have the lowest fuel cycle costs.
3. Burnup and inventory are the major factors in fuel cycles for slightly enriched uranium. These costs alone exceed the complete cycle costs for natural-uranium fuel.

24.7 Radiochemical Plant Safety Studies

Radioisotope-source fabrication and Pu^{239} and U^{233} fuel fabrication in privately owned radiochemical plants are expected to increase greatly during the next decade. The potential economic loss from off-site damage due to accidents in such plants was evaluated. With the safeguards in design and operation normally included in a radiochemical plant the worst contained accidents are not expected to result in a monetary loss due to damage to the surroundings which could exceed the limits of presently available insurance (60 million dollars). As in the case with large power reactors, however, catastrophic accidents involving loss of containment in these facilities, although having such an extremely low probability of occurrence as to be considered incredible, could result in damage to the surroundings amounting to billions of dollars, particularly when normal inventories of Pu^{238}, Sr^{90}, and Pu^{239} are involved. Uncontained accidents involving U^{233} or Kr^{85}, on the other hand, would result in potential liability of a million dollars or less.

The results of the study provide values of relative liability for plants that fabricate or process a variety of radioisotopes of current interest, and they provide rough estimates of the potential economic loss that could be incurred in major accidents. Radioactive material inventory, containment properties, meteorology, and surrounding population distribution all affect the potential monetary loss.

Contents

SUMMARY iii

1. POWER REACTOR FUEL PROCESSING 1
   - 1.1 Processes for Uranium and Thorium Carbide Fuels 1
   - 1.2 Hot-Cell Tests on Sulfex and Zirflex Processes 6
   - 1.3 Processes for Breeder Reactor Fuels 8
   - 1.4 Corrosion Studies 15
   - 1.5 Mechanical Processing 17
   - 1.6 Chloride Volatility Process Development [Reported in ORNL-3452, suppl 1]
   - 1.7 Rover Fuel Processing Development [Reported in ORNL-3452, suppl 2 (classified)]

2. FLUORIDE VOLATILITY PROCESSING 26
   - 2.1 Processing of Uranium-Zirconium Alloy Fuel 27
   - 2.2 Volatilization and Recovery of Plutonium Hexafluoride 42
   - 2.3 Preparation and Absorption of Tellurium Hexafluoride 44
   - 2.4 Process Engineering Studies 45
   - 2.5 Other Corrosion Studies 48
   - 2.6 Processing of Uranium-Aluminum Alloy Fuel [Reported in ORNL-3452, suppl 1]

3. WASTE TREATMENT AND DISPOSAL 51
   - 3.1 Pot Calcination of High-Level Waste 51
   - 3.2 Treatment of Low-Level Waste 78
   - 3.3 Engineering, Economics, and Safety Evaluations 92

4. TRANSURANIUM ELEMENT PROCESSING 96
   - 4.1 Chemical Process Development 96
   - 4.2 Development of Pulsed Columns 115
   - 4.3 Process Equipment Design 116
   - 4.4 TRU Facility Design 127
   - 4.5 Experimental Engineering Studies 130
   - 4.6 TRU – Evaluation of Protective Coatings 132
   - 4.7 Calculations for the Irradiation of Prototype HFIR Targets 133

5. CURIUM PROCESSING 134
   - 5.1 Flowsheet Tests for the Processing of Pu^{242}, Americium, and Curium 134
   - 5.2 The Curium Production Facility 138
   - 5.3 Calculations Regarding the Irradiation of Gram Quantities of Americium-241 143

6. THORIUM FUEL-CYCLE DEVELOPMENT 144
   - 6.1 Sol-Gel Process Development 144

6.2 Properties of Sol-Gel Oxides 147
6.3 The Kilorod Facility 152
6.4 Application of Sol-Gel Process to Preparation of ThC_2 and ThC_2-UC_2 156
6.5 Design of Thorium-Uranium Fuel-Cycle Development Facility 161

7. CHEMISTRY OF LANTHANIDES AND TRANSPLUTONIUM ELEMENTS 166
7.1 Extraction of Trivalent Lanthanides and Actinides 166
7.2 Extraction of Hexavalent Americium 167

8. SOLVENT EXTRACTION TECHNOLOGY 168
8.1 Final-Cycle Plutonium Recovery by Amine Extraction 168
8.2 Metal Nitrate Extraction by Amines 169
8.3 Metal Chloride Extraction by Amines 170
8.4 Metal Fluoride Extraction by Amines 172
8.5 Extraction Performance of Degraded Process Extractants 172
8.6 Separation of Alkali Metals 175
8.7 Cesium Recovery from Ores 176
8.8 Acid Recovery by Amine Extraction 177
8.9 Extraction of Niobium and Tantalum from Alkaline Solutions 178
8.10 New Extractants 178
8.11 Fundamental Studies on Solvent Extraction Equilibria and Kinetics 182
8.12 Engineering Equipment Studies 187

9. FISSION PRODUCT RECOVERY 189
9.1 Cesium 189
9.2 Strontium and Rare Earths 192
9.3 Other Strontium Extractions
[Reported in ORNL-3452, suppl 1]
9.4 Zirconium-Niobium 193
9.5 Extractions from Purex-Waste Concentrate with Amines 194

10. URANIUM PROCESSING 194
10.1 Radium Removal from Uranium-Mill Waste Streams 194
10.2 Amine Extraction of Uranium from Sulfate-Chloride Liquors 196

11. THORIUM RECOVERY FROM GRANITIC ROCKS 196
11.1 Drill-Core Samples of Conway Granite 197
11.2 Conway Granite Mineralogy 198
11.3 Conway Granite Processing 198
11.4 Thorium Reserves and Costs 198

12. PROTACTINIUM CHEMISTRY 199
12.1 Extraction of Protactinium by Various Amines 199

12.2 Ion Exchange of Protactinium from Sulfate Solutions 200
12.3 Polymerization of Protactinium 201

13. EFFECTS OF REACTOR IRRADIATION ON ThO_2 203
13.1 Irradiation Effects on P-82 Thoria Pellets 203
13.2 Irradiation Effects in Thoria Pellets Prepared by a Pressing and Firing Procedure Different from That for P-82 Pellets 206
13.3 Irradiation Effects on Other Thoria Preparations 207
13.4 Results of X-Ray and Metallographic Examination of Irradiated Thoria: P-82 Pellets, Arc-Fused Pellets, and Sol-Gel-Prepared Particles 208
13.5 Conclusions 209

14. RADIATION EFFECTS ON CATALYSTS 210
14.1 Conversion of Cyclohexanol to Cyclohexene with $MgSO_4$ and $MgSO_4$-Na_2SO_4 Catalysts 210

15. HIGH-TEMPERATURE CHEMISTRY 211
15.1 High-Temperature, High-Pressure Spectrophotometer System 211
15.2 Miniature Circulating-Loop System and Digital Data Output System for the Cary Spectrophotometer 212
15.3 Measurement of Liquid Densities at High Temperatures and High Pressures 212
15.4 Computer Programs for Spectrophotometric Studies 213

16. MECHANISMS OF SEPARATIONS PROCESSES 215
16.1 Activities of Nitric Acid and Water in Aqueous Solutions of Nitric Acid 215
16.2 Vapor Pressures of Tributyl Phosphate over Water–Nitric Acid–Tributyl Phosphate Solutions 217
16.3 Activities of Water, Nitric Acid, and Uranyl Nitrate in the Three-Component System 217

17. ION EXCHANGE 218
17.1 Radiation Damage to Ion Exchange Resins 218
17.2 Studies of the Separation of Some Fission Products by Ion Exchange 219

18. CHEMICAL ENGINEERING RESEARCH 221
18.1 Development of High-Speed Contactors: The Stacked-Clone Contactor 221
18.2 Studies on Coalescence in Solvent Extraction Systems 225
18.3 Dynamics of Gas-Liquid Contacting in Packed Towers 228

19. GAS-COOLED REACTOR COOLANT PURIFICATION 229
19.1 Oxidation of Hydrogen, Carbon Monoxide, and Methane by Fixed Beds of Copper Oxide Pellets 229
19.2 Characterization of Aerosols by a Light-Scattering Technique 231

20. EQUIPMENT DECONTAMINATION STUDIES 232
20.1 Decontamination of Stainless Steels Baked in Helium at 500°C 232
20.2 Decontamination of Specimens Contaminated from the Gas Phase 233

21. FUEL SHIPPING STUDIES 233
21.1 Fuel Carrier Drop Tests 233
21.2 Fuel Shipping Cost Studies 234
22. CHEMICAL APPLICATIONS OF NUCLEAR EXPLOSIVES (PROJECT COACH) 235
22.1 Recovery of Isotopes from Coach Event 235
22.2 Jet Sampling and Bubble-Tapping Studies 238
23. PREPARATION OF URANIUM-232 239
24. ASSISTANCE PROGRAMS 240
24.1 Eurochemic Assistance 240
24.2 High Radiation Level Analytical Laboratory 240
24.3 Plant-Waste-System Improvements 241
24.4 Molten-Salt Converter Reactor (MSCR) Fuel-Processing Study 242
24.5 Interim Alpha Laboratory, Building 3019 243
24.6 Fuel Cycle for Large Desalination Reactors 243
24.7 Radiochemical Plant Safety Studies 247
PUBLICATIONS, SPEECHES, AND SEMINARS 252
ORGANIZATION CHART 261

1. Power Reactor Fuel Processing

Laboratory and engineering-scale development of processes for recovering fissionable and fertile material from irradiated power reactor fuels is continuing. In the past year more emphasis was placed on basic chemical studies; however, major efforts are still in progress on chemical applications, engineering development, and final small-scale hot-cell testing of the more promising fuel recovery processes.

Hot-cell demonstration of the Sulfex process, including one cycle of solvent extraction, was completed with fuel samples irradiated to 28,000 Mwd/ton. Basic chemical studies were continued on uranium and thorium carbides and begun on the dissolution of PuO_2-UO_2 pellets. The engineering-scale development of the chop-leach process was continued, with major emphasis on the leaching operation. Both chemical and engineering-scale work was done on the optimization of a U^{233} solvent extraction cleanup flowsheet for the Brookhaven National Laboratory Kilorod program described in Chap. 6. Flowsheets for recovering protactinium by both adsorption and solvent extraction of thorium-uranium fuels were developed. Chloride volatility processes were studied for use with both U-Al alloy fuels and UC-ThC impregnated graphite fuels; this work is reviewed in ORNL-3452, Suppl 1.

The extensive corrosion-test program on candidate materials of construction for aqueous and nonaqueous head-end processes under development was continued.

A considerable effort was expended on the development of a main line and one or more backup processes for the Rover fuel. This work, because of its classified nature, is described in ORNL-3452, Suppl 2 (classified).

1.1 PROCESSES FOR URANIUM AND THORIUM CARBIDE FUELS

The hydrolysis studies with various uranium and thorium carbides were continued to the point where a very good understanding of the chemistry of these reactions is now available. To be assured of high-quality material for the experiments, many samples were prepared in the Metals and Ceramics Division under very carefully controlled conditions. The program effort was also extended to provide data on feed adjustment of the hydrolysis product and on solvent extraction compatibility.

Fuel Sample Preparation

Uranium-carbon alloys used in the hydrolysis experiments were prepared by the nonconsumable arc melting of high-purity uranium metal and spectroscopic grade graphite, using tungsten electrodes.[1-3] The maximum combined carbon-to-uranium (C/U) atomic ratio that could be obtained by arc melting or arc melting followed by heat treatments between 1260 and 2000°C was 1.85, which indicates that uranium dicarbide is a nonstoichiometric compound. Alloys with a total-C/U atomic ratio of 1.91, but with a combined-C/U atomic ratio of only 1.85, were prepared; they were essentially single-phase uranium

[1] M. J. Bradley and L. M. Ferris, *Inorg. Chem.* 1, 683 (1962).

[2] M. J. Bradley and L. M. Ferris, *Hydrolysis of Uranium Carbides Between 25 and 100°C. II. As-Cast Alloys Containing 2 to 10 wt % Carbon*, paper presented at the American Chemical Society National Meeting, Los Angeles, Calif., Apr. 4, 1963.

[3] M. J. Bradley *et al.*, *The Effect of Irradiation on the Hydrolysis of Uranium Carbides. I. Preparation of Uranium Monocarbide Pellets for Irradiation*, ORNL-3403 (March 1963).

dicarbide, based on x-ray and metallographic examination. Uranium monocarbide specimens appeared to be stoichiometric – $UC_{1.0}$. Alloys which contained less than one carbon atom per uranium atom were two-phase mixtures of uranium metal and uranium monocarbide, while as-cast specimens with compositions between UC and $UC_{1.85}$ were two-phase mixtures of the mono- and dicarbides. Heating $UC_{1.5}$ for 60 hr at 1600°C produced a material that was relatively pure uranium sesquicarbide (U_2C_3) according to x-ray analysis, but microscopy showed a considerable amount of impurity phases.

Graphite electrodes are required in the arc melting of thorium carbides to avoid extensive tungsten contamination (6 wt % in thorium dicarbide). Based on chemical and x-ray analyses, thorium dicarbide appears to be nearly stoichiometric, with a formula of $ThC_{1.95}$. The metallographic examinations of this material have not been completed.

Hydrolysis of Uranium Carbides in Water

The hydrolysis of uranium carbides at temperatures between 25 and 100°C yielded complex mixtures of hydrogen and gaseous hydrocarbons and a gelatinous, hydrous, tetravalent uranium oxide. Nonvolatile waxes were also formed when the alloy contained either uranium sesqui- or dicarbide. The volume of gas evolved decreased from 138 ml (STP) per gram of carbide to 42 ml per gram of carbide as the combined-C/U atomic ratio increased from 0.39 to 1.85 (Fig. 1.1).

The hydrolysis of uranium monocarbide[1] yielded principally methane (86 vol %), some hydrogen (11 vol %), and small quantities of higher hydrocarbons. As expected, the U-UC alloys yielded 2 moles of hydrogen per mole of free metal in addition to the UC hydrolysis products (Fig. 1.2). The gaseous hydrolysis products of specimens with compositions between $UC_{0.4}$ and $UC_{1.0}$ contained all the carbon originally present in the alloy (Table 1.1).

The reaction of $UC_{1.85}$ with water[2] yielded a water-insoluble wax, a gas containing about 40 vol % hydrogen, and a complex mixture of at least 36 hydrocarbons which were distributed as follows: methane, 15 vol %; ethane, 28 vol %; propane, 1.0 vol %; butanes, 4.6 vol %; C_5- to C_8-alkanes, 1.1 vol %; ethylene, 1.6 vol %; butenes, 4.7 vol %; C_5- to C_7-alkenes, 2.0 vol %; alkynes, 0.06 vol %; and unidentified unsaturated compounds, 1.2 vol %. Of the combined carbon initially present in the $UC_{1.85}$ specimens, 37% was found in the gas phase and 27% in the wax. The remaining carbon presumably was present as water-soluble compounds whose concentrations were too low to detect by conventional analytical procedures. No water-insoluble liquid hydrocarbons were observed. The wax had an H/C ratio of about 1.2. Preliminary infrared data indicated the presence in the wax of aromatic and aliphatic double bonds, C=O, and C–O–C bonds. Temperatures between 25

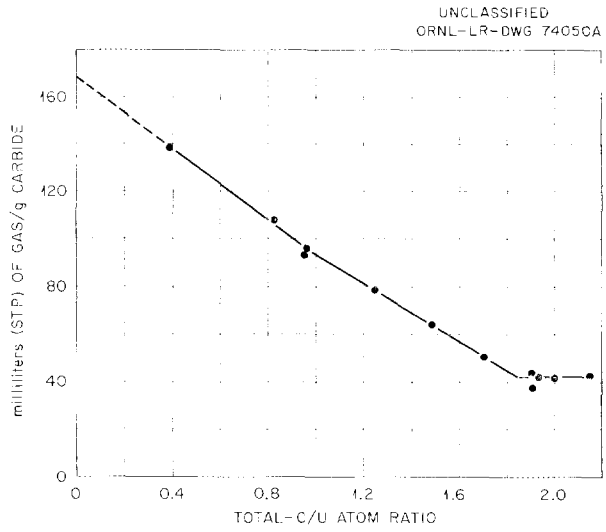

Fig. 1.1. Volume of Gas Evolved when As-Cast Uranium Carbides React with Water at 80°C.

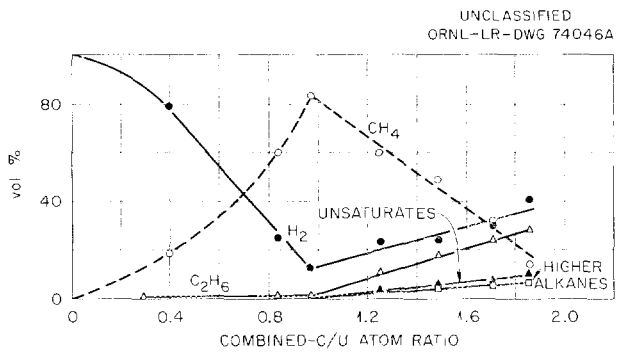

Fig. 1.2. Gaseous Products from the Reaction of As-Cast Uranium Carbides with Water at 80°C.

Table 1.1. Carbon Distribution in the Hydrolysis of Uranium and Thorium Carbides at 80°C Expressed as Percent of Combined Carbon in Alloy

Material Reacted (Combined Carbon-to-Metal Atomic Ratio)	Gaseous Products				Nonvolatile Carbon Compounds	
	CH_4	Saturated C_2- to C_8-Hydrocarbons	Unsaturated Hydrocarbons	Total Gaseous Carbon	Wax	Unaccounted
As-Cast						
$UC_{0.39}$	70	20	8.5	99		
$UC_{0.83}$	87	9	3	99		
$UC_{0.97}$	92	6.5	1.5	100		
$UC_{1.25}$	42	25	8.5	75	4.5	21
$UC_{1.48}$	24	29	11	64	11	25
$UC_{1.71}$	10.5	25	12	47	20	33
$UC_{1.85}$	4	22	11	37	27	36
$ThC_{1.01}$	83	9.5	6	98		
$ThC_{1.95}$	1	24	28	52	12	36
Heated 60 hr at 1600°C						
$UC_{1.47}$	1.5	35	16	52	11	36

and 99°C had no effect on the products of this reaction.

Hydrolysis of as-cast specimens with compositions between UC and $UC_{1.85}$ (i.e., UC-$UC_{1.85}$ mixtures) produced[2] a decrease in the methane concentration and increases in the amounts of free hydrogen, C_2- to C_8-hydrocarbons, and wax as the combined-C/U atomic ratio of the alloy was increased (Fig. 1.2 and Table 1.1). The yields of methane were considerably lower than expected from the UC concentrations in the alloys, indicating that during hydrolysis some C^{4-} units from the UC react with $(C_2)^{4-}$ units from the $UC_{1.85}$.

Heating of as-cast $UC_{1.5}$ (i.e., a UC-$UC_{1.85}$ mixture) for 60 hr at 1600°C to form uranium sesquicarbide (U_2C_3) caused a marked change in the gaseous hydrolysis products. Only 1.5% of the carbon originally present in the heat-treated alloy was found as methane compared with 24% for the as-cast specimen (Table 1.1). The heat-treated specimen yielded more saturated and unsaturated C_2- to C_8-hydrocarbons (51% of the carbon vs 40% for the as-cast specimen) and considerably more free hydrogen (0.8 atom per uranium atom vs 0.3 atom for the as-cast specimen). In both cases, 11% of the carbon was found in the wax.

Hydrolysis of Thorium Carbides in Water

The hydrolysis of thorium monocarbide was similar to that of uranium monocarbide, yielding 90 ml (STP) of gas per gram of sample; the gas consisted principally of methane (85 vol %) and hydrogen (10 vol %) (Table 1.1). On a mole basis, the amounts of the various alkanes and alkenes produced in the hydrolysis of $ThC_{1.95}$ were nearly identical with those that would be obtained by extrapolating the data for as-cast uranium carbides to a hypothetical composition of $UC_{1.95}$ (Table 1.1). In addition, thorium dicarbide yielded significant quantities of alkynes (14% of the combined carbon vs 1% from uranium dicarbide), bringing the total carbon in the gas phase to 50% for $ThC_{1.95}$ vs 35% for hypothetical $UC_{1.95}$. Thorium dicarbide yielded less wax (12% vs 27%

for uranium dicarbide) and about the same amount of organic compounds unaccounted for.

Hydrolysis of Uranium Carbides in Nitric Acid

When uranium carbides are dissolved in nitric acid, soluble organic compounds, primarily acids, are produced.[4–6] The purpose of the present work, being conducted initially with uranium monocarbide, is to determine the identities and amounts of the dissolved species under several dissolution conditions. Of particular importance is the identification of any potentially explosive components or those which might have a deleterious effect on the recovery of uranium from nitric acid solutions by solvent extraction. The results of this study are applicable both to the direct dissolution of uranium carbide reactor fuels in nitric acid and to the acid leaching of graphite-base fuels that contain carbides.

In the dissolution of uranium monocarbide (UC) in nitric acid, 20 to 40% of the carbide carbon remains in solution; the amount depends on acid concentration and reaction temperature. The rest of the carbon is volatilized, mainly as CO_2. The dissolved species were isolated by adjusting the acidity of the nitric acid solutions to 6 *N* and then removing the uranium by extraction with 20% TBP–80% Amsco solution.[4] Nitric acid was then evaporated from the uranium-free solutions at low temperatures, leaving a dark red-brown colored mixture of organic compounds that was air-dried at room temperature. These organic compounds proved to be polyfunctional, soluble only in polar solvents, and acidic. Equivalent weights were in the range of 70 to 80 g/eq (Table 1.2). The infrared spectra showed that only traces of nitro compounds were present, as expected, since the nitrogen contents of the mixtures were always less than 0.5%.

Oxalic acid and water were the major identifiable components of the acidic organic mixtures. The amount of oxalic acid decreased from 35 to about 10% as the reaction temperature was increased from 25 to 110°C (Table 1.2). This relation is to be expected since oxalic acid is oxidized to CO_2 in hot nitric acid. The number of experiments conducted thus far has been insufficient to allow evaluation of the effect of reaction time on the oxalic acid content of the mixtures. The times given in Table 1.2 are approximately those required for the complete dissolution of 50- to 200-g samples of UC. The oxalic acid was isolated by vacuum sublimation at about 100°C and was the only organic component of the mixtures that sublimed at this temperature. The water content of the mixtures varied randomly from 7 to 17%. This water was removed during the vacuum sublimation and was also titrated directly with Karl Fischer reagent.

[4] A. M. Simpson and B. A. Heath, *Products of the Reaction Uranium Monocarbide–Nitric Acid*, IG Memorandum 464(D) (June 1959).

[5] *Chem. Technol. Div. Ann. Progr. Rept. June 30, 1962*, ORNL-3314, pp 6–9.

[6] R. E. Blanco, *Quarterly Progress Report for Chemical Development Section B July–September 1962*, ORNL TM-403 (Feb. 7, 1963).

Table 1.2. Composition of the Organic Products from the Reaction of Uranium Monocarbide with Nitric Acid

Sample No.	HNO_3 Concentration (*M*)	Reaction Temperature (°C)	Dissolution Time (hr)	Analyses of Organic Species			
				C (%)	H (%)	Equivalent Wt (g/eq)	Oxalic Acid (%)
UC-16Y-2	16	25	840	30.1	2.66	74	35
UC-4Y-3	4	40	312	33.0	3.5	75	25
UC-4Y	4	105	6.5	39.1	1.5	77	8
UC-4Y-2	4	105	23	39.3	2.6	73	11
UC-16Y	16	110	24	40.9	1.8	74	

Qualitative paper chromatographic tests with ethanol-water-NH_4OH solvent[7] and partition chromatography experiments with elution from a silica gel column with chloroform-butanol solutions[8] revealed traces of benzene polycarboxylic acids in the mixtures. Preliminary data obtained thus far indicate that the benzene acids which contain up to four carboxyl groups account for less than 5% of the mixtures. Mellitic acid (benzene hexacarboxylic acid) has also been identified as a component of the mixtures; based on the weight of the insoluble ammonium mellitate salt,[9] the mixture contains about 20% mellitic acid. The remaining constituents of the mixtures appear to be higher-molecular-weight polyacids. These acids have not yet been identified, but their equivalent weights were estimated at 120 to 300 g/eq.

Preliminary experiments indicated that similar organic products are obtained from the nitric acid dissolution of uranium dicarbide ($UC_{1.85}$) and ThC.

Solvent Extraction of Uranium Carbide Fuel Solutions

The fuel solutions obtained by hydrolyzing uranium monocarbide (UC) with both water and nitric acid directly were subjected to solvent extraction tests, by use of the Purex flowsheet, to determine whether the presence of dissolved organic compounds would have any adverse effects on the flowsheet. The hydrolysis of UC with water at 80 to 100°C to produce hydrous uranium dioxide, followed by dissolution of the UO_2 in boiling nitric acid and appropriate feed adjustment, yielded a feed solution that appeared compatible with the Purex solvent extraction process. Direct dissolution of the UC in boiling nitric acid produced a solution that is much less suitable. In the current program of the hot-cell demonstration of processes for carbide fuels, head-end processes and appropriate solvent extraction flowsheets will be evaluated with fuel specimens irradiated up to 16,000 Mwd/ton.

Uranium monocarbide which contained a trace of uranium dicarbide (total carbon, 5.1 wt %) was hydrolyzed with water at an H_2O/UC mole ratio of 20 at 90°C for 4 hr, producing a thick slurry of hydrous uranium dioxide. Dissolution of the slurry in boiling 8 *M* HNO_3 was complete in 2 hr. The resulting solids-free raw-feed solution contained 350 g of uranium per liter, 4 *M* HNO_3, and trace amounts of soluble organic acids. These acids, produced from the hydrolysis of the dicarbide impurity, were found, in contacting the solution with 30% tributyl phosphate (TBP) in Adakane, to act as emulsifiers and strong complexing agents for uranyl nitrate, and therefore cannot be tolerated in the Purex system.

The organic acids were successfully degraded by oxidation to largely aliphatic compounds, possibly nitrated, that do not interfere with solvent extraction. Treatment of the raw-feed solution with either 0.02 *M* $KMnO_4$ or 0.05 *M* $Ce(NH_4)_2(NO_3)_6$ at 70°C for 3 hr was equally effective. After removal of the manganese dioxide precipitate which forms during permanganate treatment, the resulting feed solution, when tested by exhaustive extraction with 30 vol % TBP in Adakane and exhaustive stripping with 0.01 *M* HNO_3, was free of interfacial crud and exhibited normal coalescence times for the Purex system. Uranium extraction and stripping losses were each less than 0.01%. Almost identical results were obtained with feed solution treated with ceric ion. Treatment with ceric ion would be preferred in a process not requiring a feed-clarification step or not utilizing the permanganate head-end treatment for initial decontamination of fissile material from fission product ruthenium, zirconium, and niobium. A head-end flowsheet based on UC hydrolysis in water and oxidation of organic acids with $Ce(NH_4)_2(NO_3)_6$ is given in Fig. 1.3.

---

[7] A. L. Clingman and D. A. Sutton, *Fuel* **31**, 259 (1952).

[8] B. Fishwick, *J. Chem. Soc.* **1957**, 1196 (1957).

[9] B. Juettner, *J. Am. Chem. Soc.* **59**, 208 (1937).

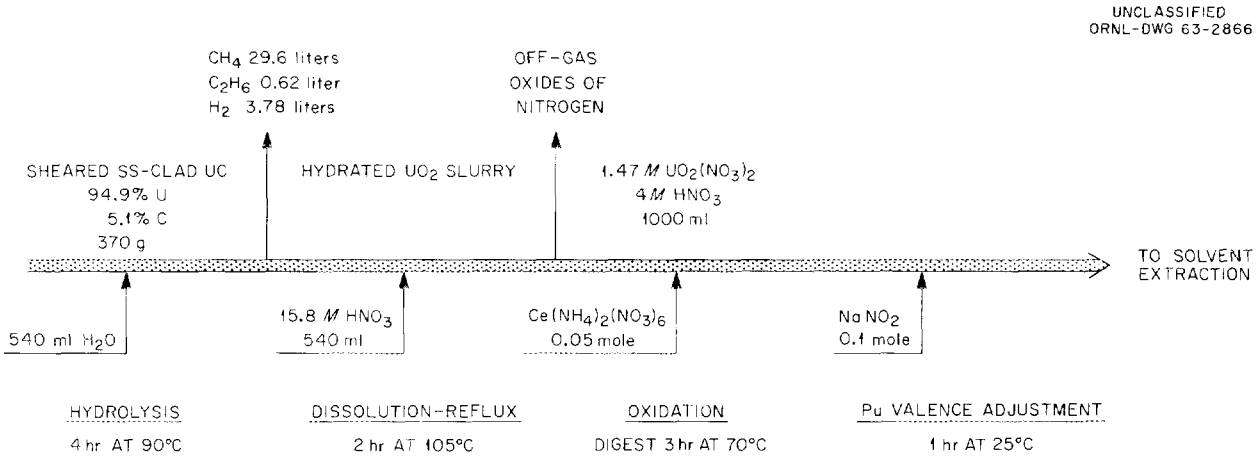

Fig. 1.3. Head-End Hydrolysis Process for Uranium Monocarbide Reactor Fuel.

1.2 HOT-CELL TESTS ON SULFEX AND ZIRFLEX PROCESSES

Chemical and engineering development of the Zirflex[10] and Sulfex chemical decladding processes for Zircaloy-2 and stainless-steel-clad UO_2 and ThO_2-UO_2 fuels was completed this year with a series of 19 Sulfex hot-cell runs with Yankee prototype fuel samples irradiated up to 28,000 Mwd/ton. The Sulfex flowsheet is given in Fig. 1.4, and a picture of the hot-cell equipment used in these runs is presented in Fig. 1.5.

In the Sulfex process, boiling 4 *M* H_2SO_4 is used to remove the stainless steel fuel cladding. The exposed uranium dioxide is then wsahed with water to remove residual sulfate and dissolved in boiling 4 *M* HNO_3 to provide a feed solution suitable for a modified Purex solvent extraction process. Similarly, washed thorium dioxide–uranium dioxide core material is dissolved in boiling 13 *M* HNO_3–0.04 *M* HF–0.1 *M* $Al(NO_3)_3$, to provide a feed for the Acid Thorex extraction process.

Nineteen Sulfex decladding runs[11–15] were conducted on type 304 or 316 stainless-steel-clad uranium dioxide pellets of 93 to 96% of theoretical density, irradiated from 1545 to 28,200 Mwd/ton. Most of the specimens were initially passive to boiling 4 *M* H_2SO_4, and contact of the cladding with iron wire was required to start the reaction. (Passivity has generally been observed with unirradiated specimens and is not thought to be an irradiation effect.) Stainless steel dissolution rates averaged 2 mg min^{-1} cm^{-2}, a value in close agreement with rates obtained with unirradiated specimens. About 5 hr was required for complete dissolution of the cladding. Soluble losses of uranium and plutonium to the decladding solution were about 0.05%, and occasionally as high as 0.3% (Table 1.3). In three runs with 6 *M* H_2SO_4 as the decladding reagent, the uranium losses were higher than those obtained with 4 *M* H_2SO_4. No significant increase in decladding losses was observed that could be attributed to irradiation effects. The decladding solutions were filtered to remove undissolved scale, uranium

[10] *Chem. Technol. Div. Ann. Progr. Rept. June 30, 1962*, ORNL-3314, pp 15–17.

[11] J. H. Goode and M. G. Baillie, *Hot-Cell Demonstration of the Zirflex and Sulfex Processes, Report No. 1*, ORNL TM-111 (Jan. 11, 1962).

[12] J. H. Goode and M. G. Baillie, *Hot-Cell Demonstration of the Zirflex and Sulfex Processes, Report No. 2*, ORNL TM-130 (Jan. 26, 1962).

[13] J. H. Goode and M. G. Baillie, *Hot-Cell Demonstration of the Zirflex and Sulfex Processes, Report No. 3*, ORNL TM-187 (May 14, 1962).

[14] J. H. Goode and M. G. Baillie, *Hot-Cell Demonstration of the Zirflex and Sulfex Processes, Report No. 4*, ORNL TM-370 (Sept. 10, 1962).

[15] J. H. Goode, M. G. Baillie, and J. W. Ullmann, *Demonstration of the Zirflex and Sulfex Decladding Processes and a Modified Purex Solvent Extraction Process Using Irradiated Zircaloy-2 and Stainless-Steel-Clad Urania Specimens*, ORNL-3404 (May 9, 1963).

dioxide fines, etc., which were returned to the dissolver prior to dissolution of the uranium dioxide core. Core dissolution in boiling 4 *M* HNO_3 was complete in about 6 hr, which is comparable to the time required to dissolve unirradiated uranium dioxide. The larger surface area presented by the fractured irradiated pellets produced a higher initial dissolution rate than did intact unirradiated pellets, but the rate decreased as the surface area was reduced.

Solvent extraction runs were conducted with the solutions produced by dissolution of the core, and the runs were made in miniature mixer-settlers simulating the first cycle of a modified Purex process. At irradiation levels from 13,100 up to 28,200 Mwd/ton, uranium extraction losses were well below 0.01%, and plutonium losses averaged 0.1%. The presence of 0.1 *M* residual sulfate in the feed had no deleterious effect on the losses.

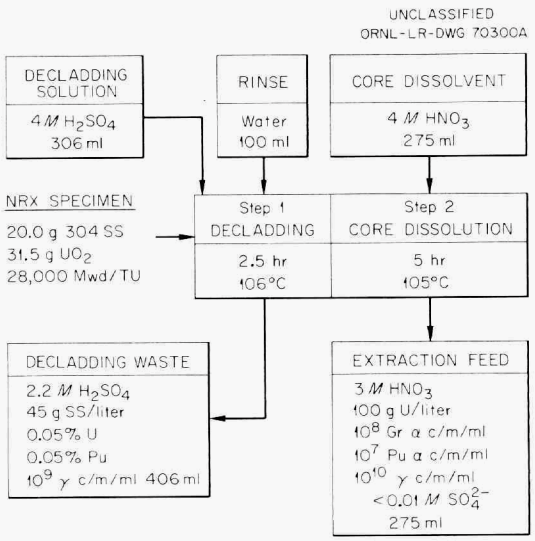

Fig. 1.4. Sulfex Head-End Treatment.

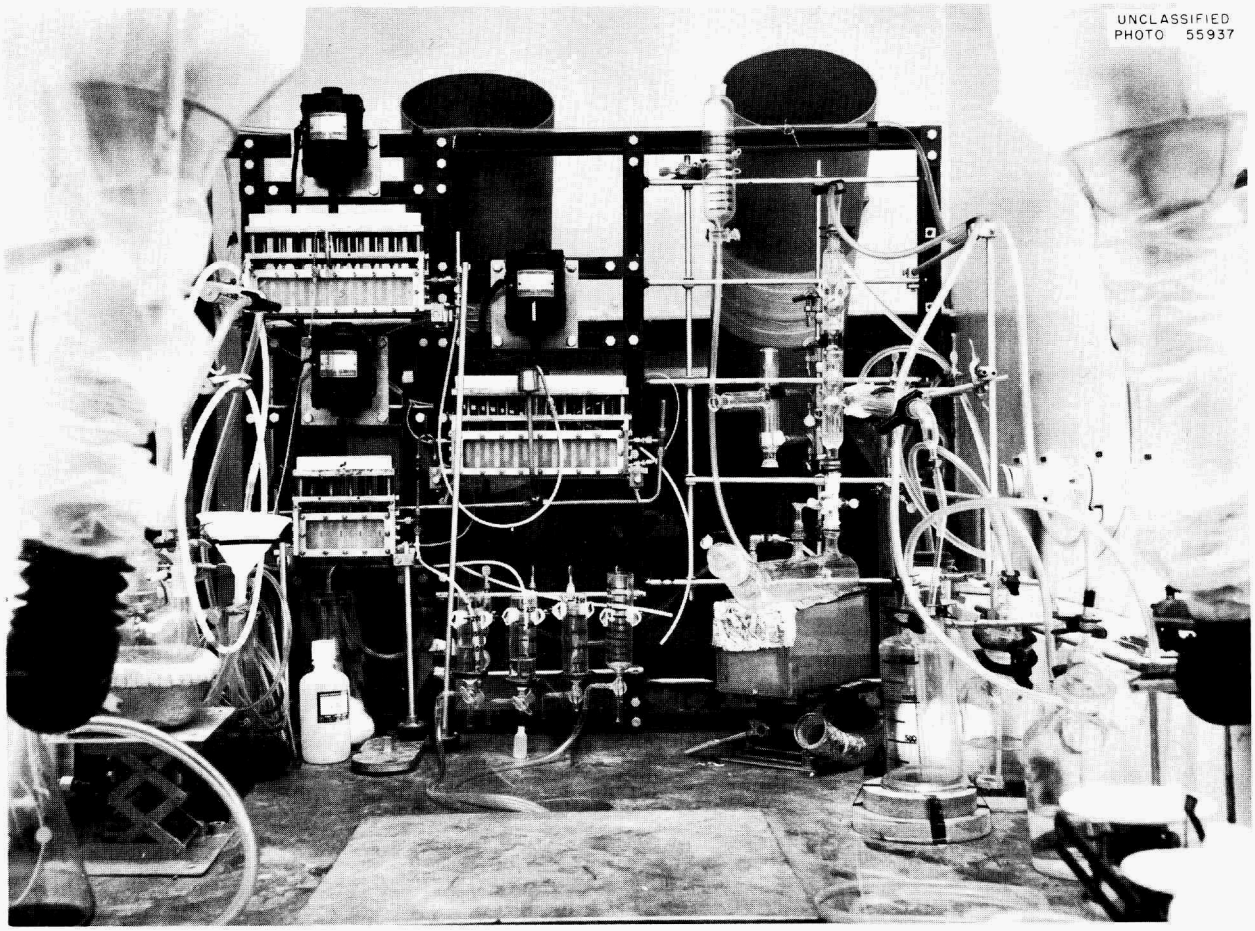

Fig. 1.5. Photograph of Sulfex Hot-Cell Equipment.

Table 1.3. Uranium and Plutonium Losses During Sulfex Decladding of Irradiated Stainless-Steel-Clad UO_2 in Boiling 4 *M* H_2SO_4

Irradiation Level (Mwd/ton)	UO_2 Density (% of Theoretical)	Pellet Condition[a]	Soluble Uranium Loss (%)	Soluble Plutonium Loss (%)
1,545	93 to 95	S	0.20	0.12
2,790[b]	93 to 95	S	0.23	0.12
7,900	93 to 95	S	0.23	0.46
7,900	93 to 95	S	0.05	0.11
7,900	93 to 95	S	0.05	0.11
9,700	93 to 95	S	0.08	0.29
9,700	93 to 95	S	0.03	0.07
12,900	93 to 95	S	0.05	0.22
12,900	93 to 95	S	0.02	0.10
20,400	93 to 95	S	0.18	0.32
20,400	93 to 95	S	0.03	0.03
22,800[b]	96	IF	0.77	0.17
22,800[b]	96	IF	0.89	0.03
22,800	96	IF	0.08	0.04
22,800	96	IF	0.06	0.04
28,200	96	IF	0.08	0.01
28,200	96	IF	0.03	0.01
28,200	96	IF	0.08	0.05
28,200	96	IF	0.05	0.00

[a]S, shattered; IF, intact or fractured.
[b]These decladding experiments conducted with boiling 6 *M* H_2SO_4.

Uranium decontamination from fission products average 3.1×10^4 and 1.3×10^4 for beta and gamma emitters respectively. Plutonium was decontaminated from beta and gamma emitters by average factors of 2.5×10^4 and 7.1×10^3 respectively. These tests show that there are no deleterious effects on uranium and plutonium losses or decontamination when feed solutions prepared from highly irradiated uranium dioxide and highly purified solvent on a once-through basis are used.

1.3 PROCESSES FOR BREEDER REACTOR FUELS

Fuel processing experiments were made with UO_2-PuO_2 fuel samples designed for fast breeder reactors and with Th-Pa^{233}-U^{233} fuel solutions obtained by dissolving fuel from thermal converter or breeder reactors. The experiments on the first type of fuel included basic dissolution studies with UO_2, PuO_2, and UO_2-PuO_2 fuel pellets, and adsorption studies of plutonium nitrate on

zirconium phosphate. Work on the thorium-U^{233} fuels included the chemical and engineering development of a U^{233} cleanup flowsheet for the BNL Kilorod program and protactinium adsorption and solvent extraction studies.

Dissolution Studies on UO_2-PuO_2 Pellets

In order to determine the dissolution characteristics of UO_2-PuO_2 fuel pellets as a function of fuel-pellet variables and manufacturing conditions, a series of basic dissolution experiments were performed with unirradiated UO_2 pellets obtained from Davison Chemical, Nuclear Materials, United Nuclear, Atomics International, and Westinghouse, with PuO_2 pellets acquired from the Nuclear Materials and Equipment Company, and with mixed UO_2-PuO_2 pellets also obtained from Nuclear Materials.

Dissolution of UO_2 Pellets. – The instantaneous dissolution rate of 90% of theoretical density UO_2 pellets in boiling 2 to 4 *N* HNO_3, or in aluminum, sodium, or lithium nitrate containing 10% HNO_3 was found to increase as the square of the nitrate concentration. For Davison pellets with a density 95% of theoretical, the dissolution rate R in mg cm^{-2} min^{-1} is defined by the equation:

$$\log R = 2.1 \log (NO_3) - 0.68 ,$$

where (NO_3) is the total nitrate molarity. In uranyl nitrate–nitric acid solutions, the rate increased as the square of the nitrate concentration due to the nitric acid, plus half the nitrate from the uranyl nitrate. The addition of hydrofluoric acid to the nitric acid was found to either increase or decrease the rate, depending upon the respective concentration of the acids; the addition of 3 moles of aluminum per mole of fluoride in the mixtures negated the effect of the fluoride. The instantaneous dissolution rates of pellets of the same theoretical density varied with the source of the pellets by as much as a factor of 50 (Fig. 1.6). Photomicrographs showed that the pellets that displayed the higher dissolution rates had larger surface areas; however, pore sizes could not be determined. No difference in dissolution rate was noted for varying oxygen-to-uranium ratio.

The time for complete dissolution of pellets with a density of 10.3 g/cm^3 was 61% of that calculated by use of the initial instantaneous dissolution rates. About 95% of the mass of the pellets dissolved in the first half of the time. The apparent surface area increased during dissolution of the first 35% of the pellet and decreased thereafter. The nitric acid consumed in dissolution ranged from 3.3 moles per mole of uranium for 14 *M* HNO_3 to 2.6 moles per mole of uranium in 6 *M* HNO_3 in the presence of air. There was no variation in dissolution time when the amount of acid used was 2 to 10 times that required. The time for complete dissolution of a Davison pellet with a density of 10.3 g/cm^3 in 14 *M* HNO_3 was about 70 min.

Dissolution of PuO_2 Pellets. – The instantaneous dissolution rate of PuO_2 pellets with a density of 10.3 g/cm^3 obtained from Nuclear Materials and Equipment Company in boiling 7, 10, and 14 *M* HNO_3 increased about as the fourth power of the nitric acid concentration. The rate R in mg cm^{-2} min^{-1} is defined by the equation:

$$\log R = 4.10 \log (HNO_3) - 6.92 ,$$

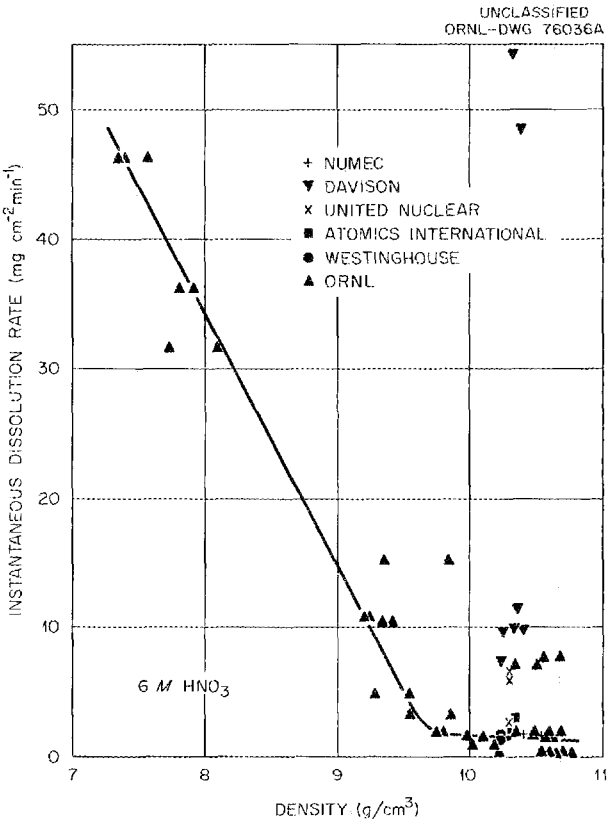

Fig. 1.6. Dissolution Rate of UO_2 Pellets from Various Sources as a Function of Pellet Density.

where (HNO_3) is the nitric acid molarity. The addition of nitrate salts to the nitric acid did not vary the dissolution rate. In mixtures of nitric acid–hydrofluoric acid, the rate increased as the 4th power of the nitric acid and the 1.41th power of the hydrofluoric acid. The dissolution rate in 14 *M* HNO_2–0.1 *M* HF was 2.1 mg min^{-1} cm^{-2}. The addition of 3 moles of aluminum per mole of fluoride to the nitric acid–hydrofluoric acid system decreased the effect of fluoride to the 0.36th power. The rate in nitric acid which contains 0.01 to 0.1 *N* $Ce(NH_4)_2(NO_3)_6$ increased as the first power of the ceric ion concentration. The addition of dichromate, ozone, or hydrogen peroxide did not vary the rate. The dissolution rate of PuO_2 in Darex dissolver solution (5 *M* HNO_3–2 *M* HCl) was only 10^{-3} mg min^{-1} cm^{-2}; therefore, there would be little plutonium loss if this reagent is used to remove the stainless steel cladding from PuO_2 seed pellets. An experiment in which a PuO_2 pellet of 90% theoretical density was dissolved in 14 *M* HNO_3–0.05 *M* HF showed that about 1% of the plutonium dissolved per hour; there was no apparent increase in the surface area during dissolution.

Dissolution of UO_2-PuO_2 Pellets. – The instantaneous dissolution rate of pellets of varying PuO_2-to-UO_2 ratio may be determined as a weighted average of the rates of PuO_2 and UO_2 alone. The dissolution rate of coprecipitated mixtures of UO_2-PuO_2 is satisfactorily expressed by the equation:

$$\log R_{mix} = \% UO_2 \times \log R_{UO_2} + \% PuO_2 \times \log R_{PuO_2} ,$$

where

R_{mix} = the instantaneous dissolution rate of the UO_2-PuO_2 in mg cm^{-2} min^{-1},

R_{UO_2} = the instantaneous dissolution rate of the pure UO_2 in mg cm^{-2} min^{-1},

R_{PuO_2} = the instantaneous dissolution rate of the pure PuO_2 in mg cm^{-2} min^{-1}.

This equation also assumes that the UO_2-PuO_2, UO_2, and PuO_2 are of the same theoretical density and that the rates for UO_2 and PuO_2 are determined or calculated for the same dissolvent. An example of the fit of calculated to experimentally determined dissolution rates for 20% PuO_2 in UO_2 (80% of theoretical density) in 10 and 14 *M* HNO_3 is shown in Fig. 1.7.

Plutonium Adsorption Studies

Initial data indicate that ionic plutonium can be removed from nitrate solutions by adsorption on zirconium phosphate or zirconium phosphate-silicate. Plutonium polymer was not adsorbed, and the extreme conditions required to convert plutonium polymer to an ionic form would probably make its recovery from waste solutions by adsorption uneconomical.

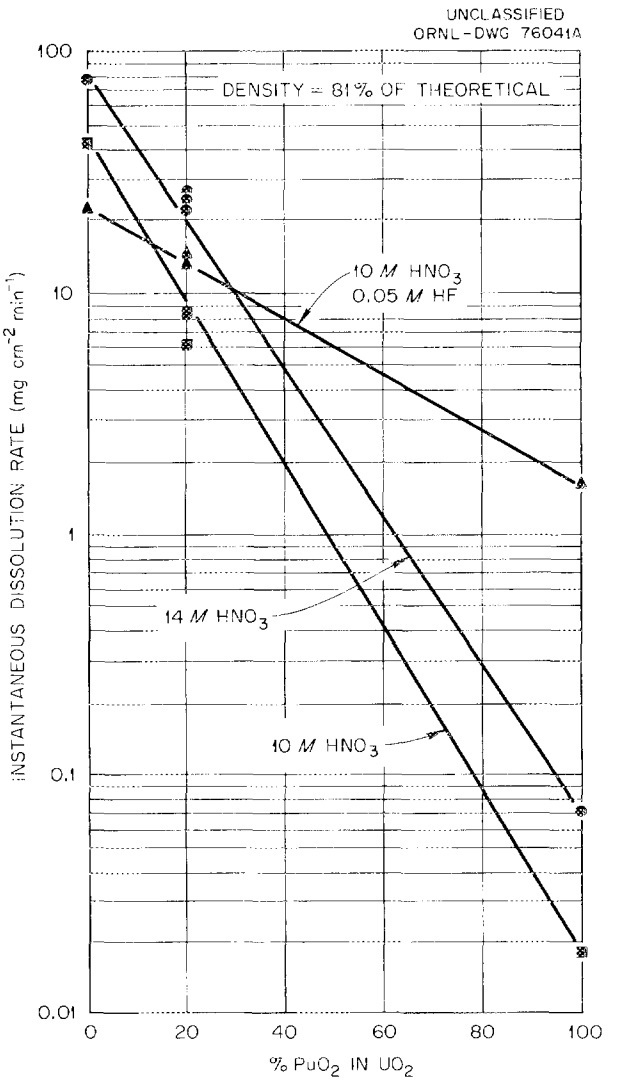

Fig. 1.7. Dissolution Rate of PuO_2-UO_2 Pellets.

In two experiments, a column 1 cm in diameter and 12 cm long, which contained 50- to 100-mesh zirconium phosphate (Bio Rad ZP-1), removed 75 and 96% of the plutonium from 50 ml of simulated nitrate waste solutions (Table 1.4), containing 4 and 1 *M* HNO_3 respectively. In both tests, 82% of the adsorbed plutonium was eluted with 100 ml of 8 *M* HNO_3. The feed solutions contained about 1.7×10^5 counts min^{-1} ml^{-1} of plutonium obtained from aged uranium-plutonium solvent extraction feed solutions. The flow rate during adsorption was about 0.75 ml/min.

Table 1.4. Concentrations of Ionic Species in Simulated Nitrate Waste Solution

Constituent	Concentration (*M*)
Al^{3+}	0.2
Fe^{3+}	0.02
Mn^{2+}	0.2
Na^{+}	2.0
PO_4^{3-}	0.02
K^{+}	0.5
HNO_3	0.1 to 4.0
Total NO_3^{-}	3.7 to 7.7

A 17-hr batch equilibration with a zirconium phosphate-silicate adsorbent (10 g per liter of solution) removed 99% of the plutonium and 86% of the gross gamma activity from a solution which contained 0.9 mg of uranium per milliliter, 0.5 *M* HNO_3, 0.01 *M* $NaNO_2$, 4.5×10^5 gross-gamma counts min^{-1} ml^{-1}, and 2.7×10^4 plutonium counts min^{-1} ml^{-1}. When the nitric acid concentration in the feed was increased to 4 *M*, the plutonium adsorption decreased to 12% and the gross gamma to 34%. The exchanger was prepared according to the method of Naumann[16] and had a ratio of ZrO_2:SiO_2:P_2O_5 of 1.0:4.8:0.7.

Zirconium phosphate, zirconium phosphate-silicate, and fired or unfired Vycor glass adsorbed less than 24% of the plutonium from simulated waste solutions which contained plutonium polymer. The waste solutions that contained 0.1 to 4 *M* HNO_3 and about 1.5 plutonium polymer counts min^{-1} ml^{-1} were contacted 30 min with 10 g of each adsorbent per liter of waste solution.

[16] D. Naumann, *Z. Chem.* 1, 247–48 (1961).

Reprocessing of Aged U^{233}

In order to minimize the shielding required for the remote fabrication of fuel elements that contain U^{233}, the uranium must be reprocessed immediately before use to remove the decay daughters of the U^{232} contaminant. This problem is of particular importance at present because of the Laboratory's commitment to produce 1000 ThO_2-$U^{233}O_2$ fuel rods for criticality experiments at Brookhaven National Laboratory. The program includes the dissolution of aged U^{233} metal returned from Los Alamos in which the U^{232} concentration was approximately 40 ppm, solvent extraction of the uranium in the Thorex Pilot Plant to remove the U^{232} daughters, preparation of ThO_2-UO_2 fuel by the sol-gel process, and, finally, the manufacture of the fuel rods by the vibratory compaction method (see Sec 6.3). In order to provide a suitable flowsheet for the first two steps, a series of experiments were made on the dissolution and subsequent solvent extraction of aged U^{233}.

Dissolution tests with uranium metal in a boiling mixture 1.5 *M* in $Th(NO_3)_4$ and 4 *M* in HNO_3 indicated a surface penetration rate of 0.001 cm/min. Assuming that the uranium to be dissolved is in the form of a 4-kg sphere, the resulting dissolution time would be 68 hr. In a boiling mixture 1.5 *M* in $Th(NO_3)_3$ and 3 *M* in HNO_3, dissolution would take 16 days.

In the solvent extraction flowsheet work, the scope of the effort included the development of a process that would provide a U^{233} decontamination factor from thorium and U^{232} decay-daughter gammas of $\geq$100 and that would be operable in the present Thorex Pilot Plant equipment. Because of the large size of the Thorex solvent extraction columns, an Interim-23 flowsheet was chosen in which stored thorium is used as the salting agent. The work included both laboratory-scale experiments and extraction-column-performance tests in 2-in.-diam columns.

In laboratory experiments, the extraction of the U^{233} with either tributyl phosphate (TBP) in *n*-dodecane (NDD), or di-sec-butylphenyl phosphonate

(DSBPP) in diethylbenzene (DEB) provided a product decontaminated from thorium and gross gamma by greater than the required factor of 100. Uranium-thorium separation was a factor of 4 higher with DSBPP, but TBP in NDD was more chemically stable than DSBPP in DEB. The extraction of uranium and thorium nitrates with DSBPP was quite similar to extraction with TBP. DSBPP and uranium combine in a mole ratio of 2. The maximum concentration of uranium in 2.5 vol % DSBPP was about 12 g/liter. DSBPP and thorium combine in a mole ratio which appears to be 3 in dilute thorium solutions; however, a deviation becomes noticeable at a thorium nitrate concentration of about 0.1 g/liter in 2.5% DSBPP, probably due to the formation of a dimer (Fig. 1.8). As a result, the uranium-thorium separation factors in systems that contain less than about 2 g of thorium per liter were about 1000 with DSBPP in DEB and only 15 with TBP in NDD. Conversely, in the presence of 100 g of thorium per liter, the separation factor was larger with TBP than with DSBPP. Therefore in the extraction section of an Interim-23 flowsheet, less thorium is extracted with TBP than with DSBPP; but in the scrub section the reverse is true. As a result of these tests, DSBPP in DEB was chosen for use in the pilot plant. The recommended flowsheet is shown in Fig. 6.3 (Chap. 6). Laboratory experiments that use these conditions, with full concentrations of U^{233}, resulted in uranium decontamination factors from thorium and gross gamma activity of 10^4 and 700 respectively. No Th^{228} or Th^{228} daughters could be detected in the product by gamma spectroscopy.

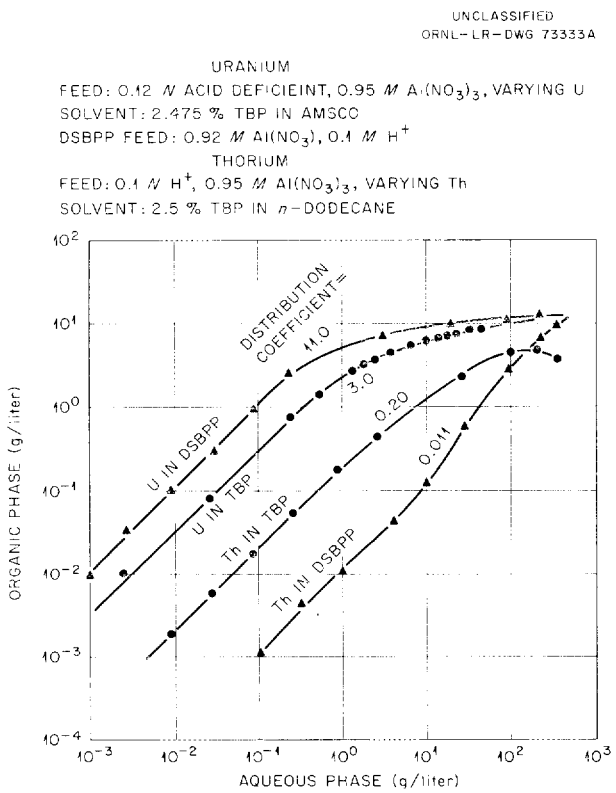

Fig. 1.8. Extraction of Uranium and Thorium from 1 *M* $Al(NO_3)_3$ with 2.5% TBP and with 2.6% DSBPP in DEB.

The use of slightly degraded solvent resulted in nearly the same decontamination factor for the product, but the uranium distribution factor in the scrub section was decreased by a factor of 2. The solvent in this experiment was stirred overnight with feed, then stripped and washed with carbonate before use. The use of aluminum as a salting agent instead of thorium did not decrease the gross gamma decontamination factor.

Engineering tests, which use the process described above, were made in 2-in.-diam stainless steel pulse columns. These tests also included stripping of uranium from the solvent product with 0.004 *M* HNO_3 and static washing of the aqueous uranium product with diethylbenzene to remove residual DSBPP.

The uranium extraction loss was only 0.03% in a 12-ft-high column with a pulse of 50 cpm and 1 in. amplitude. Decontamination of uranium from thorium was 10^4 in an 8-ft column, using the same pulse conditions. Stripping of uranium was not complete (0.6% loss) in a 12-ft column at the same pulse, but was satisfactory at a pulse frequency of 70 cpm. The static diluent-wash column, which was 7 ft high and packed with Raschig rings, was of debatable value since only about half the DSBPP was removed, leaving less than 30 ppm DSBPP in the uranium product solution. The nitrate-to-uranium ratio in the product was less than 2.3, which is within the requirement for sol-gel preparation. Most of the excess nitrate came from the 0.004 *M* HNO_3 in the strip reagent and from entrained aluminum nitrate scrub in the loaded solvent, although the samples contained less than 0.01% of the total aqueous phase.

The flow capacity (Table 1.5) of the compound extraction-scrub column was limited by flooding in the extraction section, where the total flow capacity increased from 490 to 1340 gal hr^{-1}

Table 1.5. Flow Capacity and Efficiency of 2-in.-diam Pulsed Sieve Plate Column for DSBPP Flowsheet

Flow ratio: feed 100, scrub 50, solvent 250, strip 50

Pulse Frequency[a] (cpm)	Total Flow Capacity (gal hr^{-1} ft^{-2})	HETS[b] (ft)
Uranium Extraction		
35	1340	
50	910	4.0
70	700	2.1
90	490	
50[c]	990	4.1
Uranium Stripping		
35	730	12.0
50	490	6.7
70	380	4.2
35[c]	860	12.0
50[c]	530	
70[c]	400	
Thorium Scrubbing		
50	>580	4.6
70	>410	4.1
50[c]	>650	6.2
50[d]	>530	13.0

[a]Pulse amplitude, 1 in.
[b]HETS measured at 80% of flooding capacity.
[c]Flow ratios: feed 100, scrub 40, solvent 200, strip 50.
[d]Column operated with the organic phase continuous.

ft^{-2} as the pulse frequency was decreased from 90 to 35 cpm. The flow capacity of the strip column was significantly lower at the same pulse conditions, thus limiting the total throughput of the process. The flooding capacity of the strip column increased from 380 to 730 gal hr^{-1} ft^{-2} as pulse frequency was decreased from 70 to 35 cpm. The extraction, scrubbing, and stripping efficiencies, expressed as HETS, are also given in Table 1.5.

Adsorption of Protactinium

Adsorption of Protactinium on Unfired Vycor Glass. — Earlier work[17] on protactinium adsorption on unfired Vycor glass and silica gel has been continued.[18] In current tests unfired Vycor was successfully loaded to greater than 10 mg of protactinium per gram of glass. Most of the recent experiments were performed with fuel solutions that simulated the composition anticipated from Consolidated Edison fuel irradiated to 18,000 Mwd/metric ton of thorium and cooled for 10 to 30 days. Such solutions are about 0.5 *M* in thorium, 6 to 11 *M* in HNO_3, 0.04 to 0.1 *M* in aluminum, 0.02 to 0.04 *M* in fluoride, and contain 5 g of uranium and about 50 mg of protactinium per liter. In stability tests, these solutions showed no change in protactinium concentration after storage in a plastic container for one month at room temperature or after contacting welded and unwelded type 347 stainless steel coupons for one week.

In a typical experiment such a solution that contained 54 mg of Pa^{231} per liter was passed through a column 1 cm in diameter and 8.64 cm long which contained 80- to 100-mesh unfired Vycor at a rate of 0.22 ml cm^{-2} min^{-1}. During the run, 85% of the protactinium was adsorbed, loading the column to 7.8 mg of Pa^{231} per gram of glass. The column was then washed with 11 *M* HNO_3 and eluted with 0.5 *M* oxalic acid. About 95% of the Pa^{231} that remained on the column was recovered at a concentration of 6.4 g of Pa^{231} per liter and represented a concentration factor of 120 over that in the feed solution (see raffinate and eluate concentration profile, Fig. 1.9).

The 4% initial raffinate loss was caused by the presence of an unadsorbable form of protactinium. None of the Pa^{231} was adsorbed on passage of the raffinate through a second column. The Pa^{231} product solution was reconverted to the original feed composition and then passed through a new unfired-Vycor column where 99 and 95% of the Pa^{231} was adsorbed at loadings of 2 and 5 mg of Pa^{231} per gram of glass respectively. The amount of protactinium adsorbed would probably have been higher if the feed flow rate had not been increased from 0.2 to 1.1 ml cm^{-2} min^{-1} halfway through the

[17]*Chem. Technol. Div. Ann. Progr. Rept. June 30, 1962*, ORNL-3314, pp 22–23.

[18]J. G. Moore and R. H. Rainey, *Separation of Protactinium from Thorium in Nitric Acid Solutions by Solvent Extraction with Tributyl Phosphate or by Adsorption on Pulverized Unfired Vycor Glass or Silica Gel*, paper presented at the Protactinium Chemistry Symposium, Gatlinburg, Tenn., Apr. 25–26, 1963 (to be published).

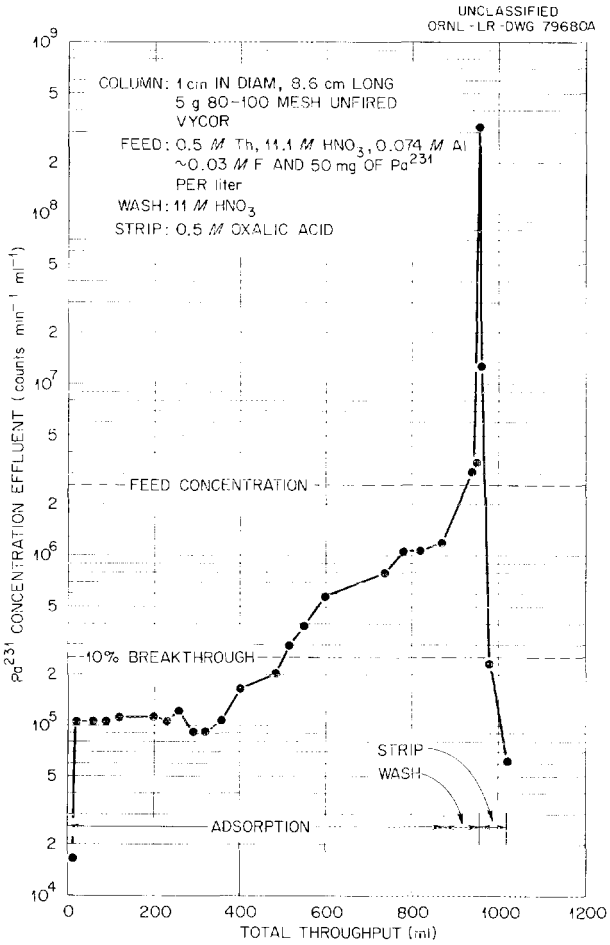

Fig. 1.9. Sorption of Protactinium with Unfired Vycor.

run. In similar experiments tartaric acid was successfully used as an elutriant, and the addition of 0.1 *M* $Al(NO_3)_3$ to the nitric acid column washes reduced the amount of Pa^{231} lost during washing. Estimates of the purity of the protactinium product were obtained in nonoptimized column experiments by use of tracer solutions of Pa^{233} and fission products. Protactinium-233 was decontaminated from thorium, uranium, ruthenium, zirconium-niobium, and total rare earths by factors of at least 6×10^3, 1.5×10^4, 4×10^3, 3, and 5.8×10^5 respectively.

Fluoride ion in the feed solution decreased the protactinium distribution coefficient and corroded the unfired Vycor adsorbent. This effect was alleviated by the addition of aluminum. The distribution coefficients of protactinium from feed solutions that contained 0.026 and 0.5 *M* thorium were decreased by factors of 1000 and about 3, respectively, when the solutions were made 0.03 to 0.04 *M* in HF. The addition of 7.5 moles of aluminum per mole of fluoride complexed the fluoride so that it exerted no influence on the distribution coefficient from the feed that contained 0.026 *M* thorium. The coefficient from the 0.5 *M* thorium solution was increased to about 70% of the value obtained with no fluoride present. Only 2.5 moles of aluminum per mole of fluoride were required to reduce the corrosion of the glass fiftyfold.

The solubility of protactinium in nitrate solutions is low but more than adequate for the processing of short-cooled Consolidated Edison fuel. For a fuel solution 0.5 *M* in thorium, the associated protactinium content would be about 70 mg of Pa^{233} per liter for ten-day cooled fuel. In stability tests, a fuel solution that contained 40 g of thorium per liter and 90 mg of Pa^{231} per liter remained free of precipitation after storage in a plastic container for one month at room temperature. Furthermore, no change in protactinium concentration was noted after contacting the solutions with both welded and unwelded type 347 stainless steel coupons for one week.

Adsorption of Protactinium on Silica Gel. – The adsorption distribution coefficient for Pa^{233} between nitric acid and laboratory-prepared silica gel is about three times the coefficient obtained with unfired Vycor and greater than five times the value obtained with commercial silica gel. Batch equilibrations with tracer Pa^{233} and 10 g/liter of 20- to 40-mesh adsorbent showed maximal adsorption coefficients of 825 and 975 at 6 and 10 *M* HNO_3 for laboratory-prepared silica gel. The maximum coefficient obtained with unfired Vycor was about 325 for 8 *M* HNO_3 and about 175 for commercial silica gel and 9 *M* HNO_3. Preliminary column runs indicated that the capacity of the laboratory-prepared silica gel is greater than 3 mg/g and is higher than that of the commercial material.

Solvent Extraction Studies

Solvent extraction studies were also made on the combining ratio of thorium and TBP, the extraction of uranium from acid-deficient or acid aluminum nitrate, and the extraction of uranium from nitric-hydrofluoric acid mixtures.

Combining Ratio of Thorium and TBP. – The combining ratio of TBP to thorium was redetermined for systems 0.5, 1.0, and 2.0 *M* in $Al(NO_3)_3$ or 6 *M* in NH_4NO_3 in 0.1 *N* HNO_3 and 0.2 to 16% TBP in *n*-dodecane. The average ratio was 3.15 when the solvent contained less than 1% TBP, but the extrapolation of the ratios calculated from more than 1% TBP indicate a ratio of about 4.

Extraction of Uranium from Acid-Deficient or Acid Aluminum Nitrate. – It was determined that the uranium distribution coefficient (DC) between dilute TBP in *n*-dodecane and aluminum nitrate which is at least 0.1 *N* acid deficient can be expressed solely as a function of the pH of the aqueous solution and when so expressed is independent of the aluminum nitrate concentration. At a given TBP concentration, the logarithm of the DC is inversely proportional to the square of the pH of the solution. The log $DC/(NO_3)^2$ is also inversely proportional to the first power of the pH of the solution. When the distribution coefficient is not expressed as a function of the pH of the solution, the distribution coefficient is a function of aluminum content, acidity, and TBP concentration. If the aqueous phase is 0.2 to 1.5 *M* in $Al(NO_3)_3$ and 0.1 *N* in HNO_3, and contains 0.5 g of uranium per liter, and if the organic phase consists of 2.5% DSBPP in DEB, the DC = $3.5\ (Al)^{3.2}$.

Extraction of Uranium from Nitric–Hydrofluoric Acid Mixtures. – The uranium distribution coefficient for the system HF–HNO_3–30% TBP increases as the 1.8th power of the nitric acid concentration when the fluoride concentration is held constant. The coefficient decreases with about the 1.6th power of the fluoride concentration when nitrate is constant. Over the range 0.5 to 4 *M* HF, the uranium distribution coefficient remains constant at 1 when the nitrate-to-fluoride ratio is 3.5.

1.4 CORROSION STUDIES

An extensive corrosion test program is being carried on in order to evaluate potential materials of construction for the various processes being developed for the processing of power reactor fuels. This work was done in the Reactor Chemistry Division by P. D. Newmann, L. Rice, and D. N. Hess. Materials for both aqueous and nonaqueous processes are being evaluated.

Corrosion studies during the past year included the evaluation of materials of construction for various chloride volatility methods (see Sec 1.6, ORNL-3452, Suppl. 1) and for graphite-fuel processing schemes which involve decomposition by burning followed by leaching with nitric acid. Studies of the corrosion of Corronel 230 in HNO_3-HF and of titanium in HNO_3-HBF_4-Cr(VI) were completed. In addition, corrosion studies on borosilicate Raschig rings, used as fixed neutron poison in large tanks, were made by the Chemical Technology Division.

Aqueous Process Corrosion Tests

One method of decomposing uncoated particle UO_2-graphite fuels and leaching the uranium from the residue is to use fuming (~20 to 23 *M*) nitric acid. Exposure of types 347 and 309SCb stainless steel in boiling 22 to 23 *M* HNO_3 which contains 1 to 2 *M* HF for times of 96 to 312 hr resulted in overall corrosion rates of 0.2 to 0.5 mil/month, with no serious localized attack. The additional presence of graphite and UO_2^{2+}, however, increased the corrosion rate of the type 309SCb to 15 to 20 mils/month and of type 347 to 4.6 mils/month. Pitting attack was observed on type 309SCb but not on type 347. Type 304L stainless steel exposed in the solution that contained graphite and UO_2^{2+} corroded at 3.9 mils/month in a 48-hr exposure test; there was no noticeable localized attack.

Aluminum alloys, 1100 and 6061, were also evaluated in these solutions. Both grades were almost completely inert in all mixtures of nitric-hydrofluoric acid with and without added graphite and UO_2^{2+} so long as the nitric acid concentration was $\geq$15.6 *M* and the HF concentration was $\geq$1 *M*. In 14 *M* HNO_3 plus 1 to 5 *M* HF, aluminum was inert for the first 24 hr of exposure time, but began to undergo accelerated attack in both solution and vapor phases for longer exposure times. At room temperature, corrosion began immediately; rates in 14 *M* HNO_3 that contained 1 and 5 *M* HF were about 65 and 290 mils/month, respectively, for 24 hr exposure. At nitric acid concentrations below about 12 *M* the rates became catastrophic at all temperatures.

Further tests on welded Corronel 230 in boiling hydrofluoric and nitric-hydrofluoric acid solutions to complete the work on this alloy reported last

year[19] showed it to be superior to other alloys tested, though rates were still unsatisfactorily high in the presence of high concentrations of uncomplexed fluoride, and the welded areas suffered preferential attack. Overall rates for 72-hr exposures were 78, 3.8, and 113 mils/month for boiling 1.0 *M* HF, 4.0 *M* HNO_3–0.3 *M* HF, and 10 *M* HNO_3–1.0 *M* HF respectively.

Cyclic oxidation–5 *M* HNO_3 dissolution tests were also made with Corronel 230. In these tests the alloy was exposed during the oxidation of graphite-UO_2, contaminated with NO_3^- and F^-, in oxygen at 800°C for 5 hr, followed by digestion of the resulting ash in 5 *M* HNO_3 for 2.5 hr. Under these conditions, Corronel 230 showed superior resistance. Rates for exposure to 22 cycles were about 0.1 mil/month for duplicate specimens. Rates for type 304L stainless steel, Carpenter 20 stainless steel, Haynes 25, and Nichrome V under the same conditions were 19.6 mils/month (9 cycles), 7.5 mils/month (18 cycles), 9 mils/month (17 cycles), and 8 mils/month (9 cycles) respectively. Intergranular attack was observed on all materials tested except Corronel 230.

Work done last year on the development of a suitable process for the continuous dissolution of U-Zr alloy fuel in titanium equipment was continued. Continuous dissolution of 2% U–Zr alloy fuel in a laboratory-scale titanium dissolver was demonstrated[20] by use of refluxing 3 *M* HNO_3–1.2 *M* HF–0.4 *M* HBF_4–0.6 *M* Cr(III)–0.4 *M* Cr(VI)–0.46 *M* Zr as the dissolvent. The zirconium dissolution rate was 8 to 16 mg cm^{-2} min^{-1}, and the titanium corrosion rate was ~1 mil/month. The dissolvent stability characteristics were in good agreement with predictions made from earlier batch studies.[21] The dissolution rate was controlled by adding the dissolvent at the rate needed to maintain a preselected potential as measured by a gold-vs-calomel electrode in the product effluent.

Other corrosion tests in which titanium was exposed in a boiling mixture of 0.465 *M* Zr^{4+}, 2.8 *M* F^-, 0.4 *M* B, 0.6 *M* Cr(III), and 0.4 *M* Cr(VI) solutions indicated that the protective film formed by treatment of the titanium in the dissolver solution followed by air drying was slowly removed during subsequent exposure. Renewal of the dissolver solution caused a temporary renewal of the film (detected by weight gain of the specimens). Overall corrosion rates for a 168-hr exposure in which there was one solution renewal varied from 4.14 to 7.75 mils/month, based on defilmed weights after exposure. Some deep pits were formed beginning after about 70 hr of exposure.

Corrosion of Pyrex Raschig-Ring Fixed Neutron Poison

Large-capacity tanks can be used for the critically safe storage of fissile solutions if the tanks are filled with a fixed neutron poison in the form of randomly packed rings of borosilicate glass. Despite its lower boron content, Pyrex glass, which contains 4.0 wt % boron, has been recommended because of its superior corrosion resistance over borosilicate glass which contains 5.8% boron. After annealing, the 5.8% boron glass lost about 0.1% by weight in 650 hr of exposure to 2 *N* and 6 *N* HNO_3 at 65°C. These same glass rings after being tempered by two methods were even more fragile after corrosion testing than the annealed rings, although their weight loss was slightly less. Tempering, therefore, did not overcome the undesirable fragility of corroded high-boron rings.

When 0.6% of gadolinium was added to Pyrex glass to raise its neutron poison effect to that of 5.8% boron glass, its corrosion resistance was not altered. Nitric acid leaching at 65°C produced no observable change in weight or appearance. Cost of such rings would probably be three to four times that of Pyrex glass which contains 5.8% boron.

In other tests there was essentially no boron leached from glass Raschig rings which contained 3.79% boron after five weeks of contact with solutions simulating solvent extraction product. Simulated product solutions that contained 100 g of uranium and 5 g of thorium per liter, 0.1 *M* in HNO_3, and solutions that contained 100 g of uranium and 0.2 g of thorium per liter, 0.4 *M* in HNO_3, were alternately heated to 65°C and cooled to room temperature in plastic containers. After five weeks there was no significant difference in the concentration of boron between solutions that contacted Raschig rings and the control solutions.

---

[19] *Chem. Technol. Div. Ann. Progr. Rept. June 30, 1962*, ORNL-3314, p 20.

[20] T. A. Gens, *Continuous Dissolution of Zirconium Reactor Fuels in Titanium Equipment: Laboratory Demonstration*, ORNL TM-395 (Jan. 23, 1963).

[21] *Chem. Technol. Div. Ann. Progr. Rept. June 30, 1962*, ORNL-3314, p 17.

1.5 MECHANICAL PROCESSING

During the past year, two approaches to the mechanical processing of power reactor fuels were studied. The major effort was expended on further development of the chop-leach process for multitubed metal-clad oxide fuels. Studies were also made on alternative methods for the mechanical decladding of stainless-steel-clad NaK-bonded fuels and the safe destruction of the released NaK bonding.

Chop-Leach Process Development

In the chop-leach process,[22] multitube stainless-steel- and Zircaloy-clad UO_2 and ThO_2-UO_2 fuel elements are sheared to ½- to 1½-in. lengths and the oxide fuel leached in acid to produce aqueous fuel solutions for subsequent solvent extraction by TBP. The UO_2 fuels are dissolved in 6 to 8 *M* HNO_3, and the solution is then extracted by the Purex process for uranium and plutonium recovery. The ThO_2-UO_2 fuels are dissolved in 13 *M* HNO_3–0.04 *M* NaF–0.1 *M* $Al(NO_3)_3$; the resulting solution is then adjusted and processed by the Thorex, Acid Thorex, or Interim-23 process for U^{235}-U^{233} recovery, and thorium recovery or discard. The leached cladding is stored as a radioactive metal waste.

The shakedown tests for the 250-ton shear were completed, for the most part, last year; this year, the effort was devoted primarily to bench-scale leaching tests with unirradiated prototype fuel and evaluation of the semicontinuous, inclined, rotary leacher. Hot-cell tests of the shear-leach process were also made on both stainless-steel- and Zircaloy-clad UO_2 fuel pins irradiated to $\geq$16,000 Mwd/ton to evaluate sheared fuel-particle distributions at high radiation levels.

Shear Evaluation Program. – Work done this year with the 250-ton shear included the careful measurement of sheared core and cladding particle-size distributions, evaluation of the life of the shear blade, further refinement of the shearing equipment to improve its operability, and the commencement of the testing of tools and methods for remote maintenance of the shear.

Further shear tests were performed with the 250-ton fuel shear on unirradiated, 36-tube, stainless-steel-clad, ORNL Mark I prototype fuel assemblies which contain porcelain, UO_2, and UO_2-ThO_2 cores. Particle-size data were obtained on sheared sections (½⁻, 1⁻, and 1½-in. lengths) to determine the amount and size of the core and jacket particles produced by shearing with the stepped blade of the shear.

The percentage of core material, *P*, that was dislodged from various sized pellets and sheared lengths (Fig. 1.10) can be expressed by the following relation:

$$P_{[UO_2(0.420\text{-in.-OD} \times 0.625\text{-in.-long pellets})]} = 35.7\,(L)^{-1.25},$$

$$P_{[UO_2\text{-}ThO_2(0.420\text{-in.-OD} \times 0.625\text{-in.-long pellets})]} = 39\,(L)^{-1.215},$$

$$P_{[\text{Porcelain}\,(0.420\text{-in.-OD} \times 3.0\text{-in.-long pellets})]} = 23.5\,(L)^{-1.388},$$

$$P_{[\text{Porcelain}\,(0.295\text{-in.-OD} \times 3.0\text{-in.-long pellets})]} = 15\,(L)^{-1.323},$$

where *L* is the sheared length in inches.

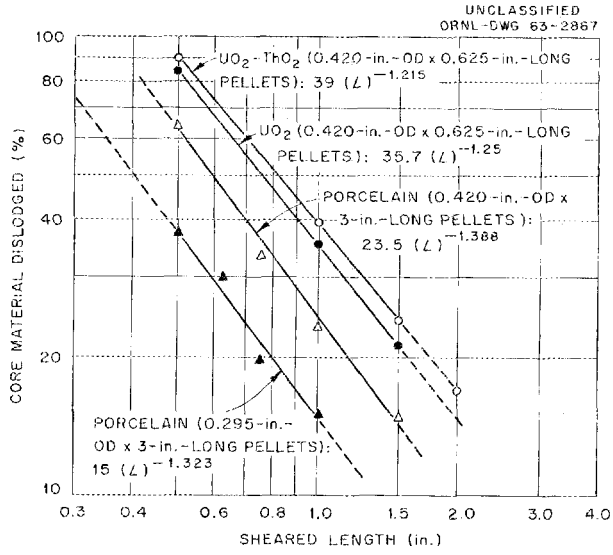

Fig. 1.10. Percentage of Core Material Dislodged vs Length of Cut.

[22] *Chem. Technol. Div. Ann. Progr. Rept. June 30, 1962*, ORNL-3314, pp 33–39.

A comparison of data on all materials sheared, including the horsepower required and the amount of cladding and core dislodged, is presented in Table 1.6.

Embrittlement of stainless steel jackets by reactor irradiation was simulated by carburizing the jackets of a porcelain-filled ORNL Mark I element to 2.6% carbon. Shearing tests with this assembly showed that more core and clad were dislodged from the carburized assembly than from an uncarburized ductile assembly (Table 1.6).

The life of the stepped, moving blade of the 250-ton shear was estimated at 10,000 cuts on a 36-tube ORNL Mark I assembly filled with porcelain, UO_2, or UO_2-ThO_2. A Squarekeen No. 3 blade supplied by the American Shear and Knife Company (composition, 0.53 wt % C, 0.31 Mn, 0.87 Si, 5.00 Cr, 1.28 Mo, 1.23 W, 0.01 S, and 0.02 P and a Rockwell C hardness of 54 to 56) was chipped on the main tooth after 5982 cuts on porcelain-filled ORNL Mark I prototype assemblies and was replaced. Based on this single measurement, one side of a blade could be used to make 5000 cuts, then turned to the other side for an additional 5000 cuts. The blade cost $250.

During the past year certain important shear components and design features were evaluated and changes made, where necessary, to achieve improved operation.

The gibs, which are long wedge-shaped devices to permit remote adjustment of the clearance between the fixed and moving blades, were difficult to remove, reinsert, and adjust. Additional development work will be required to attain the operability desired.

In general, the inner and outer gags, which clamp and restrain a fuel assembly while it is being sheared, operate satisfactorily. With the present system, a fuel assembly can be sheared to a terminal length of 1½ in. An inner gag capable of holding a 1-in.-long terminal piece is being developed.

The shear feed mechanism, which feeds a fuel assembly into the shear until a predetermined length has been sheared into the desired number of sections, operates satisfactorily. The fuel assembly stop, which is located inside the shear and sets the length of cut, was damaged on two occasions, requiring removal of the ram of the shear to effect repairs. Since it would be very difficult and perhaps impossible to make such repairs remotely in a hot cell, an internal fuel assembly stop is not recommended. Instead, it should be made a part of the external feed mechanism, where repairs could be made if needed.

Power is delivered to the shear by means of a chromium-plated stainless steel connecting rod (8 in. in diameter and 8 ft long) attached to a hydraulic piston. The present method of preventing the slow transfer of dust to the outside of the shear by this rod has not been adequate. Two packing glands now used on the connecting rod, which also serve as bearing surfaces, leak fuel particles. This design is being improved by altering the glands to serve exclusively as sealing devices.

Lubrication of the wearing surfaces of the shear by a Molykote dispersion in water appears adequate; however, it is suspected that lubrication is not needed.

The interior of the shear and discharge throat is easily cleaned of UO_2 particles by 43 spray nozzles installed in the shear (30 gal of wash water). Steady-state holdup of particulate UO_2 is about 1570 g during shearing; this powder is quantitatively removed by water washing.

An investigation of remote dismantling and maintenance of the shear has been started. Extraction tools were designed and fabricated for remote removal and installation of the gags, fixed-blade holder, and the moving blade in the shear housing, using the feed-mechanism hydraulic cylinders as the moving force. Three hydraulic cylinders were installed for remotely opening and closing the top and front doors on the shear housing and for removing and reinserting the ram in the shear housing. Lifting devices for the ram rack and ram that can be handled remotely were designed and fabricated.

Bench-Scale Leaching Studies. – An estimate of the total acid contact time required in the inclined rotary leacher to attain 99.9% UO_2 dissolution from sheared, stainless-steel-clad UO_2 fuel was attempted. A series of single-stage runs were made in which the time required for a specified uranium recovery was found to increase linearly with the reciprocal of the nitrate molarity (Fig. 1.11). Further experiments disclosed important differences between the bench-scale equipment and the inclined rotary leacher. It was concluded that the difference in configuration between the bench-scale dissolver and the full-scale rotary leacher was an important one and that the bench-scale data could only be applied to a large-scale dissolver that has

Table 1.6. Shearing Force and Size Distribution of Core and Cladding Particles from UO_2, UO_2-ThO_2, and Porcelain-Filled ORNL Mark I Fuel Assemblies Sheared into 0.5-, 1.0-, and 1.5-in. Lengths

ORNL Mark I assembly: square bundle (3.625 × 3.625 in.) of 36 type 304 stainless steel tubes $\frac{1}{2}$ in. OD × 72 in. long × 35 mil wall, assembled with $\frac{3}{8}$-in.-OD × 1-in.-long, type 304 stainless steel spacer ferrules, Kanigen or Nicro brazed at ~12-in. spacing; tubes filled with 0.420-in.-OD × 3-in.-long porcelain sections or 0.420-in.-OD × 0.625-in.-long UO_2, UO_2-ThO_2 pellets;
Shear: ORNL 250-ton, horizontally actuated stepped blade operated at 1.22 in./sec and 4.5 cuts/min

Core Material	Sheared Length (in.)	Maximum Shear Force Required		Core Material (wt %)[a]				Cladding, Stainless Steel (wt %)[b]			
				Dislodged			Retained in Clad	Dislodged			Retained
		(tons)	(hp)	<44 μ	44 to 1000 μ	1000 to 9520 μ		<44 μ	44 to 1000 μ	1000 to 9520 μ	
Porcelain (carburized, 2.6% max., clad)	0.5			9.0	51.0	28.5	11.5	0.044	0.336	18.12	81.5
	1.0	25		3.5	24.0	16.0	56.5	0.016	0.115	5.20	94.7
	1.5			1.8	10.3	4.2	83.7	0.007	0.114	5.18	94.7
Porcelain (ductile clad)	0.5			8.4	45.6	22.4	23.4	0.027	0.238	2.68	97.0
	1.0	68.5	26.5	3.2	15.8	4.0	77.0	0.030	0.108	2.50	97.4
	1.5			2.1	7.9	2.2	87.8	0.009	0.050	0.77	99.2
UO_2 (ductile clad)	0.5	58.0[c]	22.5	22.4	57.6	4.5	15.5	0.023	0.357	7.52	92.1
	1.0	63.7[c]	23.3	7.4	25.6	2.4	64.6	0.007	0.120	2.10	97.8
	1.5			4.5	12.0	1.2	82.3	0.003	0.055	2.60	97.3
UO_2-ThO_2 (ductile clad)	0.5	49.8	19.75	23.8	60.2	6.7	9.3	0.020	0.215	3.74	96.0
	1.0	62.3	23.25	9.3	26.7	3.1	61.9	0.006	0.050	1.57	98.4

[a] $\text{Wt \%} = \dfrac{\text{weight (g) of core material dislodged}}{\text{weight (g) of core material in fuel assembly}} \times 100.$

[b] $\text{Wt \%} = \dfrac{\text{weight (g) of stainless steel dislodged}}{\text{weight (g) of stainless steel in fuel assembly}} \times 100.$

[c] 70 to 75 tons through section containing ferrules.

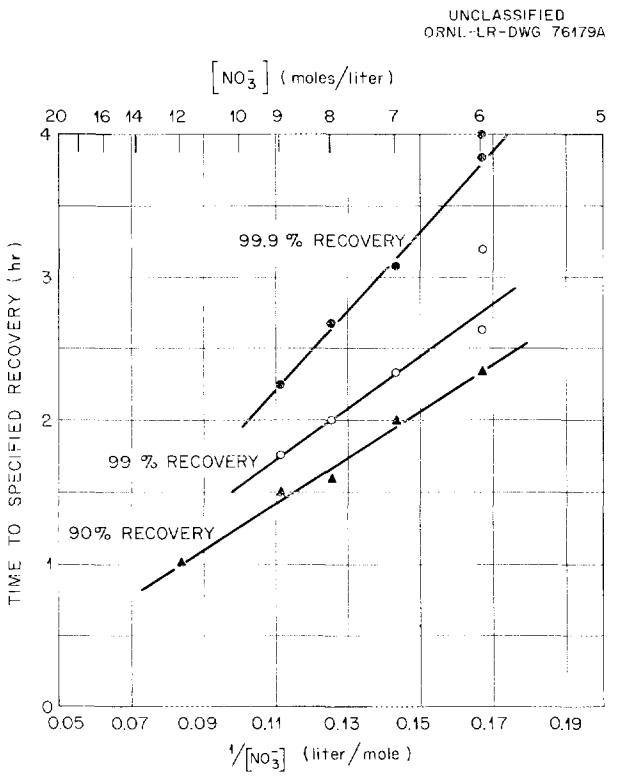

Fig. 1.11. Uranium Recovery Time vs the Reciprocal of Nitrate Concentration.

the same proportions and same acid flow pattern through the vessel.

Bench-scale leaching tests with ½-in. sheared lengths of stainless-steel-clad ThO_2-UO_2 in recirculating 12 *M* HNO_3–0.04 *M* NaF–0.10 *M* $Al(NO_3)_3$ disclosed that the leaching rate was very strongly dependent on the degree of contact between the oxide fines and the dissolvent. The leaching rate of ThO_2-UO_2 from sheared fuel in a simulated flight of the inclined rotary leacher was unacceptably low because the fines formed an impervious layer which was not penetrated by the dissolvent that flowed over the top of the bed. After changing the equipment to a recirculating batch leacher with provisions for suspending ThO_2-UO_2 fines that escaped the perforated fuel basket, a greatly improved leaching rate was obtained. In this test, dissolution was 98.5% complete in about 8 hr (Fig. 1.12), thorium concentration in the product was about 135 g/liter, and the final nitric acid concentration was about 9 *M*. Preliminary experiments indicated that if the dissolvent is added in two half-batches, the dissolution time is shorter than that for a single addition of the entire batch. With this procedure, 99.8% dissolution was obtained in 8 hr.

Engineering-Scale Leaching Studies. – The engineering-scale mechanical shear and leach complex, which consists of a 250-ton horizontally actuated shear, inclined rotary drum conveyor, and inclined rotary drum leacher, was successfully operated as a totally integrated system in which UO_2 was leached from ½-, 1-, and 1½-in. sheared sections of ORNL Mark I unirradiated prototype fuel assemblies. A series of 15 shear-leach dissolution runs were made in the inclined rotary leacher on sheared sections of aluminum- and stainless-steel-clad UO_2; hot counterflowing nitric acid was used. In these runs, a batch of sheared fuel was fed to the first flight in the leacher once an hour. Each batch contained about 24.4 g-moles of UO_2 and was obtained by shearing approximately 8 in. of a UO_2-filled ORNL Mark I assembly or UO_2-filled aluminum tubing. Each batch had a volume of

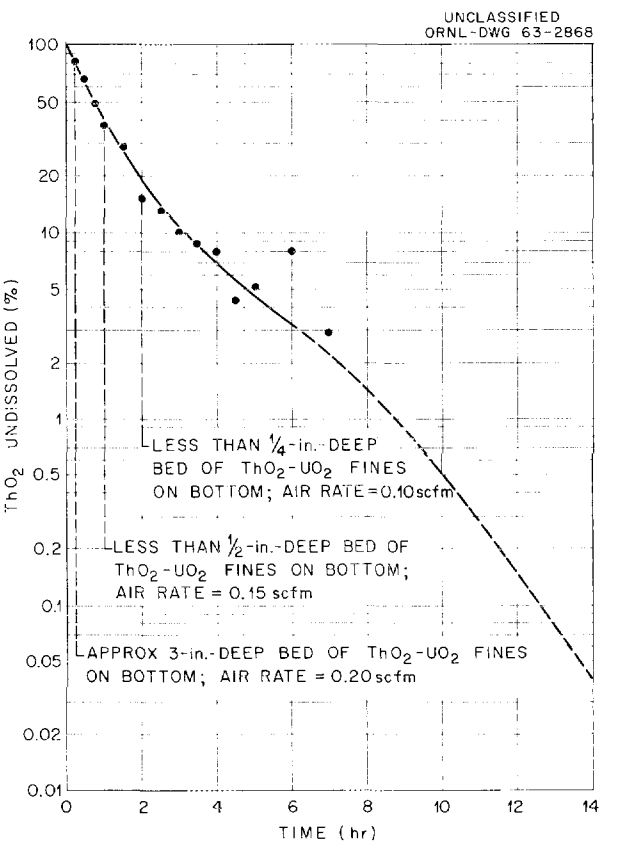

Fig. 1.12. Percentage of ThO_2 Undissolved vs Time.

about 2.25 liters. The fuel was contacted continuously and countercurrently with 7 to 8 *M* HNO_3 at approximately 95°C at HNO_3/UO_2 mole ratios of 4 to 6. The leacher, which contained four dissolution flights, was rotated once an hour, resulting in a leaching time of 4 hr; the leached rings were then washed countercurrently with water in four wash flights.

Two initial leaching runs were made in which UO_2 was leached from sections of aluminum-clad UO_2. The loose tubes were held and sheared as easily as a brazed assembly. It was necessary, however, to discontinue using UO_2-filled aluminum tubing because of the excessive dissolution of the aluminum (approximately 30%) by the $UO_2(NO_3)_2$ solution.

Four shear-leach runs were made using eight or nine batches of sheared UO_2-filled ORNL Mark I assemblies in each run. In these runs 7 *M* HNO_3 at 95°C was fed to the leacher at a feed rate equivalent to 4 g-moles of HNO_3 per g-mole of UO_2. A typical plot of instantaneous and hourly composite uranium and H^+ leacher-product concentrations as a function of dissolution time and material balance during the apparent steady-state portion of the run are presented in Fig. 1.13. A leaching flowsheet is given in Fig. 1.14. The product attained an apparent steady-state composition of 500 to 525 g of uranium per liter and 1.4 to 1.8*M* H^+ after 5 to 6 hr. However, even though an apparent steady state had been attained with respect to the product composition, the hourly uranium output was less than the input, resulting in an accumulation of undissolved uranium in the leacher (Fig. 1.13). The undissolved UO_2 accumulation rate after the sixth hour was approximately 2 g-moles/hr for the ½-in. sections, and 1.5 to 1.6 g-moles/hr for the 1- and 1½-in. sections.

The uranium buildup is not completely understood; however, it probably can be attributed to the large quantity of dislodged UO_2 fines. The fines caked, drastically reducing the area available to the leach acid. In all runs, the leached and washed clad discharged from the washing section had been leached clean of UO_2 as determined by visual observations. A nitric acid leacher cleanout was required after each run in order to recover all the uranium that had been charged during the run.

A run was made to determine the effect of adding quarter batches of 1-in. fuel sections to the leacher every 15 min while continuing to rotate the leacher once each hour. This reduced the amount of UO_2 fines charged to the leacher at each addition but also reduced the residence time for three-quarters

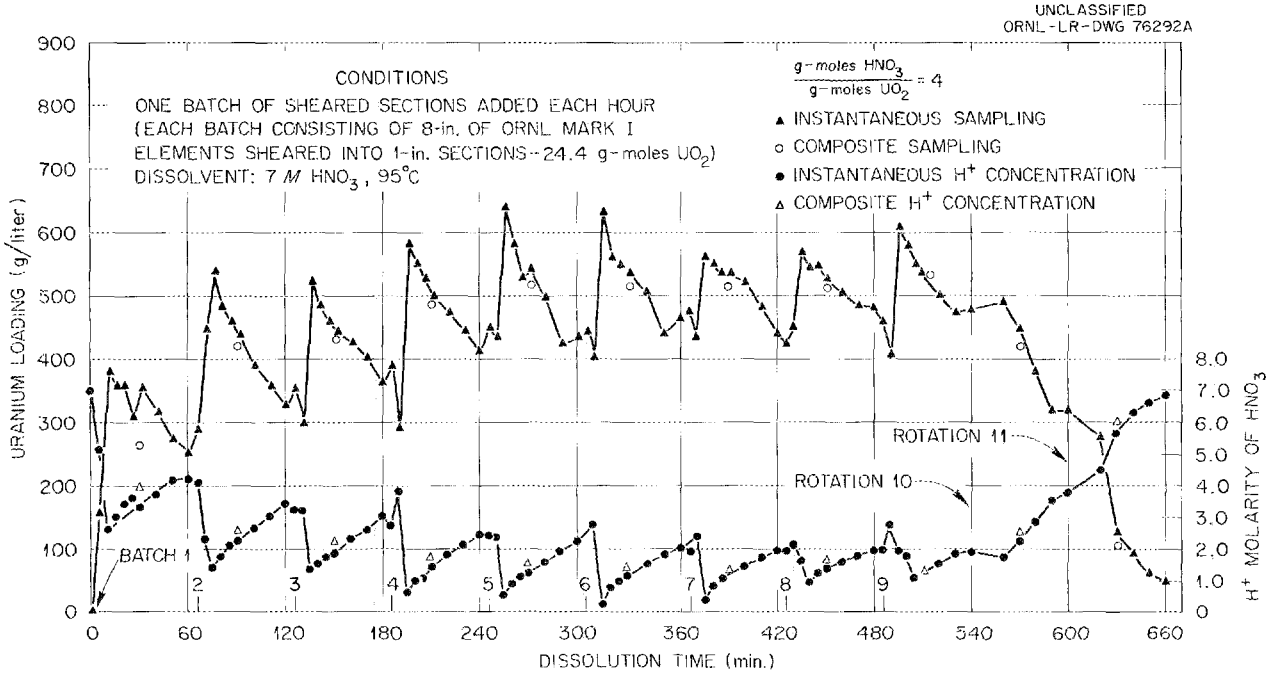

Fig. 1.13. Instantaneous and Composite Uranium Loading as a Function of Dissolution Time.

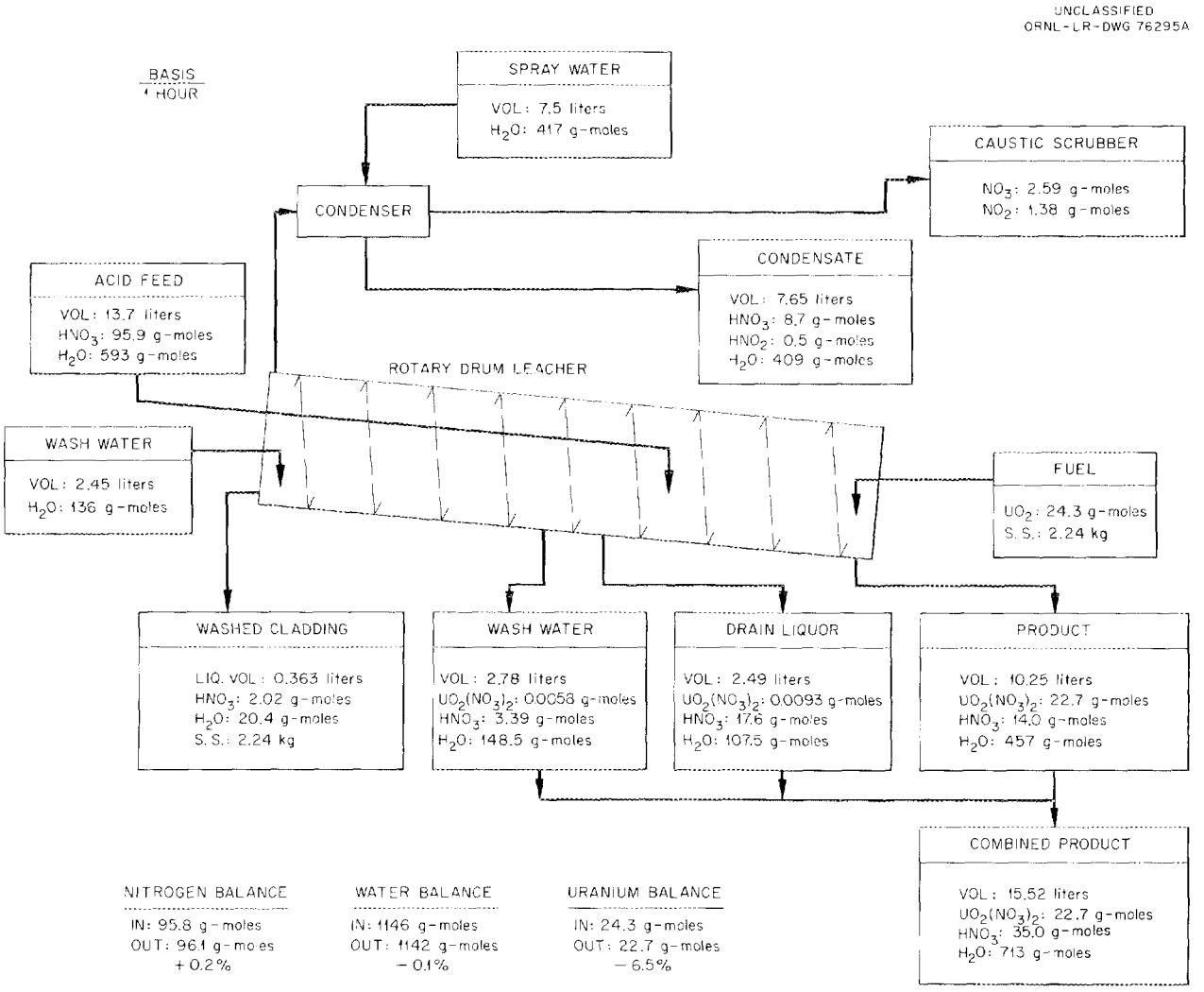

Fig. 1.14. Material Balance Flowsheet for Shear-Leach Process.

of the material added to the first flight. The uranium accumulation rate of 1.5 g-moles UO_2/hr after the sixth hour was approximately the same as that obtained by adding a full batch of 1-in. sections each hour (Fig. 1.15) (1.6 g-moles UO_2/hr); however, the total accumulation after the ninth hour approached that for ½-in. sections (35 g-moles of UO_2, compared with 37 g-moles). Apparently, the beneficial effect of smaller batch additions was more than offset by the decreased residence time.

Three additional shear-leach runs were made to investigate the effect on uranium holdup of varying the dissolvent concentration and/or flow rate. One run each was made in which the UO_2 was leached from nine batches of 1-in. sheared unirradiated fuel with 7, 7.5, and 8 *M* HNO_3 at 95°C. In these runs the HNO_3-to-UO_2 mole ratios were 6.1, 4.3, and 5.9 respectively. There was a continuing uranium buildup in the leacher run with 7.5 *M* HNO_3 at a mole ratio of 4.3, resulting in an inventory of about 28 g-moles at the end of the ninth hour. However, with both 8 *M* HNO_3 at a mole ratio of 5.9, and with 7 *M* HNO_3 at a mole ratio of 6.1, there was uranium buildup for 2 to 3 hr, after which the hourly output at apparent steady state exceeded the hourly input. With 8 *M* HNO_3 there was a 26.69 g-mole output and a 25.03 g-mole input, and with 7 *M* HNO_3 a 27.2 g-mole output and a 24.47 g-mole input. Obviously the output cannot

The shearing of stainless-steel-clad UO_2 irradiated to 16,000 Mwd/ton produced less fines than did tests with unirradiated specimens. There was almost no difference in the size distribution of small particles from either the irradiated or the unirradiated specimens; however, the sheared, irradiated, stainless-steel-clad specimens were characterized by clean-cut edges, in contrast to the torn edges of the more ductile, unirradiated material (Figs. 1.17 and 1.18). The size distribution for material in all four tests is given in Table 1.8.

Decladding of NaK-Bonded Fuels

The adequacy and versatility of the three mechanical decladding methods evaluated last year[24] during the decladding of the irradiated NaK-bonded fuel from Core 1 of the Sodium Reactor Experiment (SRE) is relatively inefficient although workable. The program to investigate other methods of reliably decladding liquid-metal-bonded fuels was continued, and several new concepts were tested and evaluated in preliminary investigations of disassembly methods and of decladding, collecting, and disposing of the liquid-metal bonding agent.

Two not entirely satisfactory methods of disassembly tried were friction sawing after casting the fuel rod ends in fusible metal or epoxy resins, and mill sawing of fuel rod ends from a mechanically clamped assembly.

[24] *Chem. Technol. Div. Ann. Progr. Rept. June 30, 1962*, ORNL-3314, pp 27–32.

Table 1.7. Stainless Steel Fines Dissolved when Using 7 *M* HNO_3 to Leach Sheared Sections of UO_2-Filled ORNL Mark I Unirradiated Prototype Fuel Assemblies

Sheared Length (in.)	Run Time (hr)	Stainless Steel (g)	Amount Dissolved (wt %)
½	11	14.8	0.076
1	11	13.7	0.066
1½	10	10.1	0.052

UNCLASSIFIED
PHOTO 59664

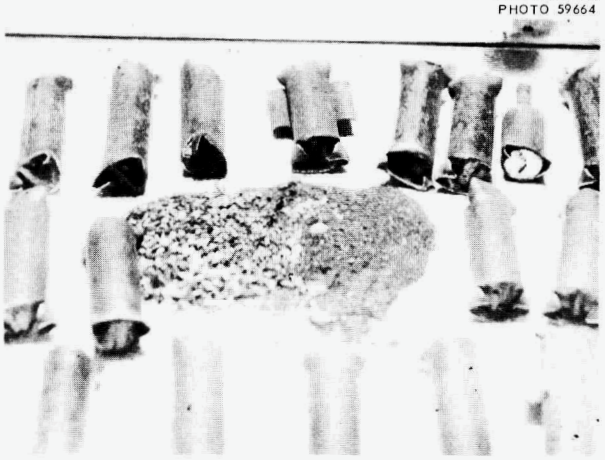

Fig. 1.17. Unirradiated Stainless-Steel-Clad UO_2 Sheared into 1-in. Lengths by Miniature Shear.

UNCLASSIFIED
PHOTO 59665

Fig. 1.18. Sheared 16,000 Mwd/ton Stainless-Steel-Clad UO_2

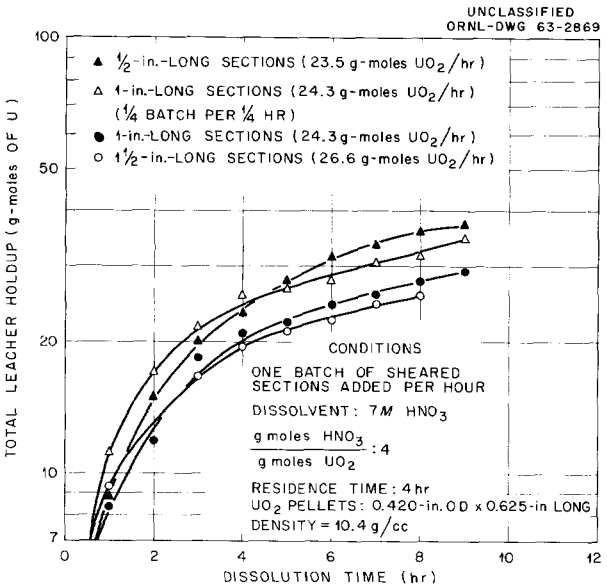

Fig. 1.15. Uranium Inventory in Rotary Leacher vs Dissolution Time.

continuously exceed the input, and had the runs been of longer duration the chosen conditions would probably have resulted in a long-term cyclic operation of the leacher. These data indicate that dissolvent flow rate and HNO_3/UO_2 mole ratio are important variables in the operation of the rotary drum leacher. The largest acid volumetric flow rate, achieved with 7 *M* HNO_3, resulted in the smallest total uranium buildup (5.5 g-moles UO_2) (Fig. 1.16).

In each of the 15 runs a negligible amount of stainless steel fines were dissolved. Typical data are presented in Table 1.7. Almost no undissolved stainless steel or UO_2 particles were carried out of the leacher; after each run, less than 1 g of solids was observed in the settler in the product line.

Following the series of 15 shear-leach runs, the conveyor-feeder and leacher were easily decontaminated from alpha activity by flooding with hot nitric acid. The two equipment pieces were then removed from cell 1A-B. New solids-inlet lines, 6 in. in diameter and with a 60° slope, were installed in each unit to eliminate plugging of the inlet lines with the sheared fuel.

Hot-Cell Shearing Tests. – Particle-size distribution of uranium dioxide fines was investigated in hot-cell equipment by means of a small hydraulic shear to cut stainless-steel-clad and Zircaloy-2-clad UO_2 fuel specimens irradiated to 16,000 and 17,000 Mwd/ton, respectively.[23] Such highly irradiated specimens are known to undergo core fracture due to thermal cycling during irradiation. Unirradiated specimens were also sheared with the same equipment for comparison.

The same quantity and size distribution of uranium dioxide particles were produced by shearing unirradiated Zircaloy-2-clad UO_2 and similar specimens irradiated to 17,000 Mwd/ton. One-inch cuts on the irradiated fuel resulted in UO_2 particles of which 6% were smaller than 2000 μ, whereas, ½-in. cuts produced UO_2 particles of which 14% were less than this particle size. The production of UO_2 particles less than 149 μ in diameter was threefold greater with ½-in. cuts than with 1-in. cuts.

[23] R. E. Blanco, *Quarterly Progress Report for Chemical Development Section B*, ORNL TM-403 (Feb. 7, 1963).

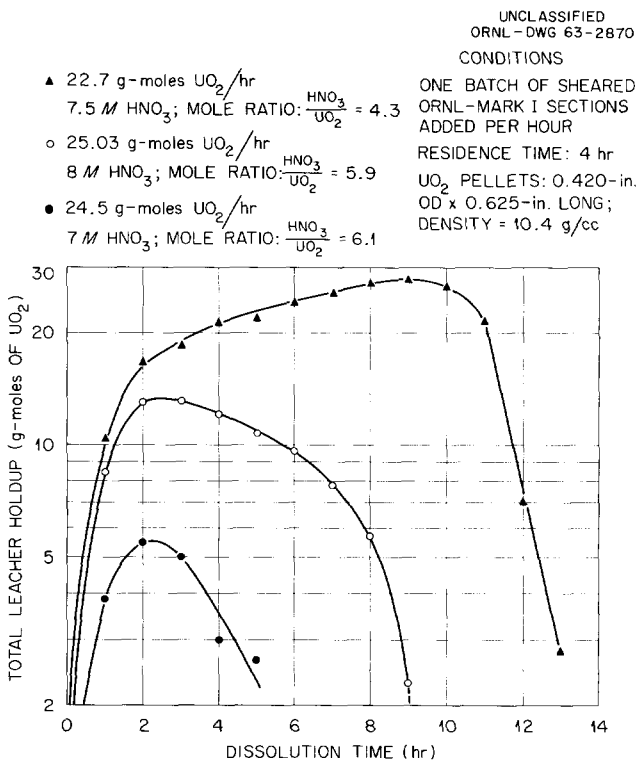

Fig. 1.16. Uranium Inventory in Rotary Leacher vs Dissolution Time.

Table 1.8. Particle-Size Distribution of UO_2 from Shearing of Unirradiated and Highly Irradiated Zircaloy-2- and Stainless-Steel-Clad UO_2 Fuel Specimens

Size of Opening in Sieve (μ)	Amount of UO_2 Retained by Sieves (%)			
	Unirradiated SS-Clad Fuel[a] (1-in. cuts)	16,000 Mwd/ton SS-Clad Fuel (1-in. cuts)	17,000 Mwd/ton Zr-2-Clad Fuel (1-in. cuts)	17,000 Mwd/ton Zr-2-Clad Fuel ($\frac{1}{2}$-in. cuts)
2000	92.5	95.9	93.9	85.9
840	0.9	0.3	0.5	2.2
590	1.1	0.6	0.8	2.4
420	0.9			
297	0.6	0.9	2.2	2.3
149	1.6	1.3	1.3	2.8
149[b]	2.5	1.0	1.3	4.3

[a]Similar results obtained with Zircaloy-2-clad fuel.
[b]Percentage of UO_2 passed by this sieve size.

Partial removal of jacketing by shearing to release or expose the sodium or NaK bond was investigated. An orbital shearing device with a rotary shearing motion was designed, built, tested, and found promising. A two-stage progressive shear die set for use as an auxiliary on the 250-ton shear was also designed and built to test further the feasibility of shearing and splitting sodium- or NaK-bonded fuel rods in short pieces to aid in sodium or NaK removal. A successful experimental test run with this single die set was made.

A study of swaging as a method for dejacketing stainless-steel-jacketed, sodium- and NaK-bonded metallic fuel is being made under a subcontract with the Torrington Company. To simulate irradidiated fuel, jackets were soft-soldered and hard-soldered to metal rods and furnished to the subcontractor for testing and evaluation. Preliminary tests were encouraging.

Equipment was also designed and built to evaluate the shearing of NaK-bonded fuel in a steam atmosphere and the disposal of the released sodium or NaK by dispersion in oil, followed by spraying the dispersion into a tank and contacting it with water under a blanket of inert gas.

1.6 CHLORIDE VOLATILITY PROCESS DEVELOPMENT

This section is reported in ORNL-3452, suppl 1.

1.7 ROVER FUEL PROCESSING DEVELOPMENT

This section is reported in ORNL-3452, suppl 2 (classified).

2. Fluoride Volatility Processing

Volatility processes are being developed at several Commission laboratories in order to provide an alternative to conventional aqueous processes for recovering uranium from spent nuclear fuels. The basic concept of all volatility techniques involves the conversion of uranium to a volatile compound such as uranium hexafluoride as the principal method of separating it from fission products. The processing of zirconium-uranium fuels is currently of primary interest at ORNL, although the enriched uranium was recovered from the homogeneous molten-salt reactor fuel, $NaF-ZrF_4-UF_4$, in 1957–58. In the current ORNL zirconium-uranium process, fuel elements are dissolved in 37.5-37.5-25.0 mole % $NaF-LiF-ZrF_4$ at 650–500°C, and the UF_4 is converted to volatile UF_6 with elemental fluorine at 500°C. An NaF sorption-desorption cycle provides further separation of volatile fission product fluorides from the UF_6. Passing the UF_6 through a bed of MgF_2 and collection by cold trapping are the final steps in the process.

The molten-salt fluoride-volatility process has several inherent advantages over conventional aqueous processes, including the following: (1) Solid, highly concentrated waste is produced without further treatment. (2) Fewer process steps are required. (3) It may have the ability to cope with certain refractory fuels not amenable to aqueous processes.

The molten-salt process for zirconium-uranium fuels has been studied here on both long- and short-decayed fuel on a laboratory scale and in the Volatility Pilot Plant in a series of 11 non-uranium-bearing runs, in 12 runs with nonirradiated fuel elements containing enriched uranium, and in 6 runs in which the enriched uranium was recovered from fully irradiated fuel elements decayed 5.4 to 6.5 yr. The pilot plant was shut down 30 weeks for decontamination and modifications to the equipment. Since then, it has been tested with three nonradioactive runs. One run each was then made with fully irradiated zirconium-uranium alloy fuel decayed 13 and 6 months, respectively. Plans for future operation of the pilot plant call for more runs with zirconium-uranium alloy fuel decayed less than one year and the processing of longer-decayed fuel as required for extended operability studies. Then enriched uranium from the residue from the EBR-1, Core 2 meltdown will be recovered as a demonstration that uranium can be recovered from a mixture containing relatively low percentages of stainless steel. Further pilot-plant efforts will then be devoted to demonstrating a molten-salt fluoride-volatility flowsheet for recovering uranium from aluminum-uranium alloys and from refractory oxide fuels such as those containing BeO, ThO_2, and ZrO_2. Progress on development of a process for aluminum-uranium alloy fuels is reported in Sec 2.6, ORNL-3452, suppl 1.

The processing of low-enrichment fuels appears to be amenable to the molten-salt fluoride-volatility process if suitable methods can be developed for separating the plutonium, presumably as PuF_6. Laboratory studies indicate that plutonium can be fluorinated from the molten salt after most of the UF_6 has been evolved. The method favored here for separating UF_6 and PuF_6 is by a sorption-desorption step, using beds of CaF_2 and NaF in series. The PuF_6 is sorbed on the CaF_2, while only UF_6 is sorbed on the NaF bed. The principal improvement needed in this area is reduction in the time required to remove the PuF_6 from the molten salt.

Other process development and refinement activities in progress are: (1) the development of specific chemical process flowsheets for the aforementioned reactor fuels; (2) determination on an engineering scale of the feasibility of using a single vessel for both the hydrofluorination (dissolution) step and the fluorination step; (3) investigation of the kinetics of sorption and desorption of UF_6, PuF_6, and other volatile fluorides on solid sorbents such as NaF, CaF_2, and MgF_2; (4) better understanding the oxidation and reduction reactions in fused salt systems; (5) a study of the kinetics of UF_6 and PuF_6 volatilization; (6) the formulation of a molten-salt system having a higher solvent capacity than the present system for common structural materials of fuel elements (jointly with the Reactor Chemistry Division); (7) the cosponsoring of the development of instruments for continuously measuring hydrogen in the presence of HF and for measuring UF_6 in the presence of fluorine; and (8) methods of decontamination of equipment. In addition to Chemical Technology Division laboratory- and engineering-scale studies of the corrosion problems inherent in the process, Battelle Memorial Institute, under subcontract, determines

the relative corrosivity of the constituents specified in new flowsheets and modifications, studies the corrosion that has occurred in experimental volatility equipment at ORNL, and evaluates and/or develops new materials of construction for the process. The Metals and Ceramics Division has assisted in corrosion studies.

2.1 PROCESSING OF URANIUM-ZIRCONIUM ALLOY FUEL

Laboratory Studies of the Decontamination of Equipment

After the series of runs in which long-decayed zirconium-uranium alloy fuel was processed, the Volatility Pilot Plant was shut down for equipment decontamination and revision. Laboratory studies were the basis for nickel and INOR-8 equipment decontamination procedures used in the Volatility Pilot Plant.

Basically, a degree of controlled corrosion by aqueous decontaminating solutions was found necessary to decontaminate nickel or nickel alloys exposed to radioactive fused salts at ~500°C or higher. More corrosion is necessary for nickel than INOR-8 since intergranular corrosion in the first case allows contamination of the base metal to a greater depth. The laboratory work generally confirmed previously reported work[1] showing that a number of operational steps are desirable in decontaminating fused-salt equipment, for example, (1) flushing with nonradioactive salt, (2) removing residual salt with boiling ammonium oxalate solution, (3) using a controlled corrodent solution, and (4) using a complexing solution to remove back-adsorbed activity. Laboratory results indicate that use of the fourth step could be avoided if a spray operation is carried out for the third step, that is, where the activity liberated from the metal is carried off by the corrodent solution instead of being allowed to back-adsorb on the surface.

The laboratory work was conducted on metal specimens dissected from the INOR-8 dissolver vessel and the nickel fluorination vessel used in laboratory process-evaluation tests.[2] All the specimens had a radiation level of about 100 to 200 mr/hr at 8 in. distance, with the source of the activity being about 75% Ru^{106} and 25% Sb^{125}. Small amounts of Nb^{95} and Zr^{95} were also present. Presumably the large amount of ruthenium was due to its diffusion into the base metal at the elevated process temperatures employed.

The high susceptibility of nickel to corrosion in aqueous media at a pH of less than 3 is markedly different from INOR-8, an alloy relatively resistant to aqueous acidic solutions. However, numerous tests demonstrated that the use of corrodent solutions on INOR-8 was necessary to obtain significant decontamination. Alkali solutions containing organic acids (tartaric, oxalic) and H_2O_2 removed some activity since these solutions are mildly corrosive, but their effectiveness was much greater when used after an acid corrodent solution. For example, a decontamination factor (DF) of 30 was obtained for nickel when using six cycles of alternating treatment with a corrodent solution [0.03 *M* $Al(NO_3)_3$] and a complexing solution (2% KOH–2% potassium tartrate–2% H_2O_2).

Corrosion tests, carried out in conjunction with activity measurements, established that suitably controlled corrosion of nickel is achieved most easily using 0.01 to 0.1 *M* $Al(NO_3)_3$ solutions. Nickel corrosion rates of 0.05 to 0.5 mil/hr were obtained in batch tests at reflux. However, these are instantaneous rates; in practice the rates are generally lower due to consumption of acid in the dissolution process. The addition of nitric acid to the original solution was recommended as a correction for acid consumption in pilot-plant usage.

Steam spray tests with corrodent solutions on both nickel and INOR-8 specimens gave the most consistent results (Fig. 2.1). Such treatment avoids the use of complexing solutions since the uncovered activity is immediately washed away instead of being back-adsorbed on the metal surface. The data presented show a decontamination factor of about 100 for both metals, with a total corrosion of 0.15 and 6.6 mils for the INOR-8 and nickel, respectively. The spray corrosion rates shown in Fig. 2.1 are higher than those given above. A high $Al(NO_3)_3$ concentration of 0.9 *M* was required for INOR-8; an alternative solution is

[1] R. L. Jolley *et al.*, *Equipment Decontamination Methods for the Fused Salt–Fluoride Volatility Process*, ORNL-2550 (Aug. 19, 1958).

[2] G. I. Cathers, R. L. Jolley, and E. C. Moncrief, *Laboratory-Scale Demonstration of the Fused Salt Volatility Process*, ORNL TM-80 (Dec. 6, 1961).

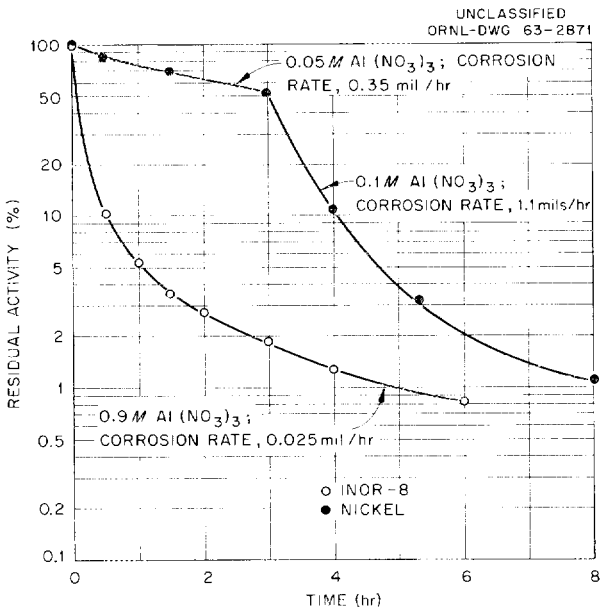

Fig. 2.1. Decontamination of INOR-8 and Nickel Specimens from Process Equipment with Steam-Sprayed Solutions.

simply 0.1 M HNO_3 with some Al^{3+} present to complex any F^- that may be present.

Decontamination of Pilot-Plant Equipment

Decontamination of Volatility Pilot Plant cell equipment was carried out following a six-run series on 5- to 6.5-yr-decayed zirconium-uranium alloy. The decontamination solutions (Table 2.1) were pumped through the equipment in several different paths so that both static and circulating conditions existed. On occasion, the top half of the fluorinator (FV-100, Fig. 2.2) or hydrofluorinator (FV-1000, Fig. 2.2) was empty; however, the bottom of these vessels always contained solution during each cycle of the decontamination.

Four principal solution cycles were used during the decontamination: (1) a molten-fluoride-salt flush, (2) an ammonium oxalate wash, (3) an aluminum nitrate–nitric acid dissolution, and (4) a caustic-peroxide-tartrate treatment. The salt flush reduced equipment activity by dilution, while the

Table 2.1. Decontamination Program for Volatility Pilot Plant Equipment

Number of Cycles	Solution	Concentration	Temperature (°C)	Time[a] (hours per cycle)	Remarks
1	Salt from simulated fuel dissolution (run T-11)	37.5-37.5-25.0 to 27.5-27.5-45.0 mole % NaF-LiF-ZrF_4	Normal operating (650–500)	~100	Normal operating conditions plus salt melt-down from dissolver walls
1	Waste salt from run TU-12	27.5-27.5-45.0 mole % NaF-LiF-ZrF_4	650–500	25–30	Normal operating temperature plus melt-down
6	Ammonium oxalate	0.35 M	50–95	40–120	Solutions both circulating and static; fluoborate added to first cycle as nuclear poison
3	$Al(NO_3)_3$-HNO_3	0.03-0.10 to 0.10-0.01 M	50–95	50–80	Solutions both circulating and static
2	$NaOH$–H_2O_2–sodium tartrate	5-1-1 to 5-2-2 wt %	Ambient	10–20	Solutions circulating
13	Water[b]		Ambient and 50–95	4–55	Solutions circulating and static

[a]By a rough estimate, the upper half of the fluorinator was empty 50% of the time; solutions were probably circulating only 75% of the time in the fluorinator bottom and about 85% of the time in the hydrofluorinator lower section.

[b]Water rinses normally followed each "soak" with the three solutions listed immediately above the last one in the column under "Solution."

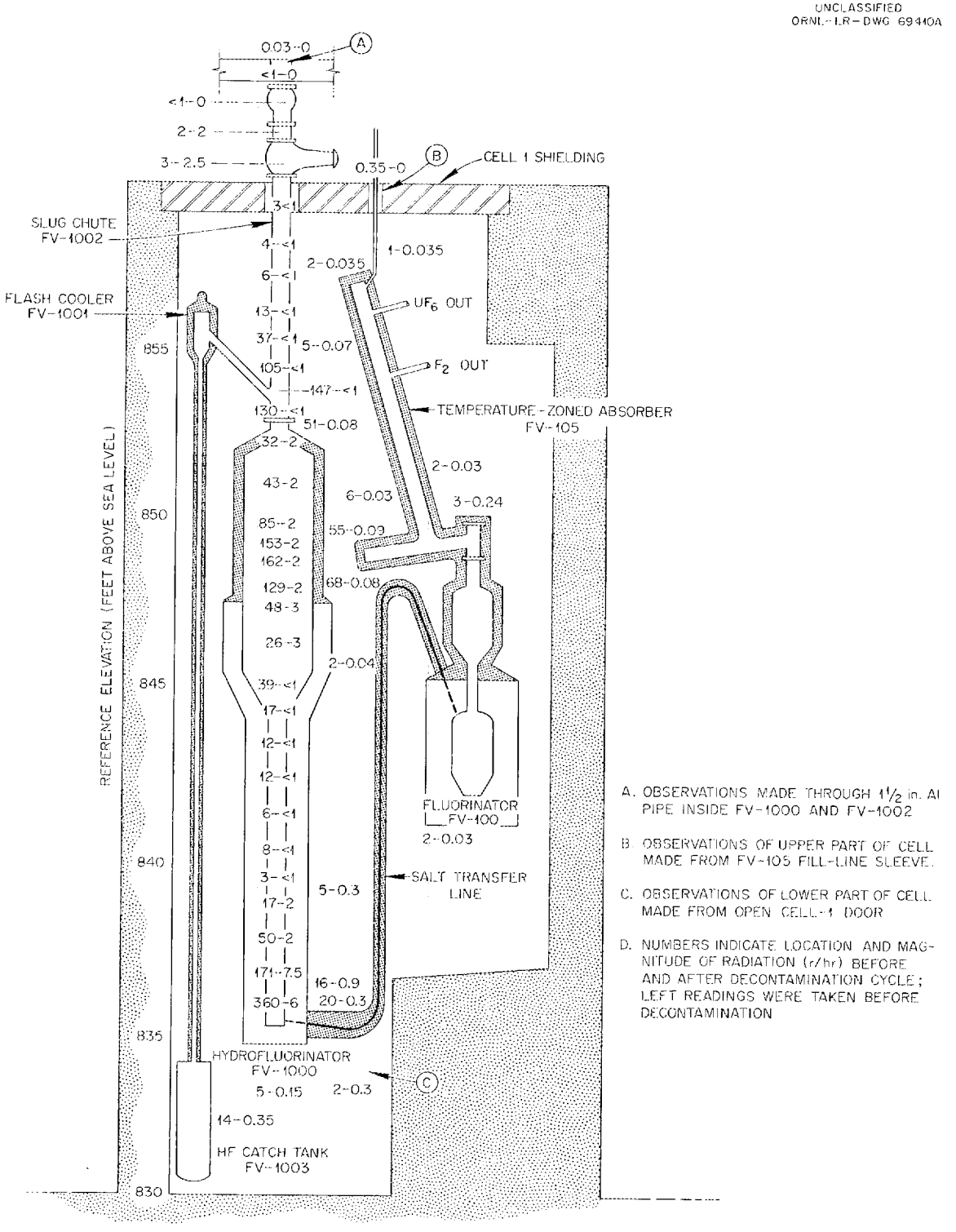

Fig. 2.2. Results of Decontamination of Volatility Pilot Plant Cell 1 Equipment.

oxalate wash removed residual salt deposits, particularly ZrF_4. During the initial oxalate treatment, 8 liters of NH_4BF_4 solution, 20 g/liter, was added to the hydrofluorinator and fluorinator as a nuclear poison. This amount would be adequate for at least 1500 g of U^{235}. The aluminum nitrate–nitric acid dissolvent removed metallic deposits and corrosion films by corroding the internal surfaces of the vessel. The caustic-peroxide-tartrate treatment removed plated activity (mainly Ru^{106}) from vessel walls.

Activity measurements were made in cell 1 before and after decontamination (Fig. 2.2). The internal hydrofluorinator readings were made by inserting an ion chamber (inside an aluminum pipe) into the vessel. Observations outside the dissolver in the upper part of the cell were made by inserting the ion chamber through the absorber fill-line sleeve, while those in the lower part of the cell were made through the open cell-1 door. Following decontamination, general cell-1 activity levels were 30 to 60 millirems/hr.

Residual activity on the equipment was sufficiently low after the decontamination program to permit direct maintenance on all cell-1 equipment. During subsequent equipment modification and repair, the average cell-1 personnel exposure rate was about 30 millirems per man-hour.

Corrosion During Decontamination of Molten-Salt-Handling Equipment in the Volatility Pilot Plant

Following decontamination of the molten-salt-handling equipment, the lower half of the fluorinator was radiographed and visually inspected with a borescope. Since thin areas and some pits were indicated in the welds, two 4-in.-diam samples were cut from the fluorinator. The weld joining the bottom cone to the shell of the vessel was roughened and concave with respect to the base metal. The weld joining the upper dished head of the lower half of the vessel to the shell showed severe undercutting at the line of fusion between the weld metal and the base metal. This severe attack of the INCO-61 weld metal was not typical of any past experience with welded nickel corrosion rods exposed to molten fluorides and fluorine.

The specimens were examined metallographically, and the aqueous decontamination procedure was simulated in a laboratory experiment at Battelle Memorial Institute, under subcontract. During this experiment L-nickel specimens corroded in boiling 0.1 *M* $Al(NO_3)_3$–0.01 *M* HNO_3 (ANN) at rates ranging from 250 to 16 mils/month.[3] Solutions of 5-2-2 wt % NaOH–sodium tartrate–H_2O_2 (CTP) at room temperature gave rates for L-nickel ranging from 1.2 to 8 mils/month. This INCO-61 weld-rod specimens corroded at rates less than half those of L-nickel, but the INCO-61 weld in L-nickel specimens cut from the Volatility Pilot Plant fluorinator showed a definitely higher rate of attack than the base metal (see Fig. 2.3). Coupons welded with INCO-61 also showed a region of accelerated attack at the junction of the weld and the base metal. Specimens of INOR-8, the metal from which the hydrofluorinator is fabricated, were attacked only very slightly by ANN and CTP.

[3]P. D. Miller *et al.*, *Corrosion of the ORNL-VPP-Mark 3 Fluorinator and Group V Rods*, BMI-X-218 (Feb. 15, 1963).

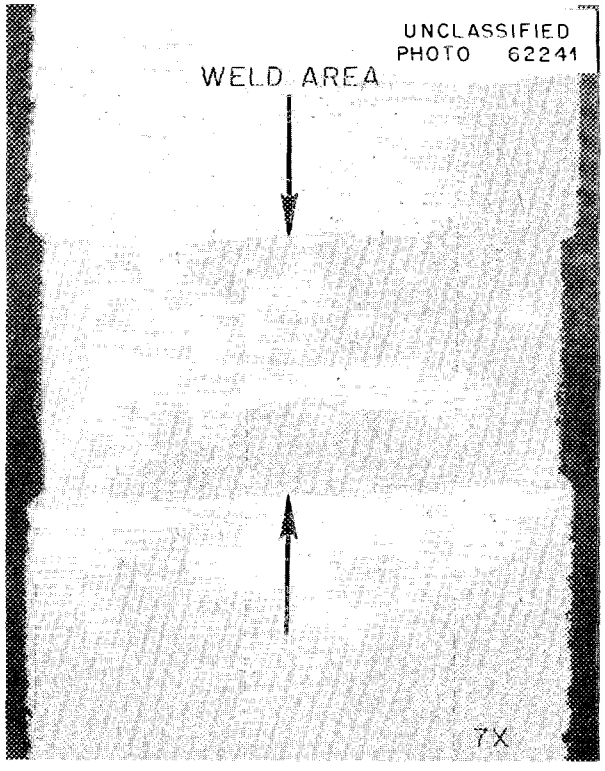

Fig. 2.3. Corrosion of INCO-61 Weld Metal in L-Nickel Volatility Pilot Plant Fluorinator Specimen During Simulated Aqueous Decontamination. Vertical faces were flat before exposure to solutions.

By metallography of the trepanned specimens, intergranular attack of the L-nickel base metal inside the lower portion of the fluorinator (in contact with molten salt during use) was 2.0 mils as-polished and 6 mils after etching, and the exterior surface showed 0 and 11 mils, respectively. Based on the sound metal remaining, as indicated by etching, and the thickness of the original stock, corrosion rates were 8.3 mils/month, based on 1920 hr of molten-salt exposure, and 0.38 mil/hr based on 57.7 hr of fluorine exposure time. If the metal loss of 7 mils obtained in the simulated aqueous decontamination regime is subtracted from the maximum attack of 22 mils, the adjusted overall corrosion rate excluding aqueous decontamination for the base metal in the lower part of the fluorinator is 7.8 mils/month of salt exposure time and 0.26 mil/hr of fluorine exposure time. However, these values should not necessarily be used as the maximum corrosion rate for the fluorinator since earlier measurements[4] indicated that the maximum corrosion rate was in the neck of the vessel, presumably because of contact with gas and splashed salt.

A HyMu 80 corrosion rod that was in the fluorinator during the last 20.8 hr and 625 hr of fluorine and molten-salt time, respectively, as well as during the aqueous decontamination, was corroded very severely, in contrast to the usual excellent performance of HyMu 80 in the presence of molten salt and fluorine. The simulated aqueous decontamination regime was found to be very corrosive to HyMu 80. Thus, the particular set of conditions under which ANN was used in the pilot plant appears to be satisfactory for INOR-8, but not satisfactory for either the L-nickel–INCO-61-weld-metal combination or HyMu 80 base metal.

Cracks in Pilot-Plant Hydrofluorinator

During examination of equipment in cell 1 following aqueous decontamination, a crust of salt, indicating a leak, was found on the outside and near the bottom of the hydrofluorinator. The salt contained both process salt and aluminum nitrate from the decontamination solutions. Thermocouple-failure data indicated that the leak probably developed during the first run made in the series of six in which irradiated zirconium-uranium alloy fuel was used. The interior of the vessel was examined with the Questar telescope, and the site of the failure was plainly visible. Figure 2.4 shows the failure area after the lower section was removed for metallurgical examination; Fig 2.5*a* is a magnified view showing it in more detail. The leakage was through two intersecting cracks – one horizontal and about $1\frac{1}{8}$ in. long between the lowest girth weld and the welds attaching two stainless-steel-sheathed thermocouples to the vessel exterior and the other a vertical crack about $\frac{3}{8}$ in. long between the thermocouple welds. Figure 2.5*b* is an x-ray picture of the crack, showing the external weld beads. Examination of the interior of the vessel with the telescope also showed several areas of short surface cracks or scratches below the girth weld located about 18 in. from the bottom.

The bottom of the hydrofluorinator was severed just above the lower girth weld and submitted for remote metallurgical examination. A replacement

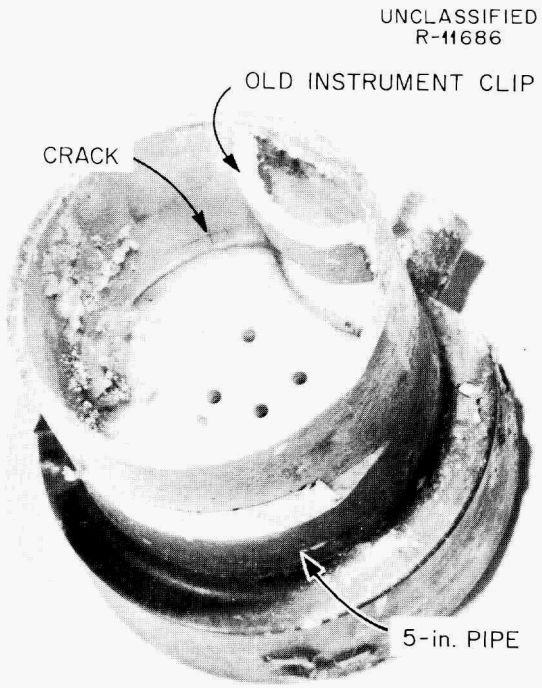

Fig. 2.4. Lower Section of Hydrofluorinator After Failure by Cracking.

[4]A. P. Litman, *Corrosion of Volatility Pilot Plant Mark I INOR-8 Hydrofluorinator and Mark III L-Nickel Fluorinator After Fourteen Dissolution Runs*, ORNL-3253 (Feb. 9, 1962).

UNCLASSIFIED
PHOTO 62242

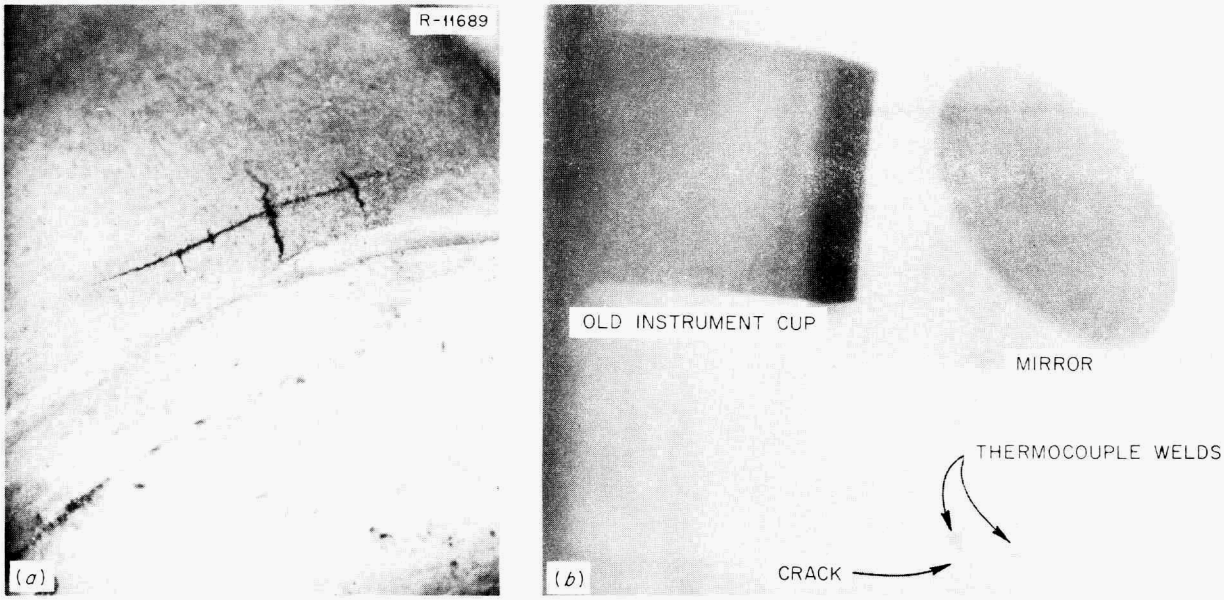

Fig. 2.5. Crack Viewed from Inside Hydrofluorinator. The crack is about an inch long.

section was made and installed during the equipment modifications. Typical sections of the horizontal crack and a thermocouple attachment bead and the main vertical crack and the other bead were prepared as two 100X composite photomicrographs. Significant features of both cracks were: (1) the much greater width of the cracks at the vessel exterior, compared with those on the interior; and (2) the rounded edges of the grain boundaries of the outer three-fourths of the length of the cracks. Another external surface crack was noted immediately below the girth weld attaching the bottom block to the 5-in. section and slightly to the right of the thermocouple beads and failure cracks. This crack was about 40 mils deep and about 10 mils from the edge of the weld metal. A series of horizontal cracks was noted on the internal surface of the lower section. These cracks were fairly uniformly spaced, and those photographed varied from about 15 to 30 mils in depth. The ones examined in detail were about 1 in. to the left of the failure area, but similar cracks were seen in other areas of the lower section. Microfissuring at the junction of the weld and base metal was noted, and it was similar to that observed in certain INOR-8 heats in 1961.[5] Samples of metal from both the lower section and from the ring above the upper girth weld of the failed section were analyzed to determine the heat number of the metal. The heat from which the hydrofluorinator was apparently fabricated (as revealed by the chemical analyses) was involved in the microfissuring difficulties, which were later traced to the melting practices of a particular vendor.

Tensile tests were made on two specimens removed from the failure area. Results were within the limits of the original specification and were comparable to those obtained on the original heat of INOR-8, indicating no significant embrittlement or strength loss.

Tentatively, the major cracks that resulted in the salt leaks were concluded to be of external origin and related to the attachment of the thermocouples to the vessel. There was no indication that interior corrosion by fused salt was a factor in initiating the cracks. On the other hand, exterior corrosion was extremely severe, as is normal with molten fluorides in air. Fabrication of the vessel from one of the substandard heats which were susceptible to microfissuring and to damage by high temperatures was thought to be a factor in the crack formation. The internal cracks may have

[5] *Molten-Salt Reactor Program Progr. Rept. Mar. 1 to Aug. 31, 1961*, ORNL-3215, pp 106–7.

been present in incipient form before the vessel was built.

Modifications to the Pilot Plant

After the six long-decayed zirconium-uranium alloy runs and the equipment decontamination, several modifications were made to the Volatility Pilot Plant. Briefly, these consisted of (1) efforts to improve purity by the addition of a magnesium fluoride bed between the sodium fluoride movable-bed adsorber and the cold traps for removal of technetium and neptunium, the installation of solids filters in the product stream, and relocation of the desorption fluorine inlet line to permit desorption of UF_6 from the movable-bed adsorber without desorbing the fission products in the hot trap zone; (2) piping changes and equipment rearrangement to allow recycle of off-specification product through the movable-bed adsorber and more convenient desorption of the main sodium fluoride chemical trap; (3) elimination of future potential failure areas by the installation of a solids rod-out device in the hydrofluorinator off-gas line and elimination of flanges in the head-end of the plant; and (4) the addition of the necessary shielding for future higher radiation levels.

The Critical Path Method (CPM) of planning was used and was of significant value. Modifications were completed in 30 weeks – two weeks beyond the original scheduled completion date because of the replacement of the leaking hydrofluorinator bottom section, the removal and replacement of fluorinator corrosion rods, and several minor items. Comments on some of the modifications are listed below.

Hydrofluorinator Off-Gas Rod-Out System. – The rod-out system installed to prevent or remove plugs in the 2-in. hydrofluorinator off-gas line consists of a tightly-wound steel spring inserted through a ½-in. line from the penthouse to the 2-in. pipe. When the spring is not in use, it is partially retracted into a flanged, nitrogen-purged casing in the penthouse. A shielded cask for disposing of contaminated spring was built.

Gas-Solids Separators. – The filters installed in the UF_6 system between the magnesium fluoride bed and the cold trap use nickel wire-mesh packing and coarse nickel disks as filter elements. A nickel wire-mesh filter was also installed in the hydrofluorinator exhaust line 1 to localize a radiation hazard by reducing the quantities of radioactive particles passing through a line in the penthouse area to the ventilation-air scrubber. A settling chamber was installed in the waste salt off-gas vent line from cell 1a to reduce the amount of entrained solids.

Pilot-Plant Runs

Five processing runs were completed in the Fluoride Volatility Pilot Plant on zirconium-uranium alloy fuel following a 30-week shutdown for equipment decontamination and modification. Three of the runs, TU-13 to TU-15, were performed to check plant equipment performance and also to study selective desorption as a method of improving product quality (by separating MoF_6 from the UF_6). Two runs, R-7 and R-8, were made to study fission product behavior and uranium decontamination from fission products while processing 13-month- and 6-month-decayed alloy, respectively.

In the flowsheet used (Fig. 2.6), the fuel elements were dissolved by HF at 650 to 500°C in molten equimolar NaF-LiF containing 25 to 45 mole % ZrF_4. During dissolution, the zirconium-uranium alloy was converted to ZrF_4 and UF_4, both soluble in the fluoride salt. Submicron-size solids generated during the dissolution operation were scrubbed from the hydrofluorinator off-gas by liquid HF. After transfer to a separate vessel, the UF_4 was converted to volatile UF_6 by fluorination at 500°C with elemental fluorine. The fluorination step separated the uranium from the bulk of the nonvolatile fission products. Further decontamina- of the UF_6 from trace amounts of volatile and entrained fission products was accomplished by adsorption on and desorption from an NaF bed at 100°C and 400°C, respectively. To improve product quality, MoF_6 was removed from the sorbed UF_6 by desorption at 150°C. Technetium and neptunium, which followed the UF_6 during desorption, were removed from the UF_6 during runs on irradiated alloy by sorption on MgF_2 at 100°C. The product UF_6 from all runs was collected in cold traps.

Dissolution of Alloy. – Of the five dissolution runs, three were made on fully enriched, nonirradiated alloy. Dissolution rates (based on 90% completion) ranged from 2.0 to 2.9 kg/hr with HF

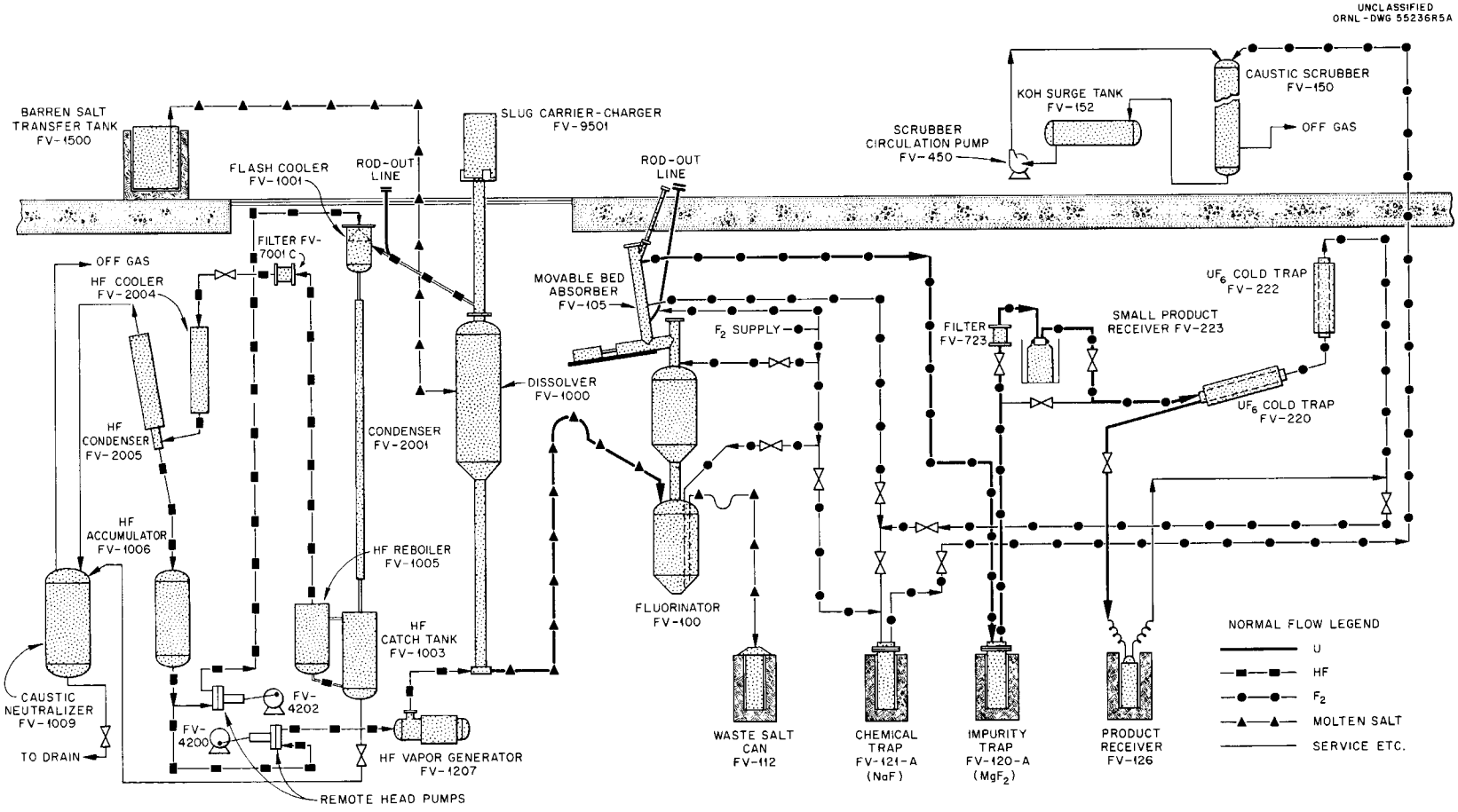

Fig. 2.6. Schematic Diagram of Volatility Pilot Plant.

utilization efficiencies per pass through the dissolver of 24 to 34% (Table 2.2). Previous experience had shown that dissolution-rate correlation was improved by basing the experimental rates on 90% completion, thereby minimizing tail-out effects. The dissolution rates obtained during the three cold runs, although acceptable, were below the previous average rate for the TU series (2.9 kg/hr).[6]

Two dissolutions (R-7 and R-8) were made with 13-month- and 6-month-decayed alloy (burnup greater than 15%). Preliminary results from the 6-month-decayed alloy run showed a dissolution rate of 3.4 kg/hr. The dissolution rate for the 13-month-decayed alloy was also higher (3.7 kg/hr) than in cold runs, but the higher rates may not be a result of fuel burnup. Previous runs on 5- to 6.5-yr-decayed alloy showed no apparent effect of burnup on the dissolution rate.

Uranium Recovery. – Uranium was separated as UF_6 from the molten fluoride melt in all runs by reaction with fluorine. The average fluorine utilization efficiency was about 5% during cold runs and 14% during the run with 13-month-decayed alloy (Table 2.3). A preliminary result for the 6-month-decayed run R-8 gave a fluorination efficiency of 7%. The 13-month value was the highest efficiency obtained in the pilot plant during the alloy program. Nonrecoverable uranium losses, mainly in the waste salt, during all fluorinations were less than 0.46%. Salt recycle would reduce this loss to less than 0.2%. The correlation of fluorination efficiency with conditions in the system has consistently been poor for the low uranium concentrations processed during the alloy program. The spread in the fluorine utilization efficiencies for the cold and hot runs was attributed to low uranium concentration in the salt.

Separation of Molybdenum and Uranium Hexafluorides. – Molybdenum hexafluoride has been shown to behave like UF_6 during the sorption-desorption cycle on NaF and to follow the uranium to the product trap.[7] Temperatures to produce vapor pressures of 1 atm over the MoF_6-NaF and UF_6-NaF complexes are 225°C and 360°C, respectively. This difference in volatilities was used during recent runs to improve product quality by separating MoF_6 from the UF_6. During desorption operations, the uranium-rich region of the absorber (12-in. section of bed below the lower side outlet) was heated from 100 to 150°C in the presence of a fluorine sweep to desorb MoF_6

[6] *Chem. Technol. Div. Ann. Progr. Rept. May 31, 1962*, ORNL-3314, pp 39–45.

[7] G. I. Cathers, R. L. Jolley, and E. C. Moncrief, *Laboratory-Scale Demonstration of the Fused Salt Volatility Process*, ORNL TM-80 (Dec. 6, 1961).

Table 2.2. Summary of Dissolution Runs in the Volatility Pilot Plant[a]

Run No.[b]	Salt Temperature (°C)		Average Dissolution Rate[c] (kg/hr)	Time[c] (hr)	Average HF Flow Rate (g/min)	Average HF Utilization Efficiency per Pass Through Dissolver[c] (%)
	Maximum	Minimum				
TU-13	690	495	2.15	18.3	75–150	25.5
TU-14	660	500	2.06	19.7	100–150	24.1
TU-15	645	500	2.89	13.1	75–140	33.7
R-7	680	495	3.67	11.4	75–125	49.0
R-8	660	500	3.36	10.2	75–120	40.6

[a] See *Chem. Technol. Div. Ann. Progr. Rept. May 31, 1962*, ORNL-3314, p 41, for data on previous runs.

[b] Runs TU-13 through TU-15: nonirradiated fully enriched zirconium-uranium alloy fuel, ~1% uranium, ~40 kg of fuel per run. Run R-7: enriched zirconium-uranium alloy fuel, decayed for about 13 months; ~40 kg of fuel; burnup greater than 15%. Run R-8: enriched zirconium-uranium alloy fuel, decayed for about 6 months; ~40 kg of fuel; burnup greater than 15%.

[c] Based on 90% completion of dissolution (complete dissolution would take about 30% longer).

Table 2.3. Summary of Fluorination Studies in the Volatility Pilot Plant[a]

Run No.	Uranium Concentration in Salt (ppm)		Fluorine Flow (standard liters per min)	Fluorination Time (min)	Fluorine Utilization Efficiency[d]	Fluorination Time to Obtain 10 ppm Uranium in Salt (min)	Total Nonrecoverable Uranium Losses	
	Initial[b]	Final[c]					(g)	(wt %)
TU-13	3987	13	6	101	5.3		2.1	0.32
			13	39				
TU-14	2207	4	6	101	5.8	104	0.8	0.20
			13	19				
TU-15	2383	11	6	101	5.3		2.2	0.46
			13	19				
R-7	4485	4	6	101	13.7	105	0.9	0.09
			13	19				
R-8	4337	1	6	113	7.0	104	0.2	0.02
			13	30				

[a]See *Chem. Technol. Div. Ann. Progr. Rept. May 31, 1962,* ORNL-3314, p 43, for data on previous runs.
[b]May include uranium heel from previous runs.
[c]Final concentration prior to hot trap dump; concentration normally lower after NaF discharge to waste salt.
[d]Based on time required to obtain 10 ppm in waste salt (or final uranium concentration if greater than 10 ppm).

through the side outlet to the chemical trap (FV-121A, Fig. 2.6). After molybdenum removal, uranium desorption was accomplished by heating the entire bed to 400°C, the UF_6 leaving the absorber through the top outlet.

During run TU-13, approximately 90% of the molybdenum initially on the NaF in the absorber was desorbed to the chemical trap with 2 std liters/min of sweep gas (1-1 F_2-N_2) at 160°C for 60 min. Under these conditions and assuming equilibrium, a 12-min desorption would theoretically have been adequate. Uranium appeared to be removed at about 90% of the equilibrium transpirational rate. The total (recoverable) uranium loss was 0.2 g.

Product Quality. — Metallic cation impurities in the product from cold runs TU-13 through TU-15 totaled about 3200 ppm (Table 2.4). AEC buyback specifications for UF_6 call for less than 300 ppm total cation impurities. However, the total cation concentration of less than 171 ppm achieved in run R-7 using 13-month-decayed alloy was well within the allowable value. A higher total cation content (<712 ppm) was obtained in run R-8 on 6-month-decayed alloy.

During previous pilot-plant runs, high metallic cation impurity levels were practically always associated with high HF contamination of the UF_6 product. Runs TU-13 through TU-15 further substantiated this observation. Up to 30 wt % HF was found in the latter runs.

The source of the HF dilution was probably moisture inleakage into the product-recovery system during movable-bed-absorber operations (pellet addition and bed measurement operations). The moisture, initially adsorbed on the NaF pellets, reacted with elemental fluorine during fluorination and desorption operations to form the HF. Product quality was excellent in run R-7 when the HF was removed by pretreating (prior to fluorination) the top zone of the absorber bed *in situ* by heating to 300 to 400°C in a fluorine atmosphere. However, some HF contamination (0.5%) of the product occurred during run R-8 indicating inadequate bed

Table 2.4. Cation Impurities in the Uranium Hexafluoride Product from the Volatility Process

Run No.	Average Product Impurity Level (ppm of U)											
	Cr	Cu	Fe	Li	Mo	Na	Ni	Sn	Zr	Np	Tc	Total
TU-13[a]	<4	487	122	<2	2040	365	11	155	<22			<3208
TU-14[a,b]												
TU-15	137	890	357	16	665	1070	44	<20	<20			<3219
R-7	<2	3	3	<1	9	129	15	<3	<1	4	<1	<171
R-8	<1	150	100	<1	43	327	30	<7	<1	48	4	<712
AEC specification[c]	<200			<10	<200							<300

[a]Yorkmesh and micrometallic filter in product line inadvertently bypassed during run, allowing NaF dust to transfer to product cold trap.

[b]Product cylinder was water washed to recover uranium for sampling (cylinder valves plugged by NaF particles). Total uranium recovered in wash solution was <1 g.

[c]*Federal Register* **25**, 2817 (1960).

pretreatment. Moisture was also limited by avoiding air inleakage, whenever possible, throughout the entire process system.

Molybdenum hexafluoride removal from the UF_6 by desorption at 150°C was not quantitative during cold runs, probably because of the high HF contamination of the product. However, during run R-7, when no HF dilution occurred, the molybdenum content of the product was only 9 ppm, the lowest value obtained during the entire zirconium-uranium alloy program. The product molybdenum level was 43 ppm in run R-8 when 0.5% HF contamination occurred. The variable quantities of copper, chromium, iron, and tin found in the cold-run products may also have been due to contamination by HF.

Sodium contamination of the product occurred when NaF fines were entrained from the absorber during desorption operations. A filter system was installed for NaF removal prior to the runs, but it was inadvertently bypassed during runs TU-13 and TU-14. Although the filter was in service in run TU-15, sodium contamination of the product was still 1070 ppm (probably from residual fines in the system being swept to the product trap). Improvement in the sodium level was obtained in run R-7 (sodium, 129 ppm), but the level increased in R-8 to 327 ppm, indicating ineffective filtration.

Final removal of Tc^{99} from the UF_6 (to less than 1 and 4 ppm in the product) was accomplished in runs R-7 and R-8 by complexing with MgF_2 at 100°C. The total Tc^{99} found on the MgF_2 was substantially below the fuel content; therefore, the NaF bed may also have been effective in Tc removal. Substantial quantities of uranium (at least 200 g) were also retained on the MgF_2 bed during run R-7 by physical adsorption and possibly deposition (as UO_2F_2) in the presence of moisture. The MgF_2 bed size was reduced from 10 kg to 1 kg between runs R-7 and R-8. The uranium retention was reduced somewhat more than proportionately – to 14 g. The MgF_2 also was effective for neptunium removal (4 and 48 ppm, respectively, in runs R-7 and R-8).

Fission Product Behavior. – The separation of uranium from fission products in the Fused-Salt Fluoride Volatility Process is accomplished by making use of the vapor pressure differences of uranium and the fission product fluorides or complexes. Several nuclides – Ru, Nb, I, Te, Mo, and Sb – form highly volatile fluorides, while others – Zr, Sr, and Cs – form relatively nonvolatile fluorides. The fission product, Tc^{99}, is principally a chemical contaminant.

Overall-process DF's ranged from greater than 10^8 to nearly 10^{11} for volatile fission products (Sb^{125}, Te, Ru^{106}, and Nb^{95}), and from greater than 10^9 to greater than 10^{10} for nonvolatile fission products (Zr^{95}, Sr^{90}, and Cs^{137}) during run

R-8 on 6-month-decayed alloy. Generally lower DF's were obtained during run R-7 on 13-month-decayed fuel. The overall DF's represent the magnitude of the uranium decontamination from fission products in both major steps of the process, dissolution and product recovery. The dissolution DF's were determined by the ratio of the calculated activity of each nuclide in the alloy to the measured activity in the fluorinator feed salt. In each case, the specific activities in the alloy were evaluated[8] from reactor operating data with the fuel burnup calculated by the CRUNCH code[9] on the IBM 7090 computer. Without exception, the dissolution DF's were small compared with the product-recovery DF's.

For the dissolution step, decontamination factors for the volatile fission products ranged from a low of 5 for Sb^{125} to a high of 5×10^3 for Te (Table 2.5). The Sr^{90} DF of 2 and the Cs^{137} DF of 1 to 3 are measures of the precision of calculation of the feed activity rather than "entrainment" decontamination factors.

Decontamination factors for the product recovery step of the process during run R-8 were greater than 10^9 for Zr^{95}, Sr^{90}, and Cs^{137}, greater than 10^{10} for rare earths, and ranged from 10^5 to greater than 10^9 for Sb^{125}, I^{131}, Te, Ru^{106}, and Nb^{95} (Table 2.5). Product-recovery DF's were based on the ratio of the measured nuclide activity in the fluorinator to the measured activity in the product receiver. When the product activity was below the analytical limit of detection, the lower limit was used as the product activity for the DF calculation.

The UF_6 product from runs R-7 and R-8 met AEC specifications for gamma activity. The product natural beta activity is being evaluated to determine if AEC beta specifications were also met. All specific fission products (with the exception of Tc^{99} in R-8) were at or below the analytical lower limit of detection in both run R-7 and R-8.

Performance of the Pilot-Plant Equipment. – The pilot-plant equipment performed generally

[8] J. O. Blomeke and M. F. Todd, *Uranium-235 Fission-Product Production as a Function of Thermal Neutron Flux, Irradiation Time, and Decay Time*, ORNL-2127 (Aug. 19, 1957).

[9] M. P. Lietzke and H. C. Claiborne, *Crunch – An IBM 704 Code for Calculating N Successive First-Order Reactions*, ORNL-2958 (1960).

Table 2.5. Approximate Fission Product Decontamination Factors for Fused-Salt Volatility Process During Processing 6-Month and 13-Month-Decayed Alloy

Radionuclide	Uranium Decontamination Factors					
	13-Month-Decayed Alloy (Run R-7)			6-Month-Decayed Alloy (Run R-8)		
	For Alloy Dissolution[a]	During Product Recovery[b]	Overall Process	For Alloy Dissolution[a]	During Product Recovery[b]	Overall Process
TRE β		$>1 \times 10^9$			$\sim 5 \times 10^{10}$	
Zr^{95}	50	$>1 \times 10^8$	$>5 \times 10^9$	10	1×10^9	1×10^{10}
Sr^{90}	2	$>5 \times 10^8$	$>1 \times 10^9$	2	$>1 \times 10^9$	$>2 \times 10^9$
Cs^{137}	3	$>1 \times 10^9$	$>3 \times 10^9$	1	$>5 \times 10^9$	$>5 \times 10^9$
I^{131}	10	$>5 \times 10^4$	$>5 \times 10^5$		$>1 \times 10^6$	
$Te^{(as\ 132)}$	300	$>1 \times 10^5$	$>3 \times 10^7$	5×10^3	$>3 \times 10^5$	$>1 \times 10^9$
Sb^{125}	250	$>1 \times 10^5$	$>2 \times 10^7$	5	$>1 \times 10^8$	$>5 \times 10^8$
Ru^{106}	750	$\sim 1 \times 10^5$	$\sim 1 \times 10^8$	1×10^3	$\sim 1 \times 10^5$	$\sim 1 \times 10^8$
Nb^{95}	100	$>1 \times 10^7$	$>1 \times 10^9$	50	1.6×10^9	8×10^{10}

[a] Based on ratio of calculated nuclide activity in alloy to measured activity in fluorinator.

[b] Based on ratio of measured nuclide activity in fluorinator to measured activity in product receiver. When product activity was below analytical limit of detection, the lower limit was used as the product activity for the DF calculation.

satisfactorily during the runs. All difficulties encountered were relatively minor, and in each case it was possible either to continue operations or to repair or modify the equipment.

One source of difficulty was in molten-salt sampling, both from the standpoint of obtaining samples and of moisture inleakage into the system during sampling. These difficulties were corrected by a combination of design and procedure changes.

Evidence was found that certain items of the mechanical equipment had deteriorated. For example, several valves were recently replaced because of either bellows failure or excessive seat leakage, the liquid HF feed pump capacity had gradually decreased, and the maintenance frequency had increased on the UF_6 refrigeration units (which were installed about seven years ago).

The shielding installed on the main process lines and tanks in preparation for short-cooled operation was adequate. However, additional shielding was required at certain points, such as valves, where unexpected activity deposition occurred.

Corrosion of Volatility Pilot-Plant Fluorinator Corrosion Rods (Groups 1 to 5)

During the year, results were reported covering the metallography of the five groups of corrosion rods exposed in the Volatility Pilot Plant fluorinator during the zirconium-uranium run series.[10–13] Table 2.6 summarizes test conditions and maximum corrosion rates for the 36 specimens reported. These data supplement similar information gathered during the ARE fuel recovery program.[13] The maximum corrosion rates of the L-nickel specimens exposed in both the ARE and the zirconium-uranium series are summarized in Table 2.7. Some of the more apparent conclusions from these tests are as follows:

1. The combination of operating temperatures of about 500°C and lithium fluoride present in the salt melts generally produces about the same bulk metal losses on nickel and nickel-base alloys as was found by operating at 650°C without lithium fluoride but with much larger quantities of uranium.

2. Bulk metal losses on L-nickel and the nickel binary alloys containing manganese, iron, cobalt, aluminum, or magnesium are about the same during fluorination at 500°C with lithium present in the fluoride salt baths. However, the presence of the alloying elements, iron, aluminum, or magnesium in nickel, drastically reduces or eliminates the intergranular attack practically always found in unalloyed nickel exposed to the fluorination environment. Extra-high-purity nickel is the most susceptible to bulk metal losses and intergranular attack in the fluorination environment of all the nickel alloys tested, including L-nickel.

3. Although direct comparisons are not possible because of differing degrees of corrosivity of the various run groups, the following alloys showed significantly improved performance over L-nickel and thus are possible materials of construction for a fluorination vessel: nickel filler metal 61 (INCO-61), E-nickel, Ni–5 Fe, Ni–1 Al, INOR-8, and HyMu 80. Some of the results for Ni–1 Al, Ni–5 Mo, INOR-1, and HyMu 80 are clouded by having been obtained during the group 5 series of corrosion tests, which was concluded by the use of 0.1 *M* $Al(NO_3)_3$–0.1 *M* HNO_3 as a part of the decontamination procedure. A simulated laboratory test[14] showed this reagent to be highly corrosive to HyMu 80.

The differences between the corrosivity to L-nickel of the various runs making up the exposure conditions for the last five exposures are of interest. Table 2.7 indicates that groups 3 and 4 runs were particularly corrosive and that the corrosion of L-nickel during the group 5 runs, even considering the aqueous decontamination, was very mild. In fact, if aqueous decontamination losses found in the simulation experiment were subtracted from the final losses, the attack due to molten salt and fluorine exposure would be almost zero. Variations in HF content of the salt in the fluorinator, temperature excursions, and variations in sulfur content of the salt have all been postulated as explanations for the differences in corrosion between these melts. Insufficient information is available on either sulfur or HF content of the fluorinator melts to assess their effects on L-nickel. Although

[10] T. M. Kegley, Jr., and A. P. Litman, *Corrosion of Nickel-Base Specimens Exposed in the Volatility Pilot Plant Mark III Fluorinator*, ORNL TM-411 (Jan. 4, 1963).

[11] P. D. Miller *et al.*, *Corrosion Analysis of ORNL Pilot Plant Components*, BMI-X-201 (May 15, 1962).

[12] P. D. Miller *et al.*, *Corrosion of the ORNL VPP Mark III Fluorinator and Group V Rods*, BMI-X-218 (Feb. 15, 1963).

[13] A. P. Litman and A. E. Goldman, *Corrosion Associated with Fluorination in Oak Ridge National Laboratory Fluoride Volatility Processing*, ORNL-2832, sec IV (June 5, 1961).

[14] See pp 30–31 of this report.

Table 2.6. Comparison of Maximum Corrosion Rates for Groups 1 to 5 VPP Fluorinator Corrosion Rods

Nominal salt composition — 27.5-27.5-45 mole % $NaF-LiF-ZrF_4$ + 0.3 wt % U (no U during group 1)

Group	1	2	3	4	5[a]
Runs					
T-	1–7 (plus F_2 sparge tests)			8–10	11
TU-		1–5	6–7	8–10	11–12
R-					1–6
Molten-salt exposure					
Time, hr	367	205.5	99	601	625
Temperature, °C	485–605	490–575	550–580	500–750[b]	
Fluorine exposure					
Time, hr	12.0	10.5	3.1	5.8	20.8
Temperature, °C	535–570	500–515	500–510	505–535	490–520

Group No.	Metal	Specimen No.	Notation[c]	Corrosion Rate (mils per hr of F_2 exposure)		
				Metal Loss[d]	IG[e]	Total[f]
1	L-nickel, conditioned[g]	51	L	0.09	0.96	1.1
	INCO-61, conditioned[g,h]	51	L	0.10	0.17	0.27
	Nickel HPVM[i]	39	L	0.06	10.4	10.5
	E-nickel[h]	32	L	0.07	0.29	0.36
	Ni–5 Fe	24R	L	0.09	0.06[j]	0.15
	Ni–10 Fe	27	V	0.08	0.83	0.91
	Ni–20 Fe	29	S	0.08	0.42	0.50
2	L-nickel, conditioned[k]	52	L	0.34	0.67	1.0
	INCO-61[k]	52	L	0.64	0	0.64
	L-nickel	55	L	0.34	0.67	1.0
	INCO-61	55	IF	0.65	0	0.65
	Ni–5 Co	17	L	0.57	3.71	4.28
	Ni–10 Co	21	IF	0.78	0.33	1.11
	Ni–1 Al	1R	IF	0.55	0	0.55
	Ni–3 Al	5	IF	0.82	1.48	2.29
3	L-nickel, conditioned[k]	53	L	2.0	0.9	2.9
	INCO-61, conditioned[k]	53	IF	3.7	0	3.7
	L-nickel	54	IF	2.5	1.6	4.1
	INCO-61	54	IF	3.2	0.8	4.0
	Ni–1 Mg	8R	IF	2.8	0	2.8
	Ni–0.1 Mg	34R	IF	3.3	0	3.3
	Ni–0.05 Mg	37R	IF	2.9	0	2.9
	HyMu 80[h]	47	IF	1.3	0	1.3

Table 2.6 (continued)

Group No.	Metal	Specimen No.	Notation[c]	Corrosion Rate (mils per hr of F_2 exposure)		
				Metal Loss[d]	IG[e]	Total[f]
4	L-nickel	44	L	0.9	5.3	6.2
	INCO-61	44	L	0.3	0.4	0.7
	L-nickel	45	IF	0.4	2.1	2.5
	INCO-41[h]	45	L	0.6	0.9	1.5
	Ni–10 Fe	27	L	1.3	0.7	2.0
	HyMu 80	47A	L	1.2	0.4	1.6
	INOR-8[h]	48	L	1.0	0	1.0
5[a]	L-nickel	60	L	0.18	0.14	0.32
	Ni–1 Al	1R	L	1.83	0	1.83
	Ni–5 Mo	70	L	0.99	0	0.99
	INOR-1[h]	65	L	1.31	0	1.31
	INOR-8	48	V	0.53	0	0.53
	HyMu 80	47	L	2.62	0	2.62

[a]Group-5 rods were subjected to an aqueous decontamination procedure (sec 2.1).

[b]Temperatures of 750 and 715°C were reached during runs T-8 and T-9 in presence of salt only. No F_2 during runs T-8, T-9, and T-10.

[c]V = vapor; L = liquid; IF = vapor-liquid interface.

[d]By micrometer readings.

[e]Intergranular attack as indicated by etching. Corresponds to ORNL Metals and Ceramics Division "Grain-Boundary Modifications" designation.

[f]Based on sound metal remaining, assuming that intergranularly attacked and leached portion is unsound.

[g]F_2 conditioned for 5.3 hr at 600°C prior to exposure.

[h]Alloy compositions (nominal percentages):
INCO-61 (Ni filler metal) – Ni, 93 min; Cu, 0.25; Mn, 0.60; Fe, 1.0; Si, 0.75; Al, 1.5 max; Ti, 2–3.5
E-nickel – Ni–2 Mn
HyMu 80 – Ni, 79.0; Mo, 4.0; Mn, 0.50; Si, 0.15; Fe, bal
INCO-41 (Ni filler metal) – Ni, 97 min; Cu, 0.25; Mn, 0.35; Fe, 0.4; Si, 1.0; Ti, 0.5 max
INOR-1 – Ni, 78; Mo, 20; Fe, 0.3; Mn, 0.5; Si, 0.5.

[i]HPVM = high purity vacuum melted.

[j]Surface attack included (see ORNL TM-411, p 17).

[k]F_2 conditioned for 3.2 hr at 600 to 645°C.

there were temperature excursions during runs T-8 and T-9 during the group 4 series, they both occurred when no fluorine or UF_6 was present and consequently would not have been expected to have been significant. The exponential form of the curve of L-nickel fluorination exposure time vs corrosion rate seems to be the most likely explanation of corrosivity variations in the last five exposures.

Specimens currently being exposed in the fluorinator are: INOR-8, L-nickel, HyMu 80, and an alloy, Ni–0.1% Mg. The corrosion characteristics of as-welded metal are also being studied in two test bars made up of various combinations of L-nickel and INOR-8 welded with Inconel weld filler metal 82, INOR-8, nickel filler metal 61, and L-nickel.

Table 2.7. Maximum Corrosion Rates of L-Nickel Specimens

Specimen Type	Run	Approximate Temperature Range (°C)	Initial Bath Composition (mole %)				F_2 Exposure (hr)	Intergranular Penetration (mils)		Corrosion Rate (mils per hr of F_2 exposure)
			NaF	LiF	ZrF_4	UF_4		Section As Polished	Section Etched	
Rods	M-21–M-48	505–700	50		50		10		>27	>4.0
Rods	C-9–C-15	500–650	48		48	4	37		10	1.2
Rods	E-3–E-6	540–660	48		49.5	2.5	16.5		8	0.8
Rods	L-1–L-4	560–710	54		41	5	34		3	1.5
Rods	L-5–L-9	540–700	52		45.5	2.5	18		5	0.7
Group 1 rods	T-1–T-7	485–605	43	30	43		12.0	4.5	11.5	1.1
Group 2 rods	TU-1–TU-5	490–575	29	29	42	0.2	10.5	6	7	1.0
Group 3 rods	TU-6–TU-7	500–510	32	29	39	0.2	3.1		6	4.1
Group 4 rods	T-8–T-10; TU-8–TU-10	500–750	28	32	40	0.2	5.8		31	6.2
Group 5 rods	TU-11–T-11	490–510	28	32	40	0.2	20.8	2.5	3	0.3

2.2 VOLATILIZATION AND RECOVERY OF PLUTONIUM HEXAFLUORIDE

The recovery of plutonium in the fused-salt volatility process is essential if the method is to be adapted to the processing of low-enrichment uranium fuels. In previously reported work with molten salts containing about 2 ppm of plutonium, the volatilization of PuF_6 by fluorination was demonstrated along with recovery of the PuF_6 on fluoride salt beds.[15] Extension of this work was carried out at higher concentrations, that is, at about 1000 ppm of plutonium in the salt, for the purpose of examining whether the volatilization rate is significantly different at the higher concentration and whether the same sorption effects are observed with the larger quantity of plutonium. Some preliminary work has also been conducted in examining what the rate-controlling step is in the volatilization step and whether process conditions could be adjusted to achieve reasonable volatilization rates.

Fluorination Tests

The results of fluorination tests with 31-24-45 mole % LiF-NaF-ZrF_4 mixture containing about 1000 ppm of plutonium gave rates similar to those obtained at the concentration level of 2 ppm. The PuF_6 volatilization rate has a first-order dependence on the concentration, with the half time of the reaction being about 5.3 hr at 500°C and about 3.0 hr at 600°C (Fig. 2.7). These results were obtained in 10- and 17-hr tests, respectively, at the two temperatures, with 55 g of salt in a 1-in.-diam reactor with a fluorine flow rate of 100 ml/min at atmospheric pressure. In a recent test, preliminary results indicated a reduction in reaction

[15] G. I. Cathers and R. L. Jolley, *Recovery of PuF_6 by Fluorination of Fused Fluoride Salts*, ORNL-3298 (Sept. 24, 1962).

half time to 1.5 hr by the use of fluorine at 40 psig, which is an acceptable rate for process use provided the use of pressurized fluorine does not markedly increase corrosion rates in the fluorinator.

A number of diffusional rate-controlling mechanisms can be postulated as the reason for the relatively slow volatilization rates obtained with plutonium in fused salt. However, the results of two stirred reactor experiments showed that the PuF_6 volatilization rate was not increased by violent agitation (Fig. 2.7). Another hypothesis to account for the slow rate is that the fluorinating agent (fluorine) has too low a solubility. A test run made with intermittent additions of UF_4 was therefore carried out with the idea that the fluorinating potential of the salt would be enhanced at intervals by the presence of the higher intermediate valent states of uranium. This run, however, had a half-time reaction value of 4.0 hr, indicating that there was little effect. While more tests with agitation and using other fluorinating agents are planned, it is presently believed that the best possibility of volatilizing PuF_6 without excessive corrosion due to the long times required lies in the use of salt-spray fluorination in order to minimize contact with metal reactor walls.

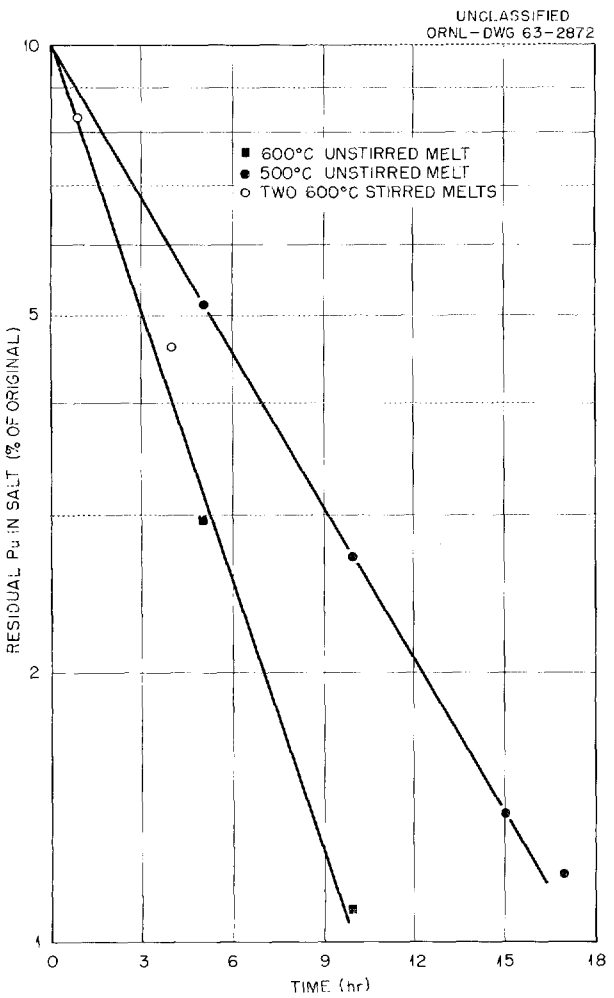

Fig. 2.7. Volatilization of PuF_6 from 31-24-45 mole % $LiF-NaF-ZrF_4$ Containing 1000 ppm of Plutonium: Comparison of Stirred and Unstirred Melts.

In all of the above fluorination tests conducted with about 1000 ppm of plutonium in fused $LiF-NaF-ZrF_4$, that is, with about 55 mg of plutonium, material balances of 95 to 100% were obtained. This corresponds quite well with the behavior exhibited in volatilizing UF_6 from fused salts in laboratory work, and it indicates that a PuF_6-volatilization process would be feasible on an engineering scale if means can be found to control corrosion.

Sorption Tests on Plutonium Hexafluoride

The volatilized PuF_6 in the above fused-salt tests was sorbed in various solid fluoride beds to examine further some sorption effects reported previously.[15] An absorption process using CaF_2 or LiF may be feasible as a means of separating PuF_6 from UF_6. In general the absorption effects observed in the present work were similar to those found in tests with less plutonium. Absorption beds of CaF_2, MgF_2, LiF, and NaF exhibited a definite selective trapping effect for PuF_6. A yellow color observed in tests made with CaF_2 and NaF indicated that complexes or compounds were formed.

The absorption results given in Table 2.8 were used in achieving the 95 to 100% material balance reported in Sec 2.2. The lithium fluoride used was prepared by fusing and fluorinating Li_2CO_3 and had a high area. The NaF (regenerated from $NaHF_2$), the CaF_2 (prepared by fluorinating $CaSO_4$), and the MgF_2 (prepared from slurried and dried powder) had surface areas, respectively, of 1.7, 14, and 60 m^2/g. Chemisorption thus appears quite probable in accounting for the quantity of PuF_6 sorbed on the materials of lower surface areas.

Table 2.8. Effects Observed in Plutonium Hexafluoride Absorption Tests by Using Two Consecutive Beds

8-g beds of 12–20 or 20–40 mesh material in ½-in.-diam tubes held at 100°C

Amount Pu Volatilized (mg)	Bed 1		Bed 2	
	Material	% Pu Found	Material	% Pu Found
45.5	CaF_2[a]	91.4	NaF	8.6
9.7	MgF_2	97.7	NaF	0.3
28.8	LiF	>99[b]	NaF	0.01

[a]Yellow color observed, which is indicative of compound formation.

[b]Specific surface area of LiF was 42 m^2/g.

2.3 PREPARATION AND ABSORPTION OF TELLURIUM HEXAFLUORIDE

Reduction of Tellurium Hexafluoride in the Fluorinator

Tellurium as a fission product has to be considered in the processing of short-decayed fuel (less than 200 days) since several volatile fluorides (TeF_4, Te_2F_{10}, and TeF_6) may be formed. The results of several "dry" attempts to prepare TeF_6 and absorb it in caustic indicated that the tellurium fluorides are probably quite easily reduced by nickel metal at intermediate process temperatures (up to 300°C). This leads to the conclusion that in the fused-salt fluorination process at 500°C, TeF_6 (bp, 39°C) would probably be formed and volatilized, but that it would subsequently be reduced again upon contact of the gas with the cooler nickel wall at the top of the reactor or in the Monel UF_6-gas process lines held at about 100°C. A study[16] made of the processing of irradiated UO_2 with a 15- to 30-day decay period appears to confirm this since the material balance for tellurium was low. Possibly tellurium acts like sulfur in the presence of nickel or of some nickel alloys at moderate temperatures.

[16]G. I. Cathers, R. L. Jolley, and H. F. Soard, *Use of Fused Salt–Fluoride Volatility Process with Irradiated Urania Decayed 15–30 Days*, ORNL-3280 (Sept. 6, 1962).

Altogether, seven runs were made in attempting to make and volatilize TeF_6 by using elemental tellurium and fluorine. A nickel reactor and boat were used at 300°C. In all runs, using a definite excess of fluorine, the 1 g of elemental tellurium employed was totally reacted and volatilized; however, a maximum of 10.5% was found absorbed in a 10% KOH trap. In most of the runs, recovery in the caustic was less than 2.5%, with this minimum figure due mainly to an analytical limit. A recovery of less than 2.5% was found when using a packed column for the potassium hydroxide solution, operating at 75°C.

Absorption of Tellurium Hexafluoride in 10% Aqueous Potassium Hydroxide

The absorption of TeF_6 in 10% KOH solution proceeded fairly rapidly in absorption tests at 50 to 70°C. This, together with the reduction effect discussed above, probably indicates that the caustic spray tower used for fluorine disposal in the ORNL Volatility Pilot Plant will be satisfactory in preventing the release of radioactive tellurium to the atmospheric environment. However, TeF_6 is more difficult to absorb in caustic than fluorine; so traces of tellurium may be detected in the plant ventilation exhaust.

A gas mixture of about 12% TeF_6 in fluorine was used to study the absorption or hydrolytic effectiveness of aqueous KOH solution. The absorption system consisted of a column (20 in. long and 1 in. in diameter) packed with ¼-in. Alundum Berl saddles and mounted over a heating flask. A finger pump was used to circulate the 10% aqueous KOH solution at a rate of about 250 ml/min. The countercurrent gas flow rate was about 100 ml/min. The TeF_6-F_2 mixtures were made by using flow measurements.

Preliminary trials established that TeF_6 (from General Chemical) was readily absorbed in a single packed column but that the use of consecutively coupled columns would be advisable in order to study the relative effectiveness for TeF_6 and F_2. Data from three tests at temperatures of 25, 50, and 70°C showed that the higher temperatures are much more effective (Table 2.9). Almost all the fluorine was absorbed in the first of two columns in all of the tests, but the TeF_6 was only partly trapped, leaving an appreciable fraction to pass into the second column. The reliability of the tellurium

Table 2.9. TeF_6-F_2 Gas Absorption Tests in 10% Aqueous KOH Using Two Consecutive Packed Columns

	Test 1	Test 2	Test 3
Column temperature, °C	25	50	70
Weight tellurium input, g	3.20	4.47	3.16
Tellurium recovery, %			
1st column	35.6	54.7	51.1
2d column	6.7	13.3	16.0
2d column, revised[a]	10.4	29.4	32.8
Tellurium material balance, %	46.0	68.0	67.1
F_2 recovery, %[b]			
1st column	104	166	115
2d column	0	0	0.1
KOH neutralized, %	43	73	50

[a]Recovery recalculated on basis of 100% entering 2d column.

[b]Based on a fluorine flow rate of 100 ml/min.

data is high because the recoveries were calculated from analytical data and the actual input determined by weighing the TeF_6 supply tank. The fluorine recovery calculations are less reliable since they were based in part on difference calculations and flow-rate control.

2.4 PROCESS ENGINEERING STUDIES

Recycle and Single-Vessel Process Testing

In order to improve the present Fused Salt Volatility Process, the concepts of single-vessel dissolution by hydrofluorination followed by fluorination, and of salt recycle, are being evaluated on a unit-operations scale with process materials. Dissolution experiments with Zircaloy-2 and zirconium-uranium alloy elements indicated that salt recycle has no significant effect on rate and also showed that filtration and/or settling steps for salt purification are not required. Corrosion rates measured during a series of single-vessel dissolutions and fluorinations were not significantly different from the sum of the rates noted when the two process steps are carried out in separate vessels.

Salt Recycle Studies. – Various lengths (2 to 12 in.) of Zircaloy-2 simulated elements and 6-in.-long sections of zirconium-uranium alloy prototype elements were dissolved with anhydrous HF in a waste ZrF_4-NaF-LiF mixture from preceding dissolutions, with enough NaF-LiF added as diluent to obtain the desired initial charge composition. Control dissolutions of each type of element in fresh salt were made for comparisons.

Specific dissolution rates in recycled salt for the Zircaloy-2 elements varied between 1.3 mg cm^{-2} min^{-1} for 12-in.-long elements and 5.2 mg cm^{-2} min^{-1} for 2-in.-long elements. Specific dissolution rates in recycled salt for the 6-in.-long zirconium-uranium alloy elements during the single-vessel studies were about 1.1 mg cm^{-2} min^{-1}. In all cases, the rates obtained in recycled salt compared favorably with those obtained when fresh salt was used.

The iron, nickel, and chromium content of the salt after each dissolution showed no significant buildup of these corrosion products. The largest increase was in nickel content after six recycles: it was about three times the average in unrecycled product salt. The concentration of iron and chromium in all recycled product salts, and that of nickel in all recycled product salt (except that recycled six times), was less than twice those of unrecycled product salt.

Determination of the iron, nickel, and chromium content of the discharge salt after each dissolution and each fluorination of the single-vessel series indicated some buildup of nickel in the fluorination discharge salt near the end of the series. After the fifth fluorination, the nickel content was about twice that after the first, and after the seventh it was about six times that after the first. The iron had increased by a factor of 2 and the chromium by a factor of 3. The nickel content of the product salt from each dissolution was less than its feed salt. This is best explained by the reduction of NiF_2 by zirconium and the deposition of this metallic nickel on the surfaces of the vessel. This metallic nickel is subsequently oxidized to NiF_2 during fluorination and returns to solution.

Single-Vessel Corrosion Studies. – Each dissolution of the zirconium-uranium alloy elements was followed by fluorination with elemental fluorine in the same INOR-8 vessel. During the dissolution-fluorinations, one INOR-8 and two Alloy 79-4 corrosion specimens were suspended through the vapor-salt interface. After the dissolution-fluorination series, only the vessel was subjected to a decontamination procedure using 0.1 *M* $Al(NO_3)_3$–0.01 *M* HNO_3 solution.

During the single-vessel dissolution-fluorinations, the corrosion bars were in contact with molten salt (550 to 585°C) for 550 hr. Of that time, 64 hr was dissolution time with anhydrous HF present, and 32 hr was fluorination time with elemental F_2 present. The INOR-8 vessel acquired an additional 50 hr of contact with molten salt, 19 hr with HF, and 4 hr of F_2 contact time. Maximum metal penetration of the bars, as determined by micrometer measurements, was 11 mils for INOR-8 and 6 mils for Alloy 79–4; metallographic examination of the lower tip of each bar showed no intergranular attack. As determined by Vidigage (ultrasonic) thickness measurements, the maximum vessel-wall penetration during the single-vessel series was 25 mils; including the corrosion due to the aqueous decontamination procedure, the maximum penetration was 30 mils. Corrosion rates are summarized in Table 2.10.

Table 2.10. Corrosion Rates During INOR-8 Single-Vessel Dissolution-Fluorination (Engineering Scale)

Penetration Rates	Molten Salt Time (mils/month)	F_2 Time (mils/hr)
Test bars (by micrometer)		
INOR-8	14.4	0.3
79-4	7.9	0.2
INOR-8 vessel (by Vidigage)		
No decontamination	30	0.7
After decontamination	43.2	0.8

A more detailed study of the single-vessel corrosion of nickel-base alloys was made on a laboratory scale. This work was done at the Battelle Memorial Institute under subcontract. The primary corrosion specimen was the test vessel, a length of 2-in. NPS, sched-40 INOR-8 pipe. The experiment consisted of ten cycles of alternating exposure to HF and F_2 in 37.5-37.5-25 mole % NaF-LiF-ZrF_4, with helium purges during transition periods. At the beginning of each hydrofluorination phase, Zircaloy-2 and Zircaloy-2–3% uranium alloy were added to the salt melt. During each hydrofluorination cycle, HF was added for 20 hr at 9.2 g/hr at 650°C followed by a 1-hr helium purge as the temperature was lowered to 500°C. Each fluorination phase consisted in adding fluorine at 200 ml/min (room temperature) for 2 hr at 500°C. The temperature was then returned to 650°C while the melt was again purged with helium for 1 hr.

In all cases, maximum penetration of the specimens contained in the vessel occurred at the interface. The usual intergranular attack occurred in the L-nickel specimens, with none present for Ni–5 Fe and Ni–1 Al, and only a trace for HyMu 80. Grain boundary modifications were noted in the INOR-8 specimens but not in the INOR-8 vessel wall. The INOR-8 grain boundary modifications were less severe than the L-nickel intergranular attack in that grains separated when the L-nickel specimens were bent but did not in the case of the INOR-8 specimens. A summary of penetration rates obtained from micrometer readings and metallography (appreciable differences are indicative of intergranular attack or grain boundary modifications) are shown in Table 2.11.

Tentative conclusions of this study thus far are that, based on 12 completely successful dissolutions of Zircaloy-2 or zirconium-uranium alloy simulated elements in recycled salt, salt recycle is a feasible and desirable method of operating the Fused Salt Volatility Process; corrosion of INOR-8 based on fluorine exposure alone during six engineering-scale single-vessel runs is apparently comparable to that of L-nickel in the pilot-plant fluorinator. HyMy 80 (Alloy 79-4), Ni–5 Fe, and Ni–1 Al, either in laboratory- or engineering-scale tests, show some possibility of providing corrosion rates lower than those for INOR-8 in single-vessel service. (Another series of engineering-scale single-vessel tests will be made with an Alloy 79-4 vessel plus test bars in order to obtain more corrosion data.) Thus, the single-vessel concept using INOR-8 is also regarded as feasible, assuming that the single vessel is approximately 1 in. thick and is replaced once in 600 operating days or 400 batches. Two approaches to the application in the pilot plant of the combined recycle and single-vessel concepts are shown in Fig. 2.8.

Table 2.11. Corrosion of Nickel-Base Alloys During Alternating Hydrofluorination of Zirconium-Uranium Alloy and Fluorination in 37.5-37.5-25 Mole % NaF-LiF-ZrF_4

	Maximum Penetration Rate According to:			
	Micrometry		Metallography	
	Total Cycle (mils/month)	F_2 Contact Time (mils/hr)	Total Cycle (mils/month)	F_2 Contact Time (mils/hr)
INOR-8	7.5	0.13	20[a]	0.33
HyMu 80	9.0	0.15	11	0.18
Ni–5 Fe	5.3	0.09		
Ni–1 Al	9.8	0.16		
L-nickel	11.5	0.19	24	0.4

[a]See text for discussion of significance.

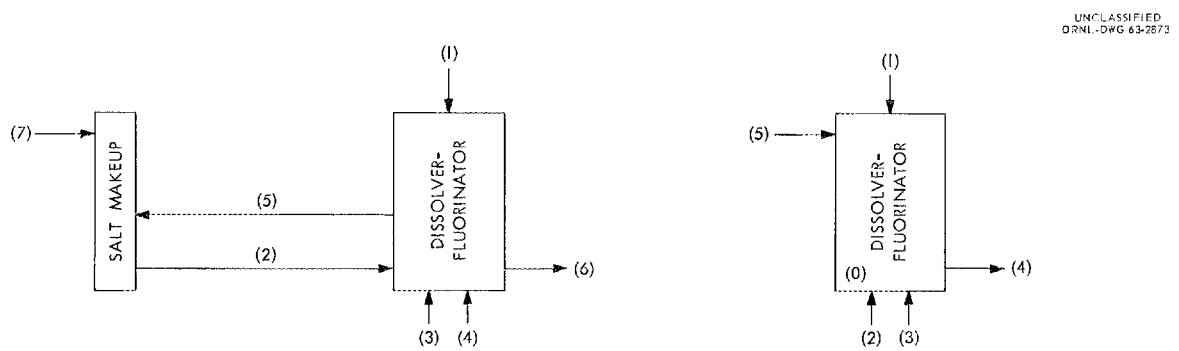

	WEIGHT (kg)		WEIGHT (kg)
(1) CHARGE WITH Zr-U ALLOY FUEL ELEMENTS	44.3	(0) BEGIN WITH INITIAL CHARGE OF 37.5-37.5-25.0 mole % NaF-LiF-ZrF_4	100.
(2) TRANSFER 37.5-37.5-25.0 mole % NaF-LiF-ZrF_4	100.	(1) CHARGE WITH Zr-U ALLOY FUEL ELEMENTS	44.3
(3) DISSOLVE ELEMENTS WITH HF		(2) DISSOLVE ELEMENTS WITH HF	
(4) REMOVE U BY FLUORINATION TO UF_6		(3) REMOVE U BY FLUORINATION TO UF_6	
(5) TRANSFER TO MAKE UP VESSEL 27.5-27.5-45.0 mole % NaF-LiF-ZrF_4	77.5	(4) TRANSFER TO WASTE 27.5-27.5-45.0 mole % NaF-LiF-ZrF_4	103.9
		REMAINING	77.5
(6) TRANSFER TO WASTE 27.5-27.5-45.0 mole % NaF-LiF-ZrF_4	103.9	(5) ADD 50.0-50.0 mole % NaF-LiF REPEAT FROM STEP (1)	22.5
(7) ADD 50.0-50.0 mole % NaF-LiF REPEAT FROM STEP (1)	22.5		

Fig. 2.8. Examples of the Application of the Single-Vessel and Salt-Recycle Concepts to Processing Zr-U Alloy Fuels in the Volatility Pilot Plant.

Mathematical Model for Sorption of Uranium Hexafluoride on Sodium Fluoride

The data on the sorption of UF_6 from a flowing stream of UF_6-N_2 by differential beds of ⅛-in. NaF pellets in the temperature range 29 to 100°C and UF_6 concentration range 0.57 to 8.5 mole % UF_6 were correlated by use of a mathematical model which took into account the effects of temperature, UF_6 concentration, gas flow rate, and pellet characteristics. The assumptions necessary for constructing the mathematical model include the following:

1. UF_6 transfer into the pellet occurs by molecular diffusion of UF_6 through an inert gas in the pore space of the pellet.
2. The point rate of reaction of gaseous UF_6 with unreacted NaF is:

$$\frac{dq}{dt} = ae^{-E/RT}e^{-bq}C ,$$

where

q = quantity of UF_6 reacted at a point,

t = time,

E = energy of activation for chemisorption,

R = gas constant,

T = absolute temperature,

a, b = constants,

C = concentration of unreacted UF_6 in the pore space of the pellet.

3. Variation of void fraction at a point in the pellet with UF_6 loading is of the form:

$$\epsilon = a(1 - q/q_{max}) ,$$

where

ϵ = void fraction,

q_{max} = maximum capacity of pellet material for sorption of UF_6,

a = constant.

4. Negligible radial temperature variation occurs in the pellet.

Calculational methods based on this model were developed for predicting simultaneous adsorption of volatile fluorides such as UF_6, MoF_6, etc., by fixed beds of NaF. A computer program based on the model and the differential bed data was written for the IBM 7090 digital computer and is suitable for design calculations on fixed-bed NaF adsorbers for UF_6 removal from a flowing gas stream below about 120°C. Equipment was designed and installed for obtaining rate and capacity data in the temperature range 75 to 300°C on the other volatile fluorides of interest; these data are necessary for the determination of constants within the mathematical model.

2.5 OTHER CORROSION STUDIES

Corrosion Resistance of Experimental Nickel-Base Alloys Under Hydrofluorinator Conditions

The search was continued for a more corrosion-resistant metal for the hydrofluorinator or a combination vessel (laboratory-scale studies made at Battelle Memorial Institute under subcontract). Based on the promising results reported last year[17] for Alloy 79-4 (79 Ni, 4 Mo, balance Fe – similar to HyMu 80), an attempt was made to determine whether its composition was optimum for at least the hydrofluorination conditions. Small heats of experimental alloys were prepared to check other Ni-Mo-Fe combinations and to explore the effects of vanadium and aluminum. To achieve accelerated test conditions, the alloys were first exposed to HF in the highly corrosive 50.5-37-12.5 mole % NaF-LiF-BeF_2 mixture at 650°C, with no zirconium dissolution. The most favorable alloys were then tested in 37.5-37.5-25 mole % NaF-LiF-ZrF_4 at 650°C again with no zirconium dissolution for a somewhat lesser degree of accelerated corrosion.

Alloy compositions, test conditions, and corrosion results for this series of experiments are summarized in Fig. 2.9. Figure 2.10 shows the relationship of the composition of Alloy 79-4 (HyMu 80) to the experimental Ni-Mo-Fe alloys. Test conditions apparently were not adequately standardized, as several inconsistencies resulted. Run 34, for unknown reasons, was exceptionally corrosive, and HyMu 80 fared very poorly in that run; otherwise HyMu 80 and its BMI experimental version, Alloy

[17] *Chem. Technol. Div. Ann. Progr. Rept. June 30, 1962*, ORNL-3314, pp 53–54.

UNCLASSIFIED
ORNL-DWG 63-2874

RUN NO.	ALLOY	ALLOY COMPOSITION							NOMINAL SALT COMPOSITION (mole %)				ADDITIONS	HF RATE av (g/hr)	TIME (hr)	MAXIMUM CORROSION RATE (mils/month)	REFERENCE[a]
		Ni	Mo	Fe	Cr	V	Al	OTHER	NaF	LiF	ZrF_4	BeF_2				40 80 120 160 200 240	
31[b]	INOR-8	71	16	5	7				50.5	37.0		12.5	ZIRCALOY-2	9.6	200		BMI-X-184
	HyMu 80	80	4	16													12/1/61
32	INOR-8	71	16	5	7				50.5	37.0		12.5		9.3	95		BMI-X-198
	HyMu 80	80	4	16													4/20/62
	NO. 1	90	10														
	NO. 2	85	10	5													
	NO. 15[c]	86					14									COMPLETELY SEVERED	
	NO. 23[c]	84					13	3 Si								COMPLETELY SEVERED	
33	INOR-8	71	16	5	7				50.5	37.0		12.5		10	95		BMI-X-198
	HyMu 80	80	4	16													4/20/62
	NO. 1	90	10														
	NO. 2	85	10	5													
	NO. 3	86	5	4		5											
	NO. 4	82		8		10											
34	INOR-8	71	16	5	7				50.5	37.0		12.5		10	70		BMI-X-213
	HyMu 80	80	4	16												TO 375	12/5/62
	NO. 2	85	10	5													
	NO. 31	85	2	13													
	NO. 32	80	2	18													
	NO. 33	80	15	5													
	NO. 34	75	10	15													
	NO. 35	75	5	20												TO 295	
	NO. 36	80	7.5	12.5													
	NO. 37[d]	80	4	16													
	NO. 38	85	5	10													
35	INOR-8	71	16	5	7				37.5	37.5	25.0			10	200		BMI-X-213
	HyMu 80	80	4	16													12/5/62
	NO. 2	85	10	5													
	NO. 4	82		8		10											
	NO. 32	80	2	18													
	NO. 37[d]	80	4	16													

[a] THESE REFERENCES BY P.D. MILLER AND CO-WORKERS OF BATTELLE MEMORIAL INSTITUTE.
[b] CHEMICAL TECHNOLOGY DIVISION ANNUAL PROGRESS REPORT, JUNE 30, 1962, ORNL-3314, p54.
[c] P.D. MILLER *et al.*, DEVELOPMENT OF CONTAINER MATERIAL FOR THE FUSED CHLORIDE-ELECTROLYTIC FUEL-RECOVERY PROCESS, BMI-1539, AUG 28, 1961.
[d] SIMILAR TO HyMu 80 AND ALLOY 79-4.

Fig. 2.9. Comparative Corrosion Resistance of INOR-8, HyMu 80, and Experimental Alloys to HF in Fluoride Melts. Runs made in 4-in.-ID Vessel at 650°C.

37, gave results comparable to, or slightly better than, INOR-8, as did Alloys 1 (Ni–10 Mo) and Alloy 2 (Ni–10 Mo–5 Fe). Alloy 15 (Ni–14 Al) and Alloy 25 (Ni–13 Al–3 Si) suffered catastrophic corrosion even though they gave favorable results in a high-temperature chloride system.[18] The addition of vanadium, as illustrated by Alloy 3 (Ni–5 Mo–4 Fe–5 V) and Alloy 4 (Ni–8 Fe–10 V), did not increase corrosion resistance.

[18] P. D. Miller *et al.*, *Development of Container Material for the Fused Chloride–Electrolytic Fuel–Recovery Process*, BMI-1539 (Aug. 28, 1961).

Comparative Corrosivity of $NaF-LiF-BeF_2$ at 650°C and $NaF-LiF-BeF_2-ZrF_4$ at 500°C During Hydrofluorination

As previously reported[19] 50.5-37.0-12.5 mole % $NaF-LiF-BeF_2$ was considered as a possible melt for hydrofluorination of zirconium-base fuels at 650°C. However, this proved to be an exceptionally corrosive composition. A study was then

[19] P. D. Miller *et al.*, *Corrosion of the ORNL VPP Mark III Fluorinator and Group V Rods*, BMI-X-218 (Feb. 15, 1963).

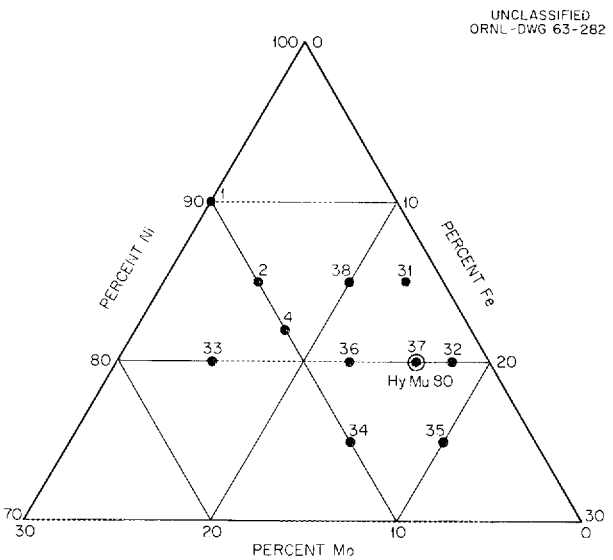

Fig. 2.10. Relationship of HyMu 80 (Alloy 79-4) Composition to Experimental Alloys Prepared for Hydrofluorination Corrosion Study.

undertaken to determine the corrosivity and zirconium dissolution rates for the same melt plus sufficient ZrF_4 to allow its use at 500°C (laboratory-scale study performed at Battelle Memorial Institute under subcontract). Specimens of INOR-8, HyMu 80, L-Nickel, BMI Alloy 2 (Ni–10 Mo–5 Fe) and Ni–5 Fe were exposed to 36.9-27.0-27.0-9.1 mole % $NaF-LiF-ZrF_4-BeF_2$ for 200 hr at 500°C. An HF sparge of about 10 g/hr was used in the 4-in.-ID BMI hydrofluorination test vessel. Zircaloy-2 was added periodically, and the specimens were raised to maintain a constant interface position.

The melt was only slightly corrosive, with all weight-loss corrosion values being less than 0.6 mil/month.[20] Only L-nickel and Ni–5 Fe showed appreciable intergranular attack. INCO-41 weld metal in nickel specimens showed slight intergranular attack, with virtually none apparent for INCO-61 weld metal in nickel. Initial Zircaloy-2 dissolution rates were significantly lower than for the $NaF-LiF-BeF_2$ melt. Operational problems prevented an accurate measurement of the total H_2 evolved and recovery of any undissolved metal as required for confirmation of overall dissolution rates. Table 2.12 summarizes differences in INOR-8 corrosion and initial Zircaloy-2 dissolution rates for the applicable BMI experiments.

Present plans are to repeat this experiment to confirm the low corrosion rates and obtain more meaningful Zircaloy-2 dissolution-rate data.

Table 2.12. Corrosion and Zircaloy-2 Dissolution Rates for $NaF-LiF-BeF_2$ at 650°C and for $NaF-LiF-BeF_2-ZrF_4$ at 500°C During Hydrofluorination

BMI run No.[a]	31	32	34	37
Salt composition, nominal, mole %	*b*	*b*	*b*	*c*
Temperature, °C	650	650	650	500
Maximum INOR-8 corrosion rate, mils/month	110	107	115	0.2
Initial Zircaloy-2 dissolution rate, mg cm^{-2} hr^{-1}	24			7

[a]Zircaloy-2 was only dissolved during runs 31 and 37.
[b]50.5-37.0-12.5 mole % $NaF-LiF-BeF_2$.
[c]36.9-27.0-27.0-9.1 mole % $NaF-LiF-ZrF_4-BeF_2$.

2.6 PROCESSING OF URANIUM-ALUMINUM ALLOY FUEL

This section is reported in ORNL-3452, suppl 1.

[20]P. D. Miller *et al.*, *Corrosion Resistance of Nickel-Base Alloys in a $NaF-LiF-BeF_2-ZrF_4$ Salt Mixture Under Hydrofluorinator Conditions with Zircaloy-2 Dissolving at 500°C*, BMI-X-227 (Apr. 25, 1963).

3. Waste Treatment and Disposal

This program is concerned with the development and demonstration (on a pilot-plant scale) of processes for the treatment and final disposal of both high- and low-level radioactive wastes resulting from power reactor operations and fuel processing. The effective, economic management of radioactive effluents is a prerequisite to the natural growth of a nuclear power industry.

Emphasis continued to be placed on high- and low-activity liquid wastes. Engineering studies of the pot-calcination process for converting high-activity wastes to solids were devoted to gathering data and operating experience needed in the design of a pilot plant to be constructed at Hanford. Improvements were made in the control system and de-entrainment devices for a continuous evaporator closely coupled to the pot. A rack was built for simultaneous testing (under process conditions) of pumps for feeding the calciner. Studies of the effect of fission product heat in the calciner showed that carefully programmed operations will be required, and liaison was maintained with Hanford on the pilot-plant design being carried out there. A program for testing the mechanical equipment and the manipulations required for the process was successfully completed. To take advantage of the versatility inherent in this process, work included (1) the development of mixes and procedures for fixing the waste fission products in low-solubility glassy solids, (2) corrosion studies, (3) measurement of thermal conductivities of solidified waste products, and (4) preparation of equipment to be installed in a hot cell for tests on actual wastes.

In the area of low-activity waste treatment, processes based on scavenging, ion exchange, and foam separation are under study for decontaminating very dilute salt solutions such as cooling water and canal water. A process utilizing scavenging precipitation and ion exchange was tested in a 600-gph pilot plant and shown to be capable of decontaminating 750,000 gal/day of ORNL process waste to an activity level less than 3% of the maximum permissible concentration (MPC) for water (for continuous occupational exposure) for a cost of 75 to 80¢ per 1000 gal of waste. Laboratory studies were devoted to the problem of phosphate interference with the precipitation-scavenging step. The pilot plant was modified by the installation of a new clarifier, an alumina column, and a continuous ion exchange column for advanced studies. Foam separation studies in the laboratory and in engineering-scale equipment yielded encouraging results and will be extended to tests in the pilot plant with ORNL waste during the ensuing year.

An economic and safety evaluation of alternative methods of waste management was undertaken jointly with the Health Physics Division. During the past year, studies of the effect of fission product removal on the costs of waste management and the cost of the interim storage of solidified high-activity wastes were completed.

3.1. POT CALCINATION OF HIGH-LEVEL WASTE

The pot-calcination process (Fig. 3.1) involves introducing the waste into an evaporator, where it is concentrated and where nitric acid is steam stripped by the addition of water, and then feeding this concentrated solution into a calciner pot (with a constant liquid level and heated by a furnace), where the waste is denitrated, brought to a solid cake, and calcined in place.[1] The pot of solids is then disconnected from the system, sealed, and used as the container for the waste during final storage at a suitable site. Studies so far indicate that special salt mines may be most suitable.

[1] *Chem. Technol. Div. Ann. Progr. Rept. Sept. 24, 1962*, ORNL-3314, pp 78–85.

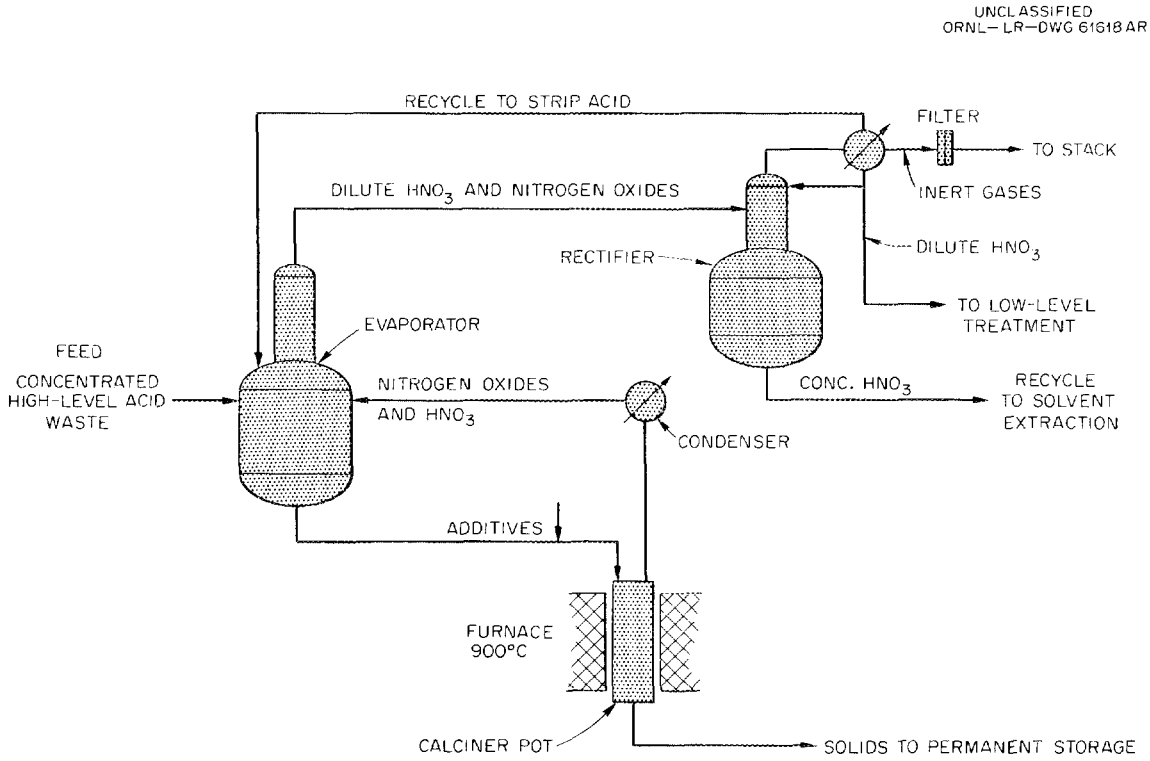

Fig. 3.1. Flowsheet for Converting High-Level Wastes to Solids.

An important condition placed on the evaporator is that the acidity (nitric acid) not exceed a given value (depending on the type of waste) to avoid the oxidation of ruthenium to a volatile form. For this reason water is added. The evaporation is the primary decontamination step in the process; the 1.6 *M* HNO_3 vapors from it are sent to a distillation tower, where water is separated from entrained radioactivity and the nitric acid. The water that is not recycled for process use can be released after, perhaps, ion exchange treatment, and the nitric acid product can be reused in the fuel reprocessing plant.

Large amounts of gases are neither introduced or produced, and the off-gas volume from the process is very low, 1 or 2 ft^3 per liter of feed, primarily from inleakage and instrument probes.

Experimental work has been carried out with synthetic TBP-25, Darex, and Purex wastes (Table 3.1). Since the process pilot plant at Hanford will use waste produced there as feed material, a second Purex waste, expected to be produced there in 1965, has been included in experimental studies. This waste (FTW-65) is different from current Purex 1WW in that it will have been treated with formaldehyde to reduce the nitric acid concentration, will be more dilute in dissolved salts, and will contain lesser amounts of such major constituents as iron, sulfate, and aluminum. Important minor constituents (silicate, fluoride, chloride, and phosphate) may be present.

During calcination, the solids are brought to 900°C, causing the nitrate wastes to revert to refractory oxides containing only traces of nitrate. When mercury salts are present, the mercury volatilizes, but sulfate is retained in the cake by the addition of calcium nitrate to the pot in proportion with the feed to form calcium sulfate, which stays in the cake almost quantitatively. It is intended to retain all the fission products in the cake, but there is some entrainment and some volatilization of ruthenium, which is caught in the evaporator. The steady-state concentration of ruthenium in the evaporator is therefore slightly higher than that in the feed. The maximum calcination temperature, 900°C, was selected because of the properties of

Table 3.1. Compositions and Characteristics of Simulated High-Level Wastes

Constituent	Waste Compositions (moles/liter)			
	TBP-25	Darex	Purex 1WW	Purex FTW-65
Al^{3+}	1.72		0.1	0.05
Fe^{3+}		1.25	0.5	0.10
Cr^{3+}		0.38	0.01	0.02
Ni^{2+}		0.18	0.01	0.01
Hg^{2+}	0.02			0--0.0035
Mn^{2+}		0.04		
Na^{+}	0.1		0.6	0.3
NH_4^{+}	0.05			
H^{+}	1.26	2.0	5.6	0.5
Ru	0.002	0.002	0.002	0.002
SO_4^{2-}			1.0	0.15
PO_4^{3-}				0.005
SiO_3^{2-}				0.01
F^{-}				0.0005[a]
Cl^{-}		0.001		
NO_3^{-}	Bal	Bal	Bal	Bal
Density (g/ml)	1.32	1.33	1.30	
Gallons/ton U	106[b]	24[b]	40	82

[a]Previously listed as 0.02 *M*.
[b]Gallons of waste per kg of U^{235} processed.

stainless steel and because adequate nitrate removal was obtained. The same temperature, therefore, was adopted as the maximum allowable in the calcined cake during storage.

Engineering Studies

The calciner pots used for development work were 8-in.-IPS, generally 88 in. from the bottom to the neck, with the lower 78 in. in an electrical resistance furnace. The pots operated with a 76-in. liquid level (Fig. 3.2). The pots were made of type 304L stainless steel and had wall thicknesses of 100 and 340 mils. Various pot closures were tested, and the one selected for the pilot plant is a modified Grayloc connector that will simultaneously seal two feed lines and an off-gas line. Two vertical thermocouple wells are provided in the pots, one along the axis of the vessel and the other positioned 1 in. from the wall. Thermocouples extend inside the wells to the center of each of the six furnace zones, and six additional thermocouples are tacked to the outside surface of the pots at the same elevations.

Studies of Continuous and Batch Evaporation. — Two alternatives were tested in the engineering development of the pot-calcination process: batch and continuous evaporation. In the batch operation (Fig. 3.3), the tanks and evaporator are large enough to accommodate enough waste to fill one pot. The pot is fed from a tank of concentrated waste either by gravity or by pumping. Concurrently, the vapors from the pot are returned to an evaporator filled with the waste for the next batch, which is undergoing concentration and acid removal. The continuous process uses a smaller evaporator and returns the condensed pot vapors to the evaporator, from which the feed to the pot is pumped. This evaporator is fed with raw waste and continuously removes the nitrate from the system (Fig. 3.4). The batch flowsheet offers the advantage of simplicity of control and operation but has disadvantages due to larger equipment and larger holdup. The continuous process has the advantages of smaller holdup, smaller equipment, and more reasonable application to a plant with several pot lines fed from the single evaporator. The control of the continuous evaporator is more complex, however, since the flowsheet is not truly continuous in that the pots are filled batchwise, and the evaporator must follow the transient filling of the pot.

During a continuous evaporator run, the acidity of the evaporator vapor (measured by an electrical conductivity probe in the condensate) is controlled by the addition of water; the density, or solids concentration, is controlled by the boilup rate; and the liquid level is controlled by the waste feed rate under the varying loads of product withdrawal and pot condensate return. The liquid level in the pot is maintained by use of a temperature probe that correlates the high wall temperature and the cooling effect of the liquid (Fig. 3.5). A 0 to 100% signal is obtained over a liquid-level variation of 8 in. Because this controller worked over a flow rate range in which the highest rate was more than 10 times the lowest, a logarithmic

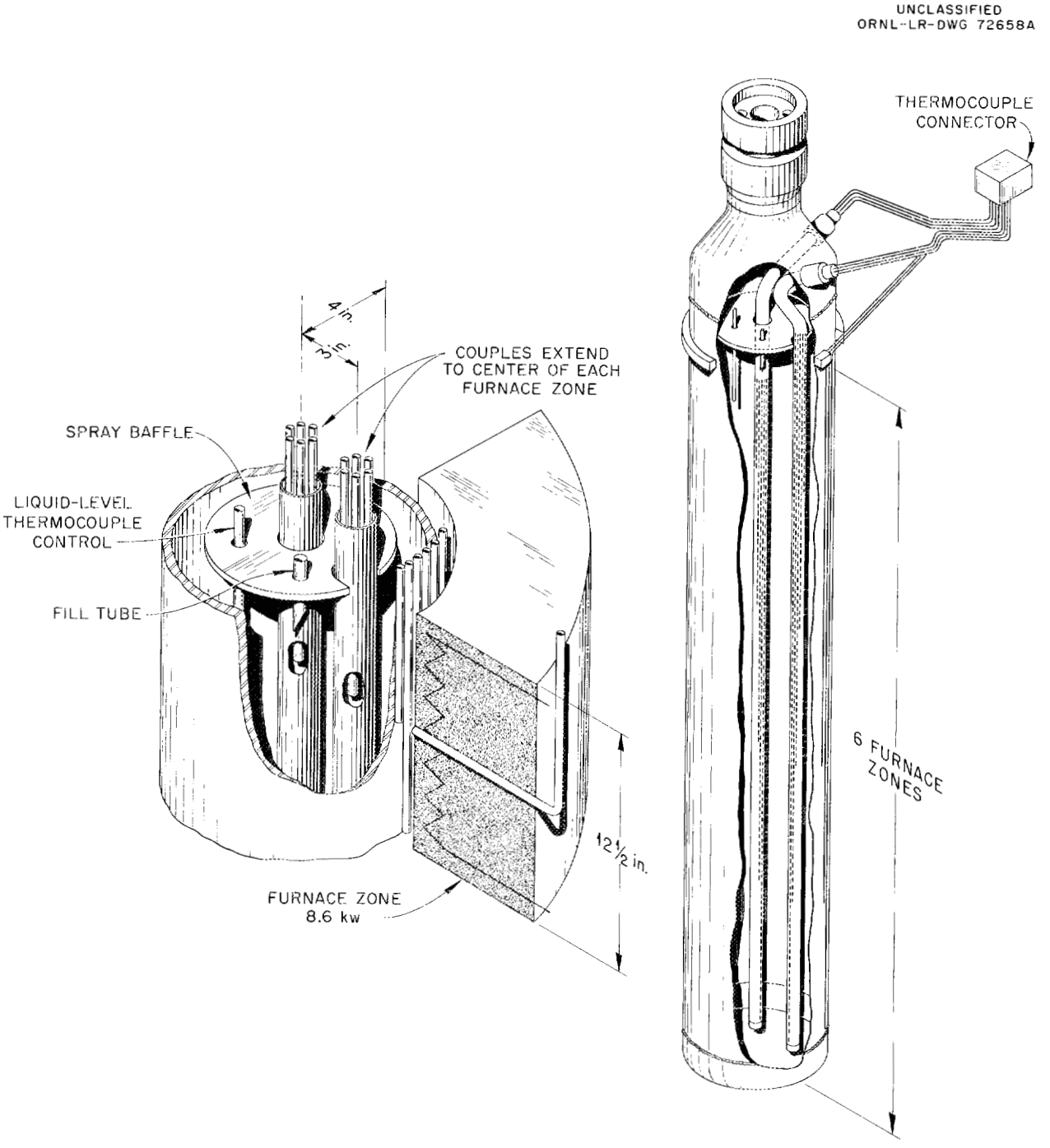

Fig. 3.2. Waste Calciner Thermocouple Detail.

valve was used with a 200% proportional band and a 5-hr reset time on the controller. Intermittent fouling of the control valve with the concentrated solution caused some fluctuation in control, but this was eliminated by using an electromagnetic flowmeter in the calciner feed line and cascading the control. In this case, the signal from the calciner sets the feed rate, which is measured and met by another controller operating the feed valve in a short-response-time loop. The pot behaves as though it always has foam at the liquid level. Sudden changes in the feed rate can cause the buildup or the collapse of foam to give a momentary signal change in the wrong direction, resulting in an upset, but this can be avoided by using warm feed to the pot and a large proportional band on the controller.

Correlations for Pot-Filling Time.[2] – The recognition of the consistent occurrence of circular stratification of the calcined waste cakes suggested the mathematical treatment of the rate by a radial-deposition model. The equations that were derived for various cases are as follows:

Case 1: No internal heat generation,

$$t = \frac{\lambda\beta R^2}{4k(T_w - T_b)}\left[1 + \left(\frac{r_0}{R}\right)^2 \ln\left(\frac{r_0}{R}\right)^2 - \left(\frac{r_0}{R}\right)^2\right].$$

[2]M. E. Whatley, C. W. Hancher, and J. C. Suddath, *Engineering Development of Nuclear Waste Pot Calcination*, ORNL TM-549.

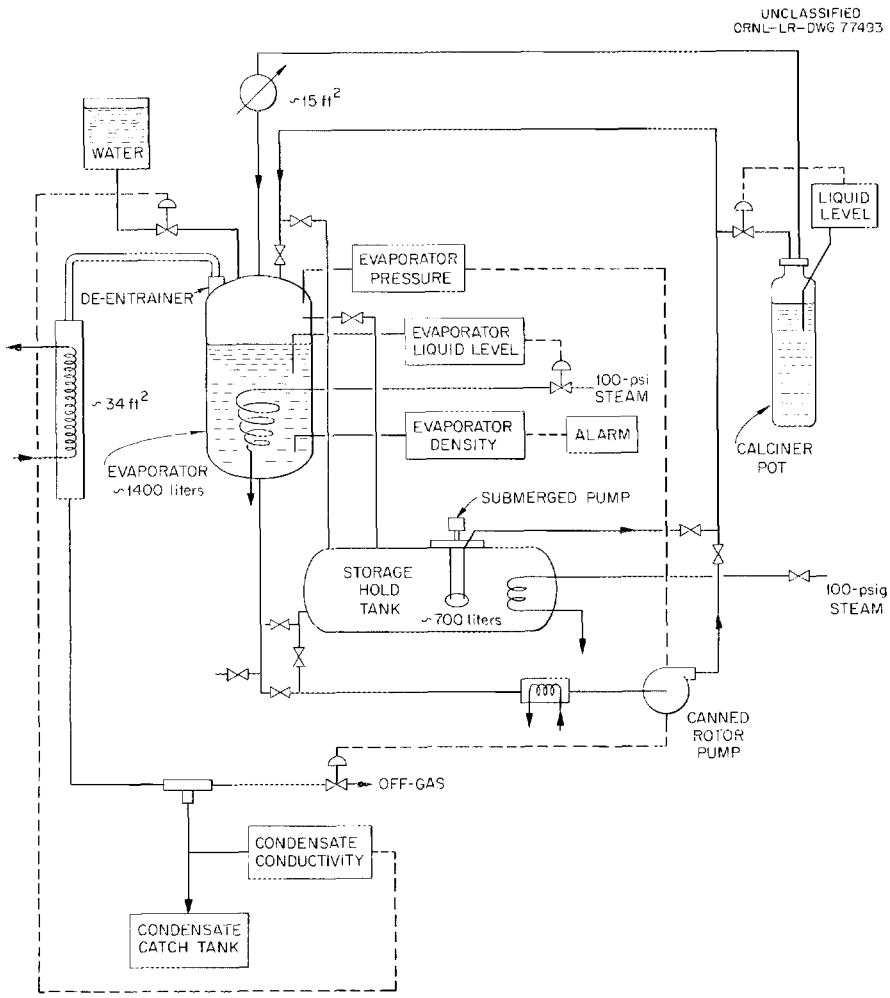

Fig. 3.3. Flowsheet for Engineering Batch Evaporation Tests for Pot Calcination.

Case 2: With internal heat generation; wall temperature constant,

$$t = \frac{\lambda\beta}{Q} \ln \times \frac{T_w - T_b + \frac{QR^2}{4k}\left[1 + \left(\frac{r_0}{R}\right)^2 \ln\left(\frac{r_0}{R}\right)^2 - \left(\frac{r_0}{R}\right)^2\right]}{T_w - T_b} .$$

Case 3: With internal heat generation; constant temperature T_m at $dT/dr = 0$,

$$\frac{dr_0}{dt} = \frac{Q}{2\beta\lambda}\left[\frac{r_m^{\,2} - r_0^{\,2}}{r_0}\right] ,$$

$$T_m - T_b - \frac{Qr_m^{\,2}}{4k}\left[1 - \left(\frac{r_0}{r_m}\right)^2 + \ln\left(\frac{r_0}{r_m}\right)^2\right] = 0 ,$$

$$T_w = T_b - \frac{QR^2}{4k}\left[1 + \left(\frac{r_m}{R}\right)^2 \ln\left(\frac{r_0}{R}\right)^2 - \left(\frac{r_0}{R}\right)^2\right] .$$

Since all nonradioactive engineering work must be done in the absence of internal heat generation, only case 1 has been validated experimentally. For mathematical convenience it expresses time as a function of the radius to the liquid-solid interface r_0. The parameters are: R (pot radius); λ (latent heat of vaporization per liter of feed); β (ratio of the feed volume to cake volume); k

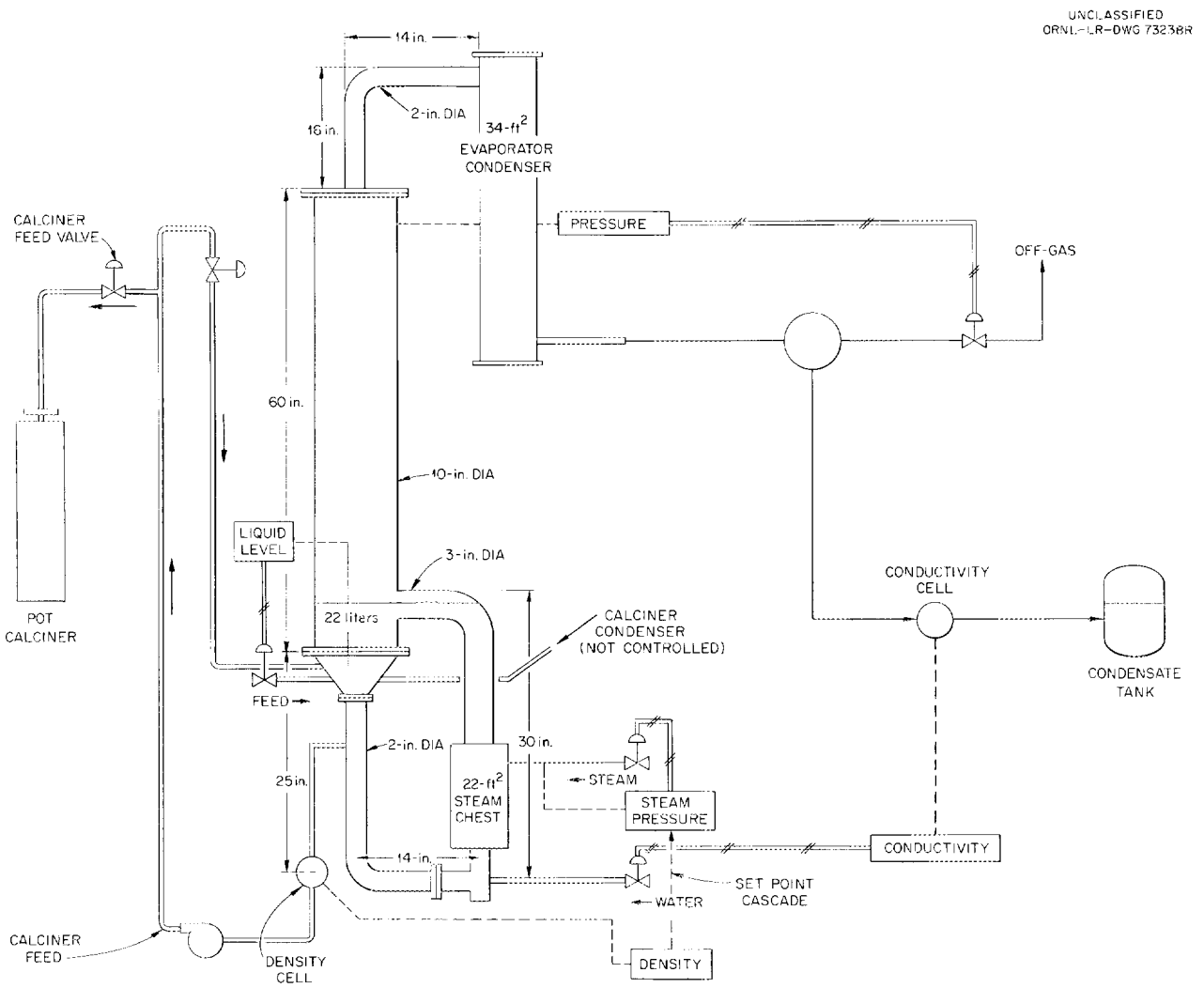

Fig. 3.4. Flowsheet for Engineering Continuous Evaporation Tests for Pot Calcination.

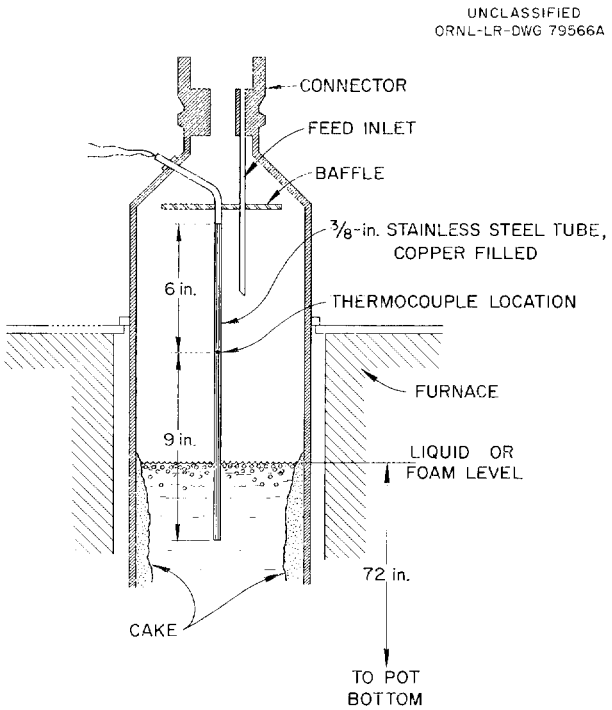

Fig. 3.5. Calciner Liquid-Level Sensing System.

(effective thermal conductivity of the cake); and T_w and T_b (wall temperature and boiling temperature respectively). The assumptions involved in this equation are: (1) that the parameters are essentially constant during the run, (2) that the cake deposits radially and uniformly, and (3) that the rate of change of the liquid-solid boundary is small compared with the temperature transients within the cake. Since these assumptions are also required for the equations for deposition with internal heat generation, it was felt that validation of the equation would lend credence to the equations for the internal-heat-generation cases. In these studies, the group in the brackets, termed the "F factor," was plotted against time to evaluate the filling-rate coefficient, which embodies all parameters.

Internal heat generation is both an asset and a detriment. Since this kind of heat source is close to the liquid-solid interface (where it is needed), filling times will be decreased by 10 to 20%, and calcination times will be reduced to a matter of 2 or 3 hr. Internal heat does create the problem of avoiding excessive temperatures (>900°C) during calcination and storage. Consequently, a pot radius must be chosen such that during storage the center-line temperature will be the maximum allowable (i.e., less than the maximum calcination temperature), while the temperature of the wall remains near ambient. Obviously, if the pots were allowed to calcine with the wall at 900°C, the center-line temperature would very much exceed this. In most cases it will be necessary to decrease the wall temperature before the end of the filling period.

The equation for case 2 is the feeding-rate equation, using a constant wall temperature as a boundary condition. The heat generation rate per unit volume is Q. An alternative boundary condition was imposed in case 3. At the time that the heat flux at the wall goes to zero, that is, when the temperature gradient at the wall becomes zero, the wall temperature is programmed so that the maximum temperature in the cake is maintained at a constant value and the location of this maximum, r_m, moves toward the center of the pot. It was not possible to get an analytical solution for this case. The differential equation for r_0 involves the location of the maximum temperature, r_m, which is given by the implicit relation of r_0 and r_m involving the two known temperatures, the maximum temperature and the boiling temperature. The wall temperature, which must be programmed, is given by the last equation.

Figure 3.6 is a plot of the F factor vs time for run R-70. The ratio r_0/R was actually computed from the feed, using the ratio of solids fed to the solids necessary to fill the pot. The adequacy of this correlation is the basis for confidence in the radial-deposition model. The slope of this line is the filling-rate coefficient, which will later be presented as a characteristic index to the overall rate for the run. The reciprocal of the filling rate coefficient is the theoretical time required to completely fill the pot but is not useful because of the low rates toward the end of the run in the absence of internal heat generation. Further, at half the theoretical filling time, when the F factor equals 1/2, the pot is about 81% full. Figure 3.7 shows calculated temperature profiles in the cake during filling, with and without internal heat generation. The steeper temperature gradients toward the end of the run for the internal-heat-generation case give rise to the higher rates. The internal temperature in this case gets higher than the maximum wall temperature, a condition which is presently thought intolerable.

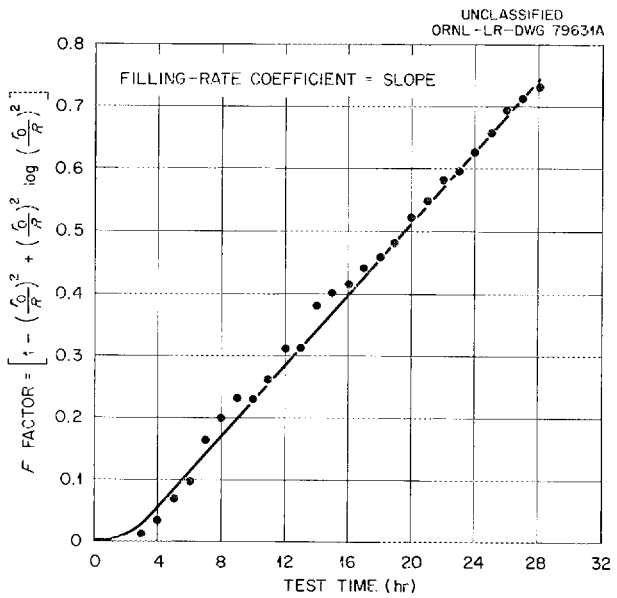

Fig. 3.6. *F* **Factor Test vs Time for Purex FTW-65 Run R-70.**

Figure 3.8 shows the progression of the temperature profile in the case for an ideal calcination run with internal heat generation. Early in the run the deposition rate is limited by the heat output from the furnace, and the wall temperature increases as the cake deposits. Then the wall temperature is held constant as the cake continues to build. At the point where the heat flux at the wall goes to zero, the temperature of the wall is decreased. The maximum temperature then moves away from the wall. At some predetermined degree of fullness, probably dictated by vapor velocity in the decreasing center zone, the feed is turned off and the now dry inner boundary begins to heat. The location of the maximum temperature continues to move toward the center, while the wall temperature must be further decreased. At the end of the run the wall temperature should be not much higher than the temperature intended for storage, and the center temperature should be at the maximum.

Practical calcination operating conditions will, of course, require reasonably wide control limits. By relaxing the requirement of maximum temperature, there are methods of using this prediction to program wall temperature safely. The simplest of these, which allows only about a 200°F rise above the intended maximum, uses a linear approximation for the wall-temperature program (Fig. 3.9). This program involves heating the pot wall at 1650°F for 0.8 hr and then cooling to the required equilibrium wall temperature in 1.1 hr, assuming a thermal conductivity for the cake of 0.2 Btu hr^{-1} ft^{-1} $°F^{-1}$ and an internal heat generation rate of 4000 Btu hr^{-1} ft^{-3}. The program was determined for the situation where the calcination pots are filled until the slope of the temperature gradient at the pot wall is zero, indicating that no heat is being added or removed at that point. In Fig. 3.9, T_0 is the wall temperature, T_5 is that at the surface of an internal cavity 1 in. in diameter along the axis, and the other temperatures are at equally intermediate points on the radius of an 8-in.-diam pot.

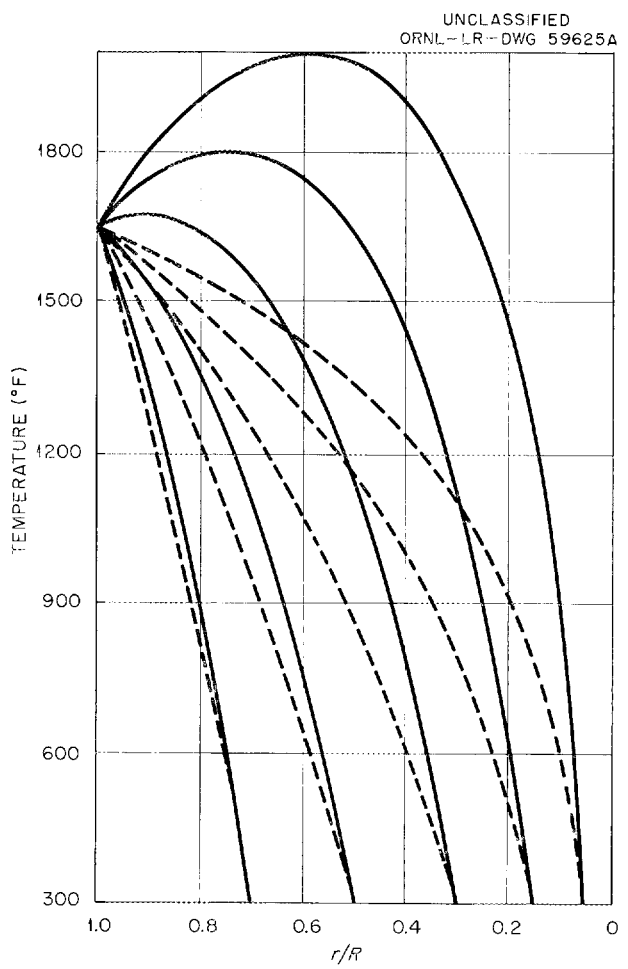

Fig. 3.7. Temperature Profiles in Deposited Purex Solid Waste in a 12-in.-diam Vessel. Solid line, Q = 5000 Btu hr^{-1} ft^{-3}; **dashed line,** $Q = 0$.

UNCLASSIFIED
ORNL-LR-DWG 79746A

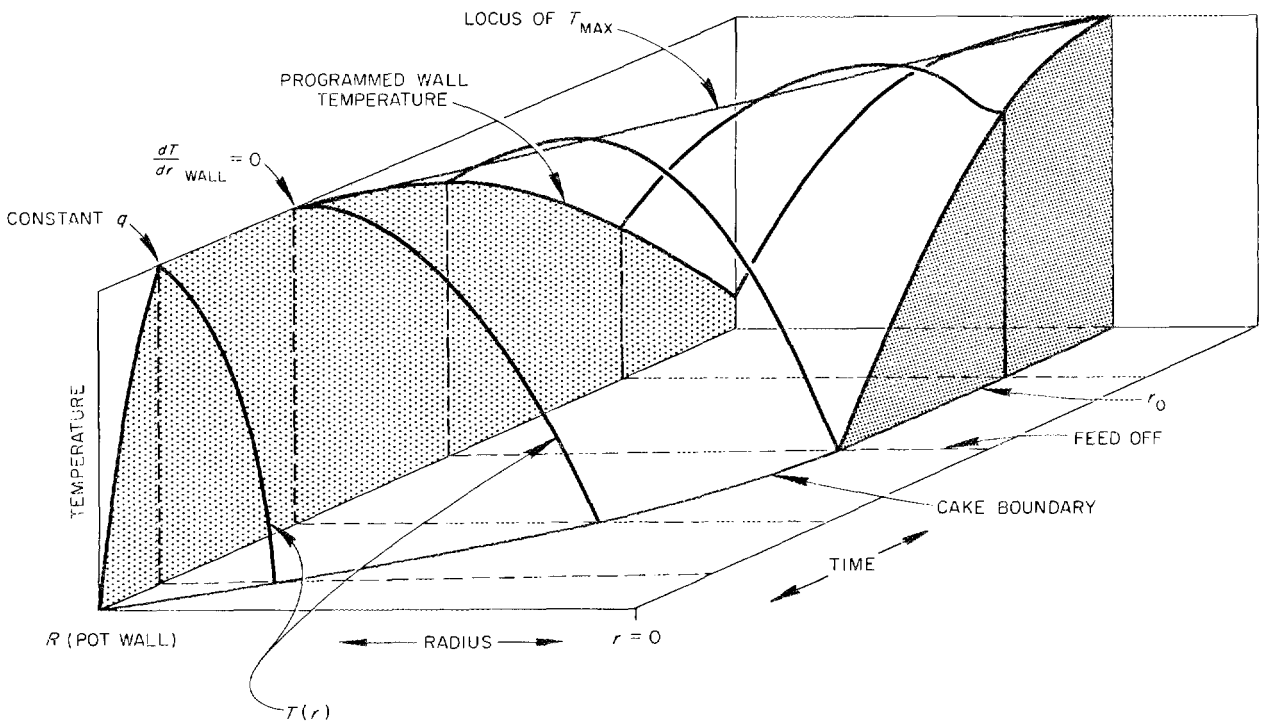

Fig. 3.8. Cake Temperature During an Ideal Pot-Calcination Run with Internal Heat Generation.

UNCLASSIFIED
ORNL-LR-DWG 69388A

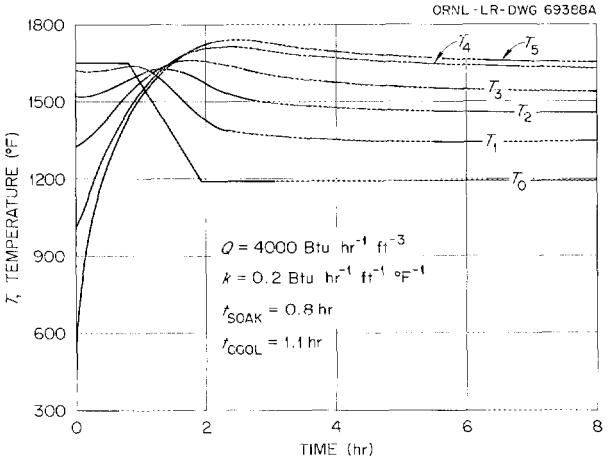

Fig. 3.9. Calcination Cooling Program for 8-in.-diam Pot.

Pot-Calcination Tests. – During the past year, 11 tests, numbers 65 through 75, were carried out (Table 3.2). Five of the tests were made with TBP-25 waste and six with Purex (FTW-65) wastes. In some runs a small amount of the solvent degradation products, mono- and dibutylphosphate (MBP and DBP), was added to the feed. In the 11 tests it was shown that feeding by either gravity or pump would be acceptable for plant application. The organic additives promoted foaming, but not to a detrimental extent.

In the TBP-25 calcination, the variation in feed volume to the pot is primarily an operational variable and could have been made more consistent. The water-to-feed volume ratio, the amount of water necessary to strip the nitric acid from the evaporator, should be about 2.3. Higher values indicate an unnecessarily low setpoint for the acid in the evaporator overhead. The feed to the

Table 3.2. Summary of Engineering-Scale Tests

Run No.	Feed Type	Feed Volume (liters)	Water to Feed Volume Ratio	Calciner Feed Al^{3+} or Fe^{3+} Concentration (g/liter)	Average System Feed Rate (liters/hr)	Filling Rate Coefficient[a] (hr^{-1})	Calcination Time (hr)	Nitrate Remaining in Solids (wt %)	Solid Bulk Density (g/cm^3)
65	TBP-25	476	3.1	115.5	20.6	0.034	9	0.19 to 0.06	0.68
66	TBP-25	449	6.4	55.0	20.4	0.037	17	0.04	0.65
67	TBP-25	391	2.8	45.1	17.0	0.003	20	0.007	0.50
68[b]	TBP-25	343	2.6	47.5	26.4	0.056	20	0.019	0.54
69[b]	TBP-25	469	5.4	45.0	15.6	0.025	17	0.111	0.64
70	FTW-65	1818	0.75	46.9	67.3	0.029	28	0.04 to 0.01	1.25
71	FTW-65	1843	0.57	34.6	68.3	0.028	36	0.02 to 0.01	1.30
72	FTW-65	1912	0.10	26.7	40.0	0.023	24	0.026 to 0.004	1.33
73[c]	FTW-65	1838	0.20	40.2	31.1	0.017	9	0.103 to 0.006	1.23
74[c]	FTW-65	1968	0.34	49.2	53.0	0.022	23	0.016 to 0.015	1.30
75[c]	FTW-65	1793	0.72	33.8	26.0	0.012	11	0.01	1.26

[a]Equal to $[4k(T_w - T_b)]/\lambda\beta R^2$.
[b]Gravity feed.
[c]1 ml of 50% MBP–50% DBP added per 200 liters of feed.

pot is only slightly more concentrated than the original waste feed to the evaporator. The feed to the evaporator contains about 23 g of aluminum per liter and the feed to the pot contains 45 to 55 g of aluminum per liter. A successful run was made in which the calciner feed contained 115 g of aluminum per liter, but this is assumed to be impractical since the solution will crystallize at room temperature. The average system feed rate was 20 liters/hr, with a maximum of 26 and a minimum of 17. The filling-rate coefficients were determined from plots of the F factor from the radial-deposition equations against time. The only term in this coefficient not computable through other data is the effective thermal conductivity of the cake. The term β, which is the ratio of calciner feed volume to cake volume, is proportionally related to the aluminum concentration in the calciner feed and was nearly constant.

The nitrate concentration remaining in the solids depends on the calcination time. At 20 hr of calcination the residual nitrate was reduced to acceptably low levels. In all cases the low numbers are characteristic of the bulk of the cake, and the high numbers represent the center top part of the calciner product. When fission product heat is available, there should be no problem in removing nitrate to any desired level.

Bulk densities of about 0.62 g/cm^3 were achieved with TBP-25 waste. The bulk density is defined as the ratio of the weight of solids in the pot to the volume of the pot up to the liquid-level point, including the void that occurs in the center.

The behavior of mercury during tests with TBP-25 waste was of interest since mercury compounds are unstable at 900°C, and volatilized mercury must be removed from the system. A trap for removing mercury compounds from the calciner off-gas stream was installed but was only partially effective. The calciner off-gas line was heated to 400 to 500°C, while the trap was maintained at about 150°C for condensation of mercury compounds. Subsequently, the solids deposited in the trap were dissolved with nitric acid and removed from the system. On the average the trap contained 19% of the mercury, the evaporator about

40%, and the solids in the calciner about 13%. The remainder deposited on the process piping and equipment throughout the system. A more satisfactory method of handling mercury is necessary, but none has been developed.

In the tests with FTW-65 waste, the large feed volumes reflect the diluteness of the feed. The initial iron concentration was about 12 g/liter, so the evaporator concentrated the feed three- or fourfold, and the water-to-feed volume ratio was less than 1. The filling-rate coefficients were uniform, showing two groups: those without organic in the feed and those with it. The presence of organic halved the filling-rate coefficient. The nitrate in the residual solids was reduced to an insignificant level by adequate calcination time, and the solid density was about 1.3 g/cm^3.

Mercury compounds in FTW-65 waste were again a problem, and the mercury trap was employed with little success. In three experiments, condensate was collected in a separate tank near the end of the calcination period, when the temperature of the cake reached about 600°C. Since most of the mercury is volatilized during this final stage of heating, it was expected to condense with the last 10 to 30 liters of condensate. However, only 8, 28, and 54% of the mercury was recovered.

In tests with FTW-65 waste containing 0.005 *M* F^-, severe corrosion of the calciner pot was encountered even in the presence of calcium added (as the nitrate) to reduce sulfate volatilization. Little corrosion was observed in the absence of fluoride. The calcium-addition procedure was modified to ensure precise continuous addition and hence a uniform action to retain sulfate and reduce corrosion by fluoride. The maximum fluoride concentration expected is 0.005 *M* (see Table 3.1), and satisfactory corrosion rates are expected at this concentration.

Run 72 contained 0.087 g of natural ruthenium per liter. As predicted from laboratory work, the ruthenium concentration in the calciner condensate increased steadily to a maximum when the last water and nitrate were evolved. The evaporator condensate generally contained 1/5000 of the evaporator concentration, and the overall decontamination factor was about 3000.

Evaporator Impingement Sieve-Plate De-entrainer. – A stainless steel Yorkmesh de-entrainer in the 10-in.-diam continuous evaporator corroded rapidly in the presence of the HNO_3-H_2SO_4 vapors from boiling Purex waste. Replacement of the Yorkmesh with an impingement de-entrainer reduced entrainment from up to 7 ppm to below 3 (Table 3.3). The impingement de-entrainer designed for the continuous evaporator was based on the work of Schlea and Walsh.[3] Of the two impingement plates provided, the first removes the bulk of the entrained liquid at impingement velocities up to 38 fps. The second plate is designed to remove particles of

[3] C. S. Schlea and J. D. Walsh, *De-entrainment in Evaporators*, paper presented at A.I.Ch.E. 42nd National Meeting, Feb. 21–24, 1960.

Table 3.3. Efficiency of De-entrainers

Run No.	De-entrainer	Iron Concentration in Evaporator (g/liter)	Maximum Iron Concentration in Condensate (ppm)	Maximum Boilup Rate (lb/hr)
70	Yorkmesh	29–64	4	490
71	Impingement plates	30–39	3	390
72	Impingement plates	10–48	1.6	280
73	Impingement and sieve plates	23–63	0.65	370
74	Impingement and sieve plates	26–56	0.50	350

diameters ranging from 3 to 10 μ at impingement velocities up to 90 fps. At higher velocities, reentrainment will occur. The maximum design vapor rate was 500 lb/hr.

The minimum decontamination factor for the impingement plates, based on 3 ppm Fe in the vapor, was about 1×10^4. To increase the decontamination factor tenfold, a sieve plate was installed above the impingement plates, starting with run 73 (Fig. 3.10). The plate has 504 holes (1/8 in. diam), giving a 4.65% free area based on the cross-sectional area of the vapor bonnet. Reflux is added to the plate at a rate of 50 cm^3/min and discharged over the weir in the center of the plate. It drains to the evaporator liquid through a dip leg and is vaporized along with the evaporator overhead. The plate liquid level is maintained at 1 in. by the weir. Table 3.3 indicates that the entrainment during runs 73 and 74 was reduced to a maximum of 0.65 ppm, which corresponds to a minimum decontamination factor of 7×10^4. However, since the average entrainment was about 0.4 ppm for the two runs, the average decontamination factor was about 1×10^5.

Pump-Test Loop. — Four pumps for the pot-calcination pilot plant are being tested simultaneously in a pump-test loop under simulated

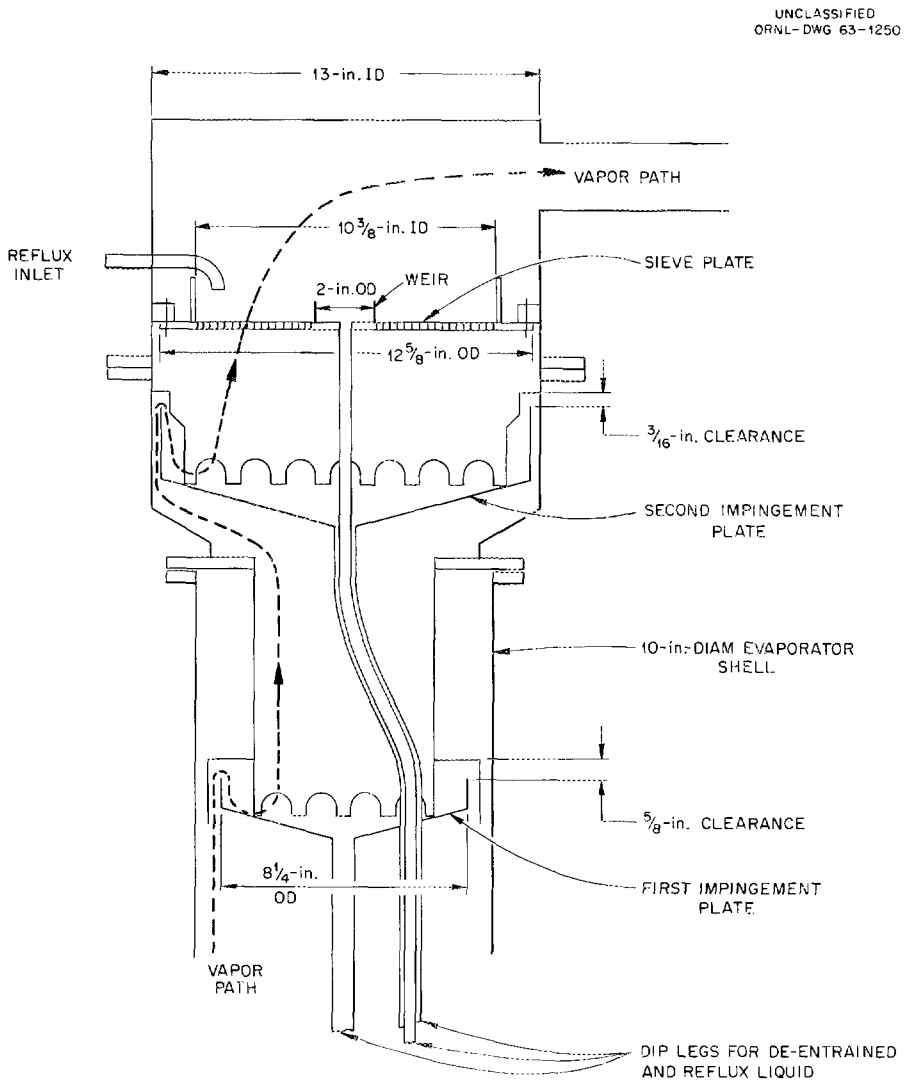

Fig. 3.10. Impingement-Sieve Plate De-entrainer.

process conditions (Fig. 3.11). Purex waste containing a small quantity of calcined solids is circulated in the loop at its boiling point. Purge water introduced at the pumps is vaporized in the head tank in order to maintain a constant density and liquid inventory in the system. The following pumps are currently installed in the loop: Byron-Jackson canned-rotor pump, designed by ORNL; Chempump, model GA-1-1/2K; Chempump, model CFT-1-1/2-3/4S; and Allis-Chalmers, model C-10BS.

The bearings in all the pumps except the Byron-Jackson are of carbon or graphite; a special aluminum oxide bearing is used in this pump. Bearing dimensions will be checked periodically.

Mechanical Development

A mechanical development program was successfully conducted at Lockheed Nuclear Products Facility—Georgia Nuclear Laboratory under subcontract with ORNL. After completion of this program, the demonstration equipment (Fig. 3.12) was disassembled and shipped to Hanford. Program objectives were to (1) develop a permanent seal for calciner pots, (2) demonstrate functional reliability of the remote mechanical equipment, (3) study thermal behavior of the pot with simulated fission product heat, (4) develop and demonstrate remote equipment replacement and repair, and (5) recommend design changes for better equipment performance and easier in-cell repair.

Closure Tests. – Both a welded and a mechanical closure (Grayloc connector) were tested as permanent seals for the calciner pots. Two basic joint designs were welded remotely: a threaded plug (sketch A, Fig. 3.13) and a shrink fit (sketch B, Fig. 3.13). The specimens were mounted on a rotatable face plate attached to a Boston gear reducer and a Graham variable-speed drive. Preliminary welds to determine optimal machine settings were made on stainless steel bar stock machined to approximate the joint configuration being tested. Specimens were pressure purged with NO before welding, in order to simulate actual process conditions.

After visual and dye-penetrant inspection, the specimens were heated to 300°C and leak tested while under 100-psi internal pressure. The specimens were then cooled rapidly to induce excessive stress. After five heating cycles, stress cracks were detected, and leak rates for all specimens were still below the reliable detection limit of 0.054 cm^3/yr. Leak rates of the Grayloc connector under similar conditions were 72 cm^3/yr.

Burst tests were made on a welded specimen of each basic design. The shrink-fit design sustained a hydraulic pressure of 20,000 psi without failure; the threaded plug design failed at 9000. The tests are summarized as follows:

1. The welded closures were at least a factor of 100 lower, and the Grayloc closures were a factor of 2.5 higher than an assumed maximum permissible leak rate of 32 cm^3/yr. The value of 32 cm^3/yr is subject to change, pending a hazards evaluation of pot storage.
2. Sound, crack-free fusion welds were made with both designs, without the addition of filler metal. Radiography showed all welds to be free of internal flaws, and incomplete penetration was verified visually.
3. The electrode must be accurately positioned over the weld joint to obtain complete fusion of the bottom edges of the joint.
4. "Arc blow" was present during the welding of all samples. The arc was deflected in a radial direction, away from the center of rotation of the test piece.
5. The cover for the shrink-fit closure tended to cock and jam during assembly of the cover into the preheated body.
6. No detrimental pressure buildup occurred in the closed vessel attached to the test pieces.
7. The NO gas present had no apparent effect on the stability of the welding arc.
8. The threaded-plug design failed at 9000 psi, but since internal pot pressure should never reach this value, both weld designs are satisfactory.

Remote Equipment Reliability Tests. – Positioning tests were conducted with the furnace dolly fully loaded (about 10,000 lb) to determine the average deviation from standard horizontal and vertical positions of the furnace at the filling station. Fifty tests were successfully completed, with a high degree of positioning accuracy and reliability. An additional 50 tests were conducted, with 2000 lb of lead in the dolly, in which maximum lateral dolly positions and extreme malpositioning in the direction parallel to the tracks were induced in order to permit evaluation of the capability of the filling station to align, accept, and clamp a pot that might arrive off-station. The limit switches proved reliable in controlling the dolly and furnace

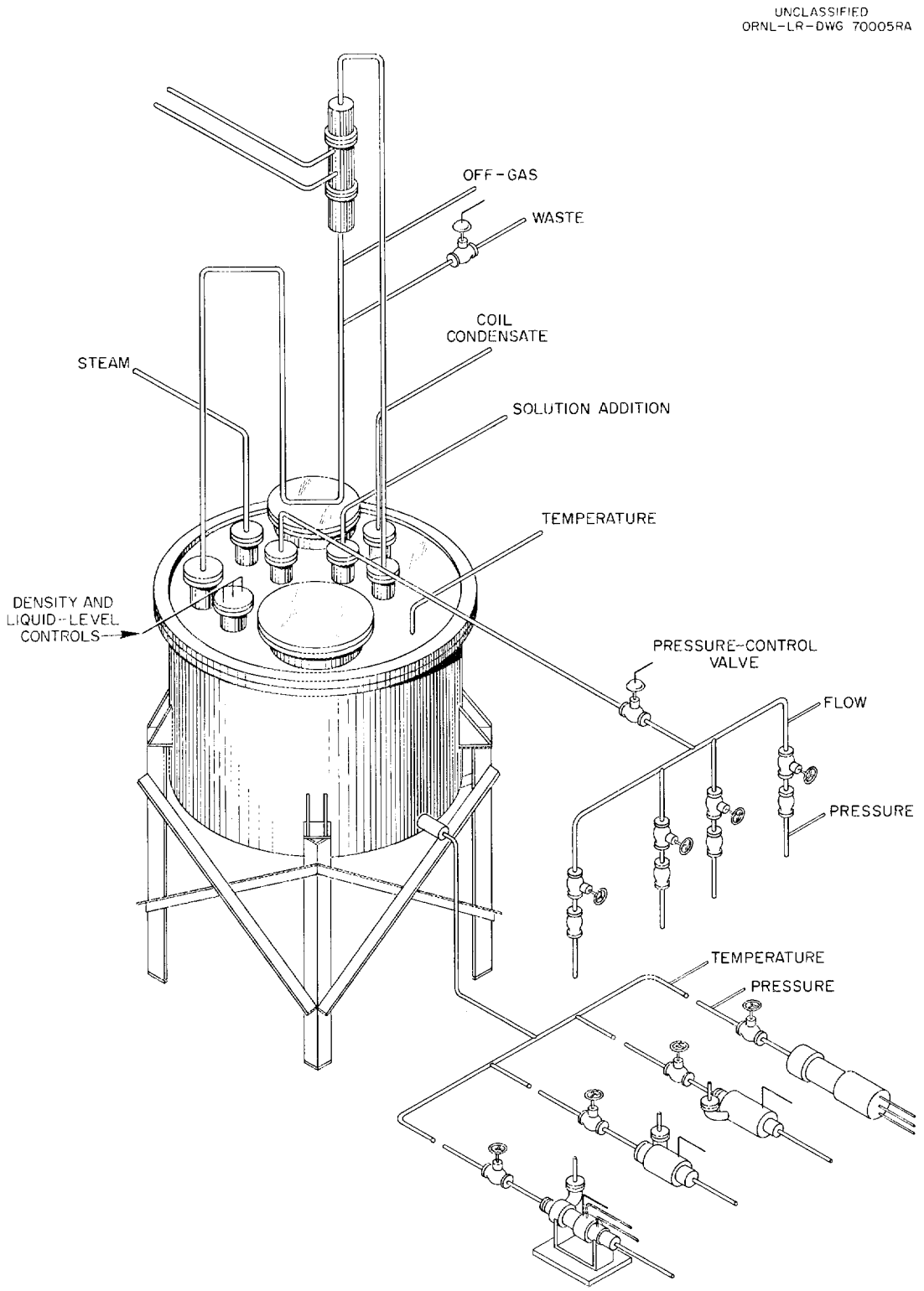

Fig. 3.11. Pump-Test Loop.

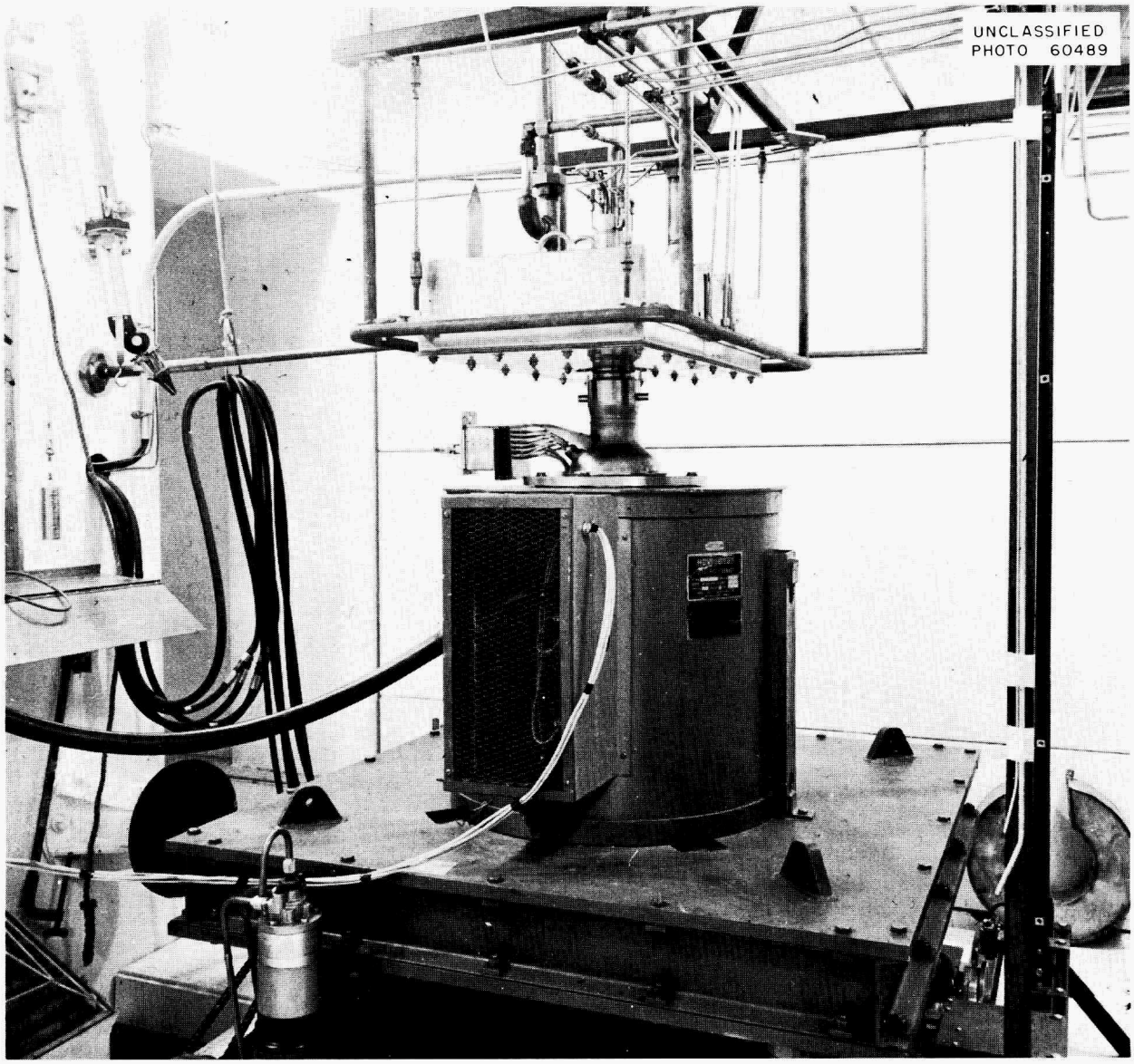

Fig. 3.12. Remotely Operated Equipment Developed for Pot-Calcination Process.

movements within design tolerance, and induced misalignments at the filling station did not prevent proper connections of the pot to the filling-station cap.

Connect-Disconnect Leakage Tests. – Gasketed and Grayloc connectors were satisfactory for sealing the calciner pot to the process filling head. Leakages past blue asbestos and stainless-steel-clad asbestos gaskets and through the Grayloc connector were determined as pressure changes at temperatures from ambient to 300 and at 900°C for 10-min test periods (Table 3.4). The static pressures were nominally 8 in. Hg in the vent line and 22 psig in the fill line. The use of stainless-steel-clad gaskets is preferred because of their ability to remain with the pot rather than to adhere to the fill head when the connection is broken. Closures with the conventional Grayloc ring seal gave comparable results.

Design Recommendations. – (1) Ease of disassembly of the filling station for maintenance would be improved by removing the entire assembly from

UNCLASSIFIED
ORNL-LR-DWG 69416A

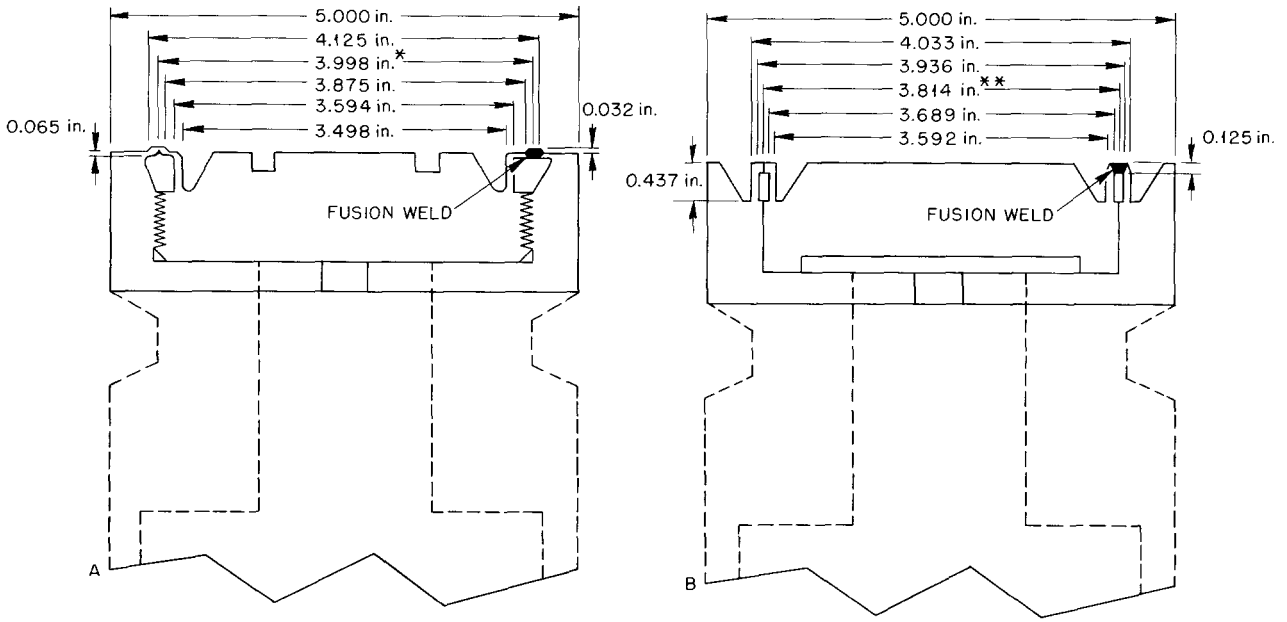

Fig. 3.13. Cross Section of Weld Joint Designs A and B. Solid lines show simulated weld test sample; broken lines show its orientation to the calcining pot neck. * Joint clearance for assembly is 0.001 in. ** Male dimension shown; female dimension 3.811 in. for shrink fit.

its frame and moving it to a table in front of the cell window for remote disassembly. (2) Either flex lines or piping sections with disconnects on either end should be used for the services and vapor lines to the filling station to permit clear access at the top of the station for easy removal of components. (3) The pneumatic actuator on the dust-cap slide mechanism should be eliminated. Simple operation of the slide by a manipulator is considered to be more reliable. (4) The screws on the Grayloc clamp for permanent sealing should be lengthened to facilitate installation of the clamp and realignment of the clamp jaws. (5) A pot thermocouple connector fabricated from Cannon connectors with ceramic insulation should be used. (6) A limit switch on the filling-station clamp assembly should be used to prevent accidental lowering of the furnace while the pot is clamped to the filling station.

Remote Maintenance Times. – Remote disassembly, repair, and reassembly of the filling station will require several man-days of effort when performed in a radioactive hot cell. Experience obtained in cold tests is summarized in Table 3.5. Remote assembly of the filling-station parts will require about the same time as disassembly. Normal operations such as the installation and removal of the pot thermocouple connector or the pot screw-cap installation require about a minute.

Pilot-Plant Design

A pilot plant will be located at Hanford in the new Fuels Recycle Pilot Plant building[4] to demonstrate the pot- and spray-calcination processes on radioactive wastes. The cell will have a 22 × 25 ft floor and a height of 27 ft to the bottom of the crane hook. A pipe trench is provided outside the east wall of the cell for connecting service piping to vessels in the cell and for connecting vessels

[4] *Design Criteria for Fuels Recycle Pilot Plant, Project CHH-916*, HW-69666 (June 28, 1961).

across the east-west axis of the cell, thus keeping the floor free of piping. Four feet of high-density (200 lb/ft^3) concrete shielding will be provided on one wall and at the windows; the remaining exterior walls will have at least 5.33 ft of normal-density concrete. Shielding calculations, for an array of 39 pots (8 in. diam) containing Purex waste cooled 180 days and stored at least 24 in. from the 4-ft wall, gave a maximum dose rate of about 1 mrem/hr. Results for other cooling times and for Consolidated Edison Darex or APPR Darex wastes are shown in Fig. 3.14.

A high-activity-level vault outside the cell will be used to contain the waste feed and the alkaline and acid wastes from the process. A low-activity-level vault will contain the sample and condensate

Table 3.4. Connect-Disconnect Leakage Tests[a]

Test No.	Type of Closure	Test Conditions	
		Cold: Ambient to 300°C	Hot: 900°C
1	Blue asbestos gaskets		
	Vent line (in. Hg/min) vacuum	0–0.44	0–0.38
	Fill line (psig/min) pressure	0–0.1	0–0.27
2	Stainless-steel-faced gaskets		
	Vent line (in. Hg/min) vacuum	0–0.04	0–0.08
	Fill line (psig/min) pressure	0–0.03	0–0.03
3	Grayloc seal ring		
	Vent line (in. Hg/min) vacuum	0–0.03	0–0.17
	Fill line (psig/min) pressure	0.05–0.13	0.01–0.10

[a]System was leak-tightened between tests 1 and 2.

Table 3.5. Summary of Operations in the Remote Maintenance of the Pot-Calciner Mockup

Operation	Time Required	Tools Required
Pot thermocouple connector: connect-disconnect	15 sec	Connector and two model 8 manipulators
Dust-cap installation	2 sec	One model 8 manipulator
Pot screw-cap installation	1.3 min	Special wrench and two model 8 manipulators
Filling-station disassembly: Disconnect 1-in. vacuum line, two 1/2-in. fill lines, two 1/4-in. water lines, cap-heater lines, and remove limit switch	4.6 hr	Standard hot-cell tools
Disconnect two 1 1/2-in. vent lines and filling-station air-supply "tee" and remove cap and cap deck	1.5 hr	Standard hot-cell tools
Remove clamp assembly, screw, bearings, and springs; remove slide assembly and cap-loader actuator	1.7 hr	Standard hot-cell tools

storage vessels. Feed for the process will be brought in by shielded cask from the Purex and Redox plants.

The process flowsheet for the pot-calcination portion of the pilot plant is shown in Fig. 3.15. It will include an induction furnace for heating pots of up to 12 in. in diameter and 6 ft long. The evaporator can be operated batchwise or continuously. For batch operation the calciner feed tank will be the pot feed source, while continuous operation will require that the evaporator be directly connected to the pot. Provision is also made to catch the pot condensate separately or to feed it continuously by gravity to the evaporator. The overhead vapors from the evaporator will be condensed and then fractionated to produce water and nitric acid. The noncondensable gases will be filtered, passed through a silica-gel trap for ruthenium, scrubbed in a packed tower, and refiltered before discharge into the cell-exhaust system.

A spray calciner will be operated using the same off-gas system as the pot calciner and also the batch calciner feed tank and pump for feeding. Provisions will be made to use the same external induction-heating equipment for both processes.

A layout of the major equipment items is shown in Fig. 3.16. A unique system that combines remote and direct maintanence is used. The vessels will be mounted on racks, with remote disconnects on the piping between racks so that an entire rack can be removed remotely, decontaminated, and maintained directly in an air-lock cell located just outside the calcination cell. Service

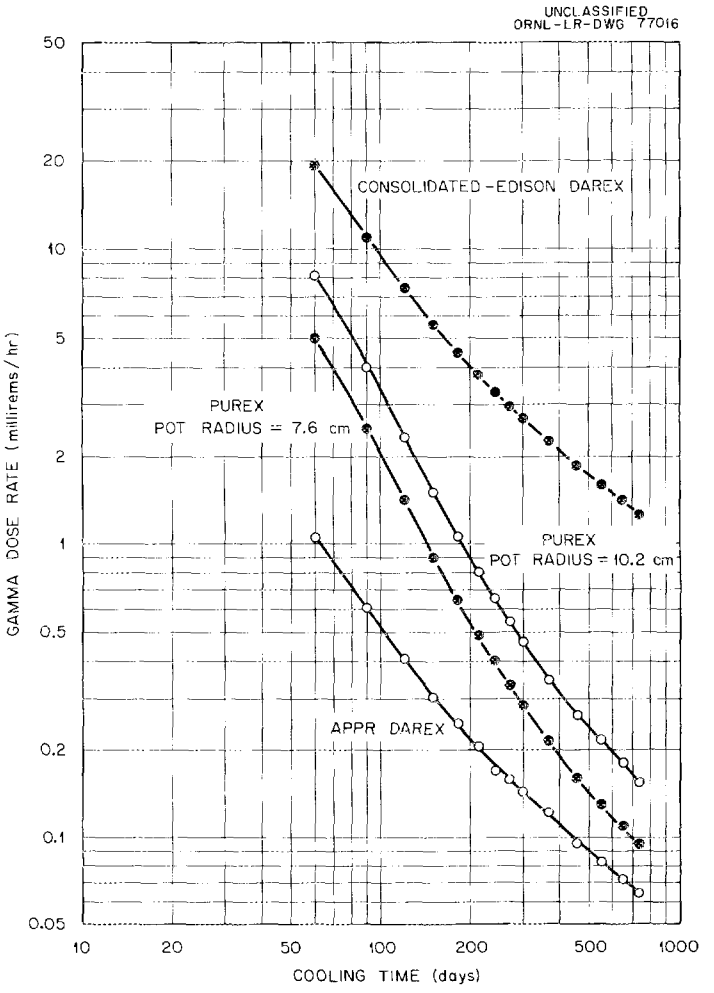

Fig. 3.14. Comparison of the Gamma Dose Rates from the Different Wastes (Mechanical Cell).

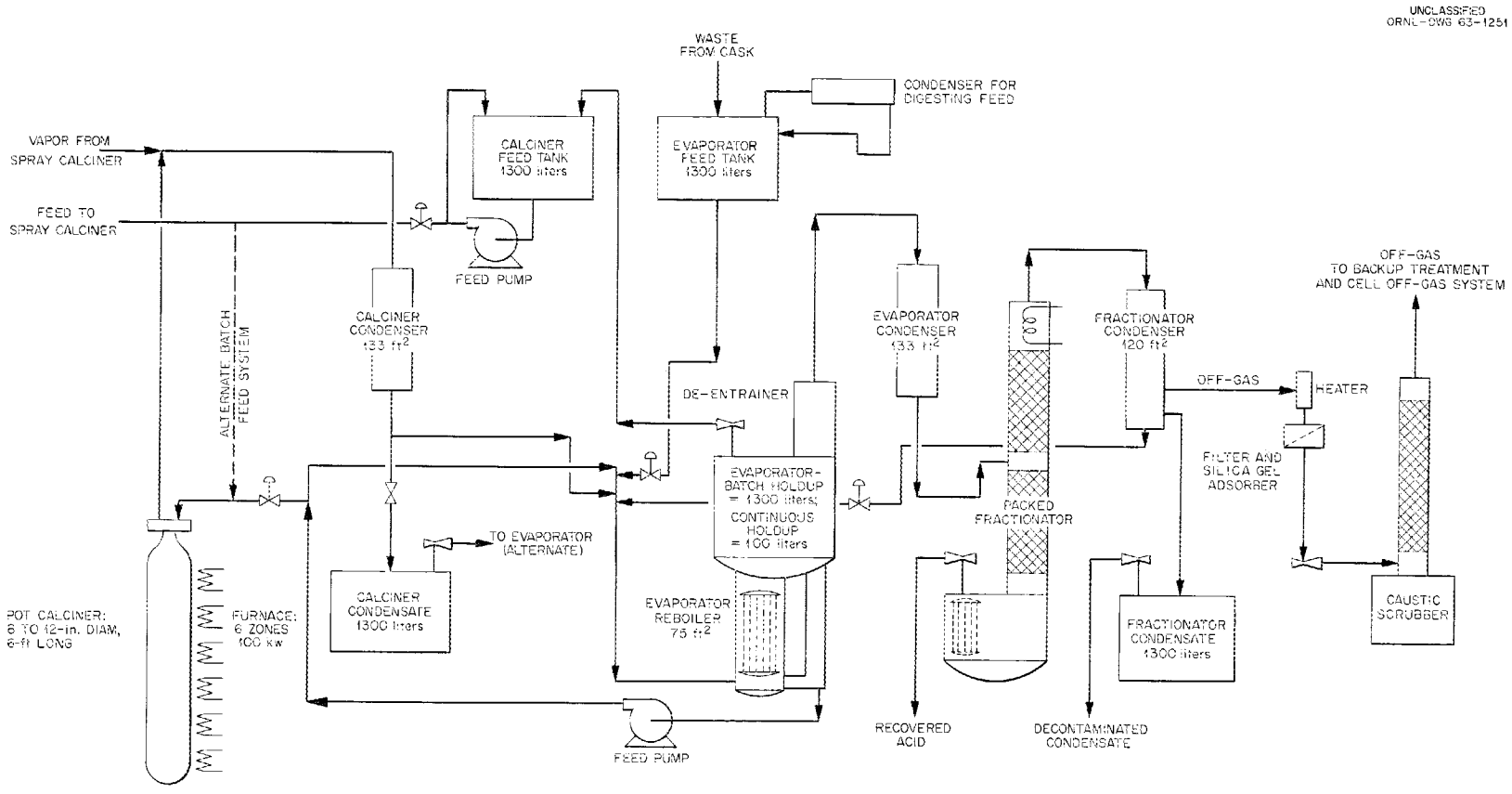

Fig. 3.15. Hanford Pot-Calcination Pilot Plant: Flow Diagram.

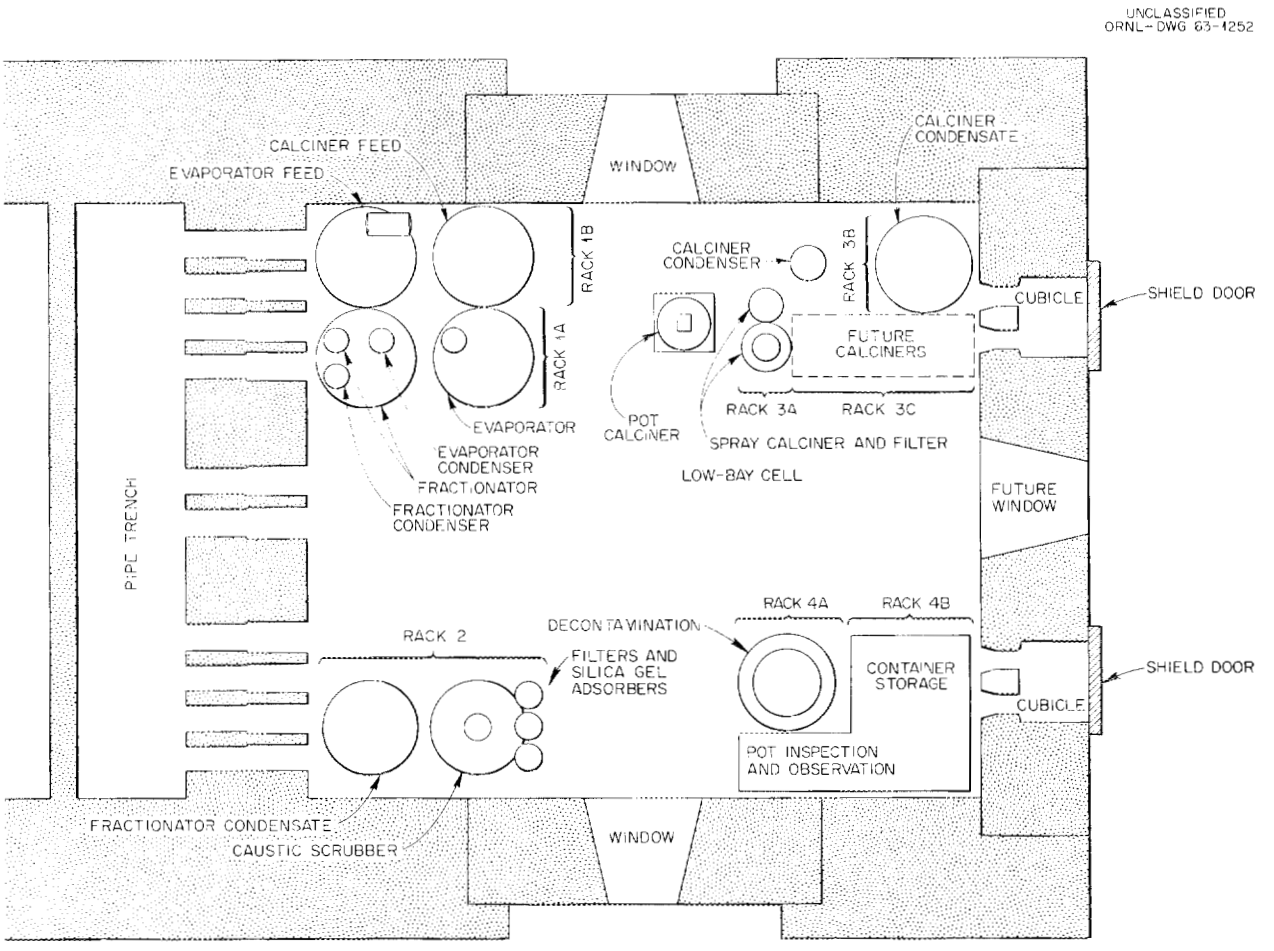

Fig. 3.16. Hanford Pilot Plant: Vessel and Rack Arrangement.

connections to each rack will be made at the shielded cubicles. This will permit the direct connection of the lines from the operating area after a plug (containing the pipes and fastened to the rack) has been inserted in the cubicle from the cell side. A door on the operating-area side will shield these lines, so it will be necessary to partially decontaminate them before the connections can be broken after hot operation.

Laboratory Studies

Laboratory work included characterization of liquid-vapor equilibria, determination of waste boil-down characteristics, glass formation, and sulfate loss during glass formation from Purex FTW-65 simulated wastes. Further work was also done on the leaching characteristics of Darex glasses, on glass formation and sulfate loss from high-sulfate Purex waste, on the x-ray structure of the glassy products, on the removal of mercury salts from the waste prior to glass formation, on the thermal conductivity of powders and solid materials, and on the corrosion of types 304L and 347 stainless steel under conditions expected for glassmaking both for the pots and the off-gas system. Semi-continuous, semiengineering-scale glass-fixation experiments were carried out with TBP-25, Darex, and FTW-65 waste types. Synthetic nonradioactive wastes were used in all experimental work.

Fixation in Glassy Solids. — The objectives of this program are (1) to fix the fission products in a mechanically strong, insoluble solid suitable for

storage for an indefinitely long time with minimum or no surveillance; (2) to achieve a large reduction in the volume of the waste in order to decrease the storage space; (3) to form a dense product to allow the maximum transfer rate of fission product heat to the surroundings and to permit the use of large storage containers (pots); (4) to incorporate all fission products into the solid in order to eliminate the recycle of intermediate- and low-level side streams; and (5) to hold the maximum temperature as low as possible (~900°C and <1050°C as an upper limit) in order to allow the use of stainless steel containers.

The successful incorporation of TBP-25 wastes in phosphate glasses that soften at temperatures as low as 800°C was reported previously.[5] Several semicontinuous, semiengineering-scale (4-in.-diam × 24-in.-high pot) experiments were performed to study the fixation of tracer ruthenium and promethium in order to distinguish between volatile and entrained ruthenium. About 0.1% entrainment occurred from the pot along with the volatilization of 12 to 25% of the ruthenium. In previous small-scale batch and semicontinuous experiments operated at a fixed liquid level, the presence of hypophosphite or phosphate in the fixation pot reduced the volatility of ruthenium to about 0.1%. Operation with a slowly rising liquid level (which is the preferred method for glass formation) did not reproduce these results. Apparently, ruthenium is voltalized from the material that spatters on the hot walls of the pot during the thermal decomposition of the nitrates. In engineering tests, passage of the off-gas from the pot through a continuous evaporator gave a ruthenium decontamination factor (DF) of about 1000. The volatility of ruthenium from the evaporator can be decreased further, if necessary, by the presence of 0.1 to 0.2 *M* phosphite in the evaporator.[6]

Darex products spiked with Cs^{137} and subjected to leaching tests in circulating distilled water showed that a ceramic containing about 25% waste oxides leached about 1000 times faster than a glass containing about 15% waste oxides (melts 2 and 3, Table 3.6). This is consistent with previously reported results on TBP-25 and Purex products (Fig. 3.17). A 4-in.-diam stainless steel fixation pot, 24 in. long and about two-thirds filled with a lead phosphate glass containing 25 wt % TBP waste oxides, developed a vacuum that slowly increased to about 30 in. of water when heated to 900°C for 24 days. The internal pressure never exceeded atmospheric. Subsequent sectioning of the pot and comparison with a pot subjected only to the fixation process revealed that no significant corrosion had taken place during the extra heating period. The solid remained glassy.

Semicontinuous, semiengineering-scale fixation of Darex waste in an aluminophosphate ceramic (No. 4, Table 3.6) produced an extremely hard and strong solid representing a volume reduction of 5.1. This solid was unsatisfactory because it expanded slightly on cooling, causing the fixation pot to stick in the furnace liner.

Melts in which barium and lead oxides were added to simulated Purex 1WW waste (plus the standard additives calcium, sodium, magnesium,

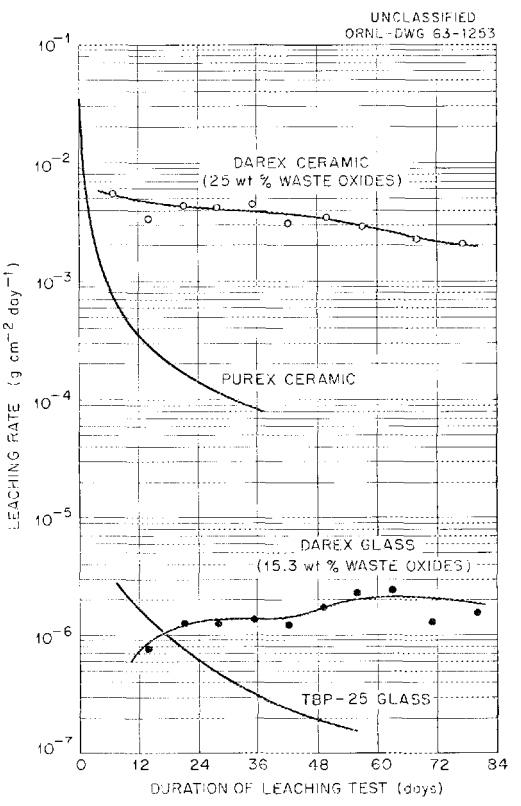

Fig. 3.17. Leach Rate of Glasses Made with Purex, Darex, and TBP-25 Waste Solutions in Water at 25°C.

[5] *Chem. Technol. Div. Ann. Progr. Rept. May 31, 1961*, ORNL-3153, p 46.

[6] H. W. Godbee and W. E. Clark, "The Use of Phosphite and Hypophosphite to Fix Ruthenium from High-Activity Wastes in Solid Media," *Ind. Eng. Chem., Prod. Res. Develop.*, June 1963 (in press).

Table 3.6. Compositions of TBP-25, Darex, and Purex Glassy Products Produced in Scouting Experiments

	Melt Designation and Type					
	No. 1, TBP-25; Semiengineering-Scale Fixation Leach Test and Prolonged Heating	No. 2, Darex; Leach Test	No. 3, Darex; Leach Test	No. 4, Darex; Semiengineering-Scale Fixation	No. 5, Purex 1WW; Leach Test	No. 6, FTW-65; Semiengineering-Scale Fixation
Additive (g-moles per liter of waste)						
H_3PO_3				0.4	1.52	
$NaH_2PO_4 \cdot H_2O$	2.0	3.0				
$NaH_2PO_2 \cdot H_2O$		2.0	2.8	2.4		0.34
$Na_2B_4O_7 \cdot 10H_2O$		0.32	1.44		0.172	
B_2O_3			1.0	1.1		
$Al(NO_3)_3 \cdot 9H_2O$		4.3		1.5		0.08
$Ca(OH)_2$						0.07
MgO					0.80	
PbO	0.250					
NaOH		0.4			1.67	0.38
Composition of the solid (wt % of oxides, theoretical)						
Al_2O_3	25.0	22.9	12.3	13.2	1.4	7.9
CaO						5.0
Na_2O	18.6	19.7	15.4	13.2	21.8	27.2
MgO					8.7	
Fe_2O_3	0.06	10.5			10.7	10.0
Cr_2O_3		3.0			0.2	1.9
NiO		1.4			0.2	0.5
MnO		0.4				
PbO	15.9					
RuO_2	0.01	0.003			0.1	0.4
P_2O_5	40.5	37.3	35.3	35.3	29.0	30.9
SO_3					21.5	15.7
B_2O_3		4.8	12.0	13.2	6.4	
SiO_2						0.1
F^-						0.5
Total	100.0				100.0	100.1

Table 3.6. (continued)

	Melt Designation and Type					
	No. 1, TBP-25; Semiengineering-Scale Fixation Leach Test and Prolonged Heating	No. 2, Darex; Leach Test	No. 3, Darex; Leach Test	No. 4, Darex; Semiengineering-Scale Fixation	No. 5, Purex 1WW; Leach Test	No. 6, FTW-65 Semiengineering-Scale Fixation
Waste oxides (wt %)	26.0	15.3	25.0	25.0	39.1	45.0
Softening temperature, (°C)	900	800	900	850	840	850
Bulk density	2.84	2.61	2.86	2.65	2.70	
Volume reduction from liquid waste	8.1	2.5	4.9	5.1	7.5	30.3
Leach rate[a]	4.3×10^{-7}	1.4×10^{-6}	4.0×10^{-3}		1.03×10^{-3}	
SO_3 lost[b] (%)					51.2	2–9[c]
Appearance	Greenish-white glass	Brown-black glass	Black ceramic; glassy if quenched	Black rock; very hard	Green ceramic; glassy if quenched	Dark-brown crystalline rock; hard

[a]Grams cm^{-2} day^{-1} after 30 days in contact with circulating distilled water at ~25°C; rate is based on removal of Cs^{137} from the solid.

[b]Based on weight lost when held 100°C above the softening temperature.

[c]The higher figure was obtained from thermogravimetric measurements; the lower was obtained from analysis of the off-gas from the fixation experiment.

phosphate, and borate) showed little improvement over previously reported compositions, either in physical properties or in the retention of sulfate. Waste oxides varied from 19 to 40 wt % in these tests. Variation of standard additives produced a few melts, containing 39 to 42 wt % waste oxides, which retained up to 97% of the SO_3 when heated at 100°C above their softening temperatures for 100 min (Table 3.7). Melts that contained a stoichiometric excess of alkali and alkaline-earth metals over the anions PO_3^-, SO_4^{2-}, and BO_2^- generally retained more sulfate; melts with an anion excess lost more sulfate and were more likely to produce a glassy product. No simple correlation was possible.

Solubility and vapor-liquid equilibrium data were obtained for simulated FTW-65 waste. The waste can be concentrated fourfold without inducing the precipitation of solids. Ruthenium volatility during equilibrium distillation of FTW-65 was as predicted from the plot of the logarithm of [Ru (vapor)]/[Ru (soln)] vs HNO_3, published previously.[6] Solid fixation products containing 45% waste oxides were made by the addition of phosphite, sodium, calcium, magnesium, and aluminum (Table 3.8). Several had excellent physical properties, and a few lost less than 10% of the sulfate. One of these (No. A-1, Table 3.8; No. 6, Table 3.6) was also tested in a semicontinuous run in a pot 4 in. in diameter and 24 in. long. Less than 2% of the sulfate was found in the condensate and off-gas, and the volume reduction factor from the unconcentrated FTW-65 solution to the melt was > 30.

Removal of Mercury. – Mercury compounds in waste solutions present a problem during calcination-fixation. The compounds are unstable at 700 to 1000°C, and mercury is volatilized with the last of the water vapor, nitric acid, and oxides of nitrogen. Attempts to selectively condense mercury resulted in the collection of about 50% of it in both laboratory- and engineering-scale experiments. The remainder was distributed throughout the off-gas system.

Passage of the waste solution through a column packed with copper shot and turnings removed more than 99.9% of the mercury from FTW-65 waste, but added two to three times as much copper to the waste as would be predicted from the simple displacement of mercury by copper.

Thermal Conductivity. – Effective thermal conductivities were measured for magnesia, alumina, and zirconia powders in air at atmospheric pressure at temperatures from 200 to 1500°C. The volume fraction of the solid in the heterogeneous systems varied from 0.49 to 0.70. Measurements were made by a steady-state method based on radial heat flow in a hollow cylinder. A few measurements were made by an unsteady-state method in order to corroborate the steady-state measurements. The unsteady-state method is based on the heating of a cylinder of a perfect conductor surrounded by an infinite amount of the material whose conductivity is being measured.

The powders had mean particles sizes ranging from about 255 to 895 μ, as determined by screening. The particles had little or no porosity, as would be expected for powders prepared from fused and crushed oxides. The surface area (determined by the BET nitrogen-adsorption method) of the powders ranged from 0.03 to 0.12 m^2/g.

The effective thermal conductivity of all the powders increased with increasing temperature (Fig. 3.18). The variation of effective thermal conductivity was approximately quadratic with temperature. Since the thermal conductivity of both theoretically dense zirconia and air increases with temperature, the effective thermal conductivity of a zirconia powder would be expected to increase with increasing temperature. However, the thermal conductivities of theoretically dense magnesia and alumina both decrease with increasing temperature (over the range of temperature studied); therefore, *a priori* argument would not necessarily predict that the effective thermal conductivities of these three powders would increase with increasing temperature. The increase in conductivities with increasing temperature means that the gas conductivity has more influence on the conductivity of the composite body than does the solid conductivity. For a specific powder the effective thermal conductivity increases with increasing volume fraction of the solid (Fig. 3.19).

Corrosion. – The limiting factor in the design of the fixation pot is believed to be the corrosion of the top of the pot when filled with glass and subjected to a high temperature (up to 1050°C) just before its removal from the furnace. Since the pot is suspended from top flanges, the entire weight of the pot and its charge must be held by the pot wall. Corrosion work was done by members of the Reactor Chemistry Division.

Experiments were performed in which simulated high-sulfate Purex waste mixed with glassmaking

Table 3.7. Sulfate Volatility from Experimental Melts Containing 39 to 43% Simulated High-Sulfate Purex Waste Oxides

(Purex waste composition, *M*: 6.1 NO_3^-, 5.6 H^+, 1.0 SO_4^{2-}, 0.5 Fe^{3+}, 0.1 Al^{3+}, 0.01 Cr^{3+}, 0.01 Ni^{2+}, 0.02 Ru)

	Melt Number							
	1	2	3	4	5	6	7	8
Additives (g-moles per liter of waste)								
$NaH_2PO_2 \cdot H_2O$	1.26	1.26	1.26	1.26	1.46	1.56	1.46	1.26
H_3PO_3				0.50				0.51
NaOH	1.36	0.61	0.76	0.86	0.42	0.98	1.08	
$Ca(OH)_2$	0.41	0.41	0.41	0.41	0.92	0.40	0.53	0.92
MgO			0.30					
$Na_2B_4O_7 \cdot 10H_2O$		0.125						
Composition of melt (wt % of oxides, theoretical)								
Fe_2O_3	11.8	11.5	11.7	10.9	11.1	11.2	11.2	11.0
Al_2O_3	1.5	1.5	1.5	1.4	1.5	1.5	1.5	1.5
Na_2O	29.4	24.2	23.9	23.0	21.7	27.6	27.5	16.0
Cr_2O_3	0.2	0.2	0.2	0.2	0.2	0.2	0.2	0.2
NiO	0.2	0.2	0.2	0.2	0.2	0.2	0.2	0.2
RuO_2	0.1	0.1	0.1	0.1	0.1	0.1	0.1	0.1
SO_3	23.6	22.9	23.5	21.8	21.0	21.2	22.1	20.9
P_2O_5	26.2	25.8	26.4	34.2	29.5	31.7	29.6	35.5
CaO	5.9	8.8	9.0	8.4	14.8	6.3	8.5	14.7
MgO			3.6					
B_2O_3		5.0						
	99.9	100.2	100.1	100.2	100.1	100.0	99.9	100.1
Wt % of waste oxides, theoretical[a]	42.7	41.6	42.6	39.5	39.1	39.4	39.4	38.8
Excess cation equivalents	0.79		0.79		0.86	0.38	0.74	
Excess anion equivalents		0.21		0.21				0.07
Ratio $\left(\frac{\text{g-equiv. Na} + Ca^{2+} + Mg^{2+}}{\text{g-equiv. } SO_4^{2-} + PO_3^- + BO_3^-}\right)$	1.24	0.944	1.24	0.944	1.25	1.11	1.21	0.982
Approximate softening temp (°C)	850	850	880	800	875	800	850	950
SO_3 lost during 100 min at 100°C above softening temp (wt %)	5.3	22.0	2.1	Excessive	19.0	12.5	995	14.3
Appearance	Gray-white; crystalline; strong	Light-tan; weak; glassy only if quenched	Dark-brown; strong; crystalline; some voids	Gray; crystalline; weak	Light-green; crystalline	Light-gray; crystalline	Light greenish-gray; crystalline	Shiny; gray; metallic

[a]Assumes all Hg to be volatilized.

Table 3.8. Fixation of Simulated FTW-65 Purex Waste in Glassy Products Containing 45 wt % of Waste Oxides

(Waste composition, *M*: 0.5 H^+, 0.3 Na^+, 0.05 Al^{3+}, 0.10 Fe^{3+}, 0.02 Cr^{3+}, 0.01 Ni^{2+}, 0.0035 Hg^{2+}, 0.15 SO_4^{2-}, 0.005 PO_4^{3-}, 0.01 SiO_3^{2-}, 0.02 F^-, NO_3^- to balance)

	A-1	A-2	A-3	A-4	A-5	B-1	B-2	B-3	B-4	B-5	B-6
Additives (moles/liter)											
$NaH_2PO \cdot H_2O$	0.34	0.34	0.34	0.34	0.34	0.34	0.34	0.34	0.34	0.34	0.34
NaOH	0.38	0.38	0.38	0.38	0.38	0.26	0.26	0.26	0.26	0.26	0.26
$Ca(OH)_2$	0.07	0.14	0.07			0.21	0.14	0.07		0.14	
MgO			0.10	0.20	0.10		0.10	0.20	0.30		0.20
$Al(NO_3)_3 \cdot 9H_2O$	0.08				0.08					0.08	0.08
Waste oxides, theoretical[a] (wt %)	45.0	45.0	45.0	45.0	45.0	45.0	45.0	45.0	45.0	45.0	45.0
Al_2O_3	7.9	2.9	2.9	2.9	7.9	2.9	2.9	2.9	2.9	7.9	7.9
CaO	5.0	10.0	5.0			15.0	10.0	5.0		10.0	
MgO			5.0	10.0	5.0		5.0	10.0	15.0		10.0
Na_2O	27.2	27.2	27.2	27.2	27.2	22.2	22.2	22.2	22.2	22.2	22.2
Fe_2O_3	10.0	10.0	10.0	10.0	10.0	10.0	10.0	10.0	10.0	10.0	10.0
Cr_2O_3	1.9	1.9	1.9	1.9	1.9	1.9	1.9	1.9	1.9	1.9	1.9
NiO	0.5	0.5	0.5	0.5	0.5	0.5	0.5	0.5	0.5	0.5	0.5
RuO_2	0.4	0.4	0.4	0.4	0.4	0.4	0.4	0.4	0.4	0.4	0.4
SO_3	15.7	15.7	15.7	15.7	15.7	15.7	15.7	15.7	15.7	15.7	15.7
P_2O_5	30.9	30.9	30.9	30.9	30.9	30.9	30.9	30.9	30.9	30.9	30.9
SiO_2	0.1	0.1	0.1	0.1	0.1	0.1	0.1	0.1	0.1	0.1	0.1
F^-	0.5	0.5	0.5	0.5	0.5	0.5	0.5	0.5	0.5	0.5	0.5
Total	100.1	100.1	100.1	100.1	100.1	100.1	100.1	100.1	100.1	100.1	100.1
Approximate softening temperature (°C)	850	900	900	875	850	950	950	925	925	925	900
Approximate melting temperature (°C)	900	950	950	925	900	1050	1050	1000	1000	1000	950
Maximum TGA temperature (°C)	950	980	980	960	950	1100	1100	1100	1100	1100	980
SO_3 loss for 100 min at maximum temperature (%)	9.2	9.0	9.6	9.6	12.4	33.2	29.9	38.8	28.7	44.3	19.7
Description	Hard, microcrystalline rock; dark-brown	Hard, microcrystalline rock; dark-brown	Hard, microcrystalline rock; black	Hard, microcrystalline rock; gray	Crystalline rock; brown	Very hard, microcrystalline rock; gray	Very hard, microcrystalline rock; black	Very hard, microcrystalline rock; brown-black	Segregated; yellow-brown; microcrystalline	Brown; microcrystalline rock	Mottled; rock-like; corrosion of crucible evident

[a] Assumes all mercury to be volatilized.

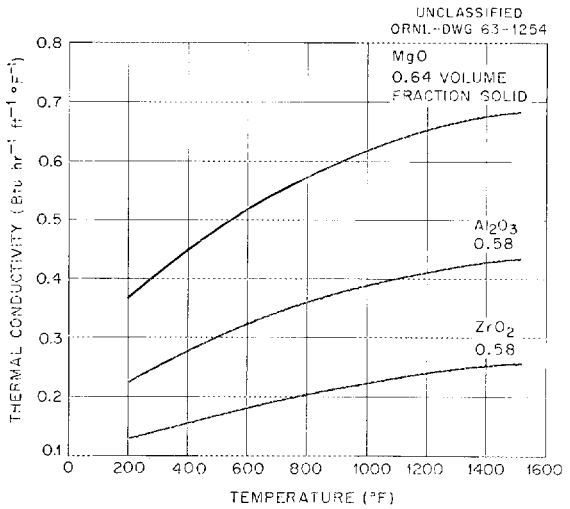

Fig. 3.18. Variation of Thermal Conductivity with Temperature for MgO, Al_2O_3, and ZrO_2 Powders in Air at Atmospheric Pressure.

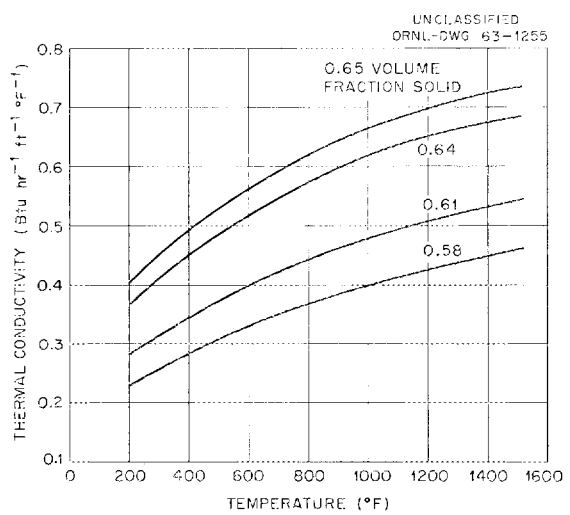

Fig. 3.19. Variation of Thermal Conductivity with Temperature, with Volume Fraction Solid as a Parameter, for an MgO Powder in Air at Atmospheric Pressure.

ingredients was evaporated in a type 304L stainless steel pot that was heated to 1050°C for 96 hr under a tension of 315 psi. Maximum elongation was 1.49×10^{-3} in./in. At 150 psi elongations of 9.4×10^{-5} to 5.4×10^{-4} in./in. were measured. Coupon specimens exposed inside the pot showed corrosion rates of 19 to 47 mils/month, and a weld that indicated porosity before the test showed localized attack.

In tests in which FTW-65 waste was evaporated and calcined at 900°C with and without added calcium nitrate, the most aggressive corrosion occurred when water was retained in the product up to high temperature. The presence of 0.02 *M* F^- increased the amount of corrosion. The addition of sufficient calcium (as nitrate) to fulfill the ratio

$$\frac{\text{Chemical equivalents } (Na^+ + Ca^{2+})}{\text{Chemical equivalents } (SO_4^{2-} + PO_3^- + F^-)} \geq 1.1$$

prevented excessive corrosion, provided that the additive was uniformly mixed in the calcined product. Calcium addition was incorporated into the standard procedure. Type 304L stainless steel is recommended as the best stainless steel for use as the material of construction for fixation pots.

Types 304L and 347 stainless steel exposed at 305°C in off-gases from the evaporation of Purex 1WW corroded at maximum rates of about 3 mils/month, indicating that either of these steels can be used for the off-gas system immediately above the pot. Welded specimens of type 304L stainless steel, Hastelloy F, titanium 45A, and 304L stainless steel–titanium 45A couples all showed slight weight gains after 1584 hr of exposure in the solution, interface, and vapor phases of refluxing FTW-65 waste; hence they are also satisfactory materials of construction for the off-gas system.

Welded specimens of type 304L stainless steel tested at 300°C for 672 hr in contact with sodium chloride (with and without added water, $MgCl_2$, or $CaSO_4$, and a combination of the three) showed a maximum corrosion rate of 0.03 mil/month. Unless more aggressive attack occurs with increased exposure time, corrosion rates of pots stored in a dry salt mine should be satisfactorily low.

Hot-Cell Demonstration with Radioactive Waste

Stainless steel equipment was assembled for use in experiments on the calcination of radioactive wastes on a 10- to 30-liter scale. Concentrated liquid waste from the Hanford and Idaho radiochemical separations plants (see Fig. 3.17 in ref 1) will be used. The tests will include evaporation, continuous addition and evaporation

of the adjusted feed in a resistance-heated calciner pot, and calcination of the residue at about 900°C. Gases evolved during evaporation and calcination will be condensed and collected. Noncondensable gases will be scrubbed with caustic and recycled continuously. The loaded calciner pots, after cooling, will be disconnected, equipped with instruments to monitor temperature and pressure, and then transferred to a storage site for long-term observation. Ten calcination, three glass-fixation, and five evaporation experiments are planned, and high-level radioactive Purex wastes from the Hanford and TBP-25 waste from the Idaho chemical processing plants will be used. In addition, one experiment will be made with Purex waste containing no sulfate. A liquid-waste shipping carrier was constructed and tested for the shipment of Purex 1WW from Hanford to ORNL.

3.2 TREATMENT OF LOW-LEVEL WASTE

The development of a scavenging-precipitation ion exchange process for the routine removal of trace amounts of fission products from large volumes of process water has progressed through the laboratory, design, and pilot-plant phases. In a series of 16 runs in a 600-gph pilot plant, the economic, chemical, and equipment factors of the process were evaluated. A complete description of the process and an evaluation of results have been published.[1,7,8]

In this process, slightly radioactive waste water from the million-gallon ORNL equalization basin is pumped into the plant at 10 gpm, where it is made 0.01 *M* in NaOH in a flash mixer with an 18-sec holdup. Ferrous sulfate is added to the mixer as a coagulant (final iron concentration, 5 ppm). The solution then flows by gravity to a lightly agitated 270-gal flocculator, where the floc of insoluble carbonates, algae, foreign sediment, and ferric hydroxide agglomerates into large particles, which carry a significant fraction of the fission products. The solution and floc flow, again by gravity, to a 1980-gal clarifier, where the solutions pass up through a 4- to 5-ft-thick sludge blanket. The sludge, containing 60% of the Sr^{90}, is continuously withdrawn, filtered, and packaged for disposal. The clarifier effluent is transferred to a surge drum and then pumped through a sand or anthracite polishing filter for additional hardness and turbidity removal. The filtered solution is pumped through one of two resin columns filled with 28 gal of Duolite CS-100 cation exchange resin to remove the remaining hazardous fission products, principally Cs^{137} and Sr^{90}.

When 2000 resin-bed volumes (56,000 gal of waste water) have been passed through the bed, the feed is stopped, the fission products are eluted with 10 volumes of 0.5 *M* HNO_3, and the resin is washed with water and regenerated with 0.1 *M* NaOH.

The pilot-plant equipment was recently revised to test an improved flocculation unit, continuous ion exchange, inorganic and organic exchange media for the removal of ruthenium and phosphate, and foam separation. The revised pilot plant will be in operation in late 1963.

Scavenging-Precipitation Ion Exchange Process

Pilot-Plant Performance. — Seven additional runs were completed in the 600-gph pilot plant[1,8] for testing the scavenging-precipitation ion exchange process. Volumes of 42,000 to 90,000 gal of ORNL process waste water (Table 3.9) were treated per run, representing 1500 to 1940 resin-bed volumes. During the eight-month demonstration period (16 runs), 1.3×10^6 gal of ORNL process waste was treated.[8]

In all but two runs (HF-12 and HF-14, Table 3.10), the average activity of the process effluent was less than 3% of the MPC_w values[9] for all isotopes for continuous occupational exposure (Table 3.11). The isotopes considered the greatest health hazards (Sr^{90} and Cs^{137}) average 1.10 and 0.30%, respectively, of the MPC_w for continuous occupational exposure in the effluent. Other principal fission product contaminants, Co^{60} and

[7] R. R. Holcomb, *Low-Radioactivity-Level Waste Treatment. Part I. Laboratory Development of a Scavenging-Precipitation Ion-Exchange Process for Decontamination of Process Water Wastes*, ORNL-3322.

[8] R. E. Brooksbank *et al.*, *Part II. Low Level Waste Treatment and Pilot Plant Demonstration of the Removal of Activity from Low Level Process Waste by a Scavenging-Ion Exchange Process*, ORNL-3349 (May 13, 1963).

[9] *Maximum Permissible Body Burdens and Maximum Permissible Concentrations in Air and in Water for Occupational Exposure*, NBS Handbook 69, June 5, 1959.

total rare earths, were 0.17 and 0.35% of MPC_w respectively. Decontamination factors for Sr^{90} and Cs^{137} ranged from 2000 to 12,000 and from 77 to 3400, respectively, for all but four runs of the demonstration series. Low decontamination in these runs was caused by hexametaphosphate in the feed water (HR-12 and HR-14), low pH of the water (11.3 rather than 12.0) fed to the ion exchange columns (HF-15), or the use of excessive amounts of Na_2CO_3 added to reduce the effects of the phosphate (HR-16).

The scavenging–ion exchange process produced significantly better removal of major fission products than the lime-soda process (Table 3.12) for a five-month period (November 1961 to March 1962). During this period, 43×10^6 gal of low-level waste was treated in the lime-soda plant and 0.6×10^6 gal in the waste pilot plant.

Premature breakthrough of Sr^{90} to the effluent occurred in runs HR-12 and HR-14 (Table 3.10). The breakthrough (at the 1%-of-MPC_w level) occurred after 760 and 1160 resin bed volumes of water, respectively, had been treated. The cause of the breakthrough was the presence of 2 to 5 ppm of total phosphate (from decontamination solutions) in the influent stream. The phosphate prevented complete precipitation of calcium, and the calcium produced premature breakthrough of Cs^{137} from the ion exchange column. In the head-end, or precipitation, portion of the process, soluble calcium and magnesium are precipitated and removed to prevent their loading on the ion exchange columns. Hexametaphosphate or other phosphates in the feed water interfered with hardness precipitation by reducing the surface area of the carbonate precipitate available for seeding. This interference was overcome by the addition of 0.005 *M* Na_2CO_3 in the precipitation step in runs HR-15 and HR-16. However, the addition of an excess of Na_2CO_3 in HR-16 caused early breakthrough of Cs^{137} from the ion exchange column. Thus, the removal efficiency of Cs^{137} by ion exchange depended on the pH of the adjusted feed solution, the total hardness, and the sodium concentration in the feed to the resin column. These variables can be satisfactorily controlled to achieve specified decontamination of low-level waste, even in the presence of high phosphate concentrations.

A cost study for a 750,000 gal/day plant using the scavenging-precipitation ion exchange process was prepared, based on pilot-plant tests (Table 3.13). A cost of $0.72 per 1000 gal was calculated for normal operation with 2000 ion exchange resin-bed volumes of waste treated per cycle, with decontamination factors greater than 1000 for both cesium and strontium. However, when ORNL low-activity waste contains more than 2 ppm of hexametaphosphate (caused generally by the heavy use of hexametaphosphate cleansers for equipment decontamination), the throughput rate of the ion exchange column without the addition of Na_2CO_3 decreases to 500 bed volumes per cycle before strontium begins to break through. The operating cost at this throughput rate is $1.32 per 1000 gal (Table 3.12). Throughput can be increased to greater than 3000 bed volumes before strontium breaks through (but only 900 bed volumes per cycle before cesium breaks through) by the addition of 0.005 *M* Na_2CO_3 in the head end. The carbonate costs 10.6¢ per 1000 gal, making a total of $1.02 per 1000 gal for a throughput rate of 1000 bed volumes per cycle. Thus it is cheaper to add carbonate to overcome phosphate-induced difficulties than to reduce the number of bed volumes treated per ion exchange cycle to maintain the high decontamination specified.

Table 3.9. Average Radiochemical Analysis of ORNL Process Waste Water During Pilot-Plant Tests

Nuclide	Activity (dis min^{-1} ml^{-1})
Gross β	36.2
Gross γ	88.5
Total rare earths, β	9.3
Sr^{90}	86.4
Co^{60}	130.2
Ru^{106}	7.7
Cs^{137}	54.4
Zr-Nb	<2.3

Laboratory Studies. – Laboratory studies were directed toward describing and counteracting the tendency toward calcium and magnesium supersaturation in the scavenging-precipitation step, evaluating the effect of complexing agents on the precipitation step, and determining the quantitative effect of sodium and hardness (calcium and magnesium) on the ion exchange step.

Scavenging Precipitation. – The caustic-copperas treatment for the precipitation of hardness,

Table 3.10. Overall Removal of Activity from ORNL Waste

Run No.	Resin-Bed Volumes	Gross β DF	Gross β % Removed	Gross γ DF	Gross γ % Removed	Sr^{90} DF	Sr^{90} % Removed	Cs^{137} DF	Cs^{137} % Removed	Co^{60} DF	Co^{60} % Removed	TRE β DF	TRE β % Removed	$Zr\text{-}Nb^{95}$ DF	$Zr\text{-}Nb^{95}$ % Removed	Ru^{106} DF	Ru^{106} % Removed
HR-2	2000	30	96.70	44	97.7	2956	99.97	288	99.65	16	93.9	4	71.6				
HR-3	1500					6143	99.98	788	99.87								
	2086	46	97.80	25	96.1	2047	99.96	246	99.59	11	91.3	28	96.5				
HR-4	1959	42	97.60	10	89.9	4982	99.98	429	99.80	6	82.8	22	95.6				
HR-5	1789	37	97.3	16	93.8	5588	99.98	2520	>99.96	4	74.3	31	96.8				
HR-6[a]	1500					2316	99.96										
	2046					2316	99.96	544	99.80								
	2593					139	99.28	12	91.50								
	2711					29	96.54	4	76.10								
	3118	12	92.0	5	77.9	20	95.11	6	82.30	5	80.9	21	95.3				
HR-7	2086	34	97.0	19	94.7	12160	99.99	451	99.80	121	91.9	24	95.8				
HR-8[b]	300					8400	99.99	153	99.35								
	800					8400	99.99	809	99.88								
	1300					3360	99.97	688	99.85								
	1800					2800	99.96										
	2000	4	71.4	3	65.2	4200	99.98	3444	99.9	3	63.3	21	95.2				
HR-9	200					4098	99.97										
	800					8196	99.99										
	2131	26	95.4	14	93.1	8196	99.99	77	98.70	12	91.2	56	98.2				
HR-10	1500	95	99.0	23	95.6	2880	99.97	200	99.50	18	94.4			151	99.3		
HR-11[c]																	
HR-12[d]	360	33	97.0	49	97.9	3150	99.97			7	86.3	649	99.8				
	860	28	96.4	39	97.4	3150	99.97	116	99.1	10	90.0	325	99.7				
	1500	3	60.3	2	52.3	15	93.46	2	43.6	5	81.4	3	64.6				
HR-13[c]																	
HR-14[d]	300					698	99.86	37.6	97.34	8	87.5	135	99.3			8.3	88.0
	800					77	98.71			7	85.7	58	98.3	11	91.0	1.4	29.6
	1300					9	89.43		8.27	4	75.0	13	92.6			2.7	62.5
	1700					11	91.04		28.96	4	71.4	13	92.6			1.7	42.8
	1942	3	66.7	10	91.6	16	93.91			4	75.0	25	96.0	13	92.3	1.5	34.6
HR-15[e]	341					586	99.83		99.99								
	800					938	99.89	35.2	97.16								
<1 ppm	1240					1563	99.94	9.0	88.85								
	1791	81	98.78	13	92.6	2344	99.96	13.3	92.50	6	84.0	442	99.78				
HR-16	463					1032	99.90	76.0	98.68							2.7	63.33
	900					2580	99.96	8.9	88.82							5.0	80.00
2 ppm	1350					2580	99.96	1.2	17.11								
	1601	20	95.0	4	71.1	2580	99.96	1.6	39.47	6	84.0	587	99.83			5.45	81.67

[a]Deliberate breakthrough run to ascertain Sr^{90}, Cs^{137}, and hardness limits.
[b]High-activity run; Co^{60} spill at ORNL, 1.7×10^3 dis min^{-1} ml^{-1} Co^{60} in feed.
[c]Precipitation-clarification equipment operated only.
[d]Excess (2 to 3 ppm) PO_4, in feed solutions, polishing filter breakthrough.
[e]Use of 0.005 *M* Na_2CO_3 as process additive.

like the lime-soda process, is not very effective in cold water containing less than 100 to 150 ppm hardness. Unless special precautions are taken,[10] the water will be supersaturated with hardness salts. A residual hardness of about 20 ppm from the head-end step will reduce the breakthrough capacity of the carboxylic phenolic resin for cesium by 50% (Fig. 3.20) in the subsequent ion exchange step. High residual hardness is also accompanied by a reduction in decontamination factors for ruthenium, cobalt, total rare earths, and other nuclides normally removed by this step. Decontamination is reduced from the usual 70 to 90% to 30 to 50%.[4]

Phosphates in the waste stream prevent complete precipitation through supersaturation effects. Supersaturation encountered with ORNL low-level waste was initially attributed to hexametaphosphate, since the effect is the same as the "threshold" treatment[11] of water with a very low concentration of Calgon. This treatment depends on surface phenomena rather than on stoichiometric chemical reactions and involves isolation of nuclei from which crystals of calcium carbonate might grow; precipitation is prevented. The concentration of hexametaphosphate is much less (1 to 5 ppm) than would be required if sequestration of metal ions were accomplished (100 ppm). This effect was studied in a continuous laboratory-scale clarification unit with tap water and pure hexameta-, ortho-, pyro-, and polyphosphates; commercial detergents; and decontaminating solutions. The same residual hardness was obtained for equal concentrations of contaminant (as PO_4^{3-}) independent of the type of phosphate employed (Table 3.14).

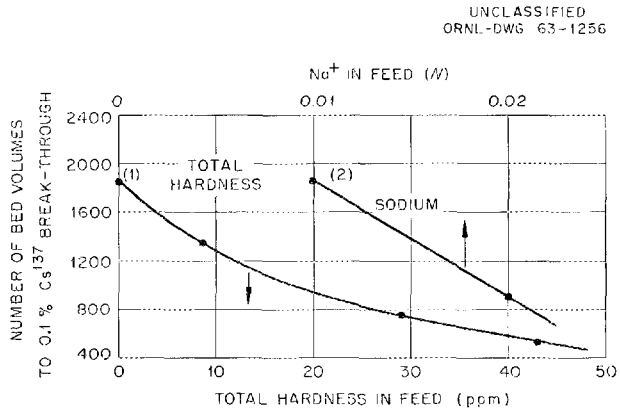

Fig. 3.20. The Effect of: (1) Total Hardness on Cs^{137} Breakthrough Capacity in Presence of 0.01 N Na^+, and (2) Sodium on Cs^{137} Breakthrough Capacity in Absence of Total Hardness.

Table 3.11. Low-Level Waste Water Decontamination in Scavenging-Precipitation Ion Exchange Process

Nuclide	Process Water Activity (% of MPC_w[a])					
	Influent			Effluent		
	High	Low	Av	High	Low	Av
Sr^{90}	7567	2081	3891	2.7	0.45	1.10
Cs^{137}	62	3	12	2.1	0.01	0.30
Co^{60}	149	<1	12	0.5	0.06	0.17
Ru^{106}	7	<1	4	4.4[b]	0.45	1.95
TRE, β[c]	12	3	6	1.1	0.02	0.35

[a]For continuous occupational exposure for a 168-hr week.

[b]Runs HR-14, -15, -16 only.

[c]Calculated as Y^{91}.

[10]P. Hamer, J. Jackson, and E. F. Thurston, *Industrial Water Treatment Practice*, pp 22–37, Butterworths, in association with Imperial Chemical Industries Limited, London, 1961.

[11]*Calgon in Industry*, Hagan Chemicals and Control, Inc., Pittsburgh.

Table 3.12. Activity Removal from ORNL Low-Level Waste by Lime-Soda and Scavenging-Precipitation Ion Exchange Process for Five-Month Period

Process	Water Treated (millions of gal)	Activity Removal from Low-Level Waste (%)			
		Sr^{90}	Co^{60}	Cs^{137}	TRE, β
Lime-soda	43	62.2	30.8	72.6	72.8
Scavenging–ion exchange	0.6	>99.99	84.9	>99.7	89.7

Table 3.13. Operating Costs for Various Throughput Rates of Ion Exchange Columns, Scavenging-Precipitation Ion Exchange Process for Low-Level Waste Treatment
(All costs are in ¢/1000 gal of waste fed to process)

	Bed Volumes			
	2000	1500	1000	500
Fixed costs				
Utilities	1.0	1.0	1.0	1.0
Labor	16.4	16.4	16.4	16.4
Maintenance	7.0	7.0	7.0	7.0
Amortization	7.0	7.0	7.0	7.0
Total fixed costs	31.4	31.4	31.4	31.4
Chemical costs				
NaOH for pH adjustment	13.4	13.4	13.4	13.4
NaOH for column backwash	1.4	1.9	2.8	5.7
NaOH for regenerant waste neutralization	1.7	2.2	3.4	6.6
HNO_3 for resin regeneration	2.6	3.4	5.1	10.2
Total chemical costs	19.1	20.9	24.7	35.9
Waste-handling costs				
Evaporation of regenerant waste	8.8	11.7	17.6	35.1
Tank storage of regenerant waste concentrate	6.3	8.4	12.6	25.2
Burial of scavenging sludge	6.0	6.0	5.0	4.0
Total waste disposal costs	21.1	26.1	35.2	64.3
Total operating costs	71.6	78.4	91.3	131.6

Table 3.14. Effect of Phosphates on Hardness Precipitation and Hardness Removal by Ion Exchange

Phosphate in Waste (ppm)	Residual Hardness in Clarifier Effluent (ppm)	Number of Bed Volumes to Hardness Breakthrough on Amberlite IRC-50 Resin
0	0–2	$> 10^4$
1	8–9	$> 10^4$
2	30–40	8400
3	60	2400
4–5	70	1200
> 5	70	1200

The "threshold" effect of up to 3 ppm phosphate was counteracted by the addition of 0.005 *M* Na_2CO_3 (53 ppm), which reduced the residual hardness from about 60 ppm to less than 5. Decontamination efficiency for ruthenium, cobalt, total rare earths, etc., in the precipitation step was restored. The removal of the calcium also restored the efficiency of the ion exchange column for strontium decontamination. However, the increase in sodium concentration from the normal content of the water (0.01 *N*) to 0.02 *N* (from the 0.005 *M* Na_2CO_3) reduced the ion exchange capacity of the resin for cesium by 50% (Fig. 3.20).

Ion Exchange. – Another approach to the supersaturation problem is to accept the high residual hardness from the precipitation softening when phosphates are present and to maintain high decontamination of cesium and strontium by more frequent regeneration of the resin. This is less

favorable economically (Table 3.13) than treating with Na_2CO_3 when using the carboxylic-phenolic resin Duolite (CS-100), which has a capacity of 0.4 to 0.5 meq of calcium per milliliter of wet sodium-form resin. Another carboxylic resin (Amberlite IRC-50) achieved a loading of 1.45 meq of calcium per milliliter of wet sodium-form resin (Table 3.14).

Amberlite IRC-50 resin has little capacity for cesium and thus cannot be used to replace Duolite CS-100. It will protect the capacity of the phenolic resin from saturation with hardness when used as a pretreatment column. In this case, sodium carbonate is not required with the attendant addition of sodium ions, which decrease the cesium decontamination. The Amberlite IRC-50 ion exchange method introduces only a stoichiometric amount of sodium and thus protects the loading capacity of the phenolic resin for cesium. Since the residual hardness reaches a maximum at about 70 ppm (the fraction of hardness due to calcium), the ion exchange method of removing hardness is independent of phosphate concentrations over 4 ppm. Conversely, the sodium carbonate requirement is dependent on the phosphate concentration – 0.01 *M* Na_2CO_3 at 4 to 5 ppm of phosphate and 0.015 *M* at 5 to 6 ppm of phosphate.

Alumina Adsorption. – By pretreatment of the neutral waste with alumina, phosphate concentrations can be reduced to where their effect is negligible. Passing 2000 bed volumes of actual waste through 0.6 bed volume of alumina removed enough phosphate to allow precipitation to less than 10 ppm of residual hardness. The residual hardness increased to 15 ppm after 260 hr (about three cycles of the ion exchange system) of continuous operation. The residual hardness reached 73 ppm within 24 hr after the alumina was taken off-stream, and reduced to 8 ppm when replaced on-stream. A colored band of ruthenium containing about 4 μc of Ru^{106} was removed, along with some cobalt, on elution of the alumina column with 1 *M* NaOH. The efficiency of ruthenium and cobalt removal is unknown since the experiment was optimized for phosphate removal. Further experiments are in progress to define the overall efficiency of alumina and anionic organic resins for the removal of ruthenium, cobalt, and phosphate.

Pilot-Plant Modifications. – Changes in the equipment and piping for the ORNL Low-Level Pilot Plant were made in order to demonstrate the operation of the fixed-bed and continuous ion exchange processes (proposed by Higgins[12]) and a new agitated clarifier for the scavenging-precipitation ion exchange process. The fixed-bed and continuous ion exchange processes have a potential advantage over the scavenging–ion exchange process in that they may require less chemicals for wastes that have less than 400 ppm of hardness. Laboratory-scale tests on an agitator-clarifier produced satisfactory precipitation and separation of hardness at throughput rates up to four times higher than those used in the present pilot-plant clarifier. Following these tests, the pilot plant will be modified to test foam separation (see the section on "Foam Separation," following in this chapter).

Fixed-Bed Ion Exchange Process. – The Fixed-Bed Ion Exchange Process involves the use of two cation beds in series: a weak-acid resin followed by a strong-acid resin. The weak-acid resin removes the bulk of the calcium and magnesium and can be regenerated by dilute nitric acid in almost stoichiometric proportion to the exchange capacity of the resin. The strong-acid bed is thus free to sorb cesium, strontium, and other fission products and is regenerated with 5 *M* HNO_3. This acid-regenerating solution containing excess acid is used to regenerate the weak-acid bed at more frequent intervals. Decontamination factors of 1000 and 100 for strontium and cesium, respectively, are expected for this process.

A flowsheet for the Low-Level Pilot Plant equipment is shown in Fig. 3.21. The first of the two existing 28-gal beds is filled with Amberlite IRC-50 resin and the second with Dowex 50. An anthracite filter is used upstream of the beds to remove algae and suspended matter. At a feed rate of 10 gpm, it is estimated that the Amberlite IRC-50 resin will require regeneration daily, while the Dowex 50 might operate for two days, based on a feed hardness of 115 ppm (as calcium carbonate). The Dowex 50 resin is regenerated upflow with a 0.72 bed volume of 5 *M* HNO_3. Two acid cuts are used to regenerate the IRC-50 bed: the first is the final 0.56 bed volume cut from the prior IRC-50

[12]Letter from I. R. Higgins to R. E. Blanco, January 1963. Final report to be prepared by Chemical Separation Company on ORNL contract following pilot-plant tests.

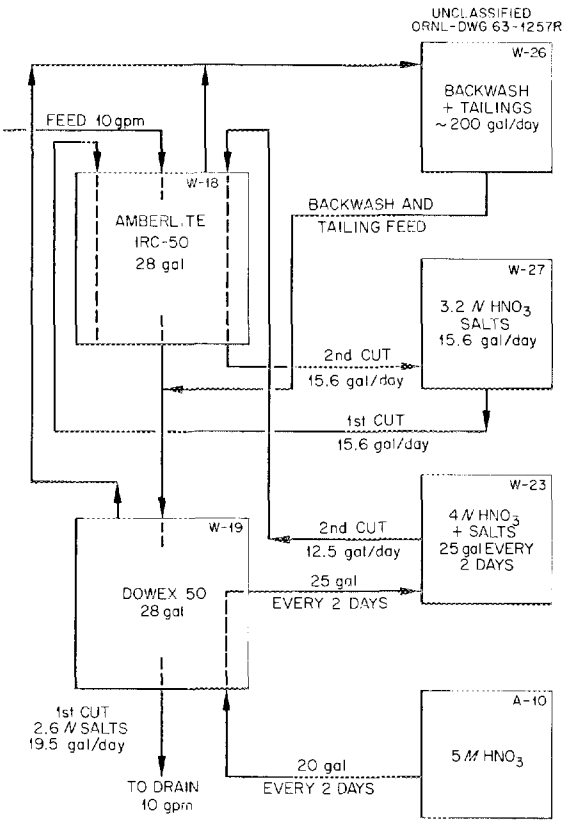

Fig. 3.21. Flowsheet for Weak- and Strong-Acid Fixed Bed Ion Exchange Process for the Low-Level-Waste Pilot Plant.

regeneration, and the second is the 0.45 bed volume of acid collected from the Dowex 50 regeneration. The second cut is stored for use as the first cut in the next IRC-50 regeneration. Nearly all the acid should be used in regeneration of the beds, producing an approximately 2 *N* calcium and sodium nitrate salt solution. Washes from both regenerations are collected and recycled.

Agitated Clarifier. – The present nonagitated clarifier in the Low-Level Pilot Plant has a velocity of 15.6 gal hr^{-1} ft^{-2} in the main blanket section; this is considerably lower than the velocities used in industrial practice (25 to 100 gal hr^{-1} ft^{-2}). Studies with agitated clarifiers up to 9 in. in diameter (see "Laboratory Studies," this section, and also Sec 1.2) showed that the outlet turbidities were not significantly higher for rates up to 60 gal hr^{-1} ft^{-2}. These studies were performed on Oak Ridge tap water and ORNL low-level waste adjusted to 0.01 *M* in caustic and 5 ppm in iron (same treatment as used in the Low-Level Pilot Plant). Therefore, the design basis of the new 4-ft-diam agitated clarifier (see Fig. 3.22) for the Pilot Plant used a maximum velocity of 60 gph/ft^2 for the 10-gpm rate.

The clarifier design includes a bottom conical inlet section for forming the floc and the sludge blanket. A distributor is positioned directly above the inlet to prevent channeling of the inlet waste through the center of the bed. The two removable four-bladed agitator paddles can be positioned at any point along the shaft. The purpose of the agitator is to promote precipitation of the hardness in the sludge blanket and to provide a better distribution of the solids in the blanket, thereby preventing channeling. The required speed range for the agitator (0.5 to 5 rpm) was scaled up from laboratory data by using a constant volumetric power input according to the following equation:

$$N_P = N_L \left(\frac{d_L}{d_P} \right)^{2/3} ,$$

where

N_P = speed of pilot-plant agitator,

N_L = speed of agitator used in laboratory,

d_P = diameter of pilot-plant agitator,

d_L = diameter of agitator used in laboratory.

Foam Separation

Laboratory Studies. – Studies of the application of foam separation for decontaminating low-radioactivity-level process waste water (LAW) were continued both with synthetic and ORNL waste water. Since Sr^{90} is the most deleterious contaminant, much of the experimental work was devoted to its removal. Since it has been shown[1] that the large amounts of calcium (60 to 70 ppm as $CaCO_3$) present in the LAW interfere with Sr^{90} removal by foam separation, it was necessary to precipitate a large fraction of the calcium as a carbonate or phosphate prior to foam separation.

Two basic flowsheets were developed (Fig. 3.23). The first, a two-step process, involves the precipitation of calcium as the carbonate or orthophosphate in a slowly stirred, upflow sludge column that produces a clear effluent having a low calcium concentration (2 to 6 ppm as $CaCO_3$)

(Fig. 3.23*a*). This effluent, without filtration, is fed to the countercurrent, continuous foam column contactor. The second, a one-step process, involves contacting the waste water with the precipitation-inducing chemicals plus surfactants (phosphate, ferric iron, dodecylbenzenesulfonate (DBS), and Armeen Z) (Fig. 3.23*b*) in a small mixing chamber, wherein calcium precipitates as the phosphate. Solids plus solution are fed to the foam column, in which ionic contaminants are removed as a result of the homogeneous foam process, and the solids are removed by frothing or flotation.

Two-Step Process. – The agitation of the upflow sludge bed is important since this movement prevents channeling in the bed. This agitation produces other advantages, such as a faster precipitation rate in the lower part of the bed and better filtration in the upper zone, not only of inorganic solids but also of the algae and organic matter that carry contamination.

Calcium carbonate precipitation is slow and is sensitive to impurities such as phosphates. This was a problem in continuous contactor experiments, and a series of beaker tests was performed to determine the effects of impurities that are present periodically in ORNL process waste water.[13] Of these impurities, the household detergent Fab and the decontaminating agent Turco 4324, both of which contain large amounts of phosphates, cause a serious reduction in the rate of calcium precipitation. A few parts per

[13] E. Schonfeld, *Use of Alkali Carbonate and Alkali Phosphate to Eliminate Inhibitory Effects of Some Impurities on the Precipitation of Calcium and Magnesium from Process Water Waste*, ORNL TM-505 (in press).

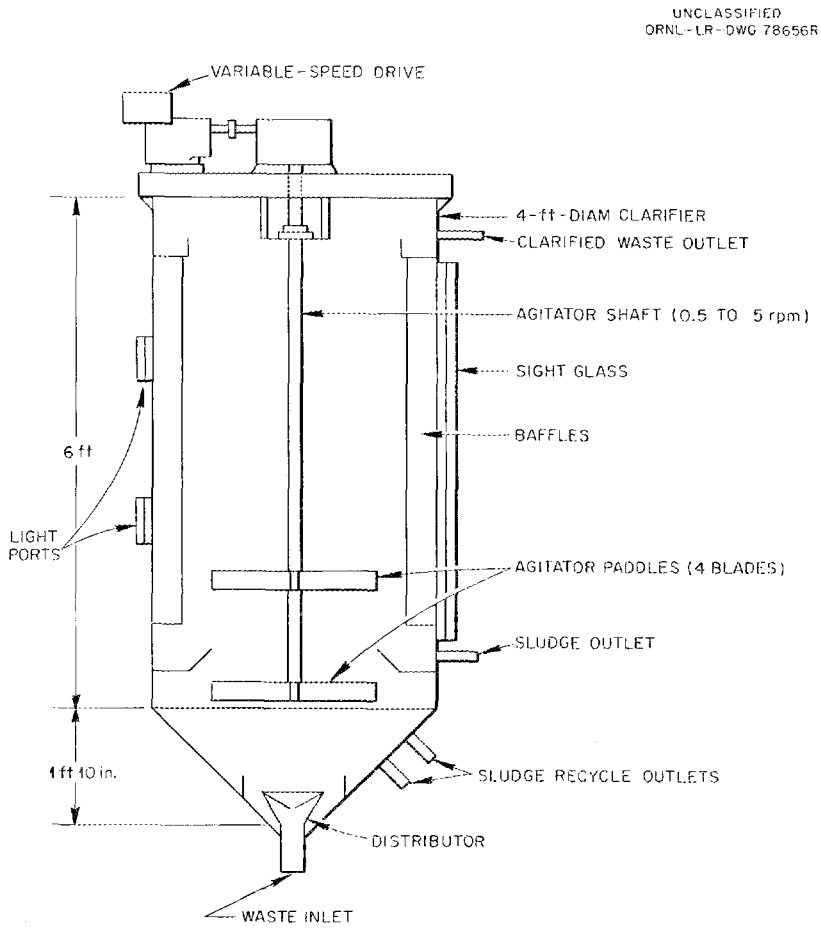

Fig. 3.22. Agitated Clarifier for the Low-Level-Waste Pilot Plant.

million strongly inhibits calcium carbonate precipitation when the solution is made 0.005 or 0.01 *M* in NaOH but does not affect the precipitation of calcium as the orthophosphate. When sodium carbonate (0.005 *M*) and ferric iron (2 to 8 ppm) were added, the inhibitory effect of phosphate was nearly eliminated. The completeness of calcium precipitation, that is, the efficiency in eliminating the detrimental effects of phosphate impurities, was proportional to the iron concentration and dependent on the order of addition of the chemicals. With LAW containing 5 ppm of PO_4^{3-}, the total hardness (initially 110 to 140 ppm), after adding ferric iron and caustic-carbonate

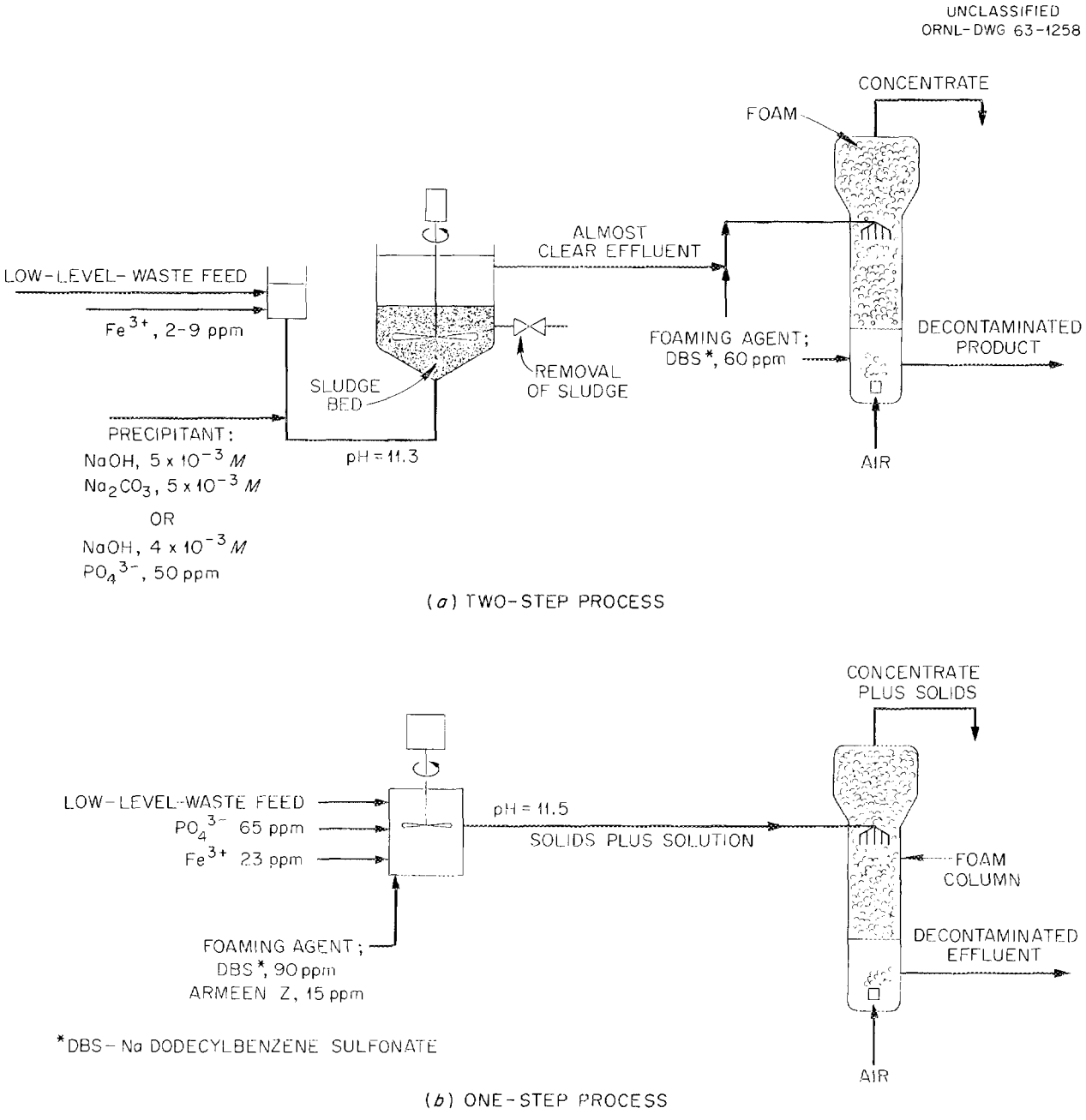

Fig. 3.23. The (*a*) Two-Step, Precipitation–Foam Separation and (*b*) One-Step Flotation–Foam Separation Processes.

at the same point to make the water 8 ppm in Fe^{3+} and 0.005 *M* each in NaOH and Na_2CO_3, was reduced to 25 ppm (as $CaCO_3$); when only the iron (up to 20 ppm) was initially added to water containing 10 to 14 ppm of PO_4^{3-} and then caustic-carbonate was introduced after a 4-min holdup, the hardness was reduced to 2 to 5 ppm.

Studies showed the absence of any effect of sludge-height/column-diameter ratio, which was varied from 2 to 0.5, on the chemical and mechanical behavior of the column when linear water flow rates and roughly equal peripheral speeds of the paddle were used.

Continuous sludge-column experiments with LAW were performed in columns having diameters of 2, 3, 4, and 9 in. at flow rates from 7 to 60 gal ft^{-2} hr^{-1} (Table 3.15). For comparison, data from the existing lime-soda treatment plant are given. Filtration of the effluent with quantitative-grade paper produced little increase in sludge-column decontamination factors for Cs^{137}, Sr^{90}, and Ru^{103}-Ru^{106}, which were 1.1, 10 to 15, and 2 respectively. The Ce^{144} and Co^{60} decontamination factors, which ranged from 10 to 30 and 30 to 40, respectively, were increased about 40% by filtration. The Cs^{137} decontamination is poor; but the addition of grundite clay, 0.5 lb per 1000 gal of simulated waste, gave a decontamination factor between 10 and 40 (ref 14). This sludge contactor produces a clear effluent for many potential secondary treatment processes, in addition to sizable decontamination factors for many isotopes. The sludge bed, after settling an hour, had a volume 1/1200 that of the liquid treated. A solid waste was obtained by adding 59 g of cement per 100 g of decanted sludge (12% solids), corresponding to a cement cost of $0.05 per 1000 gal of water treated.

The composite laboratory unit for the two-step process (Fig. 3.23*a*) was a 3-in.-diam sludge column (20 gal ft^{-2} hr^{-1}) and a 1.5-in.-diam countercurrent, continuous foam column (60 gal ft^{-2} hr^{-1}). The foaming agent, sodium dodecylbenzenesulfonate, was used as described above, and the alkali content of the water was adjusted to 0.005 *M* each in Na_2CO_3 and NaOH. The iron concentration ranged from 4 to 9 ppm. In a four-day run with ORNL tap water spiked with Sr^{85}, the overall strontium decontamination factors were 10^3 to $>10^4$. The flow rate ratios of gas to liquid in the foam column were 10 to 15. Better strontium decontamination was obtained at the higher ratio. The decontamination factor across the foam column was in excess of 100.

Initial scouting runs were performed with actual ORNL low-level process waste water. The foam surface area rate to liquid feed rate was lower in these experiments, because of a wider range in bubble diameters (0.1 to 1 mm), than that obtained with tap water, but other conditions were the same. Based on gamma-ray spectrometry (rather than on radiochemical analyses), decontamination factors larger than 15, 20, and 210 were obtained.

One-Step Process.[15] – Calcium phosphate precipitation is fast and is not inhibited by the polyphosphates or other phosphates; hence a simpler one-step process may be practical. Instead of using a large holdup upflow sludge column as a precipitator, a small premixer-precipitator is used, and the feed to the foam column consists of solution containing suspended solids. Experiments with this process were conducted with synthetic waste water of the following composition:

$MgCl_2 \cdot 6H_2O$	58.5 ppm
$NaHCO_3$	28.5 ppm
$CaCl_2 \cdot 2H_2O$	98.5 ppm
Sr^{2+}	10^{-6} *M*
pH	7
Sr^{85} tracer	$\sim 10^{-10}$ *M*

About 67 ppm of PO_4^{3-}, 23 ppm of Fe^{2+}, 90 ppm of foaming agent Siponate DS-10, and 15 ppm of the flotation agent Armeen Z were added, and the pH was adjusted to 11.5 with sodium hydroxide. The solution and the precipitate that was formed after the pH adjustment and during the holdup of 10 to 20 min in the premixer were fed continuously into a 2-in.-diam multistage foam separation column. The liquid feed throughput was 30 gal ft^{-2} hr^{-1}, and the gas-to-liquid-feed ratio for the best decontamination factor for strontium was 12.4. Under these conditions a strontium decontamination factor in excess of 1000 was achieved.

[14] E. Schonfeld and W. Davis, Jr., *Head-End Treatment of Low-Level Waste Prior to Foam Separations*, ORNL TM-260 (May 29, 1962).

[15] E. Rubin and E. Schonfeld, *Quarterly Progr. Rept. Oct. 1, 1962 to Dec. 31, 1962*, RAI-110.

Table 3.15 Head-End Precipitation of Calcium and Magnesium from ORNL Process Waste Water

Stirred, 9-in.-diam, Sludge Column[a]								Present ORNL Lime-Soda Treatment Plant			
Feed	Effluent		Decontamination Factor					Feed	Effluent		Decontamination Factor for Sr^{90}
Flow Rate (gal ft^{-2} hr^{-1})	Total Hardness (ppm as $CaCO_3$)	Turbidity (ppm)	Ce^{144}	Cs^{137}	Co^{60}	Ru^{106}	Sr^{90}	Flow Rate (gal ft^{-2} hr^{-1})	Total Hardness (ppm as $CaCO_3$)	Turbidity (ppm)	
10	2.0–3.5	1–1.5	~40	1.1	30	1.7	11–15	21	~35	30–40	3.7
15	2.0–4.0	0–1.5		1.1	20		10	21	~35	30–40	3.7
20	2.0–4.0	0–3.5	~40	1.1	10	2.2	11–15	21	40–60	30–40	~3.0
26	2.0–2.5	0–1.5		1.1	15		11.5–13	21	40–60	30–40	~3.0
40	2.0–4.0	1–2.0	~30	1.1	30		11–14	21	40–60	30–40	~3.0
60	2.5–4.5	1–5.0		1.1	50		10	21	40–60	30–40	~3.0

[a]Water was made 0.005 *M* in NaOH, 0.005 *M* in Na_2CO_3, and 2 ppm in ferric iron.

The decontamination factor increased as the gas-to-liquid ratio and the height of the foam column below the feed distributor was increased. Initial tests of the one-step process with ORNL process waste water gave strontium decontamination factors of 200 to 300.

Engineering Studies. – Engineering studies included the effects of parameters on column efficiencies as measured by HTU_x, evaluation of foam drainage and condensation methods, and consideration of foam columns for low-level-waste decontamination.

Foam-separation-column HTU_x values were measured experimentally for stripping of Sr^{89} from aqueous solutions of DBS in a 6-in.-diam column. The lowest HTU_x values of about 1 cm required use of spinneret gas spargers, of liquid flows of 100 gal ft^{-1} hr^{-1} or less, and of uniform liquid feed distribution with low inlet velocities. The most important property of the gas sparger with respect to low HTU_x values was the ability to give a uniform bubble size. There was little variation in HTU_x values for countercurrent column lengths of 10 to 28 cm. The chief effects of liquid and foam flow rates and of liquid distributors on HTU_x values were due to their effects on the amount of channeling. It appeared that uniform liquid feed distribution in large columns might be partly achieved by allowing an extra length of countercurrent flow.

The performances of centrifugal, cyclonic, and sonic foam breakers were evaluated. Capacities for a 120-mesh screen in a 4-in.-diam centrifuge bowl were about 1 ft^3 ft^{-2} min^{-1} for a 150-*g* centrifugal field and 2.5 ft^3 ft^{-2} min^{-1} at 230 *g*. The fraction of uncondensed foam was decreased for 100- or 120-mesh screen as compared to 40 or 200 mesh, for low rates of dry foam as compared to a high rate of wet foam, and for a Teflon stationary wall around the bowl instead of glass. The fraction of foam uncondensed was less than 1% for the Teflon wall and the normal foam densities. The air-operated sonic whistles had a foam-breaking capacity of 0.05 to 0.10 ft^3 of foam per standard cubic foot of operating air. The fraction of foam uncondensed by a 0.4-in.-diam cyclone was from less than 0.2% for a dry foam to 4% for the wetter foams.

Foam densities and the drainage of liquid from the foam were studied. Experimentally measured densities for countercurrent flows of foam and liquid were from 0.065 to 0.360 g of liquid per cubic centimeter of foam; values of 0.12 to 0.32 g/cm^3 were observed for the usual ranges of operating conditions. Drainage to 0.001 g of liquid per cubic centimeter of foam was obtained without excessive foam condensation in either enlarged or horizontal drainage sections at reasonable flow rates.

The operation of foam columns and the recovery of surfactant for low-level-waste decontamination were investigated. A system combining a clarifier for removing calcium and magnesium by precipitation, a foam column, and two single surfactant (recovery) stripping stages was recommended for the ORNL low-level-waste (LLW) pilot plant (Fig. 3.24). A 2-ft-diam column was installed for studies of scaleup and flow problems for this pilot plant (Fig. 3.25). Good distribution of the liquid feed in large columns was obtained only by using orifices or capillary tubes to split the flow into equal streams, which are introduced separately over the column cross section. Probably 30 or more such streams are necessary for the 24-in.-diam column since 19 streams for this column gave visible channeling for up to 30 in. below the feed point. Strontium distribution factors after the addition of DBS to clarifier effluent were 0.6 to 2.4×10^3 $(moles/cm^2)/(moles/cm^3)$; these agree with values measured for 5 ppm Ca^{2+}. Solutions containing 0.01 to 0.02 *M* Na^+ could probably be stripped to about 5 ppm DBS in a surfactant recovery system; experimental surfactant concentrations achieved in a three-stage recovery system agreed with those calculated by using a distribution factor of 7×10^{-4} $(moles/cm^2)/(moles/cm^3)$ for the DBS. The results indicate that the recommended LLW system will give the desired strontium decontamination and use only about 1/2 lb of DBS per 1000 gal of waste water.

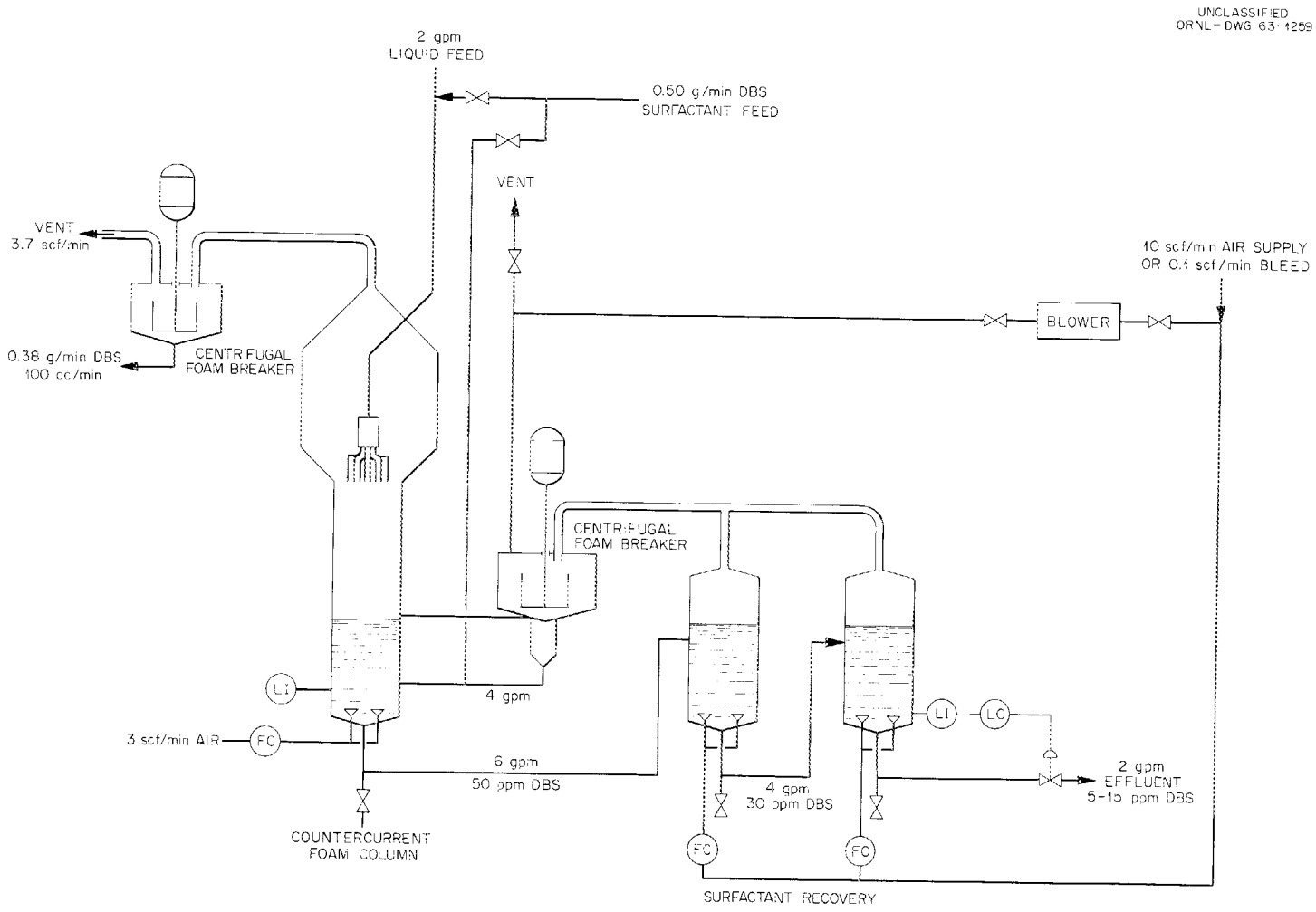

Fig. 3.24. Proposed Pilot Plant LLW Foam Column Flowsheet.

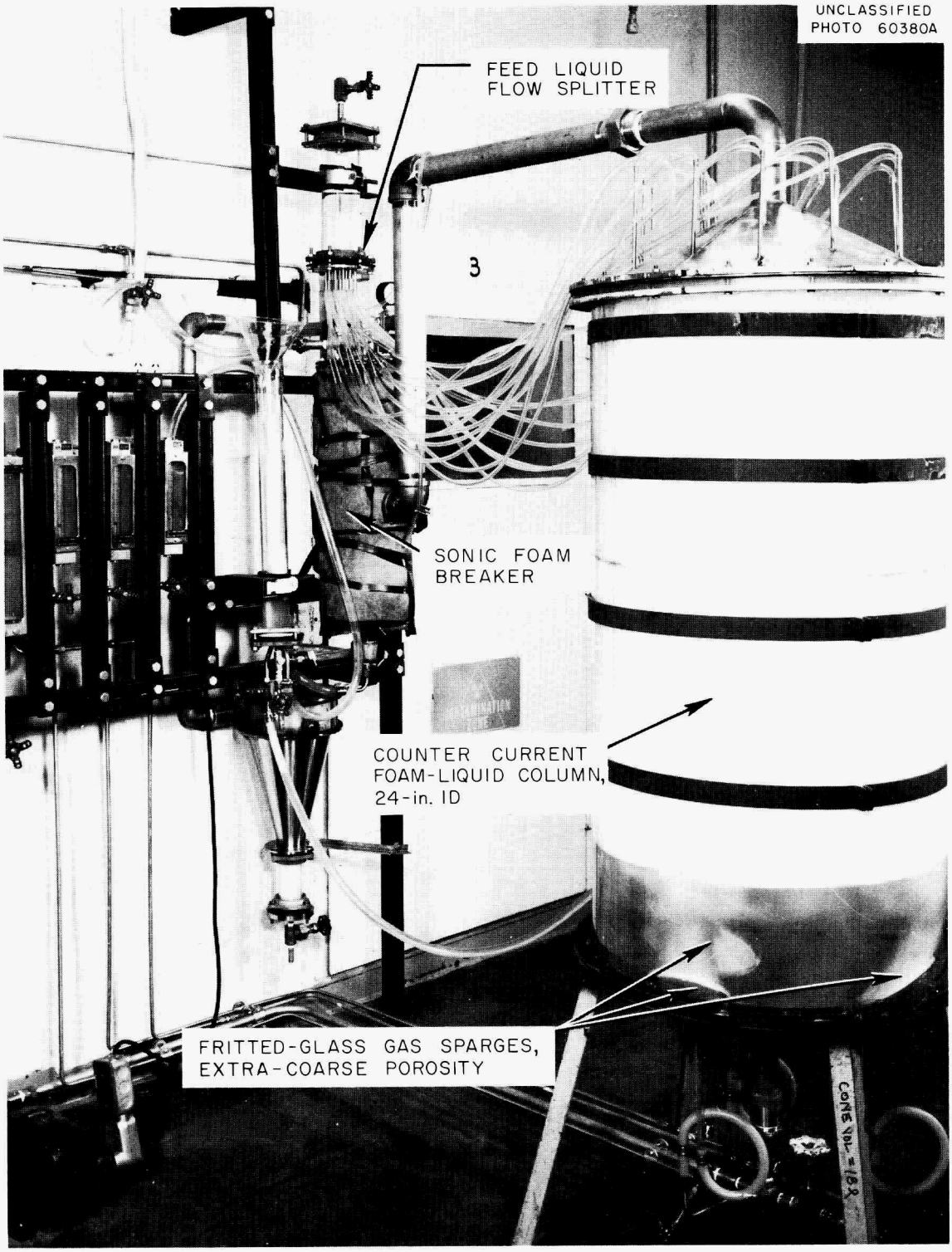

Fig. 3.25. Foam Separation Column.

3.3. ENGINEERING, ECONOMICS, AND SAFETY EVALUATIONS

This study, undertaken in cooperation with the ORNL Health Physics Division, has as its objective the evaluation of the economics and safety associated with alternative methods for the ultimate disposal of highly radioactive liquid and solid wastes. All steps between fuel processing and ultimate storage are being considered, and the study should define an optimum combination of operations for each disposal method and indicate the most promising methods for experimental study.

A 6-metric-ton (tonne) per day fuel processing plant is assumed, processing 1500 tonnes/yr of uranium converter fuel at a burnup of 10,000 Mwd/tonne, and 270 tonnes/yr of thorium converter fuel at a burnup of 20,000 Mwd/tonne. This hypothetical plant would process all the fuel from a 15,000-Mw (electrical) nuclear economy, which may be in existence by 1975. The preliminary operations to be evaluated are interim liquid storage, conversion to solids by pot calcination, interim storage of solids, and shipment of calcined solids. The ultimate disposal methods to be evaluated include the storing of calcined solids in salt deposits, in vaults, and in vertical shafts, and of liquids in salt deposits, in porous geologic formations by deep-well injection, and in tanks. Cost studies of the preliminary operations which have been completed and reported previously were devoted to interim liquid storage,[16] conversion to solids by pot calcination,[17] and shipment of calcined solids.[18] Studies of interim storage of solidified wastes[19] and the effects of fission product removal on waste-management costs[20] have recently been completed.

[16] R. L. Bradshaw *et al.*, *Evaluation of Ultimate Disposal Methods for Liquid and Solid Radioactive Wastes. I. Interim Liquid Storage*, ORNL-3128 (Aug. 7, 1961).

[17] J. J. Perona, *Evaluation of Ultimate Disposal Methods for Liquid and Solid Radioactive Wastes. II. Conversion to Solid by Pot Calcination*, ORNL-3192 (Sept. 27, 1961).

[18] J. J. Perona *et al.*, *Evaluation of Ultimate Disposal Methods for Liquid and Solid Radioactive Wastes. IV. Shipment of Calcined Solids*, ORNL-3356 (Oct. 4, 1962).

[19] J. O. Blomeke *et al.*, *Evaluation of Ultimate Disposal Methods for Liquid and Solid Radioactive Wastes. III. Interim Storage of Calcined Solid Wastes*, ORNL-3355 (in press).

Interim Storage of Solidified Wastes

Interim storage facilities were designed to handle cylinders of solidified wastes produced by the pot-calcination plant described previously.[17] It was assumed that Purex and Thorex wastes were converted to solids and calcined in cylinders (6, 12, and 24 in. in diameter by 11 ft high). Calcination after storage of the wastes as both acid and neutralized solutions and the production of a glass from acid Thorex waste were considered.

Interim solids storage periods of 1, 3, 10, and 30 yr in water-filled canals were considered for cylinders with contents aged for 120 days, 1, 3, and 10 yr by interim liquid storage. Although the wide range of conditions resulted in facilities of different sizes and configurations, they consisted, in essence, of a central-facility canal for the receiving and removal of cylinders, canals for the storage of cylinders, and a service area containing the equipment for cooling and purifying the water, a personnel office, and a change room.

The central-facility canal was designed for receiving cylinders of solid waste from the calcination plant, for storing them briefly to permit the detection of defective containers, and for routing them to the proper canal for interim storage. It also served for the underwater loading of the cylinders into casks prior to shipping offsite. It was equipped with an overhead 100-ton bridge crane for lifting the shipping casks and with a 5-ton bridge crane for manipulating the individual cylinders under water.

The cylinders of solidified waste were assumed to be stored upright in canals adjoining the central facility. It was assumed that they were arranged in parallel rows, each row consisting of two cylinders staggered back to back, with a space between rows for moving them in and out. The length of canal required for the storage of these wastes in this array is a function only of interim storage time and is independent of cylinder diameter. The lengths of 48-ft-wide canal required for the various waste types for different storage times (Table 3.16) were broken into more economically and practically sized segments. To provide for drainage and maintenance, 25% excess storage capacity was added to the facility, and each

[20] J. J. Perona *et al.*, *Evaluation of Ultimate Disposal Methods for Liquid and Solid Radioactive Wastes. V. Effects of Fission Product Removal on Waste Management Costs*, ORNL-3357 (in press).

Table 3.16. Lengths, in Feet, of 48-ft-wide Canal Required for Interim Storage Solids from Different Types of Wastes

Type of Waste	Length Required for an Interim Storage Time of:			
	1 yr	3 yr	10 yr	30 yr
Acid Purex	14.5	43.3	145	433
Reacidified Purex	36.2	108	362	1085
Acid Thorex	21.7	65.0	217	650
Reacidified Thorex	64.1	192	640	1920
Thorex glass	28.1	84.5	281	845

segment was sized to handle no more than 25% of the total cylinders, except in those cases where the central facility was larger than a segment. The canals were assumed to be made of 1-ft-thick reinforced concrete around the sides and on the bottom, with interior walls 2 ft thick separating them from the central facility and from each other. The concrete was assumed to be painted with an epoxy-base paint, and each canal segment was equipped with a 5-ton bridge crane for underwater manipulation of the cylinders.

The depth of the water required for shielding varied from 15.4 ft for 120-day-old acid Purex waste to 10 ft for 10-yr-old reacidified Thorex waste, which, together with an additional fixed depth of 13 ft for cylinder height and freeboard, determined the total depth.

As an aid in locating defective cylinders during storage, the canals were provided with aluminum partitions 8 ft apart along their length in order to channel the water for monitoring.

The canal water was recycled for demineralization and cooling. Filters and demineralizers were provided to process the water at a turnover rate of once a week. The cooling system consisted of primary and secondary loops, with pumps, intermediate heat exchangers, and a cooling tower, and was designed to handle the maximum heat-generation rates computed for Purex and Thorex wastes of different ages and for various storage times.

It was assumed that a masonry building would enclose the central facility, service area, offices, and change rooms and that the storage canals would be housed in a frame building of lighter construction.

Capital costs expressed on an annual basis were computed as the sum of the costs of the various components, allowing 4% interest. Excavation, concrete, and buildings were amortized over 50 yr; aluminum partitions and cranes over 25 yr; cooling systems 20 yr; and demineralizer system, epoxy lining, and radiation monitors 10 yr. The total capital costs ranged from about $35,000/yr for 1-yr storage of 10-yr-old acid Purex waste to $521,000/yr for 30-yr storage of 120-day-decayed reacidified Thorex waste.

Labor costs were assumed to be $113,000/yr for all cases considered. This allowed for 9 man-years (4 shift operators, 1 supervisor, 1 health physicist, and 3 maintenance craftsmen).

Total costs, expressed in terms of mills per electrical kilowatt-hour, were computed for handling each waste type separately and for the combination of acid Purex–acid Thorex and reacidified Purex–reacidified Thorex wastes. Highest costs were for the storage of 120-day-decayed wastes and ranged from 0.018 mill/kwhr (electrical) for 30-yr storage of reacidified Thorex waste to 0.0019 for 1-yr storage of acid Purex. Lowest costs were for storage of 10-yr-decayed wastes, which ranged from 0.017 mill/kwhr (electrical) for 30-yr storage of reacidified Thorex to 0.0015 for 1-yr storage of acid Purex. Although costs did decrease with age of waste at time of storage, this effect was not very pronounced, usually amounting to less than a 15% reduction in costs for storage of 10-yr-decayed wastes compared to an equivalent length of storage of the same wastes aged only 120 days.

The costs of storage of Purex and Thorex wastes together in the same facility ranged from 0.0015 mill/kwhr (electrical) for 1 yr of storage to 0.0048 for 30 yr of storage for the calcined acid wastes, and from 0.0018 to 0.0063 mill/kwhr (electrical) for the calcined reacidified wastes (Fig. 3.26). The storage of acid wastes as solids was cheaper by factors of from 2 to 2.7 than the storage of the same wastes as liquids, reported previously.[16] However, for most storage times, the storage of neutralized liquid wastes was slightly cheaper than that of reacidified Purex and Thorex calcined solids.

Effects of Fission Product Removal

The object of this study was to compare two costs: management costs for wastes from which

large fractions of fission products have been removed by improved processes (representative of the best future technology) and the costs for managing the original wastes with all fission products present. Three cases were studied, each representing a different degree of uniform removal of all fission products: 0, 90, and 99%. The waste from which fission products were removed was assumed to be acid Purex.

Although removal of 90 and 99% of the fission products simplifies the subsequent handling of the wastes from the standpoints of heat dissipation and shielding requirements, the isotopes remaining represent a hazard requiring management under essentially the same conditions of safety as are demanded for the original waste. Costs were estimated in each case, therefore, for the interim storage of liquid waste, pot calcination of waste, interim storage of calcined waste, shipment of the calcined solids, and disposal of the solids in a salt mine. Treatment and disposal schemes were then worked out to minimize the total costs.

No attempt was made to estimate the costs of fission product removal or subsequent disposal of used fission product sources, because there is not yet sufficient information about the separations processes or source characteristics to permit accurate cost estimates.

The compositions and volumes of the waste from the fission product separation plant (in liquid and solid forms) were assumed the same as the neutralized Purex waste previously treated in this study;[16,17] that is, the processes for the removal of the fission products did not greatly increase the volume or solids content of the waste produced per ton or amount of uranium processed (an optimistic assumption). With these assumptions, adjustments in the costs of waste management are attributable to the reduced heat removal and shielding requirements caused by fission product removal.

Costs of interim liquid storage were less for fission-product-depleted wastes because of the reduced amount of heat to be dissipated and because mild steel tanks could be used rather than stainless steel. These costs were about the same for 90- and 99%-depleted wastes, ranging from 0.0011 to 0.0025 mill/kwhr (electrical); costs for acid Purex waste ranged from 0.0018 to 0.0069 mill/kwhr (electrical) for storage periods of 1 to 30 yr.

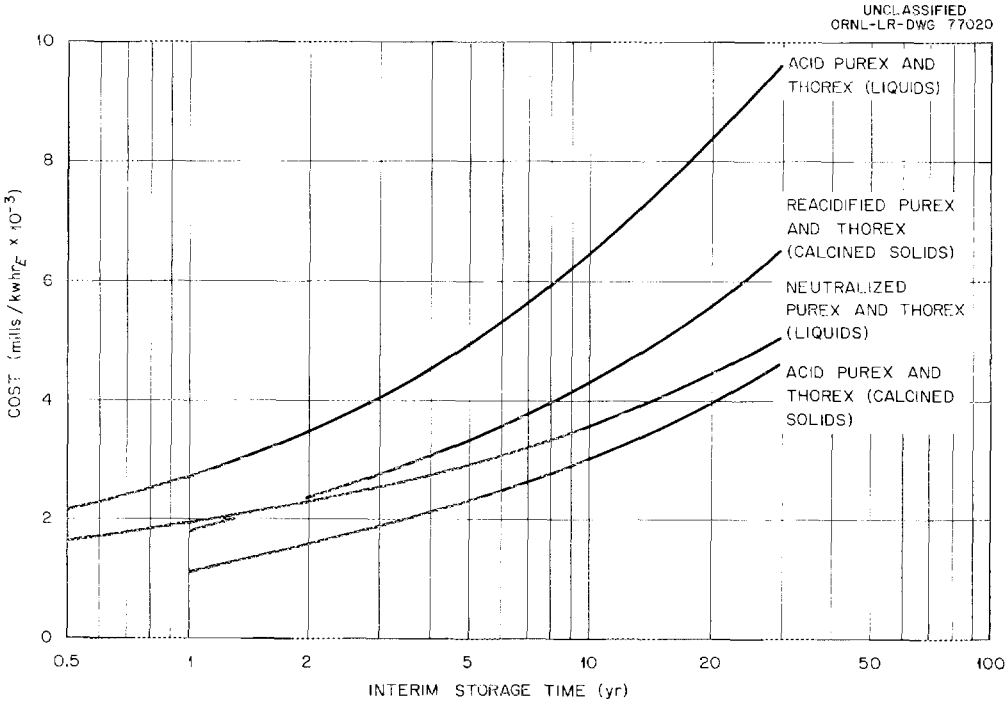

Fig. 3.26. Comparative Costs of Interim Storage of Liquid and Calcined Wastes.

Pot-calcination costs were the same for depleted wastes as for neutralized Purex waste, because these costs were not affected by heat removal considerations and the variations in shielding requirements had negligible effect on the costs. They varied from 0.0215 to 0.0113 mill/kwhr (electrical) for fission-product-depleted and neutralized wastes (which require reacidification before calcination) and from 0.0123 to 0.0081 mill/kwhr (electrical) for acid Purex for cylinder diameters of 6 to 24 in.

Interim solids storage costs were less for depleted wastes than for calcined acid Purex for a short storage period (up to 3 yr), where cooling systems costs were important; however, these costs were higher for depleted wastes for longer storage periods as their greater volume, resulting in more cylinders to be stored, became the predominating effect.

Both 90- and 99%-depleted wastes could be shipped immediately on discharge from the calcination plant in the largest shipping casks considered feasible, which hold four 24-in.-diam cylinders. A minimum aging of 11 yr is required before shipping acid Purex waste in this manner. Shipping costs were generally lower for acid Purex than for depleted wastes if shipping in 6- or 12-in.-diam cylinders and were about the same if shipping in 24-in.-diam cylinders. These costs fell in the range of 0.0005 to 0.005 mill/kwhr (electrical) for 1000-mile shipments.

Ultimate disposal costs of calcined wastes in a salt mine were roughly half as much for depleted wastes as for acid Purex, 0.0037 to 0.0056 mill/kwhr (electrical) for depleted wastes vs 0.0067 to 0.0132 mill/kwhr (electrical) for acid Purex.[21] The removal of fission products would decrease the heat-generation rate of the waste and thus allow closer spacing of the cylinders in the floor of the room. For fission-product-removal wastes the limiting salt temperature of 400°F was controlling rather than the limiting calcination temperature of 1650°F at the axis of the waste cylinder. Mine space requirements range from 2 to 6 acres/yr for acid Purex waste, 0.2 to 1.3 acres/yr for 90%-depleted waste, and 0.04 to 0.17 acres/yr for 99%-depleted waste. Minimum center-to-center spacings were assumed to be 2, 5.3, and 8 ft for 6-, 12-, and 24-in.-diam cylinders. The minimum age at which acid Purex waste in 24-in.-diam cylinders can be placed in the salt formation is about 30 yr; however, 6- and 12-in. cylinders filled with 99%-depleted waste would be stored at the minimum spacing for all ages.

The term "total waste-management costs" is used here to mean the cost of disposal in a salt formation plus the costs of all necessary preliminary steps. The disposal cost is a function of the age at burial, diameter of the cylindrical container, and degree of fission product removal. Thus, total waste-management costs reflect these functions.

In computing total costs, consideration must be given to the minimum ages for calcination and disposal in vessels of a given diameter, as determined by fission product heat-generation rates. Minimum ages for burial in salt are 2.3, 5.5, and 30 yr for untreated acid Purex waste in 6-, 12-, and 24-in.-diam vessels; and 1.2 yr for 90%-depleted waste in 24-in.-diam vessels. For all other cases for depleted wastes, the minimum age is 0.33 yr, the assumed age at the time of discharge from the fuel processing plant. Minimum pot-calcination ages for acid Purex waste are 0.6, 2.2, and 6.5 yr for 6-, 12-, and 24-in.-diam vessels.

Prior to computing the costs of interim storage, it next must be observed that storage as calcined solid is cheaper than storage as liquid for acid Purex; but for the depleted wastes, liquid storage is cheaper. Even so, some liquid storage must be used for untreated acid Purex waste due to economically justified decay cooling of this waste prior to calcination. In obtaining the total waste-management costs, the minimum cost of interim storage was used, subject to the various minimum age requirements.

The results are shown graphically in Fig. 3.27. For the case of untreated acid Purex in 6-in.-diam cylinders, the largest shipping cask, which results in lowest costs, cannot be used prior to a waste age of 2.8 yr; hence the break in the curve in Fig. 3.27.

Total waste-management cost for acid Purex decreased as age at burial increased, and at 30 yr (the upper limit used in the study), it was about 0.025 mill/kwhr (electrical) with both 12- and 24-in.-diam cylinders. Costs for depleted wastes were cheaper with 24-in.-diam vessels and not so strongly affected by age, falling in the range of

[21] R. L. Bradshaw *et al.*, *Evaluation of Ultimate Disposal Methods for Liquid and Solid Radioactive Wastes. VI. Disposal of Solid Wastes in Salt Media*, ORNL-3358 (in press).

0.017 to 0.019 mill/kwhr (electrical) for both 90- and 99%-depleted wastes for ages from 0.33 to 30 yr. Relatively little cost reduction (about 7%) is achieved by increasing the fraction of fission products removed from 90 to 99%.

A rather optimistic estimate of the amount to be gained in waste-management costs with removal of 90 to 99% of the fission products is about 0.006 mill/kwhr (electrical), which is equivalent to about $400 per tonne of uranium processed. Thus, the cost of managing wastes that contain only 1% of the fission products is 70% as much as the cost for wastes containing all the fission products, representing a savings of 30%. Because this savings is not nearly enough to pay for fission product separation, packaging, and disposal, such practices would not be carried out as part of a waste-management scheme but would necessarily depend on a large and diverse market for fission products to pay the major portion of these costs. If such a favorable large market exists, then, obviously, wastes depleted in fission products (particularly from strontium and cesium) will be calcined and stored with a lower cost than wastes containing all the cesium and strontium. Conversely, if no large market exists (i.e., for all the cesium and strontium), then savings which result from the ultimate storage of cesium- and strontium-free waste cannot justify the cost of removal of specific fission products.

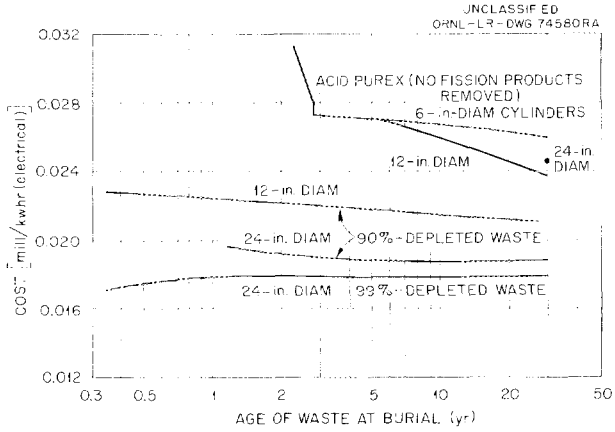

Fig. 3.27. Total Costs for Interim Storage, Calcination, Shipment, and Disposal in a Salt Mine.

4. Transuranium Element Processing

4.1 CHEMICAL PROCESS DEVELOPMENT

The Transuranium Processing Plant (TRU) and a very-high-flux reactor, the High Flux Isotope Reactor (HFIR), are being built here in order to provide gram quantities of many of the transuranium elements and milligram quantities of some of the transcalifornium isotopes. These materials will be used for research purposes in laboratories throughout the country.

Long-term irradiation of 10-kg batches of Pu^{239} in the Savannah River production reactor produces about 600 g of Pu^{242} and a 300-g mixture of Am^{243} and Cm^{244}, the starting materials for further irradiation in the HFIR. After an irradiation of 12 to 18 months, the transcurium elements will be recovered as products, and the curium isotopes will be returned to the reactor for additional irradiation.

Chemical processes are being developed, and equipment is being designed in order to make the target rods, dissolve and recover the transuranium elements from the irradiated targets, and then prepare and ship the recovered chemicals to customers as required. This report summarizes the development of the chemical separations processes, equipment design, and the design and development of TRU. Development of the procedures for making the targets is under the direction of the Metals and Ceramics Division and is not reported here. Corrosion studies being done in the Reactor Chemistry Division are also reported elsewhere.

After plutonium-aluminum alloy has been irradiated in the Savannah River production reactor to greater than 99.9% burnup of the Pu^{239}, the

residual plutonium, which is primarily the mass-242 isotope, will be recovered (also at SRL) by conventional solvent extraction or anion exchange procedures. Alternative methods which are being developed at ORNL for recovering Am^{243} and Cm^{244} from the raffinate of the plutonium-recovery step are outlined in Fig. 4.1. One method consists in concentrating americium, curium, and rare-earth (RE) fission products by anion exchange, converting to a chloride system by amine extraction of nitric acid from mixed hydrochloric-nitric acid solution, and separating americium and curium from rare earths by the Tramex process. In the second method, concentration of Am-Cm-RE and conversion to a chloride system are combined into a single extraction cycle. Americium, curium, and rare earths are extracted into tertiary amine from neutral nitrate solution and are stripped into dilute hydrochloric acid.

The main-line HFIR target processing method (Fig. 4.2) consists in target dissolution in hydrochloric acid; actinide separation from fission products and aluminum by the Tramex process; transcurium element separation from americium and curium by phosphonate extraction from dilute hydrochloric acid; berkelium separation from californium, einsteinium, and fermium by dialkyl phosphate extraction of Bk(IV) from concentrated nitric acid; and californium, einsteinium, and

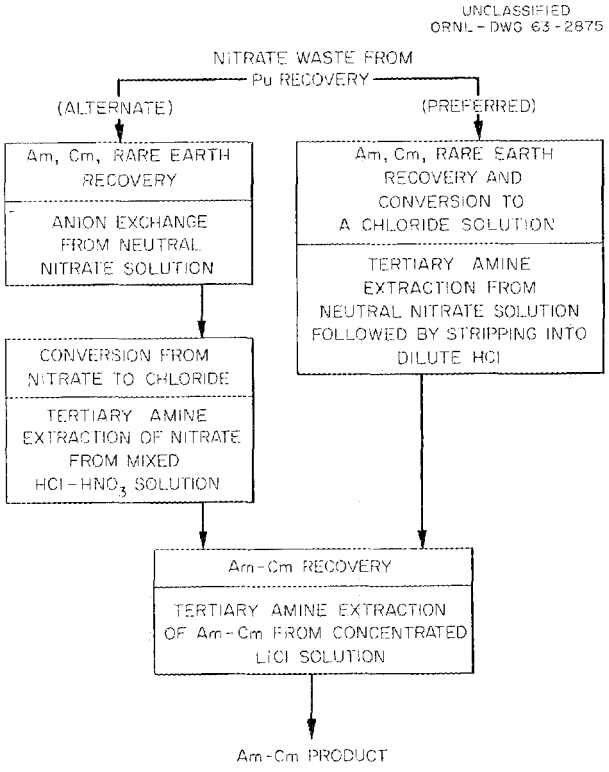

Fig. 4.1. Summary Flowsheet for Americium-Curium Recovery for Plutonium Process Waste.

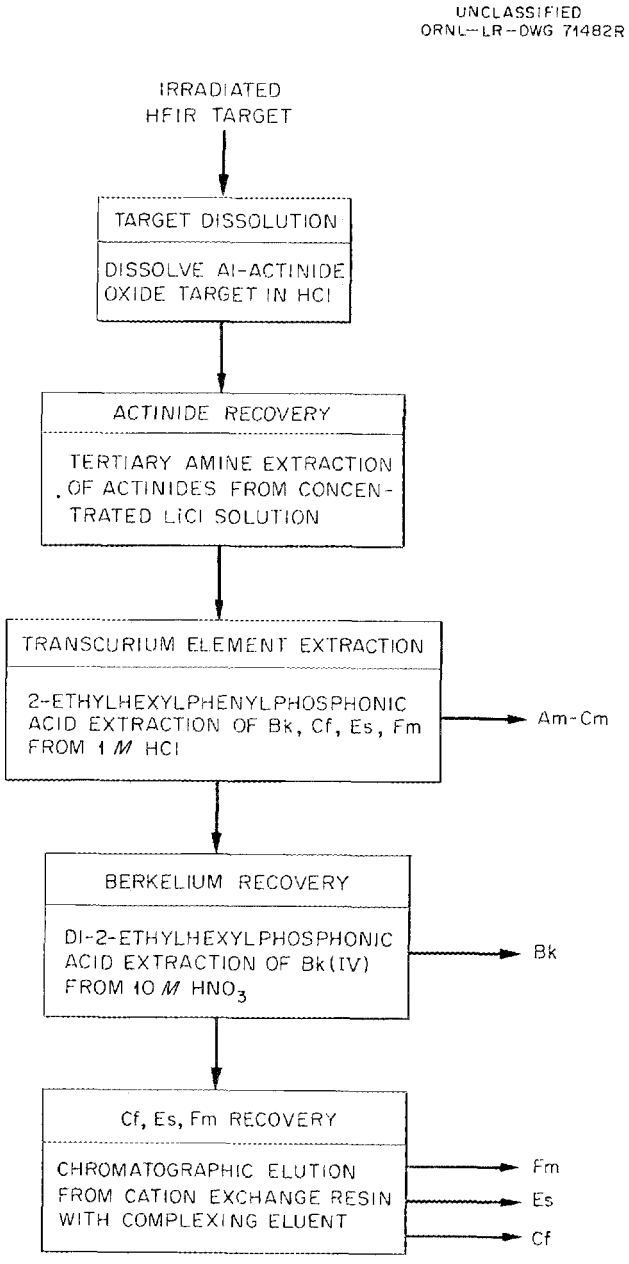

Fig. 4.2. Summary Flowsheet for HFIR Target Processing.

fermium isolation by chromatographic elution from a cation exchange resin.

In addition to development of the main-line process methods, scouting tests were made in order to find methods for separating americium from curium, to determine the possibility of actinide-lanthanide separation in a carbonate system, and to develop a method to prepare PuO_2 for HFIR targets.

Recovery of Americium, Curium, and Rare Earths from Nitrate Solutions

Additional laboratory studies were made of variables affecting the anion exchange recovery of americium and curium from nitrate solution,[1] and an attractive alternative procedure, based on teritary amine extraction, was developed. A full-activity-level demonstration of the ion exchange process was provided by the americium-curium recovery program (Sec 5.1) in which eight plutonium-aluminum alloy rods irradiated to produce Pu^{242}, Am^{243}, and Cm^{244} for HFIR targets were processed in cell 1, Building 4507, to recover plutonium and the americium and curium contained in the plutonium waste effluent. Difficulty in operating this anion exchange process at a production scale clearly indicates that the solvent extraction method using tertiary amine is to be preferred.

The anion exchange process makes use of the sorption of americium, curium, and rare earths on an anion exchange resin from concentrated aluminum nitrate solutions of low acidity, whereas the amine extraction process[2] depends on the extraction of these elements into tertiary amine solvent from neutral nitrate solution. With either process, americium and curium can be recovered in dilute nitric acid solution, free of aluminum, corrosion products, and most fission products except the rare earths. The nitrate product can be converted to chloride by adding HCl and extracting the HNO_3 with a tertiary amine;[1] the americium and curium can then be purified by the Tramex process.

The concentration of Am-Cm-RE and their conversion to chlorides can be combined into a single extraction cycle by extracting from the nitrate solution and stripping with hydrochloric acid.

Recovery of Americium-Curium from Nitrate Solution by Anion Exchange. – Laboratory studies of this process have been concerned with the effects of rare-earth concentrations in the feed, flow rate through the column, and acid deficiency in the feed. The capacity of Dowex 1-X10 resin for cerium was investigated; however, values for total resin capacity were not obtained since equilibrium was not reached in the 96 hr of contact time. No evidence of radiation damage was noted when full-activity-level feed was in contact with the resin for 21 days.

Effect of Feed Variables: Rare-Earth Concentration, Flow Rate, and Acid Deficiency. – The behavior of europium tracer, which sorbs slightly less than curium, was used to measure the effects of these variables. Tests were made with a 1-in.-diam glass column filled with resin to a depth of 45 cm. Europium losses were measured during sorption at 60°C from 15 column-displacement volumes of feed and during subsequent washing with 5 displacement volumes of 8 *M* $LiNO_3$.

Increasing the rare-earth concentration above 0.5 g/liter in 2.6 *M* $Al(NO_3)_3$ feed adversely affected europium recovery (Fig. 4.3). With a flow rate of 2 ml cm^{-2} min^{-1}, europium recoveries were 89, 87, 77, 62, and 40% for rare-earth feed concentrations of 0.5, 1.0, 1.5, 2.0, and 5.0 g/liter respectively. This effect can be offset by decreasing the flow rate, as shown by the results plotted in Fig. 4.4. Europium recovery from feed containing rare earths at a concentration of 2 g/liter was increased from 62% to 89% by decreasing the flow rate from 2 to 1 ml cm^{-2} min^{-1}. The same effect is shown in Fig. 4.5 for feed containing a 5 g/liter concentration of rare earths; however, europium losses were 40%, even at a flow rate of 0.6 ml cm^{-2} min^{-1}. Since there was no appreciable europium loss during loading from the first 10 displacement volumes of feed, complete europium recovery can be obtained by limiting the amount of feed to less than this volume.

Since acid-deficient aluminum nitrate is more soluble than neutral aluminum nitrate, and since the highest possible aluminum concentrations are required for satisfactory americium-curium recovery, the effect of acid-deficient feed on europium recovery was investigated. With 2.6 *M* Al^{3+} it was found that europium recovery was unaffected

[1] F. L. Culler *et al.*, *Chem. Technol. Div. Ann. Progr. Rept. June 30, 1962*, ORNL-3314, pp 133–34.

[2] R. E. Leuze *et al.*, *Transuranium Quarterly Progress Report for Period Ending August 31, 1962*, ORNL-3375, pp 11–12.

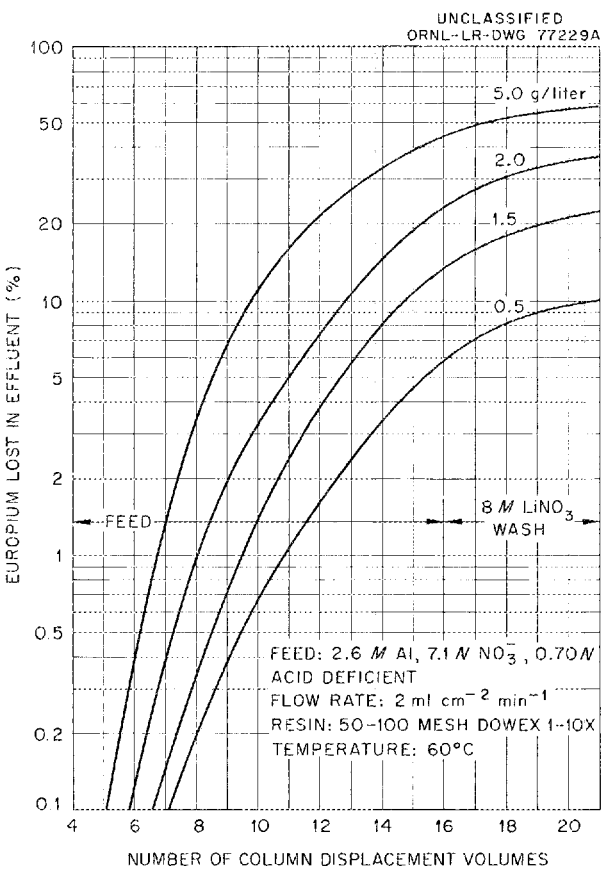

Fig. 4.3. Europium Losses During Rare-Earth Loading on Anion Exchange Resin: Effect of Rare-Earth Feed Concentration.

in changing from neutral feed to 0.7 *N* acid-deficient feed. However, by increasing acid deficiency from 0.7 to 1.17 *N*, europium recovery was decreased from 90% to about 81%.

The effect of acid-deficient feed on the behavior of iron was investigated, and it was found that 2 g of iron per liter in the 0.5 *N* acid-deficient feed did not affect europium recovery. Iron did not load or precipitate on the column, and only 0.8% was found in the product cut.

Resin Capacity. – An attempt was made to determine the cerium loading capacity for three mesh sizes of Dowex 1-X10 resin. However, equilibrium was not attained in 96 hr at 25°C. In these experiments, a gram of dry resin was tumbled in 10 ml of 9 *M* $LiNO_3$ which contained cerium (20 g/liter) as $Ce(NO_3)_3$, plus cerium tracer. The results are shown in Fig. 4.6. Resin loading increased with decreasing particle size, and equilibrium was approached more rapidly with finer resin. In 96 hr, it appeared that equilibrium was nearly reached for –400-mesh resin but not for 100- to 200-mesh or 50- to 100-mesh resin.

Resin Stability at Full Activity Levels. – Dowex 1-X10 resin in contact with high-activity-level feed for 21 days showed no evidence of radiation damage. Two grams of resin was in contact for 21 days with 4 ml of 2.6 *M* $Al(NO_3)_3$ containing 3.14×10^8 gross alpha and 1.68×10^{10} gross gamma counts per minute per milliliter. This solution was prepared from full-activity-level plutonium waste effluent. There was no visible discoloration of the resins, and the gross alpha distribution coefficient K_d increased slowly during the first eight days and then remained constant at about 50. This behavior is similar to that for cerium, noted above.

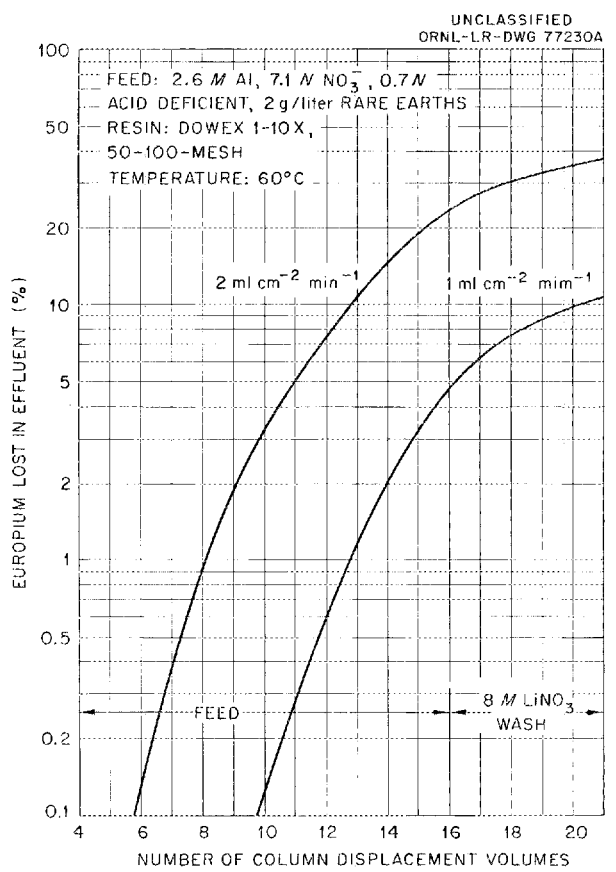

Fig. 4.4. Europium Losses During Rare-Earth Loading on Anion Exchange Resin: Effect of Flow Rate for Feed Containing Rare Earths at a Concentration of 2 g/liter.

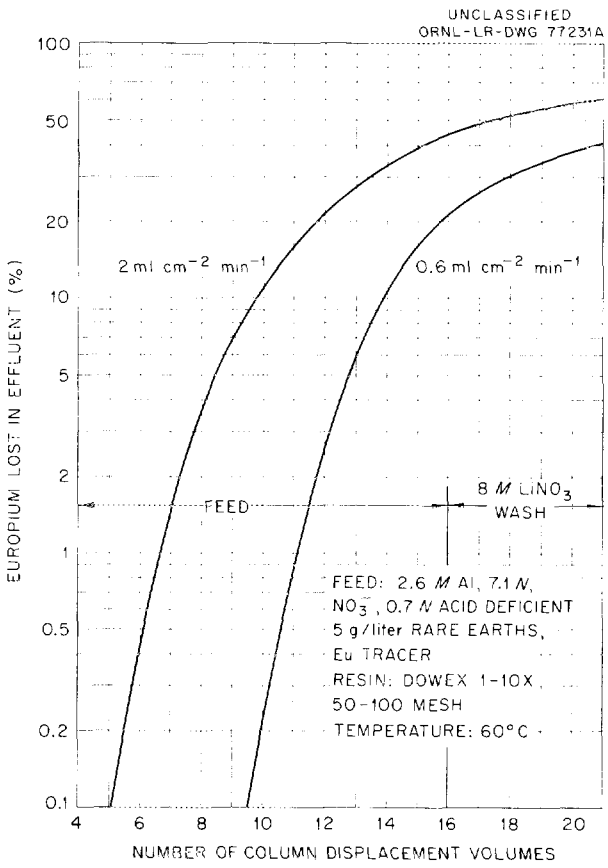

Fig. 4.5. Europium Losses During Rare-Earth Loading on Anion Exchange Resin: Effect of Flow Rate for Feed Containing Rare Earths at a Concentration of 5 g/liter.

Amine Extraction of Americium-Curium from Nitrate Solution. – Laboratory-scale mixer-settler runs demonstrated excellent curium extraction by 0.6 *M* Alamine 336·HNO_3 in diethylbenzene (DEB) and good decontamination from corrosion products aluminum and nitrate. Distribution coefficients determined for curium and for a number of possible contaminants from $LiNO_3$ solution vs 0.6 *M* Alamine 336·HNO_3 in DEB also confirm the possibility of good decontamination. The most effective salts for maximum curium extraction are those nitrates that form higher hydrates. Americium and curium distribution coefficients varied by a factor of over 40 for different diluents. The solvent, 0.6 *M* Alamine 336·HNO_3–DEB, is a satisfactory extractant, giving an americium distribution coefficient of 8 when contacted with 3 *M* $LiNO_3$–1 *M* $Al(NO_3)_3$.

Flowsheet and Mixer-Settler Demonstrations. – The flowsheet for americium-curium recovery from neutral nitrate is shown in Fig. 4.7. Americium, curium, and rare-earth fission products are extracted with 0.6 *M* Alamine 336·HNO_3 in DEB from 1 to 2 *M* $Al(NO_3)_3$ solutions, scrubbed with 8 *M* $LiNO_3$, and eluted with 3 *M* HCl. Eight extraction and eight scrub stages are used with a feed/scrub/extraction ratio of 1:1:2. Stripping is accomplished with 3 *M* HCl in conjunction with a neutral amine scrub.

In laboratory demonstrations of this process, a curium recovery of 99.8% was achieved with 1 *M* $Al(NO_3)_3$ feed that contained Cm^{242} and

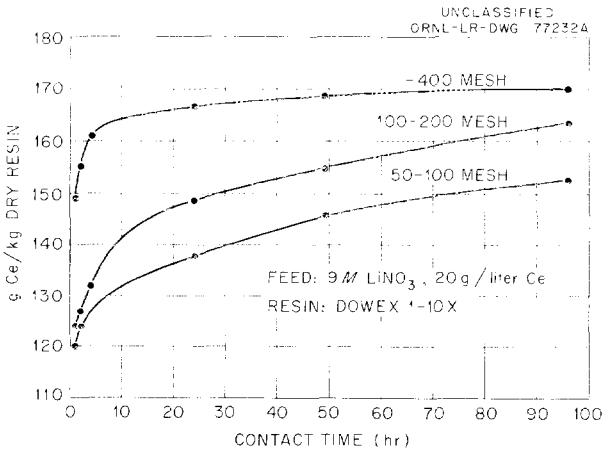

Fig. 4.6. Cerium Loading on Dowex 1-X10 Resin at 25°C.

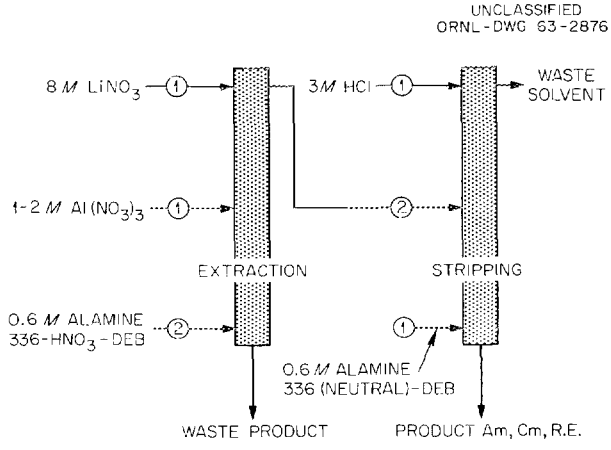

Fig. 4.7. Flowsheet of Amine Extraction Process for Recovery of Americium and Curium from Nitrate Solutions.

$Ru^{103-106}$. About 60% of the ruthenium extracted. The pregnant organic extractant was stripped with half a volume of 3 *M* HCl and then with half a volume of organic scrub [0.6 *M* Alamine 336 (neutral)–DEB]. Ruthenium remained in the organic phase, and an overall decontamination factor of 10^3 from ruthenium was obtained. The curium product was 2.4 *M* in HCl and <0.01 *M* in NO_3^-, which is suitable for feed adjustment for the Tramex process.

A similar laboratory-scale mixer-settler test demonstrated almost complete recovery of rare earths decontaminated from corrosion products. The 2 *M* $Al(NO_3)_3$ simulated feed contained rare earths (5 g/liter) as stand-ins for americium and curium, and it also contained chromium, nickel, and iron (1 g of each per liter). Rare-earth losses in the aqueous waste were only 0.005%, and the extraction of chromium, nickel, and iron was so slight that they could not be detected in the extractant. Aluminum content in the extractant was 0.09 g/liter; this represents an aluminum decontamination factor of about 300.

Distribution Coefficients for Curium and Possible Contaminants. – Distribution coefficients for curium from 3 to 8 *M* $LiNO_3$ into 0.6 *M* Alamine 336·HNO_3 in DEB were determined (Fig. 4.8) and are proportional to about the seventh power of the $LiNO_3$ concentration. Aluminum nitrate and lithium nitrate were interchangeable, with no noticeable difference in extractability. The distribution coefficients were proportional to the square of the Alamine 336·HNO_3 molarity in DEB (Fig. 4.9).

Most contaminants, except the rare-earth fission products, are so inextractable they will remain in the aqueous waste. Distribution coefficients between 0.6 *M* Alamine 336·HNO_3–DEB and 1 *M* $Al(NO_3)_3$–3 *M* $LiNO_3$ were less than 0.001 for Mn, Co, Ni, Cr, Ba, and Sr and less than 0.1 for Fe, Cu, Zn, Ag, Sn, and Zr. Distribution coefficients for Cd, Y, and Pd were 0.6, 2.4, and 120 respectively.

Effect of Metal Cation on Curium Extractability. – Curium extraction into the tertiary amine depends strongly on the type of cation used in the nitrate salting solution. Distribution coefficients between 0.6 *M* Alamine 336·HNO_3–DEB and 6.0 *N* nitrate solutions made from a number of different nitrate salts are given in Table 4.1. The large variation in distribution coefficients from 0.051 for 6 *N* NH_4NO_3 to 5.4 for 6 *N* $Be(NO_3)_2$ appears to be associated with the ability of the smaller

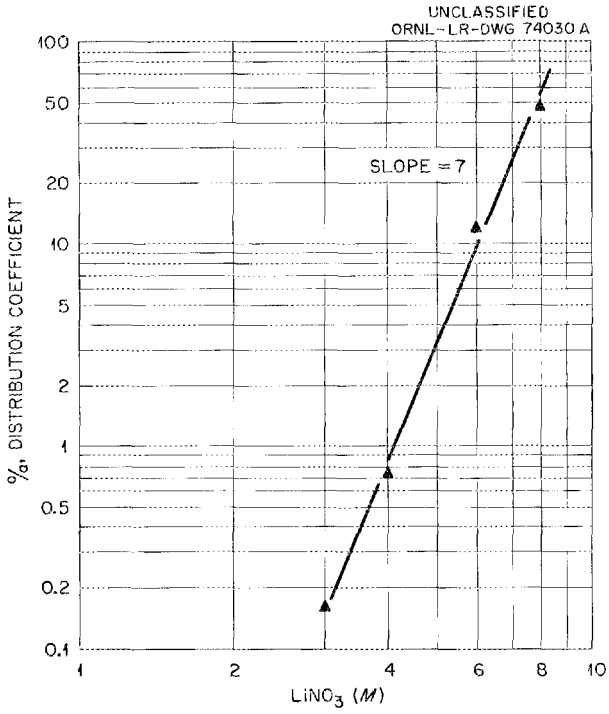

Fig. 4.8. Effect of $LiNO_3$ Concentration on Curium Extraction by 0.6 M Alamine 336·HNO_3–DEB.

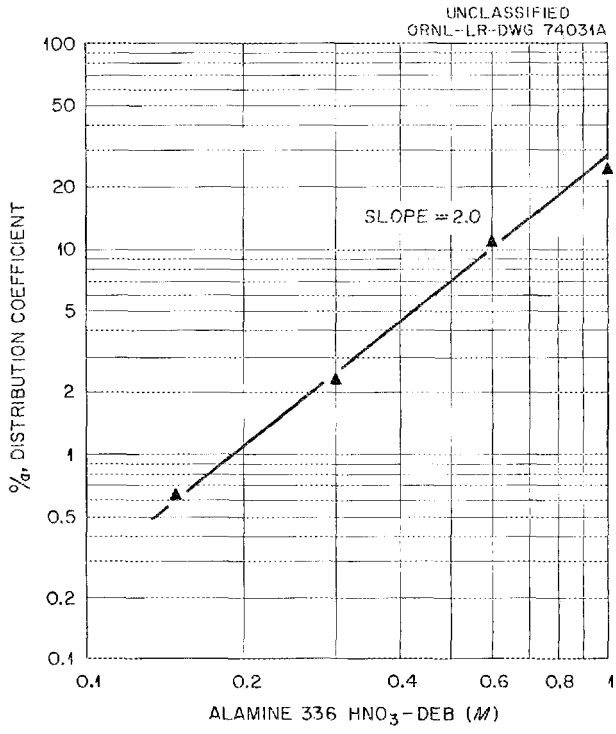

Fig. 4.9. Effect of Amine Concentration on Curium Extraction from 2 M $Al(NO_3)_3$.

ions to tie up larger amounts of water by hydration, thereby increasing the nitrate activity of the solution.

Effect of Diluent on Americium and Curium Extractability. – When different diluents were used for the extractant, americium distribution coefficients varied from 0.53 to 38; curium distribution coefficients varied from 0.43 to 20; and americium-curium separation factors varied from 1.23 to 2.06 for the system 0.6 *M* Alamine 336·HNO_3 vs 3 *M* $LiNO_3$–1 *M* $Al(NO_3)_3$. These data, along with viscosity of the solvent and water content of the solvent after equilibration, are given in Table 4.2. Based on the viscosity of 5.4 centipoises and distribution coefficients of 8.0 for americium and 5.3 for curium, DEB is a satisfactory diluent and is recommended, since it is the diluent also used for the Tramex process.

Water content of the solvent was nearly constant for a wide variety of diluents and appears to be associated with the amine at the mole ratio of 4 amine molecules to 1 of water. Water content did increase slightly when 2-ethyl hexanol was added to prevent the formation of a second organic phase.

Table 4.1. Effect of Various Metal Nitrate Salting Solutions on Curium Extraction into 0.6 *M* Alamine 336·HNO_3–DEB

Cation	NO_3^- (*N*)	Distribution Coefficient, E_a^o, for Curium[a]	Ionic Radius[b] (*A*)
NH^4	6.0	0.05	1.48
Na	6.0	0.10	0.95
Ca	6.0	0.24	0.99
Mg	6.0	4.07	0.65
Li	6.0	4.04	0.60
Be	6.0	5.40	0.31

[a]Cation extraction coefficient, E_a^o = (cation concentration in organic phase)/(cation concentration in aqueous phase) at equilibrium.

[b]Linus Pauling, *Nature of the Chemical Bond*, 2d ed., p 350, Cornell University Press, Ithaca, N.Y., 1948.

Tramex Process Development

Investigations continued on developing, testing, and improving the Tramex process for separating transplutonium elements from fission products, corrosion products, and aluminum used in irradiation targets. This process is useful for recovering all known transplutonium elements as a group, and

Table 4.2. Effect of Various Diluents on Extractability of Americium-Curium into 0.6 *M* Alamine 336·HNO_3 from 3 *M* $LiNO_3$–1 *M* $Al(NO_3)_3$

Diluent	Viscosity (centipoises)	Water Content (g/liter)	Distribution Coefficient, E_a^o		
			Am	Cm	Am/Cm
1,2 Dichlorobenzene	1.97	3.90	0.53	0.43	1.23
Decane + 10% alcohol	8.15	4.29	2.95	1.52	1.94
Benzene	3.14	2.57	8.04	3.93	2.04
Amsco + 5% alcohol	13.01	3.91	8.45	4.10	2.06
Diethylbenzene	5.39	2.70	7.98	5.27	1.49
Carbon tetrachloride	5.21	2.08	9.00	5.35	1.68
Heptane + 5% alcohol	6.08	3.75	12.30	7.53	1.63
Toluene	3.06	2.43	13.02	8.48	1.53
Triethylbenzene	8.67	3.18	15.10	9.79	1.54
Xylene	3.44	2.39	20.70	12.46	1.59
Diisopropylbenzene	9.08	3.02	28.80	16.70	1.72
Cyclohexane	9.33	2.93	38.20	20.50	1.86

it is planned specifically for isolating Am^{243} plus Cm^{244} from concentrates recovered from plutonium processing raffinates, for isolating all the transplutonium elements from irradiated HFIR targets, and for isolating Cm^{242} plus the remaining Am^{241} from irradiated cermets of AmO_2 and aluminum (Sec 5).

Process conditions presently recommended for maximum decontamination are shown in Fig. 4.10. These differ from the conditions reported last year[3] in three respects: (1) aluminum chloride is added to the feed, (2) more concentrated hydrochloric acid is used for stripping, and (3) strip product is scrubbed with freshly prepared Alamine 336·HNO_2 in DEB diluent. Aluminum chloride was added because it will be present in the feed from target dissolution. This small amount of aluminum chloride is also beneficial since, by hydrolysis, it helps replenish small losses of acid. The acidity of the stripping solution was increased, and the solvent scrub was added to improve decontamination. The higher acidity is more effective in keeping Zr, Nb, and Fe in the solvent phase. The presence of HNO_2 in the solvent scrub keeps ruthenium in the solvent. Results of tests indicate that this process is satisfactory for isolating transplutonium elements from all probable contaminants except some short-lived fission products (such as Ag^{111} and possibly Te^{132}), and from nickel, which comes from the aluminum alloy used in HFIR targets and from corrosion of the process equipment. In most cases, sufficient decay time can be allowed to eliminate difficulties from the short-lived fission products, and nickel can be kept in solution when americium and curium are precipitated as hydroxides by urea hydrolysis or as oxalates from dilute acid solutions containing ammonium ion.

Tests of the basic flowsheet in 1- to 10-ml batch extractions at activity levels up to 10 w of Cm^{242} per liter indicated no serious radiation effects. Solvent exposed to 300 whr/liter, which is three times the anticipated maximum dose in the Transuranium Process Plant, performed satisfactorily. Loss of acid in Tramex feed by radiolysis at high activity level poses a potentially serious problem, since acid concentration must be kept below 0.1 *M* to ensure satisfactory extraction but greater than approximately 0.01 *M* to prevent the precipitation of metal hydroxides. Additional demonstration at full activity and at plant scale is required to firmly establish the capabilities of the Tramex process.

During the past year, work was directed at testing and improving the process and included the following: process demonstration in mixer-settlers, with simulated feed containing tracers; process demonstration by batch countercurrent extraction with high-activity-level feed containing Cm^{242}; behavior studies of short-lived fission products and ruthenium; investigation of the effect of high-level alpha activity on solvent and feed solution; development of feed-adjustment methods; determination of physical properties of Tramex solutions; investigation of acid, americium, and europium distribution coefficients as a function of HCl, LiCl, and $AlCl_3$ concentration in the feed; and evaluation of alternate solvents.

Laboratory-Scale Tests of the Tramex Process. — Laboratory-scale tests of this flowsheet were made in mixer-settlers with eight scrub and eight extraction stages in the first contactor, and eight strip and eight scrub stages in the second contractor. Each of these mechanical stages operated at about 60% efficiency. Runs made with simulated feeds containing macro amounts of rare earths and spiked with small amounts of irradiated Am^{241} (about 1 mg in 300 ml of feed) demonstrated americium and curium recoveries of greater

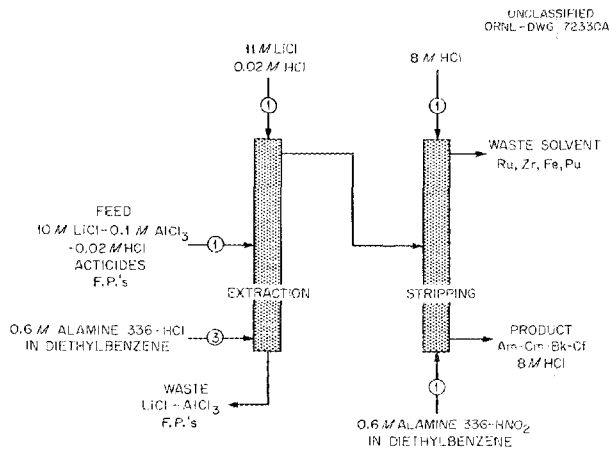

Fig. 4.10. Tramex Process Flowsheet.

[3]F. L. Culler *et al.*, *Chem. Technol. Div. Ann. Progr. Rept. June 30, 1962*, ORNL-3314, pp 128–30.

than 99.9% and fission product decontamination factors of about 10^4. In other tests, with macro amounts of corrosion products and tracer activities in the feeds, iron and chromium decontamination factors were greater than 10^3, and rare-earth, zirconium, and ruthenium decontamination factors were $\geq 10^4$.

Tramex Test at High Activity Level. – Results of testing the Tramex process in a batch countercurrent extraction at a Cm^{242} concentration equivalent to about 4 w/liter indicate no difficulties as a result of the high activity level. Distribution coefficients were in agreement with tracer-level studies, and phase separation was as good as or better than that in the absence of activity. Because of mechanical difficulties, it was not possible to operate the scrubbing and stripping contactors as planned. Two extraction stages were used, and batch stripping was accomplished by shaking the solvent with the strip solution in sample bottles. None of the operating difficulties were due in any way to the activity level of the solutions. Although it was not possible to demonstrate complete recovery and decontamination in this test, the data and operating experience indicate that the Tramex process will be satisfactory at high activity levels.

Process Description. – An Al-AmO_2 cermet target containing 40.3 mg of Am^{241} and 12.5 g of Al was prepared and irradiated in the Oak Ridge Research Reactor for 39 days at a neutron flux of 2.0×10^{14}. After cooling for two months, the aluminum was dissolved in 2.5 *M* NaOH solution. The resulting solution was decanted through a filter, and the residue (containing the americium, curium, and fission products) was washed with dilute sodium hydroxide solution and then with dilute lithium hydroxide solution. The residue was dissolved in warm 6 *M* HCl. Excess acid was distilled off, and $LiCl_3$ and $AlCl_3$ were added to adjust the extraction feed to 9.9 *M* LiCl–0.2 *M* $AlCl_3$ containing a quantity of curium equivalent to approximately 4 w/liter. Of this feed, 7.8-ml portions were contacted with 9-ml volumes of 0.6 *M* Alamine 336·HCl–DEB in two batch countercurrent extraction stages. Solvent containing extracted Am, Cm, Ru, and Zr was stripped with 5 to 8 *M* HCl by collecting each batch of solvent in a sample bottle containing the desired strip solution. These were shaken, and each phase was analyzed to determine stripping results.

Equipment Description. – The equipment pictured in Fig. 4.11 was described previously.[4] The essential features of this equipment were six countercurrent batch-operated extraction stages, a dissolver-evaporator, and associated equipment for transferring the solution, sampling it, handling the off-gas, and disposing of the waste solution. Two of the stages were planned for extraction, one for scrubbing, one for stripping, and two for washing the strip product with fresh solvent. The apparatus was mounted in an alpha-tight enclosure and installed in a cell in Building 3019 High Radiation Level Analytical Facility. Operations were performed by remote manipulation.

Operational Experience and Results. – Caustic dissolution of the aluminum jacket and matrix of the target proceeded normally. About 10% of the Cm^{242} was lost in the aluminum dissolver solution and the caustic washes. The residue was readily dissolved in warm 6 *M* HCl. Analytical results showed that this solution (270 ml) contained 7.9 mg of Cm^{242}, 18 mg of Am^{241}, and 2.1 mg of fission products (see Table 4.3). Thus about 30% of the Am^{241} was converted to Cm^{242}, and

[4] R. E. Leuze *et al.*, *Transuranium Quarterly Progress Report for Period Ending August 31, 1962*, ORNL-3375, pp 6–8.

Table 4.3. Composition of the Dissolver Solution for the High-Activity-Level Tramex Test[a]

Isotope		Quantity (mg)
Cm^{242}		7.9
Am^{241}		18
Pu^{238}		3.1
Pu^{242}		2.1
Fission products		2.1
Sr^{89}	110 mc	
Ru^{103}	360 mc	
Ru^{106}	140 mc	
Cs^{137}	1.8 mc	
Ba^{140}	290 mc	
Ce^{141}	580 mc	
Ce^{144}	85 mc	

[a] The Am-Cm was dissolved in 270 ml of 6 *M* HCl; then this solution was adjusted to 200 ml of extraction feed.

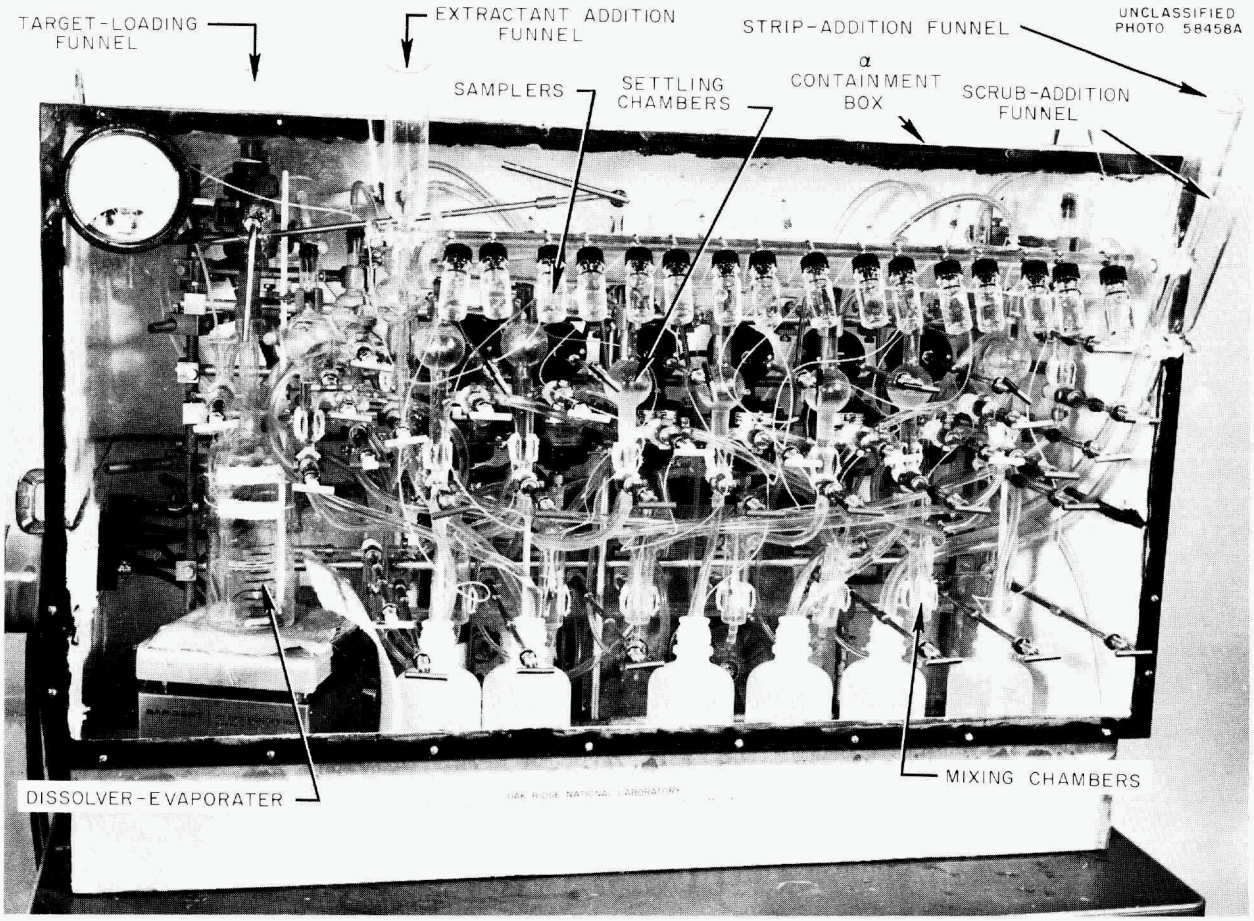

Fig. 4.11. Equipment for Tramex Test at High Activity Level.

about 6.2% of the Am^{241} fissioned during the 39-day irradiation in the ORR at a neutron flux of 2×10^{14}. The dissolver solution was adjusted to approximately 200 ml of extraction feed; the Cm^{242} concentration was about 3.5 mg/liter, equivalent to a power density of approximately 4 w/liter.

During the extended testing period (six weeks) damage to the Tygon tubing by the solvent made the transfer line from stage 3 inoperable, thus making it impossible to use the last four stages. Solution transfer and phase separations in the first two stages were comparable with operations in which no activity was present.

Distribution coefficients for Cm, Ce, Ru, and Zr in the two extraction stages are given in Table 4.4. In general, these are comparable with values obtained at tracer levels except for the zirconium distribution coefficients, which were low.

Material balances over the second extraction stage were Cm, 99%; Ce, 89%; Ru, 240%; and Zr, 103%. Since only two extraction stages were used and the solvent was not scrubbed, neither complete product recovery nor complete decontamination was demonstrated. The best results were obtained when 8 *M* HCl strip was used. Ninety-five percent of the curium was recovered, and cerium, ruthenium, and zirconium decontamination factors were 12, 17, and 5 respectively. Although these results do not offer conclusive proof of the capabilities of the Tramex process, no indications of radiation-related problems appeared at activity levels up to 10 w/liter.

Behavior of Ruthenium in the Tramex Process. – Fission product ruthenium in Tramex feed will probably exist in both the tri- and tetravalent states. Only Ru^{4+} is extracted along with the transplutonium elements; Ru^{3+} remains in the

Table 4.4. Distribution Coefficients of Cm, Ce, Ru, and Zr in High-Activity-Level Tramex Test

Element	E_a^o	
	Feed Stage	Second Stage
Cm	3.5	5[a]
Ce	0.076	0.31[b]
Ru	13	1.4[b]
Zr	3.5	0.46[b]

[a]These increases may be due to decreased acidity of the feed after one contact with the solvent.

[b]These marked decreases may be due to the presence of some inextractable species of these elements.

aqueous waste. Trivalent ruthenium is rapidly oxidized to the tetravalent form by Cl_2, H_2O_2, and nitrite. Since H_2O_2 is produced by radiolysis of the feed solution, it is difficult to keep ruthenium quantitatively in the trivalent state. Therefore, at least some, if not all, the ruthenium can be expected to extract with the transplutonium elements. The tetravalent ruthenium that is extracted is slowly reduced by the solvent to the relatively inextractable Ru^{3+}, thus allowing a small fraction of the ruthenium to be stripped along with the transplutonium elements. In a mixer-settler run with H_2O_2 added to the strip solution, the overall ruthenium decontamination factor was only 10^3. In this case, the H_2O_2 was not completely effective in reoxidizing ruthenium to Ru^{4+} during stripping operations because the H_2O_2 half-life in the strip solution is only about a minute, compared with a residence time of 15 to 20 min in the mixer-settler. In tests at alpha radiation levels of 3 w/liter, H_2O_2 from water radiolysis was not sufficient to keep the ruthenium quantitatively in the solvent during stripping. In mixer-settler tests, the addition of a side stream of $NaNO_2$ to the strip solution (or scrubbing of the strip product with 0.6 *M* Alamine 336·HNO_2) was effective in oxidizing the ruthenium or in forming an extractable complex. In these tests, ruthenium decontamination factors were $\geqq 10^4$, which is adequate for most applications.

Behavior of Short-Lived Fission Products in the Tramex Process. – The 7.5-day Ag^{111} fission product quantitatively followed americium and curium through both extraction and stripping in a laboratory-scale mixer-settler run with synthetic feed spiked with irradiated Am^{241} that had been cooled for two days. The 78-hr Te^{132} fission product was partially extracted, and a small amount was stripped with the product. Although 67-hr Mo^{99}, 8-day I^{131}, and 2.3-hr I^{132} were extracted, they remained in the solvent during stripping.

The distribution coefficient data for Ag^{111} given in Table 4.5 confirm the behavior of silver in the mixer-settler run. Silver can be kept in the solvent if dilute acid is used to strip the transplutonium elements. However, the higher acid concentrations are required for good ruthenium and zirconium decontamination. In most processing, decay times will be long enough to eliminate Ag^{111}.

Effect of Alpha Radiation on Tramex Solutions. – *Solvent.* – No difficulty in phase separation was noted when 0.6 *M* Alamine 336·HCl–DEB was in contact and intermittently mixed with 10.5 *M* LiCl containing Cm^{242} for a total solvent exposure of approximately 300 whr/liter. The most notable effect was a 30% decrease in the curium distribution coefficient, which, however, is still large enough for satisfactory processing. This test indicates that the solvent is sufficiently stable to radiation for full-activity-level processing since the maximum solvent exposure anticipated in the TRU plant is less than 100 whr/liter.

A 10-ml sample of 10.5 *M* LiCl containing Cm^{242} at a concentration of about 25 mg/liter (equivalent to about 3 w/liter) was mixed with 10 ml of a

Table 4.5. Extraction Coefficients of Ag^{111} into 0.6 *M* Alamine 336·HCl–DEB from Chloride Solutions

Composition of the Aqueous Phase (*M*)	E_a^o
1 HCl	420
3 HCl	113
5 HCl	19
7 HCl	2.6
9 HCl	0.4
11 LiCl	19
9 LiCl–0.3 $AlCl_3$	16

0.6 *M* solution of Alamine 336·HCl in DEB. The two phases remained in contact, with occasional remixing, for 116 hr. The curium distribution coefficient decreased from 3.6 to 3.2 at an exposure of approximately 60 whr/liter, and to 2.4 at approximately 300 whr/liter. After an exposure of about 200 whr/liter, some interfacial crud formed but did not cause emulsion problems. Phase separation was satisfactory when the experiment was terminated after an exposure of nearly 300 whr/liter. The curium was readily stripped from the solvent into 9 *M* HCl.

Feed Solution. — A potentially serious problem with loss of acid may result from high activity levels in the Tramex feed solutions. Tests have shown that radiation results in the destruction of acid and the eventual precipitation of those metal cations that form insoluble hydroxides. Since Tramex feed must contain <0.1 *M* HCl in order to obtain sufficiently high distribution coefficients for the transplutonium elements, the adjusted feeds will be stable for only a short time.

Acid-depletion G values (G_{-H^+}) were determined for synthetic Tramex feeds that were 10 *M* in LiCl and contained from 2.6 to 15 w of Cm^{242} per liter. These solutions were kept at room temperature and were vented to the atmosphere. Results of the experiment at 2.6 w/liter are shown in Fig. 4.12. Results of other tests were similar. The initial rate of acid loss corresponded to large G_{-H^+} values of 10 to 20. Later, at acidities below 0.4 *M*, G_{-H^+} values were 2.2 at 2.5 w/liter and 1.0 at 15 w/liter. The solutions became acid deficient, and metal hydroxides (including curium) precipitated. The radiolytic gas from solutions at 15 w/liter contained 1 part Cl_2, 3 parts O_2, and 15 parts H_2; no HCl was detected.

These data indicate that feed solutions at 10 w/liter, which is the proposed operating level, will lose acid at the rate of about 0.1 mole $liter^{-1}$ day^{-1}. Since acid must be less than 0.1 *M* for satisfactory extraction, adjusted feeds will be stable for less than a day unless the acid is replenished.

These investigations are still in progress, with emphasis on determining the acid-loss mechanism, finding methods for reducing the loss, and finding methods for replenishing the acid.

Tramex Feed Adjustment Studies. — Tests made on a 1- to 2-liter scale in laboratory glassware indicate that it is possible to prepare stable Tramex feed of low acidity by simply distilling off water and acid until the desired salt concentration is obtained. Solutions of 2 *M* HCl containing varying amounts of LiCl and $AlCl_3$ were distilled to salt concentrations of 4 to 10 *M* for LiCl and 0.2 to 0.5 *M* for $AlCl_3$. Figure 4.13 shows the approximate concentration of the residual HCl as a function of the final total salt concentration (LiCl plus $AlCl_3$). Maximum salt concentrations obtainable without incurring solution instabilities were also determined as follows:

LiCl	$AlCl_3$
10 *M*	0.2 *M*
9 *M*	0.4 *M*
8 *M*	0.5 *M*

Since Tramex feed will lose acid by radiolysis, it will be necessary to replenish the acid in some manner to prevent precipitation of aluminum and actinide hydroxides. Bubbling HCl gas through an adjusted feed will introduce HCl without diluting

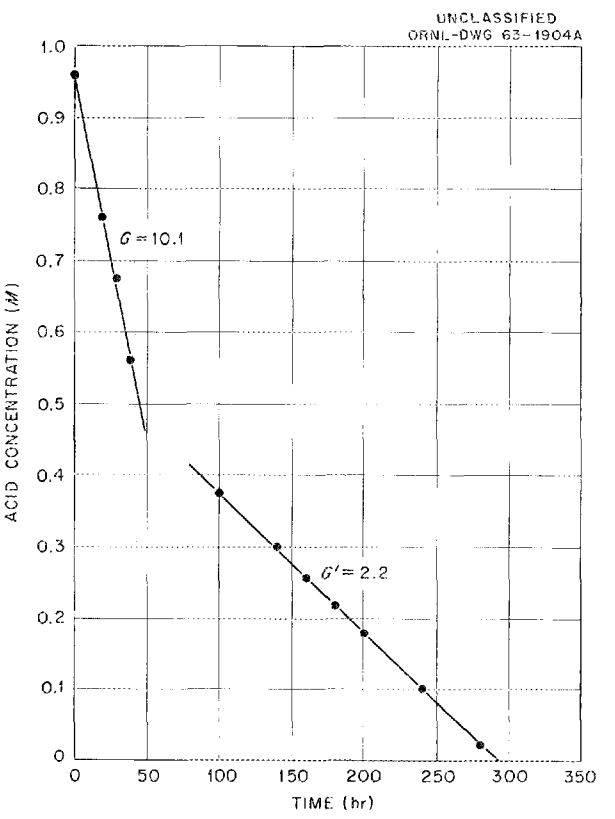

Fig. 4.12. Acid Loss by Radiolysis in 10 M LiCl Containing 2.6 w of Cm^{242} per Liter.

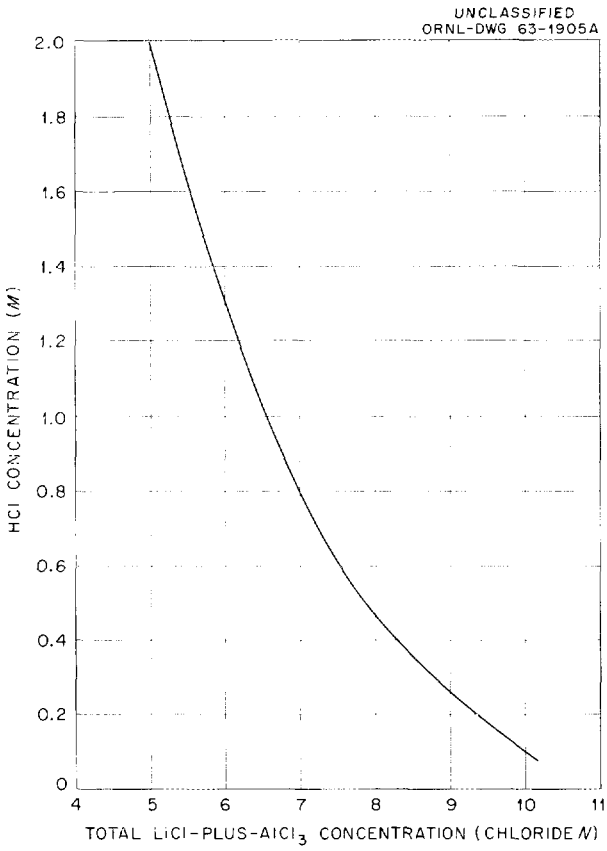

Fig. 4.13. Approximate Acid Concentration of Tramex Feeds Prepared by Simple Distillation of $AlCl_3$-LiCl-HCl Solutions.

the feed. Unfortunately, equilibrium acid concentrations of 1.35 *M* at 60°C and 0.4 *M* HCl at 120°C are too high for satisfactory extraction, and final adjustment is dependent on acid analyses at precisions difficult to obtain for these highly radioactive solutions.

Mixed gas bubbled through the feed will adjust the acidity to the desired value if the HCl partial pressure in the gas is equal to the HCl vapor pressure over the feed. Work to determine the vapor pressure of HCl over 10 *M* LiCl containing up to 0.1 *M* HCl has been started. If the vapor pressure is very low, the volume of mixed gas necessary to replace acid lost by radiolysis may be too large for practical application.

Physical Properties of Tramex Solutions. – A program was started to accumulate data on physical properties of solutions used in the Tramex process. The solubility of $AlCl_3$ in concentrated LiCl solutions was investigated, since this may determine the volume of feed solution required to process targets fabricated from aluminum. The solubility of $AlCl_3$ at room temperature, (24 ± 1)°C, decreases from 0.38 *M* in 9 *M* LiCl to 0.09 *M* in 11 *M* LiCl (see Fig. 4.14). The proposed Tramex feed is 10 *M* in LiCl and 0.1 *M* in $AlCl_3$, well below the solubility limit of 0.2 *M* $AlCl_3$ in 10 *M* LiCl.

Densities, boiling points, and refractive indices for 9, 10, and 11 *M* LiCl containing $AlCl_3$ have been measured and are given in Fig. 4.15.

Effect of Salt and Acid Concentration in Tramex Feed on Extraction. – Distribution coefficient data have been difficult to reproduce since coefficients change rapidly with small variations in acid or salt concentration, and analyses of feeds with the necessary degree of precision are difficult. A careful investigation of these variables is being made. Since it was found that the solvent extracts HCl from the aqueous phase, distribution

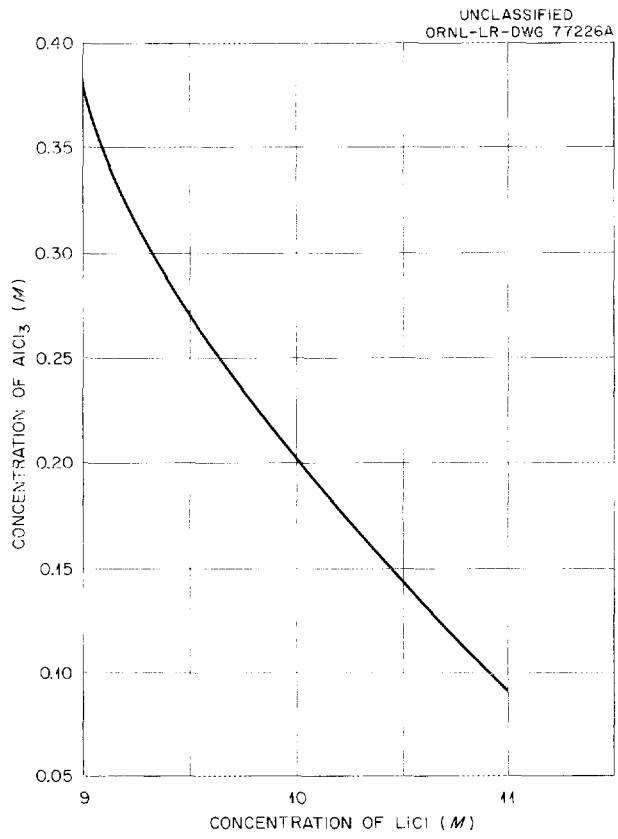

Fig. 4.14. Solubility of $AlCl_3$ in LiCl Solutions at 25°C.

coefficients were determined for HCl between 0.6 *M* Alamine 336·HCl in DEB and feeds containing 9, 10, and 11 *M* LiCl over an acid range of 0.01 to 2.0 *M*.

With well-characterized feeds, distribution coefficients were also determined for americium and europium over the above range as a function of acid concentration. The amount of acid extracted by the solvent from feeds containing 9, 10, and 11 *M* LiCl and from acid solution only is shown in Fig. 4.16. In Fig. 4.17 the logarithm of the HCl distribution coefficient is plotted against the acid concentration in the organic phase. Straight-line parallel functions were obtained for 9, 10, and 11 *M* LiCl below organic acid concentrations of about 0.3 *M*. Distribution coefficients appear to vary regularly with both acid and salt concentration. Similar results are obtained for americium and europium distribution coefficients when plotted as a function of acid concentration in the organic phase (Figs. 4.18 and 4.19). Americium distribution coefficients obtained for 10 *M* LiCl feed containing 0.15 *M* $AlCl_3$ (Fig. 4.18) demonstrate that in this system there is almost no difference between the salting strengths of LiCl and $AlCl_3$ when normalities are compared.

In order to learn the precision of the methods employed in this study, the series containing 0.15 *M* $AlCl_3$ was duplicated, starting with new feeds. Listed below are americium distribution

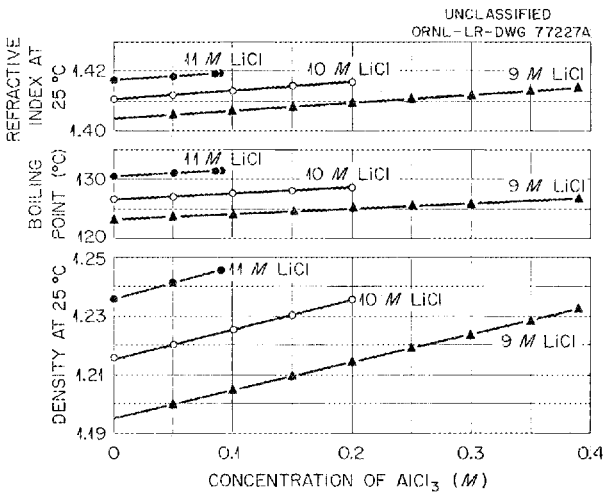

Fig. 4.15. Refractive Indices, Boiling Points, and Densities of $AlCl_3$-LiCl Solutions.

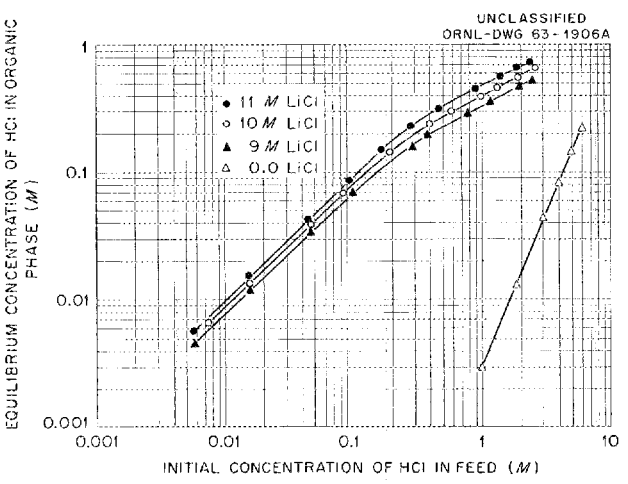

Fig. 4.16. Extraction of HCl into 0.6 *M* Alamine 336·HCl–DEB from Aqueous Feeds Containing LiCl and HCl.

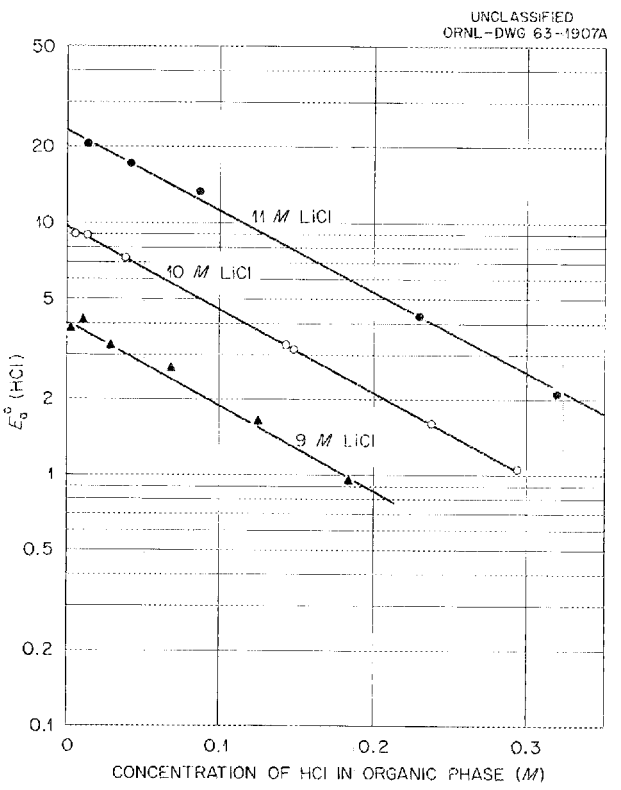

Fig. 4.17. Extraction Coefficient for HCl for the System 0.6 *M* Alamine 336·HCl–DEB and LiCl Solutions.

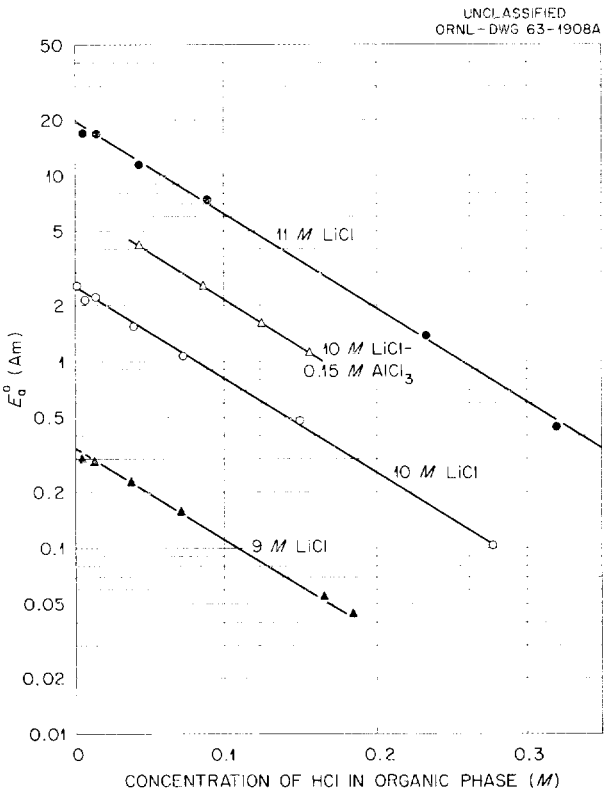

Fig. 4.18. Effect of Acid and Salt Concentration on Americium Extraction Coefficients for the System 0.6 M Alamine 336·HCl–DEB and LiCl Solutions.

coefficients obtained and the acid concentrations in the organic phase for the two feed preparations:

HCl in Organic Phase (*M*)		E_a^o for Americium	
Feed 1	Feed 2	Feed 1	Feed 2
0.042	0.043	4.27	3.87
0.086	0.081	2.58	2.44
0.124	0.125	1.65	1.60
0.156	0.156	1.15	1.06

Synthetic feed solutions were carefully prepared by volumetric combinations of 1 *N* HCl solution and saturated solutions of $AlCl_3$ and LiCl. Numerous analyses have demonstrated that saturated LiCl is 13.85 *M* and that saturated $AlCl_3$ is 3.05 *M* at 25°C. The concentration of the acid in the organic phase was determined by plotting pH vs the volume of caustic required to neutralize an acetone solution of the organic phase. The results were concordant, being within ±0.002 *M*.

Considerable scatter was obtained for europium distribution coefficient data for 9 and 10 *M* LiCl. This is apparently due to the fact that the europium counts in the organic phase were barely above background. Curves indicating probable values are shown in Fig. 4.19. These were drawn according to a comparison with europium data for 11 *M* LiCl and with data for americium.

The degree of precision necessary for Tramex feed adjustments is apparent from these data. For example, proposed Tramex feed will contain 10 *M* LiCl, 0.1 *M* $AlCl_3$, and 0.02 *M* HCl, giving an americium distribution coefficient of about 4. Data given in Fig. 4.18 indicate that the americium distribution coefficient will be decreased to 1 by either increasing the acid concentration to 0.135 *M* or decreasing the salt concentration to 9.5 *N*.

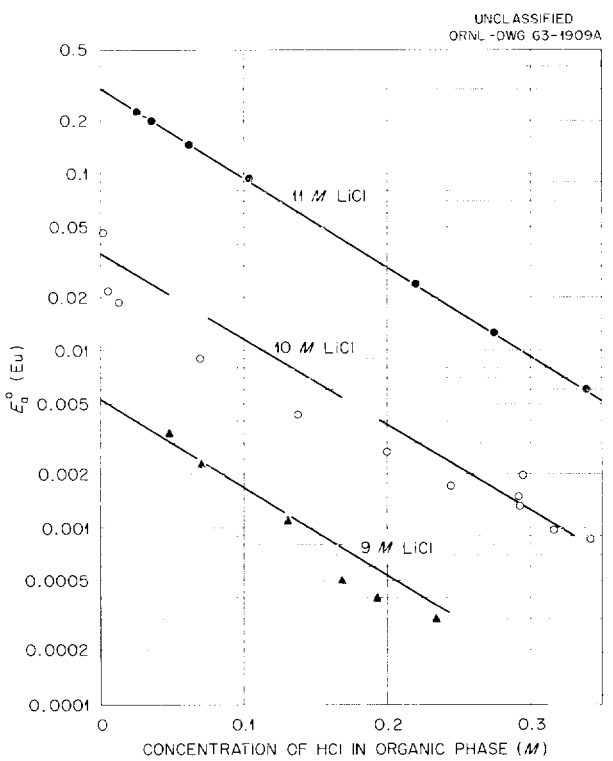

Fig. 4.19. Effect of Acid and Salt Concentrations on Europium Extraction Coefficients for the System 0.6 M Alamine 336·HCl–DEB and LiCl Solutions.

Evaluation of Other Solvents. – Triisooctylamine (TIOA) as an alternative to Alamine 336 and diisopropylbenzene (DIPB) as an alternate to DEB were investigated since both are commercially available and both give increased curium extraction. Curium distribution coefficients and viscosities for various combinations of 0.6 *M* amine in diluent are given in Table 4.6. Although it is possible to increase curium distribution coefficients by 25 to 60%, the solvents giving the highest extraction also have the highest viscosities. Since phase separations between 0.6 *M* Alamine 336–DEB and 10 *M* LiCl–0.2 *M* $AlCl_3$ are marginal, and since temperatures of 50°C are necessary for satisfactory mixer-settler operation, it does not appear to be advisable to use a solvent with a higher viscosity.

Table 4.6. Extraction of Curium from 10 *M* LiCl–0.2 *M* $AlCl_3$ into Various Solvents

Solvent	Distribution Coefficient, E_a^o	Viscosity of Solvent (centipoises)
0.6 *M* Alamine 336–DEB	6.6	4.95
0.6 *M* Alamine 336–DIPB	8.5	6.43
0.6 *M* TIOA–DEB	8.2	5.83
0.6 *M* TIOA–DIPB	10.6	7.80

Separation of Transcurium Elements from Americium and Curium by Phosphonate Extraction

A process based on the extraction of transcurium elements from 1.0 *M* HCl into 1.0 *M* 2-ethylhexyl phenylphosphonic acid [2-EH(ØP)A] in DEB has been developed for separating transplutonium elements into an americium-curium fraction and a transcurium fraction.[5,6] Data reported last year indicate that this process will be satisfactory. Nickel, the principal contaminant, will not extract but will remain with the americium and curium. Tests have not been made at high activity levels, but solvent damage was insignificant when mixed solvent and simulated feed were exposed to radiation equivalent to 100 whr/liter; a Co^{60} gamma-ray source was used. Demonstration of full activity at plant scale is required to establish the adequacy of the phosphonate process.

During the past year, investigation of this process was limited to a study of the effect of various diluents on americium and californium extraction and to a demonstration of americium-californium separation by preferential elution of americium from 2-EH(ØP)A sorbed on a column of powdered glass.

Effect of Diluent on Americium and Californium Extraction into 2-Ethylhexyl Phenylphosphonic Acid. – Americium and californium extraction depends greatly on the solvent used to dilute the 2-EH(ØP)A. Distribution coefficients between 1 *M* HCl and 1.0 *M* 2-EH(ØP)A decreased sharply as diluents of greater polarity were used (Fig. 4.20). Note that the californium distribution coefficient decreased from 45 for heptane diluent (dielectric constant of 1.9) to 3 for toluene diluent (dielectric constant of 2.4). Americium distribution coefficients with these two diluents were 0.37 and and 0.028 respectively. In a similar manner the addition of octyl alcohol (dielectric constant of about 10) or tributyl phosphate (dielectric constant of 7.9) to the solvent decreases the distribution coefficients.

It is believed that the more-polar diluents compete with 2-EH(ØP)A dimer formation by hydrogen bonding and thus decrease the effective concentration of the 2-EH(ØP)A dimer. Since the mechanism of actinide extraction involves hydrogen bonding with three dimers,[7] the presence of polar diluents results in less extraction of the actinides.

Californium-Americium Separation by Preferential Stripping from a Column of 2-EH(ØP)A Adsorbed on Powdered Glass. – Complete separation of americium and californium was demonstrated in a test which used preferential stripping from 2-EH(ØP)A into 1.9 *M* HCl. A column of 2-EH(ØP)A adsorbed on powdered Vycor glass was used, and operations were similar to those used for ion exchange resin columns.

[5] F. L. Culler *et al.*, *Chem. Technol. Div. Ann. Progr. Rept. June 30, 1962*, ORNL-3314, pp 131–33.

[6] R. D. Baybarz, *Separation of Transplutonium Elements by Phosphonate Extraction*, ORNL-3273 (July 20, 1962).

[7] D. F. Peppard, G. W. Mason, and J. Hucher, *J. Inorg. Nucl. Chem.* 18, 245 (1961).

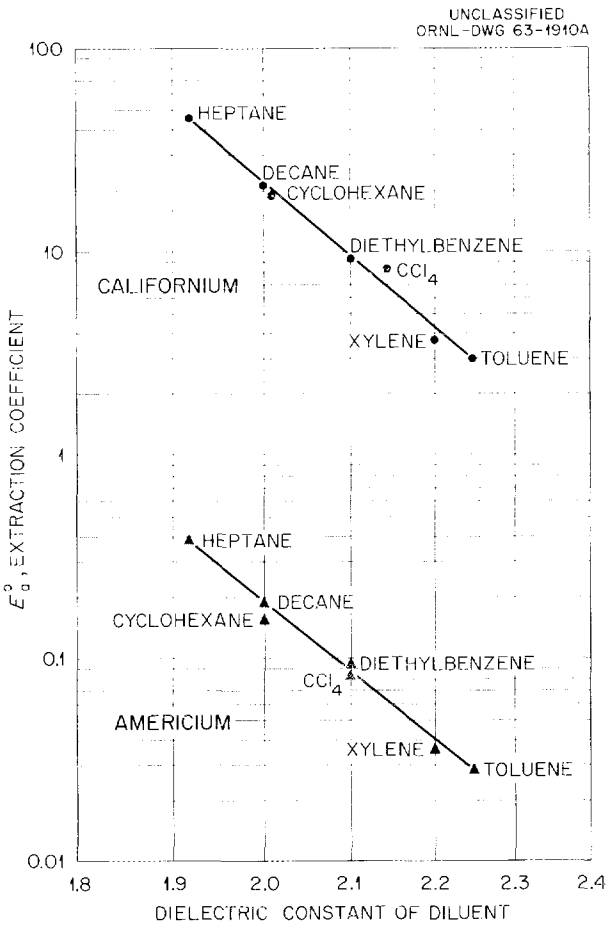

Fig. 4.20. Americium and Californium Extraction Coefficients for the System 1 *M* HCl and 1.0 *M* 2-Ethylhexyl Phenylphosphonic Acid in Various Diluents.

Vycor glass powder (100 to 200 mesh) was slurried in 2-EH(ØP)A. The glass was filtered to remove excess solvent and then placed in a 10-cm-high column 0.15 cm^2 in cross section. A small volume of 1.9 *M* HCl containing californium and americium tracer was passed through the column at 80°C. The column was washed with 1.9 *M* HCl until all the americium was eluted, and then the californium was stripped from the column with 6 *M* HCl. Excellent separation was obtained, as indicated by the elution curves in Fig. 4.21.

Americium-Curium Separation

In processing HFIR targets, americium and curium will not normally be separated; however, on special occasions it will be desirable to produce pure curium and americium. It is also possible that some americium-curium separation methods can be applied to californium-einsteinium-fermium separations. For these reasons, methods of separation of americium and curium are being investigated.

Americium and curium can be separated from each other by chromatographic elution from ion exchange resin or by precipitation methods based on differences in solubility when americium is in a higher oxidation state. The ion exchange methods are of special interest since they may be useful for separating californium, einsteinium, and fermium. The precipitation of gram amounts of $KAmO_2CO_3$ was studied, and good separation of americium and curium by chromatographic elution from cation exchange resin with ammonium α-hydroxyisobutyrate and from anion exchange resin with 4 *M* $LiNO_3$ was demonstrated at high activity levels.

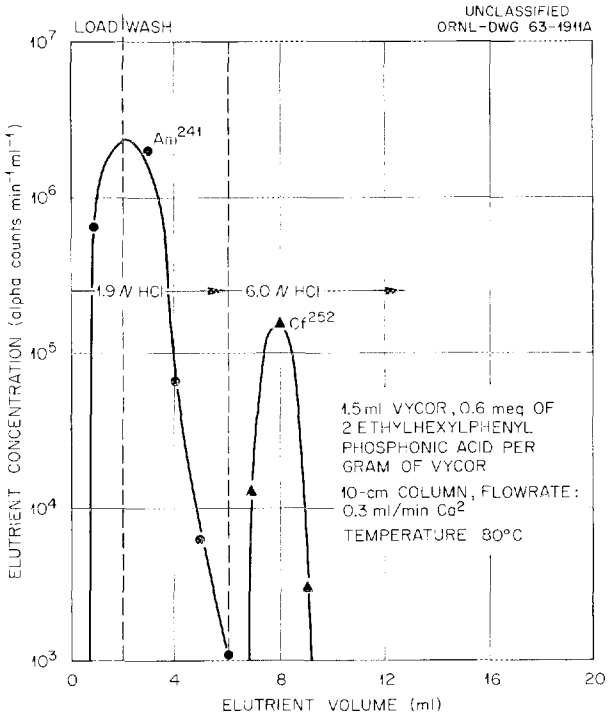

Fig. 4.21. Elution Curves for Americium and Californium. The column consisted of powdered Vycor glass onto which 2-ethylhexyl phenylphosphonic acid had been adsorbed.

Precipitation of $KAmO_2CO_3$. – A 2.5-g sample of Am^{241} contaminated with La, Ce, Fe, and Ca was purified by precipitating $KAmO_2CO_3$ from 3 *M* K_2CO_3. The precipitate contained 99.6% of the americium, free of all contaminants except cerium. This method can also be used to separate americium from curium, which will remain in solution.

A 2.5-g sample of Am^{241} contaminated with 7 g of La, 1 g of Ce, about 0.1 g of Fe, and a trace of calcium was dissolved in dilute hydrochloric acid. A carbonate solution was prepared by the slow addition and vigorous mixing of this slightly acid solution into 1 liter of 3 *M* K_2CO_3. The solution was adjusted to 0.1 *M* in NaOCl and then was heated at 80°C for 3 hr to oxidize the americium, which precipitated as $KAmO_2CO_3$. This precipitate contained 99.6% of the americium and most of the cerium, which was also oxidized by the NaOCl. The $KAmO_2CO_3$ was a very dense, light-tan precipitate, which was easy to filter. The concentration of americium in the filtrate was about 7 mg/liter. Cerium was the only contaminant found in the americium product.

Ion Exchange Separation of Americium and Curium at High Activity Level. – With fine-mesh resin, satisfactory americium-curium separation was achieved by chromatographic elution with both ammonium α-hydroxyisobutyrate from cation resin or 4 *M* $LiNO_3$ from anion resin. Since the Cm^{242} activity levels in these tests were equivalent to 0.4 and 1 mg of Cf^{252}, indications are that Cf-Es-Fm separations at the milligram level may be possible.

A quantity of Cm^{242} activity equivalent to 0.4 mg of Cf^{252} was separated from Am^{241} by chromatographic elution from a 5-ml column of –270-mesh Dowex 50 resin with ammonium α-hydroxyisobutyrate. The volume of gas formed was reduced by pressurizing the column, resulting in a successful procedure. A product containing 96% of the curium, free from americium, was obtained.

Curium-242 activity equivalent to 1 mg of Cf^{252} was successfully separated from Am^{241} on a 5-ml column of Dowex 1-X8 (–270-mesh) resin. The americium and curium were loaded from 8 *M* $LiNO_3$ and were eluted with 4 *M* $LiNO_3$, adjusted to a pH of 1.7. The elution produced a product containing 99% of the curium, essentially free of americium.

Separation of Californium, Einsteinium, and Fermium

An adequate solvent extraction process to separate transcalifornium isotopes is not available; maximum separation factors of adjacent elements for the Tramex and phosphonate systems are less than 2.5. Chromatographic elution from cation exchange resin with α-hydroxyisobutyrate solution is still the most reliable method available; however, it appears that scaleup to several-milligram quantities will be difficult because of radiolytic-gas disturbance of the resin bed.

Elution from anion exchange resin with 4.4 *M* $LiNO_3$ gave poor Cf-Es-Fm separations, compared with the excellent americium-curium separation reported above. This was a result of an unexpected reversal in elution positions of the transcurium elements.

Distribution coefficients of trivalent actinides between Dowex 1-X8 resin and 4.4 *M* $LiNO_3$ solution adjusted to pH 1.5 are given in Fig. 4.22. These were determined by batch equilibration of the resin with a 4.4 *M* $LiNO_3$ solution of the actinides, and the results were confirmed by noting the elution order from Dowex 1-X8 resin columns. The same relative behavior of trivalent actinides was noted when Alamine 336·HNO_3 was equilibrated with a 6 *M* $LiNO_3$ solution of the actinides.

Based on previously determined distribution coefficients of Pu^{3+}, Am^{3+}, and Cm^{3+}, it was anticipated that distribution coefficients of the

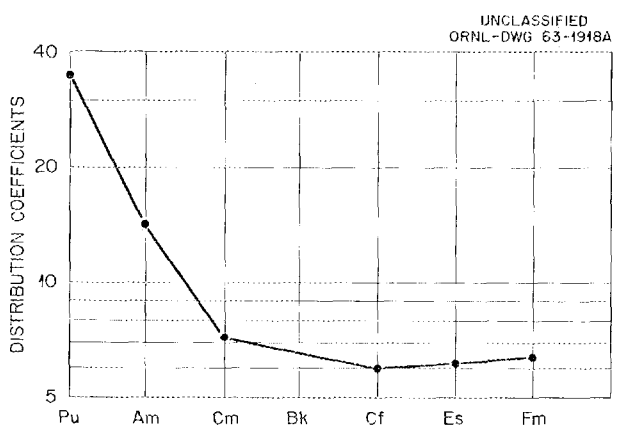

Fig. 4.22. Actinide Distribution Coefficients for the System Dowex 1-X8 Resin and 4.4 M $LiNO_3$.

transcurium elements would continue to decrease with increasing radius of the hydrated ions. The radius increases with atomic number for these elements. However, this trend reversed, with einsteinium and fermium having greater distribution coefficients than californium. It is hypothesized that, since the *f* electron half-shell is filled for curium, Li^+ may be more effective in partially stripping the hydration sheath from transcurium elements. This partial dehydration would enhance complex formation with the nitrate ion and thus result in a reversal of the sorption trend on anion exchange resin.

Actinide-Lanthanide Separations in Carbonate Solutions

Methods of separating actinides and lanthanides in carbonate solutions were investigated. If satisfactory methods could be found to replace methods that require chloride solutions, corrosion problems would be greatly reduced.

Actinides and lanthanides can be extracted into quaternary amines or loaded onto strong-base anion exchange resin from dilute carbonate solutions. There was no appreciable extraction into primary, secondary, or tertiary amines. Scouting tests indicated that it may be possible to separate americium and curium from most of the lanthanides by either extracting the lanthanides into quaternary amines or sorbing them on anion exchange resin. Group separation of actinides and lanthanides is not possible since the heavier actinides have greater distribution coefficients than the lighter lanthanides. The practical application of this method is limited by the probably poor solubilities of actinides and lanthanides in the dilute carbonate solutions.

Distribution coefficients for various actinides and lanthanides between 30% Aliquat 336 in DEB and 0.5 *M* $NaHCO_3$ are given in Table 4.7. This system is somewhat unusual since distribution coefficients of the trivalent actinide are displaced downward. Americium often behaves much like neodymium or promethium. For this system, the americium distribution coefficient is even less than that for cerium. However, there is a possibility that the cerium used in these tests was tetravalent, and the distribution coefficient for Ce^{3+} may be less than that shown in Table 4.7.

Table 4.7. Distribution Coefficients of Various Actinides and Lanthanides for Their Extraction into 30% Aliquat 336–DEB from 0.5 *M* $NaHCO_3$

Element	Valence	Distribution Coefficient, E_a^o
U	6+	13.6
Np	5+	4.6
Pu	4+	2.2
Am	3+	0.52
Cm	3+	0.65
Cf	3+	2.03
Es	3+	2.51
Ce	3+[a]	1.0
Eu	3+	4.8

[a]The cerium may have been tetravalent.

The effect of $NaHCO_3$ concentration on the distribution coefficients of americium, cerium, and europium is shown in Fig. 4.23. Over the range 0.1 to 1 *M* $NaHCO_3$, the coefficients are approximately proportional to the inverse of the cube of the bicarbonate concentration. There appears to be a slight convergence of distribution coefficients at the higher concentration. Below 0.1 *M* $NaHCO_3$, the curves are considerably flattened, with only a slight increase in extraction noted with decreasing bicarbonate concentration. The behavior of actinides and lanthanides was practically identical in $NaHCO_3$ solution or in Na_2CO_3 or K_2CO_3 solutions at half the molar concentration of the bicarbonate solution. Lanthanide and actinide sorption from these solutions onto a strong-base anion exchange resin such as Dowex 21K was similar to extraction into the quaternary amine, Aliquat 336.

Preparation of PuO_2 for HFIR Target Prototypes

When PuO_2 particles less than 10 μ in diameter are mixed with –325-mesh aluminum powder and pressed into cermets, the oxide phase is continuous, and the thermal conductivity of the pellet is low. But, with PuO_2 particles ranging from 20 to 200 μ in diameter, the aluminum phase will

be continuous, and conductivity will be satisfactory for irradiation in high neutron fluxes. Accordingly, a method was investigated for preparing dense, coarse particles of PuO_2 for use in HFIR target prototypes.

A solution of 0.5 *M* $Pu(NO_3)_4$ in 4 *M* HNO_3 was rapidly mixed with an equal volume of 8 *M* NH_4OH to precipitate $Pu(OH)_4$. The precipitate was washed thoroughly with 2 *M* NH_4OH and dried at 150°C. Firing the dried solid at 1200°C produced a glassy solid with a density of 10.99, which is 96% of the theoretical density of PuO_2. Since most of the particles were from 1 to 3 mm in diameter, this method, followed by careful grinding and screening, appears to be satisfactory.

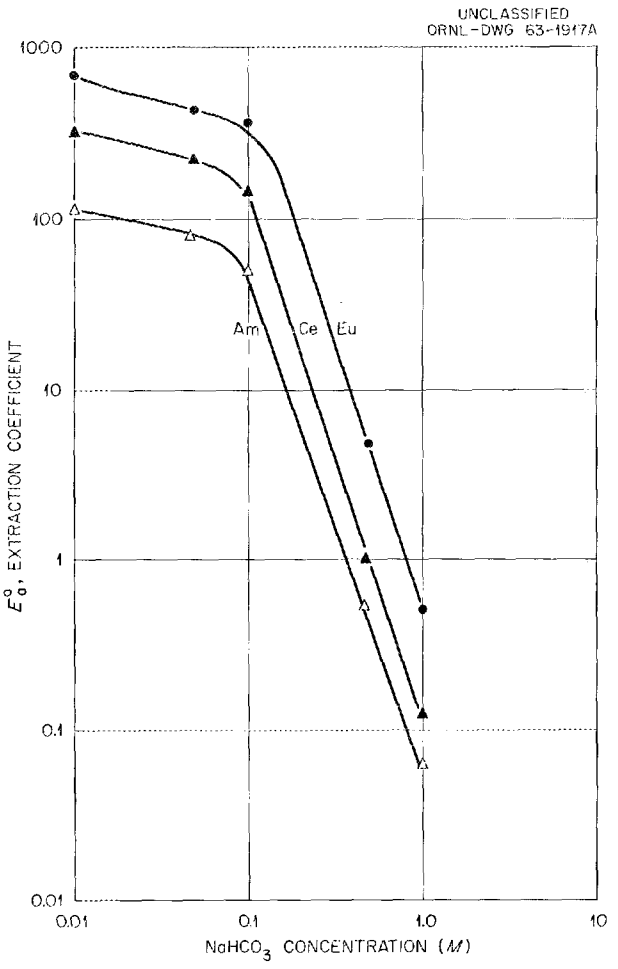

Fig. 4.23. Effect of $NaHCO_3$ Concentration on the Extraction Coefficients of Americium, Cerium, and Europium for the System 30% Aliquat 336–DEB and $NaHCO_3$ Solution.

4.2 DEVELOPMENT OF PULSED COLUMNS

Pulsed columns have been chosen as the solvent extraction contactors for the Transuranium Processing Plant (TRU) because of their inherent mechanical simplicity. Feed capacities of 1 to 2 liters/hr are required, and the cubicle concept employed in TRU limits column height to 6 ft. The program to develop these contactors for the Tramex and phosphonate flowsheets was continued in a new set of three $\frac{3}{4}$-in. glass columns with tantalum internals. All process tubing, pumps, and pulses are constructed of Teflon, making a completely corrosion-resistant system.

Scouting tests showed that the rate of transfer is slower for rare-earth scrubbing in the Tramex flowsheet than for any other of the solvent extraction processes used in TRU; consequently emphasis was placed on the study of this step. Batch-rate studies (Table 4.8) showed that the rate constant for europium scrubbing is lower than it is for other systems at the same power and temperature; however, by increasing power or temperature, the rate can be increased to permit efficient operation of conventional contactors.

The study of europium scrubbing (Table 4.9) in a small pulsed column ($\frac{3}{4}$ in. in diameter and 48 in. high), operated with the aqueous phase continuous at 50°C, showed that the stage height ranges from 19 to 28 in. when the sieve plates ($\frac{1}{32}$-in. holes, 5% free area) are spaced $\frac{1}{4}$ in. apart. The minimum stage height was obtained at pulsed volumes close to the flooding point. Profile samples showed very little backmixing, so it was concluded that efficiency is limited by diffusion in the viscous phases (3 centipoises at

Table 4.8. Mass Transfer Rates in a Batch Mixer

Power (hp/1000 gal)	Temp (°C)	Rate Constant, *ka* (min^{-1})			
		Tramex Eu Scrub	Tramex Ni Extn	Dapex U Extn	Purex U Extn
2.5	25	0.10	0.79	0.54	17
2.5	50	0.46			
2.5	70	0.77			
220	50	14			

Table 4.9. Summary of Efficiency of Pulsed Column for Scrubbing Europium from 0.6 *M* Alamine 336 by Using 9 *M* LiCl–0.3 *M* $AlCl_3$ Solution

Description of Plates	Pulse Amplitude (in.)	Pulse Frequency (cpm)	HETS (in.)
$\frac{1}{32}$-in. holes, 5% free area	0.1	40	28
	0.2	14	20
	0.2	20	27
	0.2	40	19
	0.7	7	26
	0.7	14	27
$\frac{1}{32}$-in. holes, 5% free area, with 2 graphite plates ($\frac{3}{32}$-in. holes, 40% free area) at 5-in. intervals	0.2	40	21
	0.35	30	25
	0.35	30	28
	0.35	60	19
	0.7	14	36
	0.7	45	25
$\frac{1}{32}$-in. holes, 5% free area, with a metal spiral (1 turn in 1 in.) at 12-in. intervals	0.2	40	25
	0.2	55	22
	0.7	14	37
$\frac{1}{32}$-in. holes, 5% free area, with 2-in. section of Teflon rings at 10-in. intervals	0.2	20	28
	0.2	35	25
	0.2	45	17
	0.2	45	19

50°C). Some improvement of efficiency was obtained by the insertion of coalescence sections in the column. Plastic materials work best because they are wetted by the organic droplets; but plastic is not compatible with the radiation and solvent degradation predicted in the TRU facility. With graphite sieve plates and metal spiral inserts, stage heights of 20 in. were achieved.

Hydraulic tests showed that conventional air bubbler–pressure pot control of the interface in the pulsed column is adequate for the extremes of physical properties of fluids used in the various solvent extraction flowsheets. The hydraulic behavior of the extraction, scrub, and strip sections of the Tramex flowsheet and the extraction and strip sections of the phosphonate flowsheet were studied and found to be satisfactory.

4.3 PROCESS EQUIPMENT DESIGN

The chemical processing equipment for the Transuranium Processing Plant will consist of the apparatus for dissolution, feed adjustment, two cycles of solvent extraction, and various special separations. The latter may comprise ion exchange, precipitation, or batch extraction, and much of it will be designed, built, and installed as the occasion demands. Design to data has been concentrated on the so-called "main-line" equipment. Flowsheets for this work have been developed, and detailed design of equipment components and cell layouts is approximately 20% complete (on July 1).

Flowsheets

Two sets of flowsheets were devised and issued as approved. The five equipment flowsheets depict all equipment pieces and main piping in simplified form. Composites of these equipment flowsheets are shown in Figs. 4.24 and 4.25.

In the past year the primary solvent contactors were changed from mixer-settlers to pulsed columns. Developments in this period showed that stage heights are low enough to permit the use of 6-ft-long pulsed columns, which can be fitted on the standard equipment racks. Tank sizes, throughput, and other features remain essentially unchanged.

Corrosion Studies: Choice of Materials of Construction

Corrosion studies in the past year were concentrated on zirconium alloys. Previous work had shown room-temperature corrosion rates of 5 mils/month for Hastelloy C in 3 to 6 *M* HCl, rates that are not acceptable for product streams and product storage tanks. In addition, rates accelerate rapidly with temperature. Tests this year showed that for all low-temperature service in nearly all environments, Zircaloy-2 corroded only one-tenth as fast as Hastelloy C. In addition, Zircaloy-2 can be used in boiling-HCl or -HNO_3 solutions and in mixed HNO_3-HCl systems at low temperatures. Some reservation must be exercised in the use of Zircaloy-2 at high temperatures because of slight pickup of hydrogen, which might lead to embrittlement during long exposures.

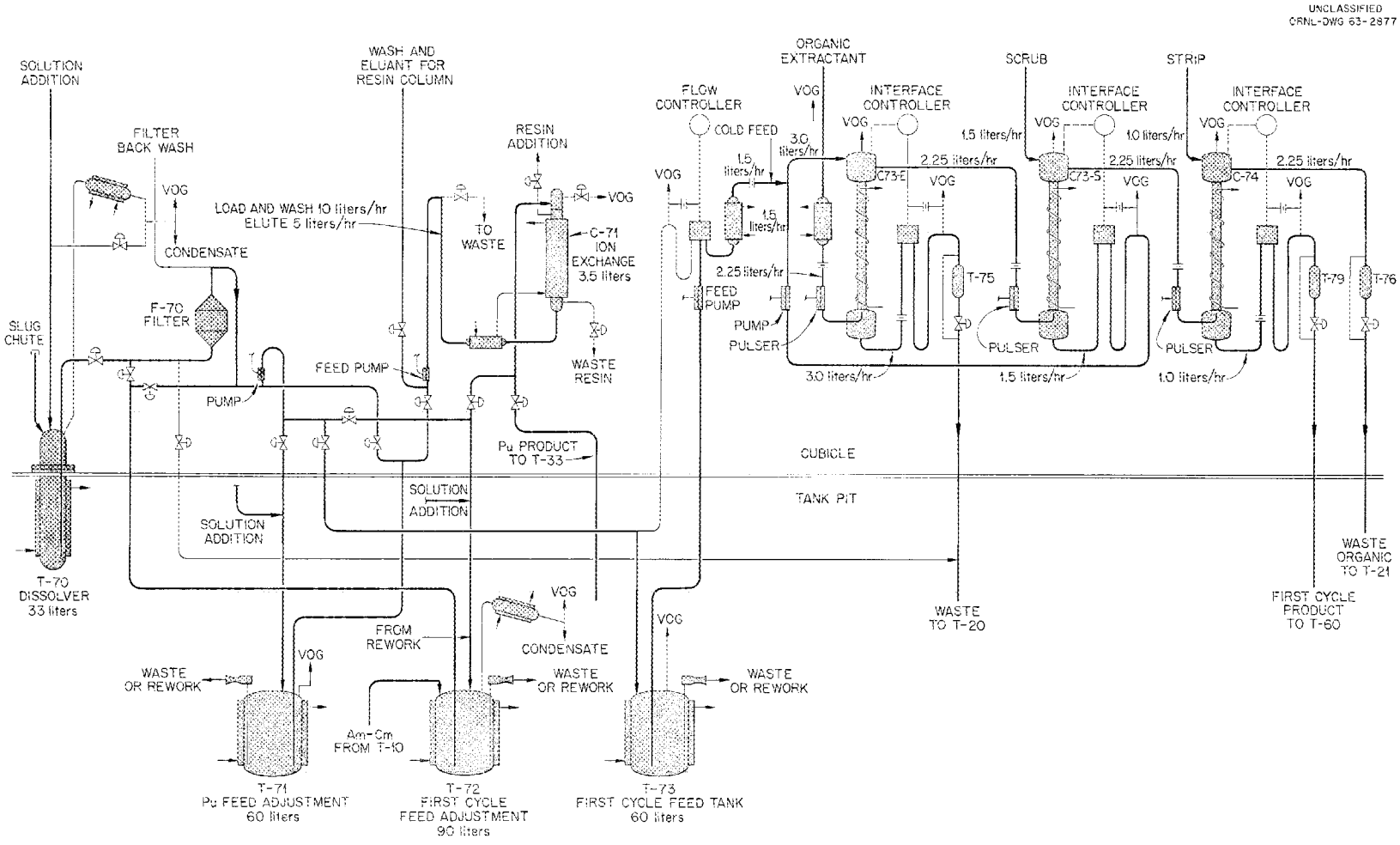

Fig. 4.24. Flowsheet for Equipment Used in Processing Targets (Cell 7).

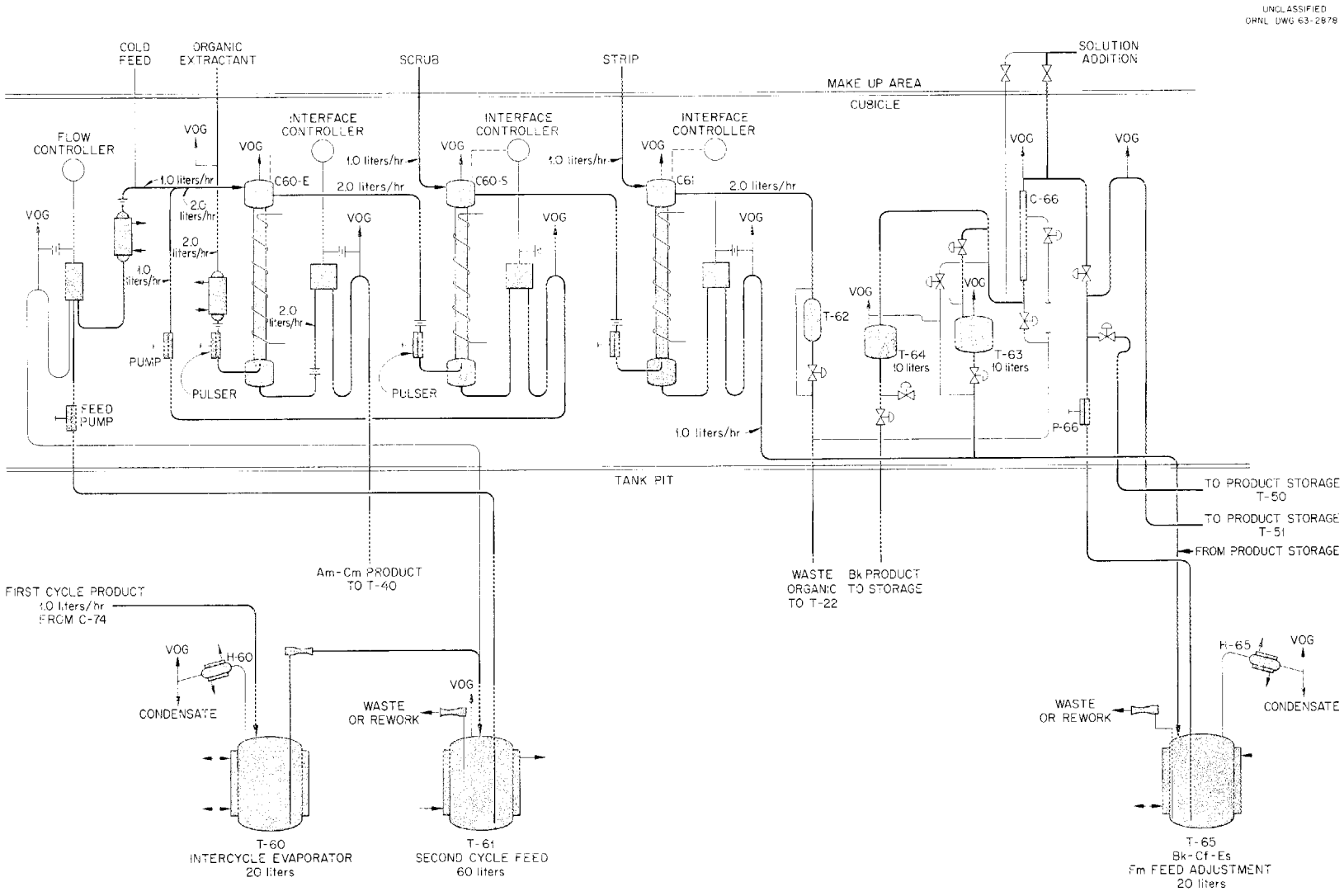

Fig. 4.25. Flowsheet for Equipment Used in Processing Targets (Cell 6).

Severe embrittlement was observed in commercial-grade zirconium in 1000-hr boiling-HCl tests.

Cost studies based on (1) firm prices for both Hastelloy C tubing and (2) an estimate of fabrication costs for the disconnects indicated that, although Zircaloy-2 was 50% more costly than Hastelloy C, an all-Zircaloy-2 piping system was slightly cheaper than a combined system that utilized Hastelloy C for certain noncritical lines, such as waste piping, and Zircaloy-2 for all product streams. The decision was made to go to an all-Zircaloy-2 piping system. Waste vessels will be of Hastelloy C, all evaporators will be tantalum lined, and product storage tanks may be either Zircaloy-2 or tantalum lined.

Detailed Component Design

Detailed design was initiated in January by the Design Group of the ORGDP Engineering Department and will continue for about 18 months. Preliminary layouts based on the detailed conceptual design have been made, and the design of several equipment components has been completed.

Process Pumps. – A design for the remote drive head of a diaphragm pump was evolved, and it is compatible both with the Building 4507 development facility and the Transuranium Processing Plant (see Fig. 4.26). Utilizing an air-pressure–vacuum drive system instead of the customary hydraulic drive, the pump is capable of suction lifts up to 22 in. of mercury. The pump is installed with two bolts, can be handled with the heavy-duty manipulators, and is sufficiently compact to fit in the conveyor canister. About 40 of the units will be used as sample pumps and 15 for feed and transfer service.

Disconnects. – The development of a single-bolt disconnect was completed. It utilizes an investment-cast clamp into which tubing adapters up to

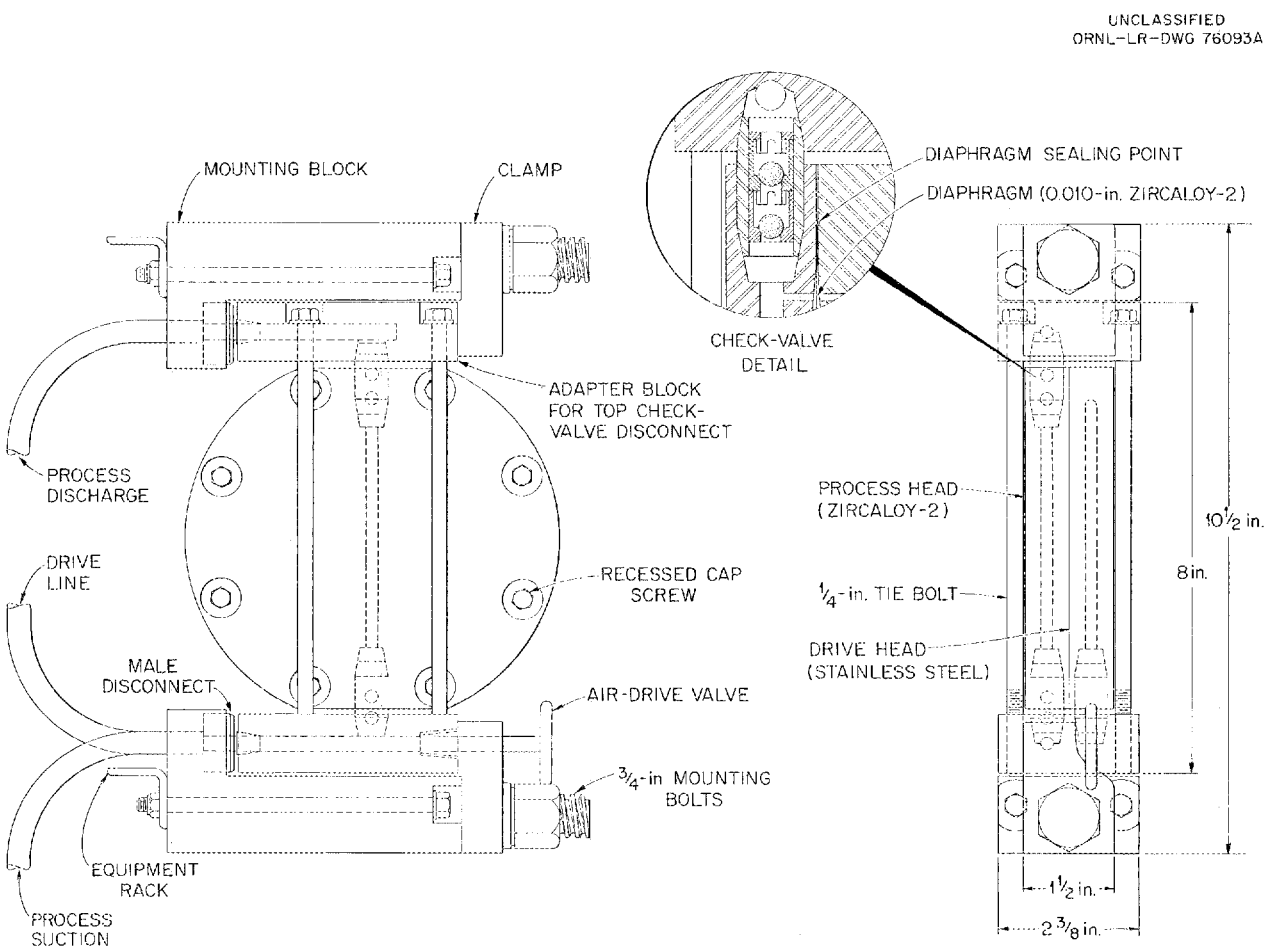

Fig. 4.26. TRU Process Pump.

$\frac{3}{4}$ in. are assembled. The disconnects are designed to be used singly or in multiple arrangements on $1\frac{1}{2}$-in. centers (Fig. 4.27). About 400 are installed in the Curium Recovery Facility, and 3000 will be required in the TRU plant. The units may be assembled with torque or impact wrenches. For in-cell maintenance with master-slave manipulators, electric impact wrenches will be used. The top half of the clamp rotates into position automatically as the nut is tightened and, conversely, is opened by means of a compression spring as the nut is loosened.

Adapters have been designed for all tube sizes up to $\frac{3}{4}$ in. and for $\frac{1}{4}$-, $\frac{3}{8}$-, and $\frac{1}{2}$-in. pipes. The design varies, depending on the material of construction. Stainless steel adapters, including butt-weld ends, are machined from bar stock and welded to the tube or pipe. Hastelloy C and Zircaloy-2 units are fabricated by machining the 1-in.-diam collar and sealing surface from solid bar stock and joining this piece to the tube by rolling techniques. Tantalum female disconnect pieces are made by flaring the end into the machined stainless steel ferrule with a simple hydraulic tool. The tantalum male pieces are made by machining the conical sealing surface from thick-walled tubing and rolling both this piece and the adjoining tube into a stainless steel ferrule. To effect a satisfactory seal with tantalum, both surfaces must be finished by a roller-burnishing operation, which smooths and hardens the surfaces.

Sampler. – A 12-unit sampler will be installed in each of the four processing cells on the back equipment rack. The sampler station can be separated as a unit from the rack so that major changes in the rack equipment may be made without replacement of the sampler. Samples are taken with the conventional two-needle arrangement. Each of the 12 units consists of a drive pump, needle block, and bottle-handling mechanism (see elevation of typical unit, Fig. 4.28). The needle blocks are contained within an enclosed housing equipped with water spray for simple decontamination following each sampling operation. All pumps in one station are driven from the same external pressure–vacuum supply system; hand-operated valves incorporated into each pump are used to actuate the desired pumps. Detailed design of the sampler is completed; mockup tests will confirm and refine, if required, the bottle-handling features of the design.

Dissolver and Other Vessel Design. – No completely satisfactory material of construction exists for the TRU dissolver. Present chemical flowsheets call for dissolution in 2 to 4 *M* HCl in the temperature range 50 to 80°C. Tests have shown that tantalum picks up hydrogen and embrittles under dissolving conditions; some minor pickup of hydrogen has been observed in Zircaloy-2 at the boiling temperatures which may be required for the dissolution of the actinide oxides. Since Zircaloy-2 has the advantage of permitting caustic dissolutions, it was chosen for the dissolver material. Design of the vessel (Fig. 4.29) is such that it may be used in both the development facilities and in the processing plant. The active region of the HFIR targets will be completely submerged in acid during dissolution in order to eliminate any problems arising from the polymerization of plutonium compounds. Temperature control will be achieved by a closed-cycle hot-water system that is capable of removing or adding heat. The jacket and the vessel are of Zircaloy-2 since in this size the cost of a flanged stainless steel jacket is as great as an all-welded Zircaloy-2 jacket.

The other boiling vessels will have flanged tops and be constructed of tantalum-plated or -lined Hastelloy C. Penetrations through the top will be rolled joints with stainless steel Swagelok fittings added above the flange for additional support. Roller tools are available with extension shafts to permit making the rolled joint through the 3-ft-long tubes that extend up to the disconnects above the vessel. Waste holdup tanks will be made of Hastelloy C. All dip tubes and nozzles will be of Zircaloy-2, installed by rolling techniques after construction of the vessel by welding. Heat treatment of welded penetrations is not practical, and the change to a second material for the penetrations does not complicate the fabrication. Product storage tanks may be either tantalum-plated vessels with Zircaloy-2 flanged tops or of all-welded Zircaloy-2 construction. The choice will be largely one of economics since both designs appear satisfactory.

Solvent Extraction Equipment Rack. – The design of the first-cycle solvent extraction equipment rack (including all components and piping) is completed, and the assembly is being fabricated from the materials of construction for use in the final facility. Early construction of this rack has two purposes: (1) The problems common

UNCLASSIFIED
ORNL-LR-DWG 75627

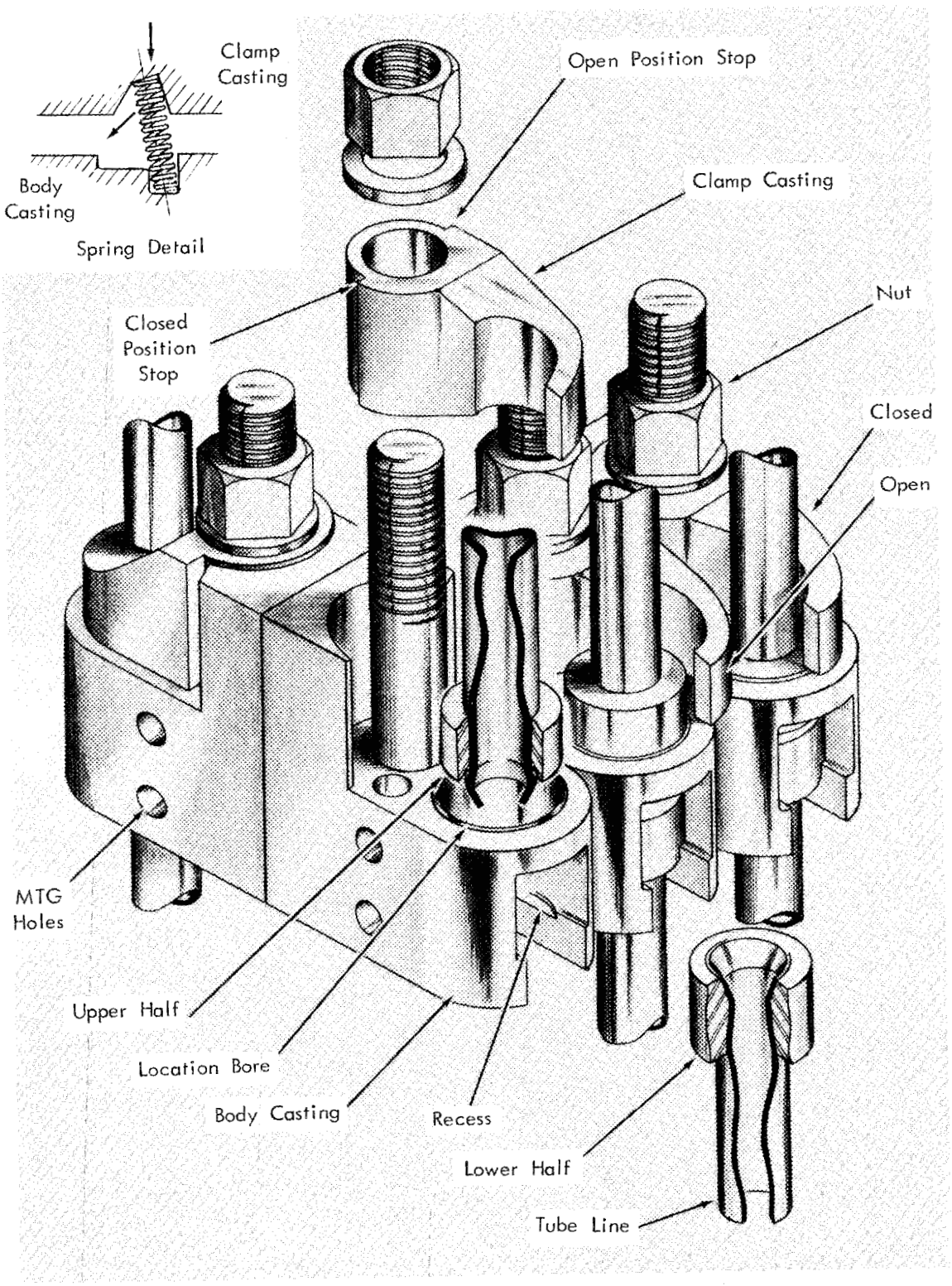

Fig. 4.27. Disconnect Assemblies Grouped.

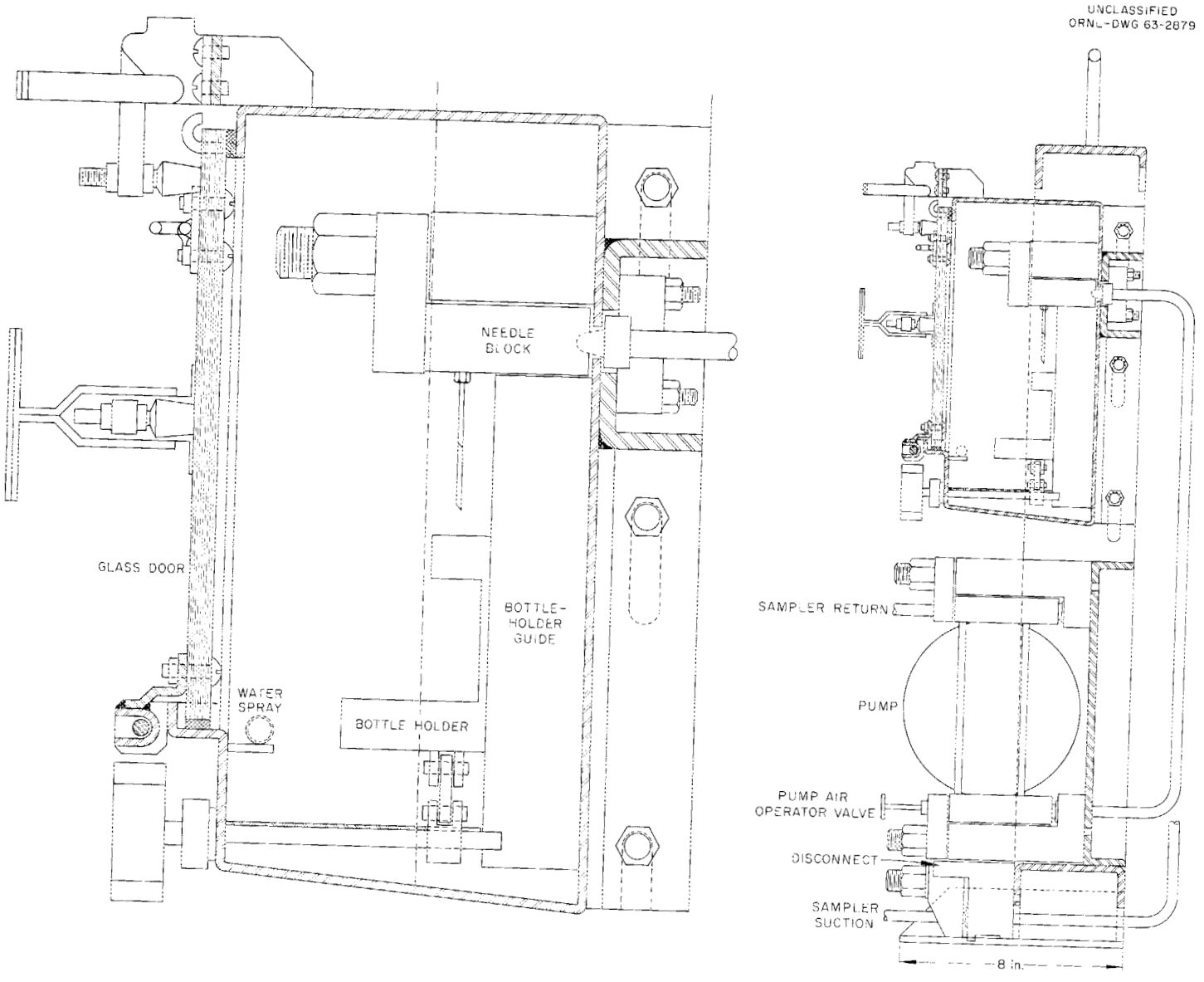

Fig. 4.28. Sectional Elevation of TRU Sampler.

UNCLASSIFIED
ORNL-DWG 63-2880

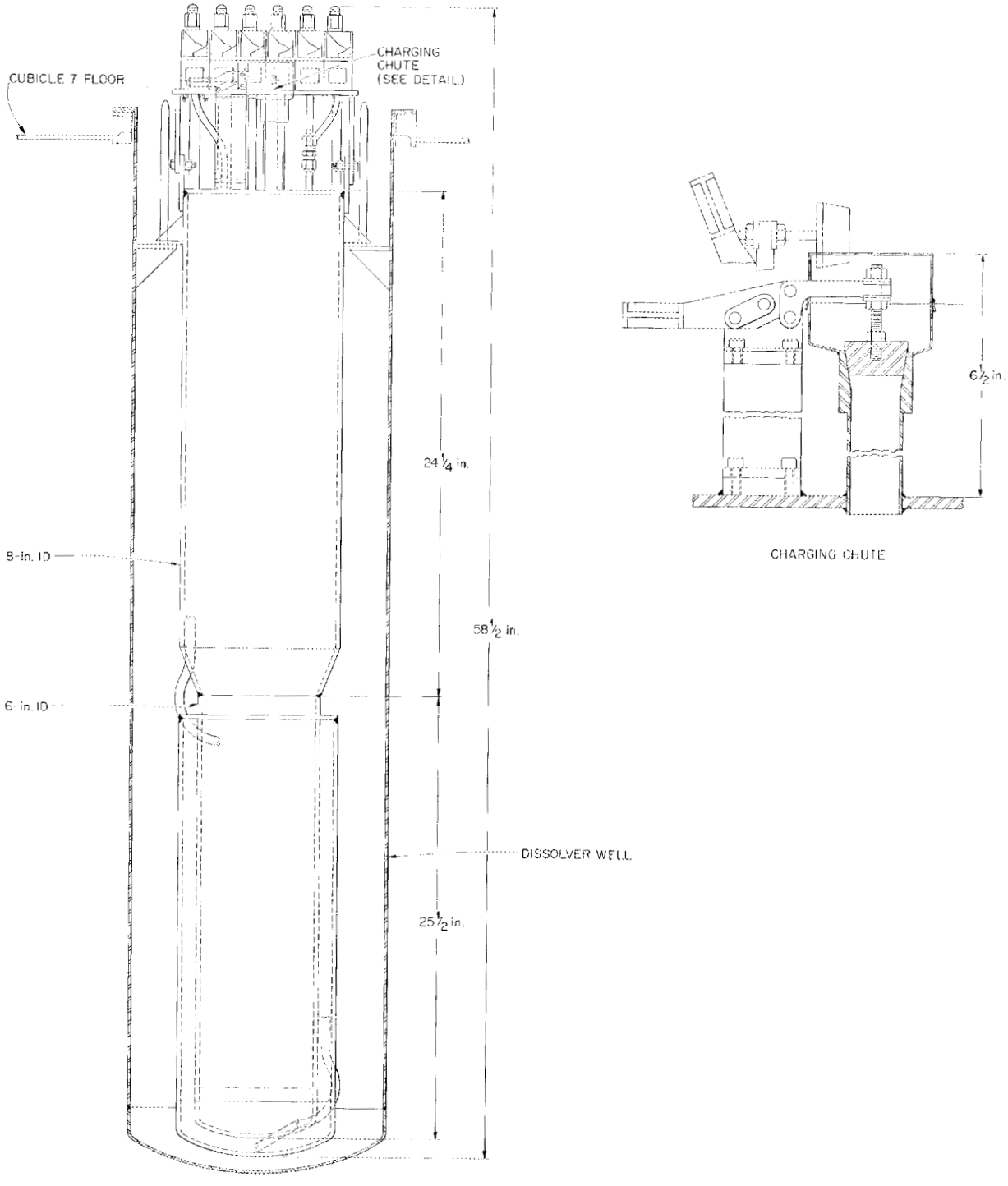

Fig. 4.29. TRU All-Zircaloy-2 Dissolver.

to all equipment racks, such as methods of joining service lines to the rack, handling problems, and maintenance operations, can be worked out in the mockup prior to final design of the remaining racks. (2) Hydraulic testing of the pulsed columns and related systems must be done with final materials and configurations. Because of the complexity of this rack, essentially all the important basic design features of the rack concept will be thoroughly tested. A typical column and associated equipment are shown schematically in Fig. 4.30. Hot feed is metered to the top of the extraction column through a specially designed flowmeter, through which flow is controlled by application of air from outside the cell to a pressure pot in the cell, analogous to the common method of column interface control. The extraction and scrub columns were separated to give additional height and still keep the columns within the 6-ft height limitation of the equipment rack. Pulsers are identical to the process pumps (Fig. 4.26) with the check valves removed. Organic flow between columns is achieved by the pumping action of the pulser, using special check valves in conjunction with the pressure changes developed by the pulse pumps. All restrictions which minimize pulse dampening are made replaceable to permit wider variation in flow rates and pulse characteristics and easy repair in case of plugging.

Ion Exchange Column. – Operation of ion exchange columns used with radioactive processes is frequently upset by gas generated by radiolysis. In downflow operation, portions of the bed may accumulate pockets of gas, and, in upflow, the gas may disrupt the bed. Various methods have been used in the past to hold the resin in place, and such a system has been designed for use in the TRU facility. A movable top screen, actuated from outside the cell by hydraulic pressure on a small piston, retains the bed. No seal between the screen support and column is provided nor is required if, under all operating conditions, the pressure drop across the screen (not the bed) is kept small. Methods to accomplish this are being worked out in a glass model of the column.

Critical-Path Scheduling

At the request of the AEC and ORNL, critical-path scheduling was initiated on the TRU project in May 1962. The method was utilized to improve planning and cost control.

For scheduling, the project was divided into two major segments: building design and construction (the responsibility of Catalytic Construction Company), and equipment design and procurement (the responsibility of ORNL). In August 1962, the arrow diagrams representing ORNL participation were combined with the building design and construction diagrams to form a master schedule that contained about 3300 activities. This master schedule was used for periodic management review meetings.

The master schedule was modified to reflect manpower leveling on ORNL design activities and ORNL procurement of special components and materials, and some resequencing of building-construction activities was developed. Important dates from this schedule are shown in the simplified arrow diagram in Fig. 4.31.

It was estimated that 8000 man-days of design were required to complete the ORNL participation. The scheduled rate of expenditure of manpower is shown in Fig. 4.32. as a percentage completion by date.

Each month, a detailed design progress report, itemizing the status of all design activities scheduled for that month, is transmitted to project personnel. The status of each activity, including design, fabrication, test, etc., is marked on the arrow diagrams by using color-coded tapes. The design report and the taped arrow diagrams are presented monthly to project management for review.

Design progress was 30% complete at the end of June 1963, slightly ahead of schedule.

The funds allocated to implement the scheduling function were as follows:

Catalytic Construction Co.	$ 30,000
ORNL	40,000
ORGDP (computer)	5,000
Construction contractor (bid alternate)	25,000
Total	$100,000

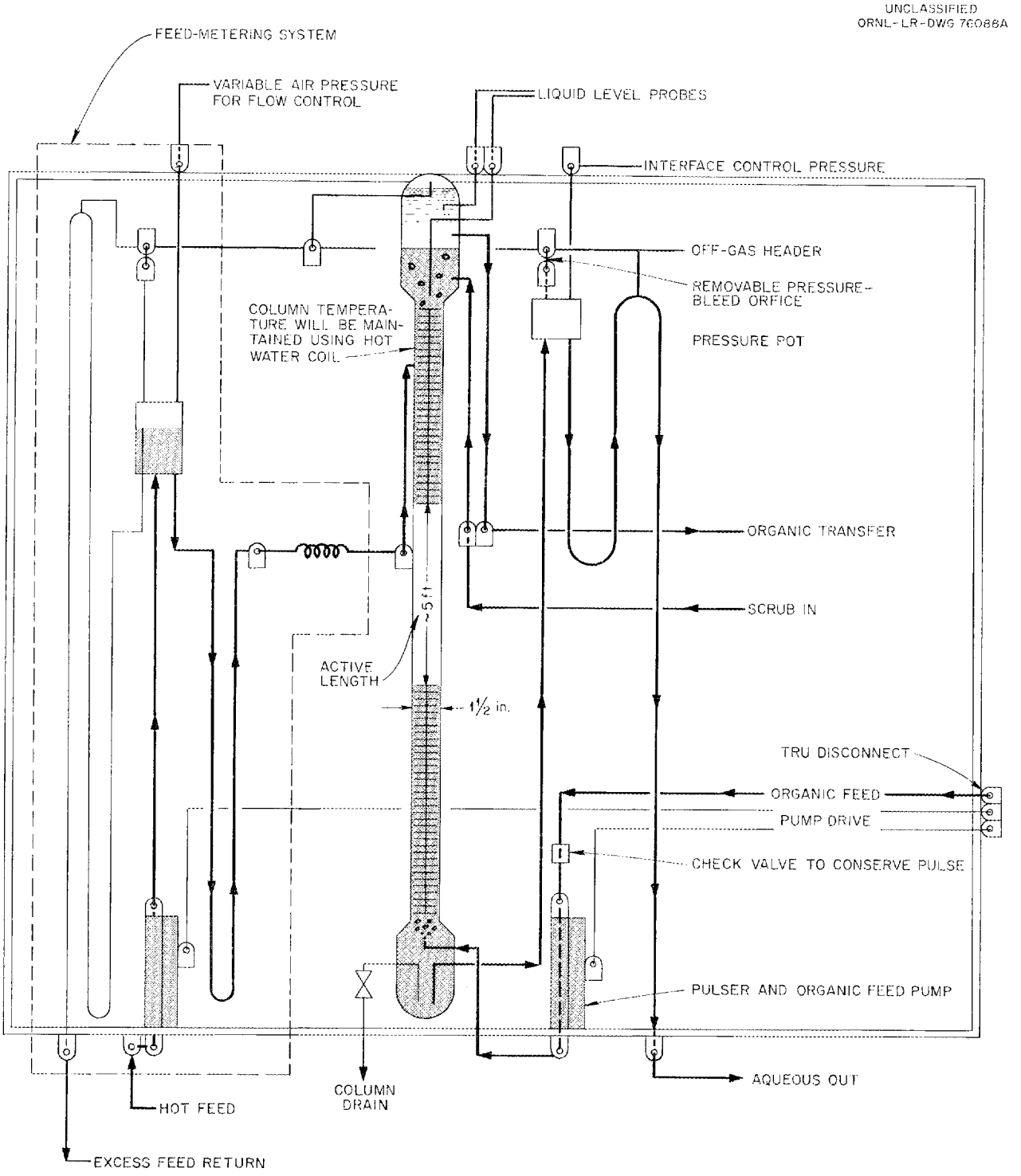

Fig. 4.30. Typical TRU Extraction Column.

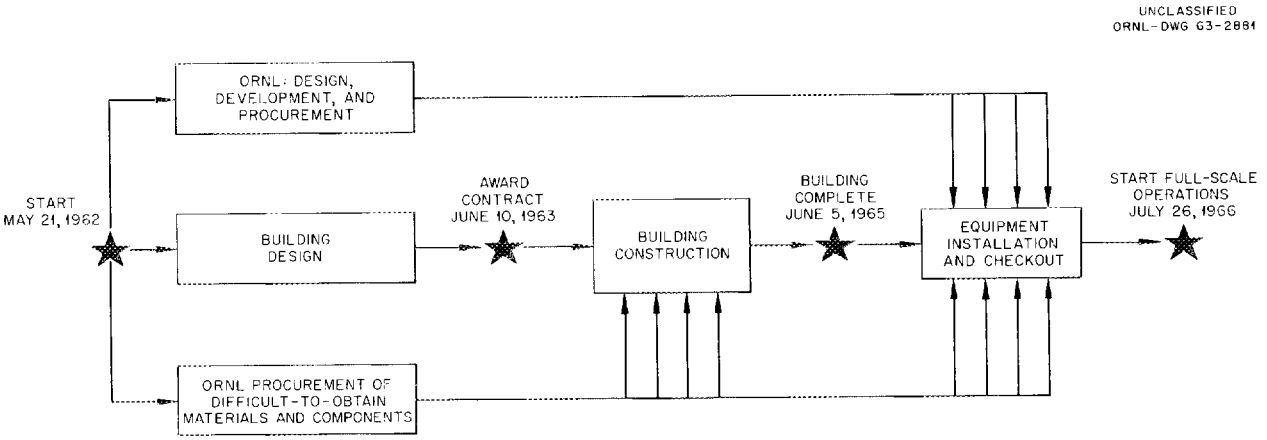

Fig. 4.31. TRU Master Schedule, May 1963.

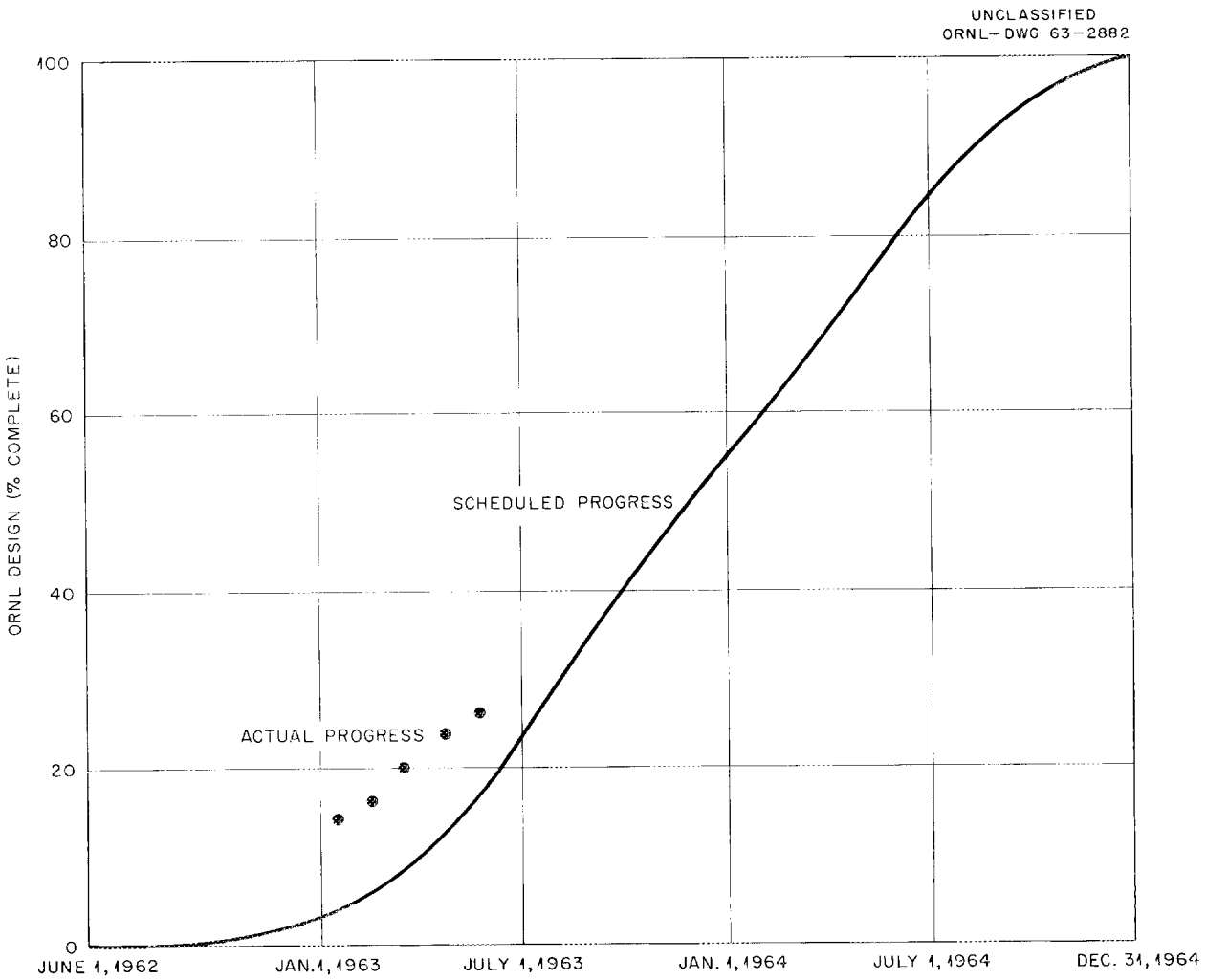

Fig. 4.32. ORNL Design Schedule and Actual Progress.

4.4 TRU FACILITY DESIGN

Building Design

The preliminary engineering (Title I) report for the Transuranium Processing Plant was prepared by the architect-engineer during FY 1962 and approved in July 1962, whereupon detail engineering was initiated and completed in February 1963. The lump-sum contract package, containing about 425 drawings and 75 specification sections, was formally advertised by the AEC-ORO for bid on March 12, 1963, and bids were opened on May 10, 1963. The low bid of $2,586,000 compared favorably with the AEC estimate of $2,716,700. The contract was awarded during mid-June. Scheduled completion date for the lump-sum portion of the construction is approximately April 1965.

Status of ORNL Procurement for Lump-Sum Contractor

Many of the materials that are difficult to procure and that require extensive lead time are being procured in advance of the lump-sum contract by the AEC-ORO and UCNC. These include such items as all Hastelloy C and special-quality stainless steel materials and fabrications, including valves, liquid eductors, pipe, and fittings; the Hastelloy C cell cubicle floor pans; the 30-in.-diam cell ventilation duct, which will be installed beneath the pipe tunnel floor; the sleeves for the cell-viewing window; certain critical Hastelloy C piping assemblies; and the hydrous iron ore aggregate from Running Wolf Mine, Montana. The procurement of these items is progressing according to the schedule established for these materials to the lump-sum contractor.

Design of Mechanical Equipment Components

Conveyor System for Intercell Transfers. – The function of the intercell conveyor system for TRU is to furnish communication between nine cell cubicles in a cell bank and a transfer cubicle. The conveyor and accessories consist of tracks and chain supports, drive mechanism, chain adjusters, chain idlers, dolly, canister, position indicator transmitter and receiver, and control box (Fig. 4.33).

The conveyor drive mechanism, tracks and chain supports, chain adjusters, chain idlers, dolly, and canister are enclosed in an alpha-tight housing approximately 95½ ft long. Openings in the top of the housing coincide with transfer ports in the nine cell cubicles and the transfer cubicle. The dolly is driven by two endless chains which extend the length of the housing. The chains are attached to the dolly mechanism and separately powered by two reversible air motors with sealed drive shafts penetrating the housing wall. The direction of rotation of the motor that is energized determines the resultant direction of the dolly or dolly elevator: right, up or down, and left, up or down. Sensor rollers located on the dolly elevator and underneath the tracks enter accurately located vertical slots in the tracks, positioning the canister at the preselected transfer port. Any transfer port or ports can be bypassed by selecting either of the "down" modes. The canister is elevated by the dolly mechanism and is sealed to the bottom of the cubicle at the transfer port. An air-actuated port closure mechanism (located inside the cell) unlocks the canister cover from the canister and locks and seals it to the port closure. Materials to be transferred are inserted or removed from the canister with the cell master-slave manipulator.

The position indicator transmitter and receiver and control box are located in the operating area. Interlocks prevent incorrect sequencing of the normal operations and resultant break of containment.

A mockup of the conveyor system has been completed, and extensive use tests have been conducted. Final design of the system for installation in the TRU Processing Plant is approximately 80% complete.

Equipment Transfer Case for Equipment Removal System. – Equipment transfers into or out of the alpha cubicles are made without breaking containment on either the cubicle or the alpha-sealed transfer case. This is accomplished by the double-door method, a close mechanical approach to bag-out techniques. The equipment transfer case must function with all cell cubicles and other components located in the limited access area incidental to the decontamination, maintenance, bagging, or burial of the large process equipment which is removed from the cell cubicles. The doors of the nine cubicles, glove box, bag rack, and burial cask are all interchangeable.

Guides are located on top of the cell cubicle to give initial alignment between the transfer case and the cubicle door (see Fig. 4.34). The guide

pins located in the top of the cubicle door will provide final alignment of the transfer case. When the case is rested on top of this door, it compresses the gasket located on the bottom of the transfer case and effects a seal to the top of the cubicle. A manual drive simultaneously unlocks the cubicle and transfer case doors and locks and seals the two doors to each other. A mechanical indicator ensures proper position of the door lock actuator when the door is being replaced or removed from the ports. A second manual drive is used to elevate the two interlocked doors into the transfer case while equipment is being removed from the cubicle. A 750-lb-capacity electric hoist

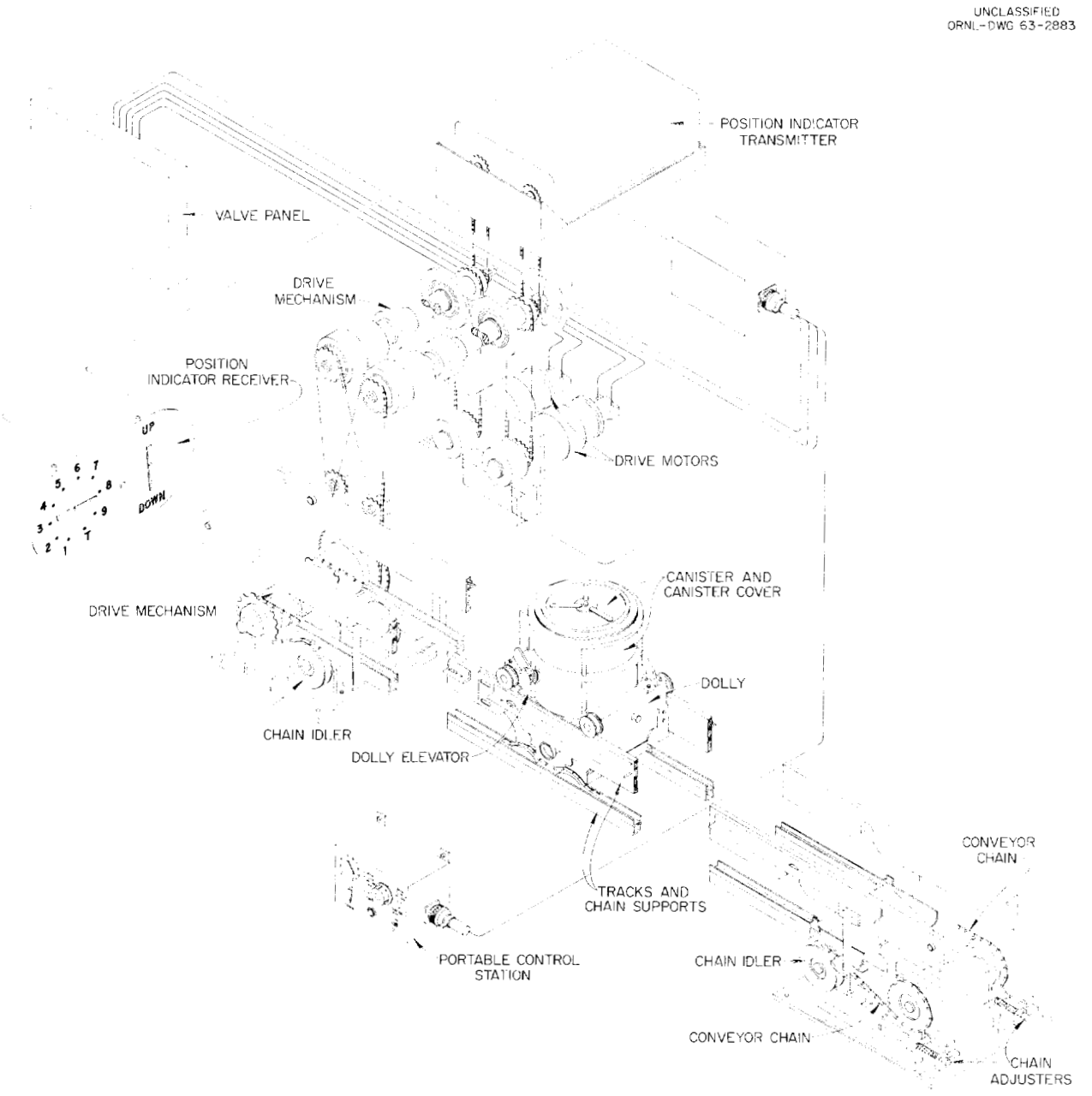

Fig. 4.33. Intercell Conveyor.

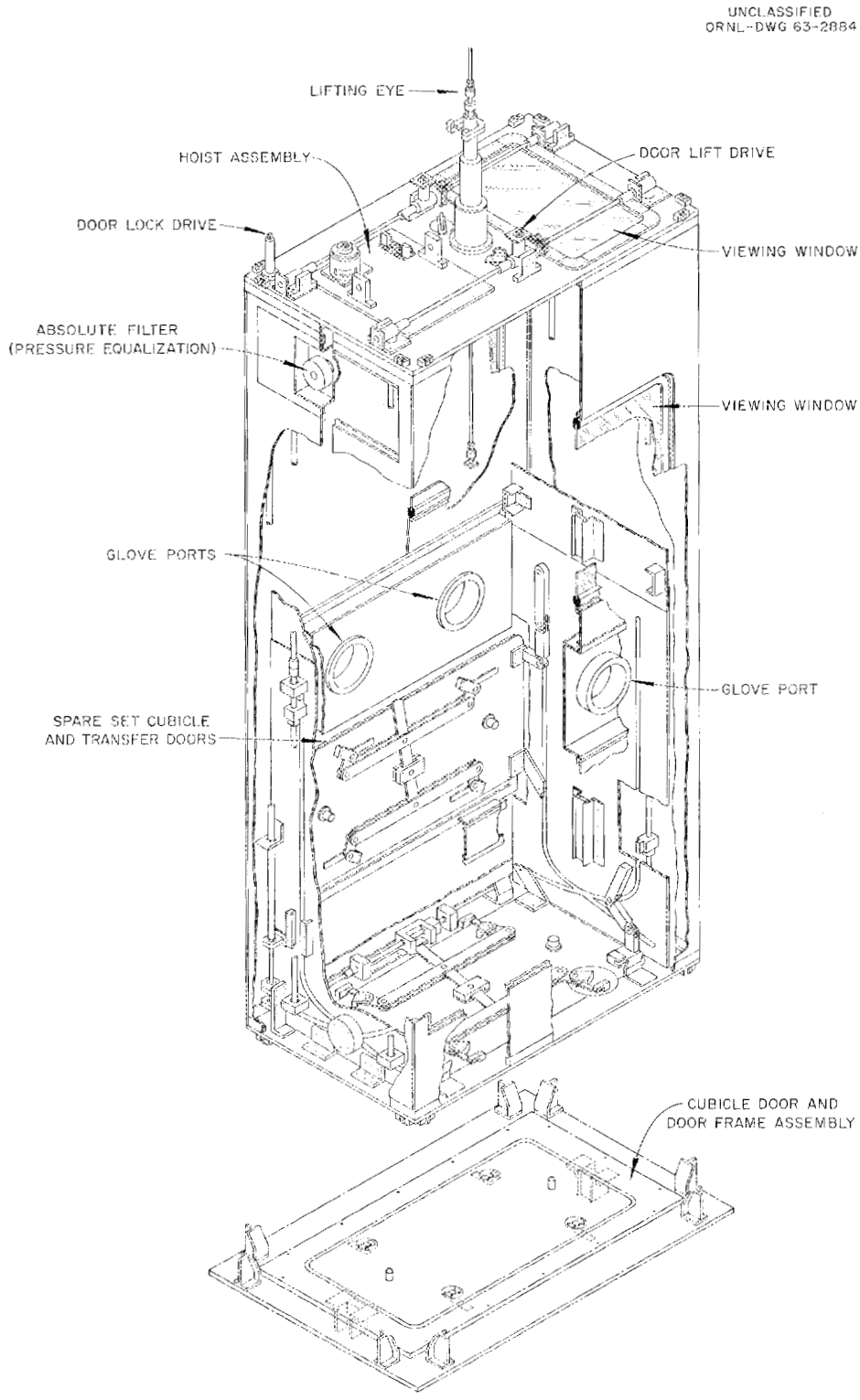

Fig. 4.34. Cutaway View of Equipment Transfer Case.

equipped with limit switches and located inside the case will be used to raise the equipment from its position in the cell cubicle.

In case of mechanical failure the doors may be replaced by means of a duplicate door combination (spare) on the opposite side of the transfer case.

The interior of the transfer case, which is of stainless steel, may be decontaminated with acid spray nozzles inserted through the top of the case. Provisions have been made to drain the case at the transfer station located in the limited-access area of the cell bank complex. Glove ports and viewing windows are also provided in the front and back of the transfer case to give access to the front and back of all equipment which will be lifted within the case.

Inspection ports are provided in the ends of the transfer case to allow adjustment of the door drive mechanisms. Under normal operating conditions no adjustment will be necessary; however, since no lubrication will be used, some adjustment may be required to compensate for wear.

Fabrication of the mockup of the equipment transfer case has been completed, and the unit has been moved to the mockup station for final testing.

4.5 EXPERIMENTAL ENGINEERING STUDIES

The suitability of design concepts and of process equipment is being determined by thorough experimental testing of full-scale apparatus in a cell mockup facility. This mockup includes cell walls, two cubicles, two tank pits, manipulators, the intercell conveyor, and a transfer area (see Fig. 4.35).

Cubicle and Cubicle Equipment Testing

Tests of the automatic port closure on the conveyor demonstrated adequate performance and little wear during 1000 cycles of operation. The port closure is operated by two air pistons and is interlocked by mechanical locking lugs and electrical limit switches. In an improved version, the fragile mechanical interlocks will be eliminated in favor of all electrical interlocks, and improvements in the electrical switching gear should minimize operator error. Improvements were made in the intercell pass-through by adding a drawer supported by ball bearing rollers. Springs were added to the door clamps to hold the clamps in open position during loading of the drawer.

An equipment rack was fabricated and fitted to tracks on the cubicle floor. Three sets of lifting arms were installed off the cubicle ceiling and were operable with the manipulators after counter weights were added. Little difficulty was experienced in the preliminary testing of the rack handling and positioning system. The equipment transfer case is essentially complete and will be tested. The cubicle top port was installed. A test device for checking the door latch seals was leak free at 20 psi air pressure.

Test work on the cell lighting system included selecting the best location for the lights, measuring the light intensity at various points, selecting proper dimensions to permit installation and removal of the electric conduit, establishing the need for light reflectors, and determining the effect of heat from the lights on the manipulator booting material. The final recommended design includes four mercury vapor lamps operating on separate ballasts if possible and two incandescent lights for color correction and emergency use. Each lamp bulb with its own protective cage will be supported by a hook mounted on a flat plate reflector. Bulbs will be replaced by unplugging the power cord and replacing the cord, porcelain lamp base, lamp cage, and lamp as a unit. This will eliminate the handling problems encountered in a multiple-bulb light fixture.

A method for removal of the alpha window is being devised which consists of (1) the removing of the segmented window frame and seal, (2) placing the window in a canvas bag, (3) shattering the window, and (4) removing the bag through the equipment transfer case. Samples of annealed and tempered glass were broken, and, since the tempered glass breaks into small particles which can be handled easily, it was selected.

Tests of Manipulators and Manipulator Boots

Master-slave manipulators for the maintenance work to be performed on the cubicles must be capable of routinely handling objects weighing up to 40 lb. A pair of AMF extended-reach manipulators was modified by the substitution of Central Research Laboratory hands and tongs and the

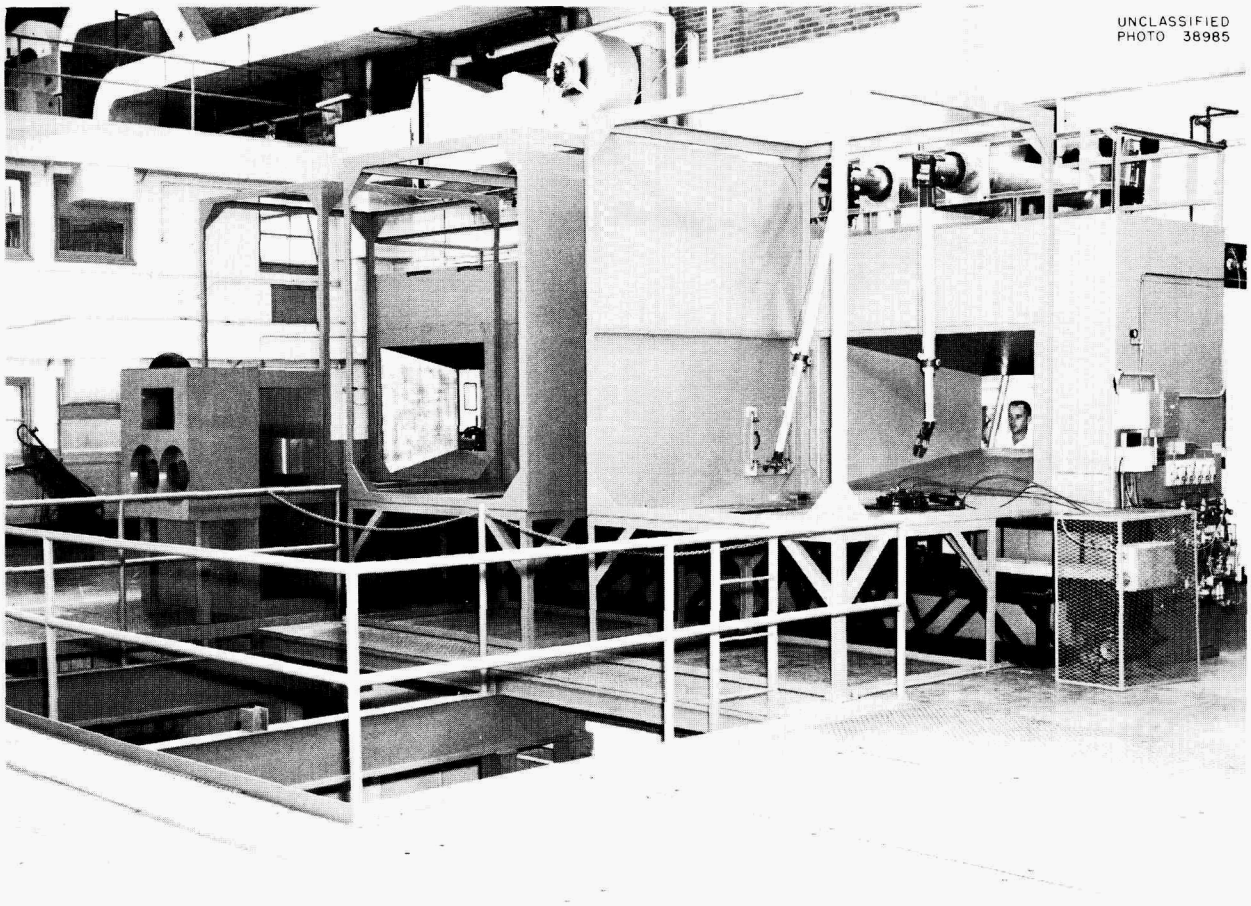

Fig. 4.35. TRU Mockup.

addition of a pneumatic power grip system. Capabilities were still less than desired. Extended-reach versions of the more-rugged CRL heavy-duty manipulators will be tested.

A manipulator booting seal changing fixture was tested, and it performed very satisfactorily. However, the seal surface must be lubricated with talcum powder to decrease the friction as the seal is forced into place.

Process Equipment Development

Development of process equipment concepts continued, and many prototype units are being fabricated and tested. An ion exchange column mockup was operated in which the resin was retained by a hydraulic piston. Flow rates were determined for optimum conditions for loading and unloading the resin. Process liquid-flow metering and control devices were successfully tested. Tests of a diaphragm sampler pump design demonstrated adequate performance and adequate life for Hastelloy C or Zircaloy-2 diaphragms. Two sampler pumps were fabricated and tested for the 4507 installation. Two electric impact wrenches were tested, along with eight torque-limiting extensions made by machining standard socket wrench extensions to give thinner springlike cross sections. Use of the larger wrench with sockets plus extensions calibrated and matched to bolt sizes was recommended to avoid bolt shearing or thread damage.

Testing of a large number of tantalum disconnect samples showed that the machined insert design for the male core and the flared tube end was superior to other designs tested. Burnishing the

seal surfaces with hardened steel rollers minimized the problem of galling. Misalignment of less than 0.5° under load was obtained for commercially fabricated disconnect clamps when the upper contact surface was machined at 1.5° to counteract the strain from loading. Initial attempts to form tantalum bellows for process valve seals by application of magneforming, explosive forming, and hydraulic forming were not successful. Fabrication by hydraulic forming at ORNL and by a commercial vendor presently appears promising.

4.6 TRU – EVALUATION OF PROTECTIVE COATINGS

Radiation-damage tests were made on protective coatings to determine the upper tolerable limits of exposure in air and in deionized water (at 40 to 50°C) to Co^{60} gamma rays at an intensity of about 1×10^6 r/hr. The coatings were considered to be potentially useful in the TRU facility, where radioactive elements must be contained or easily removed from structural surfaces.

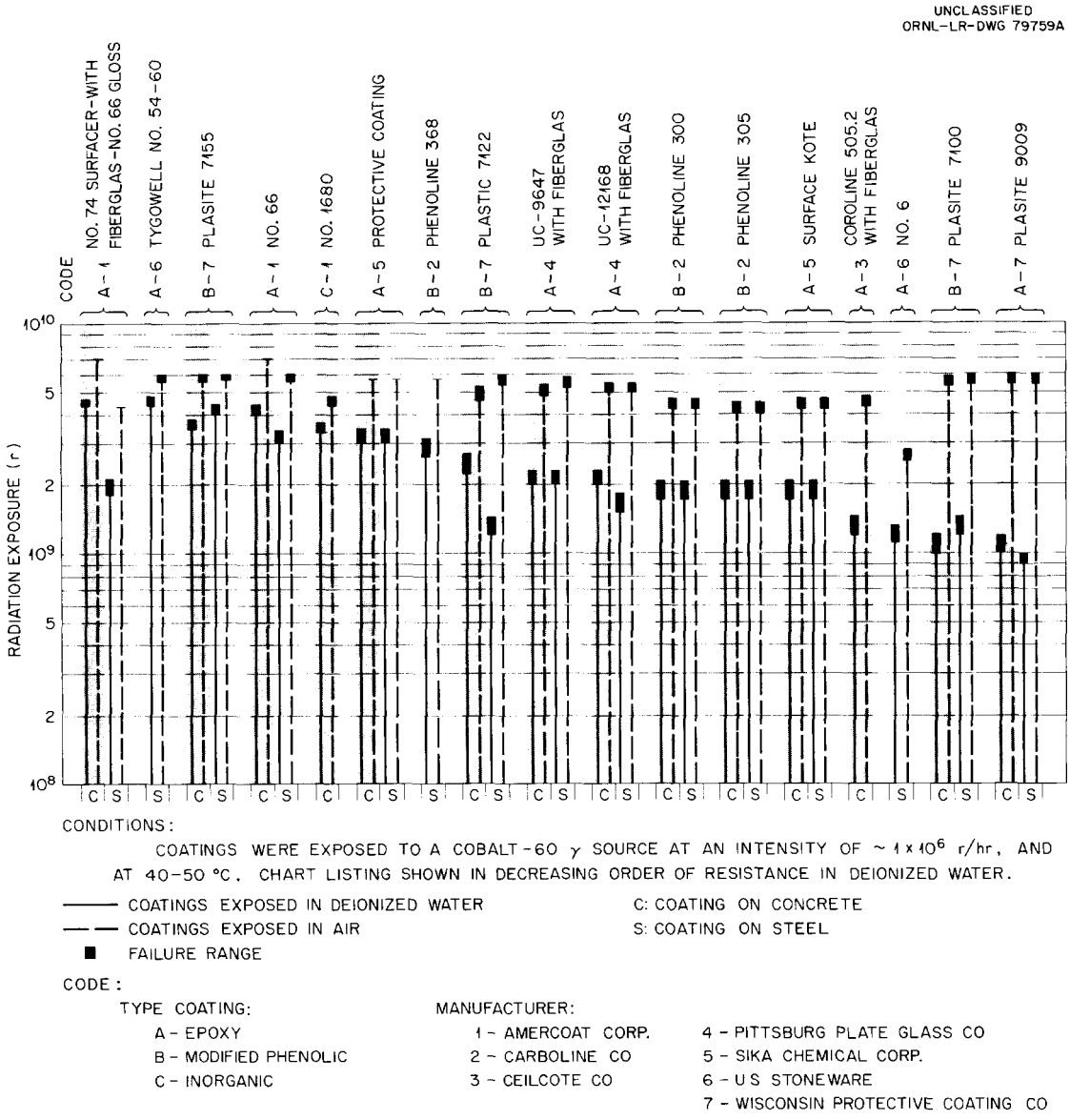

Fig. 4.36. Protective Coatings Resistant to $>10^9$ r of Gamma Radiation.

Fifty-four protective coatings were irradiated; 17 were resistant at and above 10^9 r while submerged in deionized water (Fig. 4.36), and 40 were resistant in air at 10^9 r. At 4×10^9 r, four coatings (epoxies or epoxy-phenolic formulations) were still serviceable in deionized water, and 26 in air. In general, the coatings were less affected by radiation when exposed in air than when immersed in deionized water.

The polyamide cured epoxy coatings had the best radiation resistance while immersed in deionized water. Of the 17 coatings resistant to greater than 10^9 r in deionized water, ten were epoxies, three were epoxy-phenolic formulations, three were modified phenolics (probably of the epoxy-phenolic formulation), and one was an inorganic coating. Most of the failures at the higher radiation levels resulted from embrittlement and chalking of the top seal coat, loss of adhesion, and a marked decrease in impact resistance. The coatings reinforced with Fiberglas fabric retained resistance to impact much better than the unreinforced coatings. Experimental formulations by the Sika Chemical Company and the Carboline Company, in which a dispersion of Fiberglas pigment was included in the coating, did not appreciably improve their resistance to radiation damage. The most severe attack on the submerged coatings occurred at the air-water interface, where extreme chalking, erosion, and softening were evident on most of the coatings.

Decontamination factors (DF) were determined for the various coatings by a water flush and a 3 *M* HNO_3 scrub at room temperature to remove mixed fission products (predominately $Ce\text{-}Pr^{144}$, $Zr\text{-}Nb^{95}$, and Ru^{106}) with an initial activity[8] of about 3 r/hr. The highest DF, 9.33×10^3, was obtained on a vinyl coating – U.S. Stoneware, R0221 with silicone, and TP216 top coat. An epoxy, Amercoat No. 66 gloss, gave the second highest DF (6.3×10^3). The highest and average DF's for the various types of coatings were as follows:

Epoxy: Highest, 6300 (Amercoat No. 66 gloss); average of 19 coatings, 872

Modified Phenolic: Highest, 1730 (Carboline Co., No. 300-finish, white); average of 11 coatings, 415

Polyester: Highest, 2700 (Prufcoat, epoxy modified polyester); average of three coatings, 1850

Vinyl: Highest, 9330 (U.S. Stoneware, R0-221 with silicone, TP216 top coat); average of 16 coatings, 988

Inorganic: One coating tested, 63 (Amercoat, Dimecote No. 3)

4.7 CALCULATIONS FOR THE IRRADIATION OF PROTOTYPE HFIR TARGETS

Calculations for irradiating three prototype TRU HFIR targets in the Materials Testing Reactor were completed. Each target is 24.5 in. long and $\frac{3}{8}$ in. in diameter and has an active fuel length of 14.3 in. The fuel pellets are made of a cermet, PuO_2-Al (about 17 vol % PuO_2). A peak unperturbed *nvt* of 6.4×10^{21} was requested for the three rods; however, it may be desirable to remove two of the targets for examination after shorter irradiation periods. The peak *nvt* can be obtained after 441 days by moving the targets to higher fluxes three times during the irradiation (desired peak neutron flux will vary between 1.8 and 4.4×10^{14}). At the peak *nvt*, the average target burnup should be about 760,000 Mwd per metric ton of plutonium. Assuming 100% release of gaseous fission products, the maximum pressure inside the capsule will be 750 psia, which will create a stress of 2900 psi at the end-plug welds. The average surface heat flux of the target capsule is about 600,000 Btu hr^{-1} ft^{-2}.

[8]Data of A. B. Meservey *et al.*, Chemical Development Section A, ORNL.

5. Curium Processing

5.1 FLOWSHEET TESTS FOR THE PROCESSING OF Pu^{242}, AMERICIUM, AND CURIUM

The program under which the recovery of plutonium and transuranium elements from highly irradiated Pu-Al alloy fuel rods was started has been described in a previous report.[1] Processing has been completed in cell 1, Building 4507, with the recovery of 30 g of specification-grade plutonium assaying greater than 75% Pu^{242} from eight fuel rods. Decontamination of plutonium from gross fission products by a factor of 2×10^5 was obtained. The dissolution rate of the alloy in this eight-rod lot was about the same as that obtained in earlier processing of similar fuel, averaging 0.7 mg min^{-2} cm^{-2}. Process losses were high; 20% of the processed plutonium sorbed irreversibly on the anion exchange resin, resisting even aqua regia, the strongest elutriant tried. The resin on which the irreversibly sorbed plutonium was loaded also retained ruthenium, rhodium, and palladium, under the most drastic elution conditions. Reducing the loading-scrubbing-elution cycle time decreased the radiation damage to the resin and hence the fraction of plutonium that sorbed irreversibly. Sorption and scrubbing losses to the flowing streams across two cycles of ion exchange were 5 and 3%, respectively.

The plutonium-free "waste" from the plutonium-recovery operation, containing fission products, aluminum, americium, and curium, was further processed by anion exchange to recover americium and curium free from aluminum. Only about 70% of these transuranium elements were recovered, along with most of the rare earth fission products, with the conditions given in the flowsheet (Fig. 5.1). The loss of americium and curium could have been reduced to 5% if the americium and curium contained in the pre-ion-exchange filter cake wash had been recycled. The highest loss was in the feed clarification step, where 25 to 30% of the transuranium elements were retained on the moist filter cake. Ion exchange sorption and scrubbing losses averaged 0.2 and 0.4%, respectively. The recovered product, containing 4 g of transuranium elements, was separated from aluminum by a factor of 70 and from fission products by a factor of 10. It was stored for later use as feed in the development and demonstration of amine solvent extraction separation of the transuranium elements from lanthanides. Our experience during these runs, using highly salted solutions of very high activity levels, indicates that ion exchange processes are not desirable and, in fact, may be impossible for the more difficult separations required in the Transuranium Program.

Recovery of Pu^{242} from Irradiated Plutonium Aluminum Alloy

A total of 30.4 g of plutonium containing less than 0.5% Pu^{239} was recovered from eight highly irradiated Pu-Al alloy fuel rods that were processed according to an anion exchange flowsheet.[1] The flowsheet includes dissolution of the alloy in 6 *M* HNO_3 containing 0.05 *M* Hg^{2+} and 0.03 *M* F^- as catalysts, adjustment of the plutonium to the tetravalent state, coagulation of soluble silica (both from the fuel alloy and from neutron capture in aluminum) by digestion with 10 ppm of gelatin, clarification by filtration through a sand bed filter, final adjustment of the filtrate to 7 *M* HNO_3, sorption of the plutonium on 20- to 50-mesh Permutit SK anion resin, scrubbing the loaded resin with 7 *M* HNO_3–0.05 *M* F^-, and downward elution with 0.7 *M* HNO_3.

Dissolution of the alloy proceeded at an average rate of 0.7 mg min^{-1} cm^{-2} and was conducted in the presence of an undissolved metal heel equivalent to six rods. This metal heel was required to obtain even minimum dissolution rate. Two successive cycles of ion exchange were used, and the overall sorption and scrubbing losses averaged 5 and 3%, respectively. The recovered plutonium product was decontaminated from gross fission products by a factor of 2×10^5 and had the following isotopic composition:

Isotope	Wt %
Pu^{238}	1.10
Pu^{239}	0.35
Pu^{240}	15.25
Pu^{241}	7.80
Pu^{242}	75.50

[1] *Chem. Technol. Div. Ann. Progr. Rept. June 30, 1962*, ORNL-3314, p 156.

Only 63% of the plutonium estimated to be present in the processed rods was recovered as product. The high losses during sorption and scrubbing were attributed to the low concentration of plutonium in the feed solution, partial destruction or masking of active exchange sites on the resin as a result of radiation degradation, and probable contamination of the resin bed with a small fraction of cation resin at the discharge end of the bed (possibly there from a previous program in which cation exchange was used). Examination of samples of the spent resin after exhaustive elution with 1 to 7 *M* HNO_3, which contained from 0 to 0.02 *M* F^-, and with reducing agents showed the top 20% of the 7.5-liter bed to be almost black and the remainder to be darker than freshly prepared resin. Chemical examination of these samples gave the following results:

Constituent	Amount on Resin (g/liter)	
	Top 20% of Bed	Bottom 80% of Bed
Pu	3.2	0.07
Al	0.5	
Pd	0.14	
Rh	0.03	

None of the above constituents could be completely eluted from the spent resin in extended elutions with 0.7 *M* HNO_3 or with stronger reagents, including aqua regia.

The waste effluent from the first ion exchange cycle was stored for subsequent processing to recover americium and curium.

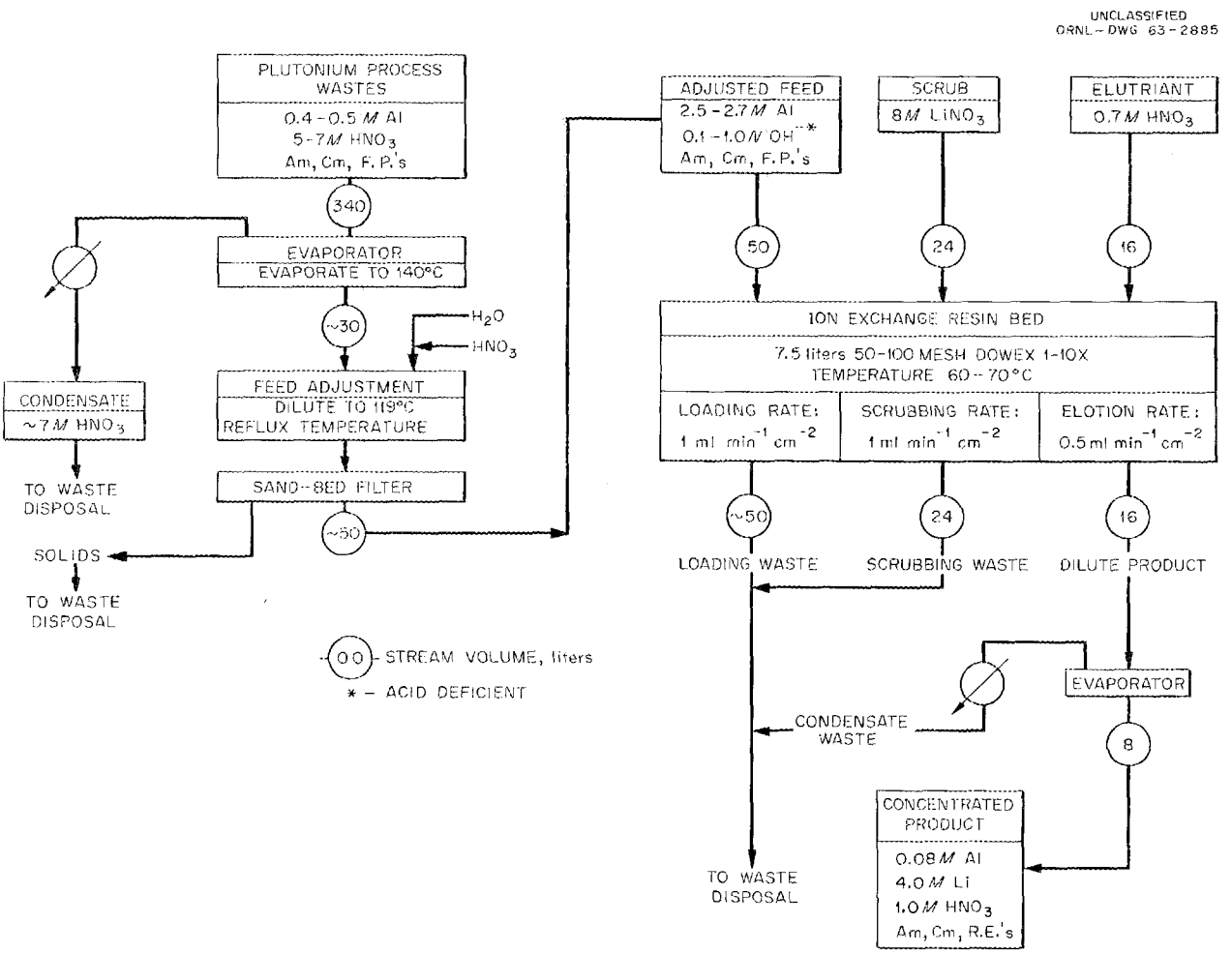

Fig. 5.1. Chemical Flowsheet for Recovery of Americium-Curium.

Recovery of Americium and Curium from Plutonium-Aluminum Alloy Processing Waste

A total of 2.6 g of Am^{241}, 25 mg of Cm^{242}, and 1.7 g of Cm^{244} was recovered from 4000 liters of wastes generated in two plutonium recovery programs processing highly irradiated Pu-Al alloy. The recovery process for the transuranium elements was conducted according to a flowsheet (Fig. 5.1) featuring concentration of the waste effluent from the plutonium recovery operation by evaporation, adjustment of the concentrate to feed specifications, sorption on anion resin, scrubbing with 8 *M* $LiNO_3$, and elution with 0.7 *M* HNO_3.

Feed Preparation. – Raw plutonium-recovery waste of the composition shown in Table 5.1 was concentrated by evaporation in the cell 1 dissolver. The wastes were added in divided portions (with evaporation between additions), until a total of 340 liters had been added, after which the temperature was raised to 140°C. All the nitric acid and a portion of the chemically bound nitrate was removed, resulting in a solution that was about 4 to 4.5 *M* in Al^{3+} and 0.5 to 2 *N* acid deficient. Condensate was discharged to waste.

Solids generated in the evaporation step were generally present in greater quantity in runs where the evaporator heating surfaces were exposed to the vapor during evaporation for long periods of time. These runs were characterized by feeds that were more acid deficient than usual. The increased acid deficiency was attributed to a steam leak that occurred during the second phase of the program in the lower of the two steam coils. (Steam had been released into the evaporating solution, resulting in an increased rate of nitric acid removal from the solution during the final stages of the evaporation step.)

Table 5.1. Composition of Raw Plutonium-Recovery Waste

Constituent	Program	
	Previous 24-Rod	Present 8-Rod
Al, *M*	0.35	0.50
HNO_3, *M*	5.2	6.2
Pu, mg/liter	1.0	1.5
Am^{241}, mg/liter	2.3	
Cm^{242}, mg/liter	0.007	0.07
Cm^{243}, mg/liter	0.12	3.9
Gross α, counts min^{-1} ml^{-1}	4.4×10^7	6.2×10^8
Gross γ, counts min^{-1} ml^{-1}	2.0×10^9	4.0×10^9

The concentrate was diluted with water to a reflux temperature of 119°C to obtain a solution that was then filtered through a bed of Ottawa sand (12 in. in diameter and 2 in. deep) that had been precoated with filter aid. Sampling this solution was difficult – the high salt content, as well as the presence of precipitated solids, often leads to plugging of the sampling unit. In addition, inhomogeneous samples were common. Concordant analytical data consequently were difficult to obtain.

The solution filtered slowly, and 25 to 30% of the americium and curium in the feed was lost to the filter cake. These losses were due to feed solution that was held in the moist filter cake rather than to selective sorption of the transuranium elements. More than 95% of the retained material could be recovered by washing the cake with 0.5 *M* HNO_3 and returning the wash to the evaporator. However, the specifications called for by the flowsheet for the ion exchange feed (high salt concentration and low acid concentration) precluded adding the wash solution to it, and since cell-1 equipment was not designed for returning the wash solution routinely, the recovery was conducted for demonstration purposes only. The clarified feed was adjusted with nitric acid to meet specification as an ion exchange feed.

Ion Exchange. – The adjusted feed solution was pumped to a heated standpipe from which it flowed to a 4-in.-ID by 40-in.-deep bed of 50- to 100-mesh Dowex 1-X10 anion exchange resin held at 60 to 70°C. Feed composition, run conditions, and results are shown in Table 5.2. The feed rate was varied from 2 to 6 liters/hr (0.3 to 1 ml min^{-1} cm^{-2}); the lowest losses were in the range 2 to 4 liters/hr.

The higher rate was beneficial in that the resin that floated in the high-density solutions could be retained in the column, with low pressure drop resulting. At the lower rate, the resin rose in the standpipe, resulting in an effectively longer resin bed with smaller cross-sectional area and consequently higher pressure drops. Sorption losses were not dependent on the acid deficiency of the

Table 5.2. Conditions and Results for the Anion Exchange Resin Run

	Program Run Number									
	1	2	3	4	5	6	8	9	10	11
Feed										
Al, *M*	2.2	1.95	2.1	2.7	2.2	2.6	2.5	2.0	2.8	2.6
A.D.(OH^-), *N*	<0.1	0.4	0.34	1.1	0.6	1.0	0.47	1.14	1.7	0.38
Rate, liters/hr	6	6	6	3	2	3.3	3	2.0	2.1	3.4
Temperature, °C	70	70	60	60	60	60	60	60	60	60
Losses, % Feed										
Loading	14	62	81	0.2	32	0.3	0.3	7.0	3.1	0.07
Scrubbing	57[a]	28	17	0.05	50	0.2	0.2	5.0	5.0	1.0
Recovery										
Am-Cm Product, % of feed	13	15	<1	95	40	70	67	62	69	100
Material Balance[b]	84	105	98	95	122	70	74	74	77	101

[a]Concentration of the $LiNO_3$ in the scrub solution: 6.2 *M*.
[b]Around the ion exchange system.

solution over the range 0.1 to 1.0 *N*, but increased slightly at values above this range. Feed solutions that were 0.1 to 0.5 *N* acid deficient were less viscous and flowed through the resin bed with greater ease. Indications were that at acid deficiencies above 1.1 *N* (OH^-), sufficient colloidal $Al(OH)_3$ was present to block the flow of feed through the resin-bed voids, which resulted in both the loss of effective resin contact and inefficient mechanical operation of the column.

Sorption losses of transuranium elements were dependent on aluminum concentrations up to 2.5 *M*. Over the range 2.0 to 2.5 *M* Al (acid deficiency at 0.1 to 1.0 *N*), sorption losses decreased from 60% to 0.3% of the feed.

After loading, the resin bed was scrubbed with 3 bed volumes (24 liters) of 8 *M* $LiNO_3$ at a flow rate of 3 to 6 liters/hr to scrub aluminum and light fission products from the bed. The temperature was held at 60 to 70°C. Scrubbing losses were dependent on $LiNO_3$ concentration and on the degree of loading. When breakthrough occurred during loading (as a result of low aluminum concentration or because of overloading), scrubbing losses were high, even with 8 *M* $LiNO_3$. Where breakthrough had not occurred, the scrubbing losses were less than 1%.

After scrubbing the loaded resin almost free of aluminum, the sorbed rare earths and transuranium elements were eluted with 2 bed volumes of 0.7 *M* HNO_3 at a rate of 3 liters/hr. The column was maintained at 60 to 70°C. The product from the resin elution was released generally in a sharp "band," and the degree of recovery varied in successful runs from 70 to greater than 99%. In those instances of low recovery on elution, severe "tailing" was observed, and extended elution was required. The cause has not been determined.

Resin Damage. – The spent resin was removed from the column after each run. The time cycle was about 40 hr. Samples of the spent resin were examined. Although it retained its bead-like shape, the spent resin had softened, become gummy, and turned jet black. Its capacity had decreased to 65% of the original value. A significant fraction of the gamma activity in the feed remained on the

spent resin after elution. The major gamma-ray contributors identified were Ru-Rh^{106}; a significant amount of Pd (Pd^{106} ?) was found on the resin.

The product fractions of each series of runs were composited separately and concentrated by evaporation to about 25% of their original volume. The concentrate was transferred to a storage tank in the cell. The average of the analyses of the concentrated products of all the runs is given in Table 5.3.

Table 5.3. Average Results of the Analyses of the Americium-Curium Product from Recovery by Anion Exchange

Al, *M*	0.08
Li, *M*	4.3
HNO_3, *M*	1.0
Gross alpha, counts min^{-1} ml^{-1}	2.6×10^9
Alpha pulse analysis, % of gross α at:	
5.5 Mev	11
5.8 Mev	47
6.1 Mev	42
Gross beta, counts min^{-1} ml^{-1}	1.7×10^{10}
Gross gamma, counts min^{-1} ml^{-1}	2.4×10^9
Ce^{144}, dis min^{-1} ml^{-1}	1.3×10^{11}
Cs^{137}, dis min^{-1} ml^{-1}	2.0×10^8
Ru^{106}, dis min^{-1} ml^{-1}	1.9×10^{10}
Sr^{95}, dis min^{-1} ml^{-1}	5.8×10^7
Zr^{95}, dis min^{-1} ml^{-1}	8.0×10^7

5.2 THE CURIUM PRODUCTION FACILITY

The hot cell facility in cells 3 and 4 of Building 4507 is being expanded from its original function as a "hot" development facility for the Transuranium Program to include also a Cm^{242} separations plant. The facility has been named the Curium Production Facility. The Tramex Process is the basic flowsheet for both operations, making the combined functions complementary. The solvent extraction equipment located in cell 4 will be served by a dissolver and general purpose chemical research type operations to be installed in cell 3.

The tentative program scheduled for the facility in the near future is as follows:

1. Low-level testing with Am^{243} and Cm^{244}.
2. Recovery, decontamination from fission products, and separation of 9 g of Am^{243} and 4 g of Cm^{244} from the initial Transuranium irradiations. Plutonium recovery and the aluminum removal steps in this process performed using ion exchange in cell 1 are reported in Sec 5.1.
3. Recovery of up to one-third of the Am^{243} and Cm^{244} from aluminum-free raffinate produced at Savannah River during the processing of the fully irradiated Transuranium target assemblies (Batch A). Approximately 170 g of Am^{243} and 220 g of Cm^{244} are in the entire batch.
4. Recovery and decontamination of 4 g of Cm^{242} from irradiated Am^{241} for subsequent fabrication into a test SNAP-13 heat source by the Isotopes Division.
5. Recovery of 12 g of Cm^{242} for the initial SNAP-11 heat source. Similar sources will be used in the Surveyor Program – which has the objective of instrumented lunar landings.
6. Recovery of the rest of the transplutonium elements from Batch A, including the isolation of microgram quantities of berkelium and californium.
7. When time permits during FY 1964, an experimental Cm^{244} heat source will be made.
8. Production of Cm^{242} for SNAP heat sources.

The first five operations are to be done in FY 1965; the routine production of Cm^{242} will follow about six months later.

Modifications of the facility for Cm^{242} production required the enlargement of the cell tankage and the installation of equipment fabricated of special materials to aqueous and high-activity levels. Glass-lined or tantalum-lined tanks are used, and process lines are of tantalum tubing. The mixer-settlers are constructed from Homalite, an allyl diglycol carbonate thermosetting plastic. This clear plastic permits observation of the settling chambers.

The apparatus shown in the equipment flowsheet (Fig. 5.2) is arranged in cell 4 as shown in the cell plan and elevation (Figs. 5.3 and 5.4).

The cell was converted from a gamma-ray-shielded facility to an alpha-gamma cell by the installation of seals on all openings and access ports. An overhead crane was installed in the cell to permit remote lifting and moving of tanks or racks of equipment.

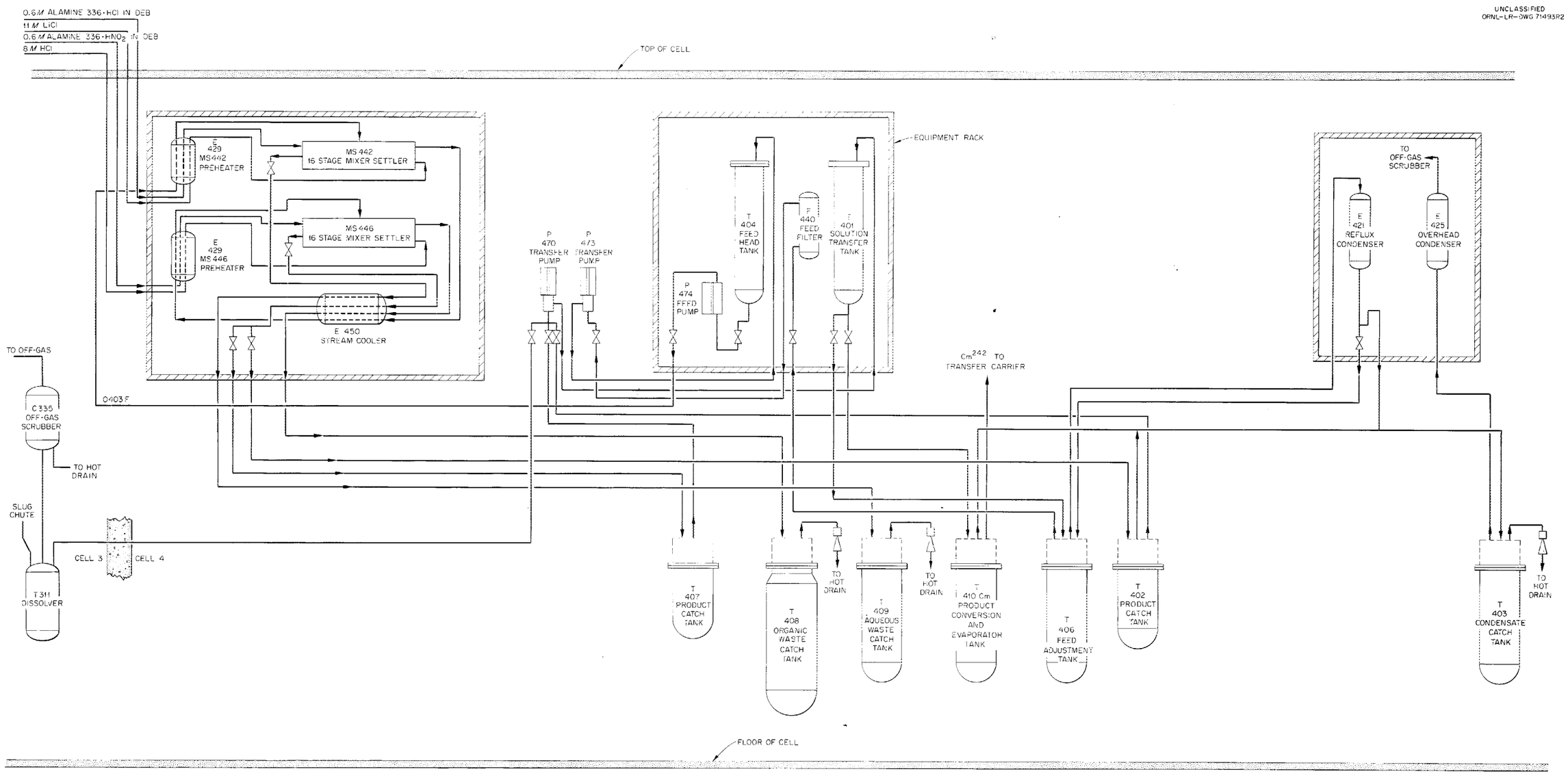

Fig. 5.2. Equipment Flowsheet for the Processing of Curium-242.

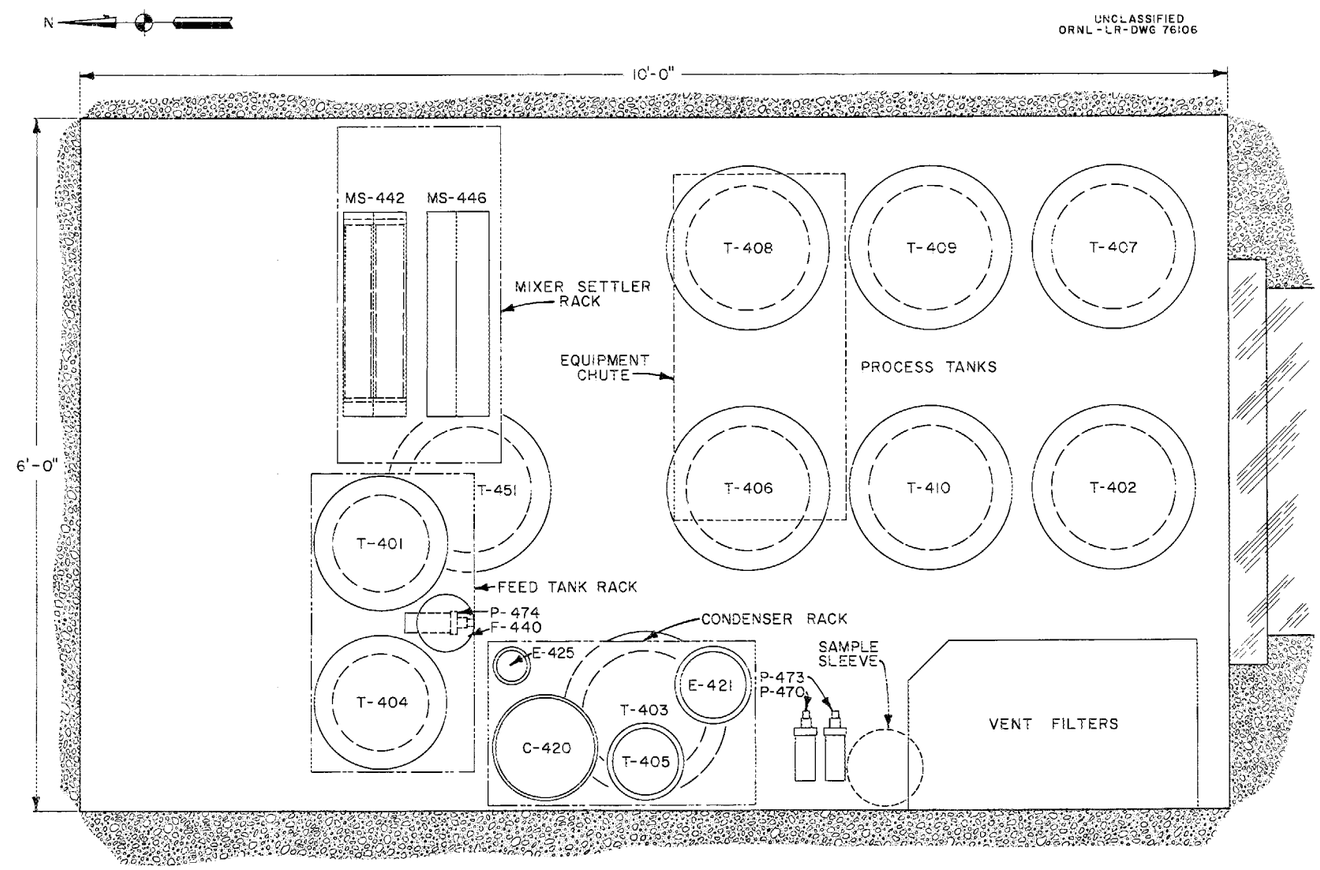

Fig. 5.3. Arrangement of Equipment in Cell 4, Plan View.

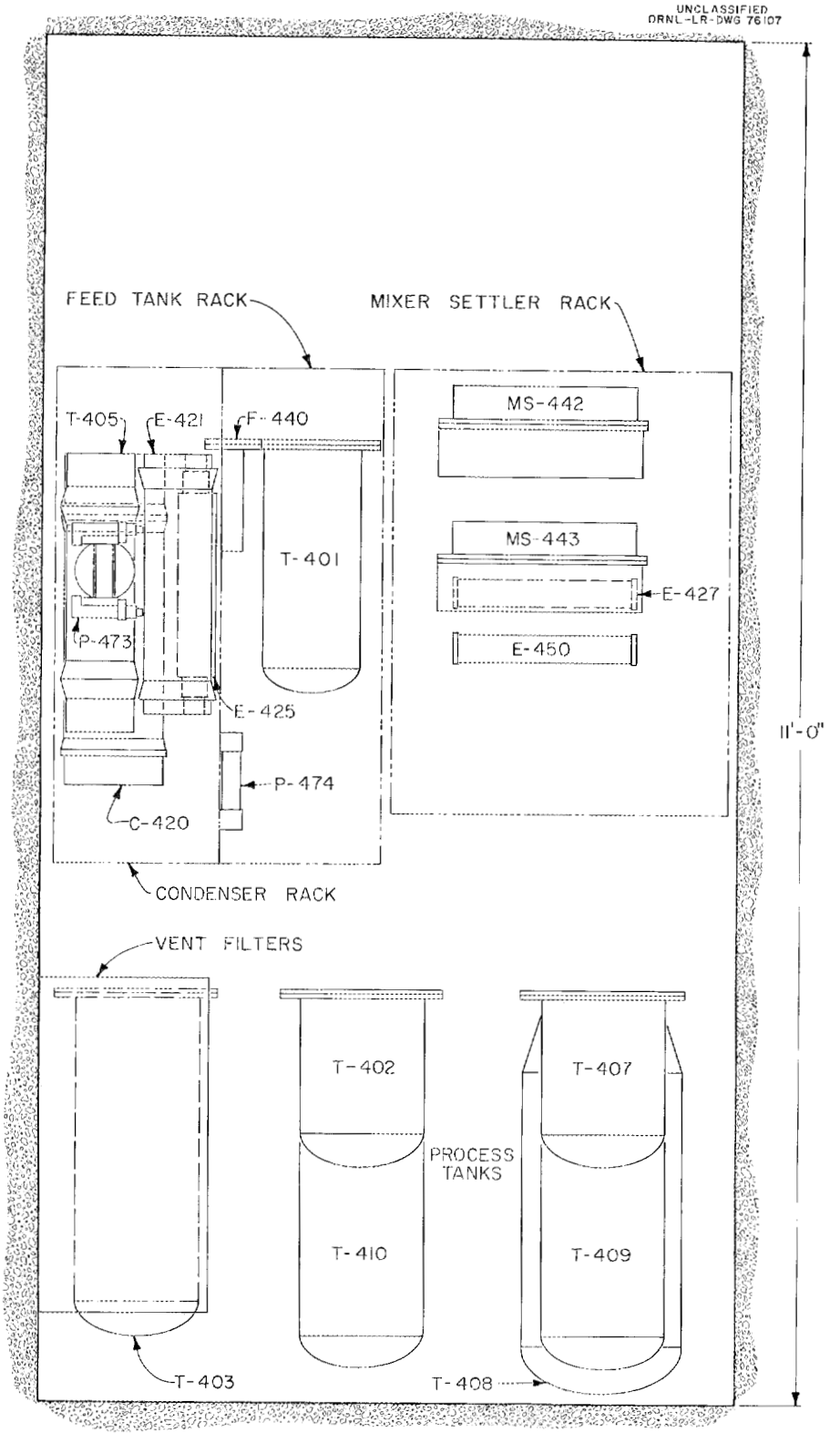

Fig. 5.4. Arrangement of Equipment in Cell 4, Elevation.

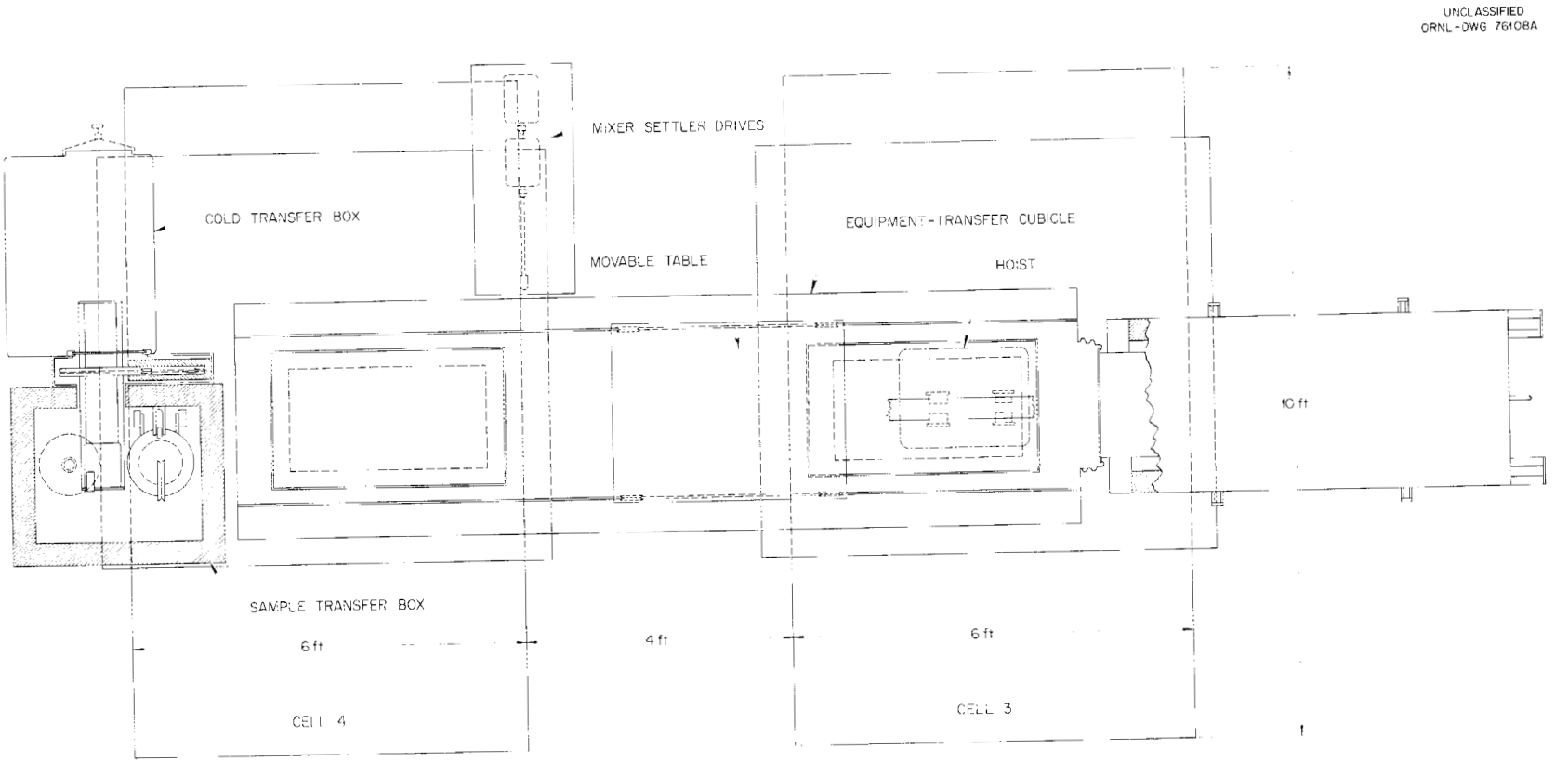

Fig. 5.5. Layout of the Penthouse Area.

All processing equipment in the cell is designed for remote manipulation and maintenance. The equipment is piped using jumpers having a remote disconnect at either end (see Fig. 4.27). Equipment or material can be transferred into the cell through a large equipment-removal cubicle located on the roof of the cell. A schematic layout of this area is shown in Fig. 5.5. Equipment can be repaired in this alpha-sealed cubicle after decontamination and then returned to the shielded cell, or it can be removed through a large "bag out" port. The equipment removal cubicle also serves cell 3, which is now being converted to alpha-gamma service.

Process solutions are sampled by a remotely operated syringe. Samples are transferred via a basket elevator to a shielded alpha-tight cubicle on the cell roof, where they are placed in a sealed can and loaded into a shielded carrier.

A pair of manipulators (double-booted model 8, heavy duty, extended reach) handle in-cell operations, which are observable through a 4-ft-thick lead-glass window. Manipulator boots can be replaced after removing the manipulators by pushing a boot-to-manipulator sleeve seal ring and boot into the cell with the new boot assembly.

Necessary "cold" chemicals are introduced into the cell from the chemical makeup area located behind the cell bank. This area also contains all potentially contaminated equipment, such as instrument transmitters and in-cell pump drive equipment.

5.3 CALCULATIONS REGARDING THE IRRADIATION OF GRAM QUANTITIES OF AMERICIUM-241

Engineering calculations for irradiating gram quantities of Am^{241} in the Oak Ridge Research Reactor (ORR) have been completed. The welded aluminum capsules (8 in. long and 0.5 in. OD) will each contain 3 g of Am^{241} as pressed pellets of AmO_2-Al. The weight of aluminum in each capsule is 60 g. An ORR core piece was designed and fabricated for irradiating up to 18 capsules. Irradiation calculations are based on an average perturbed thermal neutron flux of 3.0×10^{14}, a peak-to-average thermal flux ratio of 1.2, an irradiation time of 50 days, and an initial pellet-to-capsule gas gap (radial) of 1 mil. These conditions result in conversion of approximately 40% of the Am^{241} to Cm^{242}. Pellet center-line temperatures have been calculated for both helium- and air-filled capsules. Assuming 100% release of the gaseous fission products, the maximum stress in the aluminum capsule is 500 psi. Other conditions are shown in Table 5.4.

Table 5.4. Conditions of Irradiation

Type of Irradiation	Surface Heat Flux (Btu hr^{-1} ft^{-2})	Surface Temperature (°F)	Temperatures at Center Line of Pellet (°F)	
			He Gap	Air Gap
Average neutron flux (3.0×10^{14})	438,000	192	682	789
Peak neutron flux ($1.2\ \phi_{avg}$)	526,000	205	793	922
Peak neutron flux with 20% reactor power excursion	631,000	222	928	1082

6. Thorium Fuel-Cycle Development

6.1 SOL-GEL PROCESS DEVELOPMENT

The sol-gel process,[1,2] developed for the preparation of uranium-thorium oxide particles suitable for loading fuel elements by vibratory compaction, was tested on a 10- to 15-kg-per-batch scale in the Kilorod Facility, a pilot plant for the preparation of $U^{233}O_2$-ThO_2 fuel (U/Th weight ratio = 3/97). Engineering equipment for each step of the process was designed, built, and then successfully operated at full scale outside of shielding, with U^{238} nitrate as a stand-in for U^{233} nitrate. In the engineering-scale demonstration of the complete process, about 200 kg of the mixed oxide was prepared for vibratory compaction studies.

The steps in the sol-gel process are steam denitration of thorium nitrate to form dispersible thoria; dispersion of the thoria in aqueous uranyl nitrate to produce a stable sol; evaporation of the sol to gel fragments; and calcination of the gel to a dense mixed oxide, which is a solid solution of uranium and thorium oxides (UO_{2+x} and ThO_2). Variations in the procedure produced dense uranium oxide–thorium oxide solid solutions containing up to 10 mole % uranium, dense plutonium-thorium oxide solid solutions, spheres of thoria, up to 10 mole % UO_2–ThO_2 particles of 100 to 5000 μ in diameter, and dicarbides of thorium and uranium-thorium.

Preparation of Dispersible Thoria by Denitration of Thorium Nitrate with Superheated Steam

Equipment and procedures were developed for the dehydration-denitration of 30- to 45-kg batches of thorium nitrate crystals with superheated steam at 450 to 475°C, producing 15- to 20-kg batches of thoria. These products could be consistently dispersed to a stable, bluish, 2 *M* ThO_2 sol by the addition of 0.07 mole of 0.14 *M* HNO_3 per mole of ThO_2. Less than 1% of the oxide remained undispersed as a settled residue after a 24-hr settling period. About 700 kg of satisfactory, dispersible thoria powder was prepared while operating the electrically heated rotary denitrator (14 in. in diameter and 31 in. long) at full scale in a test demonstration for the Kilorod Facility.

Careful control of the conditions of denitration is required because differences in properties of the thoria product, not apparent from chemical analyses, greatly affect the dispersibility of the powder. The steps in the procedure that produced consistently dispersible powder were: (1) heating the thorium nitrate in the rotating denitrator to 200°C while purging lightly with air, (2) then changing to superheated steam at 450°C for 4 hr, while the wall temperature of the rotating denitrator was increased from 200 to 475°C.

The runs that produced good products showed endothermic reactions at 250, 290, and 330°C, according to temperature-vs-time plots. The residual nitrate in the thoria product was reproducibly controlled by the residence time above 450°C. Eleven runs held at about 450°C for 3 hr gave products having an NO_3^-/ThO_2 mole ratio of 0.027 ± 0.009. (The description of the equipment and a detailed discussion of the procedure are presented in another report.[1]) This procedure also produced good thoria from charges of thorium nitrate solution. In another experiment, readily dispersible 3% UO_2–ThO_2 was prepared from mixtures of uranyl and thorium nitrate crystals.

The Preparation of Uranium-Thorium Oxide Sol

Procedures that are being used in the Kilorod Facility for preparing UO_2-ThO_2 sols were developed in laboratory studies and at full scale. A full-size (30-liter capacity) critically safe slab tank, $1\frac{3}{4}$ in. thick, exactly like the one used in the Kilorod Facility except for a glass front to permit observation of the sol, was assembled and used for the full-scale sol-preparation studies. The procedure adopted was to disperse the ThO_2 in $UO_2(NO_3)_2$ solution at 80°C and then to adjust the pH of the sol with NH_4OH. A precisely measured volume of uranyl nitrate solution (50 g of uranium per liter and an NO_3^-/U mole ratio of 2.4 to 2.6) was diluted, adjusted in nitrate content to an NO_3^-/ThO_2 mole ratio of 0.077, and then circulated by a centrifugal pump through the tank and a heat

[1] D. E. Ferguson *et al.*, *Status and Progress Report for Thorium Fuel Cycle Development for Period Ending December 1962*, ORNL-3385.

[2] D. E. Ferguson *et al.*, *Preparation and Fabrication of ThO_2 Fuels*, ORNL-3225 (June 5, 1962).

exchanger to raise the temperature to 80°C. The ThO_2 powder was flushed with water into the adjusted $UO_2(NO_3)_2$ solution as the circulation and heating were continued for 1 hr to complete the dispersion. Dilute NH_4OH solution (0.017 mole of NH_3 per mole of ThO_2) was added to the suction line of the centrifugal pump in order to adjust the H^+ concentration to 10^{-3} to 10^{-4} *M*, which is the optimum for uniform distribution of the uranium on the thoria surface. Sols up to 5 *M* in ThO_2 prepared by this method were fluid and easily handled, but for the Kilorod project, a 2 *M* ThO_2 sol was adopted. A detailed description of the apparatus and an account of the development program for sol preparation are presented in another report.[1] With this procedure, the maximum deviation of the uranium/thorium atomic ratio from the mean of the entire batch was 1% for all particle sizes of final product.

When uranyl nitrate was obtained as a product of solvent extraction, the minimum mole ratio (NO_3^-/U) consistently achievable was 2.4. By the described procedure, the amount of uranium that can be incorporated while maintaining uniformity of the uranium/thorium mole ratio in the product is therefore limited to 3 mole %. However, sols containing up to 10 at. % uranium were made by adding 3 mole % uranium as uranyl nitrate and then the remainder as ammonium diuranate.

Evaporation of the Sol to a Gel

The adjusted sol is evaporated in batches in trays under a stream of heated air at 80 to 90°C. In the Kilorod Facility, the trays are arranged in cascade so that the sol from the top trays overflows to those below. The depth of the sol (¾ to 1 in.) is controlled by the height of the overflow pipe in order that the dried gel from all trays may be equal in weight, density, and volatile-matter content and have nearly uniform thickness (about ¼ in.). Drying for 48 hr at 85 to 90°C prevents the formation of bubbles and removes the volatile matter from the gel except for a residue of 4 to 6%. The density of the dried gel is 6 to 7 g/cc; the volume concentration factor during drying is about 10. The gel product is fractured during drying to particles ranging from 0.5 to 0.005 in. in diameter. The fragment-size distribution was shown to be dependent upon the flow rate and the humidity of the drying air and upon the temperature of the solids after the gel had formed. The back-addition of about 10% of its weight in water at room temperature caused the gel to fracture to particles such that 55% by weight was −4 to +16 U.S. mesh size, and 95% was −4 to +100 mesh. A blend, composed of 75% of this size distribution with 25% of −200 U.S. mesh size, obtained from ball milling gel, was mixed and fired according to the sol-gel procedure. A small batch of the product was vibratorily packed to 86.1% of its theoretical density in 3 min by a small Navco vibrator. A larger batch (420 g) was vibrated to 89.5% of theoretical density by the Branford vibrator. Since comminution of particles to sizes suitable for vibratory compaction loading prior to firing has many advantages over the conventional postfiring crushing and grinding, these studies will be pursued further.

Calcination of the Dried Gel

In the procedure developed for the Kilorod Facility, a batch of dried gel (about 11 kg) is loaded from the gel-drier trays by specially developed tray-dumping equipment into Alundum crucibles and air-fired at a temperature-rise rate of 100°C/hr up to 500°C, then at 300°C/hr up to 1150°C. After holding at 1150°C for 1 hr, the air is swept out of the retort with argon, and then a slow stream of 4% H_2–Ar (which in air makes a noncombustible mixture) is passed through the furnace retort for 4 hr to reduce the higher oxides of uranium to UO_2. The charge is then cooled under argon until the temperature is below 200°C.

Studies were made of the effects of blanket atmospheres that were used during firing and cooling and of furnace time cycles on the quality of the oxide products. The criteria for adequate quality of the oxide product for the Kilorod Facility are as follows: particle density (by toluene immersion), greater than 9.9 g/cc; oxygen/uranium ratio, less than 2.1; and total gases released when heated to 1200°C in a vacuum, less than 0.05 cc per gram of oxide. In laboratory studies with 55-g samples of oxide and well-controlled furnace atmospheres, all the quality criteria were met and surpassed by the use of argon, nitrogen, or 4% H_2–Ar as blanket gases. In a furnace like that used in the Kilorod Facility, furnace atmospheres could not be so well controlled, and the values obtained as shown in

Table 6.1 are representative of what can be expected by use of argon, 4% H_2–Ar, or nitrogen as blanket gases. Densities were greater than 9.9 g/cc for all blanket gases used. Only batches fired in 4% H_2–Ar were satisfactory with respect to oxygen/uranium ratio and gas evolution. Therefore, the 4% H_2–Ar was adopted as a blanket gas for the Kilorod Facility. Other experiments showed that if the oxides were withdrawn from the furnace directly into air at temperatures exceeding 200°C, reoxidation of the uranium occurred. More detailed data and discussion are presented in another report.[1]

The Preparation of Spheres of Thoria and Uranium-Thorium Oxide

The above-described sol-gel procedure used for preparing fragments of thoria and uranium-thorium oxide suitable for vibratory compaction was also used for preparing sol-gel spheres of the same chemical composition.[3] The dried gel fragments were comminuted by tumbling to suitable sizes, and the particles were rounded by milling them with 1200°C-fired, sharp, sol-gel-prepared thoria fragments. Figure 6.1 shows samples from kilogram batches of thoria and 3% UO_2–ThO_2 spheres of 0.2-in.-diam made by this procedure. Both products had extremely low attrition rates when tested in a standard spouted bed: 0.04%/hr for thoria spheres and 0.005%/hr for uranium-thorium oxide spheres. These rates were below the acceptable rate of 0.05%/hr.

Metals and Ceramics Division personnel produced 200- to 500-μ spheres from 3% UO_2–ThO_2 gel prepared by the Chemical Technology Division. Controlled linear shrinkage of the microspheres was demonstrated by firing them to 500 or 1000°C, depending on the degree of shrinkage desired. This shrinkage control was shown to be useful in incorporating fuel particles into pressed or extruded oxide matrices (e.g., BeO) and then firing without the danger of inducing cracking by the mismatched shrinkages of dissimilar materials.

[3] O. C. Dean and C. E. Schilling, *Preparation of Thorium Oxide and Uranium-Thorium Oxide Spheres by the Sol-Gel Process*, ORNL-3384 (in preparation).

Table 6.1. Oxygen-to-Uranium Ratio and Residual Gas Content of Calcined Product

Batch size: 5–7 kg

Composition: Uranium oxide–thorium oxide, 3/97 uranium/thorium by weight

Firing procedure: 300°C/hr to 1150° and held for 1 hr in air; calcined in indicated gases 4 hr; cooled in same gas to <100°C

Calcination Atmosphere	Oxygen/Uranium Ratio			Gas Release at 1200°C, in Vacuum (std cm^3/g)		
	+16 Mesh[a]	16–35 Mesh[b]	–35 Mesh[c]	+16 Mesh[a]	16–35 Mesh[b]	–35 Mesh[c]
Argon–4% H_2[d]	2.026	2.027	2.019	0.004	0.004	0.067
Nitrogen	2.099	2.087	2.157	0.018	0.055	0.120
Argon	2.220	2.267	2.308	0.030	0.047	0.050

[a] Comprises ~92 wt % of product.
[b] Comprises ~5 wt % of product.
[c] Comprises ~3 wt % of product.
[d] Cooled in argon containing no hydrogen.

UNCLASSIFIED
PHOTO 59580-R

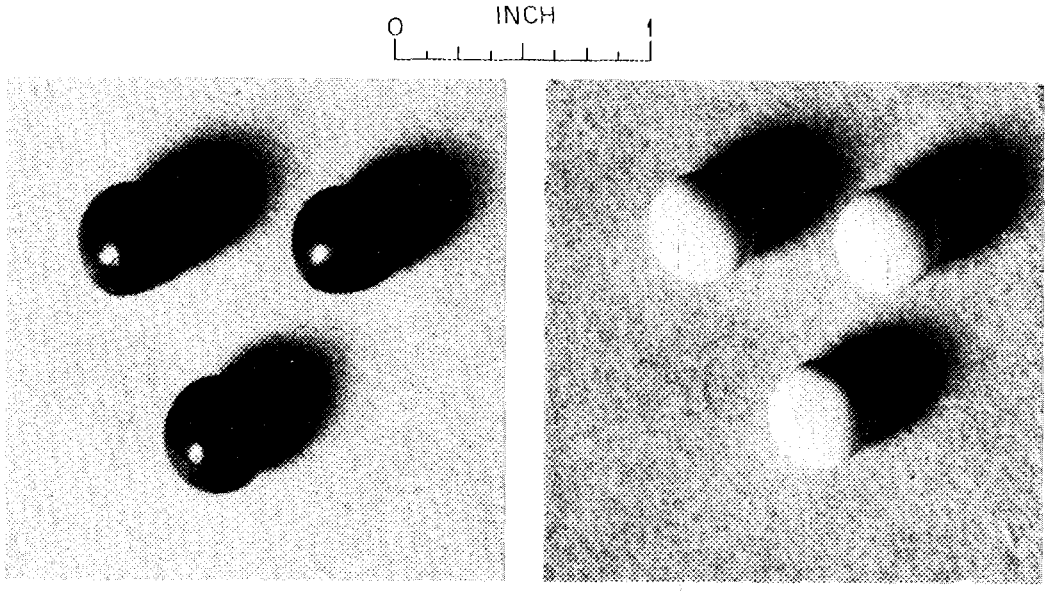

9.93 g/cc 0.005%/hr

9.87 g/cc 0.04%/hr

Fig. 6.1. Sol-Gel-Process Spheres of High Density and High Attrition Resistance.

6.2 PROPERTIES OF SOL-GEL OXIDES

Examination of the uranium-thorium oxide products by x-ray diffraction (phase identification and lattice parameter measurement), metallography, petrography, and electron micrography gave evidence that they are single-phase materials and also are probably solid solutions of UO_{2+x} in ThO_2. Products that contained 7 or less at. % uranium and which were prepared by the procedure described in Sec 6.1 had uniform mole ratios of uranium to total metal. Homogeneous physical structure and chemical compositions are desirable in fuels in order to produce uniform power density from point to point.

Homogeneity of Sol-Gel Oxides

The sol-gel process produces uranium-thorium oxide of high uniformity in the mole ratio of uranium to total metal throughout each particle, from particle to particle (regardless of particle size), and from batch to batch. Table 6.2 shows that for a single batch the deviation of the mole ratio of uranium to total metal from size fraction to size fraction was within ±1%, with one minor exception. Since the variation of the U/(U + Th) mole ratio between sizes was <1% after grinding as well as before, it was concluded that the composition of the particles was uniform. Sufficient uniformity from batch to batch has been obtained to show that a product can be made with only a ± 1% variation in uranium content; this specification was imposed on the oxide fuel product of the Kilorod program.

Photomicrographs of polished sections of sol-gel-prepared oxide particles at 150X show no evidence of grain structure, extraneous phases, gross voidage, or other inhomogeneity (see Fig. 6.2). Polished and etched sections at 500X give minimal evidence of grain structure but show a uniform distribution of very fine closed porosity. Electron micrographs of a replica of a freshly fractured surface showed closely packed grains[2] 5000 to 7500 A in diameter. The preparation represented in Fig. 6.2 released only 0.5% of the Kr^{85} formed during neutron irradiation to 14,800 Mwd/metric ton at a linear heat rating of 47,500

Table 6.2. Uniformity of Uranium Distribution in Sol-Gel-Prepared Uranium-Thorium Oxides

Weighted mean U/(U + Th) mole ratio for all size fractions = 0.0650

Batch	Particle Size, U.S. Mesh	Production Size Range (%)	U/(U + Th) Mole Ratio	Deviation from Mean U/(U + Th) Mole Ratio (%)
35-1	+16 (unsized)[a]	90–93	0.0648	–0.3
35-1-G	–6 +16 (sized)[b]	60	0.0652	+0.3
35-1	–16 +35 (unsized)[a]	4–6	0.0642	–1.3
35-1-G	–50 +140 (sized)[b]	15	0.0655	+0.8
35-1-G	–200 (ball-milled)[b]	25	0.0651	+0.2

[a]Sample was prepared by screening the product removed from the calcination furnace.

[b]Samples from size fractions prepared for vibratory compaction by crushing, grinding, and screening.

Btu hr^{-1} ft^{-1} (ref 4). Studies will be made to determine the possibility of a relation between the very small, widely distributed closed pores, whose combined volume is less than 1% of that of the solid and the fission-product-gas release of the sol-gel oxide.

Physical Properties

For typical sol-gel-prepared oxide products that are composites of all particle sizes, the specific surface areas of the unsized oxide as removed from the calcination furnace varied from 0.003 to 0.03 m^2/g, depending on particle-size distribution. When ground and sized for vibratory compaction, they varied from 0.05 to 0.25 m^2/g (Table 6.3). The average densities of particles (by the toluene immersion–pycnometric measurement) were from 99 to 99.9% of theoretical (10.035 g/cm^3). In addition to having high individual particle density, oxides prepared from sols that were optimally adjusted with respect to the NO_3^-/ThO_2 and NH_4OH/ThO_2 mole ratios had significantly higher powder sizing and "compactability" when packed by the best vibratory packing procedures than those prepared from unadjusted sols. Compactability is thought to be a function of the shape and surface roughness of the particles.

Heating an oxide sample in vacuum and collecting the evolved gases at predetermined temperatures up to 1200°C provides an out-of-pile means of predicting the amounts, partial pressures, and species of non-fission gases expected to be evolved within the element during thermal cycling in service. The measurement of the total volume of gases evolved aids in giving an estimate of the internal pressure of a fuel element that will contain the oxide. The analysis of these gases aids in predicting chemical effects of the oxide on the cladding material (e.g., H_2-Zircaloy interaction) while in service. Calcined oxides that have not been ground and sized evolve a total of 0.005 to 0.05 std cm^3/g when heated to 1200°C in vacuum (Table 6.3). Oxides that have been sized by grinding (particularly by ball milling) in air evolve 0.1 to 0.4 std cm^3/g under like treatment.

Chemical Properties

Sol-gel oxides are quite free from contaminants that would parasitically capture neutrons. One large batch containing U^{235} prepared for irradiation and sized for vibratory compaction (see Table 6.4)

[4]S. A. Rabin *et al.*, "Thorium Fuel Cycle Irradiation Program at the Oak Ridge National Laboratory," in *Proceedings of Thorium Fuel Cycle Symposium, Gatlinburg, Tennessee, December 5–7, 1962.*

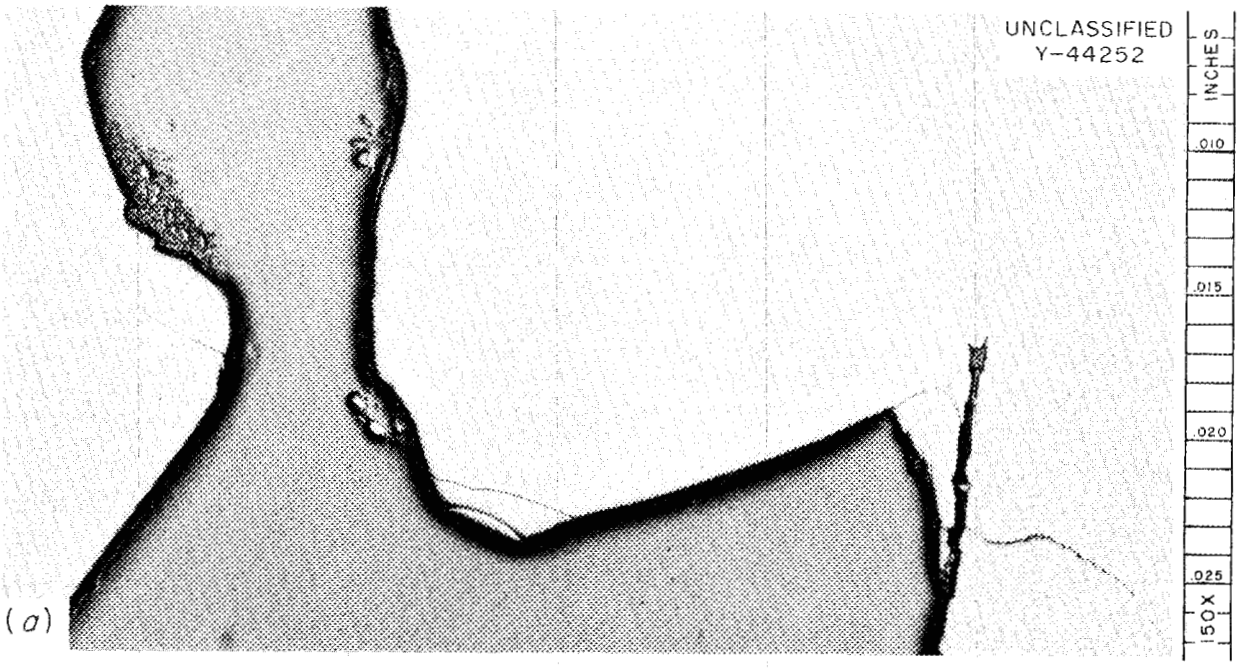

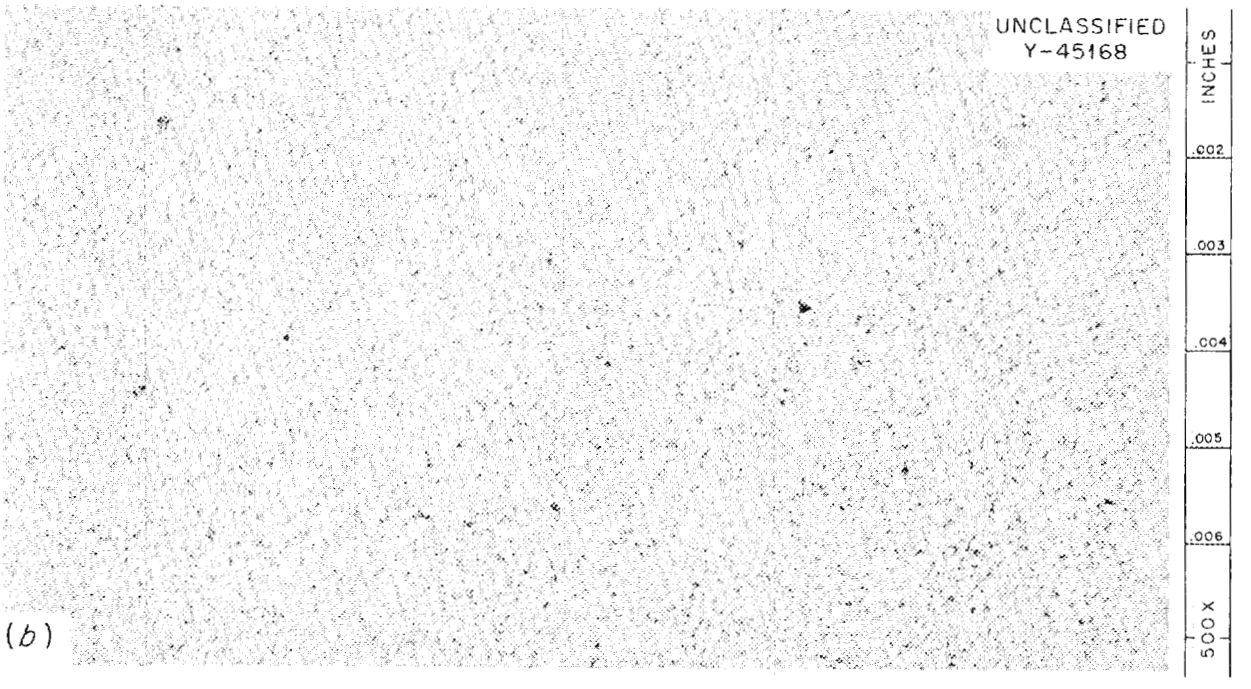

Fig. 6.2. Sol-Gel E: ThO_2–4.5 wt % UO_2 Powder. No impurities were found in this material. Small surface cracks may be seen in the particles. (*a*) 150X. As polished. (*b*) 500X. Etchant: boiling HNO_3-HF. At higher magnification the particles show a very fine natural porosity and extremely fine crystallites (spheroidal white particles). No large grain boundaries are evident.

Table 6.3. Physical Properties of Typical Sol-Gel Uranium-Thorium Oxides

Calcination procedure: in air, 25 to 1150°C at 300°C/hr; in calcining atmosphere, 4 hr at 1150°C; in cooling atmosphere to 100°C

Batch No.[a]	Furnace Atmosphere		Specific BET (N_2) Surface Area (m^2/g)		Density (g/cm^3)		Total Gases Evolved at 25–1200°C in Vacuum (std cm^3/g)	
	Calcination	Cooling	Unsized[b]	Sized[c]	Particle[d]	Packed	Unsized	Sized
26	4% H_2–Ar	Ar	0.032	0.047	9.98	8.50	0.006	0.206
35-2	4% H_2–Ar	Ar	0.005	0.213	9.91	8.95	0.005	0.101
E	H_2	Ar	0.015		9.92	8.65	0.027	
A	H_2	Ar		0.2	9.94	8.71		0.125
S	4% H_2–Ar	Ar		0.15	10.00	8.84	0.055	0.400
35-1	Air	Air	0.003	0.196	9.94	9.00	0.498	0.354
35-3	N_2	N_2	0.004	0.241	9.97	8.90	0.029	0.114

[a]Weighted average of property data for three sizes to give properties of composite mixture.
[b]Unsized, as removed from calcination furnace, not crushed.
[c]Crushed and ball milled to sizes suitable for vibratory compaction.
[d]Particle density, pycnometric (toluene immersion).

Table 6.4. Chemical Properties of Sol-Gel-Prepared Uranium-Thorium Oxides

Prepared for irradiation tests; contain fully enriched uranium
Calcination procedure: in air, 25 to 1150°C at 300°C/hr; in calcination atmosphere, 1150°C, 4 hr; in cooling atmosphere to 100°C

Batch No.[a]	Furnace Atmosphere		U (wt %)	C (ppm)	Oxygen/Uranium Ratio		Gases Evolved by Heating in Vacuum at 25 to 1200°C. (std cm^3/g)[b]					
	Calcination	Cooling			Unsized	Sized	H_2	H_2O	N_2 + CO	O_2	CO_2	Total
26	4% H_2–Ar	Ar	5.52	40	2.026	2.025	0.100	0.003	0.083	0.001	0.011	0.206
35-2	4% H_2–Ar	Ar	5.12	47	2.035	2.031	0.028	0.004	0.032	0.002	0.026	0.101
A	H_2	Ar	4.31	120		2.005	0.002	0.062	0.008	0.0	0.051	0.125
35-1	Air	Air	5.13	173	2.400	2.403	0.005	0.014	0.009	0.248	0.069	0.354
35-3	N_2	N_2	5.05	59	2.175	2.160	0.003	0.022	0.006	0.012	0.070	0.114

[a]Samples composed of a mixture of particles having a size distribution suitable for vibratory compaction.
[b]For oxides crushed and ball milled (sized) to sizes suitable for vibratory compaction.

had only 1050 ppm gross ionic impurities, 640 of which were iron, aluminum, and sodium.[4] The macroscopic cross section of the total impurities was equivalent to that of 5 ppm boron. The iron and aluminum were traced to pickup in the grinding and ball-milling equipment. Other chemical properties of typical sol-gel oxides are presented in Table 6.4. The O/U ratios of products calcined in 4% H_2–Ar (recommended in the optimized flowsheet discussed in Sec 6.1) were 2.02 to 2.03 and were not significantly affected by grinding. Experimental batches fired in air or in nitrogen in a large furnace in which atmospheres could not be well controlled had, typically, O/U ratios of about 2.4 and 2.2. In firings where the atmosphere was carefully controlled, oxides calcined in nitrogen or argon had O/U ratios of less than 2.1. For a homogeneous uranium-thorium oxide preparation containing 3 mole % uranium, an O/U ratio of 2.3 is equivalent in excess oxygen to a pure UO_2 fuel having an O/U ratio of less than 2.02 (ref 4). This indicates that less-expensive nitrogen or argon atmospheres may be used for calcination in a well-sealed, large furnace.

Gases Evolved from Products on Heating in Vacuum. – For the oxides calcined in 4% H_2–Ar or in pure hydrogen, the major gaseous components evolved on heating them in a vacuum up to 1200°C are hydrogen and carbon monoxide[4] (Table 6.4). A likely source of most of the hydrogen appears to be the reaction between water and carbon sorbed as CO_2 from the air by the thoria at any stage of processing sols or gels. Pyrolytic carbon may be collected from the calcination blanket gas. When the oxides are calcined in argon or nitrogen, the major gases evolved are water, carbon dioxide, and oxygen. Of these components, hydrogen and water are known to corrode Zircaloy-2 cladding if they are present at significant partial pressures inside the fuel element. At gas-evolution values of 0.1 std cm^3/g for oxides calcined in H_2–Ar or H_2, hydrogen partial pressures at mean fuel temperatures corresponding to those in the Consolidated Edison reactor would be 50 to 150 psi.[4] Total pressures within the element would be about 500 psi. The total pressure would be tolerable, but the hydrogen content would be destructive to Zircaloy-2. Under similar conditions, oxides calcined in argon or nitrogen give about 500 psi total pressure consisting, in part, of 25 psi of H_2O and about 200 psi of O_2. These conditions would likewise be destructive to Zircaloy-2 at reactor operating temperatures. Experience indicates that gas evolution of less than 0.05 std cm^3/g appears to be necessary for good behavior of the oxide within the cladding. When oxides are ground (particularly when they are ball milled), they sorb large volumes of CO_2 and H_2O. These react with the carbon present in the oxide to generate CO and H_2. Because of this reaction, fired oxide fuels should be ground in dry, CO_2-free air or unfired oxides should be ground prior to calcination.

Fuel-Cycle Irradiations

Since the start of the ORNL Thorium Utilization Fuel Cycle Program, 32 capsules containing different size fractions of either sol-gel or arc-fused oxide fuel have been fabricated by vibratory compaction for irradiation testing in the NRX, MTR, and ORR. The peak linear heat rating of the capsules varied between 25,000 and 60,000 Btu hr^{-1} ft^{-1}. As of Apr. 1, 1963, the in-pile tests had been completed on 18 capsules, and the present accumulated postirradiation data indicate that sol-gel oxide is a satisfactory potential reactor fuel. Ten additional sol-gel ThO_2-UO_2 capsules are being prepared for irradiation in the MTR and ETR to study the effect of higher linear heat ratings.

Thirty noninstrumented capsules have been or are being irradiated in the NRX and MTR at estimated average cladding temperatures of 200 to 210°C. The cladding is of type 304 stainless steel, with a $^5/_{16}$-in. OD and a 0.025-in. wall thickness. Sixteen of these capsules at peak linear heat ratings of 25,000 (NRX groups I and II) and 40,000 to 45,000 (MTR group I) Btu hr^{-1} ft^{-1} have been removed for examination. These examinations, performed by the Metals and Ceramics Division, include dimensional measurements, gamma radioactivity scans, fission-gas-release amounts and identification, fuel burnup measurements, and metallographic examinations of the fuel and cladding. These results are discussed in more detail elsewhere.[5] Dimensional measurements indicate negligible changes as a result of the irradiation, and the fission-gas release from sol-gel

[5] D. E. Ferguson *et al.*, *Status and Progress Report for Thorium Fuel Cycle Development for Period Ending December 1962*, ORNL-3385.

oxide compares favorably with gas release data from arc-fused oxide and UO_2 pellets. Burnup measurements on the irradiated material range from 5000 to 17,000 Mwd per metric ton of Th and U. Although the -200-mesh oxide particles agglomerated, there is no metallographic evidence of sintering.

Two 22-in.-long capsules (MTR group II), containing sol-gel S ThO_2-UO_2 vibratorily compacted to a bulk density of 8.8 g/cm^3, were inserted in the MTR on Jan. 1, 1963. These specimens are scheduled to remain there until the burnups reach 100,000 to 120,000 Mwd per metric ton of Th and U (about 2.5 yr).

Two instrumented capsules were irradiated in the ORR at average cladding temperatures of 1000 and 1300°F. Between January and September 1962, these capsules had accumulated measured burnups of 4200 and 5400 Mwd per metric ton of Th and U. The capsules (type 304 stainless steel, $\frac{5}{8}$ in. in diameter) had been loaded with sol-gel D ThO_2-UO_2, vibratorily compacted to a bulk density of 8.6 g/cm^3, and were designed to operate at a linear heat rating of 40,000 Btu hr^{-1} ft^{-1} with an active fuel length of 5.5 in. The central fuel temperatures of the two capsules were 2600 and 3500°F. Based on the design heat-generation rate, the effective thermal conductivities of the compacted oxide were 1.7 and 1.2 Btu hr^{-1} ft^{-1} °F^{-1} for respective average fuel temperatures of 1800 and 2400°F. Due to discrepancies in thermal-neutron flux measurements, the instantaneous heat-generation rate could not be determined experimentally; however, based on fuel burnup, the estimates of respective thermal conductivities of the oxide were revised to 1.2 and 1.0 Btu hr^{-1} ft^{-1} °F^{-1}.

Ten noninstrumented type 304 stainless steel capsules containing sol-gel ThO_2-UO_2 are being prepared for irradiation in the MTR (group III) and ETR (group I) at peak linear heat ratings of 85,000 and 135,000 Btu hr^{-1} ft^{-1} respectively. In addition to the higher linear heat ratings, an objective of the irradiations is to study the effect of furnace atmosphere on the in-pile performance of sol-gel ThO_2. Three firing atmospheres (air, 4% H_2–Ar, and nitrogen) were used in preparing the oxide. Then, the sized sol-gel oxide was vibratorily packed to bulk densities of 8.8 to 9.0 g/cm^3 in capsules 12 in. long and $\frac{7}{16}$ in. in diameter. The estimated peak central fuel temperature in the MTR group-III capsules will be 5000 to 5200°F, and the center temperature of the ETR group-I capsules should reach the melting point of the oxide.

6.3 THE KILOROD FACILITY

Scope of Kilorod Program

ORNL was recently assigned a development program to prepare Zircaloy-2-clad fuel rods for zero-power criticality experiments to be performed at Brookhaven National Laboratory (BNL). About 900 rods, each containing 890 g of oxide (3 wt % U^{233}–97 wt % Th), and 200 rods, each containing 310 g of the same mixed oxide, are to be made. The BNL rods will be made in the Kilorod Facility[6] using the sol-gel process[7,8] for mixed-oxide preparation, and vibratory compaction[8,9] for rod loading. The U^{233} feed will be prepared and purified of U^{232} decay products by solvent extraction.[10] The facility was designed to produce about 10 rods a day. This is a joint program with the ORNL Metals and Ceramics Division.

The Kilorod Facility is a vital part of the ORNL Thorium Fuel Cycle Program. Development programs conducted in the facility will extend thorium fuel-cycle technology by providing valuable processing and fabrication experience as well as data on worker radiation exposure while processing U^{233}.

Radiation Dose Predictions

The collection of radiation data at each step of the Kilorod process is important since the data will help determine the level of radiation that might be expected from other arrangements of the same operations and from the processing of U^{233}

---

[6] *Chem. Technol. Div. Ann. Progr. Rept. May 31, 1962*, ORNL-3314, pp 180–81.

[7] D. E. Ferguson, O. C. Dean, and P. A. Haas, *Preparation of Oxide Fuels for Vibratory Compaction by the Sol-Gel Process*, ORNL TM-53 (Nov. 27, 1961).

[8] D. E. Ferguson *et al.*, *Preparation of High-Density Oxide and Vibratory Compaction in Fuel Tubes*, ORNL-2965 (Jan. 27, 1961).

[9] J. T. Lamartine and A. L. Lotts, *Thorium-U^{233} Fuel Rod Facility – Description of the Facility and Fuel Rod Fabrication Process*, ORNL CF-62-2-26 (Apr. 27, 1962).

[10] E. C. Moncrief *et al.*, *Hazards Evaluation for the BNL Kilorod Program*, ORNL CF-62-11-16 (Nov. 8, 1962).

containing higher concentrations of U^{232}. Also, the experimental data will assist in determining shielding requirements and limits on semiremote operations at higher concentrations of U^{232}.

Calculations were made[11] to determine the gamma dose to the hands of the operators at each step of the process, using a shielding code[12] on the IBM-7090. Twelve gamma-source strengths above 0.25 Mev[13] were used in the code, which also permitted the selection of a source geometry representative of the actual equipment geometry. In the calculations, data by Arnold[14] of buildup and decay factors for members of the U^{232} decay chain were used. Basic assumptions used in the calculations were (1) U^{232} daughters were completely removed during solvent extraction purification of the U^{233}; (2) the purified U^{233} contained no fission products; (3) dose-rate contributions from Th^{228} in the ThO_2 were neglected (this contribution will be evaluated during cold testing); (4) beta dose was neglected; (5) Ra^{228}, Ra^{224}, and Rn^{220} evolution during processing was neglected; (6) uranyl nitrate feed not used during the two-week operating cycle will be repurified; (7) ten 10-kg sol-gel batches will be prepared during the two-week operating cycle; and (8) there would be negligible holdup of U^{233} in any equipment, compared with the process throughput.

The maximum hand-exposure case was evaluated in which a single operator was assumed to perform all operations in the Kilorod Facility over the two-week operating period. Although not an operating procedure, the case represents the maximum probable gamma dose to hands expected from gloved-hand operations in the facility. A maximum dose to hands of 1000 millirems would be obtained during the second week of the operating cycle. This dose is below the maximum permissible weekly hand exposure (1500 millirems/week).

[11] F. W. Davis and E. C. Moncrief, *Gamma Dose Rate Calculations for the BNL-Kilorod Program*, ORNL TM-407 (Mar. 21, 1963).

[12] E. D. Arnold and B. F. Maskewitz, *SDC — A Shielding Design Calculation Code for Fuel Handling Facilities*, ORNL-3041 (in press).

[13] D. Strominger, J. M. Hollander, and G. T. Seaborg, *Rev. Mod. Phys.* **30**, 585 (1958).

[14] E. D. Arnold, *Buildup and Decay Factors for Members of the U^{232} Decay Chain*, ORNL CF-58-7-122 (July 31, 1958).

Solvent Extraction Operations

Process Flowsheet. — The U^{233} feed to the sol-gel process was purified of U^{232} decay products and ionic contaminants by solvent extraction. The solvent extraction system used in the Kilorod program consisted of one cycle of solvent extraction using 2.5% di-sec-butylphenyl phosphonate (DSBPP) in diethylbenzene (DEB) diluent, followed by product concentration by evaporation. Existing solvent extraction equipment was modified to accommodate the flowsheet. Feed to the solvent extraction plant was uranyl nitrate solution or U^{233} metal.

Equipment modifications to the plant were completed, final flowsheet conditions were selected, and a criticality and hazards review of the system was made. Criticality control was ensured (many individual units used in the solvent extraction system are not geometrically safe) by strict control of mass and concentration of the U^{233}. In certain cases, nuclear poisoning in the form of boron-glass Raschig rings was used as a secondary control in nonsafe geometries.

Low-Activity-Level Tests. — Thorium and gross gamma decontamination factors of 1100 to 25,000 and 100 to 500, respectively (Table 6.5), were obtained in four trace-level and two intermediate-level (uranium concentration about one-tenth that of full flowsheet concentration) tests under flowsheet conditions (Fig. 6.3). Uranium loss to the extraction-column waste was less than 0.07%. The results confirmed development work and indicated that satisfactory decontamination factors, uranium recovery, and product quality could be obtained in full-level runs.

Metal Dissolution. — Dissolution of U^{233} metal was demonstrated by using 4 *M* HNO_3 under dissolution flowsheet conditions (Fig. 6.4). Criticality safety was maintained by concentration (U^{233} less than 10 g/liter) and soluble-poison control (U^{233}/Th ratio less than 0.025). Complete dissolution of the metal (a 4-kg section of the Jezebel assembly) was achieved under reflux conditions (about 108°C) in 40 hr. The uranium material balance was 100 ± 1%.

Product Quality. — Satisfactory sol-gel product depends on strict control of the concentration of the nitrate ion in the sol. This establishes an upper limit on the nitrate-to-uranium ratio (NO_3^-/U) in the solvent extraction product (in the Kilorod process this ratio is 2.5).

Table 6.5. Summary of Kilorod Solvent Extraction Tests

Run No.[a]	Overall Decontamination Factors		Distribution of Uranium Losses[b] (%)		
	Gross γ	Thorium	AW	CUW	CW
CT-2	100	1100			
CT-3[c]	130	2.5×10^4			
CT-4	100	3400			
HR-1	500	1700	0.07	0.4[d]	<0.005
HR-2		1900	0.05	0.3[d]	<0.005

[a]Run CT-2 and CT-3: column pulse amplitude, 0.8 in.; pulse frequency, 50 cpm.
Run CT-4: pulse amplitude, 1.0 in.; pulse frequency, 50 cpm.
Run HR-1 and HR-2: pulse amplitude, 1.0 in.; pulse frequency, 58 cpm for extraction, 50 cpm for stripping.

[b]Uranium losses during CT runs were not significant.

[c]Three-column operation (separate extraction, scrub, and strip column).

[d]High losses attributed to entrainment in evaporator. CUW losses were <0.01% in second half of run HR-2 when water reflux was added to evaporator top plate.

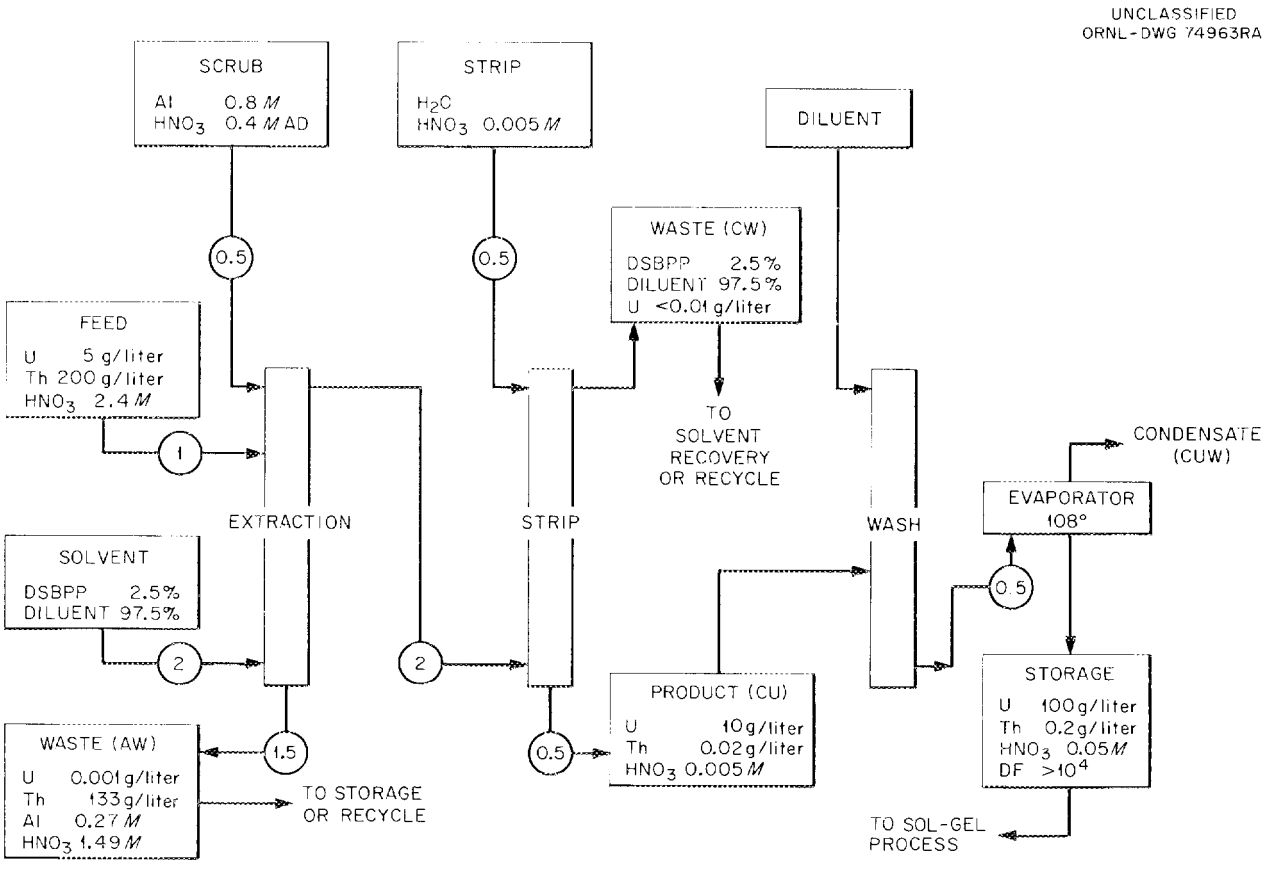

Fig. 6.3. Uranium-233 Purification Flowsheet for the Kilorod Program.

Product from the solvent extraction system normally contains a constant concentration of excess nitrate ion (nitrate from sources other than uranyl nitrate). As a result the nitrate-to-uranium ratio is high at the beginning and at the end of a solvent extraction run, since the uranium concentration is low at these times. Consequently, an off-specification product is obtained for a period at the beginning and one at the end of each run.

During operations a "product cut" is collected (Fig. 6.5) as feed to the product evaporator. The nitrate-to-uranium ratio in the composite product is controlled by diversion of the product between the product tank and the recycle tank.

In case 1 (product collected in R-3 beginning 4 hr after hot feed on), the product must be diverted to R-2 (recycle tank) no later than 13 hr after the depletion of hot feed if the NO_3^-/U ratio in the accumulated feed is to be below 2.5. About 97% of the uranium will be collected as product in this case. For case 2, the product should be diverted back to R-2 no later than 11 hr after depletion of hot feed, in which case 98% of the product will be collected. The higher recovery in case 2 results from the fact that less uranium was recycled at the beginning of the run.

Sol-Gel Operations

Equipment Performance. – Construction of the sol-gel facility and preliminary testing of the equipment were completed. Extensive alterations were required on the uranium measuring tank to avoid thermal-stress breakage, and on the tray evaporator to meet minimum capacity requirements. The minimum operating-cycle time for the batch calciner was 26 hr rather than the 18-hr cycle originally specified. The 26-hr cycle time was contingent on removing the product from the furnace at 300°C and placing it in an argon atmosphere. Thus, the calciner continues to be the production-limiting piece of equipment in the production cycle (10 kg per day, five days a week). The calciner must be operated seven days a week to meet the desired weekly capacity of 50 kg for plant.

Experience with the calciner prototype indicated a furnace-element life equivalent to 200 kg of oxide production. Preliminary Kilorod experience indicated only 50 kg per furnace element. The furnace was modified to improve element performance.

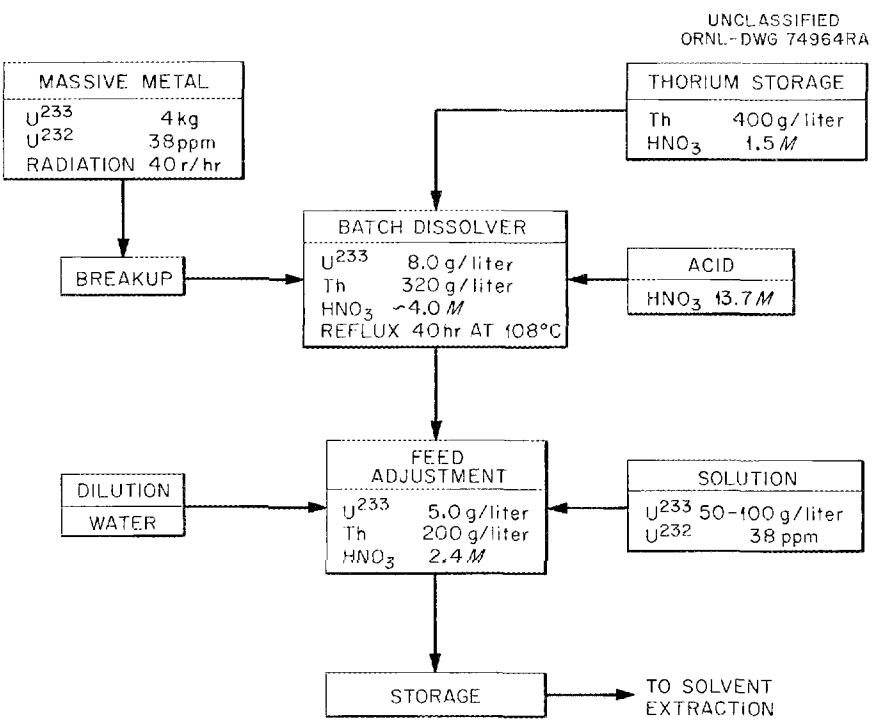

Fig. 6.4. Flowsheet for the Dissolution of U^{233} Metal in the Kilorod Program.

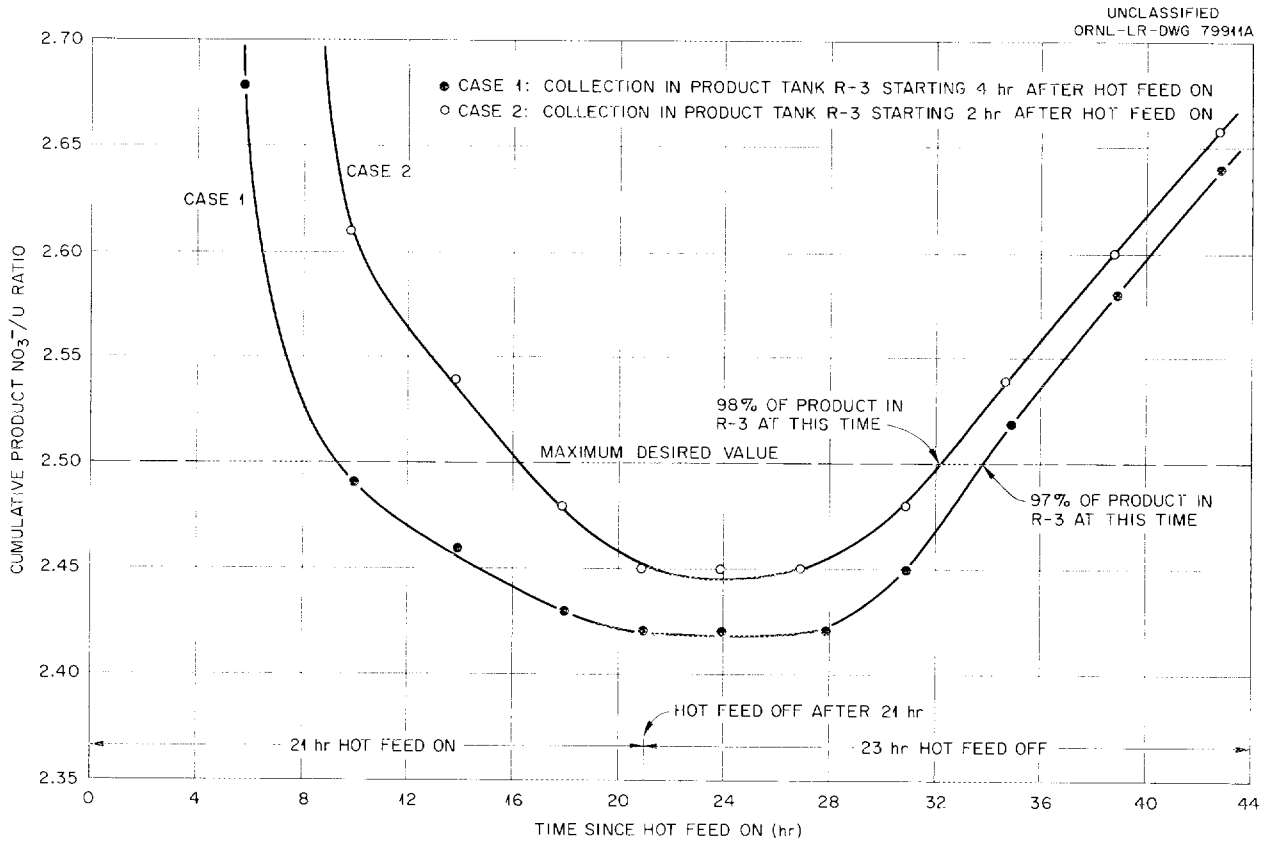

Fig. 6.5. Effect on Product Nitrate-to-Uranium Ratio of Diversion of Solvent Extraction Product Between Collection and Recycle.

Cold Preparation of Oxide. – Six cold runs were made in the sol-gel facility with thoria powder (prepared by the hydrothermal denitration of thorium nitrate) and depleted uranium as feed. The 65 kg of product prepared met specifications and was transferred to the Metals and Ceramics Division for the fabrication of fuel rods.

Denitration Operations. – A total of 450 kg of specification-grade ThO_2 powder was prepared for feed to the sol-gel process. This is equivalent to 30% of the total ThO_2 requirements for the Kilorod program.

6.4 APPLICATION OF SOL-GEL PROCESS TO PREPARATION OF ThC_2 AND ThC_2-UC_2

Rounded particles of ThC_2 and ThC_2-UC_2 were prepared by a modified sol-gel process. Spherical dicarbide particles, when coated with pyrolytic carbon or graphite and dispersed in a graphite matrix, are preferred as fertile and fuel materials for advanced, high-temperature, gas-cooled nuclear reactors.

Description of Process

Carbon, having a mean particle size of 90 A and a specific surface area of 670 m^2/g, was dispersed in an aqueous sol of thoria of similar particle size and having a specific surface area of about 80 m^2/g. The carbon-to-metal mole ratio was varied from 4.3 to 6.8 (the stoichiometric ratio for complete conversion to dicarbide being 4.0). The resultant thoria-carbon sol was dried to a gel that was fired to obtain conversion to ThC_2. Typical firing conditions for 98% conversion of ThO_2 to ThC_2 were $2\frac{1}{2}$ hr at 1650 or $1\frac{1}{4}$ hr at 1750°C in vacuum. Complete conversion was obtained in $2\frac{1}{2}$ hr at 1775°C in vacuum. The particles of

reactant ThO_2-C gel shrank in volume by approximately 30% as carburization proceeded, producing carbide particles having essentially the shapes of the reactant particles. The free-carbon content of the product ThC_2 varied from 1 to 17%, depending on the initial carbon-to-metal ratio. Uranium-thorium dicarbide with a uranium content of 3 to 10 mole % was prepared by the same procedure as that used to prepare thorium dicarbide.

Reaction Rate Studies

A study of the kinetics of the carburization of thoria and also uranium-thorium oxide was undertaken to determine the effects on reaction rates of the carbon-to-metal ratio, uranium-to-thorium ratio, size of reactant particles, and degree of dispersion of the reactants in the sol state. Information on reaction rates was obtained by measuring the volume of the evolved carbon monoxide with a positive-displacement gas meter. This information was used to obtain the apparent reaction rate, order, rate constants, and activation energy. Figure 6.6 is a plot of the volume of carbon monoxide evolved in a typical run vs time and a plot of the negative natural logarithm of the fraction of unreacted ThO_2 vs time. The linearity of this plot indicated a first-order or a pseudo-first-order reaction, having the equation

$$\frac{-d(ThO_2)}{dt} = k[ThO_2] = kC_0[1 - x] , \qquad (1)$$

where x is fraction of ThO_2 reacted, C_0 is initial concentration of ThO_2, and k is rate constant. The value for the apparent rate constant k may be obtained from the slope of the plot of $-\ln(1 - x)$ vs time. An Arrhenius plot of $\ln k'$ vs the reciprocal of the temperature is presented in Fig. 6.7. Table 6.6 is a summary of the data on reaction rates for series G12, in which ThO_2-C gels with a C/Th mole ratio of 4.3 were carburized at various temperatures. On the basis of these data and

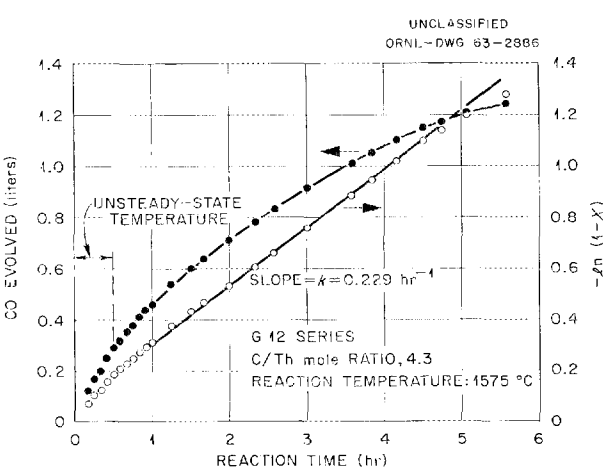

Fig. 6.6. Rate of Carburization of Thoria in Gels.

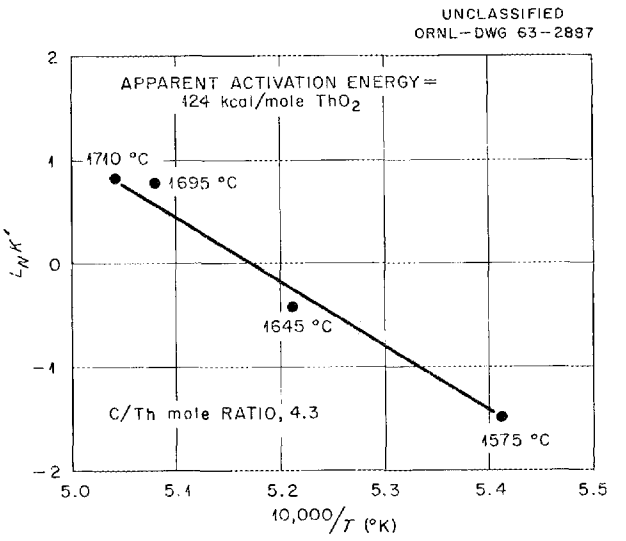

Fig. 6.7. Arrhenius Plot for Carburization Rate Study in Vacuum, G12 Series.

Table 6.6. Summary of ThO_2 Carburization Rate Data for Series G12

C/Th mole ratio = 4.3, 0% U[a]

Nominal Reaction Temperature (°C)	Apparent Rate Constant $k(hr^{-1})$	Estimated Time for 98% Conversion (hr)
1575	0.229	7
1645	0.66	4
1695	2.21	3
1710	2.27	2

[a]All firings made in vacuum.

similar data for other gels, the reaction appears to be first order with respect to thorium oxide. The apparent activation energy (for both ThC_2 and ThC_2-UC_2) ranges from 110 to 170 kcal per mole of ThO_2. These results pertain to the reaction as it is carried out in vacuum in the particular experimental apparatus used.

Preparation of Rounded Thorium Dicarbide and Uranium-Thorium Dicarbide Microspheres

Imperfectly rounded particles of thoria-carbon gels were prepared from the sol by crushing the gel, screening to obtain particles approximately 250 μ in diameter, and then tumbling to round them. The method had limited success in that it produced rounded particles; but the yield was low (15 to 20%), and the amount to be recycled was large.

An alternative method is being developed on a laboratory scale. In this method, small spheres of sol are formed by dispersing the sol in carbon tetrachloride. A paddle agitator is used to prepare the dispersion. The resultant spherical droplets are then set to gels (Fig. 6.8) by extraction of water from them by isopropyl alcohol added to the carbon tetrachloride after dispersion of the sol. As soon as the gel spheres are firm enough to support their own weight, they are separated from the CCl_4–isopropyl alcohol and further dried in air. These spheres may then be fired to produce the dicarbide (Fig. 6.9).

In six experiments with two sols, one a thoria-carbon and the other a urania-thoria-carbon sol, in which the metal concentrations were 2 M and the nominal carbon-to-metal mole ratios were 5.0, the diameters of spheres were found to be exponential functions of the rate of travel of the tip of the stirrer blade in the CCl_4 (Fig. 6.10). Modified Reynolds numbers, D^2N/γ, where D is diameter of circle described by tips of agitator blade (cm), N is agitator speed (rps), and γ is kinematic viscosity of dispersing medium (Stokes), were used to describe the flow conditions at the tips of the stirrer blade. As modified Reynolds numbers were varied from 2.2×10^4 down to 1.48×10^4, the geometric mean gel particle sizes varied from 100 to 250 μ, with geometric standard deviations of 1.45 to 3.29.

Shinnar[15] found droplet size to vary inversely with rotational speed raised to powers up to $^6/_5$ for liquid-liquid dispersions. The considerably higher dependence found here suggests that the non-Newtonian properties of the sol are important in determining the dependence of droplet size on rotational speed. These flow properties are difficult to reproduce from sol to sol. Increasing the uranium content in thoria-carbon sols increases viscosity to an abnormal degree, inducing thixotropy. As the concentration of solids and uranium increases, thixotropy also increases. Thixotropic sols do not follow the described relation in an orderly manner (note scatter of points for the sol containing uranium).

The commercial high-surface-area carbons contained about 6% volatile matter at 100 to 200°C. These volatile materials were acidic and strongly increased the stability and viscosity of the sols. From conductometric titrations with sodium hydroxide, the carbon was estimated to have on its surface (about 700 m^2/g) about 10 meq of acid per mole of carbon. However, the volatile-matter content was not uniform from batch to batch of carbon in either quantity per mole or composition, and because of this the behavior of urania-thoria-carbon is not reproducible. Apparently, the volatile components reside on the surface of the carbon and affect the flow conditions and stability of the sols by a mechanism not clearly understood at present. Studies are being made to determine optimum methods for controlling these properties.

---

[15] Reuel Shinnar, *J. Fluid Mech.* **10**, 259 (1961).

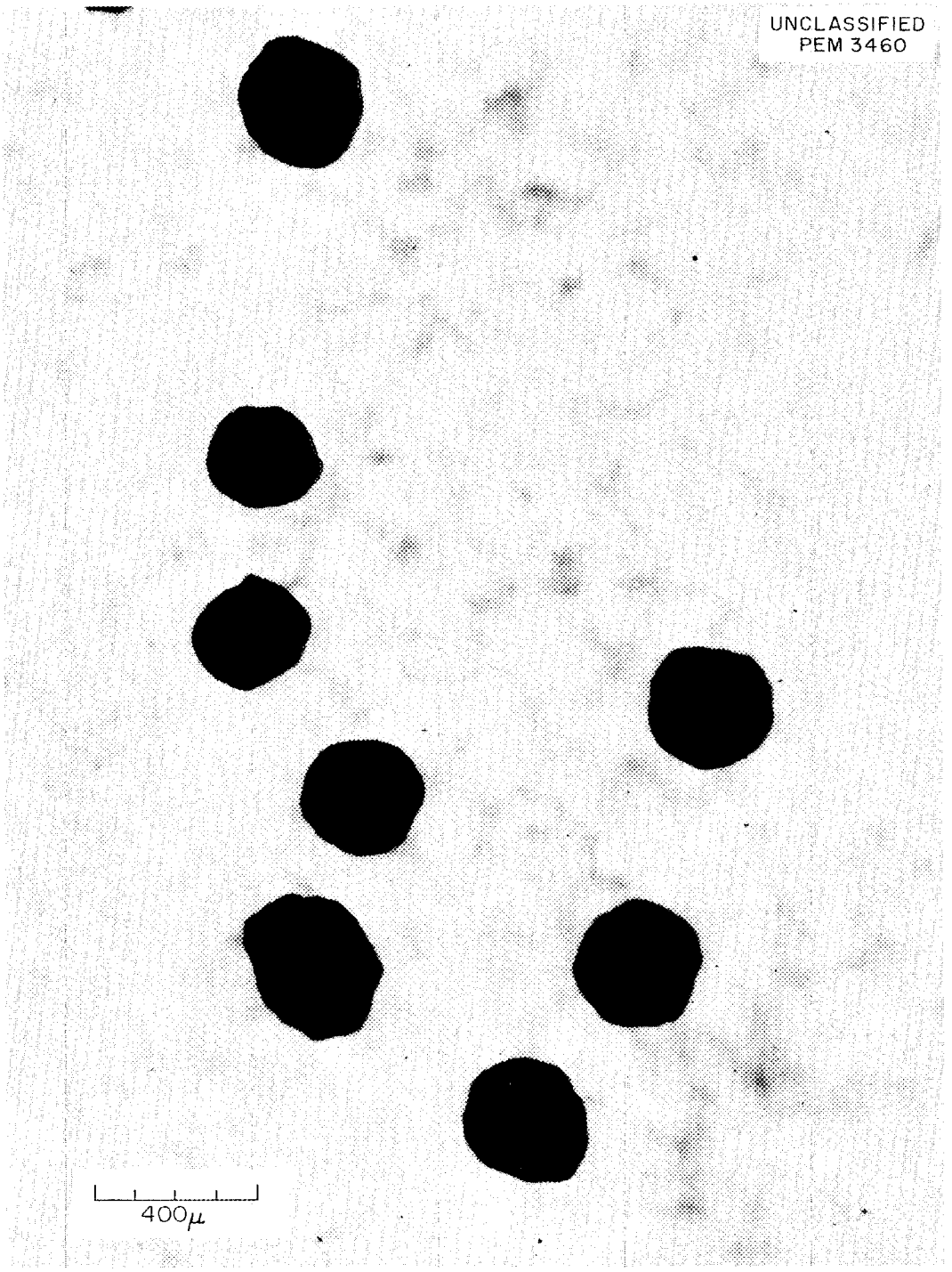

Fig. 6.8. Spheres of Thorium Oxide–Carbon Gel. Carbon/thorium mole ratio = 5; prepared from ThO_2-carbon sol; formed in CCl_4–isopropyl alcohol.

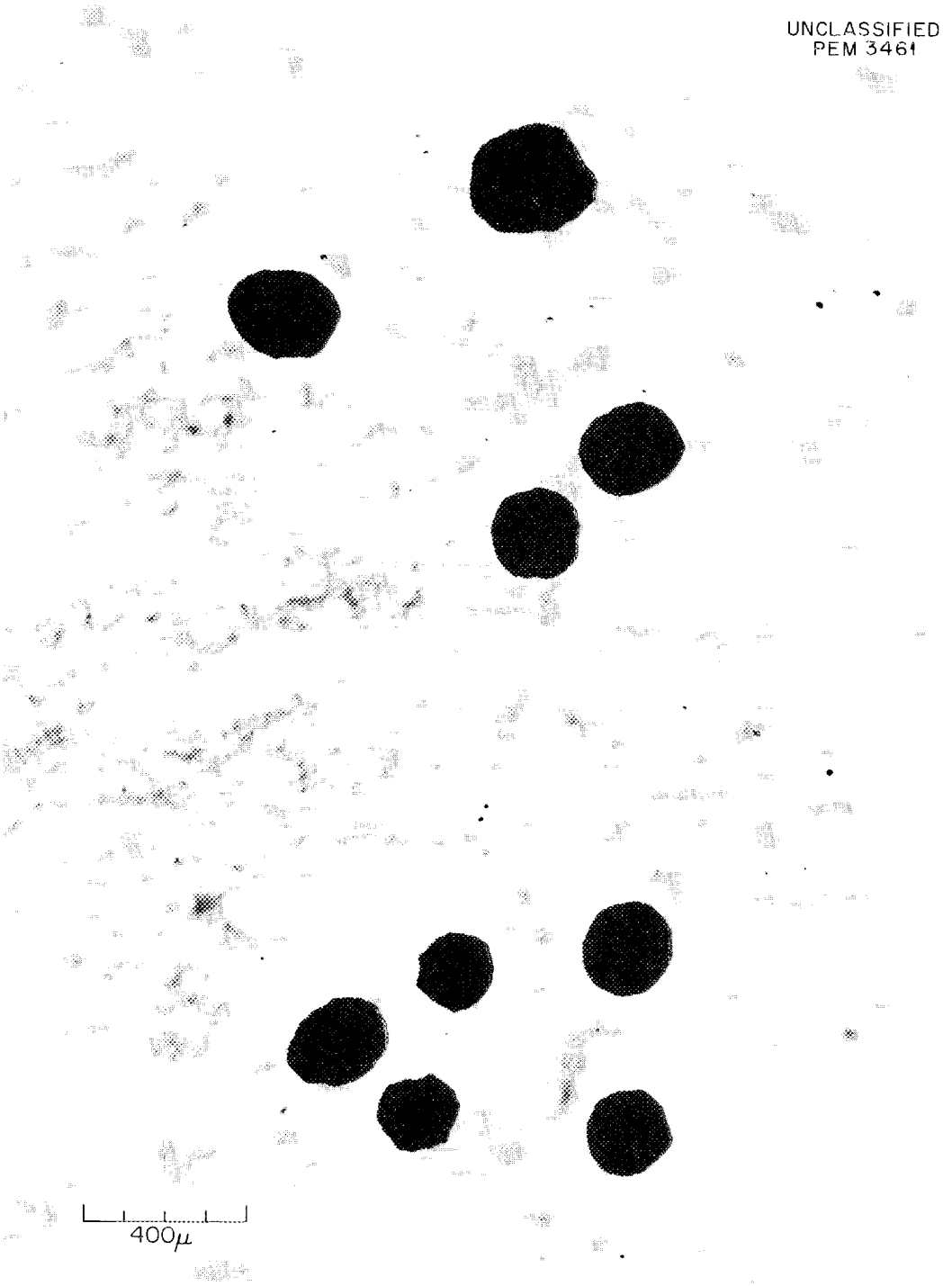

Fig. 6.9. Spheres of Thorium Carbide. Excess carbon = 7%; prepared from ThO_2-C sols; formed in CCl_4 and isopropyl alcohol; fired 2 hr at 1800°C in vacuum.

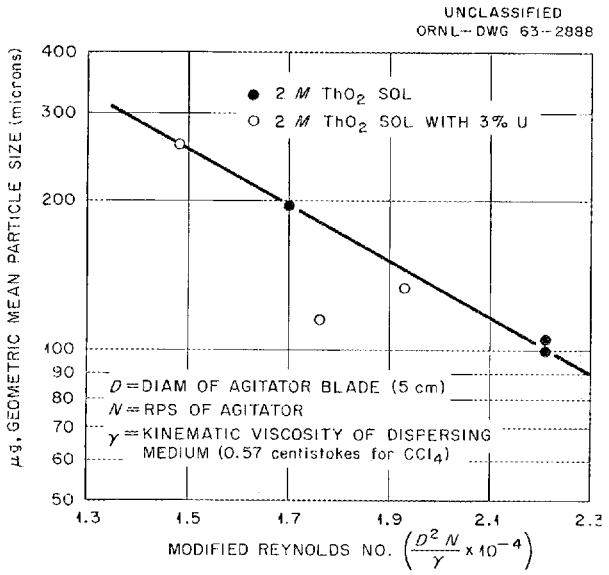

Fig. 6.10. Size of Dispersed ThO_2-Carbon Spheres in CCl_4; C/Th = 5/1.

6.5 DESIGN OF THORIUM-URANIUM FUEL-CYCLE DEVELOPMENT FACILITY

The Title I design was completed for the Thorium-Uranium Fuel-Cycle Development Facility (TUFCDF) to be built in Melton Valley for demonstration and evaluation (on an engineering scale) of the entire thorium fuel cycle. This facility is designed to house equipment for processing of fully irradiated reactor fuel assemblies, and for the reconstitution of fuels and fabrication of new fuel elements. Shielding of the cells (generally normal concrete 5½ ft thick) is sufficient to permit the processing and fabrication of highly irradiated fuels by processes achieving only minimal decontamination from fission products. Design of this facility is a joint program with the Metals and Ceramics Division.

The TUFCDF consists of four operating cells and two service cells, an unshielded but sealed glove maintenance room, plus supporting areas for equipment and workers. A plan of the first-floor area (see Fig. 6.11) shows the layout of the cells

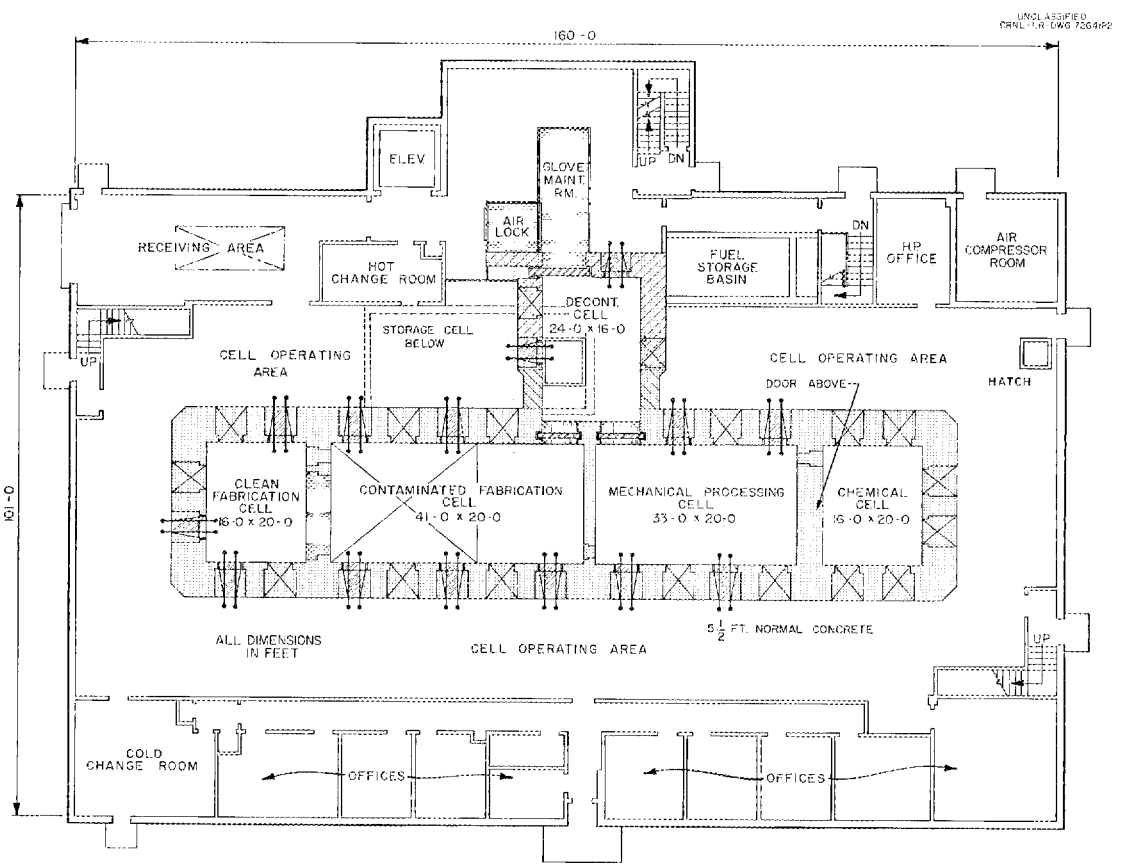

Fig. 6.11. First-Floor Plan of Thorium-Uranium Fuel-Cycle Development Facility.

UNCLASSIFIED
ORNL-LR-DWG 75591R

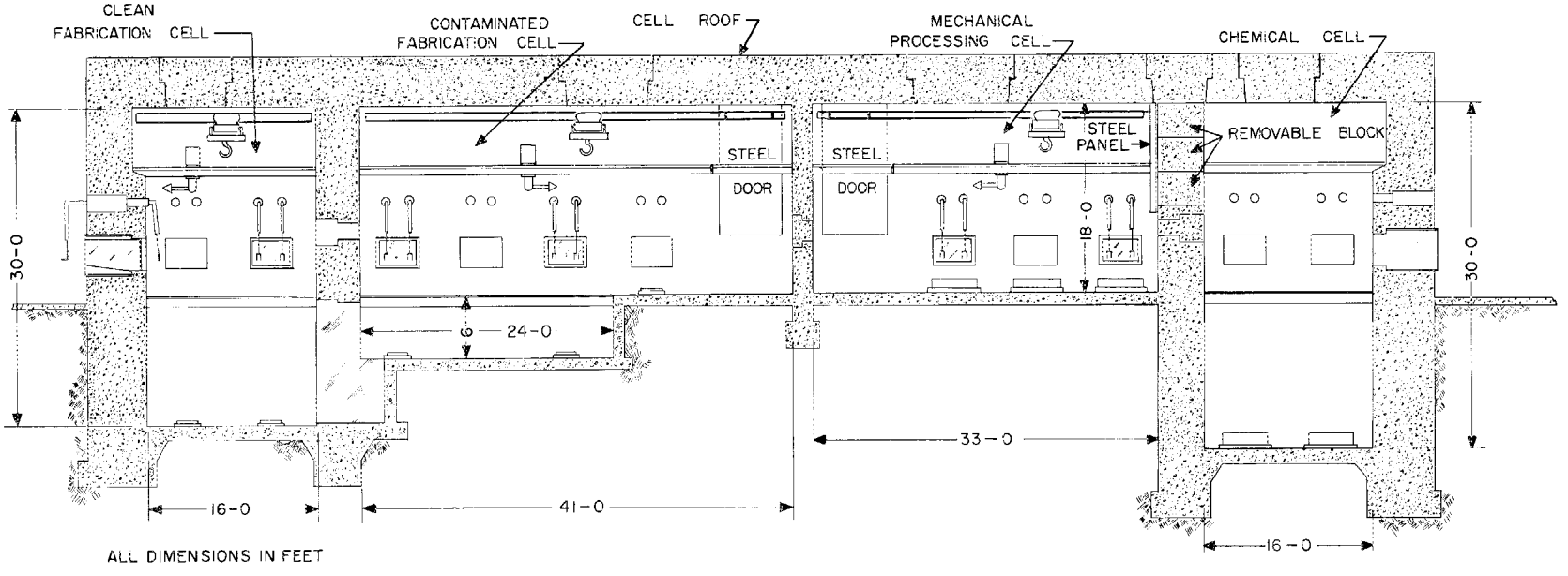

Fig. 6.12. Sectional Elevation of Operating Cells.

and service areas at this level. Figure 6.12 is a sectional elevation of the four operating cells, showing the spaces and some of the manipulative equipment. The second- and third-floor plans are shown in Figs. 6.13 and 6.14.

Five of the six cells either are or can be maintained entirely by remote devices (Fig. 6.13). The clean-fabrication cell is the exception because it is to receive fuels only after they are encapsulated in tubes or other containers. In this cell the installation and repair of equipment will be accomplished by contact methods. Either remote or contact maintenance may be used in the chemical cell. A removable wall section is to be provided so that the chemical cell can be either isolated from or joined with the mechanical processing cell. If the wall section is removed, the overhead crane and mechanical arm bridges can enter the chemical cell, and large objects can be transferred in and out.

The in-cell transportation system consists of a pair of overhead bridge cranes that can travel over essentially all the area in the glove maintenance room and the decontamination, contaminated-fabrication, mechanical processing, and chemical cells (Fig. 6.14). A special transfer bridge system is to be provided in the decontamination cell; the bridge can move in three planes and will provide for easy movement of a hoist from one area to another and will also allow removal of the operating-cell bridges to the glove maintenance room for repair. All moving parts of the crane system located in the operating cells can be remotely removed for maintenance. Cranes are also provided for the clean-fabrication cell and the storage cell. The clean-fabrication cell bridge and hoist can be lifted from the cell into the cell roof area for maintenance. The storage-cell hoist can be removed into the decontamination cell and glove maintenance room for repair.

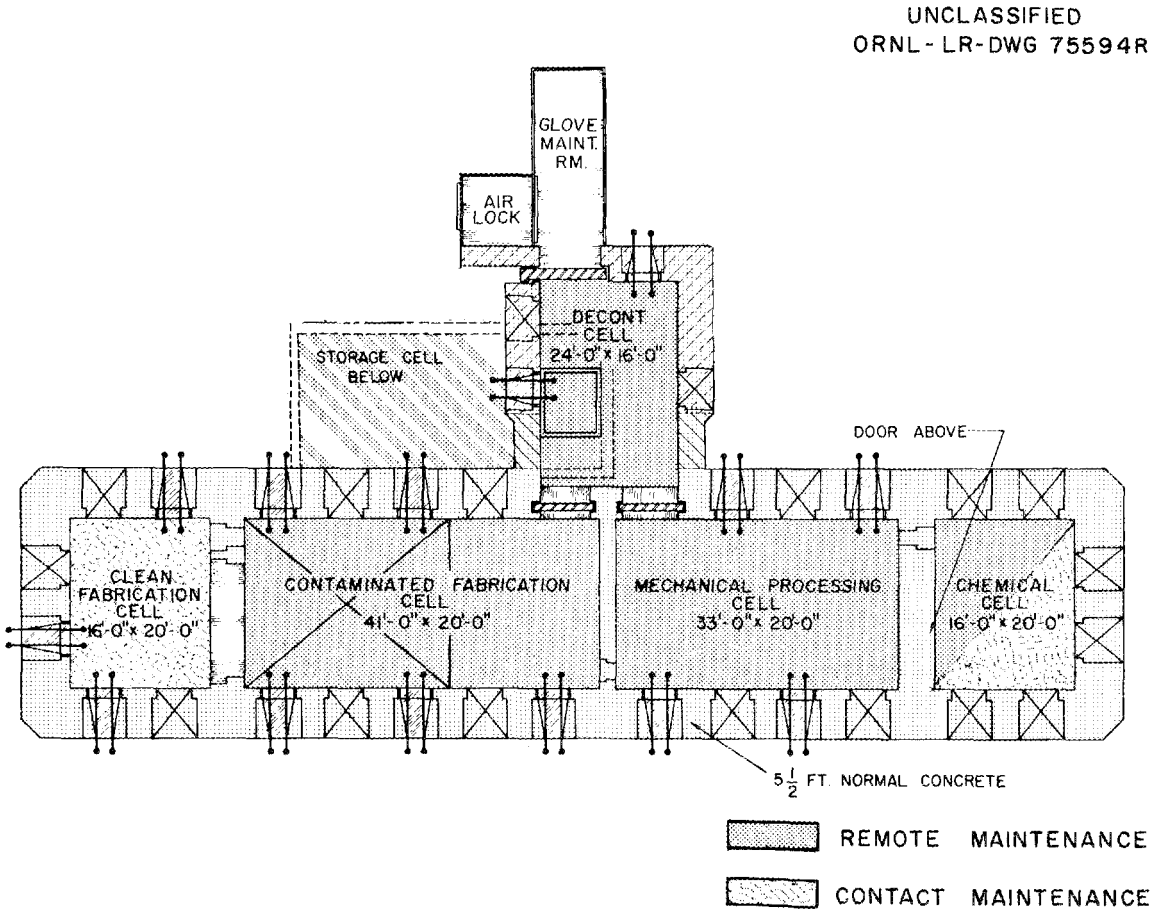

Fig. 6.13. Methods of Cell Maintenance.

Three bridge-mounted mechanical arms will be provided for the cell complex. Two of these will operate in the cells for contaminated fabrication, mechanical processing, chemical operations, and decontamination. The third unit will operate in the clean-fabrication cell. All units will be mounted for ready removal to a maintenance area.

The operating cells and the decontamination cell are laid out on a modular pattern – about 8 × 10 ft. Figure 6.15 is a view of a typical space within the shielded area. With some exceptions, each module is provided with a window liner, holes for master-slave manipulators, five 1-in. stainless steel pipes leading to the service area,

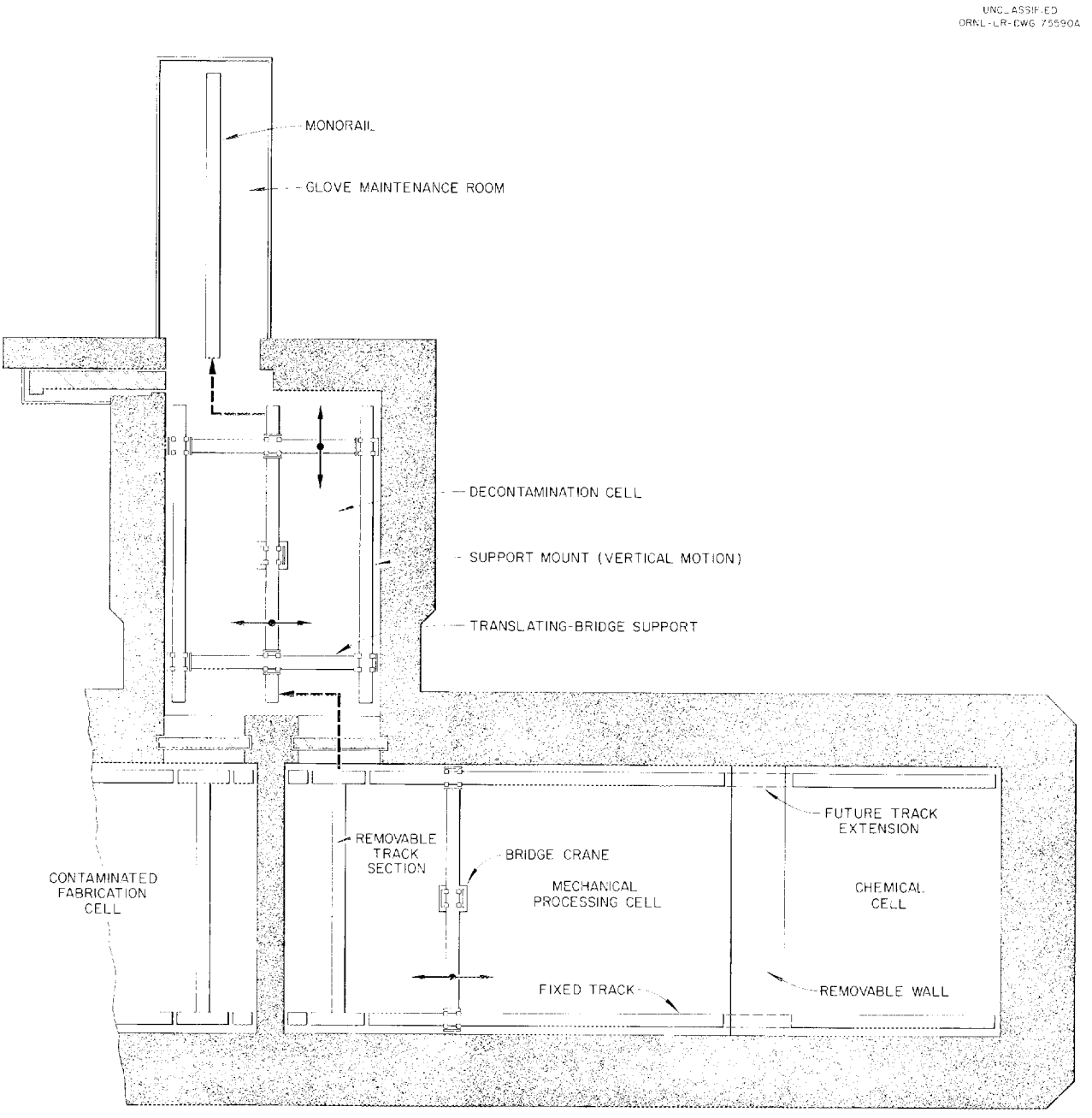

Fig. 6.14. Cell Bridge-Crane System.

UNCLASSIFIED
ORNL-LR No. 75593R

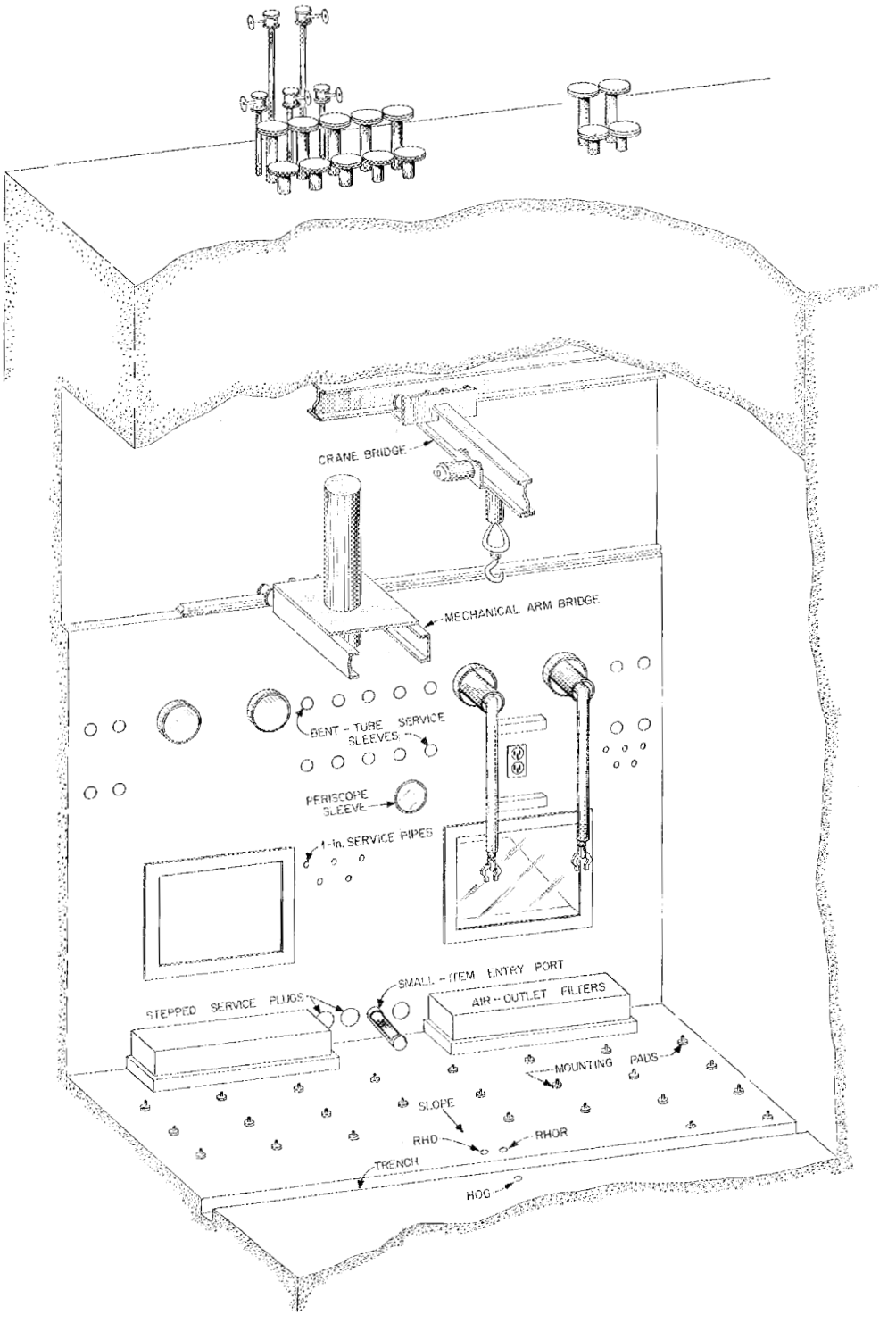

Fig. 6.15. Typical Cell Module.

ten bent-tube service access sleeves, three stepped plugs for the passage of replaceable service lines, two 1500-w iodine-quartz lamps, plus a number of precisely located foundation pads in the floor for mounting the equipment. At alternate modules, stations are provided for waste collection, hot off-gases, and future periscope installation. Windows and manipulators will be provided for about half the window liners and manipulator holes, and the remaining ones will be plugged because it appears that there will be no no need for this number of windows and manipulators in the initial phases of operation. The floors, walls, and ceilings of the chemical, mechanical processing, and contaminated-fabrication cells are to be lined with stainless steel.

The remotely maintained portion of the cell complex is to be exceptionally well sealed in order to confine radioactive materials and to allow for future use of an inert atmosphere. All openings, whether they are for viewing windows, doors, or service access, will be tightly sealed. In order to maintain a constant seal, somewhat special designs are being used for windows, service-access sleeves, manipulators, and other devices.

Title I design was initiated in January 1963 by ORNL and by Giffels and Rosetti of Detroit. The Title I design work was concentrated on the less-conventional items in the facility, such as the cranes and electromechanical manipulators, shielding doors, viewing windows, ventilation system, and service-access devices. Minimal effort was expended on conventional problems such as architecture and structure. Experience has indicated that costs for the less-conventional components in a facility frequently cause expenditure overruns because of insufficient definition early in the project. Preliminary design of equipment for the sol-gel vibratory-compaction processes was accomplished, establishing the number and functions of the various equipment pieces, their space and service requirements, and the approximate cost. The criteria used in the determination of the design and choice of equipment or process items were that the item must be of a type suitable for a large-scale production plant and that its operation be essential to a meaningful demonstration of the feasibility of the remote fabrication of fuel assemblies by the sol-gel vibratory-compaction process.

7. Chemistry of Lanthanides and Transplutonium Elements

Although extraction by tertiary amine chlorides from concentrated lithium chloride solutions (Tramex process) gives better separation between the transplutonium and lanthanide groups than any other known method, the possibilities of finding better methods from the standpoint of operation and equipment design cannot be ignored. Also, the Tramex process is not useful for separations within the transplutonium group, except for separating americium and curium from the heavier elements. Consequently, studies of the chemistry of lanthanides and transplutonium elements are being continued in search of differences that might be used in new methods for making group and intragroup separations.

7.1 EXTRACTION OF TRIVALENT LANTHANIDES AND ACTINIDES

Comparisons of the extractabilities of americium (and curium) with those of the lanthanides showed some systems in which these transplutonium elements were similar to the lightest lanthanides and other systems in which they were like the heaviest fission product rare earths, which are in the middle of the lanthanide series. These results suggest that a two-cycle process, utilizing two systems with sufficiently different separation properties, might be applicable to group separations. Part of Sec 7.1, containing additional

information on this subject, is reported in ORNL-3452, suppl 1.

With a quaternary ammonium nitrate (Aliquat 336 nitrate) the extraction coefficients for cerium and americium from 6 *N* $Al(NO_3)_3$ were greater than that for europium by factors of ~20 and ~2 respectively. It is remarkable that in previous tests with a similar compound, tetraheptyl ammonium nitrate (THAN), the separation factors (somewhat smaller) were in the opposite direction.

Extraction by Aliquat 336 carbonate from very dilute potassium bicarbonate gave high extraction of all actinides and lanthanides tested, and no useful separations were obtained. A tertiary amine, in the carbonate form, gave insignificant extractions.

A few of the many phosphonates and amides tested gave preliminary indications of unusual differences between americium and the lanthanides in extractions from 6 *N* $LiNO_3$.

7.2 EXTRACTION OF HEXAVALENT AMERICIUM

The chemistry of hexavalent americium is being studied in a search for new methods of separating americium from curium. As part of these studies, a comparison was made of the extraction of Am(III) and Am(VI) by various organophosphorus and organonitrogen reagents. In nearly all cases Am(VI) was considerably less extractable than Am(III), the reverse of the usual behavior of the actinides that can have these valences. Differences in extraction coefficients exceeded a factor of 10^4 when extracting with D2EHPA from dilute HNO_3. Differences up to a factor of 100 were obtained in extraction by tri-*n*-octylphosphine oxide (TOPO) from lithium nitrate and up to 30 with TBP from sodium nitrate solutions (Fig. 7.1). In extractions by a tertiary amine, Am(VI) was more extractable than Am(III) from lithium nitrate below 4 *N* and less extractable at higher concentrations. Extraction by a dialkylphosphoric acid appears especially promising for the separation of curium from americium as Am(VI). The separation attainable will probably be controlled by the amount of Am(VI) that is reduced with hydrogen peroxide produced from the alpha-radiation-induced radiolysis of water.

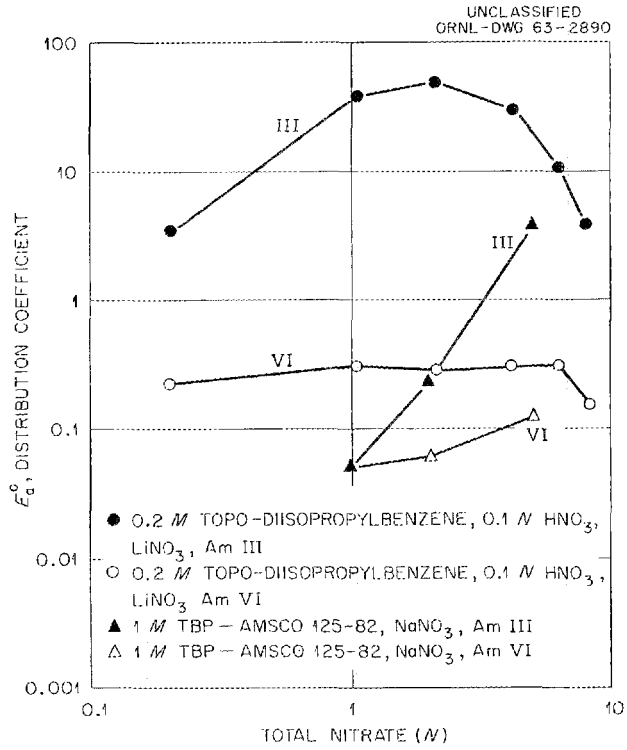

Fig. 7.1. Extraction of Am(III) and Am(VI) by TOPO and TBP from Nitrate Solutions.

8. Solvent Extraction Technology

New solvent extraction agents are being developed for wider application of solvent extraction technology, particularly in radiochemical processing. The initial intent of these studies was to extend the application of those solvents which were developed in the former ORNL raw materials program and which are used commercially in many ore processing plants. These include cation and anion exchange extractants, utilizing the principles of ion exchange technology on a liquid-liquid basis, as well as solvents extracting by various other mechanisms. More recently, additional useful extractants have been discovered as a result of continuing evaluations of new reagents. In general, it is apparent that the extraction of a large number of metals from a wide variety of aqueous solutions is possible when extraction properties are controlled by the appropriate choice of reagent structure. The present program includes a systematic experimental survey of the potential utility of these reagents in fuel processing, waste treatment, fission product recovery, transuranium recoveries, and other heavy-metal separations. Several practicable processes have already been developed as an outgrowth of this work.

Fundamental investigations, aimed at understanding the mechanisms of metal extraction by the various reagents, are also in progress, and reagents intended for use with highly radioactive solutions are being examined for radiation stability and methods of removing deleterious degradation products.

Information already obtained about extractants containing different functional groups also suggests utility outside the field of liquid-liquid extraction, as in ion exchange resins or "liquid-gel" sorbents.

8.1 FINAL-CYCLE PLUTONIUM RECOVERY BY AMINE EXTRACTION

As previously reported,[1] continuous countercurrent testing of the proposed flowsheet for final-cycle plutonium concentration and purification by tertiary amine extraction showed unsatisfactorily low gamma-decontamination factors from actual but aged Purex plant solutions, although plutonium recovery and physical operations were excellent. Subsequent batch extraction tests showed that the aged but not the fresh Purex plant solutions contain zirconium-niobium species highly extractable by the hydrocarbon diluents used with amines and other extractants, sufficient to account for the observed low decontamination factors. Batch tests with fresh process solution showed separation and decontamination factors high enough for use in the projected purification process.

The zirconium-niobium extraction from aged solution (Purex 1BP solution at ~2 *M* HNO_3, stored in stainless steel at ambient temperature for several weeks) is attributed to the slow formation of effective extractants by degradation of tributyl phosphate (TBP) and hydrocarbon diluent dissolved or entrained in the solution. Up to 15% of the gross gamma activity was extracted from the aged solution in single equal-volume contacts with the hydrocarbons diethylbenzene (DEB), Amsco 125-82, and *n*-dodecane. The extraction of gamma activity was decreased tenfold when tridecanol and tridecanol plus trilaurylamine, in concentrations typical for process use, were added to the hydrocarbon. However, the extraction of gamma activity was still higher than tolerable and high enough to account for the poor decontamination in the continuous countercurrent tests with aged solutions, as noted above.

Individual batch extraction tests with fresh Purex plant 1BP solution, completed within 70 hr after it was withdrawn from the plant process stream, showed extraction coefficients for gamma activity less than 0.01 with DEB alone and less than 0.005 with 0.05–0.15 *M* trilaurylamine in DEB. Separation factors for plutonium from gamma activity were greater than 10^4 in the individual tests, and the decontamination factor for plutonium from zirconium-niobium was 2×10^4 in a batch cascade extraction-scrub-strip test.

[1] *Chem. Technol. Div. Ann. Progr. Rept. June 30, 1962*, ORNL-3314, p 96.

8.2 METAL NITRATE EXTRACTION BY AMINES[2]

In the study of the extraction of nitrosylruthenium complexes, one of the fission product metals important in nitrate solutions, extractions by a quaternary amine and a primary amine were compared with the tertiary amine extractions previously reported,[3] and the extractions were used to provide further information about the nitrato nitrosylruthenium complexes in aqueous nitric acid solutions.[4] Extraction by Aliquat 336 (tri[octyl, decyl]methylammonium) was qualitatively similar to extraction with trilaurylamine (Fig. 8.1), but with coefficients about ten times greater. The extraction coefficient varied with about the 0.5 power of the quaternary amine concentration in contrast to the 1 to 1.5 power of the tertiary amine concentration.

Extraction by the primary amine Primene JMT was considerably different. Extraction was low near 1 *M* HNO_3 and rose instead of falling with increasing nitric acid concentration, until it exceeded extraction by the quaternary at above 8 *M* HNO_3.

In the presence of sodium nitrate used to maintain the total aqueous nitrate concentration at 6 *M*, extractions with both the tertiary and the quaternary amine were similar to those shown in Fig. 8.1 at high acidities but rose with decreasing acidity down to around 0.5 *M* HNO_3, instead of leveling off and dropping at below 2 *M* HNO_3 as when no salt was present. Extraction with the primary amine was also higher with than without salt, but only to an extent that kept it nearly constant as the acidity decreased from 6 to 0.5 *M* HNO_3, with total nitrate constant at 6 *M*.

Extraction with and without nitrate salt showed better correlation with the excess nitric acid found in the organic phase than with the aqueous nitric acid or total aqueous nitrate concentration. This may be explained on the basis that the excess organic nitric acid concentration is itself a direct function of the aqueous nitric acid activity in both acid and acid-salt solutions (Fig. 8.2).

Since equilibration is relatively slow among aqueous nitrato nitrosylruthenium complex species, both the extraction coefficients of individual complex species and their relative concentrations at equilibrium in aqueous solutions can be determined by a technique of rapid dilution and extraction at varying phase ratios. In agreement with other studies of the nitrato nitrosylruthenium system,[5] amine extractions showed that two (unidentified) species are significantly extractable, both increasing in relative concentration and decreasing

[2]Work done by the Department of Nuclear Engineering, Massachusetts Institute of Technology, under subcontract.

[3]*Chem. Technol. Div. Ann. Progr. Rept. June 30, 1962*, ORNL-3314, p 102.

[4]T. H. Timmins and E. A. Mason, *The Effect of Alkyl Amine Type on the Extraction of Nitric Acid and Nitrosylruthenium Nitrato Complexes*, MITNE-30 (Subcontract No. 1327) (Apr. 1, 1963).

[5]J. M. Fletcher *et al.*, *J. Inorg. Nucl. Chem.* 1, 378 (1955).

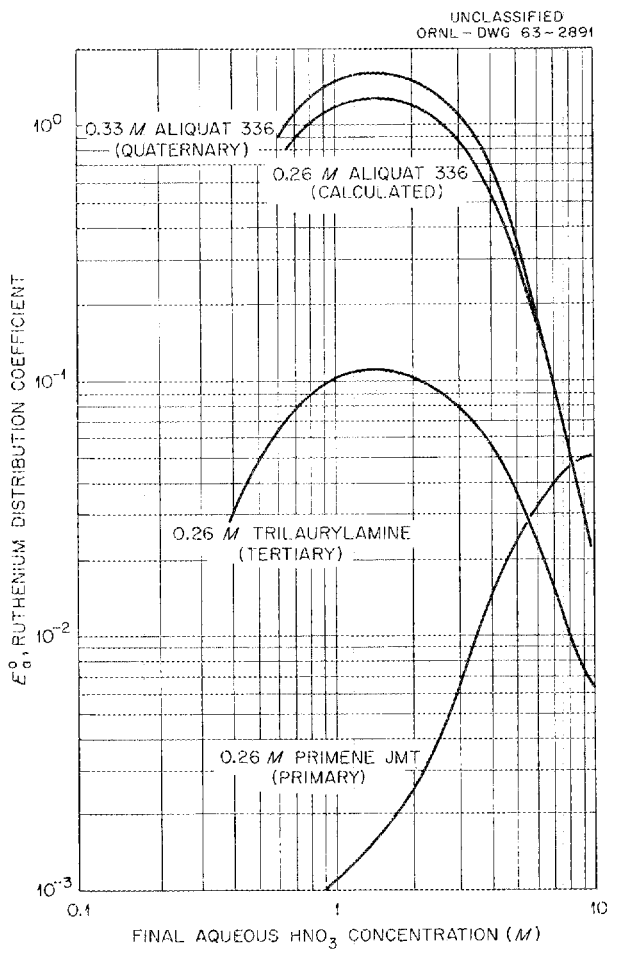

Fig. 8.1. Extraction of Nitrato Nitrosylruthenium by Amines in Toluene. Twenty-four hour extraction from aged aqueous solution.

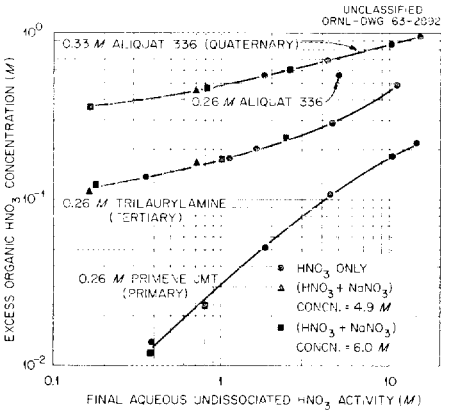

Fig. 8.2. Extraction of Excess Nitric Acid by Amine Nitrates. Acid and salt concentrations shown by circles, triangles, and squares are those in the aqueous phase.

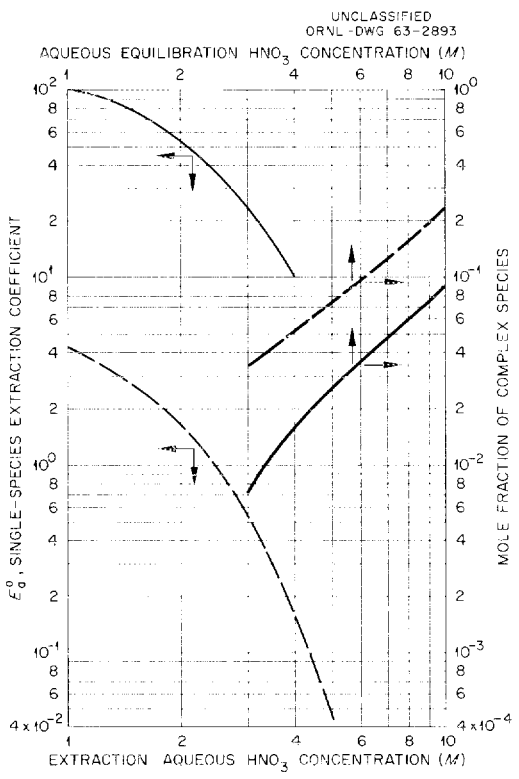

Fig. 8.3. The Two Most Extractable Nitrato Nitrosylruthenium Species. Mole fraction (heavy lines) in aqueous solution vs equilibrium nitric acid concentration, and single-species extraction coefficients (light lines) vs nitric acid concentration as adjusted for rapid extraction with 0.26 *M* trilaurylamine in toluene.

in relative extractability with increasing nitric acid concentration (Fig. 8.3). Mole fractions as determined from quaternary extractions agreed well with those from tertiary extractions.

8.3 METAL CHLORIDE EXTRACTION BY AMINES

In view of the increasing practical utilization of amine extractants, a systematic survey is being made of the extraction behavior of most representative metals from a variety of aqueous systems. This is similar to the studies already reported on anion exchange resins.

Data are shown in Fig. 8.4 for the extraction of twenty different metals from LiCl–0.2 *M* HCl over the range 0.5 to 10 *M* total chloride. Extractions of iron were reported previously.[6] In all cases the solvents were 0.1 *M* solutions of representative primary, secondary, tertiary, and quaternary amines in diethylbenzene. With few exceptions, the extraction power of the amines for the various metals varied in the order Aliquat 336 (quaternary amine) > Alamine 336 (tertiary amine) > Amberlite LA-1 (secondary amine) > Primene JM (primary amine). For most metals the extraction coefficients increased with increase in chloride concentration. Metals that extracted strongly (maximum E_a^o, >10) included V(IV), V(V), Mn(II), Co(II), Cu(II), Zn, Ga, Ge(IV), Mo(VI), Ru(IV), and Se(IV). Extractions of Sc, Ti(III), Ti(IV), As(III), As(V), Zr, Nb, and Ru(III) were moderate (maximum E_a^o, 0.1 to 10), whereas extractions of Cr(III), Ni(II), Rb, Sr, and Y were very weak or negligible (E_a^o, <0.1).

In parallel extractions from unsalted hydrochloric acid (results not reported here), the shapes of the curves were similar, but the extraction coefficients were usually slightly lower than those shown in Fig. 8.4 for the acid lithium chloride system.

[6] *Chem. Technol. Div. Ann. Progr. Rept. June 30, 1962*, ORNL-3314, p 104.

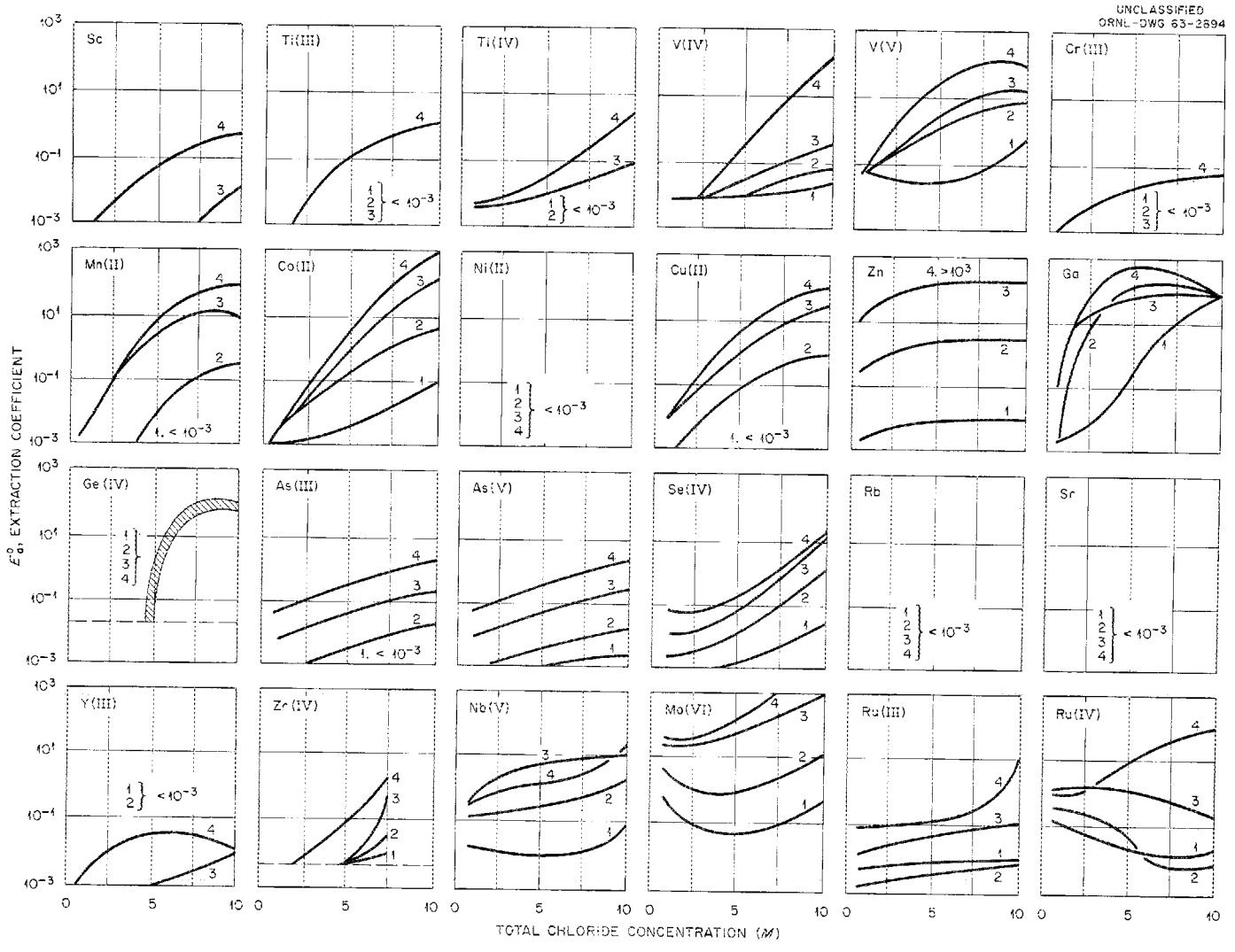

Fig. 8.4. Extraction of Metal Chlorides with Amines. Organic phase: 0.1 *M* solutions of (1) Primene JM [$RR'R''CNH_2$, 18 to 24 carbon atoms], (2) Amberlite LA-1 [$RR'R''CNHC_{12}H_{23}$, 24 to 27 carbon atoms], (3) Alamine 336 [R_3N, R = *n*-octyl–*n*-decyl mixture], and (4) Aliquat 336 [$R_3(CH_3)N^+$, R = *n*-octyl–*n*-decyl mixture] in diethylbenzene (with Aliquat 336, 3 vol % tridecanol was added to the solvent phase to prevent third phase formation); amines were in chloride form. Aqueous phase: 0.01 *M* metal ion in LiCl–0.2 *M* HCl solution (0.5 to 10 *M* Σ Cl); for niobium test, tracer only was used. Contact: 10 min at 1/1 phase ratio.

8.4 METAL FLUORIDE EXTRACTION BY AMINES

Cursory tests were made of the extraction of uranium(VI) and niobium from hydrofluoric acid with representative primary, secondary, and tertiary amines. With all the amines the extractions of both uranium and niobium were effective and decreased with increased hydrofluoric acid concentration in the range 1 to 3 *M* HF (Fig. 8.5). The primary amine extracted uranium best, and the tertiary amine extracted niobium best. Extractions of both metals were poorest with the secondary amine.

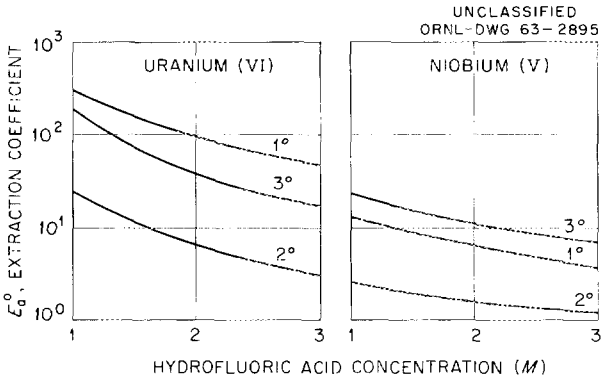

Fig. 8.5. Uranium(VI) and Niobium Extraction from Hydrofluoric Acid Solution with 0.1 *M* Amines. 1° = primary amine [1-nonyldecylamine in Amsco 125-82]; 2° = secondary amine [bis(1-isobutyl-3,5-dimethylhexyl)-amine in Amsco 125-82]; 3° = tertiary amine [trilauryl-amine in Amsco 125-82, 3% tridecyl alcohol]. Aqueous phase: 1 g of U per liter or 5 g of Th per liter initially. Contact: equal phase ratios, 10 min, room temperature.

8.5 EXTRACTION PERFORMANCE OF DEGRADED PROCESS EXTRACTANTS

Improved Amsco 125-82 Stability

Although Amsco 125-82, a specially prepared aviation naphtha, is considered to be one of the most stable of the commercial aliphatic hydrocarbons, it can be degraded severely by heating or irradiating in the presence of nitric acid. This is attributed to the fact that it is composed of 17 or more compounds in the C_{12}–C_{14} range, many of which are highly branched and are reactive toward nitric acid. For improved performance in radiochemical processing the stability of Amsco can be improved by destroying most of the reactive sites. Experimentally this has been done (1) by pretreating with concentrated sulfuric acid, and (2) by preliminary degradation in nitric acid followed by a treatment with sulfuric acid. The sulfuric acid treatment is most effective at increased temperature or when very concentrated acid is obtained by the addition of oleum.

In Fig. 8.6 results are shown for tests in which untreated Amsco and Amsco treated with sulfuric acid were made 1 *M* in fresh TBP and then degraded by boiling with 2 *M* HNO_3 for periods up to 24 hr. The extent of degradation was monitored by the usual tests,[7] which involved measurements of

[7] *Chem. Technol. Div. Ann. Progr. Rept. May 31, 1961*, ORNL-3153, p 109.

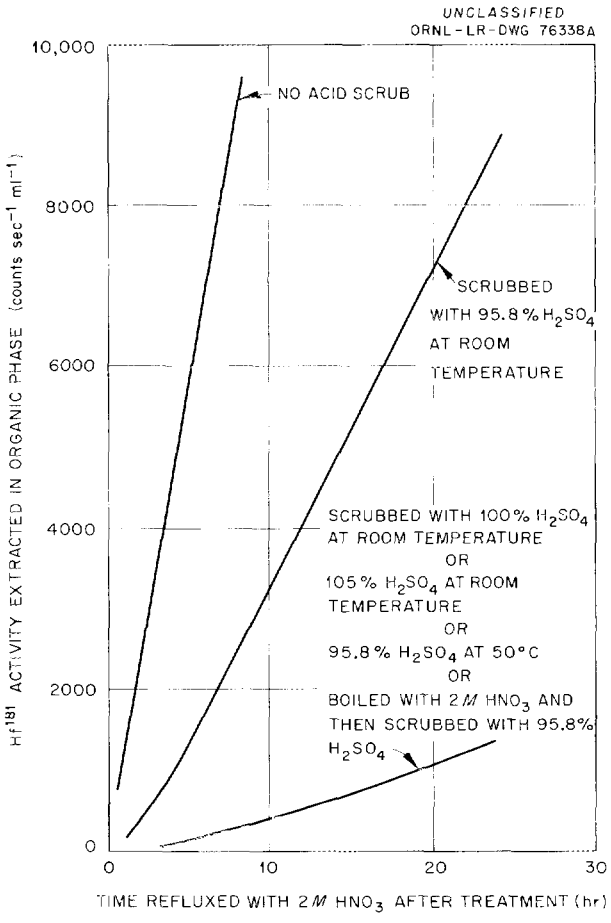

Fig. 8.6. Purification of Amsco 125-82 by Treatment with Sulfuric Acid.

Hf^{181} extractability[8] after converting the nitroparaffin in the solvent to the enol (most reactive) form by treating with sodium carbonate and calcium hydroxide. Whereas the solution in unpretreated Amsco, after 8-hr nitric acid degradation, showed a hafnium extraction coefficient of 16, those in Amsco pretreated with 96, 98, or 100% sulfuric acid showed coefficients of 0.3, 0.15, and 0.03, respectively. Solutions in Amsco pretreated with 100 and 105% acid at room temperature and with 95.6% acid at 50°C for 30 min had extraction coefficients of only ~0.15 even after a 24-hr degradation. The sulfuric acid apparently acts to destroy the reactive sites by sulfonation to sulfuric acid soluble by-products or by rearrangement of the molecule to a more stable configuration. No sulfur has been detected in the diluent after treatment.

Amsco degraded with nitric acid, scrubbed with concentrated sulfuric acid at room temperature, made 1 *M* in TBP, and then boiled for 24 hr with 2 *M* HNO_3 was as stable as Amsco pretreated with 100 and 105% sulfuric acid at room temperature or with 95.6% acid at elevated temperatures. In this treatment the sulfuric acid scrubs the nitroparaffins from the unreacted Amsco. Such scrubbing is not practical on degraded solvents containing TBP since the TBP also distributes to the sulfuric acid.

Other tests were made to determine whether additional treatment would further improve the Amsco performance. For example, Amsco was recovered from the 24-hr-degraded 1 *M* TBP solutions by extracting the TBP and nitroparaffin with concentrated sulfuric acid. The recovered Amsco was again made 1 *M* in fresh TBP and subjected to an additional 24-hr degradation with 2 *M* nitric acid. After this treatment the hafnium extraction coefficient was still ~0.15. Repetition of the cycle four additional times produced the same results. Apparently, after the initial treatments to remove or deactivate the sites susceptible to easy nitration, the remaining Amsco degrades at a consistently low rate. Its behavior is very similar to that of the relatively stable *n*-dodecane.

Aromatic Diluents to Improve Selective Uranium Extraction by TBP

It was shown previously[9] that TBP when used in aromatic rather than aliphatic diluents gave improved performance with regard to radiation stability, uranium extraction power, and separation of uranium from fission products. Similar results have now been obtained with a wider range of aromatic diluents. Solutions of TBP in diethylbenzenes, butylbenzene, or trimethylbenzenes extracted uranium from 2 *M* nitric acid with coefficients about 50% higher than those obtained with TBP in Amsco 125-82 solutions. Separation factors of uranium/hafnium were about 2 times higher (Table 8.1).

[8] E. S. Lane, *Degraded TBP-Kerosene Cleanup Using Alkanolamines and Related Compounds*, AERE-M-809 (January 1961).

[9] *Chem. Technol. Div. Ann. Progr. Rept. May 31, 1961*, ORNL-3153, p 111.

Table 8.1. Uranium and Hafnium Extraction by 1 *M* TBP in Aromatic or Aliphatic Diluents

Aqueous phase: 2 *M* HNO_3 initially, with 0.8 g U(VI) per liter, or 10^4 Hf^{181} gamma counts $sec^{-1}ml^{-1}$
Organic phase: 1 *M* TBP in indicated diluent
Test conditions: equal volumes of aqueous and organic phases; 10-min contact at room temperature

Diluent	Extraction Coefficient, E_a^0		Calculated Separation Factor, $SF = E_U/E_{Hf}$
	Uranium	Hafnium	
Diethylbenzene	65	0.07	950
1,2,3-Trimethylbenzene	65	0.09	700
n-Butylbenzene	60	0.09	650
Solvesso-100	55	0.08	700
Amsco 125-82	50	0.12	400
n-Dodecane	40	0.12	350

Stability of Aromatic Diluents

Further studies have been made of the stability of the alkyl side chains of di- and polyalkylbenzenes toward degradation by nitric acid. The previously reported[10] instability of a mixture of the isomers of diethylbenzene was shown to be a property of only the ortho and para isomers. The meta isomer was about as stable as *n*-dodecane (Table 8.2). Except for isodurene, several polymethylbenzenes tested were equally stable. Measurements of nitration of the benzene ring are not complete, but the extent of this reaction under most process conditions is expected to be low.

Several of the stable aromatic diluents have flash points acceptable for use in most plants, that is, 140°F. Those showing the best properties are not commercially available. However, the commercial mixture of diethylbenzenes (Table 8.2) is being used in the separation of thorium from uranium in the ORNL fuel recycle pilot plant (see Sec 6) and has given satisfactory physical performance. This material is available at $1.40 per gallon and is high in the meta isomer (~70%). With an established demand it should be possible to obtain preferred diluents at a reasonable cost.

[10] *Chem. Technol. Div. Ann. Progr. Rept. June 30, 1962*, ORNL-3314, p 108.

Table 8.2. Performance of Degraded Diluents

Diluent	Flash Point, Open Cup (°F)	Calcium Test[a] (counts $sec^{-1}ml^{-1}$)
1,2-Diethylbenzene	138	4000
1,3-Diethylbenzene	~138	100
1,4-Diethylbenzene	~138	>6000
Commercial diethylbenzene	~138	4000
1-Methyl-4-isopropylbenzene		4000
1,2,3-Trimethylbenzene (Hemimellitene)	124[b]	120
1,2,4-Trimethylbenzene (Pseudocumene)	125[b]	100
1,3,5-Trimethylbenzene (Mesitylene)		100
1,2,3,4-Tetramethylbenzene (Prehnitene)	163	200
1,2,3,5-Tetramethylbenzene (Isodurene)	155	1400
n-Dodecane	165[b]	125
Amsco 125-82	128[b]	4000

[a]Calcium test:
1. Boil, under reflux, diluent containing 1 *M* TBP with equal volume 2 *M* HNO_3, for 4 hr.
2. Scrub twice with equal volume 0.2 *M* aqueous Na_2CO_3.
3. Contact for 30 min with solid calcium hydroxide, about 50 g solid/liter.
4. Contact with Zr-Nb^{95} tracer solution in 2 *M* HNO_3, 10^4 gamma counts $sec^{-1}ml^{-1}$.
5. Count Zr-Nb^{95} γ activity of diluent.

[b]Closed cup.

8.6 SEPARATION OF ALKALI METALS

Extraction and separation of the alkali metals is being studied with several different types of reagents including substituted phenols, mono- and dialkylphosphoric acids, sulfonic acids, carboxylic acids, and mixtures of some of these.

The favorable separations attainable with 4-sec-butyl-2(α-methylbenzyl)phenol (BAMBP) are shown in Fig. 8.7*a*. At pH 12 to 13, where extraction coefficients are relatively high, the order of extractability is Cs > Rb > K > Na > Li. In the same pH region, separation factors are ~20 for both cesium/rubidium and rubidium/potassium.

Hanford workers[11] have discovered that combining a small concentration of di(2-ethylhexyl)-phosphoric acid (D2EHPA) with BAMBP greatly enhances cesium extraction from relatively acidic liquors where extraction with BAMBP alone is inappreciable. As shown in Fig. 8.7*b*, cesium and rubidium extraction coefficients in the pH range 3 to 8 for 1 *M* BAMBP–0.1 *M* D2EHPA in diisopropylbenzene are 2 to 4 orders of magnitude higher than for 1 *M* BAMBP alone. The separation factors, cesium/rubidium and rubidium/potassium, were ~10 and ~5, respectively, over the total pH range. It should be noted that the magnitudes of many of the extraction coefficients shown in Figs. 8.7*a*, 8.7*b*, and 8.7*c* are limited by loading of the extractant with alkali metals.

Combination of a sulfonic acid such as dinonylnaphthalenesulfonic acid (DNNSA) with a phenol also synergizes extractions of alkali metals. With 1 *M* Santophen-1 (4-chloro-2-benzylphenol) plus 0.1 *M* DNNSA in diisopropylbenzene (Fig. 8.7*c*), the extraction coefficients showed little dependence on pH in the pH range 1 to 10. The decrease in extraction at higher pH is attributed to the loss of phenol to the aqueous phase. The separation factors for cesium/rubidium and rubidium/potassium were in the range 5 to 7, whereas there was little difference in extraction coefficients for potassium, lithium, and sodium. Combination of dodecylphosphoric acid or Neo-Tridecanoic acid with the phenol extractant gave synergized alkali metal extractions, but the effect was less pronounced than with D2EHPA or DNNSA.

In extractions with 0.5 *M* DNNSA alone in diisopropylbenzene, extraction coefficients for

[11]Personal communication with HAPO personnel.

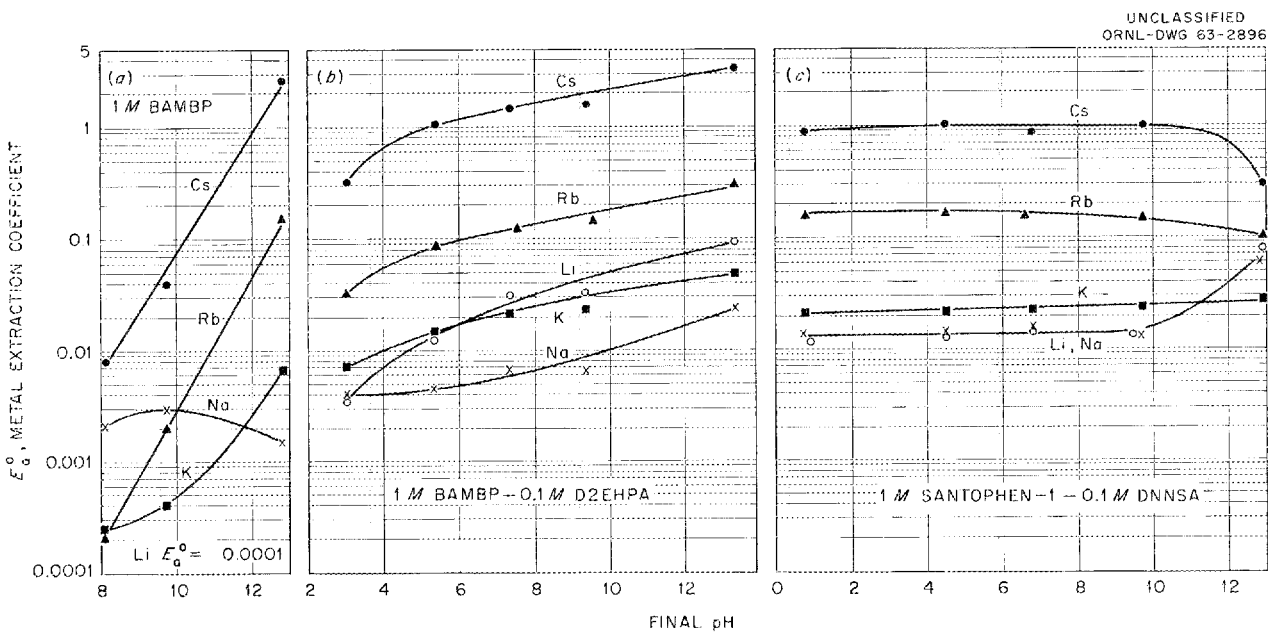

Fig. 8.7. Extraction of Alkali Metals with Phenols. Organic phase: (*a*) 1 *M* BAMBP, (*b*) 1 *M* BAMBP–0.1 *M* D2EHPA, or (*c*) 1 *M* Santophen-1–0.1 *M* DNNSA in diisopropylbenzene diluent. Aqueous phase: solution containing 0.1 *M* $CsNO_3$, 0.2 *M* $RbNO_3$, 0.4 *M* KNO_3, 0.4 *M* $NaNO_3$, 0.4 *M* $LiNO_3$; pH adjustments made with 50% NaOH. Phase ratio: 1/1.

the alkali metals (again under conditions of high solvent loading) ranged from 0.2 to 0.8 and were not appreciably affected by change in pH from 1 to 13. The extraction order was Cs > Rb > K $\cong$ Na $\cong$ Li, but separation factors between Cs and K, Na, and Li were <4. With 0.5 *M* dodecylphosphoric acid in diisopropylbenzene, the extraction order was similar, but the extraction coefficients were much lower and the separation factors were slightly higher.

8.7 CESIUM RECOVERY FROM ORES

The phenol extraction (Phenex) process, which was developed for recovering fission product cesium from reactor process waste solutions (see Sec 9.1), has been applied to the recovery of cesium from ores and its separation from other alkali metals. New uses, for example, in plasma thermionic power generators and as a fuel for ion rocket engines, are expected to create a large demand for cesium in the next few years.

The most important source of cesium is the mineral pollucite ($2Cs_2O \cdot 2Al_2O_3 \cdot 9SiO_2 \cdot H_2O$). It can be decomposed by treatment with concentrated acids or by roasting with alkaline fluxes[12] and leaching with water. The latter treatment is the better choice for use with the Phenex process, which is applicable only to alkaline liquors. In tests with a pollucite ore containing 22.9% Cs, 0.64% Rb, 0.98% K, 1.45% Na, 0.21% Li, 17.5% Al_2O_3, and 48.5% SiO_2, ~99% of the cesium was recovered by roasting one part of the pulverized ore for 2 hr at 800°C with 1.8 parts of Na_2CO_3 and 1.2 parts of NaCl and then leaching with water.

In a batch countercurrent test with 1 *M* 4-sec-butyl-2-(α-methylbenzyl)phenol (BAMBP) in diisopropylbenzene, 99.4% of the cesium was recovered from a pollucite liquor using five extraction and two scrub stages (Table 8.3). Relative flows of organic/aqueous feed/scrub (0.02 *M* NaOH) were 1/1.5/0.2. More than 95% of the cesium was stripped from the scrubbed extract in a single contact with 0.8 *M* HCl to give a solution containing about 100 g of cesium per liter. Evaporation of this solution to dryness gave a cesium chloride product containing <0.2% of the other alkali metals:

	Product Analysis (%)	Decontamination Factor (from feed solution to final product), Cs/metal
Cs	82.1	
Rb	0.011	230
K	0.137	610
Na	0.021	16,000
Li	<0.01	>10
Si	<0.02	>3000

The potassium content of the product is higher than expected in practice since the feed liquor for this test was inadvertently contaminated with potassium to about 20 times the usual amounts.

The Phenex process has also been applied to the recovery of cesium from Alkarb, a mixture of

Table 8.3. Recovery of Cesium from Pollucite Liquor with BAMBP

Organic phase: 1 *M* BAMBP in diisopropylbenzene

Aqueous phase: liquor prepared by roasting pollucite ore with Na_2CO_3-NaCl and leaching with water; liquor adjusted to pH 13.1 with caustic; analysis results expressed in grams per liter, 9.0 Cs, 0.28 Rb, 9.1 K, 37.5 Na, 0.01 Li, 0.01 Fe, 0.05 Al, 7.2 Si, 27 Cl, and 11 CO_3; traced with Cs^{134}

Scrub: 0.02 *M* NaOH

Contact: batch countercurrent; 5-min contacts

Relative flows: organic/feed/scrub = 1/1.5/0.2

Stage	pH	Cs Concentration (g/liter)	
		Organic	Aqueous
Scrub-2	12.8	13.5	9.3
Scrub-1	12.8	15.0	12.1
Aqueous feed	13.1		9.0
Extraction-1	13.1	15.3	8.5
Extraction-2	13.1	13.9	5.9
Extraction-3	13.1	9.3	2.1
Extraction-4	13.1	3.3	0.36
Extraction-5	13.1	0.49	0.04

[12] V. E. Plyushchev and I. V. Shakhno, "Interaction of Minerals Containing Rare Alkali Elements with Salts and Oxides in the Baking and Melting Process," *Chem. Abstr.* 53, 12600*d*.

alkali metal carbonates, which is a by-product of the lithium industry. The feed, prepared by dissolving Alkarb in water and adjusting to pH 13.3 with caustic, contained, in grams per liter, 1.9 Cs, 18 Rb, 37 K, 7.4 Na, and 0.18 Li. In a batch countercurrent test with 1 *M* BAMBP in diisopropylbenzene, cesium recovery was 98.5% using four extraction and three scrub stages. The organic/aqueous feed/scrub (0.01 *M* NaOH) ratios were 1/2/0.5. The extract was stripped quantitatively by a single contact with 0.5 *M* HNO_3 at an organic/aqueous phase ratio of 8.6 to 1 to give a product solution of the following composition:

	Strip Product Analysis (g/liter)	Decontamination Factor (aqueous feed to strip product), Cs/metal
Cs	38.8	
Rb	5.25	70
K	0.01	8800
Na	0.086	1500
Li	<0.00005	>70,000

The high rubidium content of the product could be reduced by increasing the number of scrub stages or using a lower concentration of caustic for scrubbing. The rubidium can also be recovered from the cesium process raffinate by extracting with BAMBP after appropriate feed adjustment.

8.8 ACID RECOVERY BY AMINE EXTRACTION

Studies of sulfuric acid recovery from Sulfex process waste solutions were reported previously.[13] The relatively weak-base sterically hindered tertiary amines were preferred for this use since they could be stripped to the free-base form with water to give a relatively concentrated acid product solution. Recent tests showed the utility of tertiary amines for the recovery and purification of phosphoric acid from the highly contaminated wet-process acid produced in the fertilizer industry. For this application, more basic amines such as Alamine 336 (tri[octyl,decyl]amine), or preferably, benzyldilaurylamine, are required for extraction. Mixtures of amines of different basicities can also be used to obtain the best balance between extraction and water stripping.

Isotherms for the extraction of phosphoric acid from pure 5 *M* H_3PO_4 solution show that an acid recovery of better than 90% and a 1.5 *M* H_3PO_4 water-strip product can be obtained in about four ideal extraction and four ideal stripping stages with Alamine 336 or benzyldilaurylamine (Fig. 8.8). For comparison, only about 50% of the phosphoric acid can be recovered in four ideal extraction

[13] *Chem. Technol. Div. Ann. Progr. Rept. June 30, 1962*, ORNL-3314, p 104.

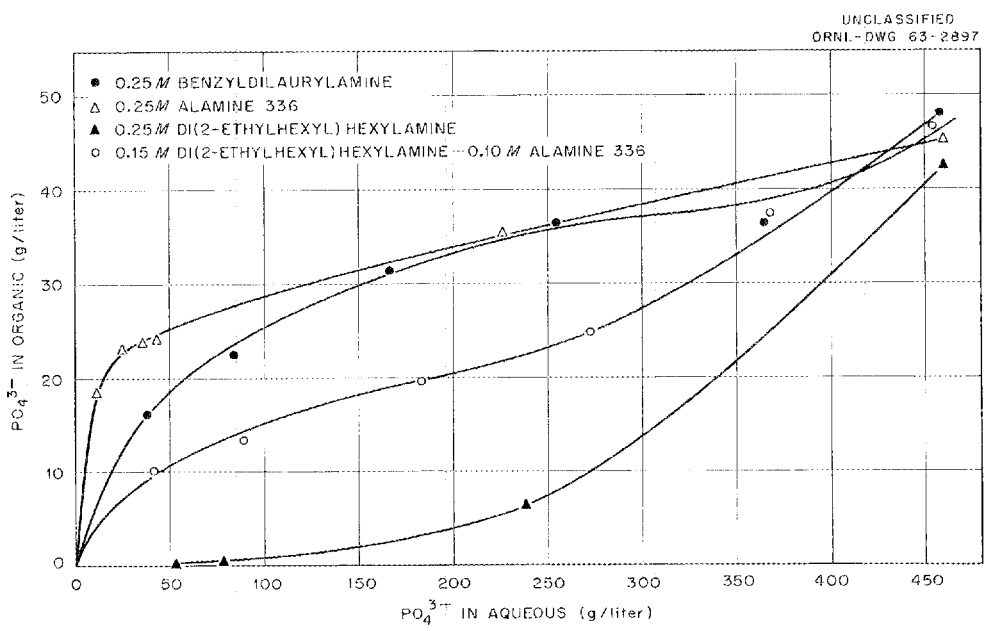

Fig. 8.8. Extraction of Phosphoric Acid from 5 *M* H_3PO_4 with 0.25 *M* Amine in 84% Amsco 125-82–16% Isodecanol at ~25°C.

stages with di(2-ethylhexyl)hexylamine. However, with this amine, water stripping would produce a 3.5 to 4 *M* H_3PO_4 product.

Tests with a synthetic wet-process phosphoric acid solution showed almost negligible iron and aluminum extraction, indicating a high degree of purification. If desired, ammonium phosphate rather than phosphoric acid can be produced as a product by stripping the amine with ammonia.

8.9 EXTRACTION OF NIOBIUM AND TANTALUM FROM ALKALINE SOLUTIONS

Niobium and tantalum have been recovered and separated by extracting from alkaline solutions with quaternary amines such as 0.1 *N* Aliquat 336 (tri[octyl,decyl]methylammonium carbonate) in 95% Amsco 123-15–5% tridecanol. The aqueous feed solutions for these tests were prepared by dissolving reagent-grade potassium niobate and potassium tantalate in K_2CO_3 or K_2CO_3-KOH solutions. Extraction coefficients decreased rapidly with increase in carbonate concentration but were sufficiently high up to 0.4 to 0.5 *M* carbonate to permit efficient recovery. Niobium was extracted preferentially, the separation factor (Nb/Ta) ranging from 5 to 10. Solutions of Na_2CO_3, NaOH, $(NH_4)_2CO_3$, K_2CO_3, chloride salts, and nitrate salts were effective stripping agents. With strip solutions containing sodium, the niobium and tantalum precipitated directly from the solvent as their sodium salts. These precipitates settled rapidly in the aqueous phase and did not cause emulsions.

Unfortunately, in later tests with ore liquors, prepared by fusing a niobium-tantalum ore with K_2CO_3-KOH and leaching the fused mass with water, the niobium and tantalum were extracted, but no significant separation factors were obtained. Likewise, significant separation factors were not obtained if solutions of the pure salts were heated on a steam bath or if the niobium and tantalum in these solutions were precipitated and redissolved in carbonate prior to extraction.

The inconsistent results are attributed to the complex chemistry of niobates and tantalates, which are affected by the preparation history of the solution. If future tests do not show ways for obtaining separable species from ore liquors, application of the process will be limited. It may be useful for the combined recovery of niobium and tantalum with separation from other elements.

8.10 NEW EXTRACTANTS

Amides

A number of amides, especially phosphoramides, examined several years ago at ORNL, gave good uranium extraction from sulfate-nitrate and phosphate-nitrate solutions of the type encountered in ore processing.[14] Work elsewhere showed *N,N*-dibutylacetamide, a carboxylic amide of moderate molecular weight, to be a useful extractant for uranium from nitrate solutions.[15] Although many of these compounds were noticeably hydrolyzed during use, their uranium-complexing properties have encouraged study of a wider variety of possibly more stable compounds. Consequently a number of different amides, covering a range of structures (Table 8.4), were examined with regard to their extraction of uranium, thorium, and several other solutes from nitric acid solutions. The results indicate that, in comparison with TBP, the *N,N*-dialkylamides extract in the same manner, are somewhat weaker uranium extractants, but have potential for considerably greater selectivity. (They also resemble TBP in synergistically enhancing uranium extraction by di(2-ethylhexyl)-phosphoric acid.) Extracted uranium was stripped with water or with dilute nitric acid ($\lesssim$0.1 *M*).

Considering first the dimethylamides of fatty acids (Fig. 8.9), the patterns of uranium extraction and thorium extraction vs nitric acid concentration are considerably different. Uranium extraction power varies considerably with length of acid chain, while each curve is rather similar in shape to the TBP and di-sec-butyl phenylphosphonate (DSBPP) reference curves. In contrast, the thorium extraction power varies only slightly with chain length but the curves are much steeper than the TBP and DSBPP curves, offering a wide range of relative uranium and thorium extractabilities. Still different patterns are shown by a branched-chain amide [$C_9H_{19}C(CH_3)_2CON(CH_3)_2$, Figs. 8.9 and 8.10], which shows much lower extraction at low acidities throughout, but moderately high uranium extraction and hence very high indicated

[14] K. B. Brown, *Progress Report: Uranium Chemistry of Raw Materials Section*, ORNL-1308 (May 23, 1952); *ibid.*, ORNL-2366 (Sept. 4, 1957).

[15] H. M. Feder and Milton Ader, *Solvent Extraction of Uranium Values*, U.S. Patent, 2,872,285 (patent applied for Sept. 6, 1956).

selectivity for uranium at high acidity. Some compounds with larger alkyls attached to the nitrogen also show higher indicated selectivities (Table 8.4).

Preliminary tests with diisopropylpropionamide and tetraethylphthalamide showed potential for separating the transplutonium group from lanthanides. Extraction was low for uranium and thorium from hydrochloric and sulfuric acid solutions, and for strontium and cesium from nitrate solutions. Nitric acid was extracted readily, reaching mole ratios of about 2.5 moles of HNO_3 per mole of amide with some of the fatty acid dimethylamides in contact with 12 *M* HNO_3.

No hydrolysis of the amides was noted during the extraction tests. In preliminary stability tests, fatty acid dimethylamides were extensively hydrolyzed by the severe treatment of boiling with 2 *M* HNO_3. Stability under moderate conditions and effects of structure are being tested.

Table 8.4. Uranium and Thorium Extraction with 1 *M* Amide-Diethylbenzene Solutions from 1.7 *M* HNO_3 (Equilibrium Aqueous Concentration)

N-Alkyls	Amide Constituent: Carboxylic Acid: Principal Components	Amide Constituent: Carboxylic Acid: Average Number of Carbon Atoms	Extraction Coefficient: U	Extraction Coefficient: Th	Calculated Separation Factor, U/Th
Dimethyl	Caprylic-capric	8.8	5.0	0.1	50
	Lauric	12	6.6	0.1	66
	Coco acids[a]	12.5	5.6	0.1	56
	Myristic	14	6.1	0.1	61
	Palmitic-stearic	16.9	16	0.1	160
	Tallow acids[b]	17	6.3	0.1	63
	Oleic	17.6	7	0.1	70
	Neo-Tridecanoic[c]	13	0.7	<0.01	>70
Diethyl	Capric	10	2.7	0.05	54
Di-*n*-propyl	Propionic	3	5.4	0.013	410
Di-isopropyl	Propionic	3	Ppt	<0.01	
Di-*n*-butyl	Acetic	2	21	0.8	26
		Diamides			
Tetramethyl	"Dimer acid"[d]	34	14	0.5	28
Tetramethyl	Phthalic	8	0.1	<0.002	
		Organophosphorus Reference Standards			
TBP			27	1.1	25
DSBPP (xylene)			38	0.1	380

[a]Principally lauric and myristic acids.
[b]Principally palmitic and stearic acids.
[c]$C_9H_{19}C(CH_3)_2CON(CH_3)_2$.
[d]Amide groups approximately 16 carbon atoms apart.

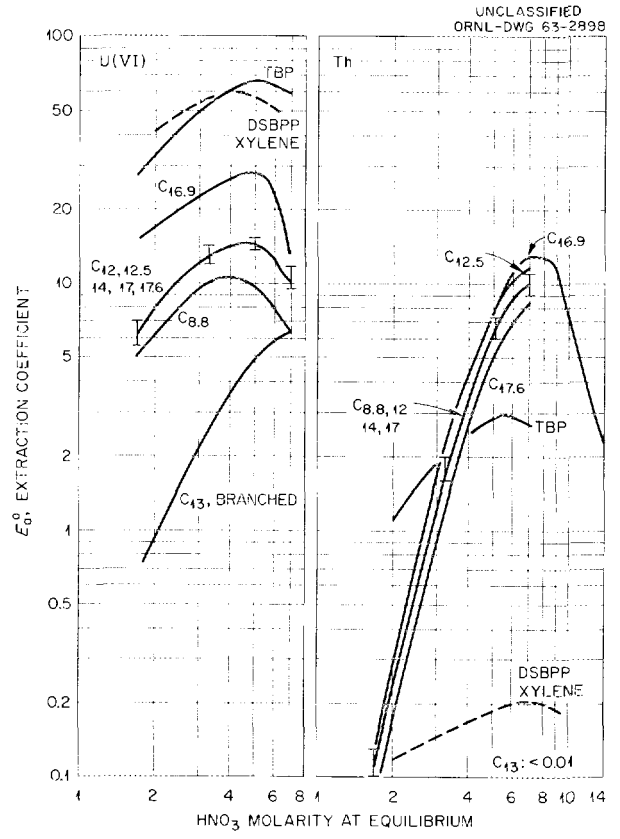

Fig. 8.9. Uranium and Thorium Extraction from Nitric Acid by 1 *M* Solutions of *N,N*-Dimethylamides in Diethylbenzene. Code numbers are the average carbon atom numbers from column 3 of Table 8.4; C_{13} is branched; all others are straight-chain compounds.

Carboxylic Acids

A systematic survey program was started of cation exchange extraction by high-molecular-weight carboxylic acids. A number of such acids have been obtained (Table 8.5), including some of recent commercial availability, and some new acids synthesized for this program. (See also "Strontium Recovery," Sec 9.3.) Their extraction characteristics were compared first by two-phase titration with sodium and potassium hydroxides, which provides a convenient indication of the relative strength of each acid, its selectivity between sodium and potassium, and its physical behavior. The acid esters[16] (the last three acids in Table 8.5) are of particular interest, since the ester carboxyl conjugated with the acid carboxyl makes them considerably stronger than the simple carboxylic acids and hence potentially usable over a wider range of conditions. Further acid esters with other alcohols and other dicarboxylic acids are being prepared.

Hydroxamic Acids

Hydroxamic acids,

$$RC(=O)-N(H)-OH\ ,$$

[16]Extraction with acid esters of tetrahydrophthalic acid was suggested by B. Emmet Reid, Baltimore, Md., in private communication to G. H. Cartledge, Jan. 14, 1963.

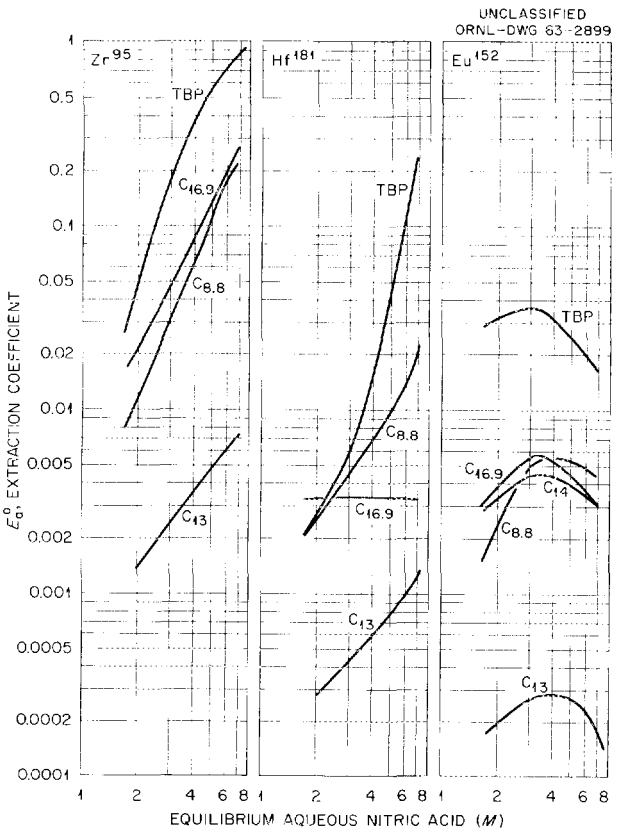

Fig. 8.10. Extraction of Zirconium, Hafnium, and Europium from Nitric Acid by 1.0 *M* Solutions of *N,N*-Dimethylamides in Diethylbenzene. Code numbers are the average carbon atoms from column 3 of Table 8.4; C_{13} is branched; all others are straight-chain compounds.

Table 8.5. Alkali Ion Extraction by Carboxylic Acids

Extraction from 2.5–5 *M* chloride solutions by ~0.1 *M* acids in diethylbenzene

$$\underset{\cdots}{HA} + M^+ \rightleftharpoons \underset{\cdots}{MA} + H^+ \text{ (ref } a)$$

$$K = (H^+)(MA)/(M^+)(HA)$$

Acid		pK'[b]	
		Na^+	K^+
Oleic	$CH_3(CH_2)_7CH{:}CH(CH_2)_7CO_2H$	8.5	8.8
Palmitic	$CH_3(CH_2)_{14}CO_2H$	Ppt	Ppt
Diheptylacetic	$[CH_3(CH_2)_6]_2CHCO_2H$	10.0	10.2
Neo-Decanoic	$C_6H_{13}(CH_3)_2C{-}CO_2H$	9.1	
Neo-Tridecanoic	$C_9H_{19}(CH_3)_2C{-}CO_2H$	9.9	
Abietic (plus congeneric acids)	$CH_2CH_2C{-}(CH_3)CCH_2CH_2CH_2$ / $(CH_3)_2CHC{:}CHC{:}CHCH_2CH{-}(CH_3)C{-}CO_2H$	9.4	9.6
Lauryl maleic	$CH_3(CH_2)_{11}O_2C{-}CH{:}CH{-}CO_2H$	5.6	5.4
Lauryl phthalic	$CH_3(CH_2)_{11}O_2C{-}C_6H_4{-}CO_2H$	6.6	
Tridecyl phthalic	$C_{13}H_{27}O_2C{-}C_6H_4{-}CO_2H$	7.1	

[a]Dots indicate the organic phase.

[b]Measured at the half-neutralization point in two-phase titration: $pK' = pH + \log \gamma_{\pm} m_{MCl}$, assuming $\gamma_{MA} \approx \gamma_{HA}$.

previously reported by workers at Harwell[17] to complex zirconium and hafnium, showed potential for extraction of zirconium, niobium, hafnium, and strontium. Octanohydroxamic acid was readily soluble in hexone, and in Amsco 125-82 containing 1 *M* TBP, but to less than 0.1 *M* in Amsco 125-82 alone or in xylene. It and other available hydroxamic acids decomposed when exposed to nitric acid or alkaline solutions, as shown by slow decrease of extraction coefficients and of characteristic infrared absorption. However, they appeared to be stable in extraction from hydrochloric acid, and may prove to be stable in other nonoxidizing acid systems. Since presumably the cations are extracted rather than their complexes with nitrate, etc., observations in the nitrate system should also indicate their general behavior in extraction from other acids.

[17]E. S. Lane, "Performance and Degradation of Diluents for TBP and the Cleanup of Degraded Solvents," presented at the Solvent Extraction Chemistry Symposium, Gatlinburg, Tenn., Oct. 23–26, 1962.

Addition of 0.1 *M* hydroxamic acid to 1 *M* TBP solution in Amsco 125-82 did not alter uranium, thorium, ruthenium, or europium extraction, but the combination did show synergistic enhancement of zirconium extraction. Strontium was extracted by 0.1 *M* octanohydroxamic acid in hexone from 0.5 *M* $NaNO_3$, with a maximum extraction coefficient of $E_a^o = 8$ and separation factor (SF) from sodium of $SF_{Na}^{Sr} \approx 50$ at pH 10.5. Cesium was not extracted.

Others

A number of substituted phenols were examined as potential cesium extractants, and several have been extensively studied in the Fission Product Recovery Program, leading to cesium recovery processes (see Secs 8.6 and 9.1). Several phenolic monomers and polymers, of specific structures suggested by the previous studies, are being prepared on subcontract.[18]

[18]Monsanto Research Corp., Dayton, Ohio.

Four potential extractants of a new type, high-molecular-weight bicyclic or "cage-structure" phosphates and phosphites, were prepared on subcontract.[18] The bicyclic phosphate of 1,1,1-trimethylolnonane

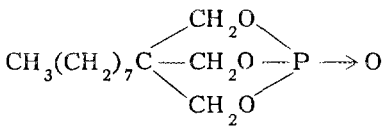

showed high extraction power for thorium and high selectivity for thorium over uranium. The extraction coefficients were $E_a^o = 6$ for uranium and $E_a^o > 200$ for thorium in extractions from 2 *M* HNO_3 with the cage phosphate reagent at 1 *M* in diethylbenzene.

The possible synthesis of phosphinic acid and phosphine oxide polymers is being investigated,[18] and some related monomeric phosphinic acids have been submitted for testing.

8.11 FUNDAMENTAL STUDIES ON SOLVENT EXTRACTION EQUILIBRIA AND KINETICS

Alkaline Earth and Alkali Extraction by Di(2-ethylhexyl)phosphate

Continued studies of strontium extraction from sodium nitrate solutions by di(2-ethylhexyl)phosphoric acid (HA, existing in benzene solution as the dimer $[HA]_2$) and its sodium salt (NaA) confirmed the previously suggested reaction[19]

$$Sr^{2+} + 3[HA]_2 \rightleftharpoons SrA_2 \cdot 4HA + 2H^+ \qquad (1)$$

and also the corresponding reaction

$$Na^+ + 2[HA]_2 \rightleftharpoons NaA \cdot 3HA + H^+ \qquad (2)$$

when the extractant is preponderantly in the acid form.[20] The stoichiometry of these extracted species is of particular interest, being markedly different from the usual stoichiometry $MA_x \cdot xHA$, or $M(A_2H)_x$, found in most extracted-metal species previously identified.

When the extractant contains significant amounts of the sodium salt, Eq. (1) must be modified, and the generalized equation

$$Sr^{2+} + (n/y)[aHA \cdot bNaA]_y \rightleftharpoons SrA_2 \cdot (n-2)[\alpha HA \cdot \beta NaA] + iH^+ + jNa^+ ,$$

$$a + b = 1, \quad \alpha + \beta = 1, \quad i + j = 2 , \qquad (3)$$

has proved to be a suitable model at least up to 50% salt form. Experimental evaluation of i from H^+-concentration dependence, n/y from extractant-concentration dependence, and y from vapor pressure measurements (see following Sec "Solvent Extraction System Activity Coefficients") leads to calculated values of n in the range 4 to 6, indicating that the extracted strontium is in the form of $SrA_2 \cdot 4HA$ or analogous adducts throughout this region.

The nature of the diluent used with di(2-ethylhexyl)phosphoric acid has moderate to large effects on its extraction of strontium nitrate. In particular, workers at HAPO[21] observed a synergistic enhancement of the strontium extraction on addition of TBP to a kerosene diluent. Figure 8.11 compares the effects of this and several other single and mixed diluents. In several cases, especially with benzene and benzene plus additives, the main effect appears to be a shift of the E-vs-pH curve along the pH scale with little change in the maximum value of E. In these cases, plots of the extractant composition ratio $[NaA]/\Sigma[A]$ vs pH would vary in much the same way, with little change in E vs $[NaA]/\Sigma[A]$. With *n*-nonane, however, there are real synergistic (TBP) and antagonistic (dodecanol) changes of E in addition to the shift vs pH. The maximum enhancement by TBP occurred at $[NaA]/\Sigma[A] \approx 1/3$, with addition of about 0.2 *M* TBP to 0.1 *M* HA (Fig. 8.12).

Thorium Sulfate Complexes

Evaluation[22] was completed of the formation constants for the thorium trisulfate and tetrasulfate anionic complexes, on the basis of amine extraction

[19] *Chem. Technol. Div. Ann. Progr. Rept. June 30, 1962*, ORNL-3314, p 112.

[20] W. J. McDowell and C. F. Coleman, *J. Inorg. Nucl. Chem.* 25, 234 (1963).

[21] Private communication from W. D. Schultz, Hanford, Wash., September 1961.

[22] K. A. Allen and W. J. McDowell, *J. Phys. Chem.* 67, 1138 (1963).

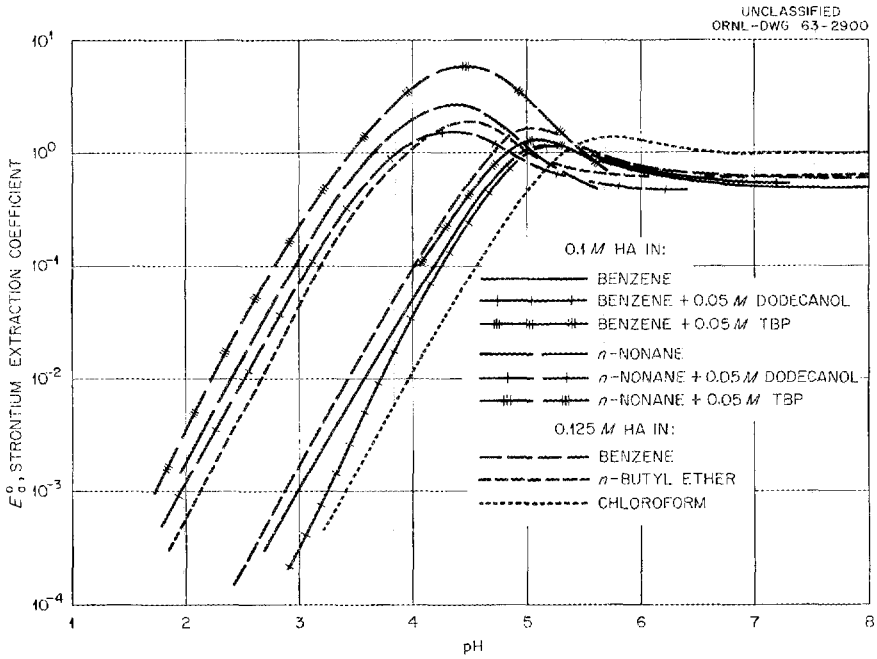

Fig. 8.11. Effect of Diluent on Strontium Extraction by Di(2-ethylhexyl)phosphoric Acid (HA). Aqueous phase: 4 M $NaNO_3$, tracer strontium.

equilibrium data.[23] A general method was developed for this evaluation. Its essential feature is the experimental maintenance of constant chemical potentials of extractable species in the aqueous phase, controlled and monitored by constant composition of the equilibrium organic phase. The aqueous solutions were made up at various combinations of sulfuric acid and sodium sulfate, each adjusted to constant sulfuric acid activity ($a_{H_2SO_4} = 6.4 \times 10^{-5}$ M) according to the data compiled by Baes.[24] The acid activity was confirmed to within ±0.5% by measurements of the equilibrium amine sulfate-bisulfate ratio, which was previously established as a function of the sulfuric acid activity.[25] The actual sulfate ion concentration was also calculated for each solution.[24] Total amine molarity was constant at 0.1 ± 0.0005, and constant total thorium content maintained the organic phase concentration constant to within 2%, this small variation being corrected in the final calculations. With the activities thus held constant, the varying aqueous-phase activity coefficients were approximated by a Debye-Hückel expression of the form:

$$\log G = -0.509\, \Lambda(Z_i^2) I^{1/2}/(1 + 2I^{1/2}) . \qquad (4)$$

Consideration of stepwise mononuclear[23] complex formation leads to a material balance relation,

$$[\Sigma M] = [MA_k] + [MA_k]\Sigma G_{tk}[A^{-j}]^{t-k} K_{kt} , \qquad (5)$$

where M is the metal ion, A the complexing anion, and G the combined activity coefficients, the double subscripts indicating the reactant and product species at each complex formation step.

For the thorium sulfate system this relation takes the form:

$$[\Sigma Th] = [Th(SO_4)_2] + [Th(SO_4)_2] G_{32} [SO_4^{2-}]^{-1} K_{23} + [Th(SO_4)_2] G_{42} [SO_4^{2-}]^{-2} K_{24} . \qquad (6)$$

Simultaneous least-squares analysis (by computer) with the thorium extraction data gave:

$$K_{23} = [Th(SO_4)_3^{2-}]/[Th(SO_4)_2][SO_4^{2-}] = 5.7 \pm 1.2;$$

[23] W. J. McDowell and K. A. Allen, *J. Phys. Chem.* 65, 1358 (1961).

[24] C. F. Baes, Jr., *J. Am. Chem. Soc.* 79, 5611 (1957).

[25] K. A. Allen, *J. Phys. Chem.* 60, 943 (1956).

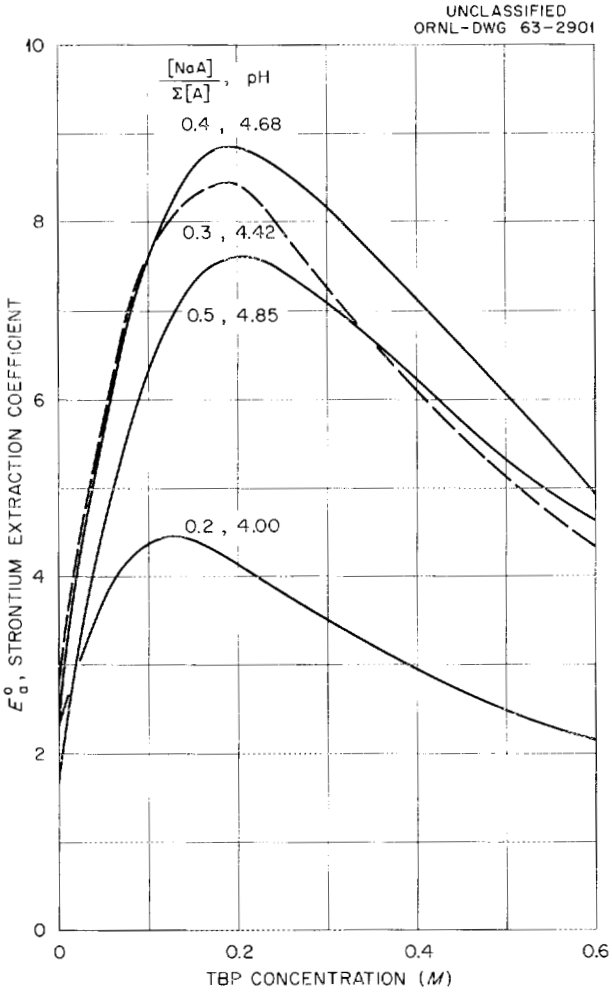

Fig. 8.12. Synergistic Enhancement of Strontium Extraction on Addition of Tributyl Phosphate to 0.1 *M* Di(2-ethylhexyl)phosphoric Acid in *n*-Nonane. Aqueous phase: 4 *M* $NaNO_3$, tracer strontium.

$$K_{24} = [Th(SO_4)_4^{4-}]/[Th(SO_4)_2][SO_4^{2-}]^2$$
$$= 0.054 \pm 0.009;$$
$$K_{34} = [Th(SO_4)_4^{4-}]/[Th(SO_4)_3^{2-}][SO_4^{2-}]$$
$$= 0.009 \pm 0.003,$$

evaluated at zero ionic strength.

These constants together with values of K_{01} and K_{12} from the literature[26] were used to calculate the fractional distribution of thorium among its aqueous species (Fig. 8.13) as a function of actual sulfate ion concentration at constant sulfuric acid activity.

Kinetics of Sulfate Transfer During Amine Extraction of Uranium

Continued investigation[27] of the rate of tagged sulfate transfer from organic to aqueous solution during amine sulfate extraction of uranyl sulfate gave evidence that both neutral complex transfer and ion transfer contribute to the uranium transfer, the former predominating in extraction from low-sulfate solutions where little of the uranyl ion is complexed, and the latter becoming important at higher sulfate concentrations where most of the uranium exists in anionic complexes. These two

[26] E. L. Zebroski, H. W. Alter, and F. K. Heumann, *J. Am. Chem. Soc.* **73**, 5646 (1951); A. J. Zielen, *ibid.*, **81**, 5022 (1959).

[27] W. J. McDowell and C. F. Coleman, "Interface Mechanism for Uranium Extraction by Amine Sulfate," *144th Am. Chem. Soc. Meeting, Los Angeles, April, 1963*, Abstract No. 62, 25K.

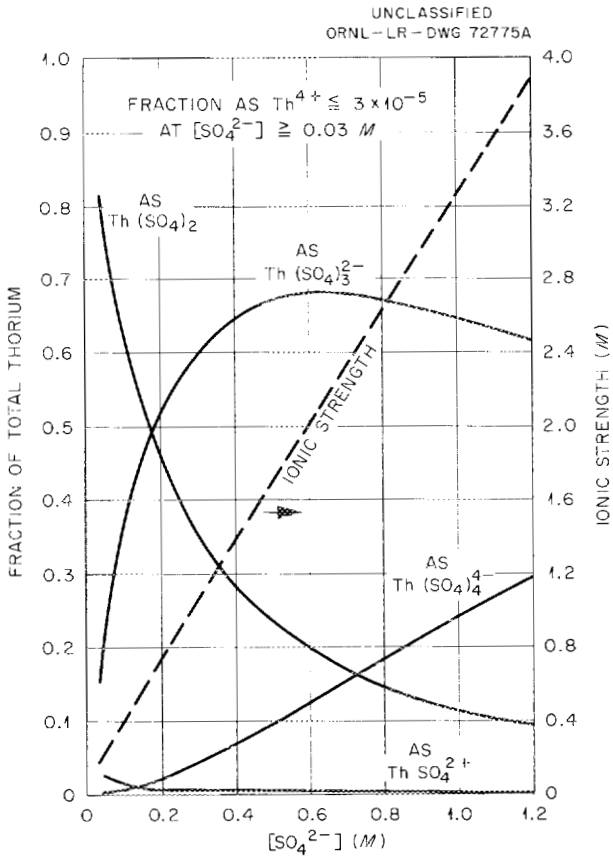

Fig. 8.13. Fractional Distribution of Thorium Among Its Aqueous Species in Sulfate Solution. Sulfuric acid activity constant at $a_{H_2SO_4} = 6.4 \times 10^{-5}$ *M*.

mechanisms cannot be distinguished by any equilibrium measurement (dots indicate the organic phase):

$$\underset{\cdots\cdots\cdots\cdots}{x(R_3NH)_2SO_4} + UO_2SO_4 \rightleftharpoons \underset{\cdots\cdots\cdots\cdots\cdots\cdots}{UO_2(R_3NH)_{2x}(SO_4)_{x+1}}, \quad (7)$$

$$\underset{\cdots\cdots\cdots\cdots}{x(R_3NH)_2SO_4} + UO_2(SO_4)_2^{2-} \rightleftharpoons \underset{\cdots\cdots\cdots\cdots\cdots\cdots}{UO_2(R_3NH)_{2x}(SO_4)_{x+1}} + SO_4^{2-}. \quad (8)$$

The extractant was 0.1 *N* di-*n*-decylamine sulfate in benzene, with the total-system acidity adjusted to maintain it essentially in the normal sulfate form and thus to avoid complication from displacement of bisulfate ion. Transfer of $S^{35}O_4^{2-}$ from organic to aqueous phase was measured (series 1) during equilibration with solutions containing $\leq$0.001 *M* H_2SO_4, plus Na_2SO_4 at 0 to 0.1 *M* and at 0.5 *M*, each adjusted to approximately 10^{-9} *M* in H_2SO_4 activity and preequilibrated before tracer sulfate was "spiked" into the organic phase. Corresponding measurements were made (series 2) during the extraction of uranyl sulfate initially at 0.012 *M* and (series 3, at low sulfate) with the same amount of uranyl sulfate present but preequilibrated.

Because of the back-transfer of sulfate ion shown in Eq. (8), if that reaction is important in extraction then the approach to isotopic equilibrium should be faster during uranium extraction (series 2) than in the other series. The isotopic equilibration did prove to be faster during uranium extraction from the 0.5 *M* Na_2SO_4 solution (Fig. 8.14), where about 75% of the uranium was estimated to exist as $UO_2(SO_4)_2^{2-}$ (ref 28). However, isotopic equilibration was slower with than without uranium extraction from the solution containing no sodium sulfate (Fig. 8.15), where more than half of the uranium was estimated to exist as uncomplexed uranyl ion and very little as the anionic complex. [The aqueous sulfate concentration changed as uranyl sulfate was depleted from this solution, but parallel series at graduated levels of sodium sulfate (Fig. 8.15) indicated that this would not seriously disturb the fractional approach to equilibrium.] Isotopic equilibration was slowed only

[28] S. Ahrland, *Acta Chem. Scand.* 5, 1151 (1931); K. A. Allen, *J. Am. Chem. Soc.* 80, 4133 (1958).

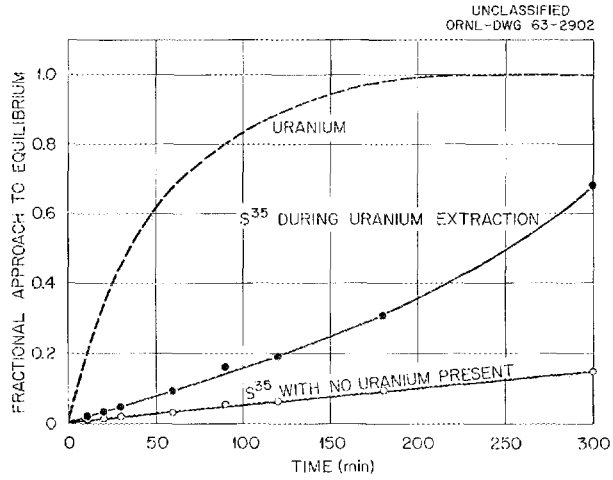

Fig. 8.14. Uranium and S^{35} Approach to Equilibrium Distribution: 0.1 *N* Di-*n*-decylamine Sulfate and 0.5 *M* $NaSO_4$; 0.012 *M* UO_2SO_4; $a_{H_2SO_4} = 10^{-9}$ *M*.

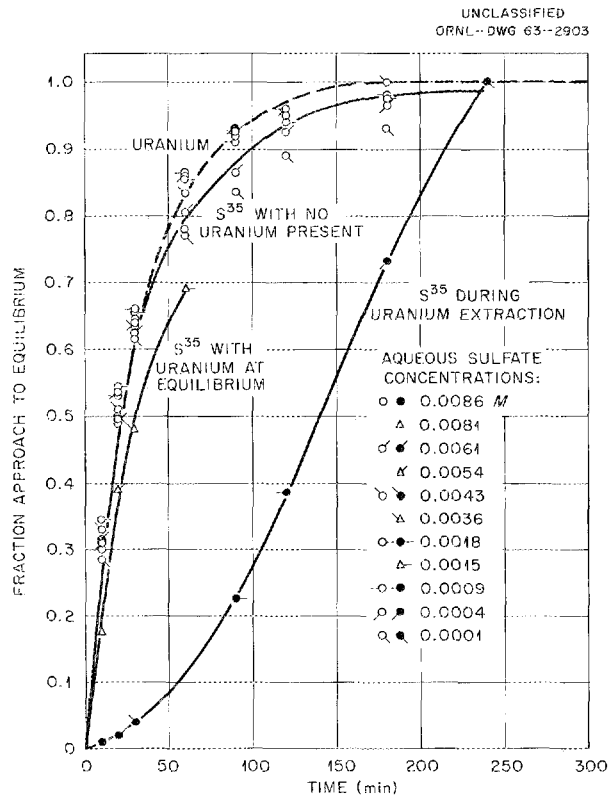

Fig. 8.15. Uranium and S^{35} Approach to Equilibrium Distribution: 0.1 *N* Di-*n*-decylamine Sulfate and <0.01 *M* Na_2SO_4; 0.012 *M* UO_2SO_4; $a_{H_2SO_4} = 10^{-9}$ *M*.

slightly by uranyl sulfate present but already at equilibrium distribution (Fig. 8.15).

These results suggest that uranium reaching the interface as $UO_2(SO_4)_2^{2-}$ does indeed displace a sulfate ion from organic to aqueous (in contrast to dissociating to UO_2SO_4 or UO_2^{2+} and then forming a new association with amine sulfate), that uranium reaching the interface as UO_2^{2+} or UO_2SO_4 simply associates with amine sulfate, and that the extracted uranium probably associates with further amine sulfates while diffusing inward from the interface, thus appreciably reversing the diffusion of tagged sulfate outward to the interface.

Solvent Extraction System Activity Coefficients

Direct, precise measurement of diluent vapor pressure differences, by the technique previously described,[29] over wet benzene solutions of di(2-ethylhexyl)phosphoric acid (HA) and its sodium salt (NaA) confirmed the dimerization of the acid over the concentration range 0.06 to 0.5 *M* HA, and showed increasing polymerization in NaA-HA mixtures as the proportion of NaA increased (Fig. 8.16). Several of the average polymerization numbers (i.e., *n* in the formula $[NaA,HA]_n$ or $[Na_xH_{n-x}A_n]$) were confirmed in dry benzene solution by isopiestic vapor balancing. The average polymerization number of NaA was 13 at 0.10 *M* and about 50 at 0.25 *M* NaA at 20°C. These polymerization data are used in interpretation of the SrA_2-NaA-HA extraction system (Sec 8.11, first paper).

Triphenylmethane has been used extensively as a reference standard in relative osmotic measurements of organic solutions by isopiestic vapor balancing. Its activity coefficients in benzene solution have now been determined by precise, direct vapor pressure difference measurements, varying from 0.98 at 0.014 *m* to 0.74 at 0.33 *m* (Fig. 8.17). Activity coefficients of azobenzene, another useful reference solute, were then determined in benzene solution by isopiestic balancing with the triphenylmethane, varying from 0.96 at 0.0134 *m* to 0.67 at 0.346 *m*. Thus, both of these reference solutes are now available for absolute as well as relative isopiestic measurements in benzene solutions. Using the triphenylmethane as reference, the activity coefficients of tri-*n*-octylamine (free-base form) were measured in benzene, ranging from 0.98 at 0.021 *m* to 0.55 at 0.354 *m* (Fig. 8.17).

Several organic liquids of low vapor pressure were examined as possible diluents for tri-*n*-octylamine (TOA) and its sulfate salts, with the objective of obtaining nonvolatile amine–amine salt solutions in which water activity can be determined by isopiestic vapor balancing. Phenylcyclohexane (vapor pressure, 60 μ at 25°C) and 95 vol % *n*-hexadecane–5% dodecanol (<5 μ) showed feasible physical performance, together with

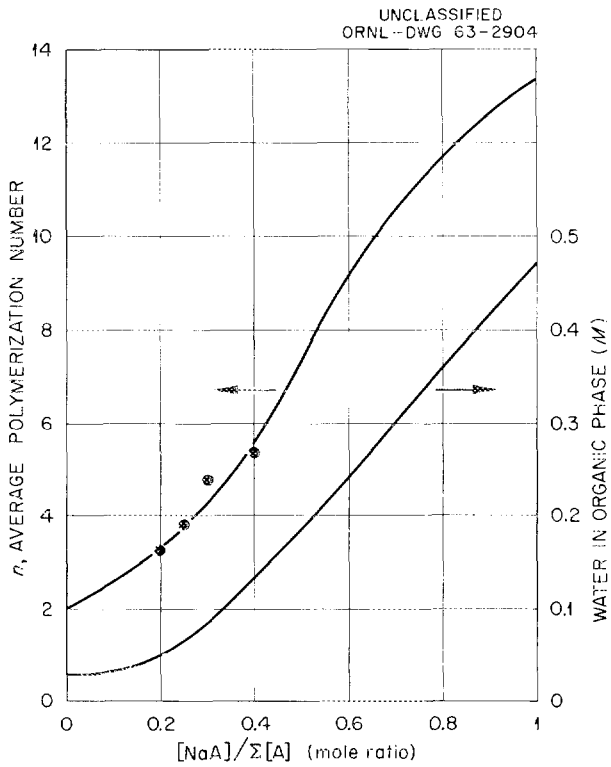

Fig. 8.16. Degree of Polymerization and Water Content of 0.1 *M* Di(2-ethylhexyl) Phosphate (HA,NaA) Solutions in Benzene. Lines: wet solutions, over saturated sodium chloride solution, by direct measurement of vapor pressure difference and Karl Fischer analysis. Points: dry solutions by isopiestic balancing.

[29] *Chem. Technol. Div. Ann. Progr. Rept. Aug. 31, 1960*, ORNL-2993, p 173.

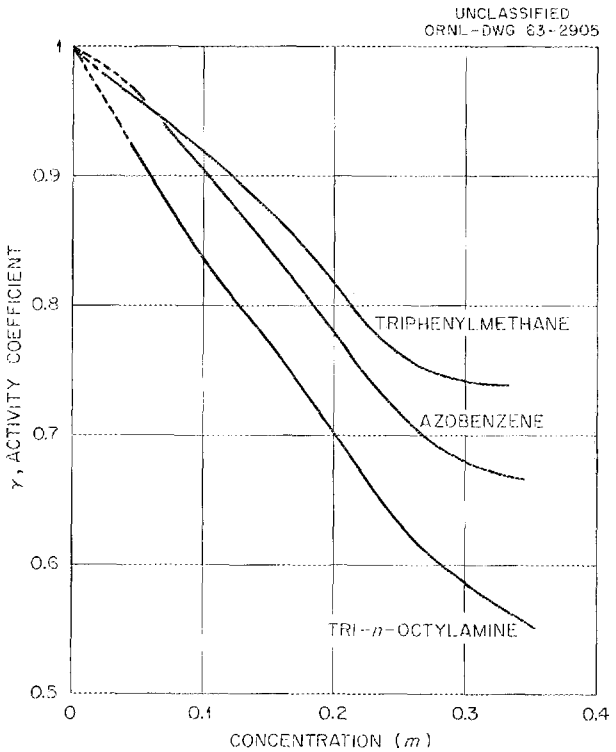

Fig. 8.17. Activity Coefficients in Benzene Solution, 20°C. Triphenylmethane: direct measurement of vapor pressure difference. Azobenzene and tri-*n*-octylamine: isopiestic balancing vs triphenylmethane.

chemical properties in amine-acid equilibrium comparable to those with benzene[30] as diluent:

Diluent for 0.1 *M* TOA	Acidity, $a^{1/3}_{H_2SO_4}$	
	Half Neutralized	Neutralized
Benzene	0.0036	0.011
Phenylcyclohexane	0.0093	0.019
n-Hexadecane + dodecanol	0.0040	0.021

8.12 ENGINEERING EQUIPMENT STUDIES

High Flow Ratios in Pulsed Columns

Development of new extraction agents with high distribution coefficients offer new methods of recovery and concentration of valuable materials such as the transuranium and fission product elements which are at low concentrations in process solutions. Preliminary studies of pulsed columns for high flow ratios (100:1 and 50:1) have been made, using 30% TBP–Amsco to extract uranyl nitrate from 4 *M* $NaNO_3$. The system was chosen because the kinetics is known to be rapid, and the distribution coefficient is high enough to permit accurate efficiency measurements at high flow ratios of the aqueous phase to the organic. The results (Table 8.6) show that the stage height (HETS) at flow ratios of 50:1 and 100:1 is only 2 to 3 times that at a conventional flow ratio of 5:1 for either the aqueous-continuous operation with sieve plates or the organic-continuous operation with nozzle plates. Furthermore, the efficiency can be increased by increased pulse frequency, with accompanying lower flow capacity. The flow capacity was virtually independent of flow ratio. The total flow capacity of the sieve plate column at a flow ratio of 50:1 increased from 520 to 3110 gal hr^{-1} ft^{-2} as the pulse frequency was decreased from 90 to 35 cpm; the flow capacity of the nozzle plate column was significantly less – ranging from 186 to 816 gal hr^{-1} ft^{-2} as pulse frequency was decreased from 70 to 35 cpm.

A comparison of the two columns shows an important advantage of operation with the major phase (aqueous) continuous because the holdup and consequently the residence time of the organic phase in the column is significantly less (0.1 to 0.5 hr per theoretical stage for aqueous continuous, 1.8 to 3.0 hr for organic continuous) at high aqueous-to-organic flow ratios. This is important in determining the time required for the system to reach steady state and in systems where solvent degradation due to radiation or chemical reaction occurs.

Measurement of drop size in the columns showed that the change of drop size and concomitant interfacial area with pulse frequency accounted for the dependency of stage height on frequency. At the same pulse conditions, the interfacial area was greater with organic-continuous operation, but this was offset by extensive backmixing of the continuous phase so that the overall stage height was not significantly lower than that with aqueous-continuous operation.

[30] K. A. Allen, *J. Phys. Chem.* **60**, 239 (1956).

Hydraulic Study of a Pulsed Nozzle-Plate Column

For the design of large pulsed columns it is important to know the maximum and minimum hydraulic pressures at the base of the column so that cavitation can be prevented in the pulser and so that the external accessories and piping can be sized. Data for 23%-free-area nozzle plates having 0.125-in.-diam holes with a 0.04-in. nozzle projecting down was obtained by using a sinusoidal pulse. The orifice coefficients, calculated at the maximum and minimum pressures developed at pulse frequencies of 30 to 80 cpm, increased slightly with increased pulse frequency and were slightly higher for downflow (0.75) than for upflow (0.70). The small difference in coefficients, which was confirmed by measuring the pressure drop with water flow through the column with no pulse, is not a significant deviation from that for conventional sieve plates.

Table 8.6. Effect of Flow Ratio on Flow Capacity and Efficiency of Pulsed Columns for Extraction of Uranium with 30% TBP–Amsco Mixture

Flow Ratio A/O	Pulse Frequency (cpm)	Flooding, Total Flow (gal hr^{-1} ft^{-2})	HETS[a] (ft)
With Sieve Plate ($\frac{1}{8}$-in. Holes, 23% Free Area), Aqueous Phase Continuous			
100	35		20.0
	50		18.5
	70	1250	13.3
	90		3.9
50	35	3110	
	50	2370	13.5
	70	1220	4.3
	90	520	
5	70	1070	4.3
With Nozzle Plate ($\frac{1}{8}$-in. Holes, 10% Free Area), Organic Phase Continuous			
100	35		6.3
50	35	816	7.5
	50	369	
	70	186	
5	35	865	3.5
	50	367	

[a]At 80% of flooding.

9. Fission Product Recovery

The objective of the fission product recovery program is to develop processes for recovering and purifying megacurie quantities of fission products from reactor-fuel processing wastes. The program includes basic chemical research, development of recovery methods, and development of engineering procedures to carry out these operations. Large quantities of certain fission product elements are now being requested for industrial, space, and other applications, and there is evidence that the demand will increase. Only relatively small amounts of these elements have been recovered in the past, principally by batch precipitation methods. From recent studies it is apparent that newer, versatile technologies (such as solvent extraction and ion exchange) offer potentially better methods for large-scale applications owing to the greater simplicity of operation and equipment.

Thus far, a solvent extraction process using di(2-ethylhexyl)-phosphoric acid (D2EHPA) has been successfully developed for recovering Sr^{90}, for which there is a large demand. The rare earths may be recovered also. A modification of this process has been operated in plant scale at the Hanford Atomic Products Operation. New processes have also been developed on a laboratory scale for recovering cesium, zirconium-niobium, yttrium, and possibly ruthenium, using extractants such as amines, phenols, and alkylphosphoric acids. These extractants, alone or in combination, are being considered for use at Hanford.

Combined with previous studies on rare-earth separation and on technetium, neptunium, and plutonium recovery, the recent studies afford an integrated solvent extraction flowsheet for the recovery of all important fission products and other components from waste liquors. Current studies are aimed at consolidating, optimizing, and completing these developments and at devising new processes that will provide even more advantages in operations and cost.

9.1 CESIUM

Continued study has confirmed the utility of the Phenex process for recovering cesium from alkaline solutions by extracting with substituted phenols and stripping with dilute acid. This process has been demonstrated successfully in batch or batch countercurrent tests with (1) simulated Hanford Purex wastes after adjusting with tartrate and caustic, (2) Hanford tank-farm supernatant solutions, and (3) caustic digests of ammonium molybdophosphate that had been used as a cesium adsorbent. Since the phenols are highly selective for cesium, excellent decontamination is obtained from other fission products, bulk contaminants of the solutions, and other alkali metals.

Continued screening of a large number of phenols of varying structure revealed several with extraction characteristics superior to those of *p*-dodecylphenol, *o*-phenylphenol, and 4-chloro-2-phenylphenol described previously.[1] Best performance was given by 4-chloro-2-benzylphenol (commercially available as Santophen-1) and 4-sec-butyl-2(α-methylbenzyl)phenol(BAMBP). The latter extractant is especially attractive owing to its low reactivity with sodium hydroxide, low loss to the aqueous phase, and compatibility with a wide selection of diluents.

The cesium extraction coefficient as a function of pH is shown in Fig. 9.1 for extractions from simulated adjusted Purex 1WW waste with 1 *M* solutions of several phenols in diisopropylbenzene. With BAMBP, the coefficient is ~2 at equilibrium pH 12, increasing to 6 at pH 12.5 and 22 at pH 13. With *o*-phenylphenol, 4-chloro-2-phenylphenol, and Santophen-1, the coefficients increase up to pH 12 to 12.3 and then decrease. The decrease at higher pH levels is due to loss of phenol, as the sodium phenate salt, from the solvent phase. At pH values of <12, where the effect of extractant loss on the coefficient is relatively small, the extraction power decreases in the order Santophen-1, 4-chloro-2-phenylphenol, BAMBP, and *o*-phenylphenol.

The measured loss of BAMBP to adjusted simulated 1WW solution increased with increase in pH but was still less than 0.5 g/liter to the aqueous phase at pH 13 (Fig. 9.2). The loss of Santophen-1 was <1.5 g/liter up to pH 11.5, but increased rapidly beyond that point, reaching ~15 g/liter at a pH of ~13. As described

[1] *Chem. Technol. Div. Ann. Progr. Rept. June 30, 1962*, ORNL-3314, p 120.

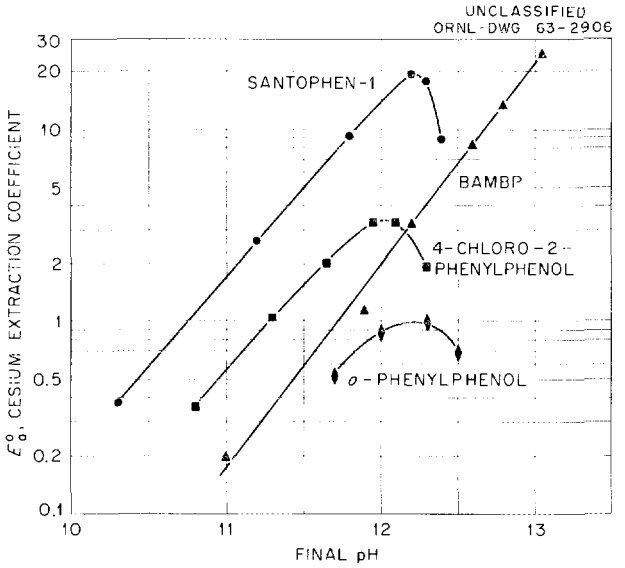

Fig. 9.1. Extraction of Cesium from Adjusted Purex 1WW with Phenols. Organic phase: 1 *M* substituted phenol in diisopropylbenzene. Aqueous phase: simulated 1WW, tartrate-complexed and diluted threefold with caustic to various pH levels. Contact: 5 min at phase ratio of 1/1.

previously,[1] high losses of phenol extractant can be avoided in a countercurrent extraction system by adding acid to the final extraction stage, converting the aqueous soluble sodium phenate to free phenol which redistributes to the solvent phase. This procedure is not necessary when using BAMBP because of its low loss and is probably not necessary with Santophen-1 when the pH of the aqueous phase is maintained at 11.5 or lower.

The type of diluent used with the phenols strongly affects their extraction behavior. Also, the extent and direction of these effects can vary with the type of phenol. With BAMBP, cesium extraction coefficients are 5 to 10 times higher with an aliphatic diluent (Amsco 125-82) than with aromatic diluents or carbon tetrachloride (Table 9.1). Conversely, Santophen-1 performs best in aromatic diluents and carbon tetrachloride.

Although the phenols are highly selective extractants for cesium, it is desirable to scrub the extract to remove entrained liquor from the solvent and to further increase the separations from contaminants. Test results demonstrated that, with the stronger cesium extractants such as BAMBP and Santophen-1, much more dilute hydroxide (0.01 *M* NaOH or 0.1 *M* NH_4OH) solutions can be used for scrubbing than were used previously[1] with *o*-phenylphenol.

In several batch countercurrent tests with BAMBP and Santophen-1 in diisopropylbenzene, the recovery of cesium from adjusted simulated Purex 1WW and simulated Hanford tank supernatants ranged from 97 to >99.7% in 6 extraction and 2 scrub stages. Typical cesium distribution results for a test with 1 *M* Santophen-1 and tartrate-complexed Purex 1WW (pH 12.3) are shown in Table 9.2. Cesium recovery was >99.7%. The aqueous-feed/organic ratio was 2/1, and the extract was scrubbed with one-third its volume with a 0.01 *M* NaOH–0.002 *M* sodium tartrate mixture. Acid was added to the last extraction stage to minimize phenol loss to the aqueous phase. The scrubbed extract was stripped quantitatively ($S_o^a = 1.5 \times 10^5$) in a single contact with 0.05 vol of 0.1 *M* HNO_3 to give a product solution containing 4.9 g of cesium and 0.035 g of sodium per liter. The overall cesium/sodium decontamination factor for the experiment was

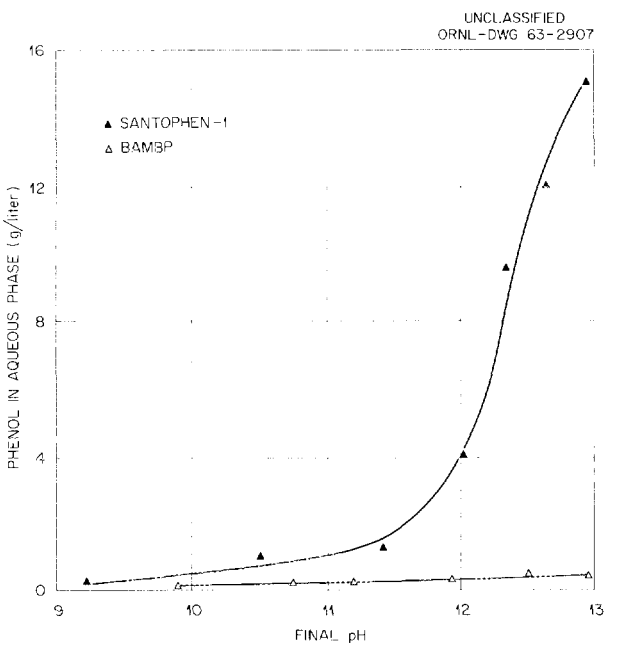

Fig. 9.2. Loss of BAMBP and Santophen-1 to the Aqueous Phase. Organic phase: ~1 *M* substituted phenol in diisopropylbenzene. Aqueous phase: tartrate-complexed 1WW adjusted to various pH levels while diluting threefold. Phase ratio: 1/1.

Table 9.1. Effect of Diluent Type on Cesium Extraction with Phenols

Organic: 1 *M* BAMBP or 1 *M* Santophen-1 in indicated diluent

Aqueous: simulated Purex 1WW,[a] tartrate-complexed (2 moles/mole of Fe), diluted threefold with caustic to pH 12.2

Contact: 2 min at a phase ratio of 1/1

Diluent	BAMBP		Santophen-1	
	Final pH	Cesium Extraction Coefficient, E_a^o	Final pH	Cesium Extraction Coefficient, E_a^o
Diisopropylbenzene	12.2	1.6	11.9	7.5
Diethylbenzene	12.2	1.5		
Xylene	12.2	0.8		
Toluene	12.2	0.7	12.0	5.1
Nitrobenzene	12.2	0.5	11.8	8.1
Amsco 125-82	12.2	7.9		*b*
98% Amsco 125-82–2% tridecanol	12.2	6.3		*b*
95% Amsco 125-82–5% tridecanol	12.2	4.9		*b*
80% Amsco 125-82–20% tridecanol			11.6	3.3
Carbon tetrachloride	12.2	1.9	11.9	18
Hexone	12.2	0.003	11.8	0.03

[a]The simulated Purex waste contained (moles/liter); 4.0 H^+, 4.45 total NO_3, 1.0 SO_4, 0.6 Na, 0.5 Fe, 0.1 Al, 0.005 U, 0.01 Ni, 0.01 Cr, 0.01 PO_4, 0.0028 Cs, 0.0066 Zr, 0.0019 Sr, 0.0034 Ce(III), 0.0058 Sm, and 0.0029 Ru.

[b]Santophen-1 is not sufficiently soluble to produce a 1 *M* concentration in these diluents.

$\sim 6 \times 10^4$. In a similar test, the overall cesium/rubidium decontamination factor was >200.

A process for recovering cesium from acid wastes by adsorption on ammonium molybdophosphate (AMP), dissolution of the AMP in caustic, and purification of the cesium by extraction with dipicrylamine in nitrobenzene has been described by British workers.[2,3] However, operation of the solvent extraction cycle is complicated by the small solubility of dipicrylamine in nitrobenzene and other diluents. Preliminary tests here indicate that the Phenex process is an attractive alternate for recovering cesium from the caustic liquor. In a batch demonstration test, cesium was adsorbed from simulated Purex 1WW (4 *M* H^+) on AMP, and the AMP was dissolved in caustic to give a solution containing ~7 g of cesium per liter. More than 99.8% of the cesium was extracted from this solution with 1 *M* BAMBP in diisopropylbenzene. Scrubbing with 0.05 *M* NaOH and stripping with 0.3 *M* HNO_3 gave a product solution containing 28 g of cesium, 0.02 g of sodium, 0.06 g of ammonium, <0.01 g of molybdenum, and <0.003 g of PO_4^{3-} per liter.

[2]J. van R. Smit, *The AMP Process for Caesium Separation. II*, AERE-R-4006 (April 1962).

[3]J. van R. Smit and F. C. W. Pummery, *The AMP Process for Caesium Separation. III*, AERE-R-4039 (February 1962).

Table 9.2. Batch Countercurrent Test with Santophen-1

Organic:	1 *M* Santophen-1 in diisopropylbenzene
Aqueous feed:	simulated Purex 1WW, tartrate-complexed (2 moles/mole of Fe), diluted threefold with caustic to pH 12.3; contained 0.12 g of Cs per liter and Cs^{134} tracer
Scrub solution:	0.01 *M* NaOH--0.002 *M* sodium tartrate
Acid (to 6*th* extraction stage):	3 *M* HNO_3
Contact:	batch countercurrent; 2-min contacts
Relative flows:	organic/aqueous feed/scrub/acid = 3/6/1/0.18

Stage	pH	Cesium Extraction Coefficient, E_a^o
Scrub-2		3.7
Scrub-1		4.2
Aqueous feed	12.3	
Extraction-1	11.7	9.7
Extraction-2	11.7	9.8
Extraction-3	11.7	9.2
Extraction-4	11.7	6.2
Extraction-5	11.1	~2.7
Extraction-6	8.7	

9.2 STRONTIUM AND RARE EARTHS

Further studies of the di(2-ethylhexyl)phosphoric acid (D2EHPA) extraction process[4,5] for recovering strontium and mixed rare earths from Purex waste included (1) investigation of rare-earth separations from yttrium, (2) comparison of tartrate and citrate as complexants for the first-cycle aqueous feed, and (3) further tests of first-cycle extraction selectivity.

In the hot-cell demonstration run[5] with Purex 1WW waste from Hanford, an apparent separation of rare earths from yttrium was obtained in the stripping cycle, but the results were not conclusive. To better define the separability, batch countercurrent runs were made with 0.3 *M* D2EHPA--0.15 *M* TBP--Amsco 125-82 that had been loaded with rare earths and yttrium (traced with Eu^{152} and Y^{91}). In tests simulating the first cycle, 98.5% of the europium but only ~5% of the yttrium were stripped with 1.2 *M* HNO_3 in 5 stages at an organic/aqueous flow ratio of 5/1. Since most of the fission product rare earths are stripped more easily than europium, stripping recoveries of the total rare earths would be higher in actual practice. Nearly the same results were obtained in tests simulating the second cycle. The results indicated that yttrium contamination of the mixed rare-earths product could be limited to <2% of the amount in the original waste solution. Following stripping of rare earths, yttrium can be recovered from the solvent with 3 to 4 *M* HNO_3.

A comparison of tartrate and citrate as complexing agents for Purex 1WW feed showed that the stability of the adjusted feed liquors and extraction results for strontium and cerium are greatly dependent on feed adjustment procedures. This is particularly true of the citrate system wherein some of the metal citrate complexes are formed slowly.[6] Because of these complications, it is difficult to obtain reproducible extraction results in these systems, and rigorous comparison of the complexing agents was not possible. However, under all conditions tested, extractions of strontium and cerium were appreciably higher from tartrate-complexed than from citrate-complexed feeds.

With 0.8 to 1.0 *M* citrate (based on the original 1WW volume) in the feed, considerable precipitation occurred when pH adjustment was made immediately following citrate addition. However, the amount of precipitate was small when the solution was aged 1 to 3 hr before pH adjustment, and the precipitate redissolved on standing. With tartrate, aging the solution before pH adjustment had no significant effect, and 0.9 *M* tartrate concentration was adequate to give stable feeds. In all these tests the complexing agent was dissolved in the simulated 1WW solution, and pH adjustment to 5 to 6 was made with 5 *M* or 19 *M* NaOH while diluting to 3 times the original 1WW volume.

[4] *Chem. Technol. Div. Ann. Progr. Rept. Aug. 31, 1960*, ORNL-2993, p 144.

[5] *Chem. Technol. Div. Ann. Progr. Rept. June 30, 1962*, ORNL-3314, p 116.

[6] R. E. Burns, *Recent Solvent Extraction Studies at Hanford Laboratories*, paper No. 23 presented at the Solvent Extraction Chemistry Symposium, Gatlinburg, Tenn., Oct. 23–26, 1962.

The coefficients for the extraction of strontium from citrate-complexed feed with 0.2 *M* D2EHPA–0.1 *M* NaDEHP–0.15 *M* TBP–Amsco 125-82 reached a maximum value of 8 at a pH of ~4 and then decreased (Fig. 9.3). From tartrate-complexed feed, the maximum coefficient was ~15 and occurred at a pH of ~5. Maximum cerium coefficients were 160 at a pH of ~3 from citrate-complexed feed, and ~250 at a pH of 3 to 5 from tartrate-complexed feed. In all these tests, the phases were mixed for 10 min and extractions were begun within 15 min after the pH adjustment.

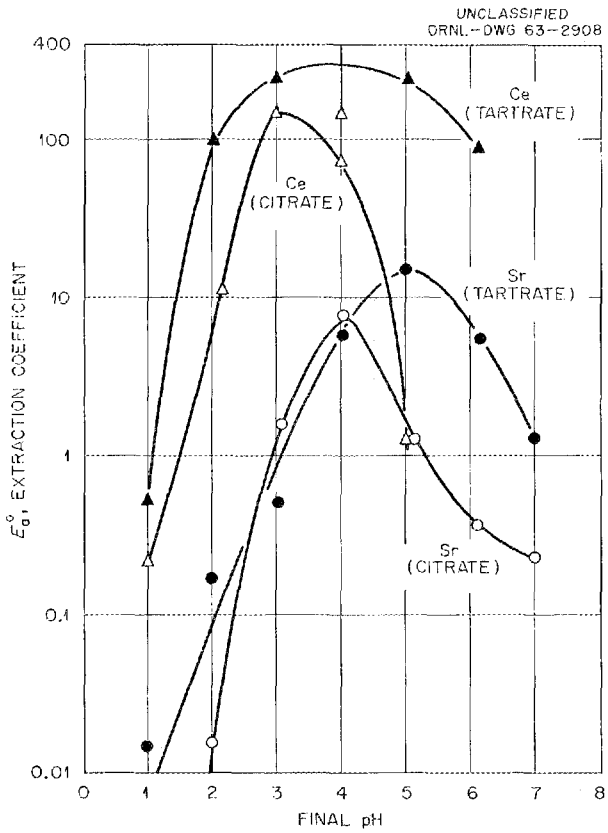

Fig. 9.3. Extraction of Strontium and Cerium from Adjusted Purex 1WW Solution. Aqueous phase: citrate or tartrate dissolved in simulated 1WW solution to 1 *M* concentration, solutions aged 1 hr, pH adjusted to 5 with caustic while diluting threefold. Organic phase: 0.3 *M* D2EHPA (portion in sodium salt form varied from 0 to 100%)–0.15 *M* TBP–Amsco 125-82. Phase ratio: 1/1. Contact time: 10 min.

As expected from earlier data,[5,6] the rates of cerium extraction at room temperature were low. For contact times of 1, 5, and 30 min, respectively, cerium extraction coefficients were 25, 78, and 220 from tartrate-complexed feed, compared with 6, 14, and 30 from citrate-complexed feed.

Batch extraction selectivity data were obtained under first-cycle extraction conditions (extraction at a pH of ~5 from tartrate-complexed 1WW) for uranium, aluminum, nickel, and chromium. Nearly all of the uranium in the feed and significant amounts of aluminum and nickel were extracted, whereas chromium extraction was inappreciable (E_a°, <0.04). Highly effective separations from uranium and aluminum are obtained in the stripping step since these elements are not removed with the strontium and the rare earths. Nickel tends to follow strontium through the process but can be eliminated by introducing 1 mole of ethylenediaminetetraacetic acid per mole of nickel in the third-cycle feed. This nearly eliminates nickel extraction without affecting strontium extraction.

9.3. OTHER STRONTIUM EXTRACTIONS

This section is reported in ORNL-3452, suppl 1.

9.4 ZIRCONIUM-NIOBIUM

The previously reported[7] slow extraction of zirconium-niobium with di(2-ethylhexyl)phosphoric acid (D2EHPA) from acid wastes can be overcome by raising the extraction temperature. For example, with 0.3 *M* D2EHPA–0.15 *M* TBP in Amsco 125-82, about 90% of the Zr-Nb was extracted upon contacting an equal volume of simulated Purex 1WW (4 *M* H^+) for 30 min at room temperature, whereas the same recovery was achieved in 10 min at 53°C and in 1 min at 83°C. Stripping of the Zr-Nb with 1 *M* oxalic acid is also temperature and time dependent. At 25°C and an organic/strip solution ratio of 5/1, Zr-Nb stripping coefficients were 0.77, 5.7, and 23, respectively, for contact times of 2, 10, and 30 min. At 50°C, the coefficients were 3.7, 14, and 41 for the same contact times.

[7] *Chem. Technol. Div. Ann. Progr. Rept. June 30, 1962*, ORNL-3314, p 123.

9.5 EXTRACTIONS FROM PUREX-WASTE CONCENTRATE WITH AMINES

Additional test results have confirmed those from earlier tests[7] that showed that nitric acid, iron sulfate, and certain fission products can be removed from Purex waste by amine extraction to produce aqueous feeds more amenable to the recovery of strontium and cesium. In a single contact, ~90% of the acid was extracted from simulated Purex 1WW waste (4 *M* H^+) with 0.24 *M* Primene JM in Amsco 125-82 at an organic/aqueous phase ratio of 15/1. This treatment also removed 72% of the ruthenium and 40% of the Zr-Nb, but <3% of the Fe, Sr, and Cs, from the waste. Except for the ruthenium and Zr-Nb content, the resulting aqueous solution is similar in composition to that produced in the process proposed for use at Hanford wherein the Purex 1WW waste is treated with formaldehyde to destroy nitrate.

By using simulated formaldehyde-treated waste (0.2 *M* H^+, 0.5 *M* Fe), the extraction of iron and acid was demonstrated in a batch countercurrent test with 0.24 *M* Primene JM (80% in sulfate salt form) in Amsco 125-82. About 94% of the iron was extracted in 2 extraction stages and 1 water scrub stage, whereas only ~5% of the cerium was extracted. The aqueous feed/organic/scrub flow ratios for the test were 1/9/0.5. Although Zr-Nb and ruthenium extractions were not followed, nearly complete removal of these elements with the iron would be expected.[7] More than 98% of the cerium was extracted later by contacting the raffinate (pH of ~1) with 6 successive volumes of 0.24 *M* Primene JM in Amsco 125-82 at an aqueous/organic ratio of 10/1.

10. Uranium Processing

10.1 RADIUM REMOVAL FROM URANIUM-MILL WASTE STREAMS

Effluents from uranium mills normally contain certain radioisotopes (e.g., Ra^{226}, Th^{230}, etc.) at concentrations too high to legally permit their direct discharge to the environment. With the exception of radium, all the isotopes can be removed adequately by lime neutralization of the acid waste. Preliminary studies, described previously,[1] indicated that radium could be removed effectively from the neutralized wastes by sorption on natural and synthetic zeolites. Recent column tests confirmed the utility of these sorbents and also showed that they can be regenerated with ammonium salt solutions, thereby effecting recovery of the radium and allowing for its permanent storage in a small volume.

The aqueous feed for these tests was synthetic lime-neutralized mill waste containing, in g/liter, 0.5 Ca^{2+}, 0.08 Mg^{2+}, 1.0 Na^+, 1.0 Cl^-, and 2.5 SO_4^{2-}, along with Ra^{226} tracer. The Ra^{226} concentration in the feed was 2200 to 2500 pc/liter (pc = picocurie = 10^{-12} curie), which is ~20 times the concentration normally expected in lime-neutralized waste solution. With Decalso (synthetic zeolite) the effluent activity was only 5% that of the feed solution after the passage of 6000 column volumes (Fig. 10.1). With clinoptilolite, the 5% breakthrough point was reached after the passage of 2000 column volumes. Elution with NH_4NO_3 solution regenerated both solids to their original capacity for subsequent cycles. Sorption during the initial portion of the subsequent cycles was somewhat less efficient (Fig. 10.1), and this is attributed to incomplete elution between cycles.

The elution of radium from clinoptilolite was much more efficient with ammonium nitrate or chloride solutions than with hydrochloric acid or sodium nitrate solution (Fig. 10.2). Elution curves for the ammonium salt solutions (~2 *M*) peaked after the passage of about four column

[1] *Chem. Technol. Div. Ann. Progr. Rept. June 30, 1962*, ORNL-3314, p 165.

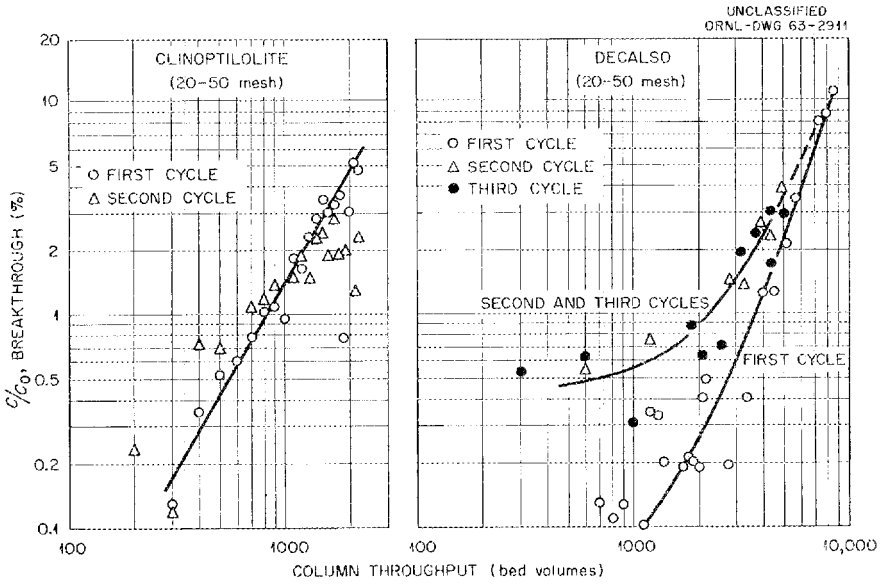

Fig. 10.1. Adsorption of Radium on Clinoptilolite and Decalso. Aqueous feed: synthetic lime-neutralized mill liquor containing, in g/liter, 0.5 Ca^{2+}, 0.08 Mg^{2+}, 1.0 Na^{+}, 1.0 Cl^{-}, and 2.5 SO_4^{2-}; spiked with 2200 to 2500 pc of Ra^{226} per liter. Column: 16-cm bed of 20 to 50 mesh clinoptilolite or Decalso in an 0.8-cm-diam column; one bed volume = 8.0 ml. Solution flow rate: 3 ml/min (90 gal hr^{-1} ft^{-2}).

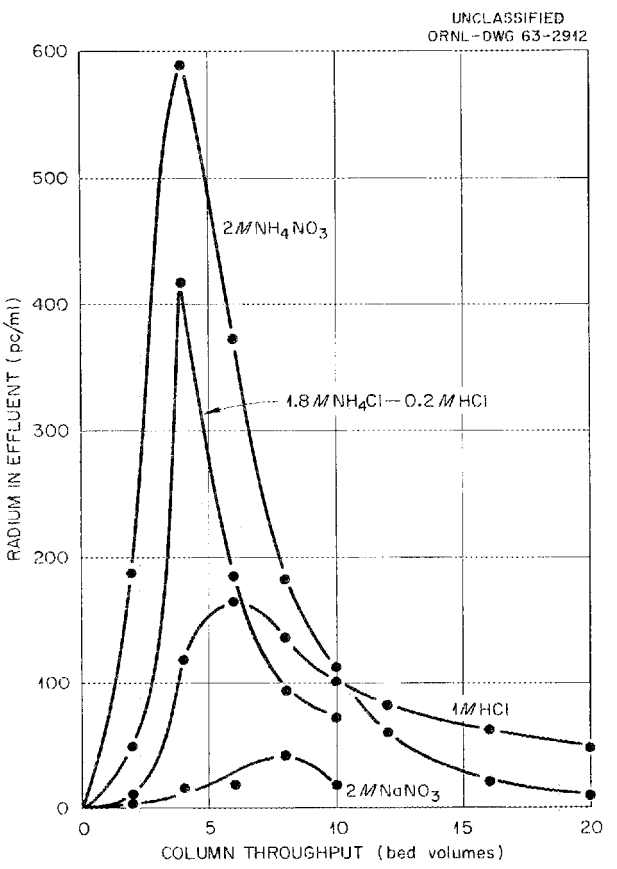

Fig. 10.2. Elution of Radium from Clinoptilolite. Eluting solution passed through column (0.8-cm-diam by 16-cm-deep bed of 20 to 50 mesh clinoptilolite) at rate of 1 to 2 ml/min; column contained 20,000 to 40,000 pc of Ra^{226} at start of tests.

volumes of eluate and then tailed off. Elution was >90% complete after the passage of ~20 column volumes.

More than 97% of the radium was removed from a 2 *M* NH_4NO_3 synthetic eluate containing 900,000 pc/liter of Ra^{226} by adding $(NH_4)_2SO_4$ to 0.02 *M* and then precipitating the sulfate[2] with a stoichiometric amount of $Ba(NO_3)_2$. The precipitate was granular and settled to <5% of the solution volume. This procedure affords recycle of most of the eluting agent with considerable saving in reagent costs. It has the additional advantage of concentrating the radium in a small volume that is easy to store.

Radium Adsorption from Acid Liquors

Decalso, zirconium phosphate, and ammonium molybdophosphate were completely ineffective as radium sorbents from a typical acid (pH 1) mill liquor. Clinoptilolite was partially effective; in a column test, radium breakthrough was ~20% after only 100 column volumes and ~100% after 1000 column volumes.

10.2 AMINE EXTRACTION OF URANIUM FROM SULFATE-CHLORIDE LIQUORS

Results from batch tests demonstrated that the *N*-benzyl secondary amines, which are unusually strong uranium extractants,[3] can be applied to recovery of uranium in plants that use the salt-roast acid-leach process for vanadium recovery. Heretofore, the use of the amine extraction (Amex) process in these plants was not feasible, owing to severe interference from chloride in the liquors on the extraction of uranium by the secondary and tertiary amines that are ordinarily used for uranium recovery. In a batch countercurrent test with 0.1 *M* *N*-benzyl-1-nonyldecylamine in kerosene and a typical synthetic leach liquor containing 1.5 g of uranium per liter and 0.3 *M* Cl^-, uranium recovery in five stages was >99.7%. The organic/aqueous flow ratio for the test was 1.7/1, and the uranium was stripped efficiently from the solvent with ammonium carbonate solution.

[2]M. H. Feldman, *Summary Report 1959–1961*, WIN-125 (Sept. 30, 1961).

[3]D. J. Crouse and K. B. Brown, *Amine Extraction Processes for Uranium Recovery from Sulfate Liquors*, ORNL-1959 (Nov. 18, 1955).

11. Thorium Recovery from Granitic Rocks

Although the reserves of high-grade thorium and uranium ores are appreciable, they are extremely limited in terms of the long-range needs. In order to satisfy anticipated power requirements, the world will eventually depend entirely on low-grade ores for its nuclear fuel supply. As an important factor in program planning, it is prudent to consider the amount and the cost of thorium and uranium that the earth can supply in support of a successful nuclear power economy. In the past, studies have been conducted at ORNL on several low-grade uranium sources such as shales, phosphate rock, and lignites. In the last three years, attention has been directed to granitic rocks, which comprise a large fraction of the earth's crust and which contain considerably more thorium than uranium. After tests of a large variety of such granitic rocks from different locations,[1–3] current interest has centered principally on the Conway granite formations in New Hampshire; these formations are especially attractive, due to their relatively high thorium content and good response to process treatment.

[1]*Chem. Technol. Div. Ann. Progr. Rept. May 31, 1961*, ORNL-3153, p 102.

[2]*Chem. Technol. Div. Ann. Progr. Rept. June 30, 1962*, ORNL-3314, p 182.

[3]H. Brown and L. T. Silver, *Proc. Intern. Conf. Peaceful Uses At. Energy, Geneva, 1955* 8, 129 (1956).

11.1 DRILL-CORE SAMPLES OF CONWAY GRANITE

Information on grade, extent, process amenability, and processing costs of the Conway granite was presented previously.[2] These data, however, were obtained from studies of outcrop samples; and predictions could not be made, with confidence, concerning the grade and properties of the deep, less-weathered material. Consequently, three drill cores were taken[4] during the summer of 1962 to depths of 500 to 600 ft at widely spaced locations in the central White Mountain batholith[5] (Fig. 11.1). Analyses by gamma-ray spectrometry showed uniform thorium concentration with depth (Table 11.1). The average thorium concentration in each of the three cores was 52, 53, and 67 ppm, in good agreement with the 56 ± 6 ppm thorium average for the entire formation, as calculated from previous analyses of several hundred surface samples. The average uranium content has not been accurately determined but is expected to be about a fourth or a fifth of the thorium content.

From the drill cores and other data, the thorium reserve in the outer 600 ft of the main Conway formations has been estimated at a minimum of 21 million tons.[4] It is probable that several times this amount could be made available by going to greater depths and by including smaller, outlying Conway granite bodies and related rocks in the White Mountain area.

---

[4]By Rice University, under subcontract to ORNL.

[5]Marland Billings, *The Geology of New Hampshire, Part II: Bedrock Geology*, New Hampshire State Planning and Development Commission, Concord, N.H. (1956).

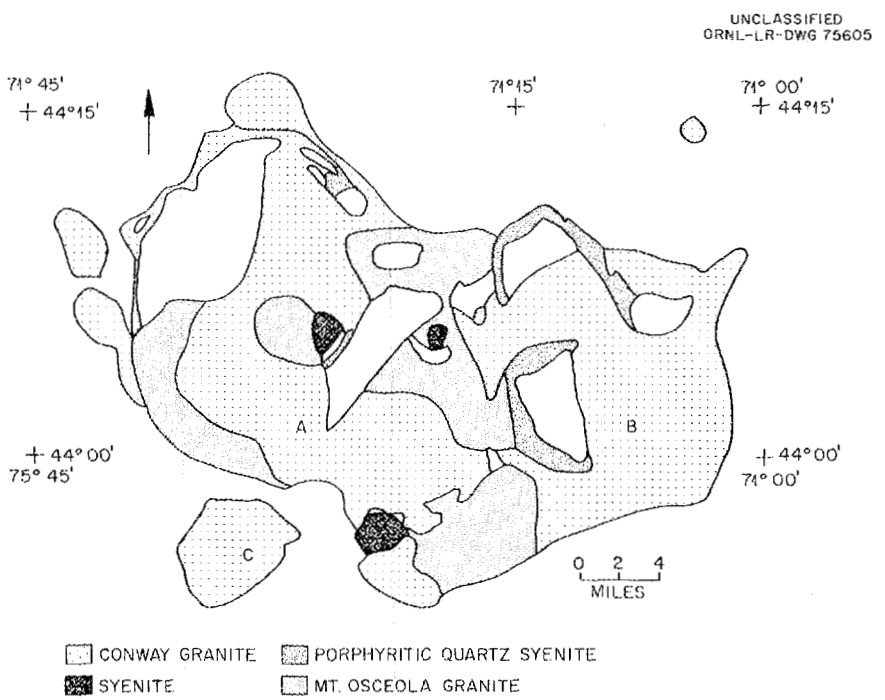

Fig. 11.1. Rock Types in Central White Mountain Batholith [as Mapped by Billings (ref 5) and Modified in Certain Areas by Rice University Geologists]. The letters A, B, and C show locations of the Kanca, Diana, and Mad River drill sites respectively.

Table 11.1. Thorium Content of Conway Granite Cores

Depth (ft)	Thorium Concentration[a] (ppm)		
	Kanca Core	Diana Core	Mad River Core
0–100	52	51	66
100–200	49	52	67
200–300	48	45	73
300–400	44	53	63
400–500	53	56	66
500–600	64	60	

[a]Average of radiometric measurements taken at 5-ft intervals.

11.2 CONWAY GRANITE MINERALOGY

Autoradiographic studies, petrographic studies, and heavy-mineral separations have been made to determine the mineral content of Conway granite. Thorite, huttonite, and zircon have been identified as the major carriers of thorium; zircon also carries uranium. In most samples, the radioactive minerals appear to be closely associated with biotite.

11.3 CONWAY GRANITE PROCESSING

Acid-leaching tests of drill-core samples showed no significant variation in thorium leachability with core depth. Thorium recoveries in a 6-hr leach with 2 N H_2SO_4 at 60% pulp density averaged 66% for the Kanca and Diana cores and 70% for the Mad River core. Total recovery costs, estimated on the same basis as that described previously,[1] were \$57, \$51, and \$37 per pound of thorium plus uranium for the Kanca, Diana, and Mad River core materials respectively.

A substantial portion of the thorium in Conway granite is dissolved rapidly by leaching with dilute acid at room temperature. Using 1 N H_2SO_4 at 60% pulp density, 45% of the thorium was dissolved from a typical sample in 10 min; and a maximum thorium recovery of about 60% was reached within 1 hr. Using 2 N and 3 N H_2SO_4, maximum thorium recoveries of about 80% and 90%, respectively, were obtained from the same sample within 3 hr. The ease of leaching is due to the liberation and exposure of most of the acid-soluble thorium minerals at this point. This is tentatively attributed to the apparent association of these minerals with biotite, which is readily reduced to thin platelets during crushing.

Other studies showed that the acid consumed during leaching should be lower in process practice than previously assumed. In earlier tests the granites were ground in a disk grinder; iron was added to the sample, which subsequently reacted with the sulfuric acid. In recent tests of samples ground in a pebble mill, the acid consumption has been 30 to 40% lower.

Physical beneficiation studies of Conway granite have shown some promise. In one test, about 70% of the thorium was recovered in a heavy-mineral separate that comprised 8% of the original ore weight. In another test, magnetic fractionation of the ore produced a magnetic product containing about 20% of the original ore weight and about 60% of the thorium.

11.4 THORIUM RESERVES AND COSTS

In contrast to the situation that seemed to exist several years ago,[6] the present information on thorium supply is highly encouraging. The recent reappraisal[7] of high-grade thorium reserves in the Lemhi Pass area has greatly multiplied the indicated reserves of low-cost thorium in the United States. At 100,000 to 400,000 tons of ThO_2, they are nearly as large, or larger, than the indicated low-cost reserves of uranium in the United States. There is apparently a sufficient supply of low-cost material to initiate a large-scale thorium fuel reactor industry, and it may be assumed that larger quantities will be found which could support the industry for an appreciable period of time.

The new information showing the sizable thorium reserves in Conway granite and in other granite formations of nearly equivalent quality gives confidence that the system could be maintained for a long period with thorium of moderate cost once

[6]Informal meeting on thorium (and uranium) reserves, held at ORNL on Feb. 29–Mar. 1, 1960, and attended by representatives of AEC Raw Materials Division, AEC Research Division, U.S. Geological Survey, Rice University, and ORNL.

[7]H. H. Adler, "The Economic Mineralogy and Geology of Thorium," paper presented at the Thorium Fuel Cycle Symposium, Gatlinburg, Tenn., Dec. 5–7, 1962.

the high-grade ores are depleted. Typical Conway granite can be processed for less than $75 per pound of recovered thorium plus uranium, and part of the material should be recoverable for less than $40 per pound. Compared with the low-grade uranium sources such as phosphates, shales, and lignites, the low-grade thorium sources are in a more favorable position from the standpoint of quantity and are equally favorable from the standpoint of cost.

By accepting lower-grade granites, immense reserves should become available, which could supply a nuclear power industry for an extremely long time at nonprohibitive costs, assuming the successful development of thermal-breeder reactor systems.

12. Protactinium Chemistry

The objective of the protactinium chemistry program is to study the nature of Pa(V) complexes in systems in which Pa(V) is reasonably soluble. The work during the past year was concerned primarily with the extractability from sulfuric acid solutions.

12.1 EXTRACTION OF PROTACTINIUM BY VARIOUS AMINES

The dependence of extraction coefficients of Pa(V) on the concentration of amine in the organic phase and of acid in the aqueous phase has been determined for several different amines. The three secondary amines *N*-benzylheptadecyl amine (NBHDA), LA-1, and S-24 dissolved in diethylbenzene were compared in most detail (Fig. 12.1). All gave qualitatively similar behavior. Highest extraction coefficients were obtained with *N*-benzylheptadecyl amine, with the benzyl group bonded to the nitrogen; intermediate extraction coefficients were found with Amine LA-1, which has a tertiary carbon atom bonded to the nitrogen and a conjugate double bond; lowest coefficients were found with Amine S-24, in which both chains have secondary carbon atoms bonded to the nitrogen. Of the amines investigated so far [the primary amines Primene JM-T and 1-(3-ethylpentyl)-4-ethyloctyl amine and the tertiary Alamine 336 in addition to the three secondary amines], there appears to be a strong correlation between the extraction power for Pa(V) and the base strength of the amine.

The variation of extraction power between different amines is so great that, by proper choice of amine system and its concentration, any reasonable extraction coefficient may be obtained. This would permit considerable flexibility should this system be used for processing application.

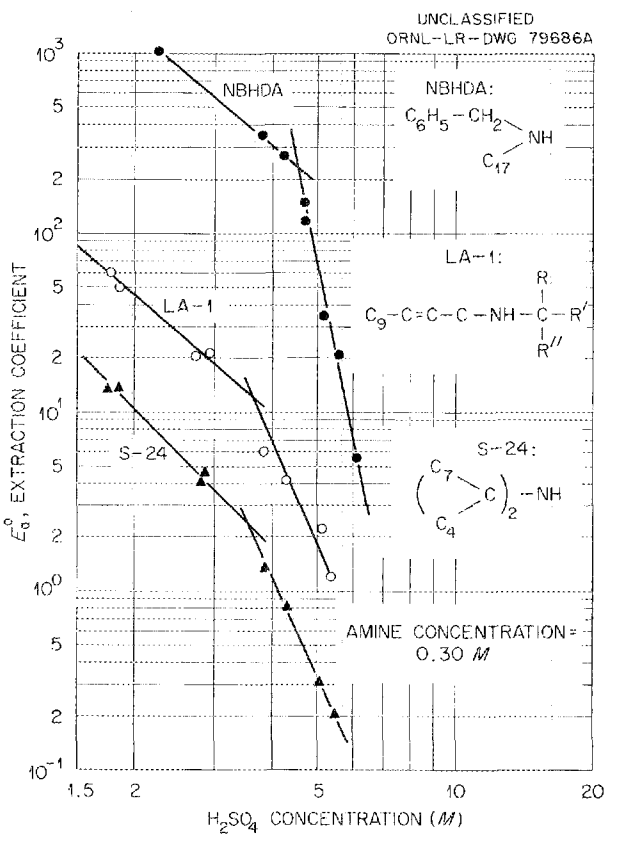

Fig. 12.1. Dependence of the Extraction Coefficient of Protactinium on H_2SO_4 Concentration in the Aqueous Phase (Extraction with Secondary Amines).

The marked decrease in extraction, observed with all amines, as the aqueous acid concentration is increased has received further attention. This effect might be attributed to a change in the aqueous-phase complexes of protactinium resulting from the change in acidity, as is often done with other acid systems; but with sulfuric acid there is also a change in organic-phase acidity with a change in aqueous acid concentration. The amine in equilibrium with aqueous sulfuric acid solutions exists primarily in two forms: the bisulfate (Amine-H^+) (HSO_4^-) and the sulfate (Amine-H^+)$_2$·(SO_4^{2-}). This is further complicated by association or aggregation of the amine. The fraction of the amine in the bisulfate form increases as the aqueous acidity increases. It has been demonstrated that some anions exchange more readily with the sulfate than with the bisulfate ion in the amine. The aqueous complex anion containing protactinium, which is the species extracting, might behave in a similar manner. In the extreme case, it might exchange, for practical purposes, only with sulfate. Then the decrease in the concentration of the sulfate form of the amine as the equilibrium aqueous acidity increased would result in a decrease in extraction, independent of any change in the aqueous protactinium complex.

A titration procedure was developed, permitting the determination of both the sulfate ion and the bisulfate ion concentration in the organic phase. It involves two potentiometric titrations of the amine dissolved in acetone, first with a standard chloride solution, which displaces sulfate preferentially and then displaces bisulfate, and second with standard NaOH to determine the bisulfate. The protactinium extraction coefficients correlate well with the sulfate concentration in the organic phase (Fig. 12.2). The extraction data for Amine S-24 are the same as that in the lower curve of Fig. 12.1, but the abscissa in Fig. 12.2 is the sulfate concentration in the amine in equilibrium with aqueous sulfuric acid. The abscissa in Fig. 12.1 is the concentration of aqueous sulfuric acid. The slope of the line is 1.7, and the data fit a linear correlation reasonably well.

Extraction experiments were also carried out with sulfuric acid–ammonium sulfate solutions at a constant total sulfate concentration of 3 *M*. As the acidity of sulfuric acid was decreased by adding 3 *M* diammonium sulfate, the extraction coefficient decreased rapidly to a broad minimum about the composition corresponding to ammonium bisulfate and then increased again as the acidity was further reduced. This is in marked contrast to the sharp increase in extraction observed when acidity was decreased by diluting sulfuric acid with water.

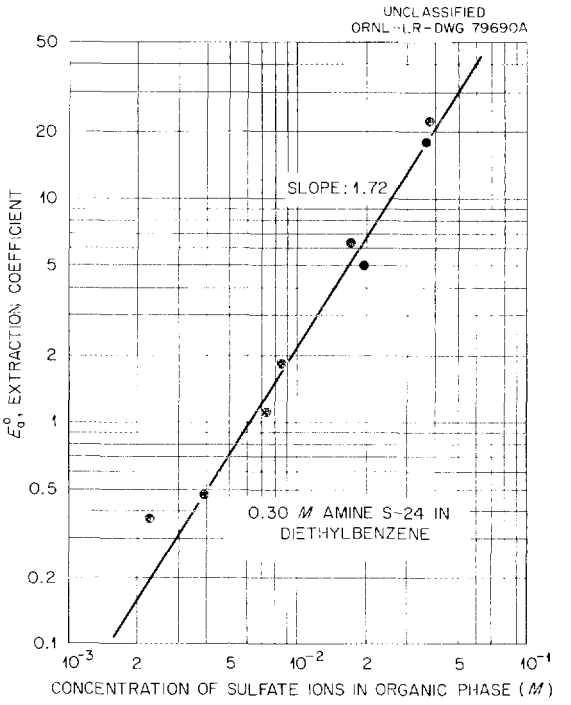

Fig. 12.2. Correlation of the Extraction Coefficient of Protactinium with Sulfate Concentration in Organic Phase (Amine S-24, 0.30 *M*).

12.2 ION EXCHANGE OF PROTACTINIUM FROM SULFATE SOLUTIONS

Extraction coefficients obtained with Dowex 1 resin varied with the amount of Pa(V) present and the phase ratio as well as with the aqueous sulfuric acid concentration. If the amount of protactinium and the phase ratio were both fixed, a smooth curve was obtained for the extraction coefficient plotted as a function of aqueous acid concentration. The curves so obtained were parallel to that reported previously by Brown *et al.*[1] It was found that all the data could be brought into approximate coincidence if the protactinium concentration in the aqueous phase in equilibrium with Dowex 1 was plotted against the aqueous acid concentration (Fig. 12.3). On a log-log plot, a

[1] D. Brown *et al.*, *J. Inorg. Nucl. Chem.* 23, 91 (1961).

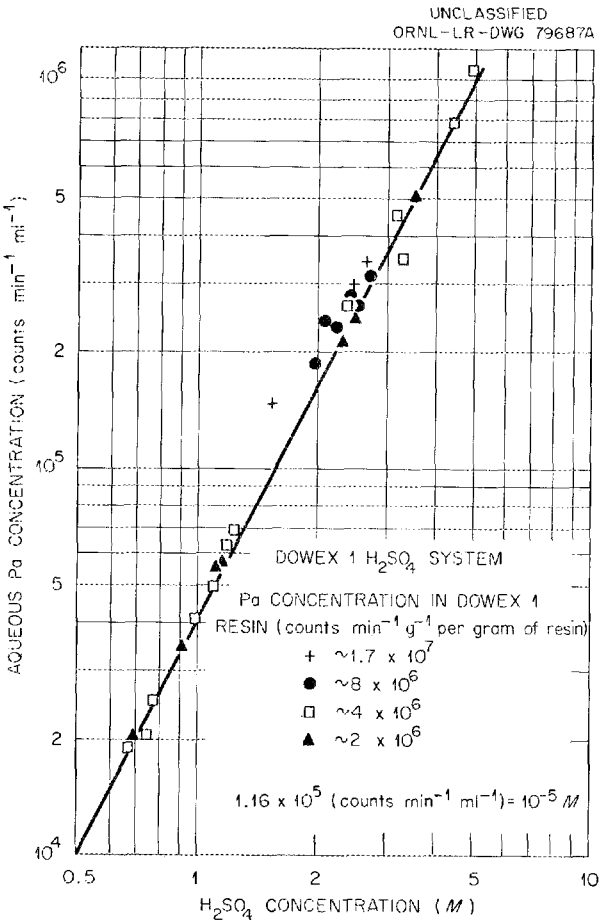

Fig. 12.3. Aqueous Protactinium Concentration in Equilibrium with Dowex 1 Resin.

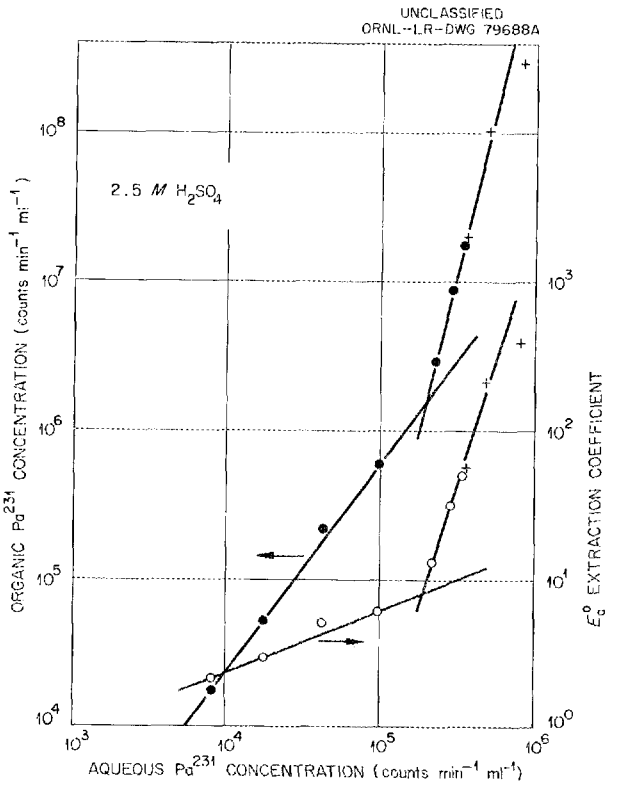

Fig. 12.4. Effect of Protactinium Concentration on Extraction into Dowex 1 Resin (H_2SO_4 = 2.5 *M*).

straight line of slope 2 fits the data over a remarkably wide range of acid concentration. As protactinium is added to sulfuric acid–Dowex 1 resin mixtures, nearly all the protactinium in excess of that given by the line in Fig. 12.3 goes into the resin phase. To elucidate this behavior, distribution measurements were also made at constant acid concentration (2.5 *M*) but at various protactinium concentrations (Fig. 12.4). The results show that at low protactinium concentrations, the extraction coefficient is nearly constant, increasing somewhat with protactinium concentration. However, at higher protactinium concentrations in the aqueous phase, at or above the concentration indicated by the line of Fig. 12.3, the protactinium concentration in the resin increases with the fifth power of the aqueous protactinium concentration. Thus, the behavior of protactinium in this system is much more complex than had been indicated previously.

12.3 POLYMERIZATION OF PROTACTINIUM

In previous solvent extraction work, extraction coefficients were large, and the aqueous protactinium concentrations were less than the values indicated for ion exchange by Fig. 12.3. In order to determine whether the dependence of extraction coefficient on protactinium concentration observed with Dowex 1 resin was a specific or a general effect, which also held for solvent extraction, a similar experiment was conducted with 0.03 *M* trilauryl amine and 2.5 *M* sulfuric acid containing varying amounts of protactinium. This amine gives relatively low extraction, so the aqueous protactinium concentrations could be conveniently increased to the range of interest. The results (Fig. 12.5) are similar to the curve for Dowex 1 resin.

The intersection of the two lines drawn asymptotic to the curve occurs at an aqueous Pa^{231} concentration of 2.2×10^5 counts min^{-1} ml^{-1} for trilauryl amine and 1.8×10^5 counts min^{-1} ml^{-1} for Dowex 1 resin, reasonably close to the same value. The corresponding organic Pa^{231} concentrations are quite different, 2.2×10^5 and 1.1×10^6 counts min^{-1} ml^{-1} respectively. The slopes of the lines are a little larger than unity for the low protactinium concentration region; that is, the extraction coefficients increase slightly with protactinium concentration. At higher protactinium concentrations, the slope is 3.2 for trilauryl amine and about 5.0 for Dowex 1 resin.

The behavior described above is in general agreement with a mechanism involving polymerization of protactinium in one or both phases (probably the aqueous phase), with both the polymer and the simpler species being extracted. The polymer is considered to be the more extractable species. Polymer formation is inhibited by increasing aqueous acid concentration, the dependence being second power, as suggested by Fig. 12.3. The polymer is small, perhaps a hexamer, and it is formed reasonably reversibly with respect to changes in both acid and protactinium concentrations. Calculations of distribution behavior based on this mechanism give results in quite good agreement with the curves in Figs. 12.4 and 12.5. However, it should be pointed out that such a mechanism does not fit all the observed data exactly and that even if it is approximately correct for these particular conditions, it is undoubtedly an oversimplification. In particular, there are some kinetic observations which indicate that more complex processes are occurring. This interesting and unusual behavior requires further study.

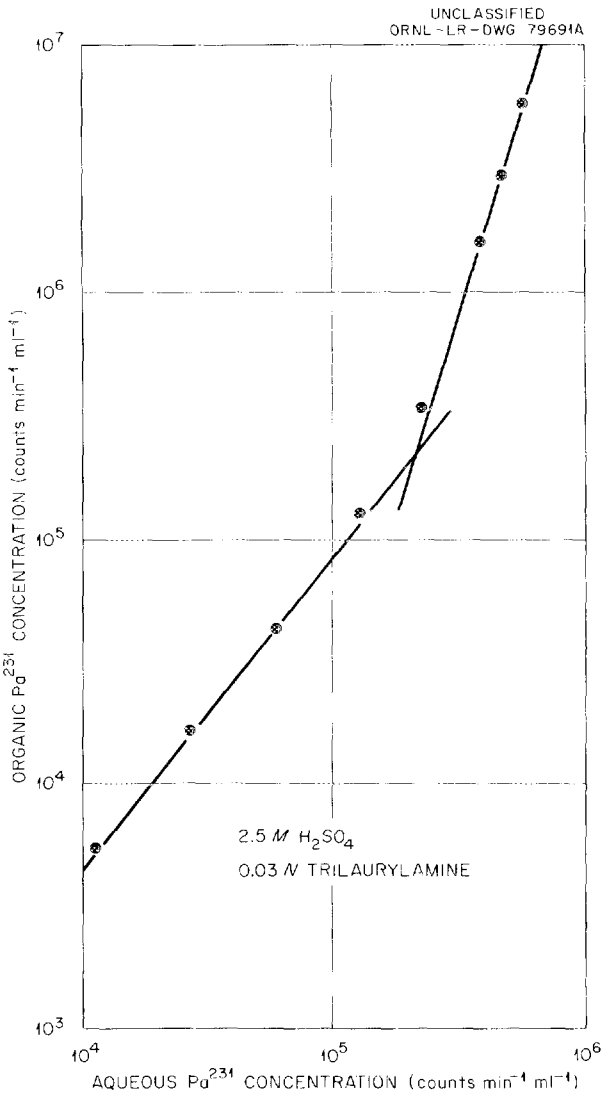

Fig. 12.5. Effect of Protactinium Concentration on Extraction into Trilaurylamine.

13. Effects of Reactor Irradiation on ThO_2

Examination of the several different thoria pellets and powder preparations irradiated in D_2O and dry in the LITR to exposures of 2.5×10^{18} fissions/gram is almost complete.[1] The preparations included the code P-82 thoria pellets;[2] sintered thoria compacts (prepared by a different method than that for the P-82 pellets);[3] shaped, arc-fused thoria pellets; fired, sol-gel-prepared thoria particles;[4] fired Houdry thoria spheres (44 to 74 μ);[5] arc-fused thoria fragments (44 to 74 μ); and 1600°C-fired thoria powder (DT-46).

The purpose of the experiment was to determine the influence of preparation method and physical condition on the irradiation effects and on any additional effects associated with the presence of water. Radiation effects were evaluated in terms of visual examination, material balances, wear tests, impact fracture tests, and x-ray and metallographic examination. Principal attention was paid to the P-82 pellets, which had shown the highest wear resistance (in attrition tests) of any pellets prepared by pressing and firing.[6]

The irradiations in D_2O were carried out in the LITR C-43 air-cooled facility at 250 to 300°C in a stainless steel autoclave especially designed for multiple-sample irradiations. The large particles or pellets were separately contained in thin-walled, annular, stainless steel tubes designed to permit thermal convection of D_2O past the pellets. The smaller-particle oxides were enclosed in single-walled, thin-walled tubes. All samples were exposed to a common gas (300 psi of oxygen at room temperature) or liquid. A wet, out-of-pile, control experiment was also carried out.

The dry irradiations of the samples were carried out in a helium atmosphere in welded aluminum capsules. The capsules were $\frac{1}{2}$ in. in outer diameter, $\frac{1}{4}$ in. in inner diameter, and $2\frac{1}{2}$ in. long. The irradiation was done in a modified fuel element in a stringer that permitted reactor cooling water (40°C) to flow over the outside of the capsules.

13.1 IRRADIATION EFFECTS ON P-82 THORIA PELLETS

The P-82 pellets irradiated under D_2O and dry showed minor weight losses but did not appear to undergo any structural damage. Evidently, however, only 13 of the 20 pellets irradiated in the wet experiment were submerged in D_2O during the irradiation, and the rest were irradiated in the vapor phase. The pellets irradiated in the vapor phase showed a significant weight loss as well as considerable surface and structural damage.

The P-82 pellets were prepared from oxalate-derived thorium oxide modified by refiring at 1425°C followed by wet ball milling in a steel mill, leaching with hydrochloric acid to remove abraded iron, mixing with 2% Carbowax, prepressing to 15,000 psi, granulating, and sizing to −35+100 mesh. Rounded-end pellets were pressed to green densities up to 6.3 g/cm^3. Roughness at the juncture of the dome and the cylinder was removed by first firing the pellets at 1450°C, cooling, and wet-tumbling. The pellets were then air fired at 1650°C in alumina. As prepared, the pellets had a pycnometric density of 9.16 g/cm^3. Pellets exposed to high-temperature water had densities of 9.6 to 9.7 before drying.

The materials irradiated dry lost less than 0.05% of their weight; those irradiated in D_2O, less than 0.4%; and the material in the vapor phase, 6.2%. During the 12-month irradiation, about 0.6% of the Th^{232} was converted to mass-233. The amount of U^{233} fissioned corresponded to a burnup of 0.11% of the original thorium atoms.

Figure 13.1 shows the original P-82 pellets and those recovered from the irradiation experiment. The pellets irradiated under D_2O and in the vapor phase were tan, similar to the originals but not glossy; those irradiated dry were gray-white. Other than the color change and an occasional chip where the domed end meets the side of the pellet, the pellets irradiated dry and under D_2O

---

[1] J. P. McBride, S. D. Clinton, and W. L. Pattison, *Chem. Technol. Div. Ann. Progr. Rept. June 30, 1962*, ORNL-3314, p 169.

[2] A. Taboada *et al.*, *HRP Progr. Rept. Nov. 30, 1960*, ORNL-3061, p 101.

[3] A. Taboada *et al.*, *HRP Progr. Rept. May 31, 1961*, ORNL-3167, p 110.

[4] Prepared by C. E. Schilling, Chemical Technology Division, ORNL.

[5] Houdry Report 58-OCR-15, June 1958; subcontract 904 under W-7405 eng-26.

[6] E. L. Compere *et al.*, *HRP Progr. Rept. May 31, 1961*, ORNL-3167, p 84.

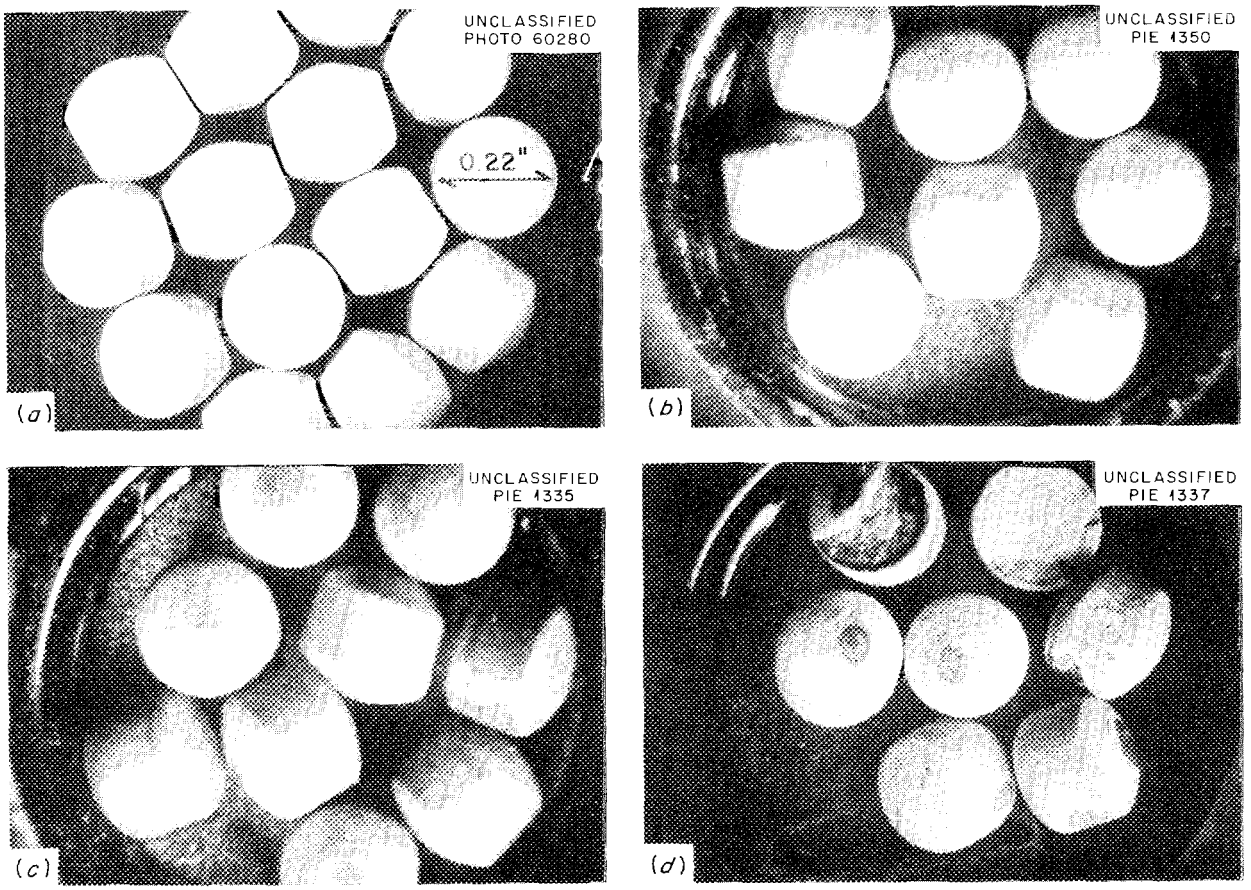

Fig. 13.1. The Original P-82 Thoria Pellets and Those Recovered from the 12 Months' Irradiation Experiment. (*a*) Original; (*b*) irradiated dry; (*c*) irradiated in D_2O; (*d*) irradiated in D_2O vapor.

appeared undamaged. Those irradiated in the vapor phase showed sand-like surfaces, and in the exposed interiors of the broken pellets a black peripheral layer just underneath the outer shell. Two of the pellets irradiated in the vapor phase were broken during a brief, relatively mild, wet stirring carried out to rid the surfaces of steel corrosion products. Extended stirring of original pellets and liquid-phase-irradiated pellets did not produce any breakage.

Pellets prepared by the procedures used in preparing the P-82 pellets have a wear-resistant, vitreous-like surface layer that appears to account for their marked stability to ordinary attrition. In spouting-bed wear tests with unirradiated materials, this layer is worn away in the first hour or two, and then the wear rate increases. Twelve months of wet and dry irradiation appears not only to have enhanced the wear resistance of this surface layer but to have made the interior of the pellet more attrition resistant (see Table 13.1). With the exception of an occasional pit, wear of the dry- and D_2O-irradiated pellets appeared to be uniform and showed little radiation-induced structural damage. Subsequent chemical analysis of material abraded from the surfaces of unirradiated P-82 pellets (about 0.4% by weight of the pellets) showed the surface to contain an aluminum/thorium weight ratio of about 0.08, in contrast with an average aluminum content of 0.02% for whole pellets. The aluminum apparently became incorporated in the pellet during the final firing at 1650°C, which was carried out in alumina. (The addition of the aluminum was therefore accidental.)

Table 13.2 gives the results of impact fracture tests on the original pellets, those from the 12-month-long D_2O-control experiment, and irradiated pellets from the 12-month and a previous 3-month

irradiation.[1] No decrease in structural strength appears to have resulted from irradiation dry and in D_2O. The pellet irradiated in the vapor phase is definitely weaker. This was also indicated by the breakage observed during the stirring mentioned above. The fracture test consisted in dropping a pestle down a loose fitting tube onto a pellet contained in a mortar. The pestle was dropped in a pattern of increasing heights until the pellet broke. In all cases, the pestle was dropped normal to the cylindrical side of the pellet.

The interiors of the 12-month, liquid-phase-irradiated pellets were similar to those in the unirradiated pellets, while those of the dry-irradiated materials were black. Heating at 400°C for an hour in air failed to remove the black color, but heating at 900°C overnight restored the original color. No weight increase

Table 13.1 Wear Rates of P-82 Thoria Pellets

Irradiation exposure: 2.5×10^{18} fissions per gram

Pellets	Weight Loss (%/hr)					
	1st	2d	3d	4th	5th	6th
Original	0.20	0.74	0.71	0.72	0.76	0.69
D_2O control	0.26	0.59	0.62	0.64	0.66	0.82
Irradiated dry	0.05	0.25	0.22	0.48	0.50	0.46
Irradiated in D_2O	0.15	0.34	0.41	0.41	0.44	0.49

Table 13.2 Results of Impact Fracture Test on P-82 Thoria Pellets

Pellet	Instantaneous Impact Energy (in.-lb)	Cumulative Impact Energy (in.-lb)
Original	0.651[a]	4.52[a]
D_2O control	0.893[b]	8.14[b]
7×10^{16} fissions/g		
D_2O liquid[c]	0.788	6.30
Dry helium atmosphere	0.683	4.78
2.5×10^{18} fissions/g		
D_2O liquid[c]	0.893	8.04
D_2O vapor[c]	0.342[b]	1.34[b]
Dry helium atmosphere	0.945	8.98

[a]Average of five tests.
[b]Average of two tests.
[c]Oxygen overpressure.

was noted as a result of the 900°C heating, and it is postulated that the black color resulted from a very slight oxygen deficiency.

The x-ray and metallographic data obtained for the P-82 pellets will be discussed in Sec 13.4, along with that obtained for the other thoria preparations.

13.2 IRRADIATION EFFECTS IN THORIA PELLETS PREPARED BY A PRESSING AND FIRING PROCEDURE DIFFERENT FROM THAT FOR P-82 PELLETS

The unirradiated and irradiated pellets prepared by what was considered a more promising method than that used in preparing the P-82 pellets are shown in Fig. 13.2. Thirteen of the twenty pellets irradiated under D_2O were badly damaged or disintegrated, the products sintering into the irregularly shaped masses shown in the picture. The vapor-phase-irradiated pellets did not appear to be as severely damaged. The dry-irradiated pellets were black but appeared undamaged.

These pellets had been formed from a very reactive thoria powder by first forming it into cubes with the aid of an organic binder and, without firing, abrading the dry cubes into spheres. The spheres were then fired at 1300°C, tumbled in water to polish the surfaces, and then given a final firing at 1800°C in a molybdenum furnace

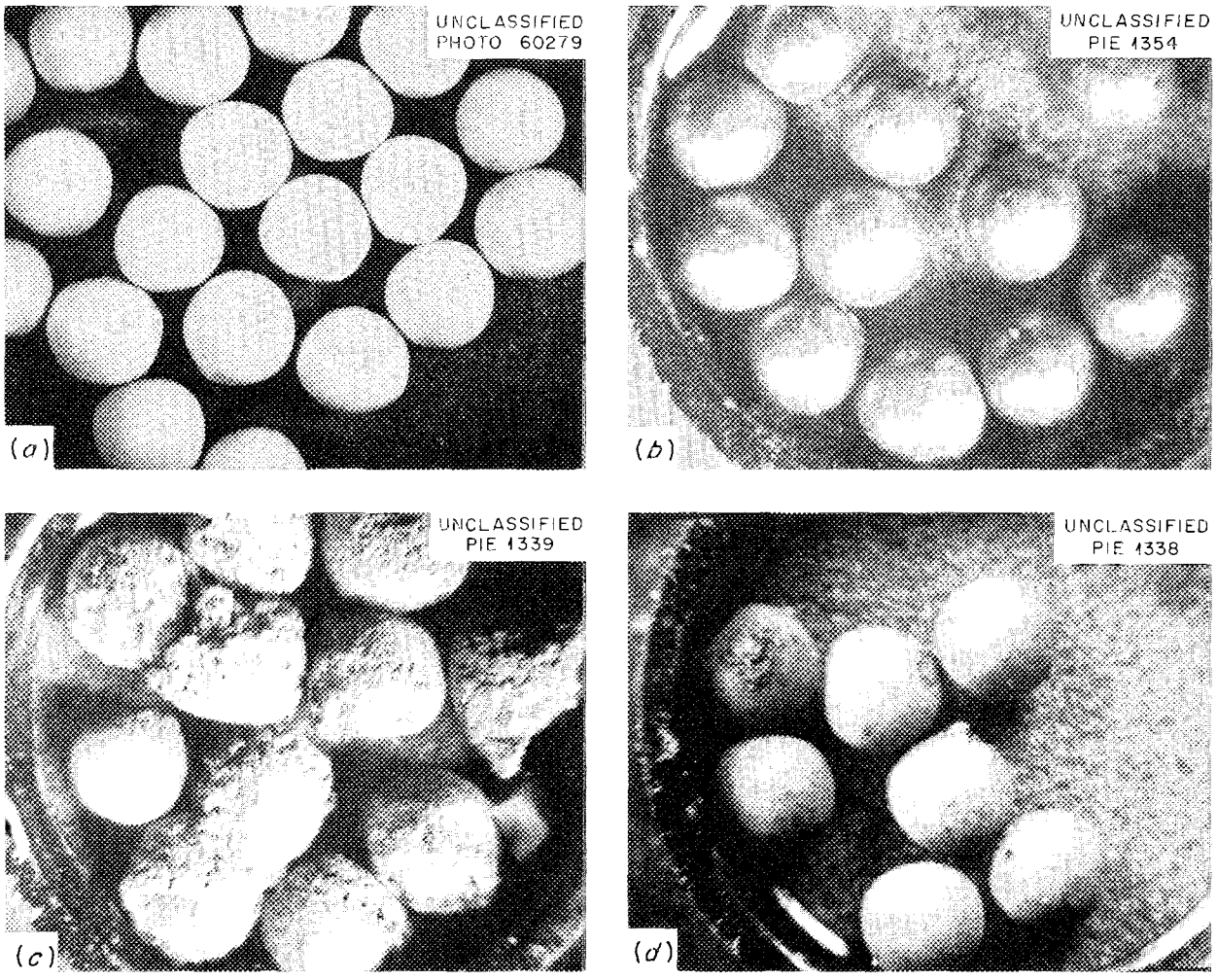

Fig. 13.2. Thoria Pellets Prepared by the Pressed-Cube Technique, As-Prepared and After 12 Months' Irradiation. (*a*) As-prepared; (*b*) irradiated dry; (c) irradiated in D_2O; (*d*) irradiated in D_2O vapor.

and a hydrogen atmosphere. The final density of the pellets was 9.8 g/cm^3.

Despite their high density, these pellets were damaged considerably by irradiation. Their low radiation resistance points up again the contribution of the surface shell to the radiation stability of the P-82 pellets and indicates the possible desirability of incorporating a small amount of another oxide, such as alumina, in thoria pellets in order to enhance their radiation stability.

13.3 IRRADIATION EFFECTS ON OTHER THORIA PREPARATIONS

Arc-Fused Thoria Pellets

Both the wet- and dry-irradiated arc-fused pellets appeared virtually undamaged by the irradiation. Those irradiated under D_2O showed a 0.5% weight loss and were gray, with occasional areas of adsorbed corrosion products (Fig. 13.3); the dry irradiated ones were opaque-black. The original pellets were partially rounded, light-red, translucent cubes. While the dry-irradiated pellets appeared opaque-black, the interior, revealed by shattering one of the pellets, appeared similar to the interior of the unirradiated ones.

The arc-fused pellets were prepared by cutting a large chunk of black, arc-fused thoria (prepared in a carbon arc by the Norton Company) into cubes, treating the cubes with moist oxygen at 1000°C (to remove carbon impurities), autoclaving them in 300°C water, agitating to eliminate cubes containing grain boundaries, and finally tumbling them in a spouting bed to round the corners. The wet-irradiated materials were especially selected cubes, evidently monocrystalline, as indicated by x-ray and metallographic examination. Pycnometric density measurements indicated them to be of theoretical density.

Fired Sol-Gel-Prepared Thoria Particles

Neither the dry-irradiated sol-gel-prepared materials nor those irradiated under D_2O appeared significantly affected by the irradiation except for color changes, although examination of the wet-irradiated materials was hampered by a deposit of corrosion products. Here and there in the wet-irradiated material a fragment showed a red discoloration, some cracks, and some surface attack, and it is presumed that these had been irradiated in the vapor phase (Fig. 13.4). The dry-irradiated solids were light orange and appeared somewhat translucent, as contrasted to the opaque whiteness of the originals.

The sol-gel-prepared materials were prepared by sol-gel methods that were still in the early stages of development, with a final firing at 1200°C; they were of theoretical density. Prior

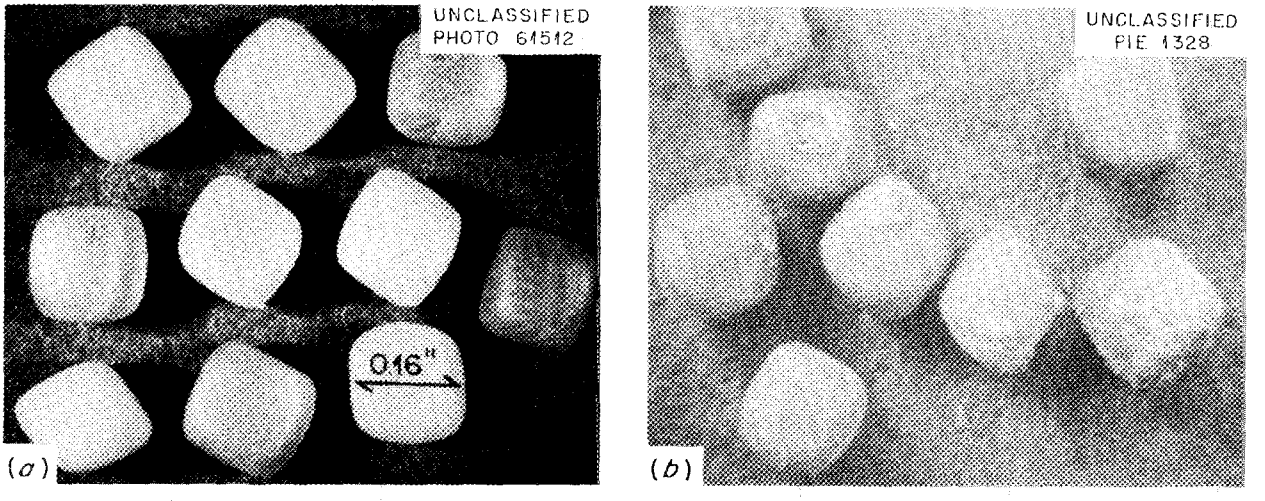

Fig. 13.3. Original As-Fused Pellets and Those Irradiated Under D_2O. Exposure: 2.5×10^{18} fissions/gram. (a) Original; (b) irradiated. 3.3X. Reduced 15%.

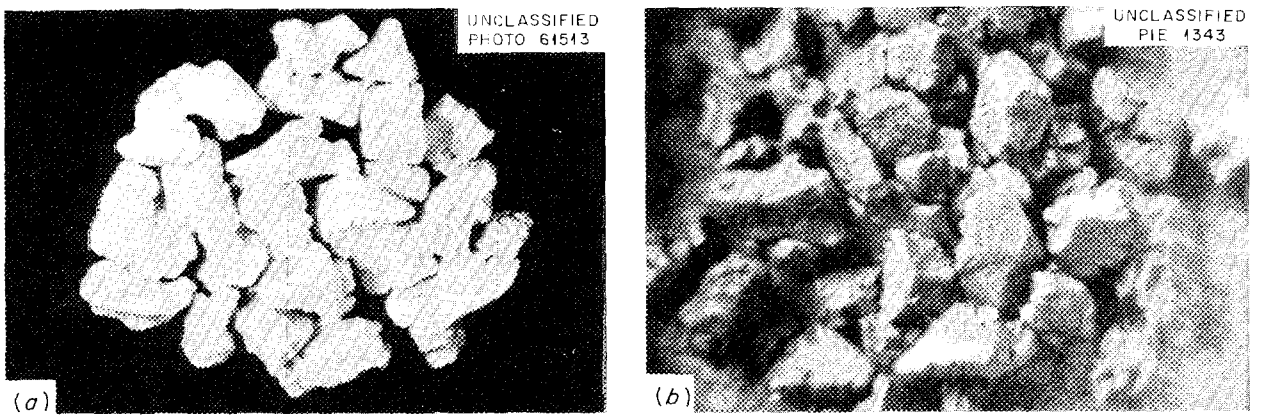

Fig. 13.4. Original Sol-Gel-Prepared Particles and Those Irradiated in D_2O. Exposure: 2.5×10^{18} fissions/gram. (*a*) Original; (*b*) irradiated. 3.3X. Reduced 26.5%.

to irradiation, the particles were rounded in a spouting-bed test.

Thoria Powders

The 44- to 74-μ materials, especially the ground arc-fused material, did not appear to be grossly changed by the irradiation. The wet-irradiated Houdry spheres showed some loose agglomeration, but their examination was hampered by a deposit of corrosion products. The dry-irradiated Houdry spheres were multicolored, reminiscent of the orange translucency encountered with the irradiated sol-gel-prepared material.

The wet-irradiated DT-46 powder had escaped from its stainless steel container around the fritted disk that formed the closure and then had settled on a lower container. It had transformed into a porous plug (readily broken in two) that contained a total of 2% iron, nickel, and chromium impurity. The dry-irradiated material had formed a chalky plug of the same shape as the interior of the aluminum container, and it broke into several pieces during its recovery (Fig. 13.5). The original DT-46 powder (prepared by thermal decomposition of the oxalate) had a surface area of 0.76 m^2/g, an average crystallite size greater than 2000 A, and a geometric mean particle size of 2.3 μ, with a geometric mean standard deviation of 1.34.

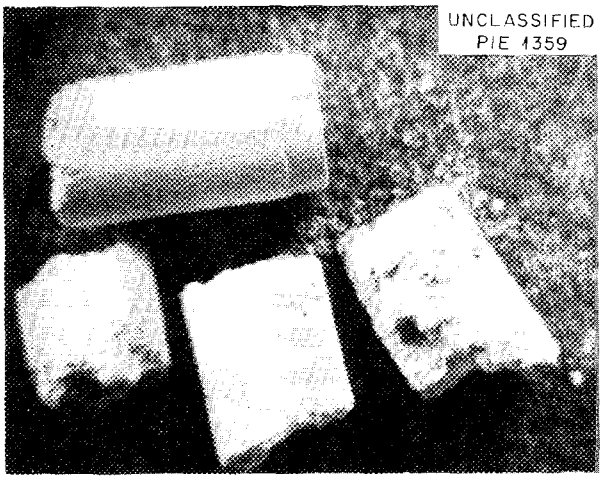

Fig. 13.5. Dry-Irradiated 1600°C-Fired Thoria Powder (DT-46). Exposure: 2.5×10^{18} fissions/gram. 3.3X. Reduced 17%.

13.4 RESULTS OF X-RAY AND METALLOGRAPHIC EXAMINATION OF IRRADIATED THORIA: P-82 PELLETS, ARC-FUSED PELLETS, AND SOL-GEL-PREPARED PARTICLES

The x-ray diffraction measurements on the P-82, arc-fused, and sol-gel-prepared materials indicated

that relatively little change had occurred as a result of the irradiation, indicative of the marked resistance of cubic structures to radiation damage.[7] The material irradiated under D_2O showed a slight lattice expansion (less than 0.5%), while that irradiated dry appeared unaffected. Apparent crystallite sizes for the irradiated P-82 and sol-gel-prepared materials ranged from 950 to 2000 A, compared with original crystallite sizes uniformly greater than 2000 A. Hence there may have been some slight crystallite damage. Diffraction patterns of the irradiated, arc-fused pellets, which were originally monocrystalline, indicated that no extensive formation of large angle boundaries occurred in the pellets as a result of the irradiation.

Polished sections, examined at low magnification, of the unirradiated and irradiated P-82 and arc-fused materials were similar. The irradiated sol-gel-prepared material exhibited extensive fracturing, as though irradiation had caused some embrittlement or had relieved strains by cracking. At high magnification, the polished and etched sections of all irradiated and unirradiated materials were similar. The irradiated P-82 pellets showed the varied density structures and grain sizes typical of this material; the irradiated arc-fused and sol-gel materials showed the typical microporosity and lack of grain structure.

13.5 CONCLUSIONS

Several very interesting facts were revealed as a result of the irradiations and the postirradiation examination. One is the marked stability of the P-82 thoria pellets compared with that of the other sintered pellets, possibly imparted by the presence of aluminum oxide in its surface shell. This points up the possible desirability of incorporating small amounts of alumina or other metal oxides in the thoria to enhance its radiation stability. It would also appear to indicate that pure thoria bodies prepared by pressing and firing are unlikely to be stable to reactor irradiation in the presence of water. Such a conclusion is not necessarily warranted in the case of the sol-gel-prepared materials since they did not exhibit the serious damage observed with the sintered thoria prepared differently from the P-82 pellets.

Another fact which complements previous information[8,9] is the sintering of the oxalate-prepared 1600°C-fired thoria powder both dry and settled under D_2O. A satisfactory reactor slurry may require the preparation of dense particles, preferably spherical, of greater than 3 μ in size and of low surface area to minimize sintering of the starting particles. If these particles degrade during irradiation and pumping to crystallite sizes of 200 A or less, as was the experience in in-pile loop tests with oxalate-prepared oxides by Compere,[10] additional studies are required to define the long-term stability of the resulting suspension.

A third fact is the marked stability of the thoria cubic lattice to irradiation damage. This agrees with irradiation data on UO_2 and lends confidence that properly prepared thoria bodies should be structurally stable to rather high irradiation exposures. Failure of irradiation to disrupt the grain structure in the P-82 pellets and to produce extensive formation of large angle boundaries in the arc-fused material further substantiates such a conclusion. Whether radiation-induced recrystallization to give small angle boundaries actually did occur in the arc-fused material can be answered definitively after the material has cooled sufficiently to obtain a Laue x-ray pattern.

---

[7] B. Lustman, p 569 in *Uranium Dioxide: Properties and Nuclear Applications* (ed. by J. Belle), GPO, Washington, 1961.

[8] J. P. McBride and S. D. Clinton, *Radiation Induced Sintering of Thoria Powders*, ORNL-3275 (July 20, 1962).

[9] J. P. McBride, *Radiation Stability of Aqueous Thoria and Thoria-Urania Slurries*, ORNL-3274 (May 18, 1962).

[10] E. L. Compere *et al.*, *Reactor Chem. Div. Ann. Progr. Rept. Jan. 31, 1963*, ORNL-3417, pp 111, 114.

14. Radiation Effects on Catalysts

14.1 CONVERSION OF CYCLOHEXANOL TO CYCLOHEXENE WITH $MgSO_4$ AND $MgSO_4$-Na_2SO_4 CATALYSTS

It has been previously reported that the incorporation of S^{35} into $MgSO_4$ and $MgSO_4$-Na_2SO_4 reduced the catalytic activity of these materials for the dehydration of cyclohexanol.[1] From the experimental evidence obtained, it was concluded that the effect was "built into" the catalyst during the crystallization and sintering procedures used in its preparation. In order to confirm that the effect resulted from the presence of radiation, and not from chemical contamination, several experiments were performed in which $MgSO_4$ catalyst was deliberately contaminated with $Mg(ClO_4)_2$, MgO, and leachings from Amberlite IR-120 ion exchange resin. The first two contaminants could be generated in the radioactive catalysts from the decay of S^{35} in the sulfate radical (beta decay to Cl^{35} to produce ClO_4^- from SO_4^{2-}) and the subsequent thermal decomposition of any $Mg(ClO_4)_2$ formed. Ion exchange resin was utilized in the purification procedure for the $H_2S^{35}O_4$ used in preparing radioactive catalysts; and, conceivably, some contamination from the resin could have survived the final distillations involved, though the chances were remote. None of the contaminants introduced had any effect on the catalytic activity. Thus it still appears that the presence of the radiation from the S^{35} is responsible for the decrease in catalytic activity of the radioactive materials.

Two experiments with nonradioactive catalysts were performed in a constant-volume closed system to determine the order of the reaction. The reaction vessel was maintained at constant temperature in a bath of Dow-Corning 550 silicone fluid, and the extent of reaction was continuously monitored by means of a Dynisco pressure transducer connected to a recorder. The pressure was recorded as a function of time until it remained constant for at least 30 min. Graphs of the logarithm of the difference between the final pressure p_∞ and the pressure p at time t vs t were found to be linear up to 88% completion in the case of $MgSO_4$ and up to 66% completion in the case of $MgSO_4$-Na_2SO_4 (see Fig. 14.1), indicating an overall reaction order of 1. Similar experiments at 350°C indicated that the reaction attained equilibrium after 25 to 30% of the cyclohexanol had been dehydrated.

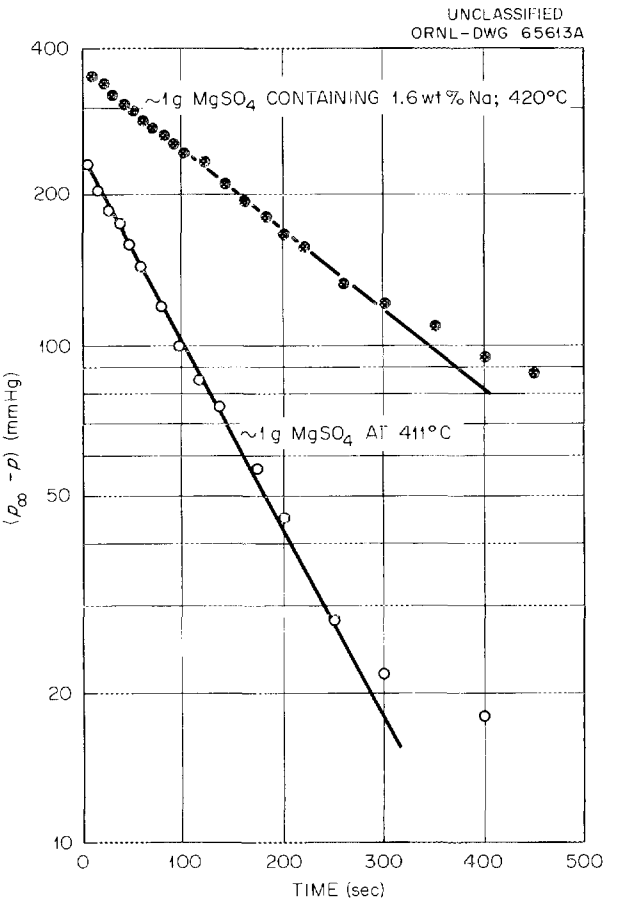

Fig. 14.1. First-Order Rate Plots for the Catalytic Dehydration of Cyclohexanol.

[1] *Chem. Technol. Div. Ann. Progr. Rept. June 30, 1962*, ORNL-3314, p 184.

15. High-Temperature Chemistry[1]

15.1 HIGH-TEMPERATURE, HIGH-PRESSURE SPECTROPHOTOMETER SYSTEM

The program for the absorption spectrophotometric study of aqueous solutions at high temperatures and high pressures has been discussed in recent reports,[2,3] and a more extensive review of the program has been given previously.[4]

A complete spectrophotometric system that can be operated at temperatures to at least 330°C and at pressures to at least 5000 psi with highly radioactive (alpha) solutions was designed under subcontract for ORNL by the Applied Physics Corporation, Monrovia, California. The general features and details of this system have been more fully discussed elsewhere.[5] A schematic layout of the cell system of the high-temperature, high-pressure spectrophotometer system and a photograph of the cell components have been presented recently.[2] Layout of the principal components and special features of the system is shown in Fig. 15.1.

A prototype high-temperature, high-pressure absorption cell was delivered by the subcontractor. A test facility for elevated temperature-pressure experiments with the cells was assembled for hydrostatic and gas pressure testing to 10,000 psi with a cell at the maximum temperatures anticipated. The prototype cell is undergoing testing to determine leak-tightness and the optimum conditions for the anticipated operating conditions. Some refinements were made in the cell design,

[1] Joint program with the Analytical Chemistry Division.

[2] *Chem. Technol. Div. Ann. Progr. Rept. June 30, 1962*, ORNL-3314, pp 187–90.

[3] *Anal. Chem. Div. Ann. Progr. Rept. Dec. 31, 1962*, ORNL-3397, pp 26–32.

[4] *Anal. Chem. Div. Ann. Progr. Rept. Dec. 31, 1961*, ORNL-3243, pp 21–22.

[5] R. E. Biggers and R. G. Wymer, *Design and Development of a High-Temperature, High-Pressure Spectrophotometer System: Status Report*, ORNL CF-60-11-96 (Nov. 12, 1960).

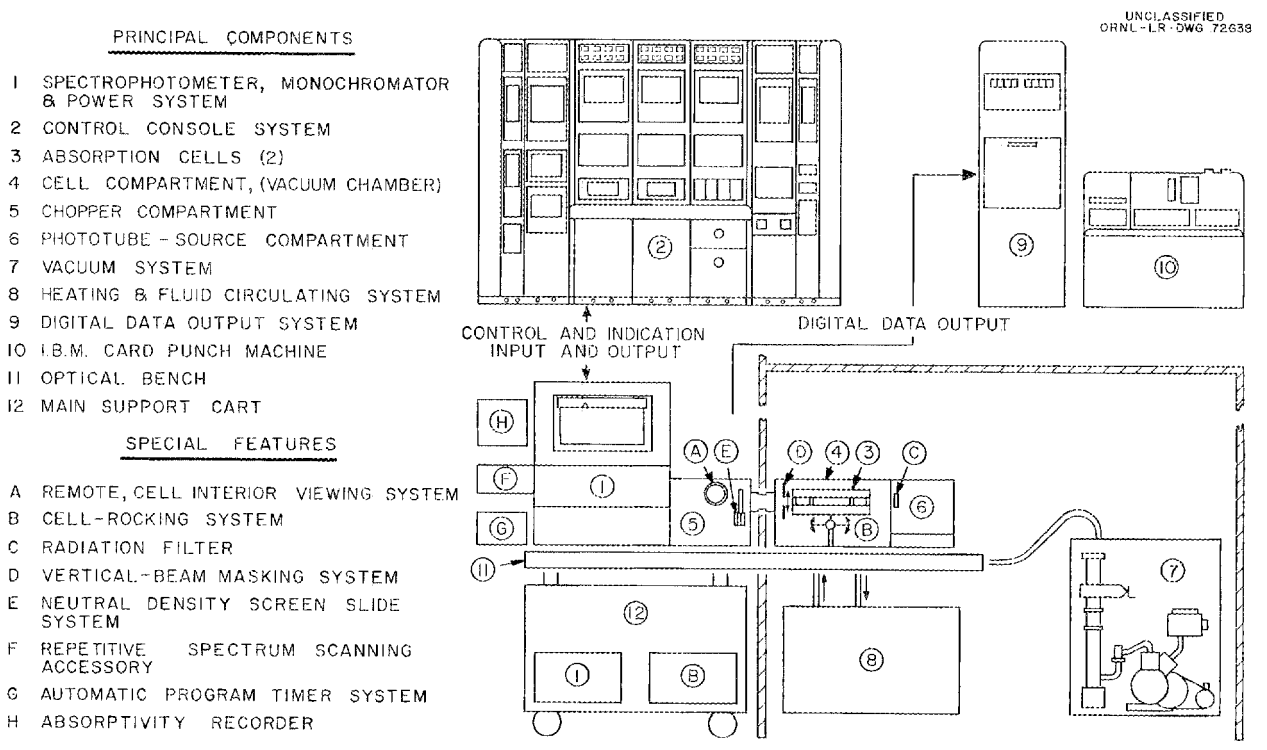

Fig. 15.1. Components of the High-Temperature, High-Pressure Spectrophotometer System.

and others will be made if they appear to be desirable. The cell has been tested at 5000 psi at 350°C and has been pressurized to 10,000 psi.

A punched-paper-tape, digitally controlled, temperature-plateau programming system was designed to replace a previously proposed mechanical cam system. The system is designed to be almost completely automatic and can operate on a program which is completely variable with respect to the operating temperature plateaus desired, the duration of any particular temperature plateau, the rate of temperature increase or decrease between plateaus, and the rate of cooldown. The desired temperature-vs-time program (any number of hours) is entered into the system continuously via the tape.

The spectrophotometer system can be synchronized with the control system in such a manner that the absorption spectra can be automatically obtained at any point on the temperature plateaus, that is, when the sample and reference cells are operating under nearly isothermal conditions. Programmed temperature shutdown (at 2°C/min) and emergency (maximum cooling rate) shutdown modes of operation can be entered automatically, if necessary, at any time during the program.

Thermal stability studies were carried out[6] to find a liquid capable of withstanding a temperature of 375°C for a prolonged time for use as the circulating heating fluid, so that the temperatures of the sample and reference cells can be thermostatically controlled. Liquids that have been considered are: Arochlor 1254 (Monsanto), tetracresyl silicate, Dow-Corning 550 fluid, and the very recently available Dow-Corning XF-1-0184. Studies are being carried out both in air and in the absence of air for prolonged heating (several weeks). The results are incomplete at present, but they do indicate that for 375°C operation, the Dow-Corning products are superior. The final decision awaits further testing.

15.2 MINIATURE CIRCULATING-LOOP SYSTEM AND DIGITAL DATA OUTPUT SYSTEM FOR THE CARY SPECTROPHOTOMETER

A Cary spectrophotometer (model 14 CMR, ultraviolet, visible, near-infrared range) was installed to serve as an auxiliary spectrophotometer for the high-temperature, high-pressure spectrophotometer system. With it the necessary preliminary and survey experiments can be carried out from below room temperature up to about 100°C in independently thermostatically controlled sample and reference cells. The spectrophotometer is equipped with a thermostatically controlled monochromator for very precise work.

The miniature circulating-loop system designed for use up to about 170°C and at moderate pressures (200 psi) with an unmodified Cary spectrophotometer has been discussed previously,[4] and a schematic layout of it was presented recently.[2] Problems encountered with some of its valves have been solved, and a loop-support system for precise vertical support (without drift or sag) and an alignment system for the present spectrophotometer installation were built and installed. The loop was designed so that the effects of gas-liquid equilibration, bubble formation, and suspended particles on spectrophotometric measurements can be studied.

The previously discussed[4] automatic, digital, data output system for the Cary spectrophotometer was transferred to the new spectrophotometer installation. Its performance is satisfactory and conforms to its design specifications. This digitizing system makes possible the rapid analysis of large amounts of complex spectral data through the use of high-speed computer methods.

15.3 MEASUREMENT OF LIQUID DENSITIES AT HIGH TEMPERATURES AND HIGH PRESSURES

As an important adjunct to this program, a method was devised for measuring the densities of aqueous solutions at accurately measured temperatures and pressures up to the critical points of the solutions. The liquid volume of a weighed solution of known composition is determined in an autoclave of suitable material, and an x-ray photograph is made in order to show the position of the vapor-liquid interface in a calibrated section of the autoclave. The density at any temperature is determined from the weight of solution and the location of the interface at that temperature. A high-pressure autoclave was designed and made of titanium. The autoclave can be operated up to at least 4000 psi at 400°C. It consists of a bulb section

[6] In collaboration with T. G. Rogers, Chemical Technology Division summer student, 1962.

of about 4 ml volume that contains an internal thermocouple well, a uniform expansion section about 12 in. long, and a high-pressure closure head with a fitting containing a titanium capillary leading to a pressure transducer. Markers on the expansion section facilitate the location of the solution interface by x-ray measurements. Densities may be determined at 370 to 371°C within a maximum error of ±0.6%, assuming all of the worst error interactions. At somewhat lower temperatures the error will be less. X-ray film can be driven past the slit in the system behind the autoclave at rates varying from about 0.05 up to about 3 in./min. All the equipment has been installed and will be used with an existing 300-kv Norelco x-ray system.

15.4 COMPUTER PROGRAMS FOR SPECTROPHOTOMETRIC STUDIES

Work continued on the development of computer programs for the analysis of large amounts of complex spectral data. Previously written programs are being converted and modified for operation on the IBM 7090 or CDC 1604-A computers. Modifications include the utilization of recent equipment additions for the off-line curve plotting from both computers. Use of the automatic, digital, data output (IBM cards) system with the spectrophotometer greatly facilitates this work.

A Computer Program for the Analysis of Spectrophotometric Absorption Data for Dynamic Multicomponent Systems[7]

The conventional method for the spectrophotometric study of multicomponent systems utilizes simultaneous equations, usually with one wavelength being used per component. The accuracy of the results depends on the accuracy with which the standard spectral data for each component is known and on the accuracy of the absorption measurements. As the number of components increases, the method becomes increasingly sensitive to small errors in either the standard spectral data for each component or in the experimental measurements at the set of wavelengths selected for the analysis of the system. However, more than one wavelength may be used for each component in order to increase the accuracy of the results by minimizing the statistical error for slight inaccuracies in either the standard data or the measurements. In order to do this a least-squares solution on the matrices involved must be carried out.

A computer program was written[8] utilizing a least-squares method in matrix form. At each of the wavelengths in the set selected, an analytical curve-fitting technique is used to obtain a polynomial function which describes the change in absorbancy of the mixture with time. From these polynomials an "instantaneous spectrum" is computed. For each experimental spectrum, an average time is selected with respect to the wavelength range and spectral scan rate used, and an "instantaneous spectrum" is computed at each of these average times. Each computed "instantaneous spectrum" is then analyzed by the method described for the equilibrium case, and the concentration of each component is determined.

The program was tested with synthesized spectrophotometric absorption data for two parallel first-order reactions involving three absorbing components, and for three series first-order reactions involving four absorbing components. For each case, the number of wavelengths selected was equal to twice the number of components.

In Fig. 15.2 is given the absorbance-time data at the selected set of wavelengths for the reacting system represented by the three series first-order reactions:

$$A \xrightarrow{k_1} B \xrightarrow{k_2} C \xrightarrow{k_3} D \ .$$

Each spectral scan corresponds to a spectrum obtained with a recording spectrophotometer at a constant scan rate. The absorbancy of the mixture was determined at the indicated set of wavelengths at which the various components of the system absorb.

The results of the analysis are given in Fig. 15.3. The concentration-time curves are shown for each component. From this type of data it is possible to determine the reaction kinetics for an experimental system.

[7] In collaboration with D. A. Costanzo, Analytical Chemistry Division.

[8] By E. C. Long and A. L. Brooks of the Central Data Processing Center, ORGDP.

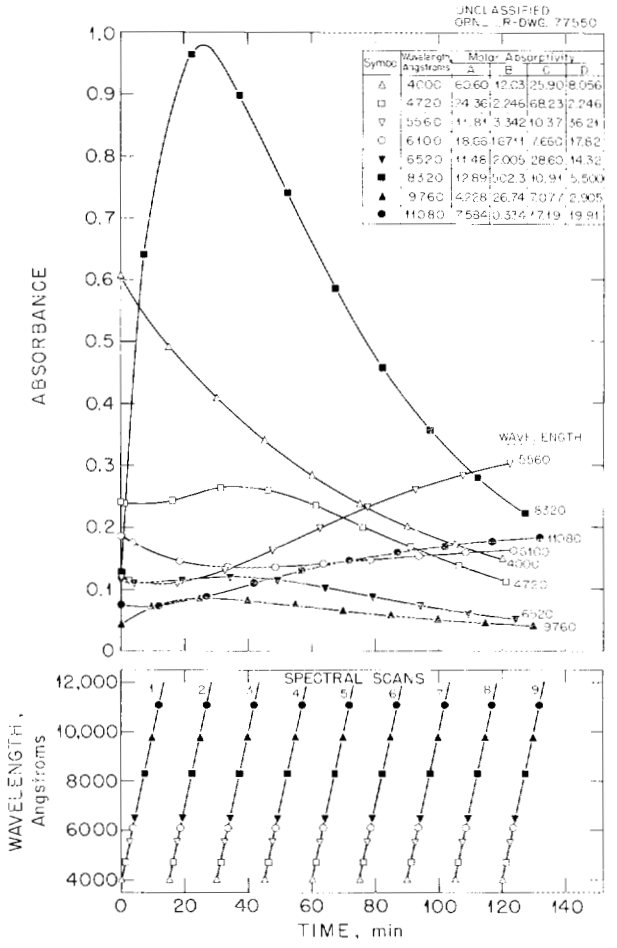

Fig. 15.2. Absorbance-Time Curves for a System Containing Components A, B, C, and D in Series First-Order Reactions.

The results obtained for the analysis of the synthesized data for a three- and a four-component system were excellent. With exact synthesized spectral data, the concentrations of each component were determined to within a relative standard deviation of ±0.5%, and within a relative error of ±0.1%.

A Program for the Convolute Smoothing of Digitized Spectral Data[9]

The output of digitized spectral data from the spectrophotometer system yields absorbancy data as a function of wavelength. At high absorbancies and low light levels there may be a significant amount of noise associated with the output from the spectrophotometer, particularly with the photomultiplier. In order to use the computer to make more-refined calculations using the spectral data, the data should be made as free as possible from the effects of random fluctuations. One of the simplest ways to do this is to take a running average. This technique, however, is not a useful one for many types of data, and particularly in the present case, because this type of average tends to distort the peaks of the spectrum.

A set of computer programs and subroutines was written for the CDC 1604-A computer to smooth spectral data. A least-squares convolution smoothing technique is employed. This technique was recently proposed and used by Savitzky.[10] The

[9] In collaboration with T. G. Kabele, co-op student from Northwestern University, January–March 1963.

[10] A. Savitzky and M. J. E. Golay (The Perkin-Elmer Corp., Norwalk, Conn.), "Some Numerical Operations on Analytical Data," paper presented at the 15th Annual Summer Symposium, Division of Analytical Chemistry, A.C.S., University of Maryland, June 14, 1962.

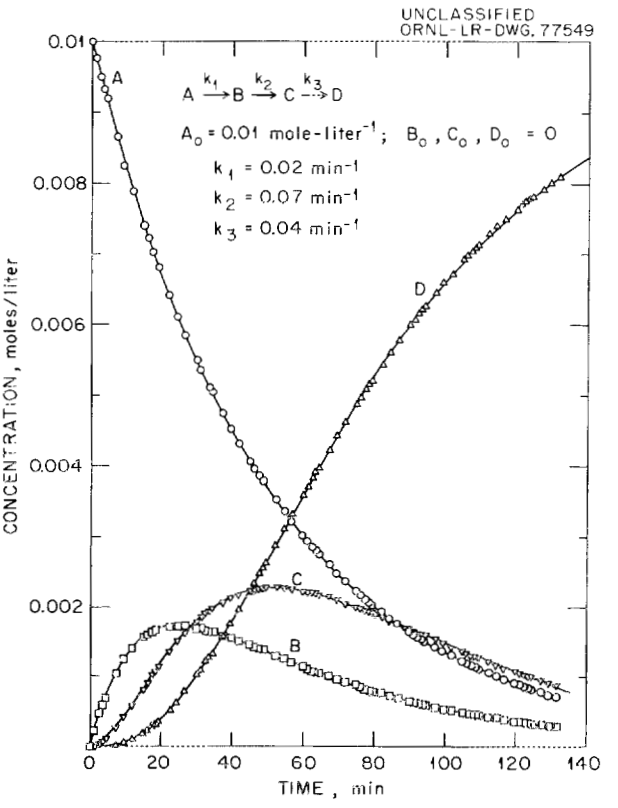

Fig. 15.3. Concentration-Time Curves for Components A, B, C, and D in Series First-Order Reactions.

smoothed value for each point is obtained from the observations in the immediate neighborhood of that point. A convolution or fitting may be done for each point over a 3- to 15-point range, utilizing a cubic function over the range of the convolute. The same technique can also be used to take the first, second, and third derivatives of curves, spectra, etc. Previously smoothed attenuator data (stored on magnetic tape) are used to correct the experimental spectral data for the additive effects of the conical-screen attenuators (nonlinear with wavelength) that are used to measure very low light transmissions (less than 1%). The program yields smoothed spectral data corrected for the effects of cell-balance zero and attenuation if this is present.

The data output may be obtained in various forms under program options: tabulated on the off-line printer, plotted as a smoothed spectrum on the Calcomp graphical plotter, and/or punched out as a card deck to be used as smoothed input for other types of programs.

16. Mechanisms of Separations Processes

In order to develop equations to describe the extraction by tributyl phosphate (TBP)–hydrocarbon diluent solutions of uranyl nitrate from aqueous nitric acid solutions, it is necessary to know the activities of each of these chemical species in the multicomponent systems. These are being obtained by combining literature data for simpler systems with additional experimental data.

16.1 ACTIVITIES OF NITRIC ACID AND WATER IN AQUEOUS SOLUTIONS OF NITRIC ACID

From literature data and measurements of partial pressures of nitric acid and water[1] over the two-component system, stoichiometric, ionic, and molecular activities for the dissociation reaction

$$HNO_3 \longrightarrow H^+ + NO_3^- \qquad (1)$$

were calculated. These calculations are based on the activity ratios

$$\frac{y_u C_u}{y_u^0 C_u^0} = \frac{(y_s C_s)^2}{(y_s^0 C_s^0)^2} = \frac{(y_\pm C_\pm)^2}{(y_\pm^0 C_\pm^0)} = \frac{p}{p_0}, \qquad (2)$$

where y_u, y_s, and $y_\pm$ are molar activity coefficients of undissociated, stoichiometric, and ionic species, respectively, C_u, C_s, and $C_\pm$ are the corresponding molar concentrations, p is the partial pressure of nitric acid, and the subscript or superscript 0 refers to pure acid. From the combination of vapor pressure data and the activity coefficients of nitric acid obtained by freezing point measurements,[2] the ratio y_s^*/y_s^0 was shown to be 1/21, where y_s^* is the activity coefficient of nitric acid when infinitely dilute in water. Values of the various quantities, each of which has been used to some extent in the literature, are shown in Fig. 16.1.

Literature data summarized in Fig. 16.1 are those of Potier,[3] of Vandoni and Laudy,[4] and of Burdick and Freed[5] on partial pressures of nitric acid over nitric acid–water solutions and, for this same system, the measurements of the degree of dissociation reported by Axtmann and Murray,[6] Krawetz and Young,[7] and Hood and Reilly.[8]

[1] *Chem. Technol. Div. Ann. Progr. Rept. Sept. 24, 1962*, ORNL-3314.

[2] F. Hartmann and P. Rosenfeld, *Z. Physik. Chem. (Leipzig)* **A164**, 377 (1933).

[3] A. Potier, *Ann. Fac. Sci. Univ. Toulouse Sci. Math. Sci. Phys.* **20**, 1–98 (1956).

[4] M. R. Vandoni and M. Laudy, *J. Chim. Phys.* **49**, 99 (1952).

[5] C. L. Burdick and E. S. Freed, *J. Am. Chem. Soc.* **43**, 518 (1921).

[6] R. C. Axtmann and B. B. Murray, *Dissociation of Nitric Acid in Aluminum Nitrate Solutions*, DP-297 (June 1958).

[7] A. A. Krawetz, University of Chicago Ph.D. thesis; data kindly made available by T. F. Young.

[8] G. C. Hood and C. A. Reilly, *J. Chem. Phys.* **32**, 127 (1960).

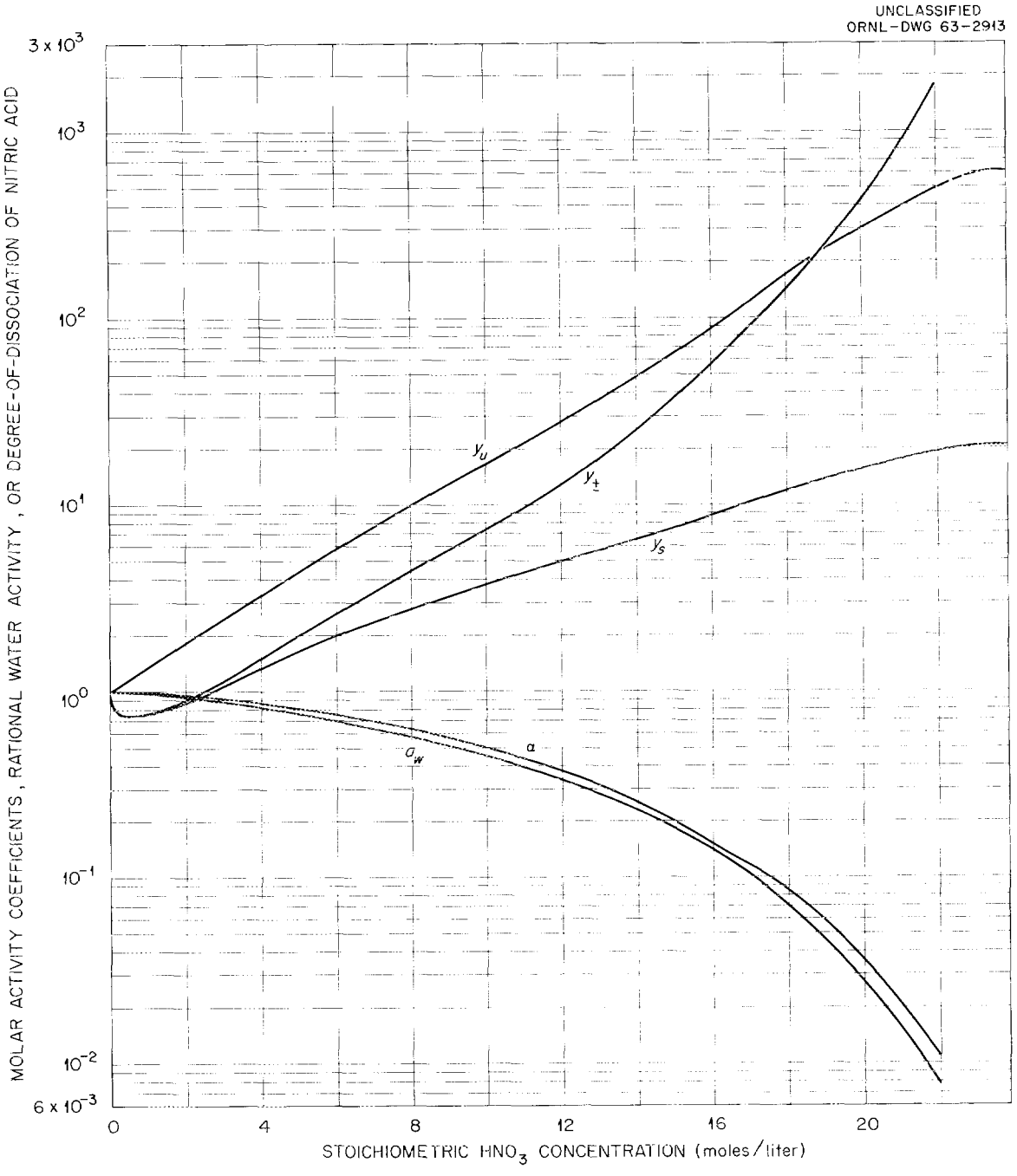

Fig. 16.1. Activities, Activity Coefficients, and Degree-of-Dissociation of Species in H_2O-HNO_3 Solutions.

16.2 VAPOR PRESSURES OF TRIBUTYL PHOSPHATE OVER WATER–NITRIC ACID–TRIBUTYL PHOSPHATE SOLUTIONS

Vapor pressures of TBP over two-phase water–nitric acid–TBP systems, at 25°C, were measured by a transpiration technique, using P^{32}-labeled TBP. Nitric acid concentrations in the aqueous phase were 0 to 15 *M*; the corresponding organic-phase concentrations ranged from 0 to 6 *M*, and the molar ratios $(HNO_3)/TBP_s)$ varied from 0 to 2.1. Average pressures of TBP over anhydrous and water-saturated TBP were 0.527 and 0.415 μ respectively. As the nitric acid concentration increased, the pressure decreased to 0.0131 μ over the most acidic solution studied. The TBP activity (Fig. 16.2), defined in terms of the water-saturated TBP, namely, $p_{TBP}/0.415$, decreased from 1 to less than 0.1 as the ratio $(HNO_3)/(TBP_s)$ increased from 0 to 1. Further addition of nitric acid caused only a slow decrease in the TBP activity.

These vapor-pressure data were used to calculate the thermodynamic equilibrium constant for extraction of nitric acid from aqueous solution by TBP and the activity coefficient of TBP in water-saturated TBP. Thus, for the reaction

$$H^+(aq) + NO_3^-(aq) + TBP(org) \longrightarrow TBP \cdot HNO_3(org) , \quad (3)$$

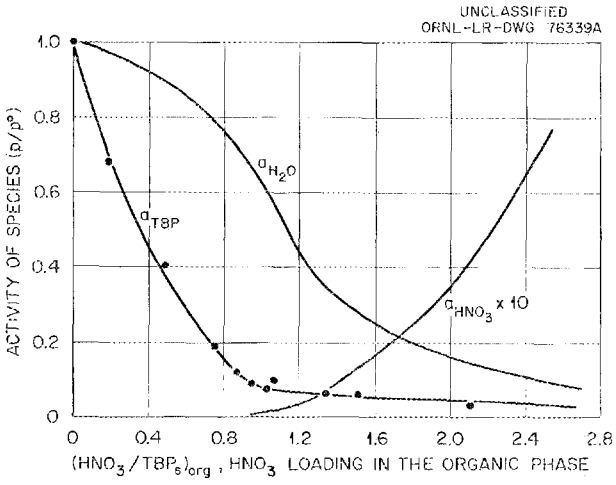

Fig. 16.2. Activities of TBP, HNO_3, and H_2O over the Two-Phase System. Water-saturated TBP is taken as the reference state for TBP.

$K/y^w_{TN} = 1.75$ (standard deviation is 0.09), where y^w_{TN} is the activity coefficient of the complex $HNO_3 \cdot TBP$ infinitely dilute in water-saturated TBP. Although y^w_{TN} is unknown at present, it is probably close to 1, which is its assigned value in the anhydrous system.

16.3 ACTIVITIES OF WATER, NITRIC ACID, AND URANYL NITRATE IN THE THREE-COMPONENT SYSTEM

The transpirational vapor-pressure technique is being used to measure vapor pressures of water and nitric acid over the three-component solutions water–nitric acid–uranyl nitrate at 25°C. Nitric acid concentrations were varied from 2.5 to 10 *M*, and those of uranyl nitrate [as $UO_2(NO_3)_2$] from 0 to 1.4 *M*. By combining these pressure measurements with those of water and nitric acid over the water–nitric acid system (Sec 16.1) and of water over the water–uranyl nitrate system,[9] the effects of uranyl nitrate on water and nitric acid activities were obtained. To a first approximation, the effect of uranyl nitrate on nitric acid acitivty is given by:

$$m_2 \ln [a_2(n_1, n_2, n_3)] / [a_2(n_1, n_2, 0)] = 5m_3 , \quad (4)$$

where m_2 and m_3 are the molalities of nitric acid and $UO_2(NO_3)_2$, $a_2(n_1\ n_2, n_3)$ is the activity of nitric acid in the three-component system, while $a_2(n_1,n_2,0)$ is the activity of nitric acid in the two-component water–nitric acid system. The exponent of the m_3 term on the right of Eq. (4) is actually a little less than 1.

The effect of uranyl nitrate on the water vapor pressure is, interestingly, given by the relation:

$$p_1(n_1, n_2, n_3)\, p_1(n_1, 0, 0) = p_1(n_1, n_2, 0)\, p_1(n_1, 0, n_2) . \quad (5)$$

In Eq. (5), the quantities n_1, n_2, n_3 refer to water, nitric acid, and uranyl nitrate, respectively, and a 0 (zero) indicates a component to be absent. This equation shows that the vapor pressure of water over the three-component system can be calculated from (1) the vapor pressure of pure water,

[9] R. A. Robinson and C. K. Lim, *J. Chem. Soc.* 1951, p 1840.

$p_1(n_1, 0, 0)$, (2) the partial pressure of water over the water–nitric acid solution, $p_1(n_1, n_2, 0)$, and (3) the partial pressure of water over the water–uranyl nitrate solution, $p_1(n_1, 0, n_3)$. The calculations refer to solutions having the same mole ratio, n_2/n_1 or n_3/n_1, in the three-component as in the two-component systems. Over the concentration ranges of acid and uranyl nitrate employed, Eq. (5) provides values of $p_1(n_1, n_2, n_3)$ that differ from measured values by only 25% of the standard deviation of the measurement.

The major purpose of these vapor-pressure measurements is to obtain the quantitative description of the variation of uranyl nitrate activity as the nitric acid concentration is changed. From such a description, the solvent extraction of uranyl nitrate by, for example, tributyl phosphate will be greatly facilitated. Although the thermodynamic techniques for using the data of these experiments are well known, they have not yet been applied.

17. Ion Exchange

17.1 RADIATION DAMAGE TO ION EXCHANGE RESINS

Anion Exchange Resins

A sample of Dowex 1-X10 (50- to 100-mesh) resin in the hydroxyl form was placed in a system of flowing demineralized water (<1 micromho/cm) and exposed in a 10,000-curie Co^{60} source to a dose of 4.2×10^8 r (~1.1 whr per gram of dry resin). Maximum specific conductance of the continuously monitored effluent was 130 micromhos/cm; the corresponding pH maximum was 10.7 (Fig. 17.1). The effluent solution had a strong odor, characteristic of amines, the active groups of the anion resin. At the conclusion of the experiment, about 62 vol % of the original resin was recovered. An additional 10 vol % was recovered as particles of less than 200 mesh; the remaining 28% had been converted to water-soluble radiolysis products.

The total dose of gamma radiation required to severely degrade Dowex 1 resin appears to depend on the resin environment. In the flowing-water experiment described above, continuously recorded pH data indicated that the resin had lost more than 90% of its strong-base capacity after an exposure of about 1.3×10^8 r (0.35 whr per gram of dry resin). Smith and Groh[1] reported that 85% of the salt-splitting capacity of Dowex 1 in the hydroxyl form was lost after a dose of 2.67×10^8 r. However, their experiments were performed in a static system with air-dried resin. According to an earlier literature survey, Marinsky and Giuffrida[2] concluded that under static conditions quaternary amine anion resins, in general, would lose 40 to 50% of their capacity after an exposure of 3.8×10^8 r and would be completely degraded after 1.7×10^9 r. Thus, under process conditions, where the resin is submerged in flowing water, there are indications that the extent of radiation-induced loss of capacity of Dowex 1 in the hydroxyl form is at least twice that for a static system. This is presumably due to the removal of radiolysis products which, in a static system, could undergo recombination reactions that would result in lower net decomposition rates.

Cation Exchange Resins

An examination was made of effluent-water solutions collected from previously reported flowing-water irradiation experiments with Dowex 50W cation exchange resin.[3] Each liquid volume was

[1] L. L. Smith and H. J. Groh, *The Effect of Gamma Radiation on Ion Exchange Resins*, DP-549 (February 1961).

[2] J. A. Marinsky and A. J. Giuffrida, *The Radiation Stability of Ion Exchange Materials*, ORNL-1978 (September 1957).

[3] *Chem. Technol. Div. Ann. Progr. Rept. June 30, 1962*, pp 196–98.

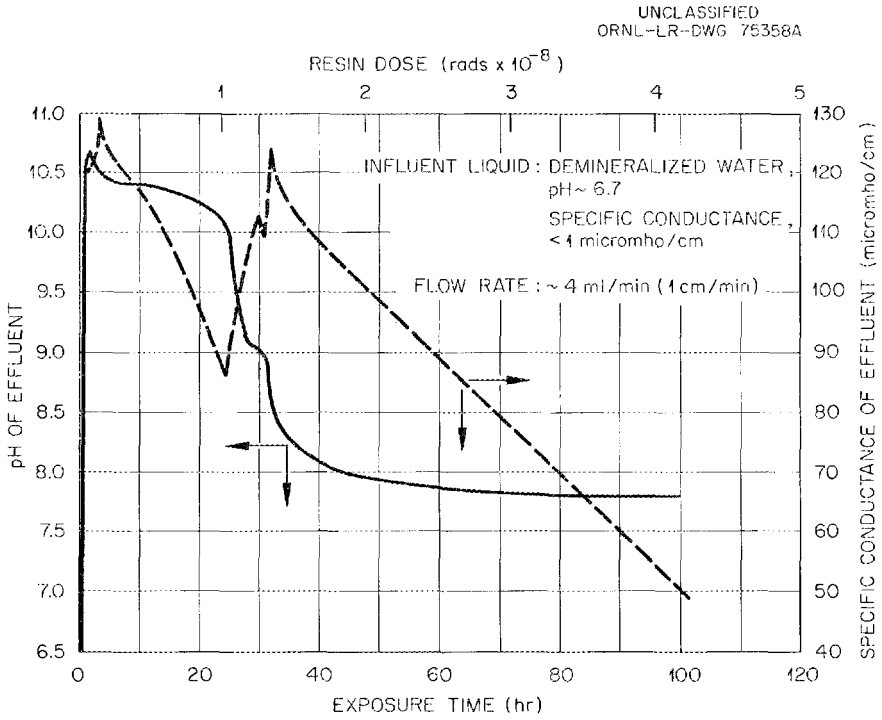

Fig. 17.1. Variation of pH and Specific Conductance of Aqueous Effluent from Dowex 1-X10 Resin (50 to 100 Mesh), Hydroxyl Form, Irradiated with Co^{60} Gamma Rays.

reduced by a factor of about 50 in a vacuum distillation unit that kept the solution at or below room temperature in order to minimize the possibility of volatilizing or decomposing any organic constituents. Chemical analyses showed that most of the concentrates of each run contained soluble sulfates and sulfonates. Visually, the first concentrates of each run were colorless, while the remaining concentrates became progressively darker, varying from light straw to dark brown and containing increasing quantities of suspended solids. Ultracentrifuge and light-scattering studies indicated that these suspended solids had a density of about 1 and a molecular weight of about several million.

One interpretation of the data on the radiation degradation of this cation exchange resin is as follows: Initially, the main degradation process involves only the cleavage of active sulfonate groups from the resin. These groups dissolve and are partly converted to sulfate in the flowing water, as indicated by the occurrence of maximum acidity in the effluent stream at the beginning of each exposure period. After a substantial fraction of the active sulfonate sites is lost, the resin matrix starts to break up, yielding water-soluble radiolysis products and small, insoluble particles of the martix. These particles, of several millions in molecular weight, break off and enter the effluent stream in some manner that does not lead to fragmentation of the resin beads.

17.2 STUDIES OF THE SEPARATION OF SOME FISSION PRODUCTS BY ION EXCHANGE

A problem sometimes associated with the recovery of fission products is the large concentration of impurity ions such as iron, aluminum, and chromium. For this reason the ability of citrate to retain these cations in solution at pH 2.5 (a higher acidity than is routinely considered), and at the same time allowing sorption of rare- and alkaline-earth elements on a cation exchange resin, was evaluated.

Distribution coefficients of Ce^{3+}, Sr^{2+}, and Fe^{3+} in synthetic Purex 1WW waste as a function of dilution (Fig. 17.2) do, indeed, show that citrate, in the acidity range 0.1 to 1.1 *N*, accomplishes the desired complexing of Fe^{3+}. At the same time citrate allows the sorption of Ce^{3+} and Sr^{2+} on Dowex 50W-X8 (100 to 200 mesh), provided that the degree of dilution of the waste is about 10 or greater. At a dilution of 20, for example, $K_d^{Sr}/K_d^{Fe} > 200$, $K_d^{Ce}/K_d^{Fe} > 600$, and $K_d^{Ce}/K_d^{Sr} \approx 3$. In these experiments the resin was pre-equilibrated with 0.5 *M* HNO_3–0.005 *M* ammonium citrate at pH 2.5. The waste solution was pretreated by adding 1.5 moles of citric acid per mole of Fe^{3+}, Al^{3+}, and Cr^{3+} and by neutralizing to pH 2.5 with concentrated ammonia.

Two resin-column runs with Purex 1WW, diluted 20-fold, largely substantiated the distribution coefficient values. In addition, major separation of rare earths, calcium, strontium, and barium from each other was achieved by elution with ammonium α-hydroxyisobutyrate[4] at successive concentrations of 0.48, 0.8, 1.0, and 2.0 *M* respectively. These results show that up to 3.3 resin volumes of Purex 1WW, diluted 20-fold, could be processed for both strontium and rare-earth recovery per volume of Dowex 50W-X8 (100- to 200-mesh) resin.

[4] L. Wish, *Quantitative Radiochemical Analysis by Ion Exchange. V. Calcium, Strontium, and Barium*, USNRDL-TR-341 (July 1959).

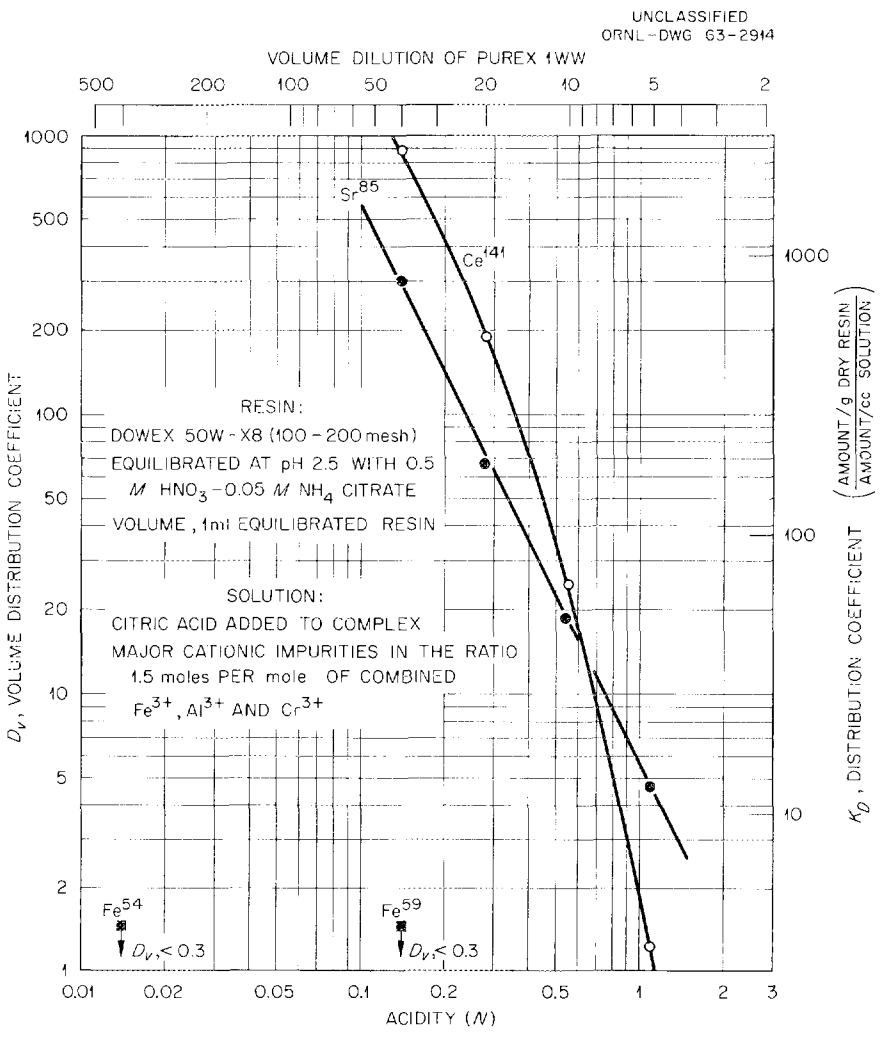

Fig. 17.2. Distribution Coefficient of Ce^{141}, Sr^{85}, and Fe^{59} in Purex 1WW as a Function of Acidity.

18. Chemical Engineering Research

18.1 DEVELOPMENT OF HIGH-SPEED CONTACTORS: THE STACKED-CLONE CONTACTOR

The development of a high-speed solvent extraction device, one having high throughput, high extraction efficiency, low contact time per stage, and low holdup, would have advantages in the processing of highly radioactive fuel solutions. The stacked-clone contactor, a cascade of axially aligned liquid cyclone stages which produces counterflow by means of the induced underflow effect, is a novel device which has, to a good degree, the properties mentioned.

Eight geometrically distinct designs of this device were tested for capacity and stage efficiency using the system uranyl nitrate in 1 *M* sodium nitrate–18% TBP in Amsco. Figure 18.1 schematically illustrates these designs. Figure 18.2 is a photograph of several stages of the assembled Mark XI stacked-clone contactor. Mark I had a $\frac{3}{4}$-in.-diam conical hydroclone stage. The others had a $1\frac{1}{2}$-in.-diam "hornical" hydroclone stage, that is, a $1\frac{1}{2}$-in.-diam top, with a conical or curved transition to a $\frac{1}{2}$-in.-diam cylindrical section. These devices have been described previously.

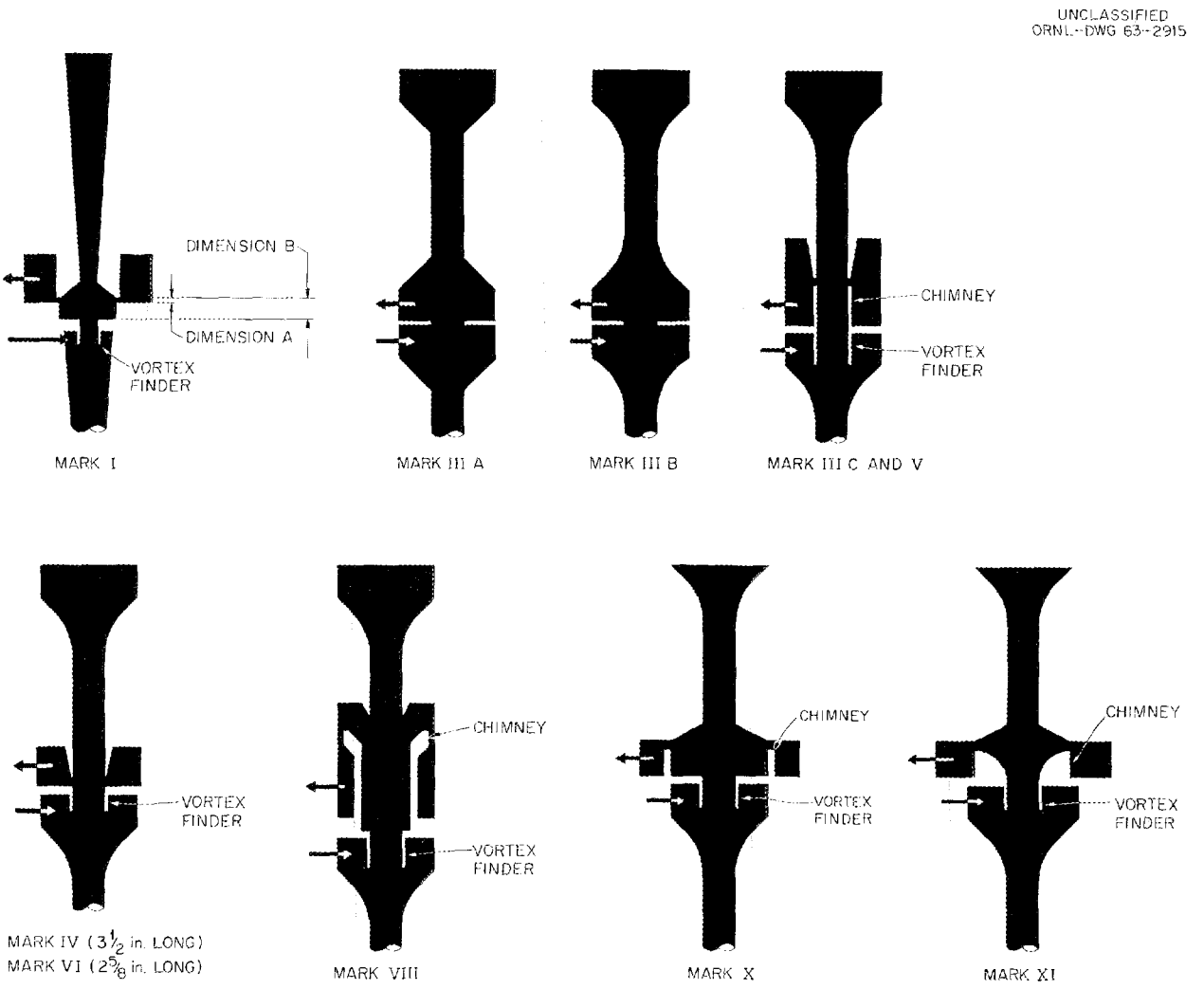

Fig. 18.1. Shapes and Underflow Chambers of Stacked-Clone Contactors.

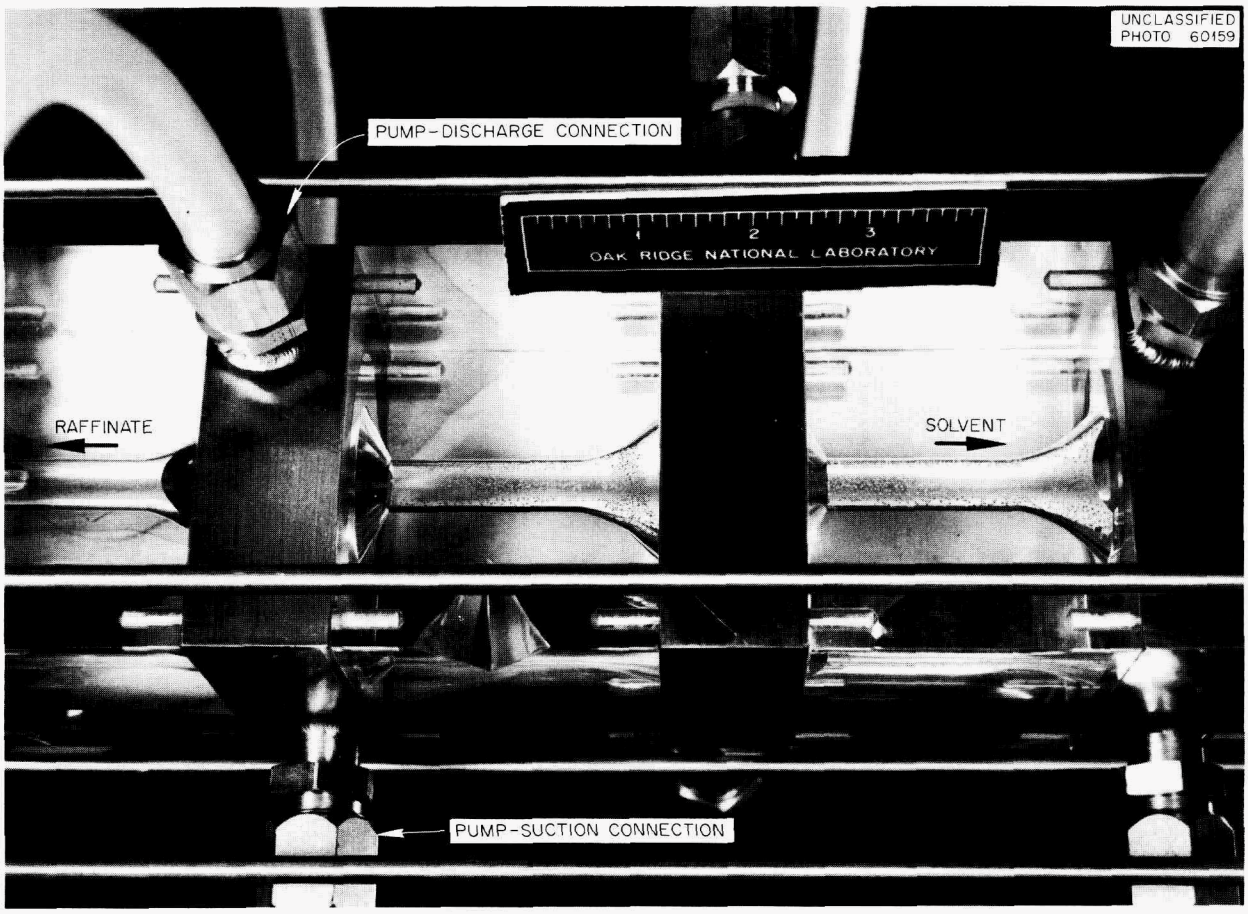

Fig. 18.2. Mark XI Stacked-Clone Contactor, Assembled.

Table 18.1 is a summary of typical test results obtained with contactors other than Mark I. Table 18.2 is a summary of typical Mark I test results. These results are averages taken over several runs at about 50 to 95% of flooding and at an aqueous-to-organic volume ratio (A/O) of about 3 to give an extraction factor near 1.

Note that the Mark I contactor gave generally high stage efficiencies but a rather moderate capacity. The larger contactors, up to Mark X, gave poor to moderate efficiencies with moderate to high capacities. Mark X and Mark XI begin to exhibit acceptably high efficiencies at high capacities. These data show the importance of the design of the underflow chamber and suggest the following criteria therefor:

1. There must be an underflow chamber for good efficiency, and there is an optimum size and shape.

2. Radial symmetry of flow to the pump suction must be ensured so that the organic-rich central vortex is maintained between stages; capacity suffers otherwise.

3. An underflow skirt is needed for both capacity and efficiency, and there is an optimum size and shape.

Mark X and XI represent the first partial application of these criteria, and the test results tend to corroborate the criteria.

Figure 18.3 correlates efficiency and capacity of the various contactors as a function of the diameter of the vortex finder. Figure 18.4 shows the product of capacity and throughput (performance factor) and the approximate retention time of both phases per theoretical stage as a function of the diameter of the finder. Since the organic holdup is less than 50% of the total, the retention time

Table 18.1. Summary of Typical Performance of Various Stacked-Clone Contactors at 40°C

Aqueous phase: uranyl nitrate in 1*M* $NaNO_3$
Organic phase: 18% TBP in Amsco
Extraction factor: $\cong$ unity

Mark No.	Vortex Finder and/or Chimney[a] Diam (in.)	Vortex Finder and/or Chimney[a] Length (in.)	Feed Port Width × Height (in.)	Flooding: Aqueous + Organic (cc/min)	Average Stage Efficiency (%)
III A	0.50	0.0	$\frac{3}{16} \times \frac{1}{2}$	1200	26
III B	0.50	0.0	$\frac{3}{16} \times \frac{1}{2}$	1300	35
III C	0.50 0.50[a]	$\frac{3}{8}$ $\frac{3}{4}$[a]	$\frac{3}{16} \times \frac{1}{2}$	2630	62
IV	0.50	$\frac{1}{2}$	$\frac{3}{16} \times \frac{1}{2}$	3820	35
IV	0.55	$\frac{1}{2}$	$\frac{3}{16} \times \frac{1}{2}$	1637	59
IV	0.45	$\frac{1}{2}$	$\frac{3}{16} \times \frac{1}{2}$	5000	21
IV	0.525	$\frac{3}{8}$	$\frac{3}{16} \times \frac{1}{2}$	2120	60
IV	0.525	$\frac{1}{2}$	$\frac{3}{16} \times \frac{1}{2}$	2850	54
IV	0.475	$\frac{1}{2}$	$\frac{3}{16} \times \frac{1}{2}$	3800	32
IV	0.475	$\frac{3}{8}$	$\frac{3}{16} \times \frac{1}{2}$	3800	41
V	0.50 0.50[a]	$\frac{1}{2}$ $1\frac{5}{8}$[a]	$\frac{3}{16} \times \frac{1}{2}$	3096	47
V	0.55 0.50[a]	$\frac{1}{2}$ $1\frac{5}{8}$[a]	$\frac{3}{16} \times \frac{1}{2}$	2095	49
V	0.45 0.50[a]	$\frac{1}{2}$ $1\frac{5}{8}$[a]	$\frac{3}{16} \times \frac{1}{2}$	3000	47
V	0.40 0.50[a]	$\frac{1}{2}$ $1\frac{5}{8}$[a]	$\frac{3}{16} \times \frac{1}{2}$	3572	44
V	0.55 0.50[a]	$\frac{1}{2}$ $1\frac{5}{8}$[a]	$\frac{3}{16} \times \frac{3}{4}$	3308	48
VI	0.40	$\frac{1}{2}$	$\frac{3}{16} \times \frac{1}{2}$	6724	43
VI	0.45	$\frac{1}{2}$	$\frac{3}{16} \times \frac{1}{2}$	6280	32
VI	0.50	$\frac{1}{2}$	$\frac{3}{16} \times \frac{1}{2}$	4084	46
VI	0.55	$\frac{1}{2}$	$\frac{3}{16} \times \frac{1}{2}$	2004	63
VI	0.55	$\frac{1}{2}$	$\frac{3}{16} \times \frac{5}{8}$	2182	66
VI	0.50	$\frac{1}{2}$	$\frac{3}{16} \times \frac{5}{8}$	4522	49
VI	0.45	$\frac{1}{2}$	$\frac{3}{16} \times \frac{5}{8}$	6748	34
VI	0.40	$\frac{1}{2}$	$\frac{3}{16} \times \frac{5}{8}$	6938	29
VIII	0.45	$\frac{1}{2}$	$\frac{3}{16} \times \frac{1}{2}$	2885	47
VIII	0.40	$\frac{1}{2}$	$\frac{3}{16} \times \frac{1}{2}$	3608	46

Table 18.1 (continued)

Mark No.	Vortex Finder and/or Chimney[a] Diam (in.)	Vortex Finder and/or Chimney[a] Length (in.)	Feed Port Width × Height (in.)	Flooding: Aqueous + Organic (cc/min)	Average Stage Efficiency (%)
VIII	0.50	1/2	3/16 × 1/2	2905	45
VIII	0.55	1/2	3/16 × 1/2	2083	45
X	0.50 1.50[a]	3/8 7/16 [a]	1/4 × 1/2	4085	57
X	0.45 1.50[a]	3/8 7/16 [a]	1/4 × 1/2	3363	62
XI	0.50 Funnel shape	3/8 7/16 [a]	1/4 × 1/2	4338	70
XI	0.45 Funnel shape	3/8 7/16 [a]	1/4 × 1/2	4630	59

[a]Chimney

Table 18.2. Summary of Performance of Mark I Stacked-Clone Contactor at 40°C

Aqueous phase: uranyl nitrate in 1 *M* $NaNO_3$ (2.5 to 3.1 g/liter)
Organic phase: 18% tributyl phosphate in Amsco
A 0.25-in.-diam vortex finder was used
Extraction factor was approximately unity

Feed Point Height (0.125 in. wide)	Dimension A Axial Gap at 7/16-in. Radius (in.)	Dimension B Finder Plate to Underflow Skirt (in.)	Flooding: Aqueous + Organic (cc/min)	Average Stage Efficiency (%)
0.125	0.0938	0.0938	2050	81
0.125	0.3125	0.3125	1403	79
0.125	0.1875	0 1875	1305	75
0.125	0.4063	0.0938	1342	73
0.125	0.0938	0.2500	1335	87
0.129	0.0627	0.0627	1410	39
0.129	0.1250	0.0627	1177	55
0.1875	0.0938	0.0938	1655	53
0.2813	0.0938	0.0938	1965	74
0.2500	0.0938	0.0938	2012	74
0.375	0.0938	0.0938	1785	69
0.129	0.5625	0.5625	1238	78

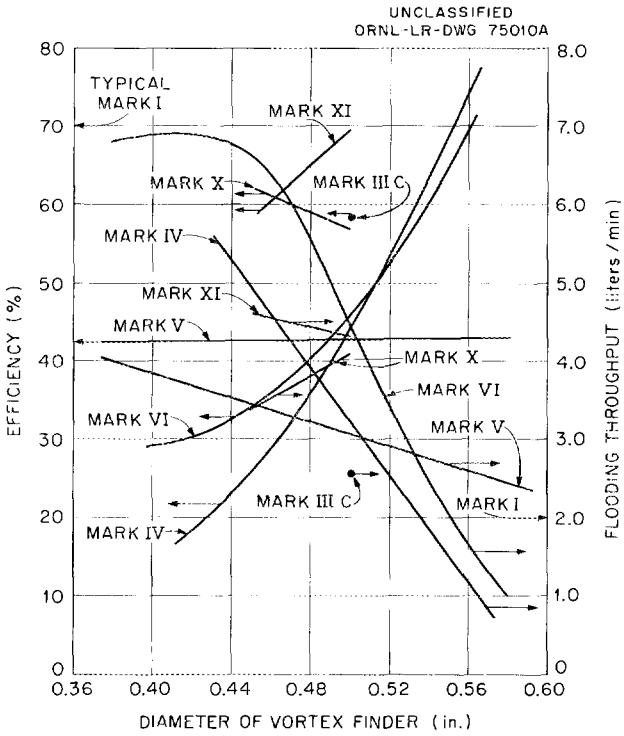

Fig. 18.3. Efficiency and Throughput vs Diameter of the Vortex Finder for Various Contactors. Temperature: 40°C.

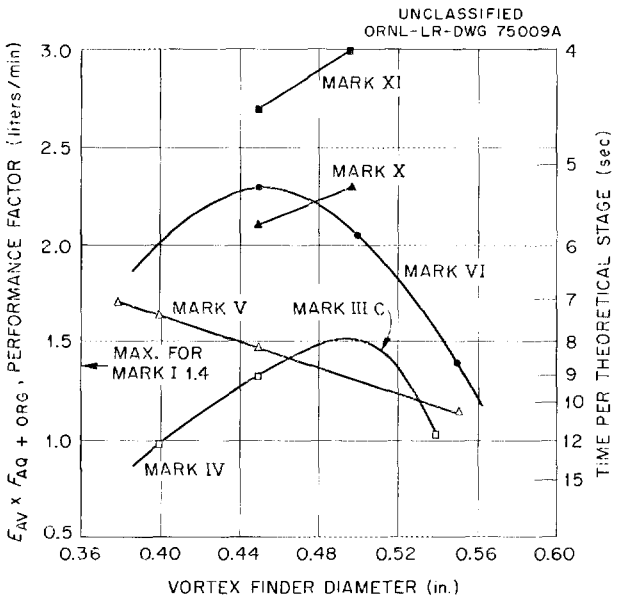

Fig. 18.4. Effect of Diameter of the Vortex Finder on Performance Factor.

of the organic phase would be less than half the times shown in Fig. 18.4.

Although a closer approach to optimum dimensions and configuration of the Mark XI type contactor, according to the criteria stated, would be desirable and profitable, the present stage of development offers a practical and useful prototype high-speed contactor for radiochemical processing.

18.2 STUDIES ON COALESCENCE IN SOLVENT EXTRACTION SYSTEMS

A study of drop coalescence in liquid-liquid solvent extraction systems has been undertaken. This work is in support of solvent extraction studies in which coalescence is frequently the most important factor in equipment design. Of particular interest is the quantitative determination of the effect of strongly ionizing radiation in promoting coalescence.

The technique used is to observe the coalescence times for single drops on a planar interface, with and without irradiation of the film between the drop and the interface. The types of radiation to be studied will include Compton electrons, alpha particles, protons, and fission fragments. The last three are produced by neutron irradiation of the appropriate target nuclide in the aqueous phase: respectively, Li^6, hydrogen, and U^{235}. Flux levels and target nuclide concentrations have been chosen to produce 10 ion tracks per square millimeter per second across the interface.

To this end, an apparatus has been designed and constructed (Fig. 18.5). A cell contains the liquids of interest, with provision for maintaining a planar interface in a raised cup and dropping upon it uniform drops of the continuous phase. The arrival and subsequent coalescence of the drop is detected by interruption of a light beam. A sample of the output is shown in Fig. 18.6. The apparatus is isolated from ambient mechanical vibration above 3 cps by suspension springs and a 600-lb lead inertia block (Fig. 18.7). The cell is mounted in a water bath, and a double-walled Lucite housing around the bath provides both acoustical and thermal isolation. This antivibration system attenuates nearby building shocks (all frequencies) by at least 15 db.

A preliminary theoretical model was constructed to describe the initiation of coalescence by heavy

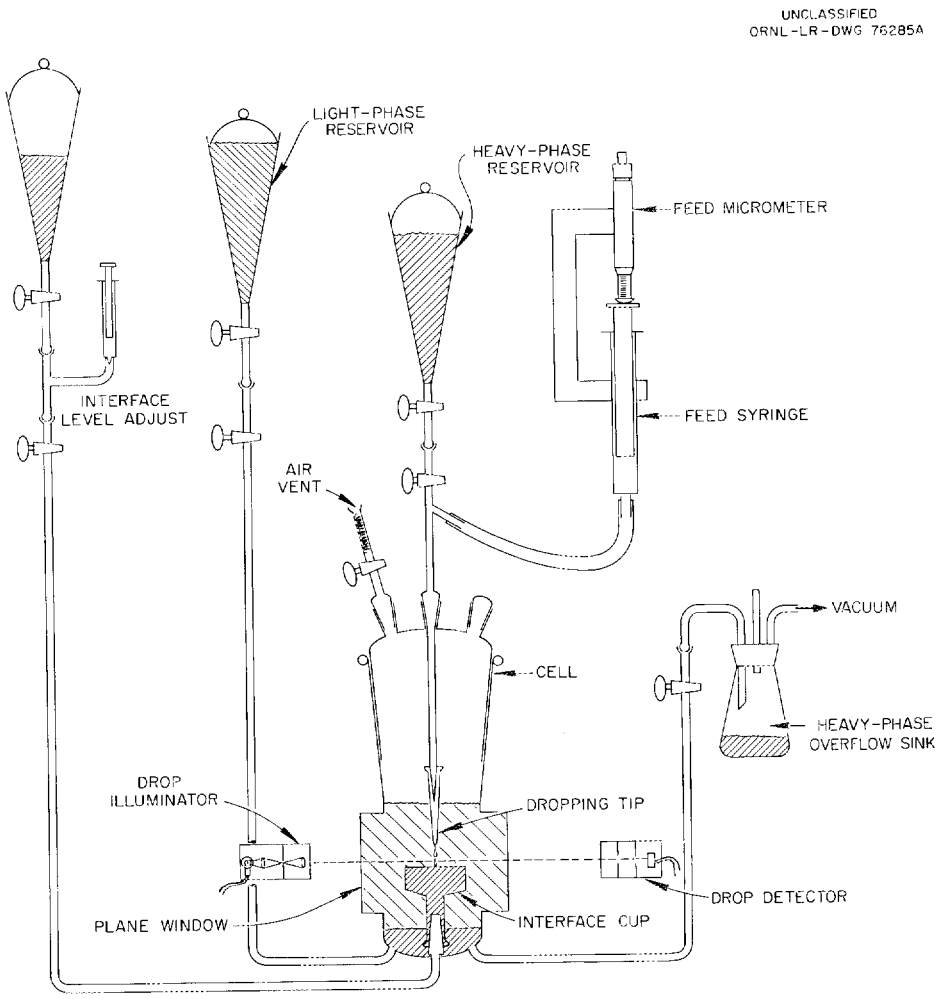

Fig. 18.5. Schematic of Coalescence Cell and Connected Equipment.

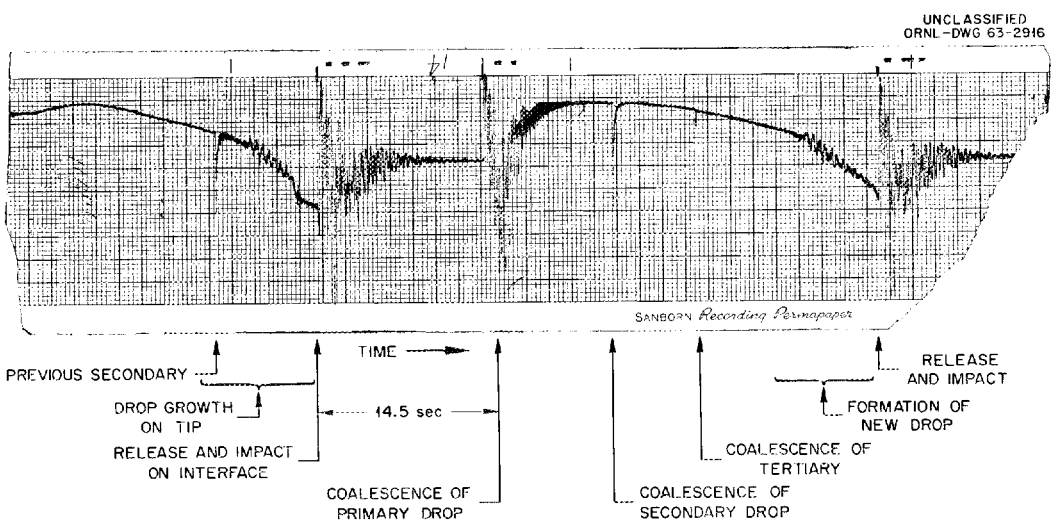

Fig. 18.6. Oscillograph from Photoelectric Drop Detector.

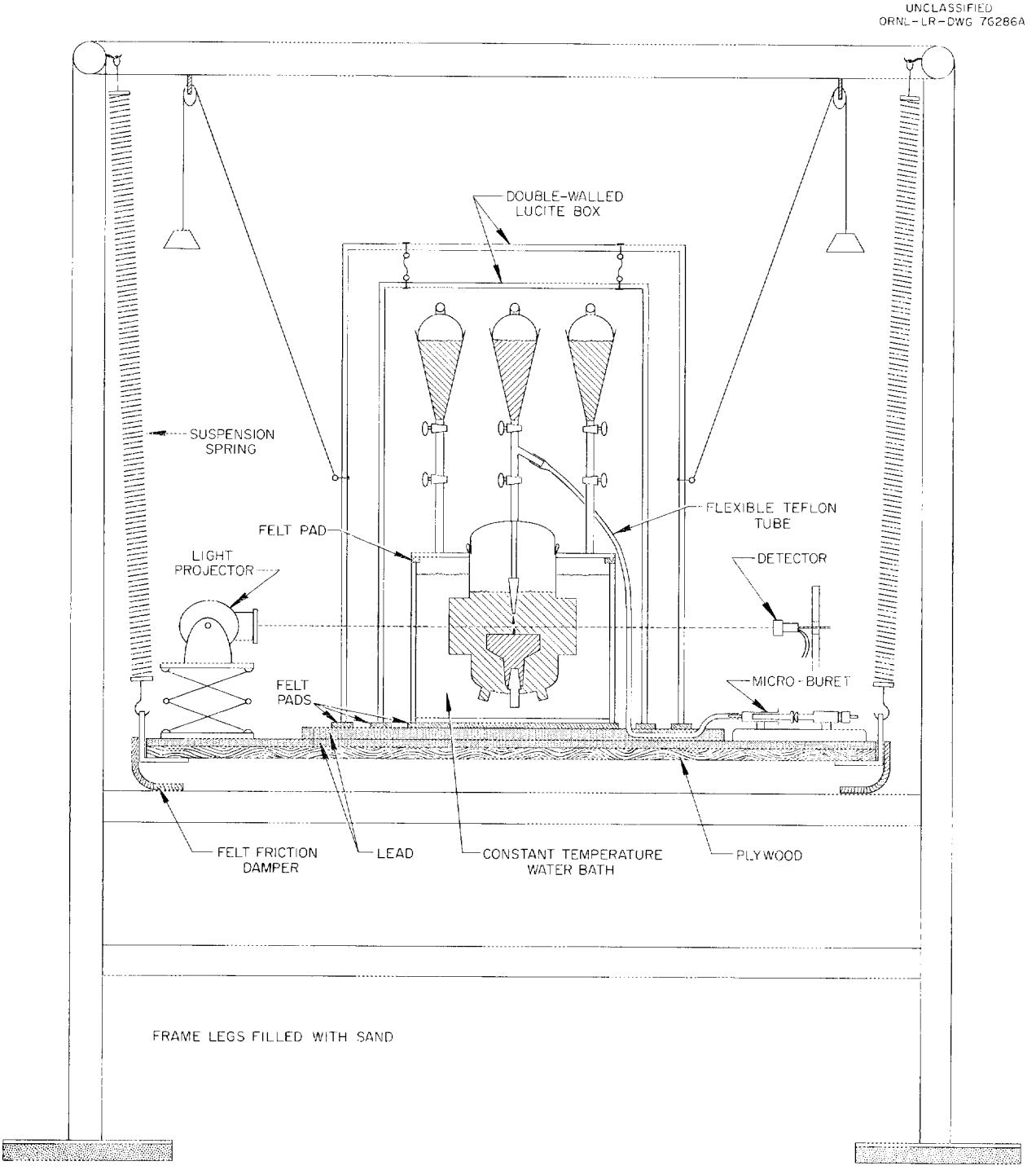

Fig. 18.7. Acoustical and Thermal Isolation System for Coalescence Cell.

ionizing particles in a manner similar to that suggested for the nucleation of bubbles in a bubble chamber. Among other things, the model predicts that particles less ionizing than alphas will not be effective in inducing coalescence.

A preliminary series of runs was made with the system water-benzene, with 10 ppm of dodecylbenzenesulfonate dissolved in the water to produce longer-lived drops. Poor reproducibility was observed, with the lifetimes averaging around 15 ± 6 sec for a 5.3-mm-diam drop. In the only neutron irradiation so far, the *n,p* reaction was used, and the lifetime was 17.5 ± 6.7 sec for neutron irradiation and 16.1 ± 6.3 sec for the control. The results show no statistically significant effect of proton irradiation on drop coalescence. The poor reproducibility was the result of nonuniform aging of the planar interface. Improvements in technique and apparatus are being made.

18.3 DYNAMICS OF GAS-LIQUID CONTACTING IN PACKED TOWERS[1]

The objectives of the study are the development of mathematical techniques for describing the transient behavior of packed, countercurrent, gas-liquid contacting equipment, and the evaluation of these techniques by experiment. The experiments were conducted with a column constructed of 6-in.-ID Pyrex pipe, packed to a depth of 5 ft with $\frac{1}{4}$- and $\frac{5}{8}$-in. ceramic Raschig rings. The system air-CO_2-water was employed, and both direct-sinusoidal and pulse forcing (i.e., varying with time) of the incoming gas composition were used for dynamic perturbation of the absorber. Overall amplitude ratios and phase shifts were obtained for liquid flows of 0 to 220 lb-moles hr^{-1} ft^{-2} and gas flows of 1 to 10 lb-moles hr^{-1} ft^{-2}. The amplitude ratio is the peak concentration leaving the column divided by the peak concentration in the incoming gas. Agreement between the two perturbation methods was good, and reproducible results from the pulse tests extended to frequencies almost twice as great as those from direct sinusoidal tests. Typical results are shown in Fig. 18.8.

[1]Work done by University of Tennessee under subcontract.

A digital computer program was written for calculating theoretical amplitude ratios and phase shifts as functions of the forcing frequency under the following assumptions: (1) the equilibrium relation is linear, (2) the operating line is linear, and (3) both phases move through the column in slug flow. Results of this program indicate that the dynamic behavior is primarily influenced by the absorption factor, the number of transfer units, and time required for liquid and gas phases to traverse one transfer unit.

Further experimental results must be obtained, including velocity distribution measurements, before dynamic models for packed columns can be evaluated.

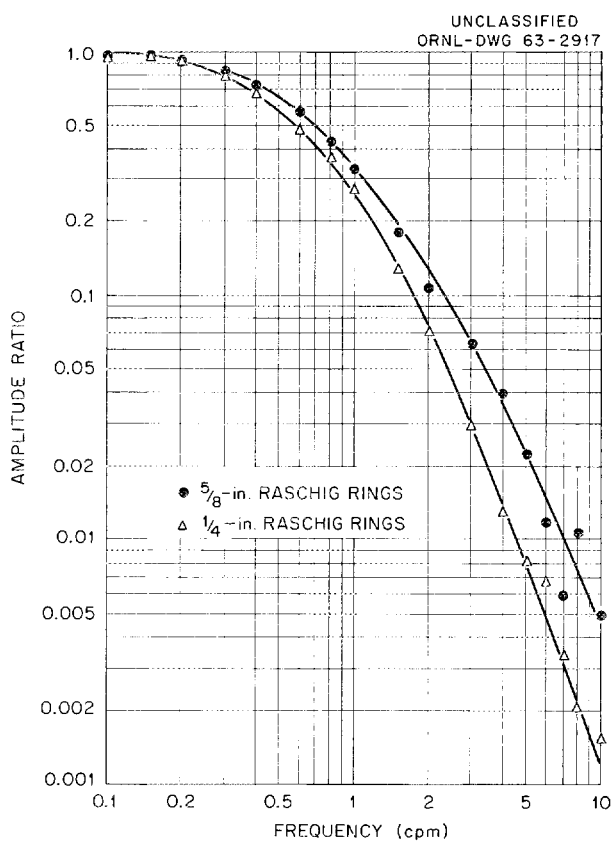

Fig. 18.8. Dynamic Behavior of Packed Tower Due to Pulse Perturbations of the Gas-Phase Concentration. Liquid flow, 55 lb-moles hr^{-1} ft^{-2}; gas flow, 1 lb-mole hr^{-1} ft^{-2}.

19. Gas-Cooled Reactor Coolant Purification

Anticipated impurities of the helium coolant in gas-cooled reactors are: (1) nonradioactive gases such as H_2, CO, CO_2, H_2O, and hydrocarbons; (2) radioactive gases such as Xe and Kr; and (3) particulate matter. These contaminants are to be maintained at low levels by continuous purification of at least a portion of the coolant.

The proposed method for removing the nonradioactive gaseous contaminants is to first oxidize all oxidizable contaminants (H_2, CO, and hydrocarbons) to H_2O and CO_2 and then to remove the H_2O and CO_2 by a co-sorption process. The experimental program has so far included the investigation of the fixed-bed CuO oxidation of H_2, CO, and CH_4 from flowing streams of He.

19.1 OXIDATION OF HYDROGEN, CARBON MONOXIDE, AND METHANE BY FIXED BEDS OF COPPER OXIDE PELLETS

Two different types of CuO pellets were tested for use as the fixed-bed oxidant for H_2, CO, and CH_4 oxidation. These two types were: (1) compacted, nominally $\frac{1}{8}$-in.-diam right circular cylinders manufactured by the Harshaw Chemical Company and (2) a material manufactured by Englehard Industries, which is extruded nominally $\frac{1}{16}$-in.-diam rods with an average length-to-diameter ratio of 4; the CuO is diluted by other metal oxides (silica and alumina).

$\frac{1}{8}$-in.-diam Right Circular Cylinders

Earlier tests made with fixed beds of nominally $\frac{1}{8}$-in.-diam right circular cylinders of CuO showed that the rate controlling factors in the range of experimental conditions tested were: (1) mass transfer of the H_2 or CO from the bulk gas stream to the CuO reaction site and (2) available Cu-CuO reaction surface in the individual CuO particles for CH_4 oxidation.[1]

Mathematical models for each type of reaction were derived, and the resulting differential equations were solved by a finite-difference technique on a high-speed digital computer.[2] The $\frac{1}{8}$-in.-diam right circular cylinders were approximated by spheres with equal surface areas.

The mathematical solution for the H_2 or CO oxidation by fixed beds of CuO has been extended to the generalized case, in which the various experimental parameters are grouped into dimensionless groups that can be used for any system in which the rate of reaction is controlled by mass transfer of the fluid component from the flowing fluid to the solid reaction site.

The generalized differential equations describing this system are:

material balance,

$$\left(\frac{\partial X}{\partial V}\right)_{ZV} = -\left(\frac{\partial Y}{\partial ZV}\right)_V ; \qquad (1)$$

specific reaction rate,

$$\left(\frac{\partial Y}{\partial ZV}\right)_V = K_E X \left[1 - \frac{K_E(1 - R_I)}{K_I R_I + K_E(1 - R_I)}\right] ; \qquad (2)$$

position of reaction interface,

$$\left(\frac{\partial R_I}{\partial ZV}\right)_V = -\frac{1}{3R_I^2}\left(\frac{\partial Y}{\partial ZV}\right)_V ; \qquad (3)$$

where

R_I = dimensionless radius of the reaction interface of the pellet,

V = dimensionless volume of the bed,

X = dimensionless concentration of the fluid impurities,

Y = dimensionless concentration of the reacted phase in the pellet,

Z = dimensionless throughput parameter,

K_E = dimensionless external mass-transport property,

K_I = dimensionless internal mass-transport property.

[1] F. L. Culler, Jr., *et al.*, *Chem. Technol. Div. Ann. Progr. Rept. June 30, 1962*, ORNL-3314, p 202.

[2] C. D. Scott, *The Rate of Reaction of Hydrogen from Hydrogen-Helium Streams with Fixed Beds of Copper Oxide*, ORNL-3292 (1962).

These equations were also solved simultaneously by a finite difference technique on a high-speed digital computer. Their solution is the basis of data presentation for design purposes. Plots of dimensionless bed effluent concentration (X) vs throughput parameter (Z) at various values of K_I and K_E were made, and these plots can be used to determine the size of the CuO bed and breakthrough time for oxidizers if the mass-transport properties K_E and K_I are known. The mass-transport properties K_E and K_I were experimentally determined for H_2 and CO reacting with the $\frac{1}{8}$-in. CuO pellets in the following range of experimental conditions:

Temperature	400–600°C
Pressure	10.2–30.0 atm
Gas mass flow rate	0.0058–0.050 g cm^{-2} sec^{-1}
Contaminant concentration	0.0008–1.21 vol %

$\frac{1}{16}$-in.-diam Rods

The rate controlling factors for the oxidation of H_2, CO, and CH_4 by the $\frac{1}{16}$-in.-diam CuO rods in fixed beds are the same as those found for the $\frac{1}{8}$-in.-diam cylinders, that is, mass transport of the H_2 or CO from the bulk gas phase to the CuO reaction site and available Cu-CuO reaction surface in the individual CuO particles for CH_4 oxidation.[3] However, cylindrical instead of spherical geometry must be used for the CuO phase.

Differential equations were derived for the mathematical model of the reaction systems for the specific cases of H_2 or CO oxidation by the $\frac{1}{16}$-in.-diam rods, in which it was assumed that the rod surface could be approximated by infinite cylinders (no end effects). These equations are: material balance,

$$\left(\frac{\partial C}{\partial t}\right)_z + u\left(\frac{\partial C}{\partial z}\right)_t = -\frac{1}{\epsilon}\left(\frac{\partial n}{\partial t}\right)_z ; \qquad (4)$$

specific reaction rate,

$$\left(\frac{\partial n}{\partial t}\right)_z = kaC\left[1 - \frac{ka \ln (r_E/r_I)}{2\pi\alpha DL + ka \ln (r_E/r_I)}\right]_z ; \qquad (5)$$

[3] M. E. Whatley *et al.*, *Unit Operations Section Monthly Progress Report, September 1962*, ORNL TM-410 (May 1, 1963).

position of reaction interface,

$$\left(\frac{\partial r_I}{\partial t}\right)_z = -\frac{1}{2\pi r_I bL}\left(\frac{\partial n}{\partial t}\right)_z ; \qquad (6)$$

where

C = concentration of contaminant in the gas phase,

t = reaction time,

z = measured distance of the bed from the gas entrance,

u = interstitial gas velocity,

ϵ = external bed porosity,

n = molar density of copper in pellet,

k = mass-transfer coefficient across external gas film,

a = effective mass-transfer area between fluid and CuO pellets,

r_E = radius of CuO pellet,

r_I = radius of Cu-CuO reaction interface in the pellet,

α = effective internal porosity of the pellet,

D = molecular diffusivity of H_2 or CO in gas phase,

L = equivalent average length of a CuO rod in in the CuO bed,

b = initial density of the CuO in the pellet.

These equations were solved simultaneously by a finite-difference technique on a high-speed digital computer, and the solution was used to confirm the reaction mechanism.

Mass-transport properties of both hydrogen and carbon monoxide in the CuO reaction were determined. The internal mass-transport property (effective pellet porosity for molecular diffusion) was determined to be 0.0373 by a number of differential bed tests and by use of the integrated form of Eq. (6). The external mass-transport property (film diffusion mass-transport factor, J_D) was determined from deep-bed tests and by a parameter-search method for the computer solution. The mass-transport factor was correlated as a function of the modified Reynolds number, N_{Re}:

$$J_D = 0.25\, N_{Re}^{-0.68} . \qquad (7)$$

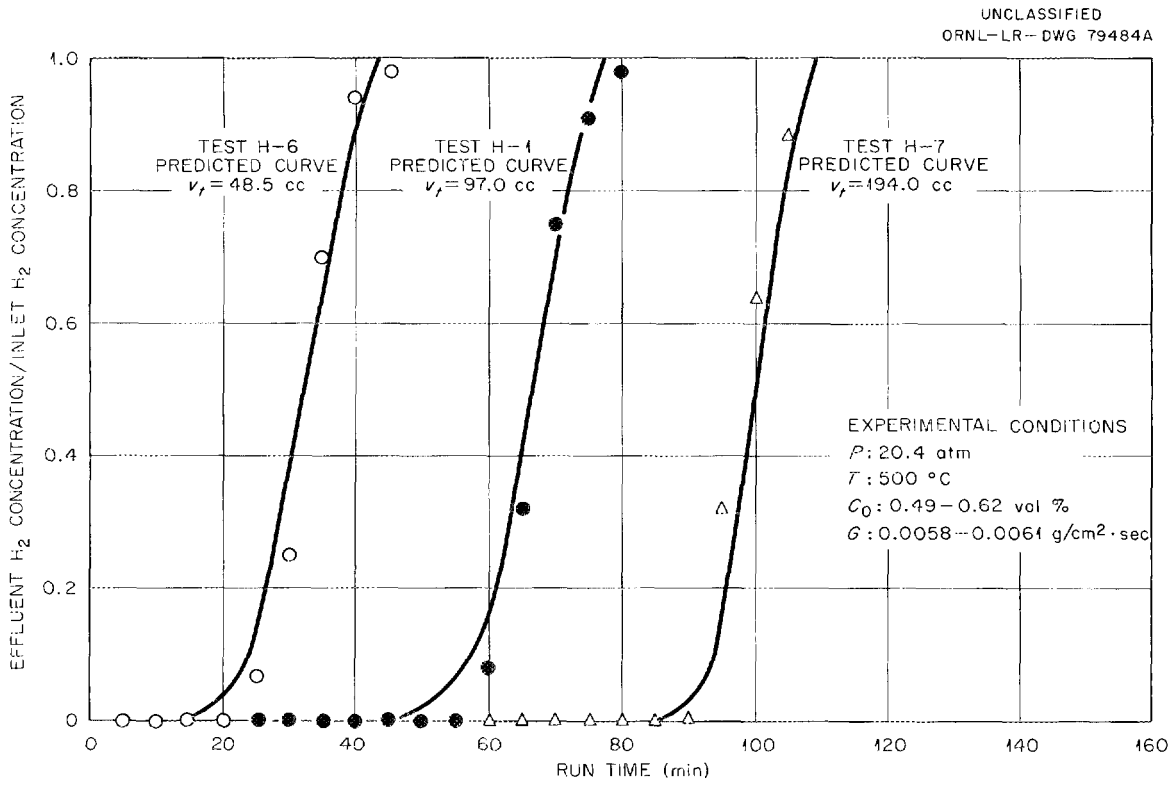

Fig. 19.1. Typical Comparison Between Experimental and Model-Predicted Results for Effluent Hydrogen-Concentration Histories for Tests H-1, H-6, and H-7, Showing the Effect of Change in Volume of the Bed of Copper Oxide.

Confirmation of the mathematical model was demonstrated by comparing the model-predicted concentrations of contaminants in the effluent with the experimental results from the deep-bed tests. The comparisons were within experimental error (Fig. 19.1).

19.2 CHARACTERIZATION OF AEROSOLS BY A LIGHT-SCATTERING TECHNIQUE

An experimental investigation has begun on the characterization of aerosols by determining their particle-size distribution and concentration in gas streams by means of a light-scattering technique. This investigation will have application in the GCR program, where it is desirable to be able to determine aerosol concentration and size distribution in the flowing gas coolant.

The principle of operation of the light-scattering device is to measure the frequency and intensity of light reflected from a known light source by individual particles in a gas stream. Both "near-forward" reflection and 90° reflection will be tested.

Equipment Development

The detecting cell for the light-scattering device has been built. This is a section of $1\frac{1}{2}$-in.-diam pipe into which four optical windows arrayed radially every 90° have been placed, and they will allow light from a primary source to enter the cell through one window and be reflected through the other three. The cell can be placed into an existing gas loop, and the optical system is such that a 1-mm^3 active volume in the middle of the cell is used for the aerosol measurement.

The necessary instrumentation for this system has been designed and is being built or procured. This includes photomultiplier tubes for each of

the detecting windows, a mercury-xenon arc lamp for the light source, a 200-channel pulse-height analyzer, and the necessary electrical circuitry. The 200-channel pulse-height analyzer will be used to count the individual light pulses and determine their light intensity, which will be a function of aerosol-particle size.

Aerosol Generator

In order to calibrate and test the aerosol-characterization device it will be necessary to generate a known aerosol that can be introduced into the detecting unit. Such a generator has been developed. It consists of multiple units which use a concentric-tube pneumatic atomizer capable of atomizing hydrosols or aqueous solutions to particles less than 10 μ in diameter.

If monodisperse hydrosols (all particles of about the same dimensions) of known particle size and concentration are atomized at a known rate into the gas system and the water is evaporated, there results an aerosol of known characteristics. Salt solutions can also be used to produce polydisperse aerosols by atomizing the aqueous salt solution into the gas stream at a known rate and vaporizing the water. The generated aerosol can be further defined by filtering known, small amounts of it through membrane-type filters and measuring and counting particles on the filters by microscopy.

20. Equipment Decontamination Studies

Details of the Gas-Cooled Reactor (GCR) Program in the decontamination research studies have been published in a progress report[1] and in semiannual reports on the GCR.[2,3]

20.1 DECONTAMINATION OF STAINLESS STEELS BAKED IN HELIUM AT 500°C

Stainless steels that had been contaminated in aqueous solutions of fission products and then baked in helium for about 1 hr at 500°C, simulating GCR conditions, were resistant to decontamination in aqueous, noncorrosive reagents.[2] Decontamination was much improved in hot oxalic acid solutions (which caused slightly higher corrosion rates) containing fluoride and hydrogen peroxide.[3] In 0.4 *M* ammonium oxalate–0.16 *M* ammonium citrate–0.34 *M* hydrogen peroxide at pH 4.0 and 95°C, with a corrosion rate for types 347 and 302 stainless steel of less than 0.001 mil/hr, the decontamination factors were 2 to 7 in 2 to 4 hr (Table 20.1). In normally corrosive 0.4 *M* oxalic acid with 0.1 *M* fluoride, in which considerable passivation was attained with 0.1 to 1 *M* H_2O_2 (0.003 mil/hr), the decontamination factors had increased to 17 to 45 in 2 to 4 hr, as shown in the table. In the same acid-fluoride solution, the corrosivity of which was increased to about 0.02 mil/hr by only 0.01 to 0.02 *M* H_2O_2, decontamination factors in 2 to 4 hr were 70 to 300. Thus a favorable prediction may be made for the decontamination of stainless steel blowers and other equipment exposed to high temperatures in the GCR.

[1] A. B. Meservey, *Peroxide-Inhibited Decontamination Solutions for Carbon Steel and Other Metals in the Gas-Cooled Reactor Program: Progress Report, November 1959–July 1962*, ORNL-3308 (Dec. 14, 1962).

[2] W. D. Manly, *Gas-Cooled Reactor Program Semiannual Progress Report for Period Ending Sept. 30, 1962*, ORNL-3372 (Jan. 25, 1963).

[3] W. D. Manly, *Gas-Cooled Reactor Program Semiannual Progress Report for Period Ending Mar. 31, 1963*, in press.

Table 20.1. Decontamination Factors (DF's)[a] Obtained with Oxalate-Peroxide Solutions on Stainless Steels Baked at 500°C in Helium

Fission Product	From Noncorrosive Solution, pH 4	From Corrosive Solution; Corrosion Rate, 0.003 mil/hr	From Corrosive Solution; Corrosion Rate, 0.02 mil/hr
$Zr\text{-}Nb^{95}$	2–4	25–45	100–200
$Ce\text{-}Pr^{144}$	6	20	200–300
$Ru\text{-}Rh^{106}$	2	17	70
$Ba\text{-}La^{140}$	7		70

[a]DF = ratio of initial to final gamma activity on sample.

20.2 DECONTAMINATION OF SPECIMENS CONTAMINATED FROM THE GAS PHASE[3]

Favorable decontamination results were obtained on stainless steels that had been contaminated from the gas phase in helium loops at Battelle Memorial Institute and also on steels contaminated by helium passed over irradiated uranium carbide in the ORNL Metals and Ceramics Division. For example, Battelle samples exposed to helium at temperatures up to 540°C were decontaminated by factors of 65 to 125 in 1 hr at 95°C in noncorrosive oxalate-peroxide at pH 4.0; more-resistant samples (contaminated at 650°C) were completely decontaminated in oxalic acid–fluoride–peroxide solutions. Samples contaminated with iodine and tellurium also responded well to noncorrosive and to slightly corrosive oxalate-peroxide solutions, depending on the temperatures at which the fission products had been deposited.

Further studies will be made on the behavior of volatilized fission products under conditions that simulate those in the GCR.

21. Fuel Shipping Studies

The AEC is currently developing criteria to ensure that the shipment of irradiated fuel assemblies will be done as safely as possible. As part of the ORNL Reactor Evaluation Program, studies were completed on damage (to prototype casks) resulting from impact loading. Assistance in this program was given by the Isotopes, Instrument and Controls, Engineering and Mechanical, and Metals and Ceramics Divisions.

Cost comparisons for two methods of shipping fuel to a southern California processing plant were made for a domestic and for an Italian reactor.

21.1 FUEL CARRIER DROP TESTS

Sixty-five drop tests were made with the eight model casks[1] built for the program and with four 100-lb lead weights. The latter were used to determine the depth of puncturing in lead without the interference introduced by a steel shell. Damage to the casks was slight for drops of 15 ft and under, except on corner and "piston"

[1]*Chem. Technol. Div. Ann. Progr. Rept. June 30, 1962*, ORNL-3314, pp 199–201.

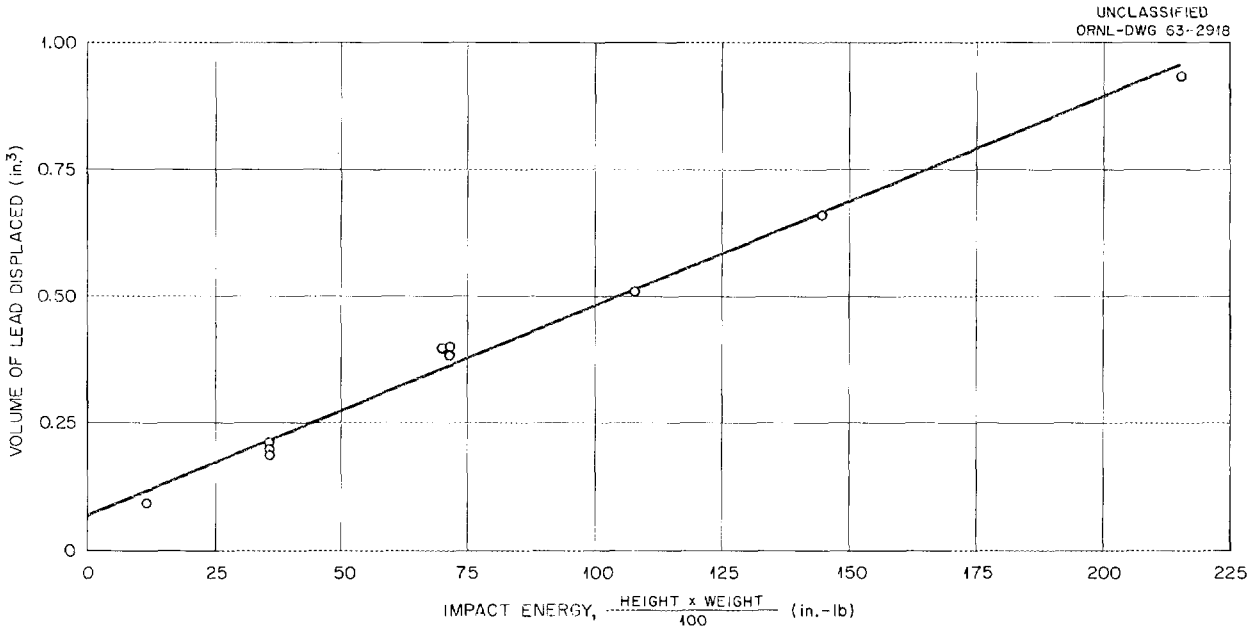

Fig. 21.1. Volume of Lead Displaced as a Function of Impact Energy. Container weight, 100 lb.

drops. Some fracturing of welds was noted; however, welding on the model casks was poor, having only about one-third penetration in some cases. With good-quality welding it is anticipated that no cracks would have been observed in 15-ft drops.

When the 1.4-ton casks were dropped onto a 2-in. piston, the steel shell was penetrated for all drops of 2 ft and above. The penetration data obtained in dropping both casks and lead weights and in more rigidly controlled laboratory tests in the Metals and Ceramics Division are now being analyzed. Figure 21.1 is a plot of the volume of lead displaced as a function of the impact energy when 100-lb lead weights were dropped on a $\frac{3}{4}$-in.-diam piston. The slope of the curve is defined as the "average dynamic-energy-absorption pressure." These results indicate that the average dynamic-energy-absorption pressure for lead under these impact conditions is about 24,500 psi. Similar plots were made for the piston drops of the 1.4- and 6-ton casks which had been dropped on 2- and 4-in.-diam pistons respectively. The slopes of these two curves were 21,300 and 12,600 psi respectively. Thus, there may be both piston and cask size dependence of the energy absorption pressure in lead, which is probably due to strain-rate effects. It has also become evident from tests performed here and at Franklin Institute[2] in Philadelphia that there is a direct correlation between the deformation of a cask and that of an exact scale model of the cask when impacted under identical conditions.

The drop tests made during the last two years indicate that the AEC criteria on cask damage under accident conditions are reasonable, although it will be difficult to meet the proposed piston-drop requirements.[3]

21.2 FUEL SHIPPING COST STUDIES

An analysis of the cost of shipping spent fuel elements from southern California to Hanford, Wash., and from Italy to southern California was

[2]H. G. Clarke, Jr., and W. E. Onderko, "Model Impact Tests Pertaining to Shipping Containers for Radioactive Materials," *Summary Report of AEC Symposium on Packaging and Regulatory Standards for Shipping Radioactive Material Held in Germantown, Maryland, December 3–5, 1962*, TID-7651, p 238.

[3]*Code of Federal Regulations*, Title 10, Part 72 (proposed).

made. The fuel was assumed to be natural uranium irradiated to a level of 8500 Mwd/metric ton.

Truck shipment of a cask filled with 13 fuel elements and weighing 24.5 tons is estimated to cost $0.60 per mile, based on Hanford experience with similar shipments. On this basis the cost of shipping spent fuel the 1175-mile distance would amount to $1.30 per kilogram of uranium at a fuel-discharge rate of 3 tons of uranium per day. This cost includes transportation, handling, and cask depreciation and assumes that a load of this magnitude would be approved by the states through which the fuel is to be hauled.

The corresponding cost of shipping the same distance by rail varied with the size of the shipment, as shown in the following tabulation:

Elements per Cask	Cask Weight (tons)	$/kg
13	24.5	2.23
26	43.5	1.86
48	75.0	1.67

In comparison the predicted cost range in shipping similar fuel 6000 miles round trip from western Massachusetts to Hanford, Wash., based on the cost of shipping spent natural uranium fuels from Chalk River to Savannah River[4] is $1.53 to $2.56 per kilogram of uranium.

The cost of shipping spent fuel 8500 miles from Italy via the Panama Canal to southern California was estimated to be $1.25 per kilogram of uranium, based on a reactor discharge of 3 tons of uranium per day and a burnup of 8500 Mwd/metric ton. This is considerably less than the cost of ocean shipment to New Orleans and overland by rail to southern California (which was estimated at $3.50 per kilogram of uranium), even though the distance is shorter. Shipping costs of this magnitude can be achieved by time-chartering a Liberty ship by the year and making approximately five round trips a year.

[4] L. Isakoff, *Economic Potential for D_2O Power Reactors*, DP-570 (February 1961).

22. Chemical Applications of Nuclear Explosives (Project Coach)

The Chemical Applications of Nuclear Explosives (CANE) Program at ORNL, a part of the Plowshare Program, is an endeavor to study and evaluate various ways in which nuclear explosions may be used to produce chemical reactions, new products, or radioisotopes which are either difficult or impossible to obtain by other means. The major effort this year was devoted to the development of a flowsheet by which the few grams of transplutonium elements to be produced in the forthcoming Coach shot can be recovered from the 10,000 to 35,000 tons of salt in which it will be dispersed. Smaller efforts were devoted to studies on the production and recovery of radioisotopes by jet sampling and on the feasibility of a bubble-tapping line to re-establish communication with the blast zone immediately after the explosion.

22.1 RECOVERY OF ISOTOPES FROM COACH EVENT

The flowsheet development of a process for recovering transplutonium isotopes from salt was done on both a laboratory and a small engineering scale. In the proposed flowsheet 10,000 to 35,000 tons of salt will be mixed and crushed by UCRL. The salt will then be water-leached, leaving a water-insoluble residue that contains 99% of the desired isotopes; and the insolubles will then be separated from the brine and acid-leached to bring the desired elements into solution. The elements from the leach liquor will be concentrated for shipment to an existing AEC site for final processing. All solid and liquid wastes will be disposed of at the Coach site.

Work at ORNL has been directed toward the determination of chemical process flowsheets for the recovery of the transplutonium elements after mining and crushing have been accomplished. The laboratory work is being performed with radioactive cores from the Gnome event.

A 2.5-to-1 weight ratio of water to salt ore was sufficient to leach all the salt from the ore, but about 10% of the ore is insoluble in water under these conditions. The insoluble residue is composed mainly of anhydrite, silicates, and clay and retains more than 99% of the activity. Solubility studies indicate that the amount of insolubles can be reduced by a factor of 2 by leaching with a 25:1 ratio of water to ore and dissolving all the anhydrite. However, the availability of water at the test site is only 50 gpm of brackish water containing 1960 ppm of sulfate and thereby precluding the use of such a high ratio. Activities that are leached by water are Sr^{90} and Cs^{137}, which are expected to have concentrations of 2.5×10^{-3} to 5×10^{-3} μc/ml and which are, respectively, 10 to 500 times the maximum permissible concentration (MPC_w) for occupational exposure. A material-balance flowsheet (based on laboratory experiments) shows that about 2×10^6 kg of insoluble residue and 5×10^7 liters of brine waste will be produced over the one-year processing period (Fig. 22.1). The salt processing rate will be 100 tons/day, as dictated by the availability of water at the site.

Nitric or hydrochloric acid is effective for leaching the water-insoluble residue. When excess acid is used, the activity leached is practically independent of acid concentration for 1 to 10 *N* HNO_3. Acid consumption is 10 to 15 meq/g. About 30 ml of acid per gram of residue is required to leach 70 to 90% of the activity; about 60 to 80% of the water-insoluble residue is soluble in the acid. At ratios less than 20 cc of acid per gram of solid, solids separation was difficult. Room-temperature leaching is as effective as leaching at reflux. Recycle of acid leach liquor to minimize waste volumes may not be possible, because a marked decrease in leaching of plutonium and gross beta activity occurs when the acid is saturated with respect to the water-insoluble residue.

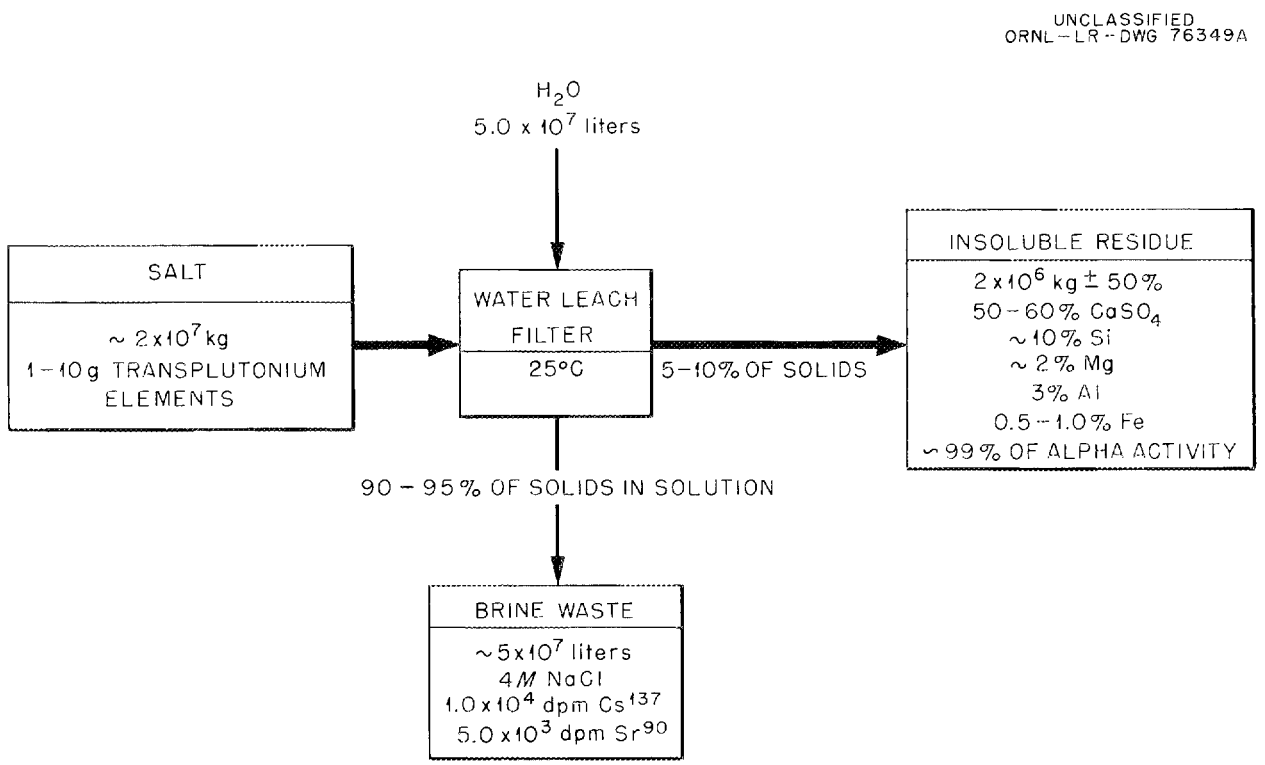

Fig. 22.1. Recovery of Transplutonium Elements from Coach Nuclear Detonation; Water Leach Step.

Partial precipitation of calcium as oxalate is effective for obtaining a primary concentrate at pH 1.0 to 1.5. Experiments with the coprecipitation of $Eu^{152-154}$ tracer from nitric acid solutions saturated with respect to $CaSO_4$ and containing ferric ion showed that 90 to 99% of the europium tracer was carried by precipitating 0.3 to 3.0% of the soluble calcium as the oxalate. A 4:1 mole ratio of oxalate to iron is required because of complex formation with ferric iron.

A material-balance flowsheet for acid leaching and primary concentration shows that about 6×10^7 liters of 1 *N* HNO_3 is required and that about 7×10^7 liters of liquid waste is produced, which must be disposed of safely (Fig. 22.2). Disposal of waste into the Coach cavity after evaporation of the waste in a surface pond is a preferred method of disposal.

Primary concentration by $Fe(OH)_3$ scavenging was investigated as an alternative to partial precipitation of calcium as oxalate. Precipitation of $Fe(OH)_3$ at pH 6 to 8 carried 99.0 to 99.9% of the trivalent actinides; but, in the expected iron concentrations of 0.2 to 0.5 mg/ml, the precipitate is voluminous and retains about 30% of the leach liquor within its gel structure. Thorough washing of the $Fe(OH)_3$ would be required to remove the mother liquor and obtain an acceptable primary concentrate of the actinides. Partial precipitation of the iron is not possible because the $Fe(OH)_3$ precipitates at pH 4.0 to 4.5 and carries only about 10% of the actinides from solution. Presently, solvent extraction systems utilizing tertiary amines and tributyl phosphate are being investigated as possible alternatives to oxalate precipitation.

A tentative equipment flowsheet (Fig. 22.3) for processing Project Coach ore salt to recover actinides was based on a few laboratory tests to characterize the settling and filtration rates of the liquid-solid separation steps. These data were compared with background information from the salt and uranium milling industries. The use of a radioactive sorter is being studied. Such a device, which has been successfully applied to sorting uranium ore, might be used to sort the melt zone salt from the rubble frozen in the melt, thereby reducing the amount of salt to be processed to about 10,000 tons. The salt dissolver probably would be a lixator type used for dissolving rock salt; thus it would be fed automatically to maintain a saturated brine and would require

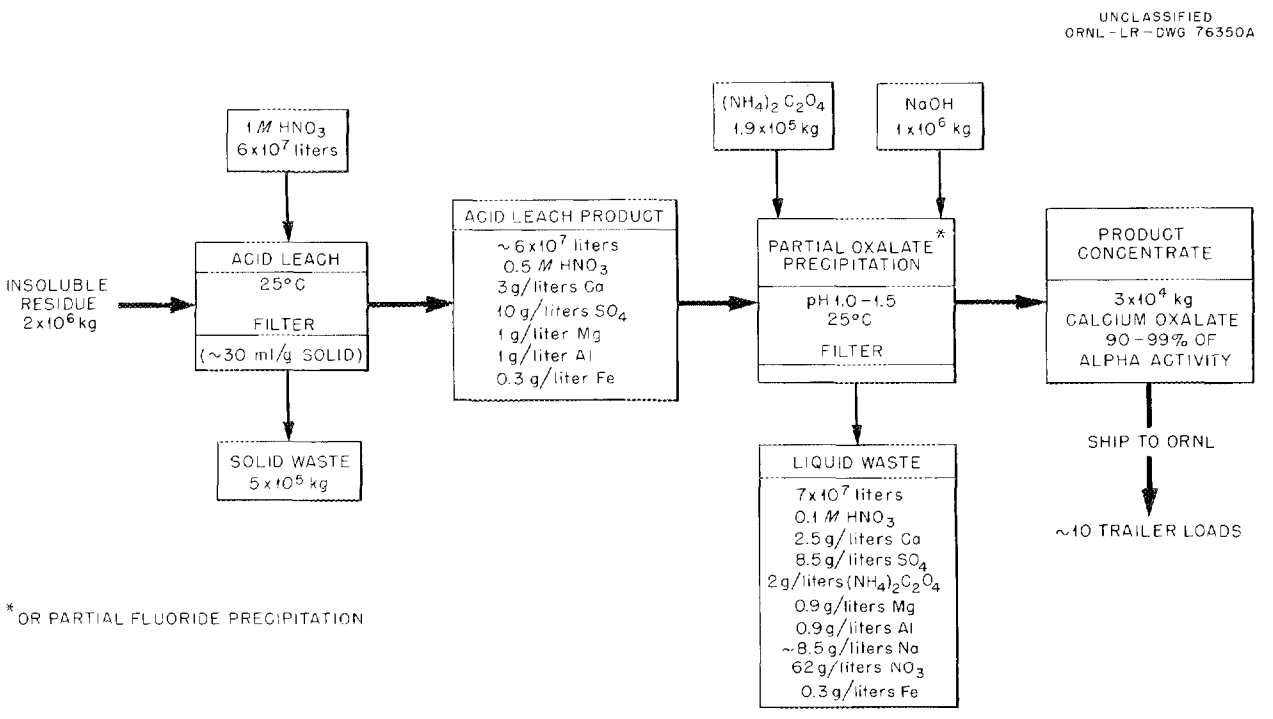

Fig. 22.2. Recovery of Transplutonium Elements from Coach Nuclear Detonation; Acid Leach and Concentration Step.

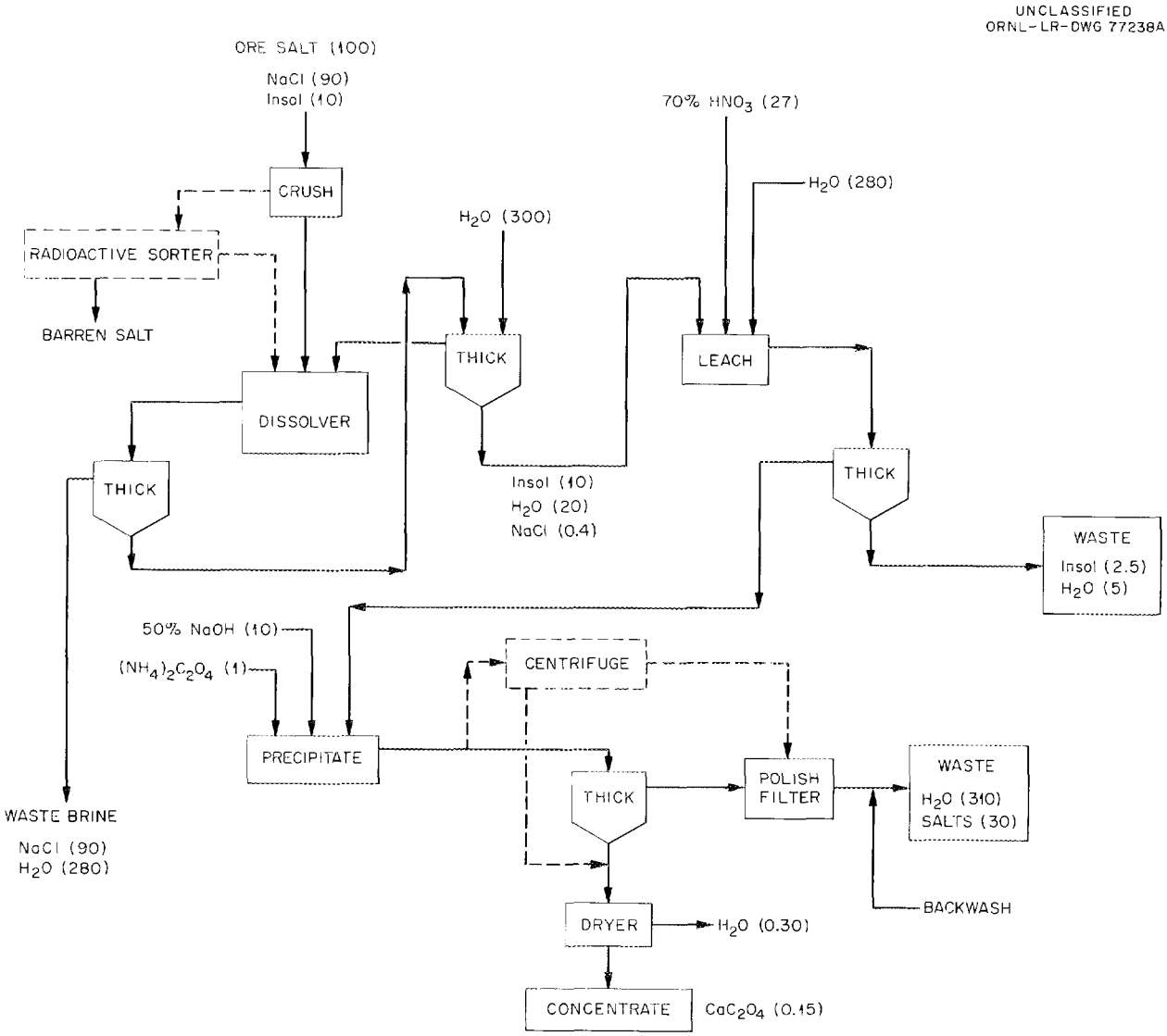

Fig. 22.3. Tentative Equipment Flowsheet for Coach Ore Salt.

no agitation. Countercurrent washing of the water-insolubles in two thickeners, which operate with low maintenance and automatic control, would remove more than 99% of the salt. After the acid-leach step, a single thickener would be adequate for washing the acid residue.

The precipitation step may require batch feed adjustment to obtain good quality control because of the effects of excess oxalate and time. The most practical method of separating the precipitate is not obvious; use of either a thickener or a centrifuge would probably require a polishing filter that could be backwashed — a precoat filter would add undesirable weight and contamination to the product. Final drying or calcining requirements depend on evaluation of shipping hazards and costs.

22.2 JET SAMPLING AND BUBBLE-TAPPING STUDIES

In support work at Frankford Arsenal, uranium target jets were successfully focused and transported about 100 ft at a velocity exceeding the

shock-wave velocity of underground nuclear detonations. The object of this work is the development of a prompt sampler that will expose a heavy-element target to neutron irradiation from a nuclear detonation optimized to maximize external neutron flux and then immediately withdraw the irradiated target from the zone of ensuing destruction so that the target material and irradiation products can be recovered. In a nuclear experiment, an evacuated iron pipe would be prepared for the target transport route so that it would seal after passage of the target and preclude any possibility of venting the detonation. A testing area and a vacuum-pipe chamber have been obtained; the sampler method is under test with high explosives at Frankford Arsenal.

Another study at Frankford Arsenal provided information necessary for proposing a bubble-tapping line to communicate permanently with an underground nuclear detonation cavity immediately after formation. This study indicated that explosives can provide counterpressures in a bubble-tapping line that are phased with the shock wave from the nuclear detonation.

23. Preparation of Uranium-232

The purpose of this program was to prepare pure U^{232} for neutron cross section measurements. Two samples were required: one of several milligrams containing only small amounts of the fissionable isotope U^{233}, and the other a 1-g sample containing up to 1% U^{233}. Preparation of 32.9 mg of U^{232} containing from 180 to 350 ppm U^{233} was discussed in the previous annual report.[1] During the past year, slightly more than 1 g of U^{232} containing 0.72 wt % U^{233} was prepared.

The production method consisted in irradiation of about 45 g of Pa^{231} as an Al-Pa_2O_5 cermet to 1.25×10^{20} *nvt* in the ORR; dissolution of the aluminum matrix and jacket in 8 *M* HCl after nine days of cooling to allow for Pa^{232} decay to U^{232}; sorption of dissolved traces of protactinium and uranium on anion exchange resin from the aluminum dissolver solution; dissolution of Pa_2O_5 in 8 *M* HCl–0.6 *M* HF; selective sorption of uranium on the same anion resin column from the Pa_2O_5 dissolver solution (protactinium forms a strong fluoride complex and does not enter the ion exchange reaction with the resin); and elution of the U^{232} with 0.5 *M* HCl. The uranium product was purified by means of a second anion exchange cycle from mixed HCl-HF solution and a final extraction into 20% TBP from 6 *M* HNO_3. This is the same procedure[1] used for preparing the 32.9-mg sample of U^{232}, with the exception of the longer irradiation and decay times required for producing 1 g of U^{232}.

The uranium product contained 1.04 g of U^{232}. The results of the uranium mass analysis (atomic percent) was 99.243 U^{232}, 0.721 U^{233}, 0.0083 U^{234}, 0.0014 U^{235}, 0.0013 U^{236}, and 0.0235 U^{238}. Alpha energy pulse analysis made within 24 hr of the final separation indicated greater than 98% U^{232}, the remainder being U^{232} daughters. Protactinium was not detectable when the product was analyzed by neutron activation. For the sample size used in this analysis, this means that protactinium contamination was less than 10 wt %, and, in all probability, it was less than 1 wt %.

All the U^{232} products were delivered to the Isotopes Division, which is responsible for the preparation of special forms required for cross section measurements.

This program has been completed except for final recovery of the residual Pa^{231}. During the coming year, it will be decontaminated from fission products, converted to the oxide, and returned to the United Kingdom.

[1] F. L. Culler *et al.*, *Chem. Technol. Div. Ann. Progr. Rept. June 30, 1962*, ORNL-3314, pp 159–64.

24. Assistance Programs

The Chemical Technology Division provided assistance to others on several projects. The Eurochemic Assistance Program was continued. Under this Program ORNL is coordinating the exchange of information between Eurochemic and the various AEC sites and is currently supplying the U.S. Technical Advisor to Eurochemic during the construction and startup periods. The Division is handling the technical liaison for the AEC, ORNL, and the construction contractors for (1) the High Radiation Level Analytical Laboratory (HRLAL) and (2) the Plant Waste Improvements projects. The Molten-Salt Converter Reactor (MSCR) conceptual design and cost estimate, done jointly with the Reactor Division, was revised to compare the economics of discarding residual Pa^{233} with recovering it. The Division designed and built an Interim Alpha Laboratory in the basement of Building 3019 for use by the Metals and Ceramics and the Chemical Technology Divisions. In a combined study program with the Metals and Ceramics and the Reactor Divisions, fuel cycle costs were evaluated for a variety of reactor stations for the production of water and possibly electricity.

24.1 EUROCHEMIC ASSISTANCE

ORNL continued to coordinate the Eurochemic Assistance Program for the exchange of information between Eurochemic and the several AEC sites participating in the program. In addition, ORNL is supplying the U.S. Technical Advisor, E. M. Shank, who will remain at Mol, Belgium, during the construction and startup phases of the Eurochemic Plant.

During the past year, 551 USAEC-originated documents and 99 drawings were sent to Eurochemic. About 37 Eurochemic documents written in English were received, reproduced, and distributed. In addition, about 15 Eurochemic documents written in French were translated and distributed.

The Eurochemic staff was expanded to about 195 people by the end of 1962; this expansion will continue until the authorized complement of 450 people is reached. The preproject designs were completed for all facilities. The plant capacity remains as previously reported except for the plutonium facility, which has been reduced from 3.0 to 1.5 kg/day. A revised cost estimate made in September 1962 gives a construction cost of 24.67 million dollars with an additional 6.03 million dollars operating cost through 1963. The civil engineering design is about 80% complete, and construction is about 50% complete; building construction is about six months behind the schedule anticipated in November 1961.

The main process consists of two solvent extraction cycles of a Purex-type flowsheet. The plutonium facility is being designed to use a 30% tributyl phosphate flowsheet. A new French stainless steel, Uranus S, is being evaluated as a material for waste evaporators. Two special studies were made relative to the processing of enriched uranium on the Eurochemic site; a final decision from the Eurochemic Board of Directors is expected by July 1963. The Board has authorized the management to start preliminary processing-contract negotiations.

24.2 HIGH RADIATION LEVEL ANALYTICAL LABORATORY

Construction of the High Radiation Level Analytical Laboratory for the Analytical Chemistry Division was started in the fall of 1962. All site-preparation work, consisting of the dismantling of Building 2005, site excavation, and the installation of the stabilized aggregate base for the new building, was done by the H. K. Ferguson Company of Oak Ridge, Tennessee, on a cost-plus-fixed-fee basis. The lump-sum contract for the erection of the new laboratory was awarded to the Foster and Creighton Company of Nashville, Tennessee. Construction by the Foster and Creighton Company throughout the period of this report was confined to the installation of concrete pits, type 304L stainless steel piping and ductwork, and Hastelloy C and Duriron drainage systems located in the stabilized aggregate base under the main floor of the building. Under the present schedule, the facility is scheduled for completion early in 1964.

24.3 PLANT-WASTE-SYSTEM IMPROVEMENTS

Several improvements and additions to the ORNL radioactive waste system (Fig. 24.1) are currently being made, based on Process Design Section studies and criteria previously described in detail.[1,2] During the past year design consultation and detailed review of all drawings and specifications were continued as an assistance effort to the ORNL Operations Division. Construction of the project is currently in progress and is being followed.

The purposes of these improvements are (1) to provide adequate water-cooled storage for acid, high-level radioactive waste; (2) to eliminate the use of soil seepage pits and trenches for disposing of intermediate-level radioactive waste; and (3) to assist in obtaining the goal of ≤ 0.1 MPC_w in low-level radioactive discharges to White Oak Creek.

Construction was started in March 1963 on the low- and intermediate-level waste collection and

[1] *Chem. Technol. Div. Ann. Progr. Rept. May 31, 1961*, ORNL-3153, p 137.

[2] *Chem. Technol. Div. Ann. Progr. Rept. June 30, 1962*, ORNL-3314, p 211.

UNCLASSIFIED
ORNL-LR-DWG 72322A

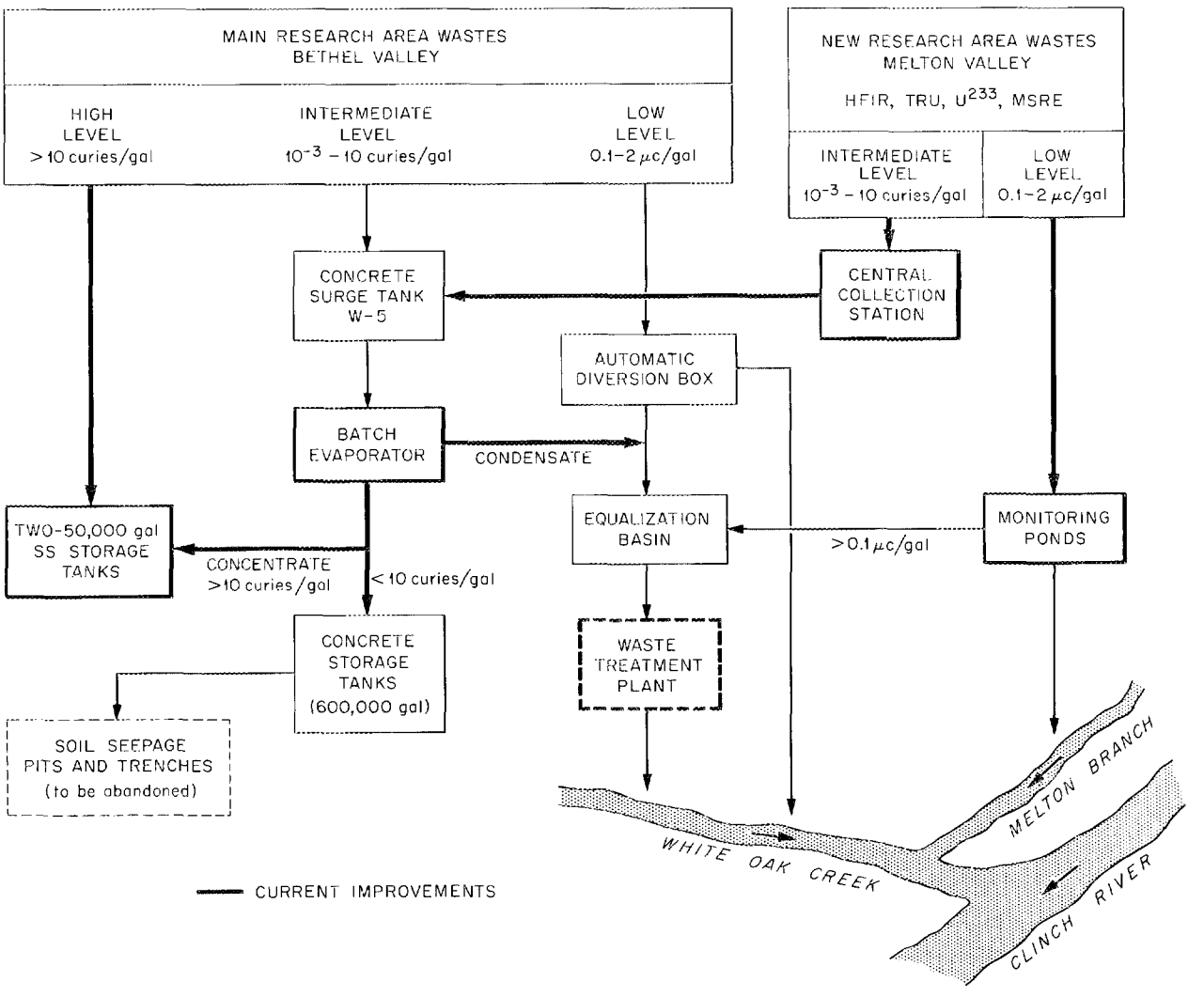

Fig. 24.1. ORNL Radioactive Waste System.

transfer systems to serve new research facilities now being built in Melton Valley about $1\frac{1}{2}$ miles south of the main ORNL area. The facilities to be served are the High Flux Isotope Reactor, the Transuranium Processing Plant, the Thorium-Uranium Fuel Cycle Development Facility (U^{233}), and the Molten-Salt Reactor Experiment. Activity monitoring ponds for low-level waste, a central collection station for intermediate-level waste, and pumping stations to deliver contaminated waste to appropriate treatment facilities in the main ORNL area should allow this new area to operate with a minimum activity release to the environment. The Melton Valley phase of the project is scheduled for completion in December 1963 at a bid cost of $159,200.

Construction was also started in March 1963 on Building 2531 to house a 600-gal/hr intermediate-level waste evaporator and two 50,000-gal stainless steel storage tanks for high-level waste. The building is scheduled for completion in December 1963 at a bid cost of $384,000, exclusive of process equipment. Title II design of the process equipment and piping, which will be installed on a cost-plus-fixed-fee contract after the building is completed, is nearly complete. The evaporator, feed tank, vapor filter, condenser, and scrubber are to be made in the ORNL shops. The evaporator should be installed and in operation by December 1964.

Because of fabrication difficulties and high cost, the design of the external cooling system for the high-level waste tanks was changed from $1\frac{1}{2}$-in.-diam stainless steel pipe welded to the tanks to segmented jackets welded to the tanks. Of several cooling methods studied, spray cooling and partial submersion of the tanks were rejected, as was the use of pentane in the jackets. The current design uses recirculated water as the primary coolant. An intermediate heat exchanger separates the primary and secondary coolants and provides double containment against activity leakage. The secondary coolant is water that is cooled in an evaporative type cooling tower.

Another design change was the removal of the stainless steel liner from the walls and floor of the storage tank vault. The bare concrete vault floor will be curbed under each tank and flooded with water to a depth of 1 in. to dilute any acid-waste leakage from either tank and thus avoid penetration of the floor by an acid leak before it is detected. A sump for each tank area will contain a liquid-level indicator, a sampler, and several jets for emptying the vault. Only one waste tank will be filled at a time, the other tank serving as a spare. A third tank is to be installed in the event of a leak in the first or when the first tank becomes filled. Hot-waste lines from Pilot Plant Building 3019, Fission Products Building 3517, and the new evaporator will connect into the first tank. Several spare lines will also connect to the first tank. The second tank will be so piped that future connections to it can be made without access to the tank or its vault. Alarm indicators for the storage tanks and the evaporator will be telemetered to the new central waste-control center in Building 3105.

24.4 MOLTEN-SALT CONVERTER REACTOR (MSCR) FUEL-PROCESSING STUDY

The MSCR Fuel Processing Study,[3,4] done as a joint effort with the Reactor Division, was completed. Because such a large part of the plant, and therefore plant cost, was required for interim salt storage for Pa^{233} decay, a subsequent study was made to determine the economics of "throwing away" the residual protactinium.

In the original design study and cost estimate, two on-site fluoride volatility processing plants were evaluated. Each plant was assumed to be processing, continuously, irradiated $LiF\text{-}BeF_2\text{-}ThF_4\text{-}UF_4$ fuel from a one-region MSCR capable of producing 1000 Mw (electrical). One plant processed fuel at a rate of 1.2 ft^3/day, the second at 12 ft^3/day; the corresponding capital investments were $\$12.5 \times 10^6$ and $\$25.7 \times 10^6$. The estimated direct operating charges were $\$1.10 \times 10^6$ per year for the smaller plant and $\$2.22 \times 10^6$ per year for the larger one.

The chemical processing scheme consisted in volatilizing uranium as UF_6 by treating the molten salt with elemental fluorine at about 550°C. The hexafluoride was then collected by absorption on NaF and condensation in cold traps, reduced to UF_4 in an $H_2\text{-}F_2$ flame, dissolved in makeup salt, and recycled to the reactor. Makeup fuel was supplied by purchasing fully enriched U^{235}. The

[3] *Chem. Technol. Div. Ann. Progr. Rept. June 30, 1962*, ORNL-3314, p 210.

[4] W. L. Carter, R. P. Milford, and W. G. Stockdale, *Design Studies and Cost Estimates of Two Fluoride Volatility Plants*, ORNL TM-522 (Oct. 10, 1962).

lithium, beryllium, and thorium components of the fuel were discarded with the waste. In the original study, the Pa^{233}-bearing waste was held 135 to 175 days until the Pa^{233} amounted to $\leq 0.1\%$ of the bred uranium, and the salt was then reprocessed for U^{233} recovery.

In the second study, in which the interim Pa^{233}-decay storage area and equipment were omitted from the smaller plant, a capital investment saving of $2,370,000 was realized, which becomes $342,000 per year at an amortization rate of 14.46% per year. Savings in operating cost were not evaluated. At $12 per gram, the amount of protactinium discarded had a value of $191,300 per year. Thus, the net gain in discarding the Pa^{233} is about $151,000 per year.

24.5 INTERIM ALPHA LABORATORY, BUILDING 3019

A general-purpose laboratory to support the Chemical Technology Division's high-alpha-activity research and development program was designed and is under construction. The laboratory, which will be 23 ft 8 in. by 66 ft 8 in., is located in the basement storage and mechanical equipment room of Building 3019, the Radiochemical Processing Pilot Plant.

Personnel access into the laboratory will be via the Building 3019 sample gallery. An existing airlock located in the personnel corridor will permit the delivery of equipment without disrupting containment. Existing windows will be removed and the openings filled with concrete block to ensure containment integrity. The interior walls and ceiling of the laboratory will be coated with acid-resistant paint. The floor will be covered with vinyl plastic sheet, heat-sealed to form a continuous surface and coved at the walls.

The laboratory will be operated as a secondary containment zone and will be served by a central year-round air conditioning system using 100% outside air on a once-through basis.

Ventilation exhaust from the laboratory will be discharged into the Building 3019 cell-exhaust system, which contains roughing and absolute filters. A backflow preventer located in the exhaust header will prevent cross contamination in the event of cell pressurization. The alpha laboratory will be operated in a contained status normally, having at least 0.15-in. (water gage), or greater, negative pressure at all times relative to less contaminated adjoining areas.

Glove boxes will provide primary containment for alpha-emitting materials. Glove-box ventilation exhaust will be given one stage each of roughing and high-efficiency filtration before discharge into the Building 3019 vessel off-gas collection system, which contains a high-efficiency deep-bed filter. The off-gas, after leaving the building deep-bed filter, passes through a final scrubber and absolute filter before discharge to the central stack.

Services will be provided to the laboratory by extension of existing systems in Building 3019 and will include hot and cold water, distilled water, compressed air, vacuum drains, hot drains, and electrical service.

The laboratory is scheduled for occupancy August 1, 1963.

24.6 FUEL CYCLE FOR LARGE DESALINATION REACTORS

Recent studies[5] indicated that large nuclear reactors with good neutron economy may produce heat at a cost low enough for the production of agriculturally suitable water from seawater by distillation. Also, electric power generation in conjunction with water production holds particular promise. Increase in the size of the various units required in a distillation–fuel-cycle complex for such a reactor was a major factor in the favorable economics.

This study was undertaken to determine the magnitude of the fuel cycle cost for several reactor fuels over a wide range of sizes. The cases studied in detail were:

A. Natural uranium, Zircaloy-clad UO_2 elements as shown in Fig. 24.2 at production rates of from 1 to 30 short tons of uranium per day.

B. The same fuel elements at 10 and 30 tons per day, with the irradiated elements discarded rather than processed (the "throwaway" case).

C. Depleted uranium and recycled plutonium so that UO_2–0.5% PuO_2 replaced the natural uranium in the above elements at 1 to 30 tons of uranium per day.

[5] R. P. Hammond, I. Spiewak, and Gale Young, *Prospects for Sea-Water Desalination with Nuclear Energy, an Evaluation Program*, ORNL TM-465 (January 1963).

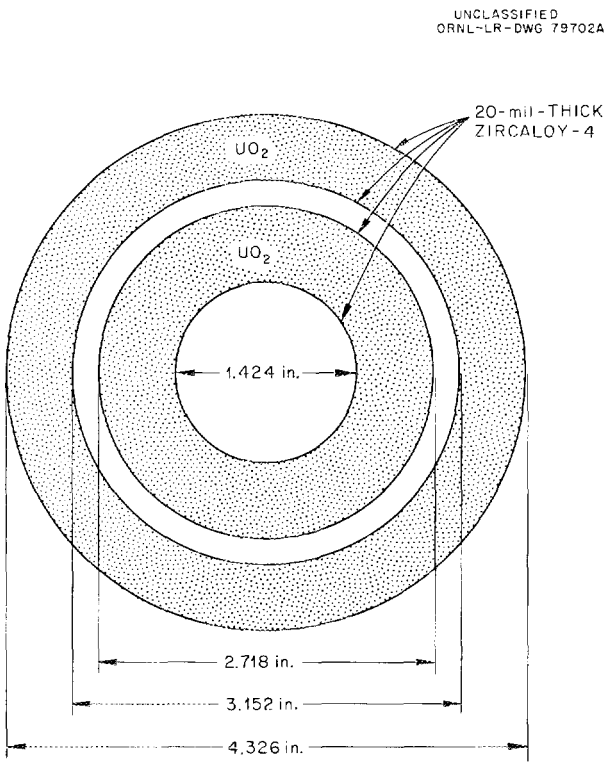

LENGTH: 72 in.

LOADING: 18.92 kg U PER FOOT OF LENGTH, 114 kg U PER ELEMENT

U/Zr RATIO: APPROX 10

Fig. 24.2. Reference Fuel Element Design.

For each of these three studies a flowsheet was prepared through equipment sizing, equipment layout, building concept, and requirements for materials and personnel, and an estimate of actual capital and operating requirements was made. The ORNL Metals and Ceramics Division followed a similar path for the fuel-fabrication step in the fuel cycle. In all cases, the plant units were considered to have a single purpose, with a continuing throughput requirement. For example, the processing of irradiated case-A fuel at 10 tons of uranium per day was done in a plant designed for and operated on case-A fuel at 10 tons per day.

In addition to the detailed estimates above, an attempt was made to study on a comparable basis the fuel cycle cost for the advanced, partially enriched reactors of the Dresden type.

The ground rules for all the studies were: capital charges at 7.7%/yr, municipal financing; inventory charges at 5.5%/yr; $13 per kilogram of uranium for natural uranium in ore concentrates; $2.50 per kilogram of uranium for depleted uranium from diffusion-plant tails; and $30 per kilogram for the cost of separative work[6] in enriching.

Case A, the base case, received the most detailed study. The reprocessing step was based on a slight modification to Farrow's estimates.[7] The results, indicating fuel cycle costs dropping from $43.55 to $0.31 per kilogram of uranium, are shown on Table 24.1 and Figs. 24.3–24.6. The tabulated cost for the refinery at 1 ton per day of uranium is probably high because costs for large plants were extrapolated to costs for plants below a practical size. The cost of Zircaloy was based

[6]M. Benedict and T. H. Pigford, p 403 in *Nuclear Chemical Engineering*, McGraw-Hill, New York, 1957.

[7]W. H. Farrow, Jr., *Radiochemical Separations Plant Study, Part 2 — Design and Cost Estimates*, DP-566 (March 1961).

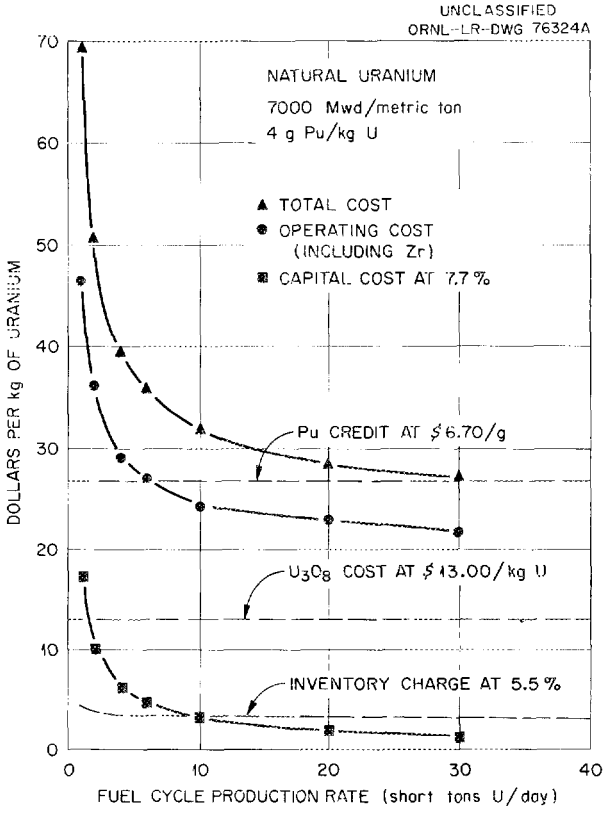

Fig. 24.3. Fuel Cycle Costs vs Production Rate.

Table 24.1. Summary of Fuel-Cycle Costs for Cases A and B

Function	Case A (Natural Uranium)			Case B (Pu "Throwaway")	
	1 Ton U per Day ($ per kg U)	10 Tons U per Day ($ per kg U)	30 Tons U per Day ($ per kg U)	10 Tons U per Day ($ per kg U)	30 Tons U per Day ($ per kg U)
Cost of U_3O_8	13.00	13.00	13.00	13.00	13.00
Refinery, U_3O_8 to UO_3	5.91	0.79	0.48	0.79	0.48
Cost of Zircaloy	4.50	3.58	3.40	3.58	3.40
Cold fuel shipment	0.05	0.05	0.05	0.05	0.05
Fabrication plant	8.04	2.50	1.04	2.50	1.04
Rejection, 5% of above, excluding ore	0.90	0.34	0.25	0.34	0.25
Subtotal, fuel element cost	32.40	20.26	18.22	20.26	18.22
Reprocessing	25.27	3.86	1.94	1.00	1.00
Pu loss at 0.25%	0.07	0.07	0.07		
Shipping irradiated fuel[a]	1.32	1.27	1.27		
Inventory costs, reactor plus fuel cycle	4.17	3.50	3.15	1.43	1.30
Subtotal	63.23	28.92	24.65	22.69	20.52
10% for uncertainty	6.32	2.89	2.46	2.27	2.05
Total	69.55	31.81	27.11	24.96	22.57
Pu credit at 6.70/g and 4 g Pu per kg U	−26.80	−26.80	−26.80		
	43.55	5.01	0.31	24.96	22.57

[a]L. B. Shappert, *An Economic Analysis of Domestic and Overseas Shipment of Spent Reactor Fuel*, ORNL CF-63-1-89 (January 1963).

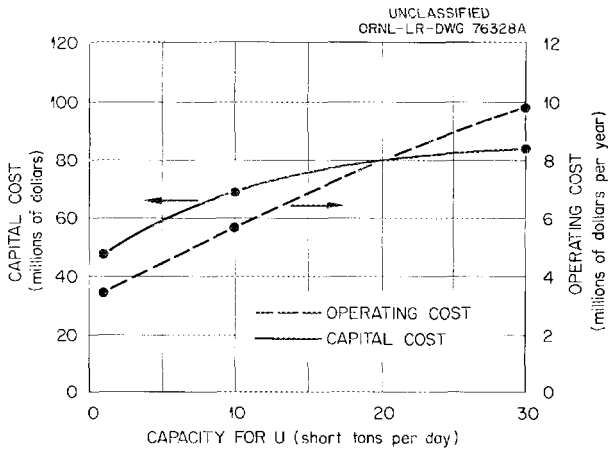

Fig. 24.4. Reprocessing Costs vs Plant Capacity.

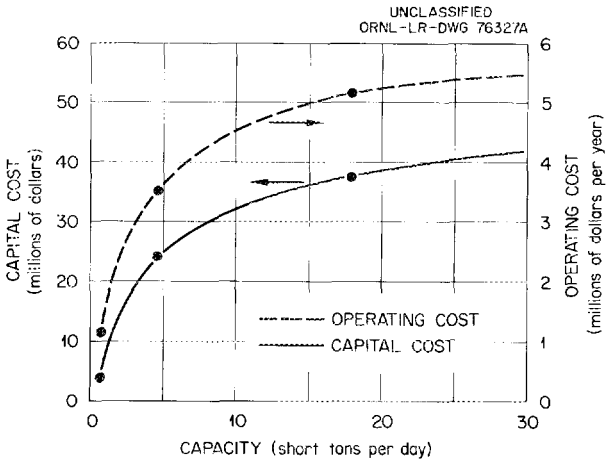

Fig. 24.5. Fabrication-Plant Costs vs Capacity.

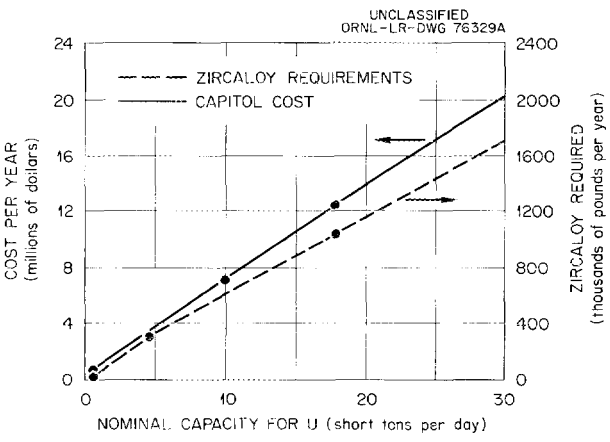

Fig. 24.6. Zircaloy Cost and Requirements vs Fuel Cycle Capacity.

on bids from producers, based on a continuing production. The value of plutonium produced and sold was taken at $6.70 a gram.

If many large reactors using the fuel cited above were in operation, the quantity of plutonium produced would likely affect the value of plutonium. To determine the upper limit of the fuel-cycle cost, the "throwaway" case was estimated at 10 and 30 tons per day of uranium. In this case, plutonium was assumed to have no value, no processing of irradiated fuel was done, and the spent fuel elements were stored under water in a constantly expanding basin near the reactor. Fuel cycle costs were $24.96 and $22.57 per kg of uranium at 10 and 30 tons per day of uranium respectively. The breakdown of the estimate is shown in Table 24.1.

The cost of a plutonium-recycle fuel cycle was determined in order to use it in reactor optimization studies still in progress. The fuel element has the same shape and dimensions as that for the base case but contains depleted uranium and recycled plutonium as UO_2–0.5% PuO_2. The preparation of reactor grade UO_2-PuO_2 was based on a large scaleup of a few successful laboratory sol-gel process experiments. Twelve inches of concrete shielding and remote operation were provided for the sol-gel and fuel fabrication steps. Fuel cycle costs were $59.74 and $22.49 per kilogram of uranium at 1 and 10 tons of uranium, respectively. A more complete summary of the estimate is shown on Table 24.2.

A rough estimate was made for a 10-ton-per-day single-purpose fuel cycle for a reactor fuel element of the Dresden type, using 1.5% enriched fuel. The resulting cost breakdown in dollars per kilogram of uranium was: burnup = 55.50; inventory = 14.30; Zircaloy = 13.40; fabrication = 25.00; reprocessing = 4.25; losses (uranium only) = 0.56; irradiated fuel shipment = 2.96; other charges = 13.78; plutonium credit (at $6.70 per gram) = 29.20; net fuel cycle cost = 100.35. Burnup and inventory charges accounted for 70% of the net fuel-cycle cost. Further details are available in ref 8.

The studies outlined above revealed:

1. Unit costs are reduced by an increase in production requirements for all fuels considered.
2. Natural uranium fuels have the lowest fuel-cycle costs.

[8]F. L. Culler, *The Effect of Scaleup on Fuel Cycle Costs for Enriched and Natural Fuel Systems*, ORNL TM-564 (April 1963).

Table 24.2. Plutonium Recycle Case (Case C)

	Dollars per kg of Uranium at 85% On-Stream Efficiency		
	1 Ton U per Day	10 Tons U per Day	30 Tons U per Day
UF_6 to U_3O_8[a]	0.77	0.23	0.15
U_3O_8 to UO_3	2.08	0.54	0.39
UO_3 to UO_2-PuO_2	3.78	1.20	0.77
Subtotal UF_6 to UO_2-PuO_2	6.63	1.97	1.31
Fabrication	18.35	8.60	
Subtotal UF_6 to element	24.98	10.57	
Processing	26.19	4.10	2.07
Shipping	1.90	1.82	1.82
UF_6 feed	2.50	2.50	2.50
Total cycle without inventory	55.57	18.99	

[a]D. C. Brater and S. H. Smiley, *Capital and Operating Cost Estimates for Conversion of Uranium Hexafluoride to Urano-Uranic Oxide at Rates of 1, 10, and 30 Tons of Uranium per Day*, KL-1559 (Apr. 22, 1963).

3. Plutonium value in the outlined recycle with depleted uranium will be determined by reactor studies now in progress. Preliminary estimates indicate it will likely exceed $3 per gram.

4. Burnup and inventory costs in a slightly enriched uranium fuel cycle exceed the complete cycle costs for natural uranium.

5. Slightly enriched uranium fuel-cycle costs are at least six times those for natural uranium fuel-cycle costs at 10 tons of uranium per day.

24.7 RADIOCHEMICAL PLANT SAFETY STUDIES

The hazards associated with a large radiochemical plant either for fuel processing or radioisotope source production may exceed those of a reactor. There are large amounts of fission products and/or nuclear materials in storage in such plants in readily dispersible form. Uncontrolled chemical reactions, fires, and nuclear accidents provide possible means for dispersal. It is imperative, therefore, that the hazards and means of combating them be assessed and understood before such a plant is built. In order to accomplish this, three general areas must be covered: (1) assessing the credible radiochemical-plant accidents and their consequences and determining which variables have a major effect on the hazards; (2) studying in detail the significant variables (e.g., the properties of aerosols produced in an accident, the mechanisms leading to a criticality accident, the maximum criticality accident possible, etc.); and (3) developing means for combating or ameliorating the consequences of radiochemical-plant accidents.

A comprehensive survey of the hazards associated with U^{233} and Pu^{239} fuel fabrication and radioisotope processing plants was made. This study served the dual purpose of (1) analyzing fuel fabrication and radioisotope processing plant accidents and (2) assessing the potential liability which might result from such accidents. The discussion presented here is essentially a summary of the study which is reported in detail elsewhere.[9]

[9]C. E. Guthrie and J. P. Nichols, *Theoretical Possibilities and Consequences of Major Accidents in U^{233} and Pu^{239} Fuel Fabrication and Radioisotope Processing Plants*, ORNL-3441 (in press).

Theoretical Possibilities and Consequences of Major Accidents in U^{233} and Pu^{239} Fuel Fabrication and Radioisotope Processing Plants

If the anticipated expansion in radioisotope sources and plutonium and U^{233} fuel for reactors is realized, several radiochemical plants for their production must be built and operated within the next 20 years. Typical 1980 yearly production is expected to be 10^4 kg of Pu^{239} fuel, 10^8 curies of Sr^{90} sources, and 100 kg of Pu^{238} isotope sources. Radiochemical plants are normally designed such that in the event of an accident one or more containment systems operate to limit the release of radioactive material to the environment (contained accident). A simultaneous failure of containment would result in the radioactive material being dispersed to the environment (uncontained accident). The simultaneous occurrence of a fire or explosion that disperses the maximum amount of material, containment failure, and unfavorable meteorological conditions (worst uncontained accident) has such an extremely low probability of occurrence as to be deemed incredible. Even so, a study of these accidents is valid in order to obtain an upper limit on liability. The final results of this study are summarized in Table 24.3. This presents the potential economic loss from the worst contained and worst uncontained accidents in Pu^{239}, Sr^{90}, and Pu^{238} fabrication plants. The worst uncontained accident in such plants would possibly result in billions of dollars of economic loss due to damage to the surrounding land and population.

There has been no major off-site contamination from radiochemical plant accidents to date. Although there is not sufficient radiochemical plant operating experience to establish a probability for a major accident, in general, the frequency and severity of accidents in such plants has been lower than in the related chemical industry. A review of the accident experience to date does serve to point out that in most cases serious accidents result from an unforeseen combination of several independent circumstances and that relatively minor accidents can start a series of events that result in a major accident.

In order to evaluate the potential economic loss from radiochemical plant accidents, contamination and personnel exposure levels were assumed, and a dollar loss value was assigned to each level. For personnel exposures of greater than 500 rem per 13 weeks to the critical organ (category A in Table 24.4), a loss of $50,000 per person was assumed; for exposures of from 50 to 500 rem per 13 weeks to the critical organ (category B), a loss of $10,000 per person was assumed; and for exposures of 5 to 50 rem per 13 weeks to the critical organ (category C), a loss of $2,000 per person was assumed. No loss was assumed for personnel exposures of less than 5 rem to the critical organ in 13 weeks. For severe area contamination (category I) resulting in long-term evacuation, total loss of property, and no crops on farmland for 5 years or greater, a loss of $10,000 per person evacuated was assumed; for moderate area contamination (category II) resulting in short-term evacuation, extensive decontamination operations, and restrictions on crops for 1 to 5 yr, a loss of $1,500

Table 24.3. Summary of Potential Economic Loss in Worst Contained and Worst Uncontained Accidents

Type of Plant	Worst Contained Accident		Worst Uncontained Accident	
	Release to Atmosphere	Potential Economic Loss	Release to Atmosphere	Potential Economic Loss
Pu^{239} fuel fabrication	40 g (2.5 curies)	$\$3 \times 10^6$	4 kg (250 curies)	$\$4 \times 10^8$
Sr^{90} source fabrication	220 curies (1.5 g)	2×10^7	50,000 curies (350 g)	5×10^9
Pu^{238} source fabrication	2.2 g (37 curies)	5×10^7	2 kg (34,000 curies)	5×10^{10}

Table 24.4. Summary of Assumed Monetary Losses and Limits for Personnel Exposure and Area Contamination

Loss Category	Effect	Assumed Loss per Person	Sr^{90}	Pu^{239}	Pu^{238}
	Personnel Exposure to Critical Organ (rems per 13 weeks)		**Exposure Limit (curies sec m^{-3})**		
A	>500	$50,000	>4.1	$>6.3 \times 10^{-2}$	$>6.3 \times 10^{-2}$
B	>50 but <500	10,000	$>4.1 \times 10^{-1}$ to 4.1	$>6.3 \times 10^{-3}$ to 6.3×10^{-2}	$>6.3 \times 10^{-3}$ to 6.3×10^{-2}
C	>5 but <50	2,000	$>4.1 \times 10^{-2}$ to 4.1×10^{-1}	$>6.3 \times 10^{-4}$ to 6.3×10^{-3}	$>6.3 \times 10^{-4}$ to 6.3×10^{-3}
	Contamination		**Contamination Limit (curies/m^2)**		
I	Severe (long-term evacuation; total loss of value; no crops $\geq$5 years)	$10,000	$>1.1 \times 10^{-5}$	$>6 \times 10^{-7}$	$>7 \times 10^{-7}$
II	Moderate (short-term evacuation; extensive decontamination; no crops 1–5 years)	1,500	$>1 \times 10^{-6}$ to 1.1×10^{-5}	$>6 \times 10^{-8}$ to 6×10^{-7}	$>7 \times 10^{-8}$ to 7×10^{-7}
III	Minor (no evacuation; minor decontamination; some crops destroyed)	0.005[a]	$>1 \times 10^{-7}$ to 1×10^{-6}	$>6 \times 10^{-9}$ to 6×10^{-8}	$>7 \times 10^{-9}$ to 7×10^{-8}

[a]Per m^2 (not per person).

per person evacuated was assumed; and for minor contamination (category III) requiring only minor decontamination operations and some destruction of standing crops and milk, a loss of $0.005 per square meter was assumed. The quantity of Sr^{90}, Pu^{239}, and Pu^{238} used for each of these categories is summarized in Table 24.4. The levels assumed for other isotopes are presented elsewhere.[9] The contamination levels for I^{131}, Sr^{90}, and Cs^{137} were based on plant uptake studies. For the other isotopes, where such data are not available, the contamination levels were based on the maximum permissible concentration (MPC) and a resuspension factor.

A population density increasing from zero at the site to 500 persons per square mile at 20 miles and farther from the site was found to be reasonably typical for fuel fabrication and radioisotope processing plants. This is essentially the same distribution used in the comparable reactor liability study.[10] A uniform population density of 100 persons per square mile was also used in calculating the loss economics to allow facile conversion of the results to various sites.

The area and downwind distance as a function of isopleths of exposure and ground contamination were calculated with the Gaussian plume-dispersion model, using experimentally verified values of dispersion coefficient, velocities conducive to deposition of particles (deposition velocities), and washout (deposition by condensation and precipitation) rates for practical, consistent sets of weather conditions.[11] The effect of weather conditions on the loss during uncontained accidents is summarized in Table 24.5. Washout maximizes contamination areas, and inversion maximizes personnel exposure. In most cases the maximum loss is for the washout condition.

The consequences of accidents involving 17 isotopes have been calculated, and the potential economic loss has been presented as a function of curies released for each. The potential loss as a function of Sr^{90} release is shown in Figs. 24.7 and 24.8. The quantity of material that must be released to cause a loss of 60 million dollars is presented in Table 24.6 for several isotopes. Release of the fission products from a criticality accident or the worst uncontained accidents involving U^{233} or Kr^{85} would result in less than 60 million dollars in damage.

The worst uncontained accident in a Pu^{239} fuel fabrication facility was postulated to result from a fire and carbon monoxide explosion in a storage area for graphite fuel elements and resulted in the release of 4 kg of Pu^{239} (4% of the inventory) as smoke to the atmosphere. The worst uncontained accident in an isotope recovery and source fabrication plant was assumed to result from a solvent explosion in the cell, dispersing 20% of the activity to the atmosphere. These and other postulated accidents are more fully described and the potential economic losses (Table 24.3) are presented in detail elsewhere.[11]

Table 24.5. Effect of Weather on Economic Loss Due to an Accident Involving a Release of 50,000 Curies Sr^{90}

Loss Category	Potential Economic Loss During: Inversion	Washout	Sunny Day
I	$\$1.0 \times 10^9$	$\$1.6 \times 10^9$	$\$9.0 \times 10^5$
II	2.3×10^9	3.0×10^9	5.8×10^5
III	4.0×10^8	4.2×10^8	6.0×10^4
A	5.0×10^7		
B	1.0×10^7	1.6×10^4	2.8×10^4
C	1.3×10^6	1.6×10^5	5.2×10^4
Total	$\$3.8 \times 10^9$	$\$5.0 \times 10^9$	$\$1.6 \times 10^6$

Table 24.6. Quantity of Material Released to Cause 60 Million Dollars in Damage Under Washout Conditions

Isotope	Amount Released (g)	(curies)
Pu^{239}	1000	60
Pu^{238}	3	60
Sr^{90}	7	1,000
I^{131}	0.6	80,000

[10] *Theoretical Possibilities and Consequences of Major Accidents in Large Nuclear Power Plants*, WASH-740, p 78 (March 1957).

[11] W. M. Culkowski and H. F. Hilsmeier, *Maximum Values of Concentration, Fallout and Washout for Radioisotope Releases*, ORO-599 (March 1963).

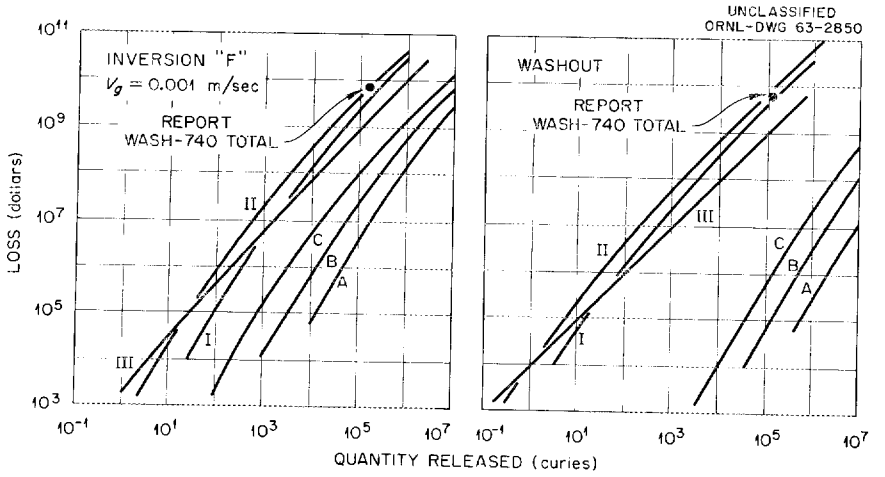

Fig. 24.7. Potential Economic Loss Resulting from Release of Sr^{90}. Typical population distribution.

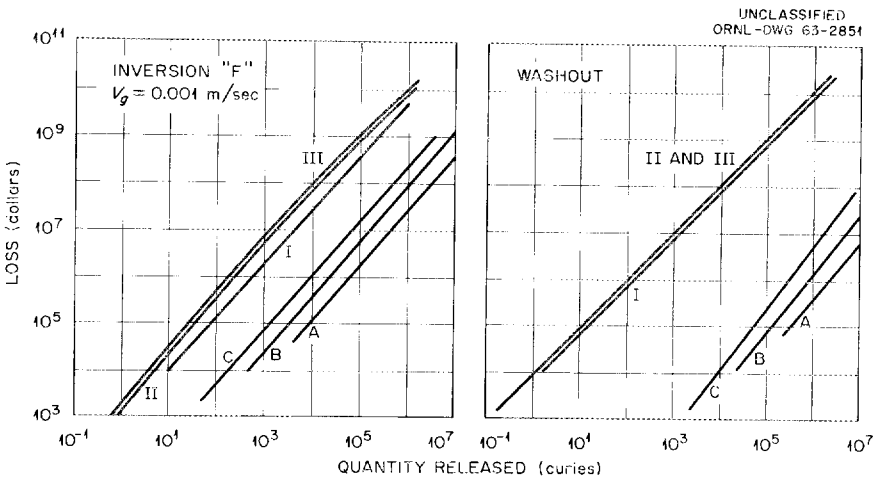

Fig. 24.8. Potential Economic Loss Resulting from Release of Sr^{90}. One hundred persons per square mile.

Nicholson, E. L., "Safety in Fuel-Storage Canals," *Nucl. Safety* 3(4), 63–66 (June 1960).

Publications, Speeches, and Seminars

POWER REACTOR FUEL PROCESSING

Arnold, E. D., and J. P. Nichols, *Hazards Analysis of Fuel Handling Facilities,* ORNL TM-346, presented at the American Chemical Society Meeting, Atlantic City, N. J., Sept. 9–14, 1962.

Blanco, R. E., "Survey of Recent Developments in Solvent Extraction with Tributyl Phosphate," presented at the Symposium on Aqueous Reprocessing Chemistry, Brussels, Belgium, Apr. 23–26, 1963.

Blanco, R. E., *Survey of Recent Developments in Solvent Extraction with Tributyl Phosphate,* ORNL TM-527 (Mar. 21, 1963).

Bradley, M. J., "Hydrolysis of Uranium Carbides Between 25° and 100°C. I. Uranium Monocarbide," *Inorg. Chem.* 1, 683 (1962).

Bradley, M. J., "Hydrolysis of Uranium Carbides Between 25° and 100°C. II. As-Cast Alloys Containing 2 to 10 wt % Carbon," presented at the 144th American Chemical Society Meeting, Mar. 31 to Apr. 5, 1963.

Bradley, M. J., *The Effect of Irradiation on the Hydrolysis of Uranium Carbides. I. Preparation of Uranium Monocarbide Pellets for Irradiation,* ORNL-3403 (Mar. 19, 1963).

Bresee, J. C., and J. T. Long, *Design Philosophy for Direct-Maintenance Radiochemical Processing Plant,* ORNL TM-153 (Mar. 7, 1962), presented at the Nuclear Congress, Radiochemical Processing of Irradiated Reactor Fuels Session, New York, June 4–7, 1962.

Clark, W. E., "Survey of Corrosion in the Atomic Energy Field," Atlanta Chapter, National Association of Corrosion Engineers, Feb. 4, 1963.

Clark, W. E., L. Rice, D. N. Hess, and E. S. Snavely, *Supplemented Studies of the Corrosion of Materials of Construction for the Darex Process,* ORNL TM-417 (Nov. 19, 1962).

Culler, F. L., Jr., R. E. Blanco, L. M. Ferris, E. L. Nicholson, R. H. Rainey, and J. Ullmann, "Proposed Aqueous Processes for Power Reactor Fuels," *Nucleonics* 20(8) (August 1962).

Gens, T. A., *Continuous Dissolution of Zirconium Reactor Fuels in Titanium Equipment: Laboratory Demonstration,* ORNL TM-395 (Jan. 23, 1963).

Goode, J. H. "Hot Cell Demonstration of Zirflex and Sulfex Decladding Processes and a Modified Purex Process at High Irradiation Levels," presented at the American Nuclear Society Meeting, Salt Lake City, Utah, June 1963.

Goode, J. H., M. G. Baillie, and J. W. Ullmann, *Demonstration of the Zirflex and Sulfex Decladding Processes and a Modified Purex Solvent Extraction Process, Using Irradiated Zircaloy-2 and Stainless-Steel-Clad Urania Specimens,* ORNL-3404 (May 9, 1963).

Johnson, H. F., *Analysis of UO_2 Dissolution in Nitric Acid,* ORNL-3297 (Sept. 4, 1962).

Kibbey, A. H., and L. M. Ferris, *U-Th Recovery from Pyrolytic Carbon-Coated Carbide Fuel Particles by Electrolysis in Nitric Acid,* ORNL TM-384 (Sept. 26, 1962).

Moore, J. G., "Separation of Protactinium from Thorium in Nitric Acid Solutions with TBP and Silicon Exchangers," presented at the Protactinium Chemistry Symposium, April 25–26, 1963.

Nichols, J. P., *Soluble Neutron Poisons as a Primary Control in Shielded and Contained Radiochemical Facilities,* ORNL-3309 (July 1962).

Nichols, J. P., "Criticality Control in Fuel Processing Plants," *Nucl. Safety* 4(4), 87–90 (June 1963).

Nichols, J. P., and J. G. Moore, *Soluble Poisons for Criticality Control,* ORNL TM-357, presented at the 142nd Meeting of the American Chemical Society, Atlantic City, N. J., Sept 9–14, 1962.

[illegible] and J. T. Roberts, *Evaluation of Ultimate Disposal*

Nicholson, E. L., "Safety in Fuel-Storage Canals," *Nucl. Safety* 3(4), 63–66 (June 1962).

Rainey, R. H., "Recent Developments in Solvent Extraction with Tributyl Phosphate," presented at the Solvent Extraction Chemistry Symposium, Oct. 23–26, 1962.

Ullmann, J. W., "Fuel Cycles," presented at the Weitzmann Institute, Rehovoth, Israel, June 3, 1963.

Watson, C. D., G. A. West, and W. F. Schaffer, Jr., *Performance of Mechanical Equipment for Dejacketing Spent SRE Core I Fuel,* ORNL TM-367 (Aug. 13, 1962), presented at the 10th Hot Lab and Equipment Conference (sponsored by the American Nuclear Society), Washington, D. C., Nov. 26–28, 1962, and published in the Proceedings of the Conference.

Watson, J. S., *Heat Transfer from Spent Reactor Fuels During Shipping: A Proposed Method for Predicting Temperature Distribution in Fuel Bundles and Comparison with Experimental Data,* ORNL-3439 (May 27, 1963).

FLUORIDE VOLATILITY PROCESSING

Cathers, G. I., and R. L. Jolley, *Recovery of Plutonium(VI) Fluoride by Fluorination of Fused Fluoride Salts,* ORNL-3298 (Sept. 24, 1962).

Cathers, G. I., and R. L. Jolley, "Recovery of PuF_6 by Fluorination of Fused Fluoride Salts," presented at the 144th National American Chemical Society Meeting, Apr. 4, 1963.

Cathers, G. I., R. L. Jolley, and E. C. Moncrief, "Laboratory-Scale Demonstration of the Fused Salt Volatility Process," *Nucl. Sci. Eng.* 13, 391–97 (1962).

Cathers, G. I., R. L. Jolley, and H. F. Soard, *Use of Fused Salt–Fluoride Volatility Process with Irradiated Urania Decayed 15–30 Days,* ORNL-3280 (Sept. 6, 1962).

Jolley, R. L., "Plutonium Recovery in the Fused Salt Volatility Process," presented at the Oak Ridge National Laboratory Volatility Symposium, Nov. 13, 1962.

WASTE TREATMENT AND DISPOSAL

Blomeke, J. O., "Treatment and Disposal of Radioactive Wastes," presented at the Chemical Engineering Graduate School Seminar, Georgia Institute of Technology, Atlanta, Feb. 25, 1963.

Blomeke, J. O., J. J. Perona, R. L. Bradshaw, and J. T. Roberts, "Estimated Costs for Management of High-Activity Power Reactor Processing Wastes," presented at the Ninth Annual Meeting of the American Nuclear Society, Salt Lake City, Utah, June 17–19, 1963.

Brooksbank, R. E., F. N. Browder, W. R. Whitson, and R. R. Holcomb, *Low-Level Waste Treatment. Part II. Pilot Plant Demonstration of the Removal of Activity from Low-Level Process Wastes by a Scavenging-Precipitation Ion-Exchange Process,* ORNL-3349 (May 13, 1963).

Clark, W. E., "Fixation of Simulated Highly Radioactive Wastes in Glassy Solids," presented at the IAEA Symposium on the Treatment and Storage of High-Level Radioactive Wastes, Vienna, Oct. 8–13, 1962.

Godbee, H. W., and W. E. Clark, *The Use of Phosphite and Hypophosphite to Fix Ruthenium from High-Activity Wastes in Solid Media,* ORNL TM-263 (rev. 1) (Jan. 14, 1963).

Godbee, H. W., and W. E. Clark, "Use of Phosphite and Hypophosphite to Fix Ruthenium from High-Activity Wastes in Solid Media," *Ind. Eng. Chem.* 2, 157 (1963).

Holcomb, R. R., *Low-Radioactivity-Level Waste Treatment. Part I. Laboratory Development of a Scavenging-Precipitation Ion-Exchange Process for Decontamination of Process Water Wastes,* ORNL-3322 (June 25, 1963).

Perona, J. J., J. O. Blomeke, R. L. Bradshaw, and J. T. Roberts, *Evaluation of Ultimate Disposal Methods for Liquid and Solid Radioactive Wastes. V. Effects of Fission Product Removal on Waste Management Costs*, ORNL-3357 (June 12, 1963).

Perona, J. J., J. O. Blomeke, R. L. Bradshaw, and J. T. Roberts, "Effects of Fission Product Removal on Waste Management Costs," presented at the Ninth Annual Meeting of the American Nuclear Society, Salt Lake City, Utah, June 17–19, 1963.

Perona, J. J., R. L. Bradshaw, J. O. Blomeke, and J. T. Roberts, *Evaluation of Ultimate Disposal Methods for Liquid and Solid Radioactive Wastes. IV. Shipment of Calcined Solids*, ORNL-3356 (Oct. 4, 1962).

Perona, J. J., R. L. Bradshaw, J. T. Roberts, and J. O. Blomeke, "Economic Evaluation of Tank Storage, Pot Calcination, and Shipping of Power Reactor Reprocessing Wastes," presented at the IAEA Symposium on the Treatment and Storage of High-Level Radioactive Wastes, Vienna, Oct. 8–13, 1962.

Schonfeld, E., *Use of Alkali Carbonate and Alkali Phosphate to Eliminate Inhibitory Effects of Some Impurities on the Precipitation of Calcium and Magnesium from Process Waste Water*, ORNL TM-505 (in press).

Schonfeld, E., and W. Davis, Jr., *Head-End Treatment of Low Level Wastes Prior to Foam Separation*, ORNL TM-260 (May 29, 1962).

Weeren, H. O., "Shale Fracturing Experiment – Descriptions and Hazards," presented before the National Academy of Sciences, Earth Sciences Committee, Washington, D. C., June 7, 1963.

Whatley, M. E., C. W. Hancher, and J. C. Suddath, *Engineering Development of Nuclear Waste Pot Calcination*, ORNL TM-549 (Apr. 29, 1963), presented at the American Institute of Chemical Engineers 50th National Meeting, Buffalo, N. Y., May 5–8, 1963.

TRANSURANIUM ELEMENT PROCESSING

Baybarz, R. D., *Separation of Transplutonium Elements by Phosphonate Extraction*, ORNL-3273 (July 20, 1962).

Baybarz, R. D., "Separation of Transuranium Elements by Phosphonate Extraction," presented at the American Nuclear Society Meeting, Boston, June 18–21, 1962.

Baybarz, R. D., Boyd Weaver, and H. B. Kinser, "Separation of Transuranium Elements from Rare Earths by Tertiary Amine Extraction," presented at the American Nuclear Society Meeting, Boston, June 18–21, 1962.

Leuze, R. E., "Chemical Processing Requirements for Transuranium Element Production," presented at the American Nuclear Society Meeting, Boston, June 18–21, 1962.

Leuze, R. E., R. D. Baybarz, and Boyd Weaver, "Application of Amine and Phosphonate Extractants to Transplutonium Element Production," presented at the Solvent Extraction Chemistry Symposium, Gatlinburg, Tenn., Oct. 23–26, 1962.

Lloyd, M. H., "Americium-Curium Recovery from Plutonium Process Waste," presented at the American Nuclear Society Meeting, Boston, June 18–21, 1962.

Mackey, T. S., *Development of a Reliable Line Disconnect for the Transuranium Processing Facilities*, ORNL-3389 (Feb. 5, 1963).

Nichols, J. P., "Hazard Control in the Transuranium Processing Facility," presented at the Transuranium Element Symposium, Argonne National Laboratory, May 15–17, 1963.

Nichols, J. P., E. D. Arnold, and D. K. Trubey, "Evaluation of Shielding and Hazards in the Transuranium Processing Facility," *Proceedings of the Tenth Conference on Hot Laboratories and Equipment, Washington, D. C., Nov. 26–28, 1962.*

Unger, W. E., B. F. Bottenfield, and F. L. Hannon, "Transuranium Processing Facility Design," *Proceedings of the Tenth Conference on Hot Laboratories and Equipment, Washington, D. C., Nov. 26–28, 1962.*

Yarbro, O. O., J. L. English, and T. S. Mackey, "Process Equipment Design and Development for Transuranium Processing Facility," *Proceedings of the Tenth Conference on Hot Laboratories and Equipment, Washington, D. C., Nov. 26–28, 1962.*

THORIUM FUEL-CYCLE DEVELOPMENT

Arnold, E. D., "Radiation Hazards of Recycled U^{233}-Thorium Fuels," presented at the Thorium Fuel Cycle Symposium, Gatlinburg, Tenn., Dec. 5–7, 1962.

Brooksbank, R. E., A. R. Irvine, A. L. Lotts,[1] and J. D. Sease,[1] "The Oak Ridge National Laboratory Kilorod Facility," presented at the Thorium Fuel Cycle Symposium, Gatlinburg, Tenn., Dec. 5–7, 1962.

Dean, O. C., C. C. Haws, J. W. Snider, and A. T. Kleinsteuber, "The Sol-Gel Process for Preparation of Thoria Base Fuels," presented at the Thorium Fuel Cycle Symposium, Gatlinburg, Tenn., Dec. 5–7, 1962 (published in the Proceedings).

Dean, O. C., R. E. Brooksbank, and A. L. Lotts,[1] "A New Process for the Remote Preparation and Fabrication of Fuel Elements Containing Uranium-233 Oxide–Thorium Oxides," presented at the Eighth Nuclear Congress, Symposium on the Fabrication of Ceramic-Type Fuel Elements for Power Reactors, Rome, Italy, June 19, 1963 (to be published in the Proceedings; issued as ORNL TM-588, June 10, 1963).

Ferguson, D. E., E. D. Arnold, W. S. Ernst, Jr., and O. C. Dean, *Preparation and Fabrication of Thorium Dioxide Fuels,* ORNL-3225 (June 5, 1962).

Irvine, A. R., and A. L. Lotts,[1] "The Thorium Fuel Cycle Development Facility Conceptual Design," Thorium Fuel Cycle Symposium, Gatlinburg, Tenn., Dec. 5–7, 1962.

Kelly, J. L., O. C. Dean, and A. T. Kleinsteuber, "The Preparation of Thorium Dicarbide and Uranium-Thorium Dicarbide Spheres by a Sol-Gel Process," presented at the Eighth Nuclear Congress, Symposium on the Fabrication of Ceramic-Type Fuel Elements for Power Reactors, Rome, Italy, June 20, 1963.

Rabin, S. A., S. D. Clinton, M. F. Osborne, and J. W. Ullmann, *Thorium Fuel Cycle Irradiation Program at ORNL,* TID-7650, presented at the Thorium Fuel Cycle Symposium, Gatlinburg, Tenn., Dec. 5–7, 1962.

SOLVENT EXTRACTION TECHNOLOGY

Allen, K. A., and W. J. McDowell, "The Thorium Sulfate Complexes from Di-*n*-decylamine Sulfate Extraction Equilibria," *J. Phys. Chem.* **67**, 1138 (1963).

Blake, C. A., Jr., W. Davis, Jr., and J. M. Schmitt, "Properties of Degraded TBP-Amsco Solutions and Alternative Extractant-Diluent Systems" (to be published in *Nuclear Science and Engineering),* presented at the Solvent Extraction Chemistry Symposium, Gatlinburg, Tenn., Oct. 23–26, 1962.

---

[1]Metals and Ceramics Division.

Blake, C. A., Jr., A. T. Gresky, J. M. Schmitt, and R. G. Mansfield, *Comparison of Dialkyl Phenylphosphonates with Tri-n-Butyl Phosphate in Nitrate Systems: Extraction Properties, Stability, and Effect of Diluent on the Recovery of Uranium and Thorium from Spent Fuels*, ORNL-3374 (Jan. 8, 1963).

Coleman, C. F., "Amines as Extractants" (to be published in *Nuclear Science and Engineering*), presented at the Solvent Extraction Chemistry Symposium, Gatlinburg, Tenn., Oct. 23–26, 1962.

McDowell, W. J., and C. F. Coleman, "Interface Mechanism for Uranium Extraction by Amine Sulfate," presented at the American Chemical Society Meeting, Los Angeles, Mar. 31–Apr. 5, 1963, and at the Tennessee Academy of Science Meeting, Nashville, Nov. 23–24, 1962.

McDowell, W. J., and C. F. Coleman, "Reagent Dependence in Sodium and Strontium Extraction by Di(2-ethylhexyl)phosphoric Acid," *J. Inorg. Nucl. Chem.* **25**(2), 234–35 (1963).

Ryon, A. D., and R. S. Lowrie, *Experimental Basis for the Design of Mixer-Settlers for the Amex Solvent Extraction Process*, ORNL-3381 (Apr. 19, 1963).

Vaughen, V. C. A., and E. A. Mason, "Equilibrium Extraction Characteristics of Alkyl Amines on Nuclear Fuels Metals in Nitrate Systems," presented at the American Nuclear Society Meeting, Washington, D. C., Nov. 26–28, 1962.

PROTACTINIUM CHEMISTRY

Campbell, D. O., "The Chemistry of Protactinium in Sulfuric Acid Solutions," presented at the Protactinium Chemistry Symposium, Gatlinburg, Tenn., Apr. 25–26, 1963.

Chilton, J. M., "Some Observations on the Behavior of Protactinium in HCl-HF Solutions," presented at the Protactinium Chemistry Symposium, Gatlinburg, Tenn., Apr. 25–26, 1963.

EFFECTS OF REACTOR IRRADIATION ON ThO_2

McBride, J. P., *Radiation Stability of Aqueous Thoria and Thoria-Urania Slurries*, ORNL-3274 (May 18, 1962).

McBride, J. P., and S. D. Clinton, *Radiation Induced Sintering of Thoria Powders*, ORNL-3275 (July 20, 1962).

McBride, J. P., S. D. Clinton, and W. L. Pattison, "Reactor Irradiation of Thoria Powders and Pellets," presented at the Thorium Fuel Cycle Symposium, Gatlinburg, Tenn., Dec. 5–7, 1962 (issued as a paper in TID-7650).

ASSISTANCE PROGRAMS

Nichols, J. P., "Radiation Characteristics and Shielding Requirements of Isotopic Power Sources for Space Missions," presented at the Symposium on Isotopic Power Fuels at ORNL, June 25–26, 1963.

MISCELLANEOUS

Bond, W. D., "A Study of the Stoichiometry of the Reduction of Alkaline Earth Sulfates by Hydrogen," presented at the Tennessee Academy of Science, George Peabody College, Nashville, Tenn., Nov. 23–24, 1962.

Bond, W. D., "Production of Tritium by Contained Nuclear Explosions in Salt: I. Laboratory Studies of Isotopic Exchange of Tritium in the Hydrogen-Water System," ORNL-3334 (Nov. 21, 1962).

Bond, W. D., "Thermogravimetric Study of the Kinetics of the Reduction of Cupric Oxide by Hydrogen," *J. Phys. Chem.* **66**, 1573 (1962).

Brown, K. B., D. J. Crouse, F. J. Hurst, and W. D. Arnold, Jr., "Thorium Reserves in Granitic Rock and Processing of Thorium Ores," presented at the Thorium Fuel Cycle Symposium, Gatlinburg, Tenn., Dec. 5–7, 1962.

Burch, W. D., and L. B. Shappert, "Behavior of Iodine and Xenon in the Homogeneous Reactor Test," *Nucl. Sci. Eng.* **15**(2), 124–30 (1963).

Chester, C. V., "Interfacial Area Measurements by Liquid Scintillation," presented at the Tennessee Academy of Science, Nashville, Tenn., November 1962.

Davis, W., Jr., "Thermodynamics of Extraction of Nitric Acid by Tri-*n*-butyl Phosphate–Hydrocarbon Diluent Solutions. Part I. Distribution Studies with TBP in Amsco 125–82 at Intermediate and Low Acidities," *Nucl. Sci. Eng.* **14**, 159 (1962).

Davis, W., Jr., "Thermodynamics of Extraction of Nitric Acid by Tri-*n*-butyl Phosphate–Hydrocarbon Diluent Solutions. Part II. Densities, Molar Volumes, and Water Solubilities of TBP-Amsco 125-82-HNO_3-H_2O Solutions." *Nucl. Sci. Eng.* **14**, 169 (1962).

Davis, W., Jr., "Thermodynamics of Extraction of Nitric Acid by Tri-*n*-butyl Phosphate–Hydrocarbon Diluent Solutions. Part III. Comparison of Literature Data," *Nucl. Sci. Eng.* **14**, 174 (1962).

Davis, W., Jr., and H. J. de Bruin, "New Activity Coefficients of 0 to 100% Aqueous Nitric Acid Based on a Relation Between Two Thermodynamic Standard States," presented at the Annual Southeastern Regional Meeting of the American Chemical Society, Gatlinburg, Tenn., Nov. 3, 1962.

Drury, J. S., R. M. Hill, B. B. Klima, and H. O. Weeren, "The Enrichment of Oxygen-17. II. Cascade Design and Construction," presented at the American Chemical Society Meeting, Los Angeles, Mar. 31 through Apr. 5, 1963.

Harrington, F. E., "Operating Practices in Contaminated-Clothing Laundries," *Nucl. Safety* 4(2), 96 (1962).

Haws, C. C., Jr., and P. A. Haas, *Pilot Plant Preparation by Flame Processes of 1-Micron Spherical Thoria Particles for Homogeneous Reactor Slurries*, ORNL-3382 (May 22, 1963).

Horner, D. E., D. J. Crouse, K. B. Brown, and B. Weaver, "Fission Product Recovery from Waste Solutions by Solvent Extraction" (to be published in *Nuclear Science and Engineering*), presented at Solvent Extraction Chemistry Symposium, Gatlinburg, Tenn., Oct. 23–26, 1962.

Horner, D. E., D. J. Crouse, K. B. Brown, and B. Weaver, "The Recovery of Fission Products and Other Metals from Aqueous Solutions by Solvent Extraction," presented at the Symposium on Unit Processes in Hydrometallurgy, AIME Meeting, Dallas, Texas, February 1963 (to be published in the Metallurgical Society Conference Series).

Krohn, N. A., "The Influence of Incorporated Radioactivity and External Radiation on the Dehydration of Cyclohexanol over Sulfate Catalysts," PhD dissertation, University of Tennessee, 1962.

Krohn, N. A., and H. A. Smith (University of Tennessee), "The Influence of Incorporated Radioactivity and External Radiations on Sulfate Catalysts," presented at the 142nd National Meeting of the American Chemical Society, Atlantic City, N. J., Sept. 1962.

Krohn, N. A., and R. G. Wymer, "Effects of Incorporated Radioactivity and External Radiation on Heterogeneous Catalysis," presented at the IAEA Conference on the Application of Large Radiation Sources in Industry, Salzburg, Austria, May 1963 (will be published in the Proceedings).

Landry, J. W., "Project Plowshare," presented at the U. S. Army Nuclear Science Seminar, Oak Ridge, Tenn., Aug. 9, 1962.

Landry, J. W., "Peaceful Uses of Atomic Detonations," presented at the U.S. Naval Research Reserve Seminar Dinner Meeting, Oak Ridge, Tenn., Dec. 1, 1962.

Landry, J. W., "Project Plowshare Applications to Highway Engineering," presented at the ORINS course in Radioisotope Applications to Highway Engineering, Oak Ridge, Tenn., Mar. 29, 1963.

Scott, C. D., *The Rate of Reaction of Hydrogen from Hydrogen-Helium Streams with Fixed Beds of Copper Oxide*, ORNL-3292 (July 23, 1962).

Shappert, L. B., "The Cask Testing Program at ORNL," p 82 in *Shipping Container Testing Program, Report of Conference Held at Johns Hopkins University, May 2–3, 1962*, TID-7635.

Shappert, L. B., "The Cask Testing Program at the Oak Ridge National Laboratory," p 211 in *Summary Report of AEC Symposium on Packaging and Regulations Standards for Shipping Radioactive Materials, Held at Germantown, Maryland, December 3–5, 1962*, TID-7651.

Shappert, L. B., "Impact Testing of Shipping Containers" [published in *Trans. Am. Nucl. Soc.* 6(1) (1963)], presented at the American Nuclear Society Meeting, Salt Lake City, Utah, June 16–19, 1963.

Shappert, L. B., "Summary of Drop Test Information," presented at the USAEC Meetings on Container Test Results, Germantown, Md., Aug. 8–13, 1962.

Shappert, L. B., "Cask Impact Testing," presented at the Meeting on Shipping Cask Testing for Reactor Evaluation Studies (sponsored by HAPO) at the University of Texas, Austin, Oct. 29, 1962.

Watson, J. S., *A Study of the Kinetics of Uranyl Sulfate Exchange with a Strong Base Anion Resin*, ORNL-3296 (July 19, 1962).

PROGRESS REPORTS

Chemical Development Section A

Ferguson, D. E., *Status and Progress Report for Thorium Fuel Cycle Development for Period Ending December 31, 1962*, ORNL-3385 (in press).

Ferguson, D. E., *Transuranium Quarterly Progress Report for Period Ending February 28, 1962*, ORNL-3290 (June 6, 1962).

Ferguson, D. E., *Transuranium Quarterly Progress Report for Period Ending November 30, 1962*, ORNL-3408 (May 31, 1963).

Burch, W. D., *Transuranium Quarterly Progress Report for Period Ending February 28, 1963*, ORNL-3482 (in press).

Chemical Development Section B

Blanco, R. E., *Summary Progress Report for Chemical Development Section B, January-July 1962*, ORNL TM-377 (Oct. 31, 1962).

Blanco, R. E., *Quarterly Progress Report for Chemical Development Section B, July-September 1962*, ORNL TM-403 (Feb. 7, 1963).

Blanco, R. E., *Quarterly Progress Report for Chemical Development Section B, October-December 1962*, ORNL TM-545 (in press).

Chemical Development Section C

Brown, K. B., *Progress Report for Chemical Development Section C, April-June, 1962*, ORNL TM-265 (Aug. 13, 1962).

Brown, K. B., *Progress Report for Chemical Development Section C, July-December, 1962*, ORNL TM-449 (Apr. 22, 1963).

Chemical Technology and Health Physics Divisions

Blanco, R. E., and E. G. Struxness, *Waste Treatment and Disposal Progress Report for February and March 1962*, ORNL TM-252 (Sept. 10, 1962).

Ibid., for April-May 1962, ORNL TM-376 (Nov. 5, 1962).

Ibid., for June and July 1962, ORNL TM-396 (Dec. 19, 1962).

Ibid., for August-October 1962, ORNL TM-482 (Mar. 25, 1963).

Ibid., for November 1962-January 1963, ORNL TM-516 (June 12, 1963).

SEMINARS

1962

July 3	Hot Cell Experiments for SRP	M. G. Baillie J. H. Goode
July 10	Glass in the Research Effort	R. W. Poole
July 24	Dynamic Analyses of Gas Absorption	John Prados (University of Tennessee)
July 31	Pot Calcination Pilot Plant	C. W. Hancher E. J. Frederick J. M. Holmes
Aug. 7	The ORNL Criticality Review Committee "Nuclear Reactors for Space (SNAP)"	J. P. Nichols Movie
Aug. 14	Foam Separations	Eliezer Rubin (Radiation Applications, Inc.)
Aug. 21	Preparation of One Gram of U-232	V. C. A. Vaughen J. M. Chilton
Sept. 11	Natural Uranium Concentrate Production from Ores Mined from the Western Slopes of the United States	J. M. Chandler
	"Production of Uranium Feed Materials"	Movie
Sept. 18	"The Story of Camp Century: City Under the Ice" "Ceramic Fuel Fabrication Development for PRTR"	Movie Movie
Oct. 9	ORNL Graduate Education Program	H. B. Willard
Nov. 6	Reactions of Uranium and Thorium Carbides with Aqueous Reagents	M. J. Bradley
Nov. 20	The Stacked Clone Contactor: A High Performance Solvent Extraction Machine	M. E. Whatley W. M. Woods
Nov. 27	Activity Coefficients of Nitric Acid and Tributyl Phosphate	W. Davis
Dec. 4	"Chemistry for the Nuclear Age" (movie)	Norman Keen (Harwell)

Dec. 11	Engineering and Economic Evaluation Studies of Waste Management	J. O. Blomeke J. J. Perona R. L. Bradshaw
1963		
Jan. 8	Visual Communications	Hubert Shuptrine (Technifax Corporation)
Jan. 15	Volatility Processing: Status of Chemical Development NaF Absorption for Uranium Purification The Combustion-Volatility Process for Graphite-Base Fuels	G. I. Cathers M. R. Bennett S. Katz
Jan. 22	Key Word Index	R. R. Dickison (Library)
Jan. 25	Kinetics of Adsorption of Silica on Thoria Surfaces by Infrared Spectroscopy Colloidal Properties of Thoria	Milton Wadsworth (University of Utah)
Jan. 29	Dissolution of UO_2-PuO_2 Pellets Recovery of Values from Uranium-Thorium Fuels	Armando Uriarte (Scientist from Spain) R. H. Rainey
Feb. 5	Chloride Volatility Studies	T. A. Gens
Feb. 19	"Fuel for Nuclear Power" and "Harwell"	Movies (from the United Kingdom)
Feb. 26	Demonstration of Electromagnetic Metal Forming Techniques Using General Atomic Corporation's Magneform Equipment	V. H. Kiplinger (ORGDP)
Mar. 26	Cesium Recovery from Ores	W. D. Arnold
Apr. 9	Recent Developments in Transuranium Element Processing	R. D. Baybarz M. H. Lloyd
Apr. 16	The Status of the Sol-Gel Process The Size and Shape of Colloidal Thoria Particles The Conductivity of Thoria Sols	O. C. Dean K. H. McCorkle A. T. Kleinsteuber
Apr. 23	Volatile and Anhydrous Metal Nitrates and Nitrato Complexes	C. J. Hardy (Harwell)
Apr. 30	Engineering Development of the Sol-Gel Process	J. W. Snider
May 7	Solvent Extraction of U-233 Sol-Gel Process Rod Fabrication	J. L. Matherne C. C. Haws J. D. Sease (Metals and Ceramics Division)
May 14	Process Technology Research at Harwell	K. D. B. Johnson (Harwell)
May 21	Summary of Protactinium Chemistry Symposium	D. O. Campbell
May 28	CINDEX and PIRTEX – Two Important ORNL Processes	M. J. Skinner (Patent Office)

CHEMICAL TECHNOLOGY DIVISION

F. L. CULLER, DIRECTOR
VIRGINIA NELLS, SECRETARY
NANCY ELLISON, SECRETARY
H. B. WHETSEL,* REPORTS EDITOR

H. B. GRAHAM, ADMINISTRATIVE ASSISTANT
BARBARA BREWER, SECRETARY*
W. O. GREEVER, PROCUREMENT
LUCILLE KUYKENDALL, SECRETARY

LONG RANGE PLANNING COMMITTEE

A. T. GRESKY
E. D. ARNOLD
C. E. GUTHRIE, RADIATION OFFICER
J. T. ROBERTS*
J. W. ULLMANN
FRANCES QUILLEN, SECRETARY

TECHNICIAN
P. P. HAYDON

APPLIED RESEARCH GROUP

R. G. WYMER*
N. A. KROHN
R. G. MANSFIELD
D. R. VISSERS

TECHNICIAN
D. M. HELTON

D. E. FERGUSON, ASSISTANT DIRECTOR
IMOGENE LOOPE, SECRETARY

J. C. BRESEE, ASSISTANT DIRECTOR
BARBARA BREWER, SECRETARY*

CHEMICAL DEVELOPMENT SECTION A

R. G. WYMER,* SECTION CHIEF
ALICE MCWILLIAMS, SECRETARY
C. F. KECK, TECHNICIAN
K. H. MCCORKLE, SPECIAL ASSIGNMENT

THORIUM OXIDE STUDIES

J. P. MCBRIDE, GROUP LEADER
L. E. MORSE
W. L. PATTISON

ALPHA MATERIAL PROCESSING

R. E. LEUZE, GROUP LEADER
R. D. BAYBARZ, PROBLEM LEADER, *TRANSURANIUM*
M. H. LLOYD
S. R. BUXTON
V. C. A. VAUGHEN, *HOT CELLS OPERATION*
D. O. CAMPBELL, PROBLEM LEADER, *Po CHEMISTRY*
J. M. CHILTON
J. E. BIGELOW, *HOT CELL EXPERIMENTS*

TECHNICIANS
R. L. HICKEY
S. A. MCCOSH
D. K. TALLENT
J. T. WIGGINS

EQUIPMENT DECONTAMINATION

A. A. MESERVEY, PROBLEM LEADER

TECHNICIAN
D. H. NEWMAN

VOLATILITY PROCESSING

G. I. CATHERS, GROUP LEADER
R. L. JOLLEY, PROBLEM LEADER
H. F. SOARD
M. R. BENNETT
S. KATZ
C. E. SCHILLING

TECHNICIANS
T. E. CRABTREE
C. J. SHIPMAN

FUEL CYCLE STUDIES

O. C. DEAN, GROUP LEADER
A. T. KLEINSTEUBER
J. L. KELLY
G. C. WALL[2]

TECHNICIAN
C. W. GREENE

CHEMICAL DEVELOPMENT SECTION B

R. E. BLANCO, SECTION CHIEF
RUTH WILLIAMS, SECRETARY
BRENDA MOSES, SECRETARY
J. E. FARMER, DRAFTSMAN
J. R. FLANARY,* *HOT CELL SUPERVISOR*

MECHANISMS OF SEPARATIONS PROCESSES, ION EXCHANGE, FOAM SEPARATION

W. DAVIS, JR., PROBLEM LEADER
ERNESTO SCHONFELD[3]
W. C. YEE
H. J. DE BRUIN[4]
M. S. LAWSON
A. H. KIBBEY

WASTE TREATMENT AND DISPOSAL

W. E. CLARK, PROBLEM LEADER
H. W. GOOBEE
R. R. HOLCOMB

TECHNICIANS
G. D. DAVIS
W. E. SHOCKLEY
J. F. EASTERLY

CANE

W. D. BOND, PROBLEM LEADER

TECHNICIAN
J. F. TALLEY

POWER REACTOR FUEL PROCESSING

J. R. FLANARY,* PROBLEM LEADER, *FLOWSHEET DEMONSTRATION ON RADIOACTIVE FUELS*
J. H. GOODE
M. G. BAILLIE[2]

TECHNICIANS
L. A. BYRD
R. C. SHIPWASH
G. E. WOODALL

L. M. FERRIS, PROBLEM LEADER, *HEAD END PROCESSING*
M. J. BRADLEY
T. A. GENS
K. S. WARREN

TECHNICIANS
E. R. JOHNS
J. F. LAND
C. T. THOMPSON

W. E. CLARK, PROBLEM LEADER, *CORROSION STUDIES*

R. H. RAINEY, PROBLEM LEADER, *BREEDER REACTOR FUEL PROCESSING*
J. G. MOORE
ARMANDO URIARTE[3]

TECHNICIAN
R. C. LOVELACE

CHEMICAL DEVELOPMENT SECTION C

K. B. BROWN, SECTION CHIEF
BETH CHRISTIAN, SECRETARY

PROCESSING OF URANIUM, THORIUM, AND OTHER METALS

D. J. CROUSE,* GROUP LEADER
W. D. ARNOLD
F. J. HURST
F. G. SEELEY

SOLVENT EXTRACTION TECHNOLOGY

C. F. COLEMAN,* GROUP LEADER, *FUNDAMENTAL CHEMISTRY AND PLUTONIUM PROCESSING*
W. J. MCDOWELL
J. W. RODDY

TECHNICIAN
G. N. CASE

C. A. BLAKE, GROUP LEADER, *PROPERTIES AND BEHAVIOR OF REAGENTS AND DILUENTS IN RADIOCHEMICAL PROCESSING*
J. M. SCHMITT

TECHNICIAN
W. E. OXENDINE

B. WEAVER, GROUP LEADER, *ACTINIDE, LANTHANIDE, AND OTHER METAL SEPARATIONS*
F. A. KAPPELMANN

TECHNICIAN
J. R. COLLINS

FISSION PRODUCT RECOVERY

D. J. CROUSE,* GROUP LEADER
D. E. HORNER
B. Z. EGAN
LEANDRO SALVADOR RAMOS[2]

TECHNICIAN
W. B. HOWERTON

WATER DESALINATION

C. F. COLEMAN,* PROBLEM LEADER

TECHNICIAN
J. P. EUBANKS

UNIT OPERATIONS SECTION

M. E. WHATLEY, SECTION CHIEF
A. D. RYON,* ASSISTANT SECTION CHIEF
J. T. LONG, *SOOK PREPARATION*
PAULA P. MAYS, SECRETARY
MARTHA M. DAWSON, SECRETARY
MILDRED I. SWANK, SECRETARY

FUEL CYCLE STUDIES AND THORIUM UTILIZATION

P. A. HAAS,* GROUP LEADER
J. W. SNIDER*
S. D. CLINTON

TECHNICIAN
D. A. MCWHIRTER

TRANSURANICS

P. A. HAAS,* GROUP LEADER
T. S. MACKEY

TECHNICIAN
H. D. ARTHUR

FLUORIDE VOLATILITY PROCESS

R. W. HORTON, GROUP LEADER
F. G. KITTS
R. S. LOWRIE
L. E. MCNEESE
W. W. PITT, JR.

TECHNICIANS
J. BEAMS
V. L. FOWLER
F. G. KILPATRICK

SOLVENT EXTRACTION DEVELOPMENT

A. D. RYON,* GROUP LEADER
C. V. CHESTER
F. L. DALEY
W. S. GROENIER
W. M. WOODS, JR.

TECHNICIANS
G. JONES, JR.
K. LADD
C. H. TIPTON

GAS COOLED REACTOR PURIFICATION STUDIES

J. C. SUDDATH,* GROUP LEADER
C. D. SCOTT

TECHNICIANS
R. O. PAYNE
W. G. SISSON

ION EXCHANGE, DESALINATION OF WATER

J. C. SUDDATH,* GROUP LEADER
S. H. JURY[4]
J. S. WATSON

WASTE PROCESSING STUDIES

J. C. SUDDATH,* GROUP LEADER
C. W. HANCHER
L. J. KING
J. J. PERONA

TECHNICIANS
W. L. COLLINS
J. S. TAYLOR

POWER REACTOR FUEL PROCESSING

C. D. WATSON, GROUP LEADER
B. C. FINNEY
B. A. HANNAFORD
H. F. JOHNSON[4]
G. A. WEST

TECHNICIANS
G. B. DINSMORE
F. L. ROGERS
J. C. ROSE
D. E. WILLIS

PROCESS DESIGN SECTION

H. E. GOELLER, SECTION CHIEF
W. E. UNGER,* ASSISTANT SECTION CHIEF
E. M. SHANK, *EUROCHEMIC ASSISTANCE*
W. M. SPROULE, TECHNICIAN
J. W. LANDRY, *CANE PROJECT*
W. G. STOCKDALE, *ECONOMIC STUDIES*
R. SALMON[1]
W. B. WINSBRO, *HRLAL*
F. E. HARRINGTON, *WATER DESALINATION*
W. L. CARTER[3]
MAY PEPPER, SECRETARY
NELLINE ROSS, SECRETARY
MARY RUTH HALL, SECRETARY
JOHANA WALKER, SECRETARY
K. F. STOOKSBURY, CLERK

DRAFTSMEN
J. H. MANNEY,[7] CHIEF
S. H. BEASLEY[7]
EVELYN BRIDGES[7]
J. W. DAY
B. G. DEVALL
O. E. DUNNING[7]
H. W. FALLON[7]
A. J. FARAFR
L. C. HUBBARD[7]
A. D. OLDHAM[7]
J. D. PHILLIPS[7]
J. N. WHEELER[7]

TRANSURANIUM PROGRAM

W. E. UNGER,* GROUP LEADER
B. F. BOTTENFIELD, *BUILDING 7920 DESIGN*
E. J. BREEDING[5]
G. B. BERRY[7]
B. N. HOBBARDS[7]
F. L. HANNON,* *MECHANICAL EQUIPMENT*
W. D. BURCH, *PROCESS DESIGN*
O. O. YARBRO
B. F. CRUMP[3]
F. L. PEISHEL, *TEST EQUIPMENT DESIGN*
W. R. WHITSON, *TEST EQUIPMENT EVALUATION*
J. P. NICHOLS, *SHIELDING AND CONTAINMENT*

POWER REACTOR FUEL PROCESSING

E. L. NICHOLSON, PROBLEM LEADER
W. F. SCHAFFER,* *MECHANICAL PROCESSING*
L. D. SHAPPERT, *FUEL SHIPPING STUDIES*
A. M. ROM, *CHLORIDE VOLATILITY*

WASTE STUDIES

J. O. BLOMEKE, PROBLEM LEADER
J. M. HOLMES, *POT CALCINATION*
B. B. KLIMA, *HOT CELL STUDIES*
E. J. FREDERICK, *MECHANICAL EQUIPMENT*
F. N. BROWDER, *PLANT WASTE CHANGES*
H. O. WEEREN, *HYDROFRACTURING*
W. F. SCHAFFER,* *DISPOSAL IN SALT*
P. L. ROBERTSON, *PLANT WATER SURVEY*
H. W. PFUHL, TECHNICIAN

THORIUM FUEL CYCLE

A. R. IRVINE, PROBLEM LEADER
J. W. ANDERSON,[7] *MECHANICAL EQUIPMENT*
J. W. SNIDER,* *PROCESS EQUIPMENT*
J. W. SHEPPARD,[7] TECHNICIAN

FLUORIDE VOLATILITY PROCESS

R. P. MILFORD, PROBLEM LEADER
J. B. RUCH
C. E. PRINCE,[1] TECHNICIAN

PILOT PLANT SECTION

R. E. BROOKSBANK, SECTION CHIEF
R. B. LINDAUER[3]
BOBBIE HOYLE, SECRETARY
JUNE DAVIS, SECRETARY

FLUORIDE VOLATILITY PROCESS

W. H. CARR, GROUP LEADER
S. MANN, *OPERATIONS*
F. W. MILES
F. L. YOUNGBLOOD
E. C. MONCRIEF,* *DATA*
R. G. NICOL

TECHNICIANS
M. C. HILL
R. R. LAXSON
H. C. THOMPSON

OPERATORS
C. W. BOATMAN
E. C. BRANTLEY
J. H. BROCK
W. J. BRYAN
H. C. CALDWELL
C. H. JONES
G. R. THOMPSON

RADIOCHEMICAL OPERATIONS

J. M. CHANDLER, GROUP LEADER
J. L. MATHERNE, *SOLVENT EXTRACTION OPERATIONS*
M. G. BAILLIE[2]
W. A. SHANNON
E. C. MONCRIEF,* *LOW LEVEL WASTE PILOT PLANT*
C. C. HAWS, *SOL GEL OPERATIONS*
R. J. SHANNON
F. W. DAVIS, *HANCOCK AND WILCOX CO. EMPLOYEE*
T. KOIZUMI[2]

DRAFTSMAN
R. B. WATERS

TECHNICIANS
W. T. BOSTIC
E. W. BROWN
J. H. GROOVER
W. A. LINDSEY
R. E. PURKEY
J. H. WALKER

*DUAL CAPACITY
[1]ON LEAVE OF ABSENCE TO IAEA, VIENNA
[2]ON LOAN FROM TECHNICAL INFORMATION DIVISION
[3]RESEARCH PARTICIPANT
[4]FOREIGN RESEARCH PARTICIPANT
[5]CO-OP STUDENT
[6]CONSULTANT, UT
[7]ON LOAN TO MOLTEN-SALT REACTOR PROJECT
[8]ON LOAN FROM REACTOR DIVISION
[9]ON LOAN FROM P AND E DIVISION

ORNL-3452
UC-10 – Chemical Separations Processes
for Plutonium and Uranium
TID-4500 (22nd ed.)

INTERNAL DISTRIBUTION

1. Biology Library
2-4. Central Research Library
5. Laboratory Shift Supervisor
6. Reactor Division Library
7-8. ORNL – Y-12 Technical Library
Document Reference Section
9-28. Laboratory Records Department
29. Laboratory Records, ORNL R.C.
30. S. E. Beall
31. D. S. Billington
32. C. A. Blake
33. R. E. Blanco
34. E. P. Blizard
35. J. O. Blomeke
36. C. J. Borkowski
37. R. E. Brooksbank
38. G. E. Boyd
39. J. C. Bresee
40. R. B. Briggs
41. K. B. Brown
42. F. R. Bruce
43. W. H. Carr
44. G. I. Cathers
45. J. M. Chandler
46. W. E. Clark
47. C. F. Coleman
48. J. A. Cox
49. D. J. Crouse
50-79. F. L. Culler
80. W. Davis, Jr.
81. O. C. Dean
82. D. A. Douglas
83. D. E. Ferguson
84. L. M. Ferris
85. J. R. Flanary
86. J. L. Fowler
87. J. H. Frye, Jr.
88. J. H. Gillette
89. H. E. Goeller
90. A. T. Gresky
91. W. R. Grimes
92. P. A. Haas
93. J. P. Hammond
94. C. S. Harrill
95. A. Hollaender
96. R. W. Horton
97. A. R. Irvine
98. W. H. Jordan
99. M. T. Kelley
100. J. A. Lane
101. C. E. Larson
102. R. E. Leuze
103. R. S. Livingston
104. H. G. MacPherson
105. R. A. McNees
106. R. P. Milford
107. E. C. Miller
108. K. Z. Morgan
109. L. Nelson
110. E. L. Nicholson
111. R. B. Parker
112. R. H. Rainey
113. A. D. Ryon
114. A. F. Rupp
115. H. E. Seagren
116. M. J. Skinner
117. A. H. Snell
118. J. C. Suddath
119. J. A. Swartout
120. E. H. Taylor
121. V. C. A. Vaughen
122. W. E. Unger
123. B. J. Young
124. C. D. Watson
125. B. S. Weaver
126. A. M. Weinberg
127. M. E. Whatley
128. G. C. Williams
129. R. G. Wymer
130. J. J. Katz (consultant)
131. T. H. Pigford (consultant)
132. P. H. Emmett (consultant)
133. C. E. Winters (consultant)

EXTERNAL DISTRIBUTION

134. R. W. McNamee, Union Carbide Corporation, New York
135. Sylvania Electric Products, Inc.
136. Research and Development Division, AEC, ORO
137. Dr. Barendregt, Eurochemic, Mol, Belgium
138. Giacomo Calleri, CNEN, c/o Vitro via Bacdisseras, Milano, Italy
139. D. J. Carswell, Radiochemical Laboratory, The New South Wales University of Technology, P.O. Box 1, Kensington, Sydney, N.S.W., Australia
140. E. Cerrai, Laboratori CISE, Casella Postale N. 3986, Milano, Italy
141. David Dyrssen, The Royal Institute of Technology, Department of Inorganic Chemistry, Kemisträgen 37, Stockholm 70, Sweden
142. Syed Fareeduddin, Indian Rare Earths Ltd., Army and Navy Building, 148 Mahatma Gandhi Road, Bombay 1, India
143. J. M. Fletcher, United Kingdom Atomic Energy Authority, Atomic Energy Research Establishment, Harwell, Berks, England
144. H. Irving, Department of Inorganic Chemistry, University of Leeds, Leeds, England
145. T. Ishihara, Chemical Engineering Laboratory, Japan Atomic Energy Research Institute, Tokyo, Japan
146. A. S. Kertes, Hebrew University, Jerusalem
147. Y. Marcus, Israel Atomic Energy Commission, Tel Aviv, Israel
148. E. Glueckauf, Atomic Energy Research Establishment, Harwell, Berks, England
149. P. Regnaut, C.E.N. Fontenay-aux-Roses, Boite Postale No. 6, Fontenay-aux-Roses, Seine, France
150. R. Rometsch, Eurochemic, Mol, Belgium
151. A. J. A. Roux, Director of Atomic Energy Research, South African Council for Scientific and Industrial Research, Box 395, Pretoria, South Africa
152. Jan Rydberg, Department of Nuclear Chemistry, Chalmers Tekniska Hogskola, Gibraltargatan 5 H, Goteborg, Sweden
153. Erik Svenke, Director, Department of Chemistry, Atomic Energy Company, Stockholm 9, Sweden
154. D. G. Tuck, University of Nottingham, Nottingham, England
155. B. F. Warner, United Kingdom Atomic Energy Authority, Production Group, Windscale and Calder Works, Sellafield, Seascale, Cumberland, England
156. R. A. Wells, Dept. of Scientific and Industrial Research, National Chemical Laboratory, Teddington, Middlesex, England
157. M. Zifferero, Comitato Nazionale per l'Energia, Nucleare, Laboratorio Trattamento Elementi Combustibili, c/o Instituto di Chemica Farmaceutica e Tossicologica dell 'Universita, Piazzale delle Scienze, 5, Rome, Italy

158-663. Given distribution as shown in TID-4500 (22nd ed.) under Chemical Separations Processes for Plutonium and Uranium Category (75 copies – OTS)